# BCL6 is a context-dependent mediator of the glioblastoma therapy response

By

Anna Kathleen Weston Tribe

A thesis submitted to Victoria University of Wellington in fulfilment of the requirements for the degree of Doctor of Philosophy

Te Herenga Waka – Victoria University of Wellington 2023

# Abstract

Glioblastoma is a rapidly fatal brain cancer with no cure. The resistance of glioblastoma tumours to available therapies means that more effective treatments are desperately needed. Previous research showed that the transcriptional repressor protein BCL6 is upregulated by chemo- and radiotherapy in glioblastoma and that inhibition of BCL6 enhances the effectiveness of these therapies. Therefore, BCL6 is a promising target to improve the efficacy of available treatments for glioblastoma. BCL6 is known as a transcriptional repressor in germinal centre B cells and an oncogene in lymphoma, as well as in other cancers. However, previous research indicated that BCL6 induced by therapy in glioblastoma may not act as a transcriptional repressor. This thesis aimed to clarify the role of BCL6 in the therapy response of glioblastoma. The effect of BCL6 inhibition on the whole proteome response of glioblastoma cells to DNA-damaging treatments was investigated. This confirmed that BCL6 was involved in the therapy response of glioblastoma and that acute irradiation appeared to cause BCL6 to switch from a repressor of the DNA damage response to a promoter of stress response signalling. Rapid immunoprecipitation mass spectrometry of endogenous proteins enabled identification of proteins associated with BCL6 in untreated and irradiated glioblastoma cells. BCL6 appeared to be a transcriptional regulator in untreated glioblastoma and its association with the corepressor NCOR2 was validated using proximity ligation assays. However, association with nuclear proteins was lost in response to acute irradiation. This was accompanied by the irradiation-induced association of BCL6 with plasma membrane proteins. Targeted long-read transcript sequencing did not reveal differential alternative splicing of BCL6 in response to acute irradiation. This indicated that the canonical BCL6 protein was expressed in irradiated glioblastoma cells and that the change in BCL6 function must be mediated by mechanisms other than the production of splice variants, such as through post-translational modification. Overall, these results support the hypothesis that BCL6 is involved in the therapy resistance of glioblastoma cells but reveal that its activity is context-dependent and may be mediated by the intensity of cellular stress.

# Acknowledgements

Thank you to my co-supervisors Melanie McConnell and Paul Teesdale-Spittle for inspiring my fascination with cancer and proteins during undergrad and for coming up with an honours project that perfectly fit my interests. Thank you so much for sticking with me for the last four years even though it looked like this project was going nowhere for the first couple of years! I want to especially thank Melanie for creating a supportive lab group environment that made me feel welcome from the beginning and Paul for going above and beyond to help me push through publication of my meta-analysis and make my plans to attend an international conference a reality.

Thank you to Mum, Dad and Tom for your endless love and support and for helping me to escape PhD life once in a while. Walks, squash, tramps, chats and dinners with you really keep me going. Thank you for spending three years asking whether I'd found BCL6 yet and for being so excited for me when I finally did, even though you're still not sure why I was looking for it in the first place! Now you can read my thesis to find out. Thank you to my wonderful partner Kadin for being beside me every step of the way. I'm not sure whether we'll ever know whether it was a great or terrible idea to start and finish our PhDs at the same time, but we've made it through together. While also slightly terrifying, it is very exciting to be starting our careers together next year. Your love and support mean the world to me. Thank you also to Bryan, Jazz and Anika for always supporting Kadin and me. Thank you to my grandparents and all of my family in the UK. You make it much easier to face the daunting prospect of moving overseas and I'm very excited to spend a couple of years much closer to you all.

Thank you so much to Lifeng Peng for your tireless work keeping the mass spectrometer running. You deserve far more recognition and support than you get and I want you to know how much I appreciate everything you do. The MMc lab group has changed a lot over the years and I owe so many people for their help and support. Thank you to Nicole Stanton for passing over your PhD project into my hands when I was a new honours student. Thank you especially to Leticia Castro, who taught me many of my lab skills, let me vent my frustrations and worked her coding wizardry for me. Thank you to Matt Rowe for being the ghost of the MMc lab and always offering your help from across the world. I'll have to become an MMc ghost myself so that I can still tap into your wisdom when I need to! Thank you to Marie-Sophie Fabre for all of your previous work on this project and for your ongoing interest and support. Thank you to Georgia Carson and Rebecca Dawson for being my PhD role models and always being generous with advice. Thank you to Devlin Forsythe for discussions about our projects and for summers spent trying to figure out our experiments while Melanie was away! A massive thank you to both Alvey Little and Sven Sondhauss for all of your help over the years, even though I wasn't in your lab groups.

Thank you to the Malaghan Institute of Medical Research for allowing me to use your equipment and thank you especially to Alfonso Schmidt for your support and advice. Thank you to George Wiggins from the University of Otago, Christchurch for your advice and for running my data through the FLAIR pipeline yourself when we were having issues with ours. Thank you also to Soleilmane Omarjee from the Cancer Research Institute UK, Cambridge, and Hamish McMillan from the University of Otago for all of your advice about RIME. Thank you to Michaela at Proteome Discoverer support for your patience and your detailed explanations.

Thank you to Hasanah Hamizan, Mackenzie Kiernan, Danielle Lewthwaite, Helena Abolins-Thompson and Kaileen Button for being there for a chat, a rant or a movie night to escape from our projects. I'm really going to miss being in the office with you all. Thank you to Déanna Shea for all of our chats and for your advice. Thank you to everyone at Pure Tough gym, especially Sophie Henkel, Ripley Shi and Sharsha Thota for keeping me sane and smiling even on the most stressful days. And thank you to my oldest friends Jess Just and Tash Miles for being there for me since I was the new girl at school.

# Table of Contents

# List of figures

# List of tables

# 1: Introduction

## 1.1: Glioblastoma

Glioblastoma (GBM) is one of the most aggressive and rapidly fatal cancers.[1,2] Historically called glioblastoma multiforme due to their extensive variability, GBM tumours are highly invasive and resistant to therapy. GBM leads to death within 12 months of diagnosis in 60% of patients.[3] While 5-year survival rates have increased slightly over the last twenty years, prognosis remains dismal and the standard of care has not changed since 2005.[3,4] Therefore, although less common than high-profile cancers such as breast, lung and colorectal cancer, the average years of life lost due to GBM are much greater.[5] Improved treatments are desperately needed to reduce the devastating impact of this disease.

### 1.1.1: Glioma

More than 80% of malignant primary brain tumours are classified as gliomas.[2] Glioma is a term encompassing multiple classifications of brain cancers with morphological similarity to glial cells.[2,6] These include astrocytoma, which account for >75% of gliomas, oligodendroglioma and ependymoma.[2] These glioma types are further divided into classifications such as diffuse astrocytoma, anaplastic astrocytoma, anaplastic oligodendroglioma and glioblastoma, among others.[7] These tumours are named for their resemblance to astrocytes, oligodendrocytes and ependymal glial cells.[2] Despite this resemblance, the origin of glioma cells remains debated, with most recent reviews concluding that multiple cell types may have capacity for transformation into glioma.[8–11] Historically, it was thought that glioma derives from differentiated glial cells which de-differentiate.[12–14] However, due to the low proliferative rate of astrocytes and experiments investigating the transformation potential of cells earlier in the glial lineage, it is now thought by many that progenitor cells are more likely candidates.[8–11,15] There is evidence that glioma may derive from the neural stem cells (NSCs) from which all glial and neuronal cells derive.[16,17] During the progression of tumours derived from NSCs, astrocyte-like or oligodendrocyte-like phenotypes and marker expression could develop, perhaps explaining the mixed characteristics of oligoastrocytomas.[8,18] However, there is also evidence that glioma tumours may derive from oligodendrocyte precursor cells (OPCs).[19] The current consensus is that glioma tumours most likely derive from various different cells of origin, especially NSCs and OPCs, and that this contributes to the intertumoral heterogeneity and molecular subtypes discussed in section 1.1.3.[8–11]

The World Health Organisation (WHO) divides central nervous system tumours into grades I-IV based on their predicted aggressiveness.[2,7] Historically, this grading system was based on histology alone, however increased understanding of molecular differences between tumour types led the WHO to include molecular information in their 2016 classification and grading system.[7] Most notably, the

isocitrate dehydrogenase (IDH) mutation status of glioma tumours is now included in the classification system.[7] Hence classifications such as 'diffuse astrocytoma' are now 'diffuse astrocytoma IDH mutant' and 'glioblastoma' is divided into 'glioblastoma IDH wildtype' and 'glioblastoma IDH mutant'.[7] Mutations in IDH1 (and sometimes IDH2) are very common in grade II and III gliomas.[7,20] Conversely, only around 10% of GBM tumours, which are grade IV, have IDH mutations.[7,20] These cases tend to correspond to tumours that have progressed from lower grade gliomas, referred to as secondary GBM.[7,20] Primary (de novo) GBM tumours tend to be IDH-wildtype.[7,20] Secondary GBM tumours usually occur in younger patients and have a better prognosis, whereas primary GBM tends to arise in patients older than 55 years.[7,20]

IDH1 is cytosolic while IDH2 is mitochondrial, however in their wildtype forms, both catalyse the conversion of isocitrate into α-ketoglutarate.[21] This reaction is coupled to reduction of NADP+ to NADPH and is reversible.[22,23] In glioma, IDH1 is most commonly mutated at R132 and IDH2 is most commonly mutated at R172.[24] These mutant enzymes convert α-ketoglutarate into 2-hydroxyglutarate.[25,26] 2-hydroxyglutarate is considered an 'oncometabolite', meaning that it is a metabolite that accumulates in glioma tumour cells and has a role in their cancerous phenotype.[27,28] 2-hydroxyglutarate is an antagonist of α-ketoglutarate.[27] Therefore, it inhibits histone lysine demethylases and the DNA demethylating TET 5-methylcytosine hydroxylases that depend on α-ketoglutarate for their enzymatic activity.[27–29] This results in increased histone methylation and hypermethylation of CpG islands, leading to the glioma CpG island methylator phenotype (g-CIMP).[30,31] This is thought to be important for glioma tumorigenesis.[27,29,32] Indeed, mutations to *IDH* genes are thought to be early events in glioma tumorigenesis.[33–35] Despite this, IDH mutant tumours tend to be slower growing than IDH wildtype tumours, possibly due to alterations to metabolism downstream of IDH mutation.[36,37] Patients with IDH mutant tumours tend to have a better prognosis.[7,38]

Although many factors have been investigated, the only environmental factor known to increase the risk of brain cancers is ionising radiation (IR) therapy for previous brain tumours.[39–41] However, the risk is stronger for meningioma than glioma.[41] Additionally some rare familial syndromes account for the development of 1-2% of glioma tumours.[6] GWAS studies have also identified single nucleotide polymorphisms (SNPs) associated with increased glioma risk, including SNPs in loci encoding *TP53*, *EGFR*, *CDKN2A-CDKN2B*, *PHLDB1* and *CCDC26*. Genetic factors are thought to account for approximately 25% of glioma cases.[42] The risk of glioma is also higher with increasing age, in males compared to females and in populations with European ancestry.[43] Incidence rates related to these factors are discussed in more detail for glioblastoma in section 1.1.2.

## 1.1.2: Glioblastoma (GBM)

At grade IV, GBM is the most aggressive type of glioma. GBM is also the most common glioma (57%) and the most common malignant brain tumour (48%).[2] Approximately 85% of GBM tumours arise in the lobes of the brain, especially the frontal and temporal lobes.[44,45] Histologically, GBM can be identified by its high mitotic index, cellular polymorphism, atypical nuclei, microvascular hyperplasia and the presence of pseudopalisading necrosis.[45,46] The latter describes the hypercellular area of migratory cells surrounding necrotic cores within the tumour.[45–47] Secretion of thrombotic factors by GBM cells and disruption of the vascular walls of blood vessels adjacent to tumour tissue leads to blood vessel occlusion and a region of local hypoxia.[46,47] This causes nearby GBM cells to either die, forming the necrotic core, or to migrate away towards normoxic areas.[45–47] The migrating cells form a pseudopalisade around the necrotic core. These hypoxic migratory cells secrete pro-angiogenic factors, leading to microvascular hyperplasia.[45,48] This results in repeating cycles of microvascular hyperplasia, followed by thrombosis and hypoxia, leading to pseudopalisading necrosis and more neovascularisation.[45] This process is intensified by the high mitotic index of GBM cells, which require high levels of the nutrients and oxygen they are deprived of under hypoxic conditions.[45] Therefore, GBM tumours are rapidly proliferating and highly infiltrative, with extensive neovascularisation and necrosis.

GBM has an incidence rate of 3.22 per 100,000 people in the USA.[2] No recent published data records GBM incidence in New Zealand, however the incidence rate for all high grade gliomas (grades III and IV) in New Zealand from 1993 to 2003 was around 4 per 100,000 people.[49] Additionally, a rate of around 2.7 per 100,000 people can be estimated for GBM from records of total brain cancer incidence in New Zealand in 2019.[50] GBM incidence varies by sex and ethnicity. GBM is 1.58 times more common in males than females. Additionally, GBM is almost twice as common in white Americans compared to African Americans and 2.39 times more common in white Americans than in Americans of Asian or Pacific Island decent.[2] Interestingly, New Zealand studies have found no statistical difference in incidence or median survival between Māori and non-Māori GBM patients.[49,51] However, it is worth noting that the sample size of Māori patients in both studies was small. The incidence of GBM also increases with age, resulting in a median age of 65 years at diagnosis.[2,6]

## 1.1.3: Subtypes of GBM

GBM tumours display extensive inter- and intratumoural heterogeneity.[52] This is thought to be one of the major impediments to finding effective treatments for GBM.[52] However, large-scale genetic profiling by The Cancer Genome Atlas (TCGA) has identified some common mutations. In 2008, the TCGA pilot project found that *EGFR* was altered, by amplification and/or mutation, in 45% of GBM tumours.[53] Additionally, *TP53* was mutated in 38% of GBM tumours and *NF1* was mutated or deleted in 23% of GBM tumours.[53] *PIK3R1* and *PIK3CA* were mutated in 10% and 7% of GBM tumours respectively.[53] From their analysis, this 2008 paper identified the p53 and RB tumour suppressor pathways and receptor tyrosine kinase (RTK) signalling as three major pathways in GBM.[53] Alterations to RTK pathways were identified in 88% of the GBM samples, including *PTEN* deletions and mutation or altered expression of *EGFR, ERBB2, PDGFRA* and *MET*.[53] Furthermore, 78% of the GBM samples had alterations to the p53 pathway, including *TP53* mutations, amplification of *MDM2* and *MDM4*, or deletion of *CDKN2A*.[53] Additionally, 77% of GBM samples had alterations to components of the RB pathway, including deletion of the *CDKN2A/CDKN2B* locus, which was seen in 55% and 53% of the samples respectively.[53] Mutation of *RB1* and amplification of the *CDK4* locus was also seen.[53] It was hoped that targeting these commonly altered pathways might prove effective in the treatment of GBM, however this has not yet materialised into any successful treatments.[54]

Further work by the TCGA used genetic and transcriptomic data to divide GBM tumours into four subtypes (Figure 1.1).[55] These subtypes were first defined by Verhaak et al. in 2010 as classical, mesenchymal, proneural and neural.[55] The classical subtype is characterised by amplification of *EGFR* and frequent *EGFR* mutations.[55] Homozygous deletion of chromosome region 9p21.3, resulting in loss of *CDKN2A*, is also common in the classical subtype.[55] Additionally, the classical subtype is characterised by a lack of *TP53* mutations, which are otherwise seen commonly in GBM.[55] The amplification of chromosome 7 paired with chromosome 10 loss was seen in other subtypes, but was present in 100% of classical subtype tumours in the Verhaak et al. (2010) study.[55]

The mesenchymal subtype is associated with mesenchymal markers, increased necrosis and an inflammatory phenotype, with increased infiltration of stromal and immune cells.[55–57] Additionally, focal hemizygous deletions of chromosome region 17q11.2, resulting in loss of *NF1*, are common in the mesenchymal subtype.[55] *NF1* mutations are also seen in the mesenchymal subtype, sometimes along with *PTEN* mutations.[55] Patients with mesenchymal subtype tumours tend to have slightly poorer survival than patients with the other subtypes.[56,57]

Proneural GBM tumours are associated with better prognosis than the other subtypes.[55] These tumours are characterised by amplification of *PDGFRA* and by mutations in or loss of heterozygosity of *TP53*.[55] GBM tumours with mutant *IDH1* (mainly secondary GBM) also fall into the proneural category.[55] The amplification of chromosome 7 paired with chromosome 10 loss seen in classical tumours occurs less

frequently in proneural tumours.[55] Additionally, the proneural subtype is associated with markers of oligodendrocyte precursor cells (OPCs) and it is thought that OPCs may be the cell of origin for this GBM subtype.[55] This supports the idea that GBM may derive from multiple different cell types and that this may contribute to the heterogeneity of GBM.[8–11,55] While Verhaak et al. originally defined a neural GBM subtype, more recent transcriptome sequencing revealed that this was likely due to contamination from non-cancerous neuronal tissue.[56] Therefore, the TCGA subtypes are now considered to be classical, mesenchymal and proneural.[54]

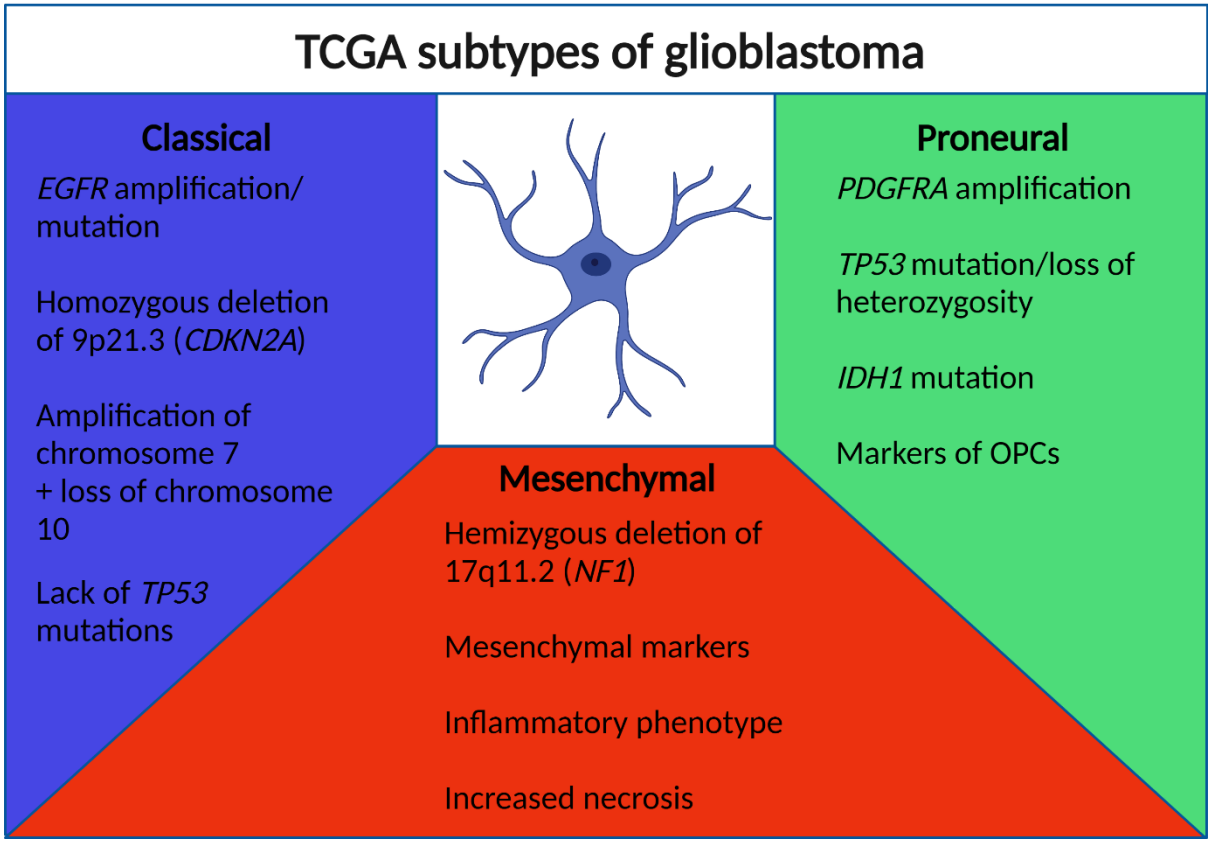


Figure 1.1: Features of TGCA subtypes of GBM
Images produced using BioRender.

Recent single cell transcriptome analysis has classified the glioma cells within each subtype into distinct types: differentiated-like, stem-like and proliferating stem-like.[57] Both classical and mesenchymal subtypes contained mainly differentiated-like glioma cells, meaning cells with gene expression patterns reminiscent of astrocytes, oligodendrocytes or mesenchymal tissue.[57] However, the mesenchymal subtype was also characterised by stromal and immune cell infiltration.[57] Contrastingly, the proneural subtype contained stem-like and proliferating stem-like glioma cells.[57] Further supporting the identification of OPCs as the cell of origin for proneural GBM, the cells in proneural tumours had characteristics of more undifferentiated progenitor cells.[57] This further differentiates the three subtypes.

As discussed in section 1.1.1, IDH mutation status has emerged as an important distinction between GBM tumours, with prognostic implications.[7,20] As IDH mutations lead to increased DNA methylation, IDH mutation status is interlinked with g-CIMP status and *MGMT* promoter methylation status, both of which are also prognostic factors.[31] g-CIMP positive tumours have a better prognosis, as do those with a methylated *MGMT* promoter.[31,58–61] As will be discussed further in section 1.1.5, $O^6$-methylguanine-DNA methyltransferase (MGMT) activity confers resistance to alkylating chemotherapies like temozolomide.[58–61] Therefore, patients with a methylated *MGMT* promoter, resulting in silencing of this gene, have a better prognosis.[58–61]

This area is further complicated by the plasticity of GBM tumours. Studies have shown that around half of IDH-wildtype GBM tumours transition from one subtype to another at recurrence, especially from classical to mesenchymal.[56,57] This plasticity appears less common in IDH-mutant GBM tumours, which are proneural at both primary and recurrent stages in 78% of cases.[57] However, the proportion of proliferating stem-like glioma cells does increase significantly in recurrent compared to primary proneural tumours.[57] This was associated with *CDKN2A* deletion and *CCND2* amplification.[57] Thus IDH wildtype and IDH mutant tumours appear to undergo very different alterations at recurrence.

The definition of the TCGA subtypes and the discoveries of the prognostic roles of IDH mutation and *MGMT* promoter methylation were major advances in the field. However, so far they have not led to improvements in the treatment of GBM.[54] It is possible that the neglect of proteomics in favour of genetic and transcriptomic analysis may be contributing to this lack of progress. It is well known that RNA expression often does not correlate with protein expression due to the multiple layers of post-transcriptional and post-translational regulation. The correlation between mRNA and protein expression changes is as low as 0.28 in gastric cancer compared to normal gastric tissue.[62] Revealingly, a recent proteomics study revealed that FGFR1, which has been targeted for the treatment of lung cancer due to its genetic amplification, is not upregulated at the proteomic level.[63] Instead, another gene encoded by the amplified region, NSD3, is highly upregulated at the proteomic level and may be a better target.[63] Similar discrepancies between genetic alterations and protein expression may be occurring in GBM.

However, studies classifying GBM tumours by protein expression are sparse. A handful of studies have examined the whole proteome of GBM tumours compared to lower grade glioma and normal brain tissue. This prompted the publication of a meta-analysis of proteomic differences between these tissue types alongside this thesis.[64] **The first study to group GBM tumours into subtypes using proteome analysis was not published until 2020**.[65] While one study found 73% concordance with the TCGA subtypes, two others found very little similarity.[65–67] Of the proteome analysis in the latter two studies, one identified two and the other three GBM subtypes distinct from the TCGA subtypes. Oh et al. (2020) found that while *EGFRvIII* and *PIK3CA* mutations were only found in one of the proteome-defined subtypes, the other well-known GBM driver mutations were found in tumours in both proteome

subtypes.[65] Interestingly, Yanovich-Arad et al. (2021) found that better predictions of survival could be made from the proteome data compared to the transcriptome data.[66] This handful of studies emphasises that proteomic analysis of GBM tumours is vital to understand their functional heterogeneity. Future large-scale studies using proteomics to classify GBM tumours may result in the identification of better therapeutic targets.

### 1.1.4: Diagnosis and first-line treatment of GBM

Symptoms suggestive of a brain tumour include the development of new neurological deficits, headaches or seizures.[68] The types of neurological deficits observed depend on which areas of the brain are infiltrated and compressed by the tumour and the peritumoral edema.[69,70] Brain tumours are typically diagnosed by contrast-enhanced MRI scans.[71–73] The contrast agent accumulates in tumour but not normal brain tissue due to the leaky walls of the tumour blood vessels.[45] Heterogeneity, invasion, edema and necrotic cores are characteristic of GBM tumours.[71,73]

Treatment for GBM begins with gross total resection of the tumour. Maximal resection increases both progression-free survival (PFS) and overall survival (OS).[74,75] However, the highly diffuse and infiltrative nature of GBM means that it cannot be cured by resection.[45] Therefore follow-up therapy is required to target the remaining cancerous tissue. One of the major impediments to this is the blood brain barrier (BBB). The BBB is a multi-layered system which protects the brain from molecules and immune cells circulating in the blood.[76,77] The first layer of defence is the tight junctions between the endothelial cells that make up the walls of the capillaries in the brain.[76,77] These cells also contain efflux pumps to remove any molecules that manage to get through.[76,77] Additionally, the extracellular basement membrane, pericytes and the glial cells within the brain are part of the BBB.[76,77] It has been estimated that > 98% of small molecules cannot cross the BBB.[78] This severely limits treatment options for GBM. Various methods have attempted to circumvent this problem, however none have entered common use for GBM treatment.[76] Therefore, the gold-standard treatment after surgery is the course of chemoradiation described in the Stupp protocol.[4] This consists of ionising radiation (IR), which can penetrate through the skull to the brain, and temozolomide (TMZ), a chemotherapy capable of crossing the BBB.[4,79]

In the Stupp protocol, IR is given at a dose of 2 Gy every day for five days, repeated for six weeks.[4] Additionally concomitant treatment with TMZ is administered every day during the six weeks of radiotherapy.[4] Adjuvant TMZ treatment is then given for 5 days in each 28 day cycle for up to six cycles.[4] The Stupp protocol was adopted after a phase III trial, published in 2005, showed that the addition of concomitant and adjuvant TMZ to radiotherapy treatment increased median OS from 12.1

months to 14.6 months.[4] In addition to this treatment regime, steroids are often administered at high doses to reduce the symptoms associated with peritumoral edema.[69,70]

Both IR and TMZ are DNA damaging therapies, however their mechanisms of action differ.[80] IR induces double-strand breaks (DSBs) in DNA, as well as single-strand breaks (SSBs) and damage to bases.[80] Healthy cells have mechanisms to detect DNA damage and activate cell cycle checkpoints to prevent replication of damaged DNA until it has been repaired.[81] However, these pathways are often altered in cancer cells, thereby supporting their very high proliferation rates.[81,82] Therefore cancer cells are more likely than healthy cells to replicate the damaged DNA, leading to cell death driven by mitotic catastrophe.[81–84]

TMZ treatment leads to methylation of adenine and guanine DNA bases, resulting in $O^6$-methylguanine ($O^6$-meG), $N^7$-meG and $N^3$-methyladenine ($N^3$-meA) lesions.[80,85,86] The $O^6$-meG lesion is critical for the cytotoxicity of TMZ.[86] When the alkylated DNA is replicated, a thymine instead of a cytosine is paired with the $O^6$-meG base.[86] This mismatch is recognised and excised by the mismatch repair pathway, however as long as the $O^6$-meG remains, the gap will be filled with another thymine nucleotide.[86] This results in repeated mismatch repair which never repairs the mismatch and eventually leads to apoptosis.[86,87]

Although it is the standard of care for glioblastoma, treatment with IR and TMZ does not greatly prolong the life of GBM patients. This is because GBM tumours display remarkable resistance to these treatments.

## 1.1.5: Mechanisms of therapy resistance in GBM

### 1.1.5.1: Resistance to irradiation (IR)

Cell line studies have shown that single dose IR treatment at the level given to patients (2 Gy) induces very little cell death.[88] However, GBM cell survival is reduced by IR in a dose-dependent manner, with higher doses (≥ 9 Gy) having a large effect, although this varies between cell lines.[88–91] Fractionated irradiation (5 doses of 2 Gy), as used in the Stupp protocol, has also been shown to induce cell death, increasing the populations of both apoptotic and necrotic cells to 20-50%.[92] However, the survival of GBM patients is extremely poor even with radiotherapy due to the high radioresistance of GBM tumours. Multiple factors have been implicated in the radioresistance of GBM tumours, however many link back to their ability to initiate cell cycle checkpoints and repair DNA.[93,94] Defects in DNA repair are linked to initiation and progression of many cancer types, however these defects also render cancer cells more vulnerable to DNA damaging therapies.[95] The ability of GBM cells to initiate DNA damage responses is critical to their therapy resistance.[93,94]

Both single dose and fractionated IR cause GBM cells to arrest in G2/M phase, which appears to be important for their ability to repair their DNA.[88–90,92] Indeed, a cell line study showed that the amount of DSBs in GBM cells peaks within hours after 6 Gy IR and is mostly repaired by 24 hours, at the peak of G2/M arrest.[88] Several studies have shown that the PI3K/AKT signalling pathway is vital for recovery after radiation damage.[96–99] AKT hyperactivation is common in GBM and is associated with poor prognosis and radioresistance.[91,100,101] The link between activation of the PI3K/AKT pathway and radioresistance has been observed in multiple cancer types.[91,96,102–107] Common genetic alterations such as *EGFR* mutation or amplification and mutation or deletion of *PTEN* lead to AKT hyperactivation.[55,108,109] Additionally, *AKT3* is commonly amplified in GBM.[53] Furthermore, IR downregulates AKT inhibitor LRIG1, leading to further AKT activation.[110] Inhibition of AKT has been shown to reduce the efficiency of DNA DSB repair after irradiation treatment of GBM cells.[96–99] This has been linked to AKT-dependent promotion of DNA-PKc activity, which is important for non-homologous end-joining (NHEJ).[98,99] A review by Han et al. (2017) showed that AKT is at the centre of a network of signalling conferring radioresistance, including DNA damage response ATM signalling and Wnt/β-catenin signalling.[93]

It has been proposed that glioma stem cells (GSCs) may be an intrinsically radioresistant GBM cell population which survive therapy and then repopulate the tumour.[111] GSCs are a small population of stem-like cells within glioma tumours.[112,113] These GSCs have characteristics of self-renewal and multipotency and are capable of tumour initiation and maintenance.[113] The study of GSCs remains controversial as there is no defined way of identifying them and the markers that are used, such as CD133, may not be specific for GSCs.[114] However, several lines of evidence indicate that GSCs are likely to be important in therapy resistance. For example, it has been shown that the proportion of cells expressing the GSC marker CD133 increases 3-5-fold after IR treatment of gliomas both *in vitro* and in mouse models.[111,115] Multiple GSC characteristics have been linked to radioresistance, including greater activation of cell cycle checkpoint proteins and more efficient repair of DNA damage in response to IR.[111] There are also suggestions that some GSCs may be quiescent.[116,117] This reversible arrest of proliferation may enable GSCs to survive therapy and later reinitiate replication, leading to tumour recurrence.[116,117] More work is needed to robustly define GSCs and to understand the complex mechanisms that mediate their radioresistance.

Aside from the properties of the GBM cells themselves, the microenvironment of GBM tumours also contributes to radioresistance. It has been shown that the radioresistance of GSCs increases *in vivo*.[118] GBM tumours are highly hypoxic and it has been known for nearly a century that hypoxia correlates with radioresistance.[119] It has generally been asserted that because most of the DNA damage induced by IR is due to production of reactive oxygen species (ROS), hypoxia inhibits the impact of IR.[94,120] However, other studies have indicated that ROS production actually increases in hypoxic cells.[121] HIF-1α, which mediates the transcriptional response to hypoxia, has been linked to the radioresistance of

tumours, including GBM.[122] While this area is still being explored, there seems to be an interplay between DNA damage response proteins and HIF-1α in response to radiotherapy which contributes to radioresistance.[122] Additionally, hypoxia promotes the self-renewal of GSCs, which occupy a hypoxic niche in GBM tumours.[123–125] This promotion of GSC stemness was dependent on both PI3K/AKT and HIF-1α signalling.[123]

Finally, autophagy has been implicated in both GBM radioresistance and IR-induced cell death. Autophagy is a cellular stress response which degrades cellular components to provide the cell with resources it needs to survive.[126] Reports on the role of autophagy in the response to IR are conflicting. The PI3K/AKT pathway is activated by IR in GBM cells and appears to be protective.[127,128] Inhibition of AKT or of a downstream target of AKT, DNA-PKc, radiosensitises GBM cells, apparently by the induction of autophagy.[127,128] mTOR, an important inhibitor of autophagy, is one of the downstream targets activated by the PI3K/AKT pathway.[129] However, other studies have shown that inhibition of autophagy sensitises GBM cells to IR.[88,130,131] It is possible that the hinderance of DNA repair due to AKT inhibition is the cause of radiosensitisation.[96–99] Autophagy may be induced to help the GBM cells deal with increased cell stress rather than being the cause of the increased stress. A recent review concluded that most of the studies indicating autophagic cell death in response to treatment were *in vitro* studies using high doses, whereas clinical and pre-clinical studies indicated that autophagy was a protective mechanism.[132] Therefore, they hypothesised that autophagy is a protective mechanism in GBM therapy response, but very high levels of stress can over-activate autophagy, leading to cell death.[132] Similarly, the authors of a review paper suggested that the level of ER stress may determine the role of autophagy.[133] They suggested that up to moderate levels of stress, the ER unfolded protein response (UPR) pathway led to initiation of autophagy to remove damaged cellular components and thereby protect cells from apoptosis.[133] However, under very high levels of stress, autophagy may instead initiate apoptosis.[133] Alternatively, it is likely that when studies refer to autophagic cell death, they are often observing the death of cells despite the activation of autophagy as a survival mechanism, rather than because of it.[126] The role of autophagy in therapeutic responses is yet to be fully elucidated.

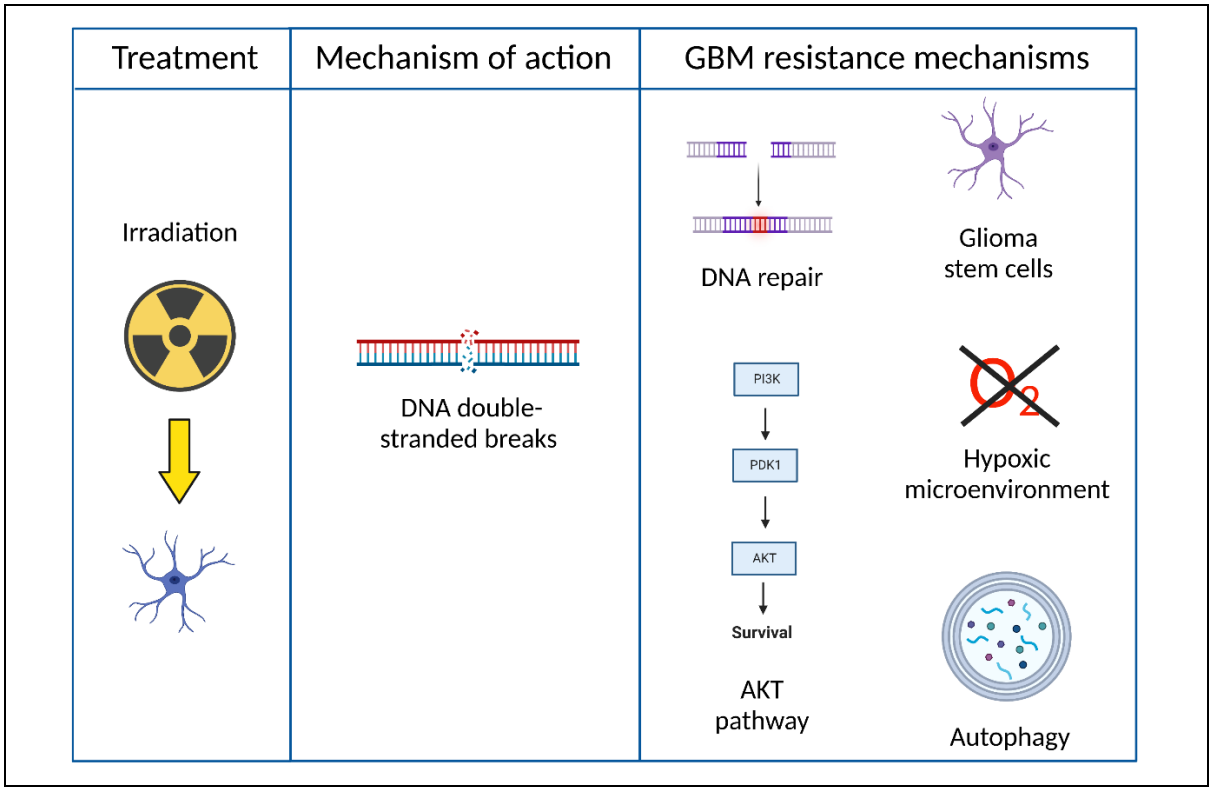


Figure 1.2: GBM irradiation resistance.
Image produced using Biorender.

### 1.1.5.2: Resistance to temozolomide (TMZ)

The Stupp protocol was adopted as the standard of care for GBM due to the slight improvement in median survival time achieved by treating patients with TMZ as well as fractioned IR.[4] However, this regimen is beneficial for less than 50% of GBM patients.[58] This is because the response of GBM tumours to TMZ is vastly different depending on their $O^6$-methylguanine-DNA methyltransferase (MGMT) status.[134,135] In about 30-50% of GBM tumours, the promotor of *MGMT* is hypermethylated.[58,136] These patients have a better response to TMZ and therefore median survival is increased to 26.5 months, compared to just 14.5 months in patients with unmethylated *MGMT*.[135] MGMT is a DNA repair enzyme that removes the $O^6$ methyl groups added to guanine nucleotides by TMZ.[137] Therefore, in GBM tumours expressing MGMT, the TMZ-induced DNA lesions are removed by MGMT before they can induce DNA damage and cell death. MGMT activity is therefore a major cause of GBM resistance to TMZ. This resistance is inherent in many GBM tumours.[58] However, in tumours with *MGMT* promotor hypermethylation, decreased methylation of this locus has been observed after TMZ treatment, indicating that resistance can also be acquired in some cases.[138,139] Various signalling pathways with established importance in GBM, such as the PI3K/AKT/NFκB pathway and STAT3 signalling, are involved in upregulation of MGMT.[140–142]

The other lesions induced by TMZ, $N^7$-meG and $N^3$-meG, are quickly repaired by base excision repair (BER) mechanisms.[143,144] Therefore, expression of BER pathway proteins is also associated with TMZ resistance.[143,144] Conversely, while MGMT and BER pathway protein expression promotes resistance to TMZ, expression of mismatch repair (MMR) DNA repair proteins is vital for the cytotoxicity of TMZ (section 1.1.4).[86,87] MMR mutations have been observed in recurrent tumours, indicating acquired resistance to TMZ.[145]s

Both GSCs and autophagy have been implicated in TMZ resistance as well as resistance to IR. Although reviews state that GSCs are an important part of GBM TMZ resistance, there seems to be little evidence indicating how they resist TMZ treatment.[146,147] As in the response to IR, autophagy in response to TMZ is generally considered to be protective but has also been linked to TMZ-induced autophagic cell death in other cases.[148–154]

TMZ is much more effective in patients with MGMT-negative GBM tumours. However, even these patients only have a median survival of just over two years, so TMZ is by no means curative.[135] A recent study indicated that while TMZ did induce apoptosis of around 20% of MGMT-negative GBM cells, the rest became senescent and remained viable.[155,156] This senescent state appeared to be dependent on the presence of un-repaired DNA DSBs induced by TMZ.[155] If these senescent GBM cells are capable of re-entering the cell cycle after a period of time, this could in part explain recurrence of even the GBM tumours that respond well to the Stupp protocol.

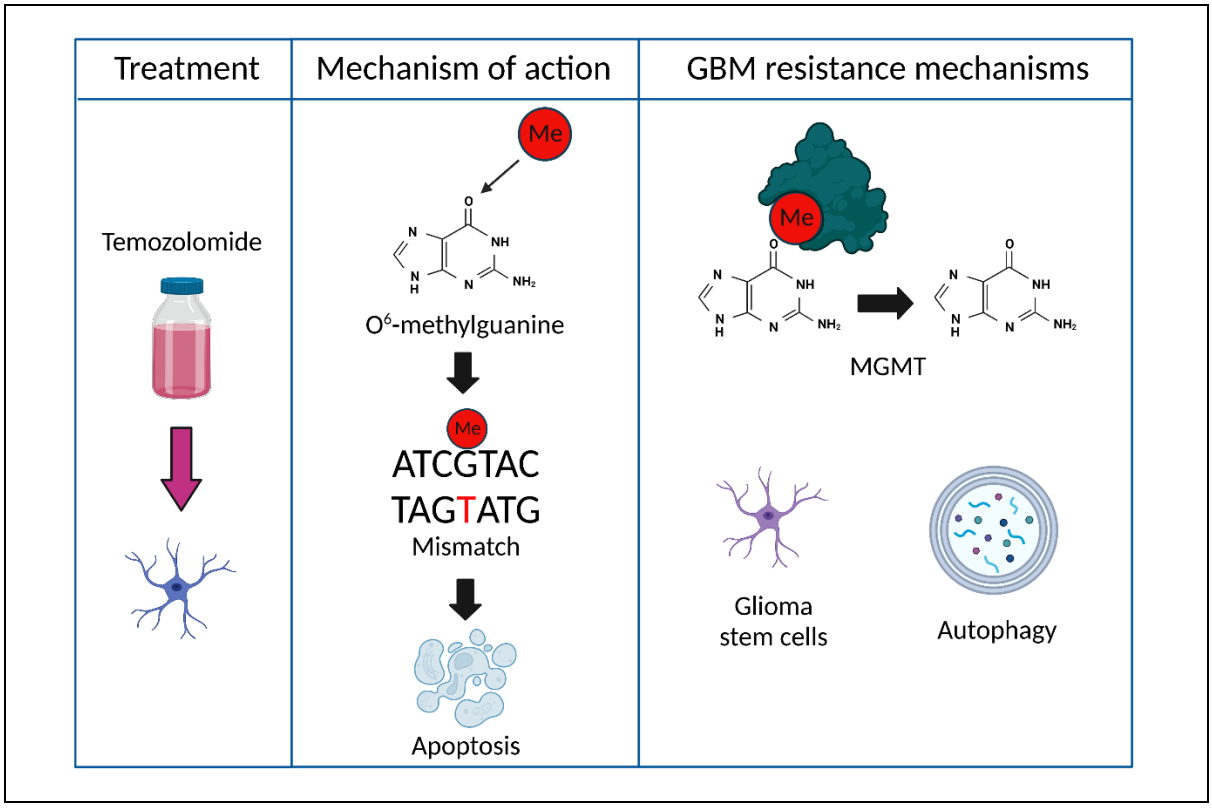


Figure 1.3: GBM temozolomide resistance.

Image produced using Biorender.

## 1.1.6: Other GBM treatments

Although the Stupp protocol is the standard of care for GBM, five other therapies have received FDA (U.S. Food and Drug Administration) approval for GBM treatment. Two of these, carmustine wafer implants and tumour treatment fields (TTFields), are approved for new diagnoses.[157] The other three treatments, bevacizumab (BVZ), lomustine and intravenous carmustine, are approved for the treatment of recurrent GBM.[157]

### 1.1.6.1 Nitrogen mustard chemotherapies: lomustine and carmustine

Lomustine (chloroethyl-cyclohexyl-nitrosourea – CCNU) and carmustine (bis-chloroethyl-nitrosourea – BCNU) are both members of the nitrogen mustard family of chemotherapies, which have been used in cancer treatment since the 1940s.[158] Nitrogen mustards are alkylating agents and their mechanism of action in cancer treatment includes alkylating and crosslinking DNA, thereby inhibiting replication.[158,159] Carmustine also inhibits glutathione reductase, resulting in interference with the cellular antioxidant response.[160]

Lomustine received FDA approval for the treatment of recurrent GBM in 1976.[161] While only minimally effective, lomustine is commonly used for the treatment of recurrent GBM, although no standard of care for recurrent GBM is clearly defined.[162] Lomustine is also part of the PVC regimen, which consists of lomustine in combination with alkylating agent procarbazine and antimitotic drug vincristine.[163] This regimen improves survival in lower grade glioma and may be used for the treatment of recurrent GBM.[162,163] Neither this regimen nor lomustine alone have been conclusively shown to have better efficacy than TMZ treatment for recurrent GBM.[157,162,164]

Intravenous carmustine was approved for treatment of GBM in 1977, however is no longer commonly used due to its high toxicity and lower effectiveness than other treatments.[165,166] Biodegradable wafers containing carmustine were approved for treatment of recurrent GBM in 1996 and for newly diagnosed GBM in 2003.[167] During tumour resection, the wafers are placed into the cavity.[168,169] This overcomes the problem of the BBB (section 1.1.4) and concentrates the drug at the site of the tumour to minimise systemic effects.[169] While some studies have demonstrated that carmustine wafers improve OS and PFS in GBM patients, they are expensive and have high rates of complications, including wound healing problems, intracranial infection and cerebral edema.[157,168]

Like TMZ, the alkylating drugs lomustine and carmustine show limited efficacy in patients with expression of MGMT.[164,170,171]

### 1.1.6.2 Bevacizumab (BVZ)

GBM tumours are characterised by microvascular hyperplasia.[45] The release of angiogenic factors such as VEGF by hypoxic GBM cells stimulates the growth of new blood vessels to provide the tumour with oxygen and nutrients.[45,48] Anti-angiogenesis drugs for GBM, most prominently anti-VEGF treatments, were predicted to limit the blood supply to the tumour and so inhibit its growth.[172,173] Bevacizumab (BVZ) (brand name Avastin®) is an anti-VEGF antibody therapy which is used for the treatment of colorectal, lung, ovarian, cervical and renal cancers.[174,175] In 2009, BVZ was approved for the treatment of recurrent GBM in the USA.[174,176] BVZ is also approved for recurrent GBM treatment in New Zealand, Japan and other countries, but not in Europe.[177,178] This is because clinical trials with BVZ and other anti-VEGF drugs have been conflicting and its effectiveness is still controversial.[173] Recent meta-analyses of clinical trials with anti-VEGF treatments highlighted the variability of the results of different studies.[173,179] Overall, they found that anti-VEGF therapies in general, and BVZ investigated separately, had no significant impact on the OS of GBM patients compared to standard or other available treatments but did significantly increase PFS.[173,179] However, although statistically significant, the median difference in PFS with BVZ treatment was only 1.1 months.[179]

### 1.1.6.3 Tumour treatment fields

Tumour treatment fields (TTFields) consist of alternating electric fields which disrupt mitotic spindle assembly and cytokinesis, leading to cell death.[180–182] TTFields are applied using a portable device attached to the scalp.[183] This treatment was approved by the FDA in 2015.[183] In 2017, Stupp et al. published a clinical trial in which patients underwent concomitant radiotherapy and TMZ treatment followed by maintenance TMZ, as in the 2005 Stupp protocol, or maintenance TMZ plus TTFields.[184] Median OS was improved from 16 months with TMZ alone to 21 months with TMZ plus TTFields.[184] Median PFS was also increased by 2.7 months.[184] Use of TTFields along with TMZ is recommended for patients who are willing and able to use the device.[185,186] At least some treatment centres have incorporated TTFields into their standard of care despite their high costs.[185,187] As well as the expense, the visibility of the device, which must be worn on the shaved scalp for 18 hours a day, is a major factor in the fairly low patient acceptance of the treatment (36% in a 2018 study).[188] However, compliance rates in patients who choose TTFields treatment are high and skin irritation due to the device is the only adverse effect in addition to those already induced by TMZ.[185,188]

### 1.1.6.4 Treatments in development

While the combination of TTFields and TMZ after concomitant IR and TMZ almost doubles median OS compared to IR alone, the prognosis of GBM remains extremely poor. Therefore, many other treatment options are under investigation.

Despite the extensive molecular characterisation of GBM tumours (section 1.1.3), all targeted therapies, with the dubious exception of bevacizumab, have so far failed to improve survival.[189] Considering the frequent amplification or activating mutation of EGFR, many clinical trials have treated GBM patients with EGFR inhibitors.[190] These inhibitors have had good results in the treatment of non-small cell lung cancer, however none demonstrated a survival benefit in GBM.[190] Furthermore, based on the importance of the PI3K/AKT/mTOR pathway in GBM survival and therapy resistance (section 1.1.5.1), multiple attempts have been made to inhibit this pathway.[191] As with EGFR, these trials have so far been unsuccessful.[191] While clinical trials targeting VEGF, EGFR and the PI3K/AKT/mTOR pathway are the most extensive, other clinical trials have targeted other proteins including MET, BRAF, RB, integrins, PKC and TGF-β.[189] None of these have shown sufficient efficacy.[189] This seems to be due to a combination of factors including the BBB, GBM intra- and intertumoral heterogeneity, tumoral plasticity and the existence of redundancy within these signalling pathways.[189,192]

DNA damage repair is of the utmost importance in the resistance of GBM to radio- and chemotherapy (section 1.1.5). Poly(ADP-ribose) polymerase (PARP) inhibitors attempt to target the DNA damage response in GBM.[193] PARP binds to sites of DNA damage and is important for the recruitment of DNA repair proteins.[193] Inhibition of PARP prevents this recruitment and inhibits BER.[193] PARP inhibition also interferes with DNA replication, leading to DSBs and gaps in the forming lagging strand.[194,195] PARP inhibitors are already in use for ovarian, pancreatic, breast and prostate cancer.[193] Several clinical trials combining PARP inhibitors with radiotherapy or chemotherapy for the treatment of GBM are ongoing.[193] It is yet to be seen whether PARP inhibitors will demonstrate any survival benefit.

Immunotherapy is at the forefront of recent advances in cancer treatment.[196] Immune checkpoint blockade, adoptive cell therapy and vaccines have been approved for multiple types of cancer.[196,197] Unfortunately attempts to develop immunotherapies for GBM treatment have so far had little success.[198] Antibodies to immune checkpoint proteins PD1/L-1 and CTLA-4 have shown great efficacy in some cancer types.[196] These immune checkpoint inhibitors remove suppressive signals so that immune cells can become activated and recognise and destroy tumour cells.[196] GBM tumours have a highly immunosuppressive microenvironment, so it is hoped that modulating this environment may improve survival.[199] Pre-clinical and early clinical trials were promising, however phase III trials of immune checkpoint inhibitors for GBM treatment have shown no survival benefit.[196,200] It is possible that access to the tumour through the BBB is part of the issue, however a trial which delivered the immunotherapy straight to the resection cavity also showed no benefit.[200]

Similarly, a phase III trial with a peptide vaccine targeting the common EGFRvIII mutation showed no survival benefit for GBM patients, despite promising results in earlier studies.[201] Other immunotherapy treatments are in ongoing phase I and II clinical trials.[202] These include dendritic cell (DC) vaccines, which involve harvesting DCs from patients, exposing them to tumour antigens and then readministering them.[203] The DCs should then present the tumour antigens to T cells to generate an anti-tumoral immune response.[203] Additionally, chimeric antigen receptor (CAR)-T cells, which have had great success in treatment of leukaemia and lymphoma, are also being tested in phase I and II clinical trials.[202,204] Several phase I and II trials are underway to investigate the use of oncolytic virotherapy for GBM treatment.[205] In oncolytic virotherapy, an oncolytic virus is targeted to infect cancer cells and replicate.[206] This can lead to cancer cell death via lysis and induce immune responses against the infected tumour cells.[206] A recent review notes that while some preliminary results are promising, they do not appear to live up to the success of preclinical work.[205] While it remains to be seen whether these treatments are successful, there are multiple barriers to overcome. The BBB, the difficulty of immune cell infiltration into the solid tumour mass and the immunosuppressive environment of GBM cells mean that multiple aspects of the immune microenvironment will likely need to be targeted to gain clinical effectiveness. Combination immunotherapy treatments targeting multiple aspects of the immune response have shown promise in pre-clinical models.[198] However, it must be kept in mind that previous immunotherapies have repeatedly failed to translate into the clinical setting.

GBM has proven extremely difficult to treat due to its location behind the BBB, its effective DNA damage response mechanisms, its intra- and intertumoral heterogeneity and its extremely immunosuppressive immune microenvironment. It is likely that combinations of treatments targeting multiple GBM survival mechanisms will be necessary to achieve significant survival benefits. Combining the current IR and TMZ treatments with targeted therapies that impair the ability of GBM cells to survive is a potential route to improved patient survival. Research by the McConnell lab group at Victoria University of Wellington and a handful of other groups has identified BCL6 as a promising target to improve the efficacy of GBM therapies.[207–211] The known functions of BCL6 in other contexts are discussed in section 1.2, followed by a summary of the research on BCL6 in glioblastoma to date.

## 1.2: BCL6

### 1.2.1: BCL6 structure and function

BCL6 (B cell lymphoma 6) is a 79 kDa transcriptional repressor protein encoded by chromosome 3q27.[212] BCL6 has an N-terminal BTB/POZ domain and six zinc-finger domains at the C-terminus.[212,213] These are connected by a central portion of the protein which contains three PEST domains thought to be important for BCL6 degradation.[214] Homodimerisation of BCL6, which is necessary for it to function, is mediated by the BTB/POZ domain.[215] BCL6 binds to DNA using its zinc-finger domains and recruits corepressors to repress expression of its target genes.[216] These corepressors include BCOR, NCOR1 and NCOR2, which bind to the lateral groove in the BTB/POZ domain.[215,217–220] Additionally, the corepressor CtBP interacts with both the BTB/POZ domain and the middle region of BCL6, while MTA3 is recruited by the middle region.[221,222] These corepressors recruit transcriptional repression complexes containing mSIN3A and histone deacetylases (HDACs) to repress transcription.[223–226] While most BCL6 targets are directly repressed by BCL6, in around 6% of cases BCL6 binds to another zinc-finger protein, MIZ1, which binds to the target gene.[227]

Chromatin immunoprecipitation sequencing (ChIP-seq) experiments have shown that in its canonical context (sections 1.2.2 and 1.2.5), BCL6 represses gene expression via two main mechanisms.[228] The most potent repression of gene promoters is carried out by ternary complexes of BCL6 homodimers bound to both NCOR1 or NCOR2 and BCOR simultaneously.[228] This repression requires the additional presence of PRC2 protein EZH2, which trimethylates H3K27.[229] This marker is required for recruitment of the BCOR corepressor complex.[229] Meanwhile BCL6 bound to NCOR1 or NCOR2 binds to and represses gene enhancers by recruiting HDAC3 to deacetylate H3K27.[228] This ChIP-seq study did not investigate the roles of MTA3 and CtBP, which are also important in repression of many BCL6 target genes.[221,222]

While BCL6 was first identified as an oncogene in lymphoma, it has important roles in the healthy immune system, particularly in germinal centre B cells.[212,230,231]

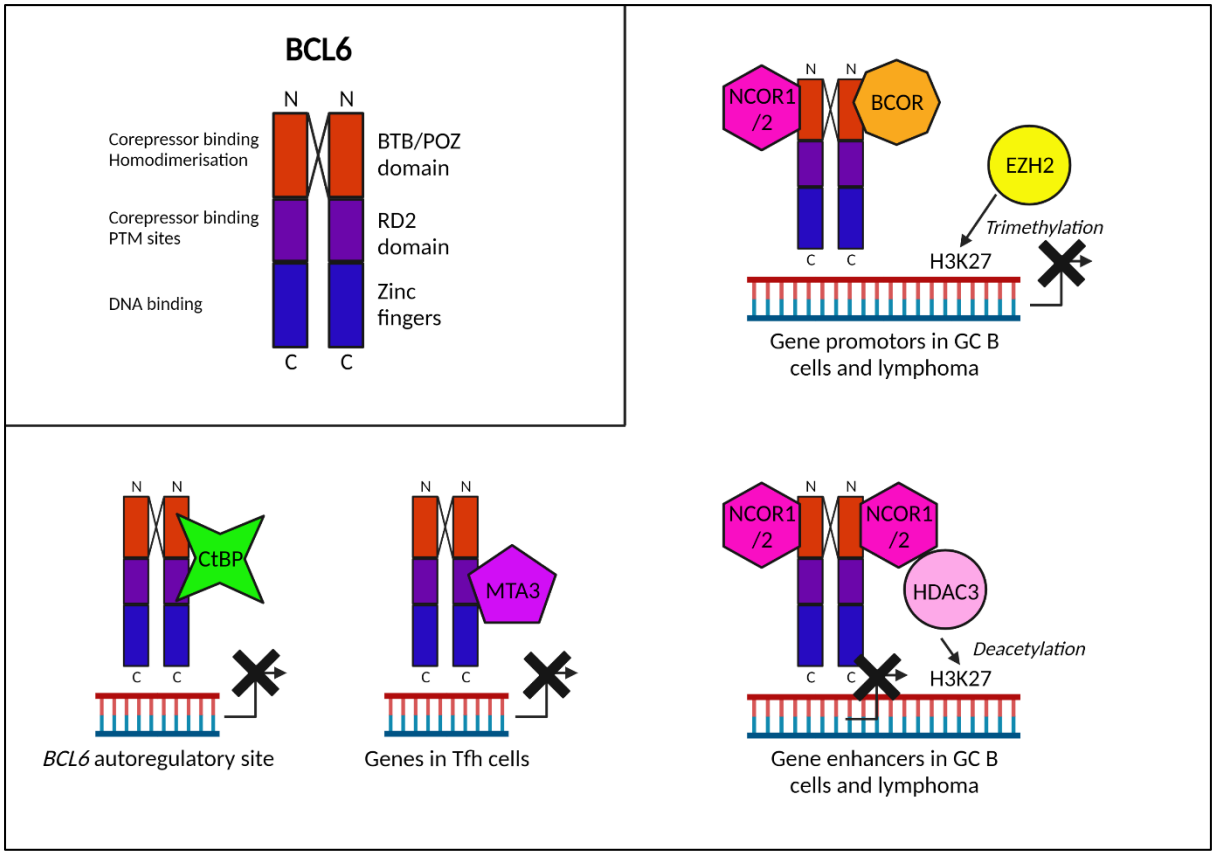


Figure 1.4: BCL6 domains and corepressor binding.
Image produced using Biorender.

## 1.2.2: BCL6 in germinal centre B cells

BCL6 is a master transcriptional regulator of the germinal centre (GC) reaction in B cells.[232–234] When naïve B cells encounter an antigen, they undergo the GC reaction in the lymph nodes or spleen.[234] In the dark zone of the GC, B cells undergo proliferation and affinity maturation.[235] Affinity maturation is the process of somatic hypermutation (SHM) of the immunoglobulin (Ig) genes until an Ig with high enough affinity for the antigen is produced.[236] After SHM, the B cells move to the light zone, where the antigen is presented to them by follicular dendritic cells.[235] The ability of the B cells to acquire the antigen and present it to T follicular helper ($T_{FH}$) cells tests the affinity of the B cell Ig for the antigen.[235] B cells are then either returned to the dark zone for further SHM, eliminated by apoptosis or committed to differentiation into plasma or memory B cells.[235] This process is tightly controlled by many factors including, vitally, BCL6.

BCL6 is involved in the GC reaction from the beginning. When naïve B cells are stimulated by an antigen, they require interaction with $T_{FH}$ cells to become GC B cells.[237] This interaction upregulates BCL6 expression, which further stabilises the interaction between B and $T_{FH}$ cells in a positive feedback loop.[237] This process is vital for GC formation, as *BCL6-null* mice are unable to form GCs.[238] BCL6 is

also very important during SHM. SHM involves a high level of DNA mutations which would usually trigger the DNA damage response, leading to checkpoint activation and apoptosis.[236,239] However, this is prevented by BCL6, which represses the transcription of DNA damage response genes including *TP53*, *ATR*, *CHEK1* and *CDKN1A*.[227,240–243] BCL6 is also involved in the repression of both pro- and anti-apoptosis genes, including *BCL2*.[227,244] It is thought that this might prime GC B cells for apoptosis if the level of DNA damage gets too high to be tolerated and the B cell receptor (BCR) is not activated by high affinity binding to the antigen.[232] BCL6 also prevents GC B cells from becoming activated and differentiated prematurely. It does this by repressing transcription of *PRDM1* (BLIMP1), *IRF4*, multiple components of MAPK, NFκB, TGF-β, STAT and Wnt signalling pathways and interferon-type, interleukin and Toll-like receptors.[227,245–247]

BCL6 is vital for the GC reaction, but it is also imperative that BCL6 activity is limited to the GC stage to allow B cells to differentiate and regain functional DNA damage response signalling.[233,234] Therefore, BCL6 expression in B cells is tightly regulated. *BCL6* transcription is activated by a ternary complex of proteins, OCAB, OCT2 and MEF2B, which interact with a locus control region 150 kb upstream of the *BCL6* transcription start site and recruit the mediator complex.[248] Interaction of the mediator complex with the *BCL6* promotor promotes transcription.[248] Additionally, IRF8 is known to directly activate BCL6 expression by binding to the *BCL6* promoter.[249] IRF8 also interacts with BCL6 and BCOR to enhance BCL6-mediated transcriptional repression.[250] IRF4, one of the targets of BCL6, also upregulates BCL6 expression during the early phase of the GC reaction.[247]

Several mechanisms ensuring the control of BCL6 expression and its elimination at the end of the GC reaction have been identified. Firstly, BCL6 binds to its own 5'-regulatory region and represses its own transcription in an autoregulatory process.[251] This function is dependent on recruitment of the corepressor CtBP.[221] When BCR and CD40 signalling is activated, triggering B cells to leave the GC and differentiate, several processes lead to BCL6 downregulation. At the transcriptional level, BCR and CD40 signalling activate NFκB, which activates IRF4 expression.[245] Although IRF4 activates BCL6 expression in the early GC reaction, unknown mechanisms cause it to switch to repressing BCL6 transcription in the late stages of the GC.[234] Other pathways inhibit BCL6 activity at the post-translational level. CREBBP and EP300 acetylate BCL6, leading to its inactivation.[252] Additionally, CREBBP acetylates the promoters of most BCL6 target genes, thereby activating their transcription.[253] CD40 signalling also stimulates the translocation of BCL6 corepressors NCOR1 and NCOR2 to the cytoplasm, further inhibiting BCL6 activity in the nucleus.[241,254] Other processes cause the degradation of BCL6. BCR signalling activates a MAPK signalling cascade which leads to phosphorylation of the PEST domains of the BCL6 protein.[214] This targets BCL6 for proteasomal degradation.[214] Furthermore, FBXO11 targets BCL6 for ubiquitination and proteasomal degradation, although it is unknown at which stage of the GC reaction this occurs.[255]

It is notable that many of the proteins which have their transcription repressed by BCL6 themselves repress BCL6 activity. These include MAPK and NFκB pathway proteins, IRF4 and p53. This suggests tight and multi-layered regulation of BCL6 activity in B cells to limit it to the GC reaction and to prevent the inhibition of DNA damage response pathways from becoming detrimental.

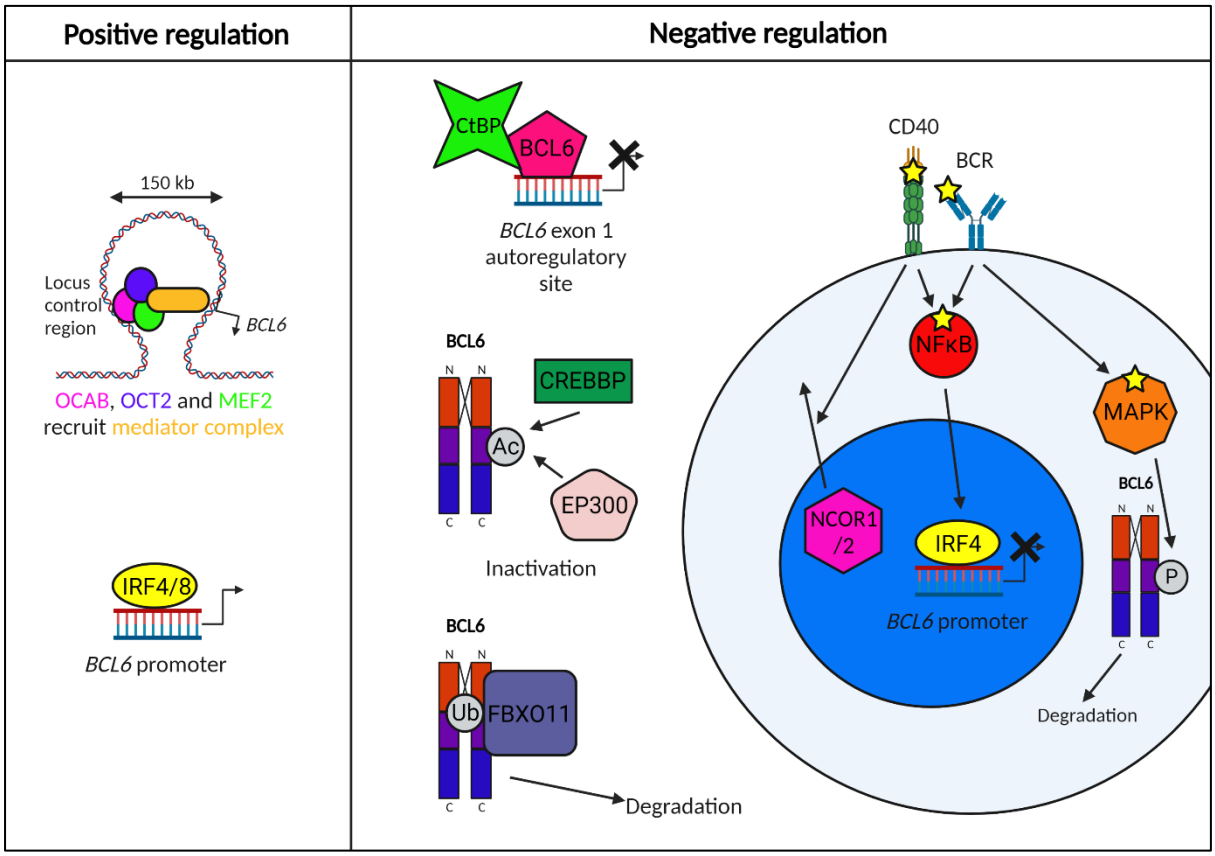


Figure 1.5: Regulation of BCL6 expression and activity in B cells.
Image produced using Biorender.

## 1.2.3: BCL6 in other immune cells

### 1.2.3.1: BCL6 in $T_{FH}$ cells

BCL6 activity is not confined to B cells. BCL6 is the lineage defining transcription factor for $T_{FH}$ cells and homozygous BCL6 deletion in mice results in failure to produce both $T_{FH}$ cells and GCs.[256,257] In $T_{FH}$ cells, BCL6 acts as a direct transcriptional repressor but also represses transcription factors which themselves repress genes important for $T_{FH}$ biology.[256] This has been described as a repressor-of-repressors circuit.[256] Through these two mechanisms, BCL6 represses genes involved in differentiation of T cells into other T cell types ($T_H1$, $T_H2$, $T_H17$ and $T_{regs}$) as well as genes involved in localisation to the T cell zone.[256,258] This ensures that $T_{FH}$ cells develop and maintain their $T_{FH}$ phenotype and that they migrate away from the T cell zone towards GC B cells.[256,258]

$T_{FH}$ cells are a vital part of the GC reaction. However, their characteristics are very different to GC B cells, making it interesting that BCL6 activity defines both cell types. Some functions of BCL6, such as repression of BLIMP1 to prevent differentiation and the presence of a negative auto-regulatory loop, are the same in GC B cells and $T_{FH}$ cells.[256] However, a ChIP-seq study showed that 49% of BCL6 DNA binding sites in $T_{FH}$ cells were unique to those cells and 66% of BCL6 DNA binding sites in GC B cells were unique to GC B cells, suggesting that the role of BCL6 in the two cell types is very different.[258] The shared DNA binding sites were mainly in gene promoters, however only 16% of these genes were repressed by BCL6 in both cell types.[258] The authors suggested that this may be due to differential expression or recruitment of BCL6 corepressors in GC B cells and $T_{FH}$ cells.[258] In contrast to GC B cells, when the BTB domain of BCL6 is mutated such that it cannot recruit corepressors, functional $T_{FH}$ cells still form.[259] Therefore, the transcriptional activity of BCL6 in $T_{FH}$ cells may be mediated by other mechanisms, such as binding of MTA3 to the middle domain. This interaction has been shown to be vital for differentiation of $T_{FH}$ cells and suppression of $T_H2$ and $T_H17$ differentiation.[260]

The BCL6 DNA binding sites unique to $T_{FH}$ and GC B cells were commonly at gene enhancers rather than promoters.[258] These binding sites corresponded to differential enrichment of enhancer-associated chromatin marks (H3K4me1 and H3K27ac) in GC B cells and $T_{FH}$ cells, suggesting that the role of BCL6 in different cell types is controlled by cell type-specific chromatin modification.[258] Interestingly, there is evidence that BCL6 is recruited to many of the target genes it represses in $T_{FH}$ cells by interaction with AP-1 bound to AP-1 binding motifs, rather than directly binding to BCL6 binding motifs.[258] It is yet to be elucidated whether BCL6 represses the transcriptional activator activity of AP-1 or forms a repressor complex with AP-1.[258] Overall, this shows that BCL6 can have very different functions in different cell types, mediated by cell context-specific protein-protein interactions and chromatin landscapes.

### 1.2.3.2: BCL6 in memory CD8+ T cells

BCL6 has also been implicated in the generation of memory CD8+ T cells in viral infection.[261,262] The role of BCL6 in these cells has been less thoroughly studied than its role in GC B cells and $T_{FH}$ cells. However, the relationship between BCL6 and the transcription factor TCF-1 seems to be important. BCL6 promotes CD8+ T cell memory precursor generation by upregulating TCF-1 expression by an unknown mechanism.[262] Additionally, TCF-1 represses pro-exhaustion factors and upregulates BCL6 expression to maintain CD8+ T cell responses during chronic infection.[263] This suggests a positive feedback loop between BCL6 and TCF-1. BCL6 also represses the expression of the cytotoxic serum protease granzyme B in CD8+ T cells, which is important to promote memory cell generation in preference to apoptosis.[264]

### 1.2.3.3: BCL6 in $T_{reg}$ cells

$T_{regs}$ are regulatory immune cells which suppress the immune response.[265] BCL6 regulates the stability of $T_{reg}$ cells and is important in their ability to suppress the $T_H2$ response.[266] This appears to be at least partly due to BCL6-mediated suppression of $T_H2$ gene expression in the $T_{reg}$ cells.[266] Additionally, BCL6 is important in maintaining the suppressive activity of $T_{regs}$ in the microenvironments of primary tumours and metastases in mice.[267] Deletion of BCL6 in $T_{regs}$ led to increased tumour infiltration of activated CD4+ and CD8+ T cells and showed synergy with immune checkpoint blockade treatment in a mouse model of colon cancer.[267] Additionally, increased BCL6 expression in $T_{regs}$ is correlated with poor prognosis in melanoma lymph node metastases and colorectal cancer in humans.[267] Furthermore, a subset of $T_{regs}$, follicular regulatory T cells ($T_{fr}$), which suppress the GC reaction are dependent on BCL6 for expression of CXCR5, which enables them to migrate to the GC.[268]

### 1.2.3.4: BCL6 in macrophages

BCL6 is also involved in suppression of the pro-inflammatory phenotype in macrophages. Accordingly, BCL6 expression is much higher in M2 macrophages than in pro-inflammatory M1 macrophages.[269] Suppression of pro-inflammatory genes by BCL6 in macrophages is dependent on its zinc finger domain but independent of its BTB/POZ domain.[259] This suggests a different mechanism of action to the canonical recruitment of corepressors and transcriptional repression of target genes (section 1.2.1). It has been suggested that BCL6 may compete with STAT proteins for binding to their target genes, hence passively inhibiting transcription of these genes.[259] More recently, it was shown that in M2 macrophages, BCL6 interacts with IκBζ to prevent it from opening the chromatin at the IL-6 promoter.[269] This prevents transcriptional activation and subsequent secretion of IL-6 and therefore suppresses the M1-associated pro-inflammatory phenotype in M2 macrophages.[269] It is conceivable that the interaction with IκBζ is mediated by the zinc finger domain of BCL6, thus explaining the dispensability of the BTB/POZ domain for suppression of the pro-inflammatory phenotype. The inhibition of IL-6 expression by BCL6 has also been linked to inhibition of STAT3 signalling in macrophages.[270] BCL6-deficient macrophages have increased IL-6 expression, resulting in increased STAT3 activation.[270] This leads to upregulation of cyclin D2 and c-Myc and downregulation of p27, resulting in accelerated G1/S transition and hyper-proliferation.[270] Therefore, BCL6 is important for the regulation of macrophage proliferation and phenotype. Unsurprisingly, given its role in the phenotype of M2 macrophages, BCL6 expression in macrophages as well as in $T_{regs}$ (section 1.2.3.3) has been linked to immunosuppressive tumour microenvironments.[271]

## 1.2.4: BCL6 in neurogenesis

BCL6 has also been implicated in neurogenesis. Unlike in GC B cells, where BCL6 prevents differentiation, BCL6 is critical for the differentiation of cortical progenitor cells into postmitotic neurons.[272,273] BCL6 promotes neurogenesis by suppressing the self-renewal promoting Wnt and Notch signalling pathways.[272,273] This transcriptional repression is dependent on recruitment of BCOR and the histone deacetylase SIRT1, as well as on physical displacement of the transcriptional activator MAML1 from Notch pathway target genes.[272,273] BCL6 is also important for the suppression of developmental cell death during cortical neurogenesis, at least in part by suppressing expression of *FOXO1*.[274] ChIP-seq experiments showed that in cortical progenitor cells, BCL6 only bound to 39% of the genes identified as BCL6 targets in GC B cells.[273] This further highlights the distinct role of BCL6 in neurogenesis.

BCL6 also recruits BCOR and SIRT1 to repress the self-renewal promoting SHH signalling pathway in neural progenitor cells in both the cortex and the cerebellum.[273,275] Unlike in the cortical progenitors, BCL6 did not bind to the Notch target gene *Hes5* in mouse cerebellar tissue.[275] BCL6 also did not bind to BCL6 target genes identified in GC B cells, such as *Tp53* and *Atr*.[275] The role of BCL6 in the differentiation of cerebellar neural progenitor cells meant that BCL6 acted as a tumour suppressor of medulloblastoma in a mouse model.[275] Given that is generally considered to be an oncogene, the very distinct role of BCL6 in neurogenesis compared to in GC B cells, other immune cells and cancers further demonstrates the diversity of BCL6 function.

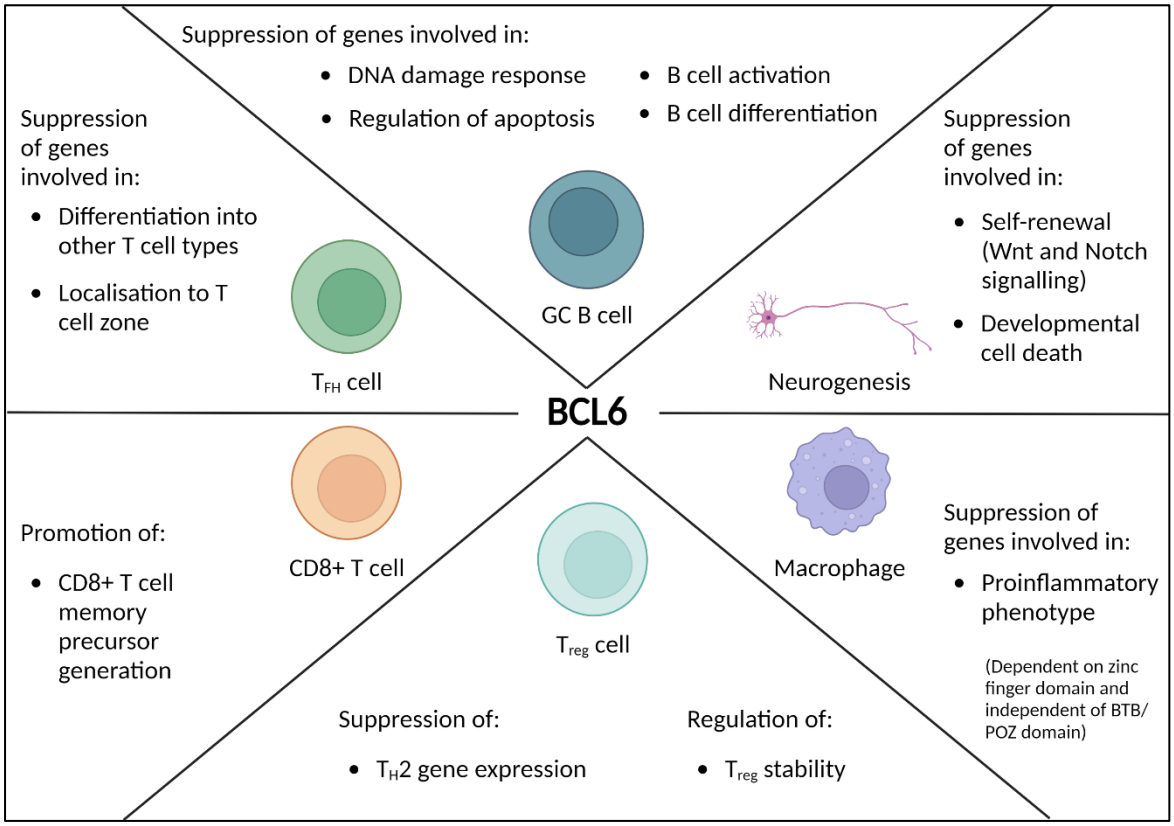

Figure 1.6: The roles of BCL6 in normal cell types.
Image produced using Biorender.

## 1.2.5: BCL6 in lymphoma

*BCL6* was first identified as the gene affected by common translocations of the 3q27 chromosome in lymphoma.[212,230,231] These translocations result in promoter switching such that *BCL6* expression is controlled by promoters for genes such as IgH, IgL, H4 and TTF.[276] As these genes are expressed constitutively in B cells, this results in constitutive expression of BCL6.[276] Additionally, these translocations often result in loss of *BCL6* non-coding exon 1, to which BCL6 binds in its auto-regulatory loop.[277,278] This provides an additional layer of deregulation. These translocations mean that genes that should only be repressed in GC B cells continue to be repressed by BCL6. It has been shown that 80% of BCL6 target genes in diffuse large B cell lymphoma (DLBCL) overlap with the target genes of BCL6 in GC B cells, indicating similar activity.[228] Therefore, constitutive activity of BCL6 means that the cells are unable to differentiate and have a suppressed DNA damage response, allowing the accumulation of oncogenic mutations.[234] This leads to lymphomagenesis.[234]

BCL6-activating translocations are found in 30-40% of diffuse large cell B cell lymphomas (DLBCLs) and 6-14 % of follicular lymphomas (FLs).[279–281] Furthermore, the enzyme responsible for SHM of IgG genes in GC B cells can also affect other genes, including *BCL6*.[282,283] This leads to mutations in *BCL6* in 30% of GC B cells.[282,283] Most of these do not affect transcription of *BCL6*, but those that do are found in lymphoma.[251,278] For example, mutations in the first non-coding exon of *BCL6* prevent BCL6 from binding to suppress its own expression in the autoregulatory loop.[251,278] Additionally, mutations in the IRF4-response element in the *BCL6* promoter prevent IRF4 from repressing BCL6 expression.[245] These aberrations lead to increased BCL6 expression and lymphomagenesis.

BCL6 deregulation in lymphoma also occurs via indirect mechanisms. These include mutations in CREBBP and EP300 that inhibit inactivating acetylation of BCL6 and prevent the re-activation of BCL6 target genes by CREBBP.[284] CREBBP is mutated in 29% of DLCBL and 33% of FL.[284] EP300 mutations are found in 10% and 9% of DLCBL and FL respectively.[284] Additionally, inactivating mutations in FBXO11 that prevent it from targeting BCL6 for degradation occur in about 6% of DLCBL.[285] Activating mutations in MEF2B in 11% of DLBCLs and 12% of FLs increase transcriptional activation of BCL6.[286] Furthermore, transcriptional activator of BCL6 expression IRF8 is mutated in 6% of FLs, which may contribute to increased BCL6 expression.[287]

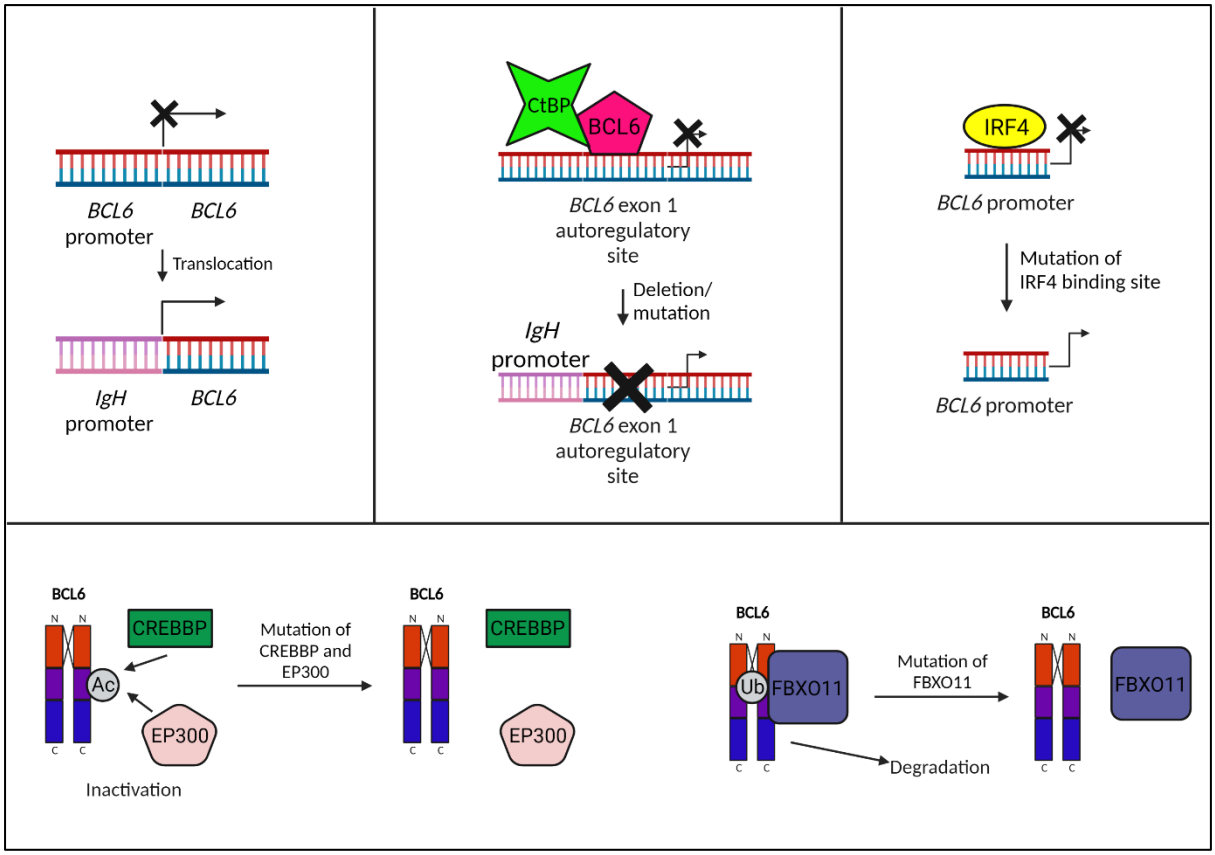


Figure 1.7: BCL6 deregulation in lymphoma.
Image produced using Biorender.

## 1.2.6: Targeting BCL6 in lymphoma

Due to the prevalence of BCL6 overexpression in non-Hodgkin's lymphomas, multiple BCL6 inhibitors have been developed.[288] Without exception, these inhibitors target the BTB domain of BCL6. This is to avoid disrupting the anti-inflammatory role of BCL6 mediated by its zinc finger domain (section 1.2.3.4).[259,289] The loss of this function due to homozygous deletion of BCL6 is rapidly lethal in mice.[259,289] The first BCL6 inhibitor was a peptide mimetic designed based on the crystal structure of NCOR2 bound to the lateral groove in the BTB domain of BCL6.[215,290] This inhibitor bound to the lateral groove and thereby inhibited recruitment of corepressors.[290] Importantly, binding was specific to BCL6 and not to other proteins with similar BTB domains.[290] This peptide mimetic increased expression of BCL6 target genes and reduced the growth and survival of BCL6-expressing cell lines but not BCL6-negative cell lines.[290] Additionally, the treatment prevented mice from forming GCs but was non-toxic.[290] This peptide mimetic was improved upon with modifications to make it more stable and efficient.[291] The resulting retro-inverso BCL6 peptide inhibitor (RI-BPI) inhibited the growth of BCL6-dependent cell lines and reactivated p53 and ATR expression in BCL6-dependent DLBCL cells.[291] Additionally, RI-BPI treatment reduced the viability of BCL6-positive primary human DLBCL cells and inhibited tumour growth in a mouse model of DLBCL.[291]

Screening of a library of peptide aptamers identified Apt48, which binds to the BTB domain but not to the lateral groove.[292] Nevertheless, Apt48 inhibited transcriptional repression by BCL6. Interestingly, it has recently been demonstrated that occupation of the region bound by Apt48 as well as the lateral groove is required for high affinity binding of NCOR2 to BCL6.[293] Like the peptide mimetics, Apt48 inhibited the growth of BCL6-expressing cell lines and increased expression of some BCL6 target genes.[292]

Small molecule inhibitors have also been designed to target BCL6. The small molecule inhibitor 79-6 was designed to bind to the lateral groove of the BCL6 BTB domain.[294] This was achieved through computer aided drug design.[294] Like the peptide inhibitors, 79-6 inhibited corepressor recruitment and inhibited BCL6 transcriptional repression, but did not affect the activity of other BTB domain proteins.[294] Additionally, 79-6 increased expression of BCL6 target genes and inhibited proliferation of BCL6-positive DLBCL cell lines.[294] The growth of a mouse model DLBCL xenograft was also inhibited by 79-6.[294] This inhibitor was non-toxic but had a much higher $K_d$ than the original peptide mimetic described above (138 μM compared to 10.2 μM).[290,294] Therefore, the design of 76-9 was improved using *in silico* site identification by competitive saturation (SILCS).[295] This generated the small molecule inhibitor FX1.[295] FX1 has a higher affinity ($K_d$ = 7 μM) for the BCL6 lateral groove than the endogenous corepressor NCOR2 ($K_d$ = 30 μM).[295] Therefore, FX1 more effectively blocks corepressor recruitment and a lower concentration is needed to inhibit the growth of DLBCL xenografts in mice.[295] A few other compounds, including pyrimidine derivatives, diphenylamine derivatives and two ansamycin antibiotics, rifamycin SV and rifabutin, have been shown to bind to the BCL6 BTB domain but have not yet been fully investigated.[296–298]

While most BCL6 inhibitors focus on blocking corepressor recruitment, one group identified compounds which cause degradation of BCL6.[299] This group screened a library of compounds to assess corepressor binding.[299] Interestingly, many of the compounds that bound the BCL6 BTB domain with high affinity led to proteasomal degradation of BCL6.[299] The level of BCL6 degradation correlated with the level of BCL6 target gene expression.[299] The compound BI-3802 was selected to treat DLBCL cell lines, which showed inhibited growth.[299] BI-3802 had no effect on cell lines without BCL6 expression.[299] It is notable that this is the only BCL6 inhibitor which not only blocks corepressor binding but also decreases the amount of BCL6 protein present. The other inhibitors have focused on preventing recruitment of corepressors to avoid inducing the inflammatory phenotype caused by homozygous deletion of BCL6. This compound was not tested in animal models due to poor bioavailability, however the authors pointed out that BI-302 induced expression of a very similar cohort of genes to inhibitors that only inhibit corepressor binding.[299]

While many of these inhibitors show great promise for the treatment of lymphoma, none have yet progressed to clinical trials. Xing et al. (2022) commented that this may be due to the relatively weak

activity of 79-6 and FX1, while higher affinity compounds developed subsequently have not been studied *in vivo*, possibly because their chemical properties make them unsuitable for use as drugs.[300] Xing et al. went on to develop the small molecule BCL6 inhibitor WK500B which they showed to be effective and orally bioavailable in mice.[300] This indicates that with some further development, BCL6 inhibitors will be able to progress to clinical trials. This will be a vital step in confirming that the effectiveness of BCL6 inhibition in the *in vitro* and pre-clinical settings translates into the clinic.

Targeted therapies often suffer from the induction of compensatory pathways within the treated tumour cells which lead to resistance (section 1.1.6.4). Indeed, it has been shown that combination therapies will likely need to target BCL2 and BCL-XL along with BCL6.[301] BCL2 and BCL-XL are anti-apoptotic proteins whose expression is repressed by BCL6.[301] Therefore, when DLBCL cell lines are treated with BCL6 inhibitors, BCL2 and BCL-XL expression increases.[301] Dupont et al. (2016) discussed the possibility that the DLBCL cells had switched their oncogene addiction from BCL6 to BCL2 and BCL-XL, becoming dependent on them for survival.[301] Treating DLBCL cell lines and mouse model xenografts with BCL6 inhibitor RI-BPI in combination with inhibitors of BCL2 and BCL-XL led to enhanced inhibition of growth compared to RI-BPI alone.[301] Therefore, while it is unlikely that BCL6 inhibitors will be useful alone, they have great promise as a component of combination therapies.

## 1.2.7: BCL6 in other cancers

Since its discovery in lymphoma, BCL6 has been revealed as an oncogene in multiple other cancer types, including leukaemia, breast cancer, non-small cell lung cancer, ovarian cancer, colorectal cancer, gastric cancer, bladder cancer and glioblastoma.

### 1.2.7.1: BCL6 in leukaemia

BCL6 has been implicated in both acute and chronic myeloid leukaemia (AML and CML) and in acute lymphoblastic leukaemia (ALL). BCL6 seems to have similar functions in leukaemia to its roles in GC B cells and lymphoma, including suppression of the DNA damage response and apoptosis, promotion of proliferation and suppression of differentiation.[302–305] BCL6 knockout or inhibition severely inhibits the survival, proliferation and self-renewal capacity of leukaemia cells and prevents them from initiating leukaemia in mouse models.[302–305] Additionally, BCL6 is involved in resistance to chemotherapy treatments in leukaemia.[302–305] In response to tyrosine kinase inhibition (TKI) treatment, CML and BCR-ABL1-rearranged ALL cells upregulate BCL6 expression.[302] This upregulation is dependent on inhibition of STAT5 and PI3K/AKT signalling and subsequent activation of FOXO proteins by the TKI.[302] The upregulated BCL6 suppresses the p53 pathway, conferring resistance to treatment.[302,303] BCL6-mediated repression of *TP53* was also necessary for the self-renewal, proliferation and survival

of CML cells.[303] Without BCL6 expression, CML cells could not form colonies and many underwent G1/S arrest followed by apoptosis.[303]

BCL6 also conferred chemoresistance to MLL-rearranged ALL by suppressing expression of the pro-apoptotic protein BIM, which is upregulated by the MLL-fusion proteins created by chromosome rearragement..[304] The rearranged MLL itself bound to the BCL6 promoter to upregulate BCL6 expression and BCL6 increased MLL expression in a positive feedback loop.[304] Furthermore, BCL6 was upregulated in AML cells compared to the cells they derive from and was further upregulated by chemotherapy.[305] Like in GC B cells and lymphoma, BCL6 was involved in upregulation of genes involved in proliferation and stem cell characteristics and downregulation of genes involved in oxidative stress response and the p53 pathway.[305] In all of these leukaemia subtypes, inhibition of BCL6 increased sensitivity to therapies.[302–305] High levels of BCL6 have also been correlated with poor prognosis in chronic lymphocytic leukaemia (CLL), although little further research has been published in this area.[306]

#### 1.2.7.2 BCL6 in breast cancer

BCL6 also has an important role in breast cancer. The BCL6 locus is amplified in 51% of breast tumours and is there is significantly higher BCL6 expression in breast cancer compared to non-cancerous mammary cell lines and tissues.[307,308] BCL6 expression is positively correlated with tumour grade and metastasis and negatively correlated with prognosis in breast cancer patients.[308] BCL6 depletion or inhibition decreased the viability and migration capacity of breast cancer cell lines, while BCL6 expression promoted the growth and invasion of cell line-derived breast cancer xenografts in mice.[308] BCL6 expression has also been linked to paclitaxel resistance in breast cancer.[309]

ChIP-seq for BCL6 in breast cancer cell lines revealed a different pattern of binding to that seen in GC B cells and lymphoma.[307] Around 50% of the genes bound by BCL6 in breast cancer were also bound by BCL6 in lymphoma, indicating at least some overlap in BCL6 function.[307] However, > 80% of the target genes of BCL6 in lymphoma were not bound by BCL6 in breast cancer.[307] Additionally, only 7% of BCL6 binding sites in breast cancer fell within promoters, compared to 23% in DLBCL.[307] This indicates that BCL6 has very different activity in breast cancer than it does in GC B cells and lymphoma.

Further analysis of four of the novel BCL6 targets found in breast cancer revealed that while BCL6 repressed expression of three of them (*HERC5*, *KLF6* and *SH3PXD2B*), it directly upregulated *MED24* expression.[307] This implies that BCL6 is not an obligate transcriptional repressor, as has been previously assumed. Interestingly, blocking BCL6 corepressor recruitment with RI-BPI repressed *MED24* expression as well as derepressing expression of *KLF6* and *SH3PXD2B*.[307] This indicates that the transcriptional activator role of BCL6 is also mediated by interactions with other proteins at the lateral

groove. *HERC5* expression was not derepressed by RI-BPI treatment, suggesting that corepressors such as MTA3 which bind to regions other than the BTB domain are also involved in BCL6 activity in breast cancer.[307]

### 1.2.7.3 BCL6 in non-small-cell lung cancer

A handful of studies have indicated a role for BCL6 in non-small cell lung cancer (NSCLC), especially in resistance to TKIs. Relatively high levels of BCL6 are expressed in lung adenocarcinoma and squamous cell carcinoma.[310] BCL6 is upregulated in NSCLC in response to BET inhibitor and EGFR inhibitor TKIs.[310,311] The upregulation of BCL6 in response to the EGFR inhibitor gefitinib was linked to the downregulation of p53 signalling and apoptosis.[310] Additionally, the combination of gefitinib and BCL6 inhibitor FX1 was synergistic and resulted in death of nearly all of the treated NSCLC cells.[310] Another study showed that combination treatment with inhibitors of STAT3 and BCL6 significantly reduced growth of NSCLC cell lines and xenografted tumours.[312] The role of BCL6 in the response of NSCLC cells to the BET inhibitor OTX015 was investigated in more depth by Guo et al. (2021).[311] BCL6 silencing increased the cytotoxicity of the BET inhibitor in NSCLC, indicating that BCL6 is involved in resistance.[311] BET inhibition disrupted the BCL6 autoregulatory loop, resulting in BCL6 upregulation.[311] This was due to the inhibition of BET protein BRD3, which was revealed to act as a BCL6 partner in the transcriptional repression of BCL6 target genes, including BCL6 itself, in NSCLC.[311] The BCL6 induced by BET inhibition repressed known BCL6 target genes *TP53*, *CHEK1*, *CDKN1A* and *CASP8*.[311]

### 1.2.7.4 BCL6 in other cancers

BCL6 has also been implicated in ovarian cancer, colorectal cancer, gastric cancer and bladder cancer. BCL6 expression is higher in ovarian cancer tumours than in surrounding healthy tissue and the level of BCL6 expression is correlated with tumour stage, metastasis and recurrence as well as with poor prognosis.[313,314] BCL6 is involved in promoting proliferation of ovarian cancer cells by inducing expression of cyclin B1 and CDC25B and in promoting metastasis and invasion by upregulating N-cadherin, MMP2 and MMP9.[313] Furthermore, BCL6 has been linked to cisplatin resistance in ovarian cancer.[315] Similarly, BCL6 is expressed at higher levels in colorectal cancer than in healthy colorectal mucosa.[316] This has been linked to promotion of proliferation via regulation of β-catenin, cyclin D1 and c-myc.[317] In contrast to its involvement in the other cancers so far described, BCL6 appeared to inhibit cell cycle progression in gastric cancer by repressing the expression of cyclin D2.[318] Meanwhile, different studies have linked BCL6 to both positive and negative prognosis in bladder carcinoma.[319,320]

Investigations into the role of BCL6 in gastric, bladder, colorectal and ovarian cancer are at very early stages and further research is needed to elucidate the role of BCL6 in these and other cancers.

#### 1.2.7.5 Summary of the roles of BCL6 in cancer

Since its original identification in lymphoma, BCL6 has been recognised as an oncogene in multiple cancer types. In most cases, BCL6 is involved in suppression of cell cycle checkpoints, apoptosis and differentiation and promotion of proliferation, with p53 expression commonly repressed by BCL6 across multiple cancer types. However, comparative ChIP-seq analysis of BCL6 target genes in breast cancer compared to lymphoma revealed very different patterns of DNA binding. Combined with the known differences in the activity of BCL6 in $T_{FH}$ cells, $T_{reg}$ cells, macrophages and developing neurons compared to in GC B cells, this indicates that BCL6 has different roles depending on the cellular context. Further research is needed to understand the differences and similarities in the activity of BCL6 in different cancer types. However, with the possible exceptions of gastric and bladder cancer, most cancer types show decreased viability and increased sensitivity to treatment when BCL6 is inhibited.

## 1.2.8: BCL6 in glioblastoma

Several studies have implicated BCL6 in the severity and therapy resistance of GBM.[207–211] BCL6 expression correlates with glioma grade.[207–211] Depletion or inhibition of BCL6 substantially decreases GBM cell line viability, long-term proliferative potential and migration as well as reducing tumour growth in GBM mouse models.[207,209–211] One study found that BCL6 depletion induced cellular senescence, although other studies have not replicated this finding.[209] Furthermore, knockout of BCL6 in GBM cell lines renders them non-viable.[207] Additionally, treatment with irradiation and the DNA damaging therapies doxorubicin and TMZ has been shown to upregulate BCL6 expression.[207] BCL6 inhibition enhances the effectiveness of GBM therapies such as IR and TMZ both *in vitro* and *in vivo*.[207,210] Together, these observations highlight that BCL6 is vital for the survival of GBM cells under unstressed conditions and plays an important role in the therapy resistance of GBM.

The mechanism of BCL6 upregulation in GBM and in response to therapy is not known. While one study showed that BCL6 translocations occurred in 37% of their sample of 30 GBM tumours, this has not been validated by any larger studies.[208,209] Additionally, large scale studies of mutations found in GBM tumours have not identified common mutations or amplifications of BCL6.[53,321] Therefore, changes in transcriptional or post-transcriptional regulation are likely to be responsible.

There are indications that the role of BCL6 in GBM may differ from its activity in GC B cells and lymphoma (sections 1.2.2 and 1.2.5). This is perhaps unsurprising given the proven alternative activity

of BCL6 in other immune cells, neurogenesis and breast cancer, which is apparently mediated by factors including cell context-specific chromatin modification and corepressor recruitment (sections 1.2.3, 1.2.4 and 1.2.7.2). In GBM, ChIP-qPCR showed that while BCL6 did appear to bind to its own exon 1 and to known target gene *TARS*, it did not appear to bind to *TP53*, *PTEN* or *CHEK1*, which are other known BCL6 targets in lymphoma.[322] Additionally, RNA sequencing of the LN18 GBM cell line treated with BCL6 inhibitor FX1 did not show de-repression of a selection of known BCL6 target genes, except for *TARS*.[322] Nonetheless, RNA sequencing and microarray analysis of gene expression in BCL6-inhibited or -depleted GBM cells showed upregulation of apoptosis and p53 pathways as well as upregulation of NFκB signalling.[207,209] However, blocking the lateral groove of BCL6 with RI-BPI or FX1 did not upregulate p53 itself, further suggesting that BCL6 does not repress p53 in GBM.[207,209] BCL6 knockdown in GBM cells resulted in upregulation of cell cycle checkpoint protein p21 and pro-apoptotic protein Bax, as well as downregulation of anti-apoptotic protein BCL2 and cell cycle promotor cyclin D2.[210] This indicates that BCL6 may retain some but not all of its known functionality in GBM.

EMSA and luciferase assays showed that overexpressed BCL6 binds to known corepressors BCOR, NCOR1 and NCOR2 in GBM and that it acts as a transcriptional repressor.[322] However, a luciferase assay for endogenous BCL6 in FX1-treated GBM cells failed to show de-repression of the BCL6 reporter.[207] This may indicate that endogenous BCL6 in GBM does not have transcriptional activity or that its transcriptional activity is not mediated by corepressor recruitment to its BTB domain or by its canonical DNA binding sequence. However, the low abundance of endogenous BCL6 in GBM cells may have prevented the true observation of BCL6 transcriptional activity in this assay.

Surprisingly, when endogenous BCL6 was upregulated by doxorubicin or IR treatment, the expression of the luciferase reporter was increased.[207] This suggests that endogenous BCL6 may act as a transcriptional activator in treated GBM cells. Another study identified BCL6 as a transcriptional activator of *AXL* in GBM and found that the expression of AXL partially mediated the positive effects of BCL6 on GBM cell viability and migration.[209] Similarly, BCL6 has been shown to activate transcription of *MED24* in breast cancer.[307] The lateral groove of the BTB domain was important for the activation of both of these genes by BCL6, suggesting that the recruitment of cofactors is involved in this activity.[209,307]

The role of BCL6 in the therapy resistance of GBM has not been thoroughly studied. Aside from the suggestion that BCL6 may act as a transcriptional activator in response to therapy in GBM, BCL6 has been shown to inhibit upregulation of p53 signalling by IR, despite not appearing to suppress p53 in untreated GBM cells.[209] Interestingly, this effect was seen at 6 Gy IR but not at 12 Gy IR, suggesting that the role of BCL6 may be modified by context.[209]

In summary, BCL6 is clearly vital for GBM cell viability and is involved in resistance to therapy. While BCL6 may retain some of its canonical functions, such as suppression of cell cycle checkpoints, apoptosis and NFκB signalling, there are also strong indications that BCL6 activity in GBM is different to in GC B cells and lymphoma. In GBM, BCL6 appears not to target many of the genes it represses in GC B cells and BCL6 may even act as a transcriptional activator in response to treatment of GBM cells. Although BCL6 seems to play a critical role in the therapy resistance of GBM, very little is currently known about what this role might be.

## 1.3: Aims of this thesis

This thesis focuses on the role of BCL6 in the response of GBM to therapy. GBM is a deadly disease for which more effective treatments are desperately needed (section 1.1). BCL6 is critical for the survival of GBM cells and is involved in the resistance of GBM to chemo- and radiotherapy (section 1.2.8). Although yet to enter clinical trials, multiple BCL6 inhibitors have been developed and have shown efficacy against multiple cancer types in pre-clinical studies (sections 1.2.6 and 1.2.7). Therefore, a promising route to improving the survival of GBM patients is to repurpose the BCL6 inhibitors already in development for the treatment of GBM, in combination with the gold-standard clinical regimen of IR and TMZ.

However, research on the role of BCL6 in the therapy response of GBM is sparse. The research that has been published suggests that BCL6 may have different functions in GBM to its canonical role in GC B cells and lymphoma (section 1.2.8). Indeed, studies of BCL6 function in other immune cell and cancer types and in neurogenesis indicate that BCL6 activity is cell context specific (sections 1.2.3, 1.2.4 and 1.2.7). Therefore, to develop BCL6 targeting therapies for GBM, it is important to first understand the role of BCL6 in the response of GBM to therapy. This gap in current understanding is addressed in this thesis with three aims:

**Aim 1:** Investigate the impact of BCL6 inhibition on the whole proteome response of GBM cells to therapy (Chapter 3).

**Aim 2:** Determine which proteins BCL6 associates with in untreated GBM cells and whether these associations change in response to irradiation (Chapters 4 and 5).

**Aim 3:** Determine whether the changed behaviour of BCL6 in response to irradiation is due to alternative splicing of its transcript (Chapter 6).

# 2: Materials and Methods

## 2.1: Reagents and materials

### 2.1.1: Cell culture

| | |
|---|---|
| eMyco mycoplasma PCR detection kit | Boca Scientific, USA |
| Gibco™ DPBS | Thermo Fisher Scientific, USA |
| Gibco™ Foetal bovine serum (FBS) | Thermo Fisher Scientific, USA |
| Gibco™ RPMI 1640 media | Thermo Fisher Scientific, USA |
| Gibco™ DMEM, high glucose, pyruvate, no glutamine | Thermo Fisher Scientific, USA |
| Gibco™ Trypsin-EDTA (0.05%), phenol red | Thermo Fisher Scientific, USA |
| 230 mm glass Pasteur pipette | Interlab, New Zealand |
| 10 cm plates | Greiner BioOne, Germany |
| 15 cm plates | Corning®, USA |
| 25 $cm^2$ Rectangular Canted Neck Cell Culture Flask with Vent Cap | Corning®, USA |
| 75 $cm^2$ U-Shaped Canted Neck Cell Culture Flask with Vent Cap | Corning®, USA |
| Gibco™ Sodium pyruvate | Thermo Fisher Scientific, USA |

### 2.1.2: Kits and enzyme mixes

| | |
|---|---|
| Duolink® Probe kit | Merck, USA |
| Duolink® Fluorescent Detection Reagent kit | Merck, USA |
| Duolink® Wash Buffers | Merck, USA |
| Duolink® Mounting Media with DAPI | Merck, USA |
| KAPA SYBR® FAST qPCR Master Mix | Sigma Aldrich (Merck, USA) |
| Micrococcal Nuclease | New England Biolabs (NEB), USA |
| NucleoSpin® Gel and PCR Clean-Up Mini Kit | Machery-Nagel, Germany |
| Pierce™ Quantitative Fluorometric Peptide Assay | Thermo Fisher Scientific, USA |
| Pierce™ Rapid Gold BCA Protein Assay Kit | Thermo Fisher Scientific, USA |
| Platinum™ SuperFi™ DNA polymerase | Thermo Fisher Scientific, USA |
| Qubit™ dsDNA Broad-Range (BR) Kit | Thermo Fisher Scientific, USA |
| Qubit™ dsDNA High-Sensitivity (HS) Kit | Thermo Fisher Scientific, USA |
| Qubit™ RNA High-Sensitivity (HS) Kit | Thermo Fisher Scientific, USA |
| *Quick*-RNA Miniprep Kit | Zymo Research, USA |

## 2.1.3: Oxford Nanopore Kits

### 2.1.3.1: cDNA-PCR sequencing

| | |
|---|---|
| Agencourt AMPure XP beads | Beckman Coulter, USA |
| cDNA-PCR Sequencing Kit (SQK-PCS109) | Oxford Nanopore Technologies, UK |
| Deoxynucleotide (dNTP) Solution Mix | New England Biolabs (NEB), USA |
| Exonuclease I | New England Biolabs (NEB), USA |
| 10X Exonuclease I Reaction Buffer | New England Biolabs (NEB), USA |
| LongAmp Taq 2× Master Mix | New England Biolabs (NEB), USA |
| RNaseOUT™ Recombinant Ribonuclease Inhibitor | Invitrogen |
| Thermo Scientific™ Maxima H Minus Reverse Transcriptase with 5× RT buffer | Thermo Fisher Scientific, USA |

### 2.1.3.2: Native barcoding amplicons

| | |
|---|---|
| Ligation Sequencing Kit (SQK-LSK109) | Oxford Nanopore Technologies, UK |
| Native Barcoding Expansion 1-12 (EXP-NBD104) | Oxford Nanopore Technologies, UK |
| Native Barcoding Expansion 13-24 (EXP-NBD114) | Oxford Nanopore Technologies, UK |
| NEB Blunt/TA Ligase Master Mix | New England Biolabs (NEB), USA |
| NEBNext FFPE Repair Mix | New England Biolabs (NEB), USA |
| NEBNext® Quick Ligation Reaction Buffer | New England Biolabs (NEB), USA |
| NEBNext Ultra II End repair/dA-tailing Module | New England Biolabs (NEB), USA |

### 2.1.3.3: Priming and washing the flow cell

| | |
|---|---|
| Flow Cell Priming Kit (EXP-FLP002) | Oxford Nanopore Technologies, UK |
| Flow Cell Wash Kit (EXP-WSH003) | Oxford Nanopore Technologies, UK |

## 2.1.4: Antibodies

| | |
|---|---|
| AMPK gamma-1 polyclonal antibody (PA5-67459) | Thermo Fisher Scientific, USA |
| Anti-β-actin AC-15 | Sigma Aldrich (Merck, USA) |
| Anti-BCL-6 antibody D-8 (sc-7388) | Santa Cruz, USA |
| Anti-BCL-6 antibody N-3 (sc-858) | Santa Cruz, USA |
| Anti-NF-κB p50 (4D1) | BioLegend, USA |
| Anti- NF-κB p65 | Sigma Aldrich (Merck, USA) |
| Anti-NCOR/SMRT antibody (ab5802) | Abcam, UK |

| | |
|---|---|
| Goat anti-mouse IgG (H+L) highly cross-absorbed secondary antibody, Alexa Fluor™ 488 | Thermo Fisher Scientific, USA |
| Goat anti-rabbit IgG (H+L) highly cross-absorbed secondary antibody, Alexa Fluor™ 568 | Thermo Fisher Scientific, USA |
| HRP goat anti-mouse IgG | BioLegend, USA |
| Invitrogen™ normal rabbit IgG | Thermo Fisher Scientific, USA |
| Mouse IgG, κ isotype control | eBioScience |

## 2.1.5: Primers

### 2.1.5.1: Quantitect primers for qRT-PCR

| | |
|---|---|
| BCL6 | Qiagen, NZ |
| HPRT1 | Qiagen, NZ |

### 2.1.5.2: Custom PCR primers

| | |
|---|---|
| SSP primer: TTTCTGTTGGTGCTGATATTGC | Integrated DNA Technologies IDT, USA |
| VPN primer: ACTTGCCTGTCGCTCTATCTTCTT | Integrated DNA Technologies IDT, USA |
| BCL6 3'-end primer: AGACGAAAGCATCAACACTCCATGC | Integrated DNA Technologies IDT, USA |
| BCL6 5'-end primer: TTGGACTGTGAAGCAAGGCATTGG | Integrated DNA Technologies IDT, USA |
| BCL6 exon 5 to exon 6 junction forward primer: CCATCACAGCCATGATGTTG | Integrated DNA Technologies IDT, USA |
| BCL6 exon 5 to exon 6 junction reverse primer: TGCCAGTGATGTTCTTCTCAA | Integrated DNA Technologies IDT, USA |

## 2.1.6: Chemicals and reagents

| | |
|---|---|
| Acetic acid | Merck, USA |
| Acetonitrile, Liquid Chromatography Grade | Merck, USA |
| 30% Acrylamide/Bis Solution, 29:1 | Bio-Rad, USA |
| Ammonium persulfate (APS) | Affymetrix, USA |
| HyAgarose™ | HydraGene, China |

| | |
|---|---|
| Ammonium hydrogen carbonate | BDH, UAE |
| Boric acid | Merck, USA |
| Bromophenol blue | BDH, UAE |
| Centrifuge grease | Dow Corning, USA |
| Chloroform | Sigma-Aldrich (Merck, USA) |
| Chloroform:isoamyl alcohol 24:1 | Sigma-Aldrich (Merck, USA) |
| Invitrogen™ DEPC-Treated Water | Thermo Fisher Scientific, USA |
| Dithiothreitol (DTT) | Bio-Rad, USA |
| Dimethyl sulfoxide (DMSO) | Thermo Fisher Scientific, USA |
| Doxorubicin hydrochloride | Ebewe Pharma, Austria |
| EDTA | Merck |
| EGTA | Sigma-Aldrich (Merck, USA) |
| Ethanol | Thermo Fisher Scientific, USA |
| Formaldehyde (37%) | Thermo Fisher Scientific, USA |
| Formic acid | Merck, USA |
| FX1 | Sigma-Aldrich (Merck, USA) |
| Gel Red® Nucleic Acid Stain | Biotium, USA |
| Glycerol | Thermo Fisher Scientific, USA |
| Glycine | Sigma-Aldrich (Merck, USA) |
| Glycogen | Thermo Fisher Scientific, USA |
| HEPES | Thermo Fisher Scientific, USA |
| HPLC-grade water | Thermo Fisher Scientific, USA |
| IGEPAL | Sigma-Aldrich (Merck, USA) |
| Iodoacetamide | GE Health Life Sciences, USA |
| Isopropanol | Thermo Fisher Scientific, USA |
| LiCl | Sigma-Aldrich (Merck, USA) |
| Methanol, Optima® LC/MS Grade | Thermo Fisher Scientific, USA |
| Methylene blue | Acros Organics (Thermo Fisher Scientific, USA) |
| Milk powder | Pams, NZ |
| Nonidet™ P 40 Substitute | Sigma-Aldrich (Merck, USA) |
| Orange G | Sigma-Aldrich (Merck, USA) |
| Gibco™ PBS tablets | Thermo Fisher Scientific, USA |
| Paraformaldehyde (PFA) | Sigma Aldrich (Merck, USA) |
| pH 4.01 Buffer | Hanna Instruments, USA |
| pH 7.01 Buffer | Hanna Instruments, USA |

| | |
|---|---|
| pH 10.01 Buffer | Hanna Instruments, USA |
| Ponceau S | Merck, USA |
| Proteinase K | Thermo Fisher Scientific, USA |
| Ribonuclease A | Sigma Aldrich (Merck, USA) |
| RNase AWAY™ Surface Decontaminant | Thermo Fisher Scientific, USA |
| Sodium chloride (NaCl) | Sigma Aldrich (Merck, USA) |
| Sodium deoxycholate (Na-DOC) | Sigma Aldrich (Merck, USA) |
| Sodium dodecyl sulfate (SDS) | BioRad, USA |
| SYBR Safe DNA Gel Stain | Thermo Fisher Scientific, USA |
| TEMED | Bio-Rad, USA |
| Trizma® base (Tris) | Sigma Aldrich (Merck, USA) |
| Trizma® hydrochloride (Tris-Cl) | Sigma Aldrich (Merck, USA) |
| Triton X-100 | Sigma Aldrich (Merck, USA) |
| Pierce™ Trypsin Protease, MS Grade | Thermo Fisher Scientific, USA |
| Thermo Scientific™ Pierce™ Water, LC-MS Grade | Thermo Fisher Scientific, USA |
| Urea | Sigma Aldrich (Merck, USA) |

### 2.1.7: Plasticware

| | |
|---|---|
| Applied Biosystems® MicroAmp™ Fast Optical 96-Well Reaction Plate, 0.1 mL | Thermo Fisher Scientific, USA |
| 10 µL, 20 µL, 200 µL and 1000 µL Barrier Tips | MultiMax™ |
| BondElut OMIX 100 µL C18 | Agilent, USA |
| CELLSTAR® 5 mL, 10 mL, 25 mL and 50 mL Serological Pipettes | Greiner Bio-One, Austria |
| Nunc™ Lab-Tek™ II 8 well Chamber Slides | Thermo Fisher Scientific, USA |
| 10 mL Combitips Advanced® | Eppendorf, Germany |
| DNA LoBind® Tubes 1.5 mL | Eppendorf, Germany |
| 10 µL, 200 µL and 1000 µL Eclipse™ pipette tips | Labcon, USA |
| 1.7 mL Eppendorf tubes | MultiMax™ |
| 15 mL Falcon® Conical Centrifuge Tubes | Corning, USA |
| 50 mL Falcon® Conical Centrifuge Tubes | Corning, USA |
| 50 mL/60 mL Luer Lock Syringe | Interlab, NZ |
| MicroAmp™ Optical Adhesive Film | Thermo Fisher Scientific, USA |
| Snap Strip 8 PCR Tubes 0.2 assorted colours | Scientific Specialties, Inc, USA |

| | |
|---|---|
| Thermo Scientific™ Low Protein Binding Microcentrifuge Tubes 2.0 mL | Thermo Fisher Scientific, USA |
| Thermo Scientific™ 0.1 mL Micro-Insert | Thermo Fisher Scientific, USA |
| Thermo Scientific™ 1.5 mL Short Thread Vials | Thermo Fisher Scientific, USA |
| Thermo Scientific™ UltraClean Closure: 9 mm PP Short Thread Caps | Thermo Fisher Scientific, USA |

### 2.1.8: Miscellaneous

| | |
|---|---|
| Coverslips | Thermo Fisher Scientific, USA |
| Invitrogen™ Dynabeads™ Protein G for immunoprecipitation | Thermo Fisher Scientific, USA |
| Kimtech KimWipes | Kimberley-Clark, USA |
| Immobilon®-FL PVDF Membrane | Merck, USA |
| Microscope slides | Thermo Fisher Scientific, USA |
| Micro-Touch® NitraFree™ gloves | Ansell, Australia |
| Prolong™ Gold antifade reagent with DAPI | Thermo Fisher Scientific |
| _-10 µL Multipipette® Plus | Eppendorf, Germany |
| Nail polish (clear) | W7®, UK |
| Parafilm® M | Sigma-Aldrich (Merck, USA) |
| Precision Plus Protein Dual Color Standards | Bio-Rad, USA |
| _-2.5 µL Research® Plus Pipette | Eppendorf, Germany |
| _-10 µL Research® Plus Pipette | Eppendorf, Germany |
| 20-200 µL Research® Plus Pipette | Eppendorf, Germany |
| 100-1000 µL Research® Plus Pipette | Eppendorf, Germany |
| Restore™ Western Blot Stripping Buffer | Thermo Fisher Scientific, USA |
| Thermo Scientific™ Halt™ Protease Inhibitor Cocktail (100x) | Thermo Fisher Scientific, USA |
| Trackit™ 1 Kb Plus DNA Ladder | Thermo Fisher Scientific, USA |
| Trackit™ 100 bp DNA Ladder | Thermo Fisher Scientific, USA |
| Western Lightning Ultra, Chemiluminescent Substrate | Perkin Elmer, USA |

### 2.1.9: LC-Mass spectrometry

| | |
|---|---|
| Acclaim™ PepMap™ 100 C18 trap column (5 µm, 0.3 x 5 mm) | Thermo Fisher Scientific, USA |
| Acclaim™ PepMap™ 100 C18 analytical column (2 µm, 100 A, 75 µm x 15 cm) | Thermo Fisher Scientific, USA |

| | |
|---|---|
| Dionex UltiMate 3000 RS Autosampler | Thermo Fisher Scientific, USA |
| Nanospray Flex™ | Thermo Fisher Scientific, USA |
| Orbitrap Fusion™ Lumos™ Tribrid™ Mass Spectrometer | Thermo Fisher Scientific, USA |
| Q Exactive™ Plus Mass Spectrometer | Thermo Fisher Scientific, USA |

## 2.1.10: Instruments

| | |
|---|---|
| Amersham Imager 600 | GE Health Life Sciences, USA |
| Bandelin Electronic™ Sonopuls™ Ultrasonic Homogenizer Mini20 | Thermo Fisher Scientific, USA |
| Centrifuge MiniSpin® with rotor F-45-12-11 | Eppendorf, Germany |
| CentriVap Cold Trap | Labconco, USA |
| CentriVap Concentrator | Labconco, USA |
| CFX96™ Touch Real-Time PCR Detection System | BioRad, USA |
| Thermo Scientific™ Shandon™ Cytospin3 | Thermo Fisher Scientific, USA |
| Dri-Bath Type 17600 | Thermolyne, USA |
| Enspire™ 2300 Multilabel Reader | PerkinElmer, USA |
| ImageScanner III | GE Health Life Sciences, USA |
| Heracell 150i CO2 Incubator | Thermo Fisher Scientific, USA |
| Labquake® Rotator | Barnstead Thermolyne Corporation, USA (Thermo Fisher Scientific, USA) |
| Laminar Flow Workstation | AES Environmental, Australia |
| LSE™ Mini Microcentrifuge | Corning Incorporated, USA |
| LSE™ Vortex Mixer | Corning Incorporated, USA |
| Mini-PROTEAN® 3 Cell | Bio-Rad, USA |
| Model 1000/500 Constant Voltage Power Supply | Bio-Rad, USA |
| Nanodrop® ND-1000 Spectrophotometer | NanoDrop Technologies, Inc., USA |
| Olympus Laser Scanning Confocal Microscope FV3000 | Evident, Japan |
| Orbit™ 1900 High Capacity Lab Shaker | Labnet (Corning Inc.), USA |
| pH510 CyberScan | Eutech Instruments, UK (Thermo Fisher Scientific, USA) |
| Platform Rocker | Bioline International, Canada |
| PowerPac 200 | Bio-Rad, USA |
| Qubit® 2.0 Fluorometer | Thermo Fisher Scientific, USA |
| Sorvall™ Legend™ Micro 21R Microcentrifuge | Thermo Fisher Scientific, USA |

| | |
|---|---|
| Sub-Cell GT Electrophoresis Cell | Bio-Rad, USA |
| Techne Large-Format Gradient Thermo Cycler with Combi Block; 100-230 V | Antylia Scientific, USA. |
| Tube Revolver Rotator | Thermo Fisher Scientific, USA |
| Typhoon FLA 9500 | GE Health Life Sciences, USA |

### 2.1.11: Software

| | |
|---|---|
| Anaconda Prompt | Anaconda, USA |
| BLASTn | National Center for Biotechnology Information (NCBI), USA |
| CellProfiler | Broad Institute of MIT and Harvard, USA |
| Fiji (ImageJ) | ImageJ |
| Geneious 2019 | Geneious |
| g:Profiler version *e104_eg51_p15_2719230* | g:Profiler |
| Integrated Genomics Viewer (IGV) | Broad Institute of MIT and Harvard, USA |
| Jupyter Notebook | Jupyter |
| OligoAnalzyer | Integrated DNA Technologies (IDT), USA |
| Primer3 | Whitehead Institute for Biomedical Research, USA |
| Proteome Discoverer 2.4 | Thermo Fisher Scientific, USA |
| PSICQUIC (Proteomics Standards Initiative Common Query Interface) | European Molecular Biology Laboratory (EMBL) – European Bioinformatics Institute (EBI) |
| SPSS | IBM, USA |
| STRING version 11.5 | © STRING CONSORTIUM |
| Xcalibur 4.2 software | Thermo Fisher Scientific, USA |
| University of California, Santa Cruz (UCSC) Genome Browser | University of California, Santa Cruz (UCSC), USA |

## 2.2: Cell culture

### 2.2.1: Cell lines

Three human glioblastoma cell lines were used in this thesis. The LN18 cell line was sourced from the American Type Culture Collection (USA). The NZG0906 and NZG1003 cell lines were previously immortalised in the McConnell lab from tumour tissue.[323] The Raji human lymphoma cell line was a gift from Ian Morison, University of Otago. The K562 chronic myeloid leukaemia cell line was a gift from Michael Berridge, Malaghan Institute of Medical Research. The hepatocellular carcinoma cell line HepG2 was used from established stocks at Victoria University of Wellington.

### 2.2.2: Cell culture media

The LN18, NZG0906, NZG1003 and K562 cell lines were cultured in RPMI 1640 media supplemented with 5% foetal bovine serum (FBS). The Raji cell line was cultured in RPMI 1640 supplemented with 5% FBS and 1 mM pyruvate. The HepG2 cell line was cultured in DMEM supplemented with 10% FBS.

### 2.2.3: Cell culture

The three glioblastoma cell lines and the HepG2 cell line were grown as adherent cultures and the Raji and K562 cell lines were grown in suspension. All cell lines were grown under conditions of normoxia, with 5% $CO_2$ and at 37 °C. Cultures were passaged as required in a sterile manner in a safety cabinet. To passage the adherent cultures, the media was aspirated and the cells were washed with DPBS. Trypsin-EDTA 0.05% was added and aspirated and cells were incubated at 37 °C, 5% $CO_2$ for 1-2 minutes. Trypsin was inactivated by addition of media. Cells were resuspended and passaged as required. The suspension cells were passaged as required by removing a portion of the cells suspended in media and replacing the media removed. All cell culture stock flasks were periodically checked for mycoplasma contamination using the eMyco mycoplasma PCR detection kit.

### 2.2.4: Cell counting

When cells were plated for experiments, they were first lifted and resuspended in media (section 2.2.3) and then an aliquot was counted using a haemocytometer.

## 2.3: Agarose gel electrophoresis

### 2.3.1: Buffer

**TBE:** 100 mM Tris, 100 mM boric acid, 2 mM EDTA in distilled water.

### 2.3.2: Gel preparation

Agarose was added to the appropriate volume of 1x TBE for the chosen gel tray and at the appropriate concentration for the desired gel (1-2%). The flask of agarose and TBE was heated in a microwave until the agarose had fully dissolved. Gel Red was added to the agarose at a dilution of 1:10,000 and the agarose was poured into the gel tray and left to set.

### 2.3.3: Gel electrophoresis

The tape was removed from the gel tray and the set gel was placed into a gel tank filled with 1x TBE. The comb was removed. Each DNA sample to be run on the gel was mixed with Orange G dye and then loaded into a well of the gel. DNA Ladder was added to another well as appropriate for the experiment. The gel was run at 70-135 V as required.

### 2.3.4: Imaging

The gel was imaged using a Typhoon FLA fluorescence scanner. Voltage was set low for the initial image and increased as needed depending on band intensity.

## 2.4: Western blot

### 2.4.1: Buffers and gels

Running and transfer buffers were used for a maximum of two western blot experiments. 10% β-mercaptoethanol was freshly added to an aliquot of Laemlli buffer for each western blot.

**4% stacking gel solution:** 6.1 mL distilled water, 2.55 mL 0.5 M Tris (pH 6.8), 100 µL 10% sodium dodecyl sulfate (SDS) (w/v), 1.33 mL acrylamide:bis (29:1), 50 µL ammonium persulfate (APS) (w/v), 10 µL tetramethylethylenediamine (TEMED).

**10% separating gel solution:** 8 mL distilled water, 5 mL 1.5 M Tris (pH 8.8), 200 µL 10% SDS (w/v), 6.66 mL acrylamide:bis (29:1), 100 µL 10% APS (w/v), 10 µL TEMED.

**Running buffer:** 120 mM glycine, 40 mM Tris, 0.1% (w/v) sodium dodecyl sulfate (SDS).

**Transfer buffer:** 120 mM glycine, 40 mM Tris, 20% methanol.

**Laemmli buffer:** 20% (v/v) glycerol, 15 mg/mL Tris-Cl (pH 6.8), 0.01% (w/v) bromophenol blue, 20 mM dithiothreitol (DTT), 40 mg/mL SDS.

**Ponceau Red:** 0.2% (w/v) Ponceau S, 3% (v/v) acetic acid.

### 2.4.2: Antibodies

Anti-BCL-6 antibody: D-8 (Santa Cruz)

Anti-β-actin antibody: AC-15 (Sigma-Aldrich)

HRP goat anti-mouse IgG: (BioLegend)

### 2.4.3: Gel preparation

Gels (1.5 mm) were prepared in a gel casting rack on the day of the experiment. The 10% resolving gel was poured and left to set. When the 4% stacking gel was added, a 1.5 mm comb was inserted into the gel cassette and the stacking gel was left to set. If the gel was not to be used immediately, it was wrapped in paper towels soaked in running buffer, placed in a plastic bag and stored at 4 °C for up to one week.

### 2.4.4: Protein extraction

LN18 cells were lifted (section 2.2.3) and pelleted at 400 *g* for 4 minutes. The cells were washed in 10 mL DPBS and centrifuged again. Next, the cells were resuspended in 1 mL DPBS and transferred into a 1.5 mL Eppendorf tube. The cells were centrifuged again at 400 *g* for 4 minutes, the DPBS was aspirated and the pellet was frozen at -80 °C. On the day of the western blot, the cells were thawed and resuspended in 200 $\mu$L 8 M urea and vortexed. The cells were then frozen at -80 °C for a few minutes before being thawed and vortexed to lyse the cells.

## 2.4.5: Protein quantification

Proteins were diluted to 2 M urea with distilled water and quantified using the Pierce™ Rapid Gold BCA Protein Assay Kit.

## 2.4.6: Gel electrophoresis

After quantification, 50 µg aliquots of each sample were taken and Laemmli buffer (with freshly added β-mercaptoethanol) was added in a ratio of 1:3 (v/v) with the sample. Samples were heated at 95 °C for 5 minutes. The gel cassette was loaded into a BioRad Mini-PROTEAN® 3 Cell gel tank and the tank was filled with running buffer. The gel comb was removed. The protein samples in Laemmli buffer were added to the wells of the gel and protein ladder was added to one well. The gel was run at 170 V until the tracking dye reached the bottom of the gel.

## 2.4.7: Transfer

PVDF membrane was cut to the size of the gel and soaked in 100% methanol. A transfer cassette was set up in transfer buffer. A sponge was placed on the transfer cassette, followed by filter paper. The gel was removed from the gel cassette and placed front-side down on the filter paper. The hydrated PVDF membrane was placed on top of the gel, followed by another piece of filter paper. A roller was used to remove any bubbles from between the gel and the membrane. Another sponge was placed on top of the filter paper and the transfer cassette was closed. The transfer cassette was placed into a gel tank along with an ice block. The gel tank was filled with cold transfer buffer and was run at 300 mA for 2 hours.

## 2.4.8: Ponceau stain

After transfer, the membrane was extracted from the transfer cassette and briefly placed front-side down in Ponceau stain. The membrane was then placed in PBS and rocked at room temperature until protein bands were clearly visible. Once it was determined that the transfer was successful, the membrane was further washed in PBS until the Ponceau stain had faded.

## 2.4.9: Membrane staining

The membrane was blocked in 5% milk powder in PBS at room temperature for 1 hour. After blocking, the membrane was incubated in 5 mL 5% milk powder in PBS containing a 1:1000 dilution of the anti-BCL6 D8 primary antibody overnight at 4 °C. The membrane was then washed three times in 0.1%

Triton X-100 in PBS. The membrane was incubated for one hour at room temperature in 5 mL 0.1% Triton X-100 in PBS containing a 1:7000 dilution of the anti-mouse HRP secondary antibody. Finally, the membrane was washed three times in 0.1% Triton X-100 in PBS.

## 2.4.10: Imaging the membrane

The membrane was dipped into ECL reagent to cover the surface of the membrane evenly. The membrane was then imaged using a CCD camera. After the whole membrane had been imaged, it was cut at the 75 kDa marker to enable better imaging of the top part of the membrane, which contained BCL6.

## 2.4.11: Re-blotting for loading control.

The membrane was stripped for 20 minutes. The membrane was then washed three times in PBS before being blocked and re-stained and imaged as described in sections 2.4.9 and 2.4.10 but with the anti-β-actin antibody.

## 2.4.12: Quantitative analysis of western blots

Western blot bands were quantified relative to the β-actin loading control.[324] The images were converted into greyscale JPEG files and opened in Fiji (ImageJ).[325] The "mean gray value" was selected under the "set measurements" menu. The rectangle tool was used to draw a box around the largest BCL6 band to be quantified. The mean gray value was measured. The same box was used to define the region of measurement for each BCL6 band and to take a measurement from a region of the membrane with no bands to obtain a background measurement. As the BCL6 blot was quite noisy, the background measurement was obtained in this way rather than taking an individual background measurement from above or below each BCL6 band individually. This process was repeated for the β-actin loading control image.

In Microsoft Excel, the pixel density was inverted for each measurement by subtracting the Fiji (ImageJ) measurement from 255. The inverted background value was subtracted from each inverted band value to obtain the net value for each band. The ratio of the net band value over the net loading control value in the same lane was calculated for each band to produce quantification values relative to the loading control. One-way Brown-Forsythe and Welch ANOVA tests with Dunnet's T3 multiple comparisons testing were performed to determine the statistical significance of BCL6 abundance changes.

## 2.5: RNA extraction

Cells were harvested (section 2.4.4) and the pellet was resuspended in the RNA lysis buffer from the Zymo Research *Quick*-RNA Miniprep Kit in a DNA LoBind® Eppendorf Tube. RNA extraction was performed as per the instructions for this kit, excluding the optional DNase step. The extracted RNA was quantified using the Qubit RNA High-Sensitivity (HS) Kit and the quality of the RNA was assessed using a Nanodrop ND-1000 Spectrometer.

## 2.6: Reverse transcription

RNA was reverse transcribed by mixing 250 ng RNA with 4 µL 5x PrimeScript RT master mix and making the reaction up to 20 µL with nuclease-free water. The 0.2 mL PCR tubes were placed into a thermo-cycler and heated to 37 °C for 15 minutes, followed by 85 °C for 5 seconds.

## 2.7: Polymerase chain reaction (PCR)

Primers were designed by using the UCSC Genome Browser to select the nucleotide sequence of the region of interest before entering the sequence into Primer3.[326,327] The primers suggested by Primer3 were investigated using the Integrated DNA Technologies (IDT) OligoAnalyzer tool.[328] This tool analysed the nucleotide sequences and calculated the predicted melting temperature and the change in Gibbs Free energy (ΔG) for predicted hairpins, self-dimerisation and heterodimerisation. The primers with the most favourable predicted characteristics overall were selected and ordered from IDT.

PCR reactions were run by mixing 12.5 µL 2x Platinum™ SuperFi™ DNA polymerase with 1.25 µL of each of the 10 µM primers (forward and reverse) and 25 ng DNA and making the volume up to 25 µL with nuclease-free water. The PCR tubes were placed into a thermo-cycler. Initial denaturation was carried out at 98 °C for 30 seconds. This was followed by 35 cycles of denaturation at 98 °C for 10 seconds, annealing for 10 seconds at a temperature optimal for the primers being used and extension at 72 °C for 15-30 seconds per kb being amplified. The final extension was then carried out at 72 °C for 5 minutes.

The PCR products were run on an agarose gel (section 2.3) to check that the DNA band was the expected size and that there was no non-specific amplification.

## 2.8: Sanger sequencing

PCR products to be sequenced were run on a 2% agarose gel (section 2.3) at 70 V for 5 hours. DNA bands were excised from the gel. The agarose was dissolved and the DNA cleaned and concentrated. The DNA was quantified using the Qubit dsDNA high-sensitivity (HS) kit.

For each extracted DNA sample, 2.5 ng DNA per 100 base pairs (or less when not enough DNA was extracted) was mixed with 0.4 µL 10 µM forward primer and made up to 20 µL with nuclease-free water. Another 2.5 ng DNA per 100 base pairs (if possible) was mixed with 0.4 µL 10 µM reverse primer and made up to 20 µL with nuclease-free water. These samples were sent to the Massey Genome Service (Massey University, New Zealand) for Sanger Sequencing. Results were opened and viewed using Geneious 2019 (https://www.geneious.com/).

## 2.9: qRT-PCR

Master mixes of Kapa Sybr® Fast qPCR Master Mix (2x) and Quantitect primers (10x) (section 2.1.5.1) were made up for each primer and 6 µL was pipetted into each required well of a 96 well reaction plate. 2.5 ng DNA was added to a final concentration of 0.25 ng/µL and the volume in each well was made up to 10 µL with nuclease-free water, diluting the Kapa Sybr® Fast qPCR Master Mix to 1x and the Quantitect primers to 1x. For each sample, reactions with each set of Quantitect primers were run in triplicate, as were no-template controls for each sample.

The qPCR plate was sealed with adhesive film and centrifuged briefly to ensure the reaction mixes were at the bottom of the wells. The plate was loaded into a qPCR machine. The program was set to 95 °C for 3 minutes, followed by 40 cycles of 95 °C for 1 second and 65 °C for 20 seconds, followed by production of a melt-curve.

Threshold cycle (Ct) values for each well were exported into a Microsoft Excel file. For each sample and primer, the average Ct value was calculated. When required, the average Ct with the experimental primer was corrected to the average Ct value with the housekeeper primer. The difference in corrected Ct (ddCt) was then calculated between samples and converted into a fold change (fold change = $2^{ddCt}$).

## 2.10: Clonogenic assay

The day before FX1 treatment, 7.5 x $10^4$ LN18 cells were plated into five wells of a six well plate. The next day, the five wells were treated with the following treatments: no treatment, 3 µL DMSO, 5 µM FX1, 10 µM FX1 and 15 µM FX1 from a 10 mM stock of FX1 in DMSO. The cells were incubated with these treatments overnight before being lifted and plated in duplicate into 6 well plates at 100, 50

and 25 cells per well. Two weeks after plating, the media was aspirated and each well was washed with PBS. The PBS was removed and each well was incubated in 1 mL methanol on a rocker at room temperature for 30 minutes to fix the cells. To stain the colonies, the methanol was replaced with 1 mL 0.5% methylene blue in 50% methanol and the plates were rocked at room temperature for 2 hours. The plates were thoroughly washed in tap water and left to dry for 3 hours. The plates were imaged using an image scanner.

Colonies were counted manually from the images. The values for each duplicate were averaged and the plating efficiency (number of colonies / number of cells plated) was calculated. One-way Brown-Forsythe and Welch ANOVA tests with Dunnet's T3 multiple comparisons testing were performed to identify statistically significant changes to plating efficiency.

## 2.11: Whole proteomics

### 2.11.1: Cell culture and treatments

LN18 cells were treated with several different treatment regimens in biological triplicate (different passage numbers). The day before every treatment, 1 x$10^6$ LN18 cells were plated into T75 flasks. The next day, the cells were given one of the treatments described below. At the end of each treatment regime, the cells were harvested and frozen at -80 °C (section 2.4.4).

The day after plating, the 'untreated' cells were treated with either 10 μM FX1 or the equivalent volume of DMSO. These cells were harvested and frozen after 24 hours.

Cells treated with acute irradiation were first treated with fresh RPMI media containing 10 μM FX1 or the equivalent volume of DMSO before being treated with 10 Gy irradiation. These cells were then harvested and frozen at -80 °C either 24 or 48 hours later. Cells treated with fractioned irradiation received a dose of 2 Gy irradiation every day for five days. Just before the first, third and fifth doses, the cells were treated with fresh RPMI media containing 10 μM FX1 or the equivalent volume of DMSO. After the second and fourth doses, cells were passaged as required back into the same media. The day after the fifth dose of irradiation, the cells were harvested and frozen.

Cells treated with temozolomide were treated with fresh RPMI media containing 10 μM temozolomide plus either 10 μM FX1 or the equivalent volume of DMSO. This treatment was repeated every second day for a total of seven doses. On the days in between doses, the cells were passaged as required back into the same media. Cells were harvested and frozen the day after the seventh treatment.

Cells treated with doxorubicin received a single 3 μM dose of doxorubicin in fresh RPMI media 24 hours after plating, plus either 10 μM FX1 or the equivalent volume of DMSO. These cells were harvested and frozen 24 hours after treatment.

### 2.11.2: Protein extraction and preparation

Cell pellets were thawed, resuspended in 200 μL 8 M urea and vortexed. The cells were frozen at -80 °C for a few minutes and then thawed and vortexed to lyse the cells. The cell lysate was transferred into a low protein binding microcentrifuge tube. To precipitate the protein from the lysate, cold acetone was added in a ratio of 4:1 and the lysate was incubated at -20 °C for 1 hour. The sample was centrifuged at 13,000 *g* for 10 minutes to pellet the precipitated protein. The supernatant was discarded and the pellet was air dried for 10-15 minutes before being resuspended in 200 μL 8 M urea. An aliquot was taken and diluted to 2 M urea with distilled water for quantification using the Pierce™ Rapid Gold BCA Protein Assay Kit. Disulfide bridges were broken by adding DTT to the protein samples to a concentration of 10 mM. The samples were incubated at 56 °C for 2 hours. Iodoacetamide was added to 40 mM and the samples were incubated at room temperature in the dark for 45 minutes. 200 μg of each sample was diluted to 2 M urea and trypsin was added in a weight ratio of 1:100. The samples were incubated at 37 °C overnight to allow trypsin to digest the proteins into peptides. Trypsin was inactivated the next day by adding formic acid to 0.1%.

### 2.11.3: Peptide desalting

Peptides were desalted for mass spectrometry analysis using BondElut OMIX 100 μL C18 tips. Tips were activated by twice aspirating and discarding 50% acetonitrile, before being washed twice by aspirating and dispensing 0.1% formic acid in HPLC-grade water. The peptide sample was then aspirated and dispensed without discarding 15 times. The tip was washed three times by aspirating and discarding 0.1% formic acid in HPLC-grade water. The peptides bound to the tip were eluted by aspirating and dispensing without discarding 50 μL 50% acetonitrile in HPLC-grade water in a low protein binding microcentrifuge tube. To bind more peptides to the tip, the original peptide sample was aspirated and dispensed without discarding a further 15 times, before being washed three times in 0.1% formic acid in HPLC-grade water. The peptides bound to the tip were eluted by aspirating and dispensing without discarding 50 μL 70% acetonitrile in HPLC-grade water in a low protein binding microcentrifuge tube. The BondElut OMIX tip was discarded. The eluted peptides in 50% acetonitrile and 70% acetonitrile were combined.

## 2.11.4: Quantification of desalted peptides

After desalting, the solvent (60% acetonitrile) was evaporated in a CentriVap Concentrator. The peptides were resuspended in 100 µL HPLC-grade water and were quantified using the Pierce™ Quantitative Fluorometric Peptide Assay as per the instructions. The water was evaporated in a CentriVap Concentrator. The majority of the peptide samples, which were to be analysed at Victoria University of Wellington, were resuspended at a concentration of 100 ng/µL in 0.1% formic acid in HPLC-grade water and transferred into glass vials. The samples treated with acute irradiation (48 hours) were sent to the Bio21 Institute at the University of Melbourne, Australia, so they were evaporated to dryness and frozen until sent.

## 2.11.5: Mass spectrometry

All whole proteome samples were run in technical duplicate.

### 2.11.5.1: Mass spectrometry at Victoria University of Wellington

The settings of the autosampler and mass spectrometer were defined using Xcalibur™ 4.2 software (version 2.1.0). 200 ng of each peptide sample was loaded by the Dionex UltiMate 3000 RS Autosampler for separation by liquid chromatography. The peptides were loaded onto an Acclaim™ PepMap™ 100 C18 trap column (5 µm, 0.3 x 5 mm) with 0.05% formic acid in 2% acetonitrile at a loading pump flow rate of 8 µL/minute. The peptides were then separated on an Acclaim™ PepMap™ 100 C18 analytical column (2 µm, 100 A, 75 µm x 15 cm). The defined mixtures of Buffer A (0.1% formic acid in HPLC-grade water) and Buffer B (0.1% formic acid in 80% acetonitrile) flowed through the column from the nanocolumn (NC) pump at a rate of 0.3 µL/minute. The flow gradient was (i) 0-5 minutes at 3% B, (ii) 5-70 minutes from 3-30% B, (iii) 70-80 minutes from 30-50% B, (iv) 82-83 minutes from 50-95% B, (v) 83-88 minutes at 95% B, (vi) 88-90 minutes from 95-3% B, (vii) 90-99 minutes at 3% B. The column was washed between every two samples with the following gradient: 0-5 minutes at 3% B, 5-6 minutes from 3-95% B, 6-9 minutes at 95% B, 9-10 minutes 95-3% B. This gradient was repeated three times with a final 14 minutes at 3% B.

The peptides eluted from the column were injected into the Orbitrap Fusion™ Lumos™ Tribrid™ Mass Spectrometer using nanospray ionisation. The ion transfer tube (25 µm) was set to 275 °C and the voltage was set to 1800 V. The MS1 scans were obtained in positive mode using quadrupole isolation with a scan range of 375-1500 m/z and with detection at a resolution of 120,000 in the Orbitrap. The maximum injection time was 50 ms and the normalised automatic gain control (AGC) target was 175%. From each MS1 scan, the 20 highest intensity ions were selected for MS2 scans on ions in an isolation window of 1.6 m/z, with charge 2-7 and intensity above 5.0E3. These ions were selected using the

quadrupole, with a dynamic exclusion duration of 60 seconds after a single detection and a mass tolerance of ±10 ppm. Precursor ions were fragmented using higher energy C-trap dissociation (HCD) with an HCD collision energy of 30%. Ions were detected in the ion trap with a dynamic maximum injection time and a normalised AGC target of 50%.

#### 2.11.5.2: Mass spectrometry at the Bio21 Institute

The following details were provided by the Bio21 Institute on request.

The LC system was equipped with an Acclaim Pepmap nano-trap column (Dinoex-C18, 100 Å, 75 µm x 2 cm) and an Acclaim Pepmap RSLC analytical column (Dinoex-C18, 100 Å, 75 µm x 50 cm). The tryptic peptides were injected to the enrichment column at an isocratic flow of 5 µL/min of 2% v/v $CH_3CN$ containing 0.05% v/v TFA for 6 min applied before the enrichment column was switched in-line with the analytical column. The eluents were 5% DMSO in 0.1% v/v formic acid (solvent A) and 5% DMSO in 100% v/v $CH_3CN$ and 0.1% v/v formic acid (solvent B). The flow gradient was (i) 0-6min at 3% B, (ii) 6-40min, 3-25% B (iii) 40-48min 25-45% B (iv) 48-50min, 45-80% B (v) 50-53in, 80-80% B (vi) 53-54min, 80-2% and equilibrated at 2% B for 10 minutes before the next sample injection.

The Q Exactive Plus™ mass spectrometer was operated in the data-dependent mode, whereby full MS1 spectra were acquired in positive mode, 70 000 resolution, AGC target of $3e^6$ and maximum IT time of 50ms. Fifteen of the most intense peptide ions with charge states ≥ 2 and intensity threshold of $4e^4$ were isolated for MSMS. The isolation window was set at 1.2m/z and precursors fragmented using normalized collision energy of 30, 17 500 resolution, AGC target of $5e^4$ and maximum IT time of 50ms. Dynamic exclusion was set to be 30sec.

### 2.11.6: Data analysis

Raw mass spectra data files were uploaded to Proteome Discoverer 2.4. Biological replicates and treatment groups were defined as categorical factors. The grouped biological replicates for each treatment were compared to other treatments in non-nested ratio analyses. The processing and consensus workflows were as shown in Figure 2.1. In the processing workflow, the Spectrum Files RC search settings defined the enzyme as trypsin and searched against the Swiss-Prot reviewed UniProt human protein database.[329] Carbamidomethyl was set as a static modification due to the use of iodoacetamide in the sample processing (section 2.11.2). MS1 precursors with a minimum mass of 350 Da, a maximum mass of 5000 Da and a minimum peak count of 1 were selected by the Spectrum Selector node. No limits were applied to retention time, charge state, minimum intensity or collision energy. In the Precursor Detector node, the signal-to-noise threshold was set at 1.5. The spectra were

matched to peptides using Sequest HT search engine against the Swiss-Prot reviewed UniProt human protein database.[329] The enzyme was defined as trypsin, with a maximum of 2 missed cleavage sites, a minimum peptide length of 6, a maximum peptide length of 144 and a maximum of 10 peptides per spectrum. The precursor mass tolerance was set to 10 ppm and the fragment mass tolerance for matching fragment peaks was 0.5 Da. Carbamidomethyl was set as a static modification. A decoy search was performed by the Percolator node. The target/decoy selection was set to concatenated, so that only the best scoring target or decoy peptide spectrum matches (PSMs) were written to the Percolator input file, and validation was based on q value. The strict target false discovery rate (FDR) (for high confidence hits) was set to 0.01. The relaxed target FDR (for medium confidence hits) was set to 0.05.

In the consensus workflow, the MSF Files node defined that all spectra with identification or quantification associated with them were stored, along with all feature traces. Only the best matched FASTA title lines of a protein were reported and there was no exclusion of peptide-spectrum masses based on the mass difference between the theoretical and found peptide. Retention time (RT) alignment with a maximum RT shift of 10 minutes was performed by the Feature Mapper node. The minimum signal to noise threshold for consensus features was 5. The PSM Grouper node grouped PSMs into peptide groups. Peptide modifications were only reported when the site probability was at least 75%. The Peptide Validator assigned PSM and peptide confidence levels based on the strict target FDR of 0.01 (high confidence) and the relaxed target FDR of 0.05 (medium confidence). The FDR values were calculated using the target/decoy method used by Percolator. The Peptide and Protein Filter node filtered out peptides which were not identified with high confidence and were shorter than 6 amino acids. Proteins were included if they were identified from at least one peptide. The Protein Grouping node formed protein groups from proteins identified from the same peptide sequences and assigned a master protein. The strict parsimony principle was applied, meaning that all protein groups not necessary to explain the peptides identified were removed. The Protein FDR validator node calculated FDR values for the proteins based on a target/decoy search. Again, the strict target FDR was set to 0.01 and the relaxed target FDR was set to 0.05. The Peptide in Protein Annotation node defined settings for the display in Proteome Discoverer.

The Precursor Ions Quantifier node defined the quantification settings. Unique and razor peptides were used for quantification. Precursor abundance was based on peak intensity and a feature only had to be included in one replicate to be used. Peptide abundance was normalised to the total peptide amount. This meant that the sample with the highest sum of all peptide abundance values was used as a reference. The peptides in all other samples in that quantification run were corrected by a constant factor per sample so that all samples had the same summed peptide abundance. The abundances were then scaled so that the average of all of the samples was 100. Protein abundances were calculated from the sum of the abundances of the connected peptide groups in that sample. Pairwise ratios of protein abundance were performed by taking the median of all possible pairwise peptide ratios between the replicates.

Fold-changes were capped at 100 and background-based t-tests were used to calculate p values for the quantification ratios. No imputation was performed.

The list of proteins identified in each quantitative analysis were exported to Microsoft Excel. All proteins identified with high and medium confidence (exp. q value ≤ 0.05) were sorted by abundance ratio. Proteins with abundance ratios ≥ 2 (3 d.p.) and abundance ratio adjusted p values ≤ 0.05 (3 d.p.) were extracted as the proteins upregulated in the comparison being made. Proteins with abundance ratios ≤ 0.5 (3 d.p.) and abundance ratio adjusted p values ≤ 0.05 (3 d.p.) were extracted as the proteins downregulated in the comparison being made.

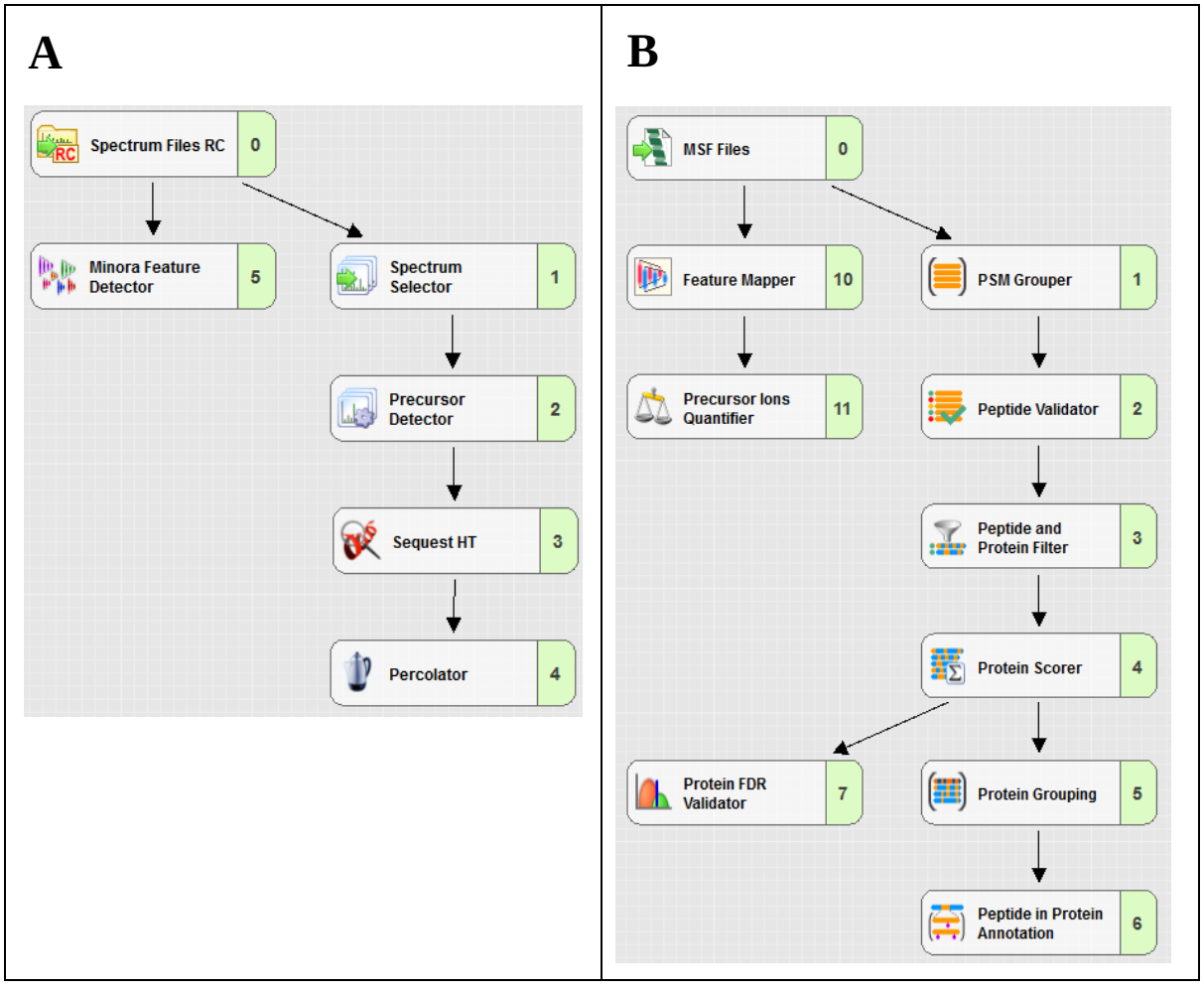


Figure 2.1: Proteome Discoverer 2.4 quantitative analysis workflows
A) Processing and B) Consensus workflows used for quantitative analysis in Proteome Discoverer 2.4.

## 2.11.7: Functional enrichment analysis

UniProt protein accession numbers assigned by the Proteome Discoverer analyses were entered into g:Profiler version *e104_eg51_p15_2719230*.[329,330] Any protein accession numbers that were not recognised by g:Profiler were converted into Ensembl gene (ENSG) IDs if available.[331] If Uniprot accession numbers were obsolete, they were replaced with the new accession number if available. Any proteins that did not have a recognisable UniProt accession number or ENSG ID, or which had an obsolete UniProt accession number but no updated accession number, were excluded from the g:Profiler analysis.

The statistical domain scope was set to 'only annotated genes', the significance threshold to 'g:SCS threshold' and the user threshold to 0.05. Data sources selected were the Gene Ontology categories GO molecular function (GO:MF), GO biological process (GO:BP) and GO cellular component (GO:MF). The term size was set to a maximum of 1000 to avoid broad, uninformative terms.

The enriched Gene Ontology terms were extracted as a CSV file and the differentially expressed proteins annotated to each enriched GO:BP and GO:CC term were compared to identify overlaps. The five most significant parent GO:BP and GO:CC terms were identified in order to display the most representative summary of the biological processes and components that were enriched in each treatment comparison.

g:Profiler multi-queries were run as described above, except that two lists of proteins were entered and the option to 'run as multi-query' was selected.

Network analysis was performed using STRING version 11.5.[332] STRING was set to show the full STRING network but disconnected nodes were hidden. The option for edge thickness to indicate the level of confidence in the interaction was selected and the minimum required confidence was high (0.7). Interaction sources textmining, experiments, databases, co-expression, neighbourhood and co-occurrence were selected. Gene ontology enrichments were inspected in the STRING Analysis tab.

## 2.11.8: Data accessibility

Mass spectra raw files and peak lists and Proteome Discover result files are available on the MassIVE database version 1.3.16 (ftp://MSV000090274@massive.ucsd.edu).[333]
Proteome Discoverer and g:Profiler gene ontology enrichment results are available as Excel spreadsheets on the Open Science Framework (OSF) repository:
https://osf.io/hs627/?view_only=0563901eb9004de7a187b5f3912bb487.[334]

## 2.12: Rapid immunoprecipitation mass spectrometry of endogenous proteins (RIME)

The rapid immunoprecipitation mass spectrometry of endogenous proteins (RIME) protocol published by Mohammed et al. (2016) was established in the McConnell lab with a few modifications as described in this section.[335]

### 2.12.1: Cell culture and treatments

For RIME experiments on irradiated cells, LN18, NZG0906 or NZG1003 cells were plated into 20 x 10 cm plates so that they would be about 50% confluent the next day. The day after plating, the cells were treated with 10 Gy irradiation. The following day, the cells were lifted and transferred into 10 x 15 cm plates to enable more effective and efficient scraping of cells during the RIME experiment. Cells were left for another 24 hours before being processed for RIME (48 hours after irradiation).

For RIME experiments on untreated cells, LN18, NZG0906 or NZG1003 cells were plated into 10 × 15 cm plates such that they would be approximately 80-90% confluent three days later. Two days after plating, the cells were lifted and then left to adhere back to the plates to mimic the transfer of the irradiated cells between plates. As with the irradiated cells, the untreated cells were left for another 24 hours before being processed for RIME.

### 2.12.2: Buffers

**RIPA buffer:** 50 mM HEPES (pH 7.6), 1 mM EDTA, 0.7% (w/v) sodium deoxycholate, 1% (v/v) NP-40, 0.5 M LiCl.

**Swelling buffer:** 50 mM HEPES-KOH (pH 7.5), 140 mM NaCl, 10% glycerol, 1 mM EDTA, 0.5% (v/v) IGEPAL, 0.25% (v/v) Triton X-100.

**Wash buffer:** 10 mM Tris-Cl (pH 8.0), 200 mM NaCl, 1 mM EDTA, 0.5 mM EGTA.

**Micrococcal nuclease reaction buffer:** 1:10 micrococcal nuclease 10 x buffer (NEB), 1:100 10 mg/mL BSA in distilled water.

**Micrococcal nuclease enzyme solution:** 1:10 micrococcal nuclease (NEB) in micrococcal nuclease reaction buffer.

**Shearing buffer:** 50 mM Tris-Cl (pH 8.1), 0.1% (w/v) SDS, 10 mM EDTA (pH 8.0).

**Dilution buffer:** 50 mM Tris-Cl (pH 8.0), 300 mM NaCl, 2% (v/v) IGEPAL, 1% (w/v) sodium deoxycholate (Na-DOC), 0.1% (v/v) sodium dodecyl sulfate (SDS).

**Elution buffer:** 1% (w/v) SDS, 100 mM $NaHCO_3$.

## 2.12.3: Antibodies

Anti-BCL-6 antibody: N3 (Santa Cruz).

Invitrogen™ Normal Rabbit IgG: (Thermo Fisher Scientific)

## 2.12.4: Use of Laminar Flow hood

All stages of the RIME experiment from cell harvesting (section 2.12.7) to peptide desalting and resuspension (section 2.12.14) with the one exception of sonication (section 2.12.9), were carried out in a Laminar Flow hood to prevent proteins in the environment from contaminating the low protein abundance samples.

## 2.12.5: Dynabead preparation

1 mg Protein G Dynabeads was added to ten low protein binding microcentrifuge tubes. The tubes were placed on a magnet and the supernatant was removed. The beads were washed with 1 mL RIPA buffer and then resuspended in 40 µL RIPA buffer. 5 µg N3 anti-BCL6 antibody was added to five of the tubes. 5 µg IgG antibody was added to the other five tubes. The tubes were rotated at 4 °C while the cells were prepared.

## 2.12.6: Fixation

The 10 x 15 cm plates of cells described in section 2.12.1 were placed on a shaker at room temperature. Formaldehyde was added to the media to a concentration of 1% (v/v) and the plates were rocked at room temperature for 8 minutes. The formaldehyde was quenched by adding 2.5 M glycine to a final concentration of 0.125 M and rocking the plates at room temperature for 10 minutes.

## 2.12.7: Harvesting

The media was discarded and the cells were washed twice with cold PBS. Next, 10 mL cold PBS was added to each plate. Cells were scraped from the bottom of the plates into the 10 mL PBS using the rubber plunger of a 50 mL syringe. The fixed cells suspended in PBS were pipetted into two 50 mL falcon tubes and centrifuged at 2000 *g* for 10 minutes at 4 °C to pellet the cells.

## 2.12.8: Nuclear preparation

The pellets were resuspended in a total of 10 mL swelling buffer with freshly added protease inhibitor and split into 1 mL aliquots across ten low protein binding microcentrifuge tubes. The tubes were rotated at 4 °C for 10 minutes and then the nuclei were pelleted at 1700 *g* for 5 minutes at 4 °C. The supernatant was aspirated and the nuclear pellets were resuspended in 1 mL wash buffer with freshly added protease inhibitor. Again, the tubes were rotated at 4 °C for 10 minutes and then the nuclei were pelleted at 1700 *g* for 5 minutes at 4 °C. The supernatant was aspirated.

## 2.12.9: DNA fragmentation

Each pellet was resuspended in 99.25 µL micrococcal nuclease reaction buffer. To each tube, 0.75 µL (150 U) micrococcal nuclease enzyme solution was added. The reactions were incubated at 37 °C for 15 minutes, during which they were vortexed every 2 minutes. Digestion was stopped by adding 10 µL 0.5 M EDTA and placing the tubes on ice. The nuclei were pelleted by centrifugation at 16,000 *g* for 1 minute at 4 °C. Each pellet was resuspended in 200 µL shearing buffer with freshly added protease inhibitor and incubated on ice for 10 minutes.

The DNA was then further fragmented by sonication with 3 × 20 second pulses with 30 seconds rest in between. The lysates were clarified by centrifugation at 9400 *g* for 10 minutes at 4 °C.

## 2.12.10: Immunoprecipitation

The samples were pooled and 12.5 µL was taken for the DNA fragmentation check. The pooled samples were diluted 1:1 in dilution buffer and were distributed evenly between the ten antibody/Dynabead tubes prepared in section 2.12.5. The tubes were rotated overnight at 4 °C to allow the antibodies on the Dynabeads to bind their target proteins.

## 2.12.11: DNA fragmentation check

To check that DNA fragmentation was successful, the DNA was extracted from the aliquot set aside before the samples were added to the beads (section 2.12.10). The aliquot of fragmented DNA was added to 125 µL of 0.3 M NaCl and 1 mg/mL RNase A in nuclease-free water and incubated at 37 °C for 30 minutes. 0.75 µL Proteinase K was added and the mixture was incubated at 65 °C for 1 hour.

For the chloroform:isoamyl clean-up, approximately 100 µL Dow Corning Centrifuge grease was squirted into the bottom of a 1.5 mL Eppendorf tube, which was centrifuged at top speed for 2 minutes to create a phase-lock tube. The DNA sample was diluted 1:1 in chloroform and vortexed until a fine emulsion formed. This was transferred to the phase-lock tube, which was centrifuged at top speed for 2 minutes. An equal volume of chloroform:isoamyl alcohol was added and the tube was vortexed. The tube was centrifuged again at top speed for 2 minutes. The aqueous layer was transferred to a new tube. The DNA was precipitated by adding 0.1× volume 3 M NaOAc, 2× volume ice cold ethanol and 1 µL glycogen. The tube was inverted and centrifuged at top speed for 10 minutes. The liquid was pipetted off and 1 mL 100% ethanol was added to wash the pellet, followed by another wash in 70% ethanol. The pellet was air dried and then resuspended in 20 µL elution buffer.

The DNA was quantified using the Qubit dsDNA broad-range (BR) kit. The DNA was then run on a 1% agarose gel (section 2.3). The modal length of DNA fragments generated using the methods in section 2.12.9 was 900 base pairs.

## 2.12.12: Washes

After the overnight incubation of the samples with the antibody-coated beads (section 2.12.10), the tubes were placed on a magnet and the supernatant, containing unbound proteins and DNA, was discarded. The beads in each tube were resuspended in 1 mL RIPA buffer and rotated at 4 °C for 5 minutes. The beads were then pelleted on a magnet and the supernatant was discarded. This was repeated for a total of 10 x 1 mL washes in RIPA buffer. A final two washes in 1 mL fresh 100 mM ammonium hydrogen carbonate were performed. Finally, the beads were pelleted on a magnet and the supernatant was discarded.

## 2.12.13: Protein digestion

The beads were resuspended in 10 µL 100 mM ammonium hydrogen carbonate containing 100 ng trypsin and incubated at 37 °C overnight. The next day, a further 10 µL 100 mM ammonium hydrogen carbonate containing 100 ng trypsin was added and the beads were incubated at 37 °C for a further 4

hours. Next, the beads were pelleted on a magnet and the supernatant was removed and retained as it contained the digested peptides from the proteins which bound to the antibody-coated beads. The samples treated with the same antibody (BCL6 or IgG) were pooled. Formic acid was added to 0.1% to inactivate the trypsin.

## 2.12.14: Peptide desalting and quantification

A 10.5 µL aliquot of each sample was taken for peptide quantification. The rest of the sample was desalted and the 60% acetonitrile evaporated as described in section 2.11.3 and 2.11.4. The aliquot taken before desalting and another aliquot taken from the sample remaining after desalting were quantified (section 2.11.4) and compared. The mass of peptides in the desalted sample was calculated. Samples run at Victoria University of Wellington were resuspended to 100 ng/µL (or a minimum of 10 µL) in 0.1% formic acid in HPLC-grade water and transferred to glass vials. Samples run at Bio21 were evaporated to dryness and frozen and then either sent lyophilised or resuspended in ≥ 15 µL 2% acetonitrile, 0.05% TFA in HPLC-grade water.

## 2.12.15: Mass spectrometry

### 2.12.15.1: Mass spectrometry at Victoria University of Wellington

Samples run at Victoria University of Wellington were run as described in section 2.11.5.1, except for the following changes. 100 ng of each peptide sample was loaded for liquid chromatography separation by the autosampler. The gradient was as follows: (i) 0-5 minutes at 3% B, (ii) 5-10 minutes from 3-10% B, (iii) 10-45 minutes from 10-25% B, (iv) 45-50 minutes from 25-50% B, (v) 50-51 minutes from 50-95% B, (vi) 51-56 minutes at 95% B, (vii) 56-57 minutes from 95-3% B, (viii) 57-70 minutes at 3% B.

### 2.12.15.2: Mass spectrometry at the Bio21 Institute

The samples sent to the Bio21 Institute were run as described in section 2.11.5.2.

## 2.12.16: Data analysis

### 2.12.16.1: Commonly identified proteins

Raw mass spectrum data files were uploaded to Proteome Discoverer 2.4 for protein identification. The nodes in the processing and consensus workflows (Figure 2.2) had the same settings as when these nodes were used for quantitative analysis in section 2.11.6, however only the nodes required for protein

identification were included. The only change was the selection of oxidation of methionine residues and deamidation of asparagine and glutamine residues as dynamic modifications in the Sequest HT search node, as advised in the RIME protocol publication.[335] No static modifications were set.

The lists of proteins identified were exported to Microsoft Excel. Any proteins identified with less than high confidence (exp. q value $\leq 0.01$) were filtered out. For each cell line, a compiled list of non-specific proteins was created by combining the lists of proteins identified in the three IgG replicates and removing duplicates. These proteins were subtracted from the lists of proteins identified in the three replicates using the anti-BCL6 antibody. This was done for each irradiated and untreated cell line. The cells identified in each replicate, minus the non-specific proteins, were compared across cell lines and replicates. Proteins identified in $\geq 3$ replicates across the nine samples for each treatment were identified as candidate BCL6-associated proteins.

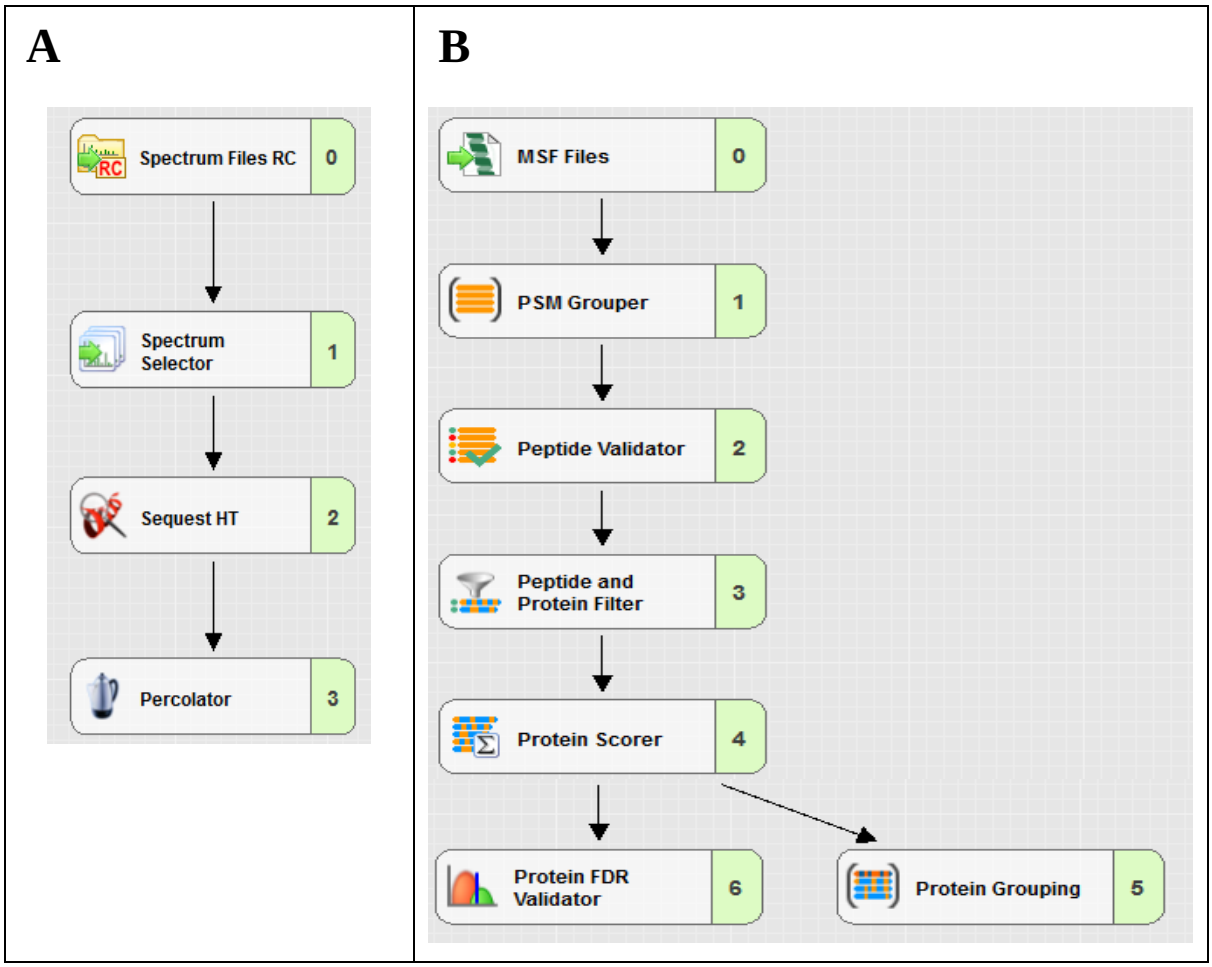


Figure 2.2: Proteome Discoverer 2.4 protein identification workflows.
A) Processing and B) Consensus workflows used for protein identification in Proteome Discoverer 2.4.

### 2.12.16.2: BCL6 vs. IgG quantitative analysis

Quantitative analysis of the BCL6 vs IgG RIME samples was performed in Proteome Discoverer 2.4 as described in section 2.11.6, except for the following changes. In the Sequest HT search, oxidation of methionine residues and deamidation of asparagine and glutamine residues were set as dynamic modifications. No static modifications were set. In the Feature Mapper node, RT tolerance was set to 0.0001 minutes and mass tolerance was set to 1E-5 ppm. This effectively prevented the match between runs (MBR) function which otherwise led to aberrant identification of BCL6 in the IgG samples. The exported quantification results were filtered to include only high confidence proteins. Only proteins upregulated $\geq$ 2-fold ($p \leq 0.05$) and not found at high abundance in any IgG samples were carried through for further analysis.

### 2.12.16.3: Irradiated vs untreated quantitative analysis

Quantitative analysis of the BCL6 RIME results from the irradiated GBM cells compared to the untreated GBM cells was performed in Proteome Discoverer 2.4 as described in section 2.11.6, except for the following changes. In the Sequest HT search, oxidation of methionine residues and deamidation of asparagine and glutamine residues were set as dynamic modifications. No static modifications were set. Additionally, proteins were normalised to the abundance of BCL6, as defined by a BCL6 amino acid sequence FASTA file. The protein abundance ratios were calculated directly from the grouped protein abundances.

### 2.12.16.4: Functional enrichment analysis

Functional enrichment analysis using g:Profiler was performed as described in section 2.11.7. Network analysis was performed using STRING version 11.5.[332] STRING was set to show either the full STRING network or the physical subnetwork and disconnected nodes were hidden. The option for edge thickness to indicate the level of confidence in the interaction was selected and the minimum required confidence was high (0.7). Interaction sources textmining, experiments and databases were selected.

### 2.12.16.5 Data accessibility

The commonly identified BCL6-associated proteins were submitted to the IMEx (http://www.imexconsortium.org) consortium through IntAct [X] and assigned the identifier IM-29565.[336]

Mass spectra raw files and peak lists and Proteome Discover result files are available on the MassIVE database version 1.3.16 (ftp://MSV000090288@massive.ucsd.edu).[333]

Proteome Discoverer and g:Profiler gene ontology enrichment results are available as Excel spreadsheets on the Open Science Framework (OSF) repository: https://osf.io/hs627/?view_only=0563901eb9004de7a187b5f3912bb487.[334]

## 2.13: Immunofluorescence confocal microscopy

### 2.13.1: Cell culture

Cells were cultured as described in section 2.2. Adherent cells were plated into chamber slide wells 24 hours before staining. When required, cells were plated into T25 flasks 24 hours before being treated with 10 Gy irradiation. The irradiated cells were then plated into chamber slide wells 24 hours after irradiation, so that staining occurred 48 hours after irradiation as in the RIME experiments (section 2.12.1). The suspension cell line K562 was transferred onto microscope slides using a Cytospin.

### 2.13.2: Antibody concentrations

Table 2.1: Antibody concentrations for immunofluorescence staining and proximity ligation assays

| Primary antibody | | Secondary antibodies | |
|---|---|---|---|
| BCL6 | 1:50 (4 μg/mL) | AlexaFluor488 | 1:1000 |
| Mouse IgG | 4 μg/mL<br>1 μg/mL | | |
| NCOR2 | 1:150 (6.7 μg/mL) | AlexaFluor568 | 1:1000 |
| AMPK | 1:300 (1.5 μg/mL) | | |
| Rabbit IgG | 6.7 μg/mL<br>1.5 μg/mL<br>0.2 μg/mL | | |
| p50 | 1:500 (1 μg/mL) | - | - |
| p65 | 1:500 (0.2 μg/mL) | - | - |

### 2.13.3: Slide preparation for immunofluorescence imaging

On the day of staining, the media was aspirated from the chamber slide wells. Each well was washed three times in PBS before cells were fixed in 4% PFA for 15 minutes at room temperature. The wells were washed three times and then permeabilised in PBS containing 0.1% Triton X-100 for 15 minutes on ice. After three more PBS washes, the cells were blocked with 3% BSA in PBS for 1 hour on ice. Primary antibodies were diluted to the optimised concentrations (Table 2.1) in PBS and added to the appropriate wells. The slides were incubated at 4 °C overnight. After three washes in PBS, the appropriate secondary antibodies were added, diluted in 3% BSA in PBS. The slides were incubated in the dark at room temperature for 1 hour before being washed three times in PBS. The wells were

removed from the chamber slides and Prolong™ Gold antifade reagent with DAPI was added to the slides. Coverslips were mounted onto the slides and sealed with clear nail polish.

## 2.13.4: Slide preparation for proximity ligation assays (PLAs)

On the day of staining, the slides were fixed and permeabilised (section 2.13.3). The cells were stained as described in the Duolink® PLA Fluorescence Protocol (Merck).[337,338] For all washes, 100 µL wash buffer was added to each well and for all other reagents 40 µL was added to each well. The PLA reagents described in the following paragraph were included in the Duolink® Probe kit and the Duolink® Fluorescent Detection Reagent Kit. The Duolink® Wash Buffers A and B and the Duolink® Mounting Media with DAPI were purchased separately.

Briefly, the cells were blocked with Blocking Solution for 1 hour in a humidified 37 °C incubator. Primary antibodies were diluted in Antibody Diluent to the same concentrations shown in Table 2.1 and added to the appropriate wells. The chamber slides were incubated at 4 °C overnight with humidity. After two 5-minute washes with Wash Buffer A, the PLUS and MINUS PLA Probes were diluted 1:5 in Antibody Diluent and added to the wells. The chamber slides were incubated for 1 hour in a humidified 37 °C incubator. After two 5-minute washes in Wash Buffer A, Ligase diluted 1:40 in Ligation Buffer was added to the wells and the chamber slide was incubated for 30 minutes in a humidified 37 °C incubator. The wells were washed twice for 5 minutes in Wash Buffer A before Polymerase was added in a 1:80 dilution in Amplification Buffer. For the NFκB positive control, the chamber slide was incubated for 100 minutes in a humidified 37 °C incubator. For all other PLA experiments, the chamber slide was incubated for 3.5 hours in a humidified 37 °C incubator. After amplification, the slides were washed twice for 10 minutes in Wash Buffer B, before being washed in 0.01x Wash Buffer B for 1 minute. The wells were removed from the chamber slides and coverslips were mounted using Mounting Media with DAPI. The coverslips were sealed with nail polish.

## 2.13.5: Confocal microscopy

Images were acquired using an Olympus Laser Scanning Confocal Microscope (LSCM) FV3000 in an inverted microscope frame IX83 (Malaghan Institute of Medical Research). Acquisition settings were adjusted to minimise the fluorescence signal in controls while still capturing signal from the experimental samples. Once optimised, acquisition settings were kept the same for all samples which were directly compared (treated vs untreated and experimental vs control).

Images were taken as z-stacks (eight stacks for immunofluorescence staining and ten stacks for PLAs) through the whole depth of the cells as assessed by DAPI staining of the nuclei. The confocal aperture

was set to 137 µm and the images acquired were 1024x1024 pixels in size. For all images, the laser power was set to 1 % and the gain was set to 1x. The voltage and offset settings are shown in Table 2.2.

Table 2.2: Confocal microscopy acquisition settings

| | | Voltage (V) | | | Offset (%) | | |
|---|---|---|---|---|---|---|---|
| **Fluorophore** | **Excitation wavelength (nm)** | **BCL6 + NCOR2 samples and controls** | **BCL6 + AMPK samples and controls** | **PLAs** | **BCL6 + NCOR2 samples and controls** | **BCL6 + AMPK samples and controls** | **PLAs** |
| **DAPI** | 405 | 510 | 520 | 430 | 4 | 4 | 5 |
| **AF488** | 488 | 500 | 480 | | 8 | 6 | |
| **AF568** | 561 | 470 | 470 | | 5 | 5 | |
| **PLA fluorophore** | 561 | | | 350 | | | 5 |

## 2.13.6: Image analysis

Images were converted to composite z-projections using Fiji (ImageJ).[325] The relative brightness of each channel was adjusted (consistently between images) using CellProfiler.[339] Adjusted single channel and composite images were exported as .npy files from CellProfiler. The .npy array files were converted into .tiff or .png files using simple python scripts utilising the conda package pillow. For the PLA images, red and blue pixels were counted in Fiji (ImageJ) using the Color Pixel Counter plugin.[340] The minimum intensity threshold for counting was set to 50 for both colours. Statistical comparisons were made with SPSS using a linear mixed model with antibody pairs and treatment as fixed effects, replicates as a random effect and images within replicates as repeated measurements with compound symmetry. Pairwise comparisons between antibody pairs and between treatments were made using sequential Bonferroni multiple comparisons adjustment.

# 2.14: Oxford Nanopore MinION sequencing

## 2.14.1: Primer design

For Oxford Nanopore MinION sequencing of BCL6 transcript variants, the BCL6 transcripts were amplified semi-specifically with one BCL6-specific primer and one universal primer. This was repeated with a primer specific to the 3'-end of BCL6 with a universal primer at the 5'-end and with a primer specific to the 5'-end of BCL6 with a universal primer at the 3'-end. This should have allowed amplification of almost all possible BCL6 transcript variants.

Primers were designed by using the UCSC genome browser to select 20-25 base pair sequences from each end of the BCL6 transcript.[326] The 3'-end primer was designed to be complementary to a sequence in the translated region of the 3'-end exon which is conserved across all known BCL6 transcripts or in the short region of the 3'-untranslated region (3'-UTR) which is also conserved across all known BCL6 transcripts. The 5'-end primer was designed to be complementary to a sequence in the first exon which is conserved across all known BCL6 transcripts. These sequences were run through the National Centre for Biotechnology Information (NCBI) nucleotide Basic Local Alignment Search Tool (BLASTn) to determine how closely they matched sequences found in other regions of the human genome.[341] The sequences with the lowest percent matches against other regions of the genome were then run through the Integrated DNA Technologies (IDT) OligoAnalyzer tool.[328] This tool analysed the nucleotide sequences and calculated the predicted melting temperature and change in Gibbs Free energy (ΔG) for predicted hairpins, self-dimerisation and heterodimerisation with the general SSP or VNP primer as appropriate. The primers with the most favourable predicted characteristics overall were selected and ordered from IDT along with the SSP and VNP primer sequences. Two T bases were added to the end of the VNP primer sequence provided by Oxford Nanopore Technologies in order to adjust the melting temperature closer to that of the 5'-end BCL6 primer.

### 2.14.2: Cell culture and treatment

For primer optimisation, LN18 cells were plated into T25 flasks so that they reached approximately 50% confluency the following day. The next day, one flask was treated with 10 Gy irradiation and the other was left untreated.

For the sequencing of semi-specifically amplified BCL6 transcripts, LN18, NZG0906 and NZG1003 cells were each plated into six T25 flasks so that they reached approximately 50% confluency the following day. The day after plating, three flasks of each cell line were treated with 10 Gy irradiation.

### 2.14.3: Harvesting and RNA extraction

Cells were harvested 48 hours after plating (24 hours after irradiation for the irradiated cells) as described in section 2.4.4. The cell pellet was resuspended in RNA lysis buffer from the Zymo Research *Quick*-RNA Miniprep Kit in a DNA LoBind® Eppendorf Tube. RNA was extracted (section 2.5). The RNA was frozen at -80 °C.

## 2.14.4: Reverse transcription

For each cell line, the three untreated RNA samples and the three irradiated RNA samples were processed together and multiplexed onto the same MinION flow cell. Reverse transcription and amplification were carried out using the Oxford Nanopore cDNA-PCR Sequencing Kit as per the SQK-PCS109 protocol, with a few changes to make the amplification semi-specific for BCL6.[342] The reverse transcription to convert mRNA into cDNA was carried out as in the protocol, except that 100 ng of RNA was used per tube instead of 50 ng.

## 2.14.5: Semi-specific amplification of BCL6 transcripts

### 2.14.5.1 Primer optimisation

The PCR was carried out as in the protocol except that instead of using 1.5 µL cPRM primers, 0.75 µL of the custom 3'-BCL6-specific primer or 5'-BCL6-specific primer and 0.75 µL of the custom SSP primer or VNP primer respectively were added instead. This enabled the semi-specific amplification of BCL6 cDNA and the production of BCL6 cDNA amplicons with the necessary end-modifications for sequencing preparation. The PCR parameters were optimised to maximise enrichment, as assessed by q-RT-PCR (section 2.9). A volume of cDNA corresponding to 2.5 ng of the total amount of RNA initially added to the reverse transcription reaction was added to each well. The amplified cDNA was added to each well at a dilution of 1:100. Hence the cDNA and amplified cDNA could not be quantitatively compared. Instead, the difference in Ct values with the BCL6 and housekeeper gene HPRT primers in the cDNA samples was compared to the difference in Ct values with the BCL6 and HPRT primers in the semi-specifically amplified cDNA samples to determine the extent of BCL6 enrichment by semi-specific amplification.

### 2.14.5.2 Amplification with optimised PCR parameters

After optimisation, the annealing temperature was set to 60 °C, the extension time to 4 minutes and 10 seconds and the number of cycles to 31 cycles. These parameters were used for the amplification step in the sequencing experiments.

For quality control, an aliquot of each PCR product was run on a 1.5% agarose gel at 135 V (section 2.3). The PCR products were cleaned-up as in the SQK-PCS109 protocol and eluted in 12 µL Elution Buffer.

## 2.14.6: Quantification of semi-specifically amplified PCR products

The cleaned-up semi-specifically amplified PCR products were quantified using the Qubit dsDNA High-Sensitivity Kit.

## 2.14.7: DNA repair, end-prep, barcoding and adapter ligation

The samples were taken through to DNA repair and end-prep with the native barcoding amplicons protocol (with Oxford Nanopore Technologies EXP-NBD104, EXP-NBD114 and SQK-LSK109 kits).[343] The end-prepped PCR products were eluted in water and quantified using the Qubit dsDNA High-Sensitivity Kit.

The end-prepped PCR products were barcoded using EXP-NBD104 or EXP-NBD114 barcodes. Although each cell line was multiplexed sequenced separately, the same MinION flow cell was washed and re-used to sequence all three cell lines, so each of the eighteen samples (three cell lines, untreated and irradiated in triplicate) needed a different barcode to avoid cross-contamination of results. The barcoded samples were quantified using the Qubit dsDNA High-Sensitivity (HS) Kit.

Next, 133 ng of each of the barcoded six samples for each cell line were pooled to give 800 ng barcoded cDNA in total. After clean-up, the pooled samples were quantified using the Qubit dsDNA High-Sensitivity (HS) Kit.

## 2.14.8: MinION loading and running

The final sample of multiplexed, semi-specifically amplified cDNA was loaded onto a R9.4 Oxford Nanopore MinION device and sequenced overnight. The next day, the sequencing run was stopped and the flow cell was washed using the Flow Cell Wash Kit (EXP-WSH003) so that it could be used for the next multiplexed sample.

## 2.14.9: Data processing

The fast5 output files were submitted for basecalling. Basecalling was performed using Guppy version 6.1 in the high accuracy configuration for basecalling (dna_r9.4.1_450bps_hac.cfg). Reads with qscores < 7 were filtered out using qscore_filtering. Additionally, the MinION quality control (QC) program outputs were observed for each run. The basecalled reads were demultiplexed using qcat in epi2me mode. Reads were skipped if they were shorter than the minimum length filter of 100.

Demultiplexing was repeated on the none.fastq file to retrieve extra reads. These were pooled with the output from the initial demultiplexing.

## 2.14.10: FLAIR pipeline

FLAIR was executed by Leticia Castro (McConnell lab group, Victoria University of Wellington, Wellington, New Zealand) to analyse the long-read sequences generated by the MinION sequencing. FLAIR was run in a Miniconda environment utilising tools as specified in the GitHub file flair_conda_env.yaml.[344]

FLAIR used minimap2 (version 2.17-r941) to align the reads with the 'no alt analysis set' of the hg38/GCA_000001405.15_GRCh38 assembly (flair align), before correcting misaligned splice junctions against an annotations file downloaded from https://hgdownload.soe.ucsc.edu/goldenPath/hg38/bigZips/genes/ (flair correct).[345] The reads with the same splice junctions were then grouped into isoform groups to form a first-pass assembly (flair collapse).[345] The raw reads were then re-aligned to this first-pass assembly.[345] The number of reads corresponding to each isoform were quantified and isoforms with fewer than three supporting reads were discarded to create a confident isoform assembly.[345] The primary read alignments were then quantified using minimap2 (version 2.17-r941) (flair quantify).[345]

The FLAIR modules flair diffExp and flair diffSplice were kindly run by George Wiggins (Logan lab group, University of Otago, Christchurch, New Zealand) due to version compatibility issues with package rpy2=2.9.4. Flair diffExp was used to analyse differential gene expression, isoform expression and isoform usage between samples, in this case between the untreated and irradiated replicates in each cell line.[345] This utilised the tools specified in the GitHub file flair_conda_env.yaml.[344] Finally, the FLAIR module flair diffSplice was used to analyse alternative 3' splicing, alternative 5' splicing, intron retention and exon skipping.

## 2.14.11: FLAIR output

The isoforms identified using the FLAIR pipeline were visualised using the Integrative Genomics Viewer (IGV) and isoform parameters and diffExp and diffSplice results were exported as Microsoft Excel files.[346] These output files are available on the Open Science Framework (OSF) repository: https://osf.io/hs627/?view_only=0563901eb9004de7a187b5f3912bb487.[334] The isoform parameters were compared between replicate, cell line and treatment samples to identify BCL6 transcripts found in multiple samples and any trends in transcript expression between cell lines and treatments. The quantification values (from flair quantify) for the commonly identified transcripts were extracted and

compared to determine the abundance of the different BCL6 transcript variants expressed in each cell line and treatment. The flair diffExp and flair diffSplice results were examined for evidence of altered BCL6 transcript expression and alternative splicing in irradiated compared to untreated GBM cells.

# 3: Investigation of the role of BCL6 in GBM responses to therapy

## 3.1: Introduction

GBM has such a poor prognosis because it is highly resistant to the available therapies. The standard treatment for GBM is maximal resection followed by radiotherapy with concomitant and then adjuvant TMZ treatment.[4] However, while this regimen extends survival by a few months, GBM tumours invariably recur and are rapidly fatal in most cases.[3,347–349] Previous studies have linked BCL6 to the therapy resistance of GBM and other cancer types.[207,210,302,309,310,350–354] This suggests that BCL6 may be a promising target to improve the efficacy of GBM therapies. The aim of this study was to gain a broad understanding of how GBM cells respond to therapy and to investigate how BCL6 activity is involved in this response. To this end, the whole proteome responses of LN18 GBM cells to five treatments with and without BCL6 inhibition were compared.

Fractionated IR and TMZ treatments were selected to mimic the regimens given to GBM patients.[4] Fractionated IR consisted of doses of 2 Gy IR given once daily for five days. TMZ (10 μM) was administered every second day for a total of seven doses. While these are the most clinically relevant treatments, three acute treatments were also selected. One of these was a single dose of 3 μM doxorubicin, with cells harvested at 24 hours. The other two acute treatments both consisted of a single (acute) dose of 10 Gy IR, but with cells harvested 24 or 48 hours after treatment. While doxorubicin is an effective treatment for many cancer types, it is not used for the treatment of GBM as it cannot cross the BBB.[355,356] However, doxorubicin treatment strongly upregulates BCL6 expression in GBM, making it useful for the *in vitro* study of BCL6 activity.[207] Additionally, despite different modes of action, doxorubicin and TMZ both result in DNA double-stranded breaks.[80,85,86,357] Although IR is used clinically, 10 Gy IR is higher than the doses that can safely be achieved in GBM patients. However, 10 Gy IR also strongly upregulates BCL6 in GBM cells.[207] Additionally, previous work investigating the role of BCL6 in the therapy response of GBM cells has used doxorubicin and acute IR treatments, so it was important to include these treatments in the proteomics analysis to provide more context for these results.

Each treatment was administered to LN18 GBM cells along with either DMSO vehicle control or the BCL6 small molecule inhibitor FX1 in DMSO. FX1 binds to the lateral groove of the BTB/POZ domain of BCL6, preventing corepressor binding and inhibiting BCL6 activity.[295] For the two most clinically relevant treatments, fractionated IR and TMZ, the LN18 cells were treated with FX1 along with the first dose of therapy and then every second day until conclusion of treatment. For the three acute treatments, LN18 cells were treated with FX1 along with the single dose of doxorubicin or IR. A schematic of each treatment is shown in Figure 3.1. The whole proteome response of LN18 cells to each treatment with

and without BCL6 inhibition was analysed to elucidate the role of BCL6 in the therapy response of LN18 GBM cells.

**Clinically relevant treatments**

Fractionated irradiation

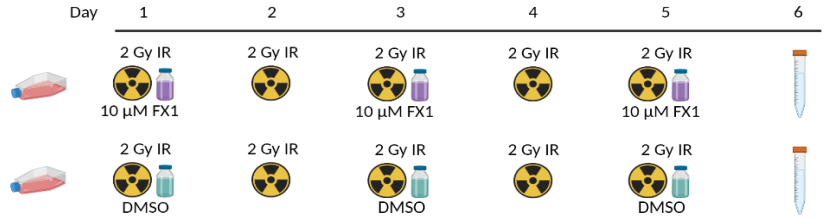


Temozolomide

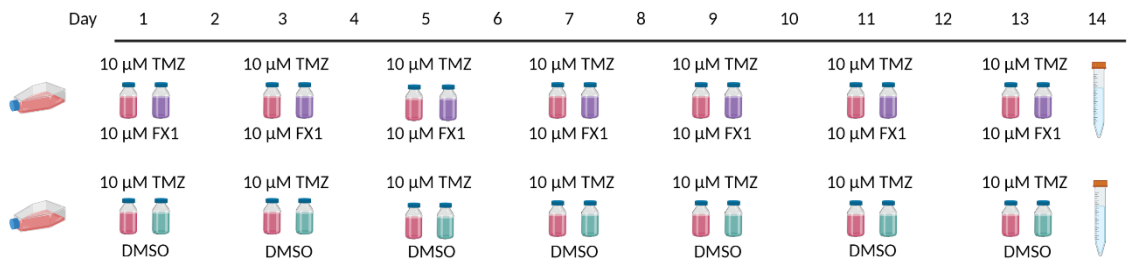


**Acute treatments**

Acute irradiation (24 hours)

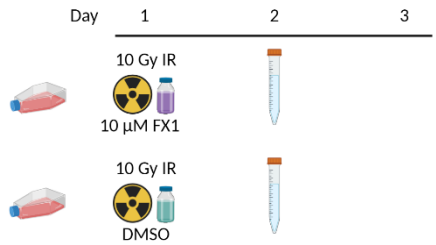

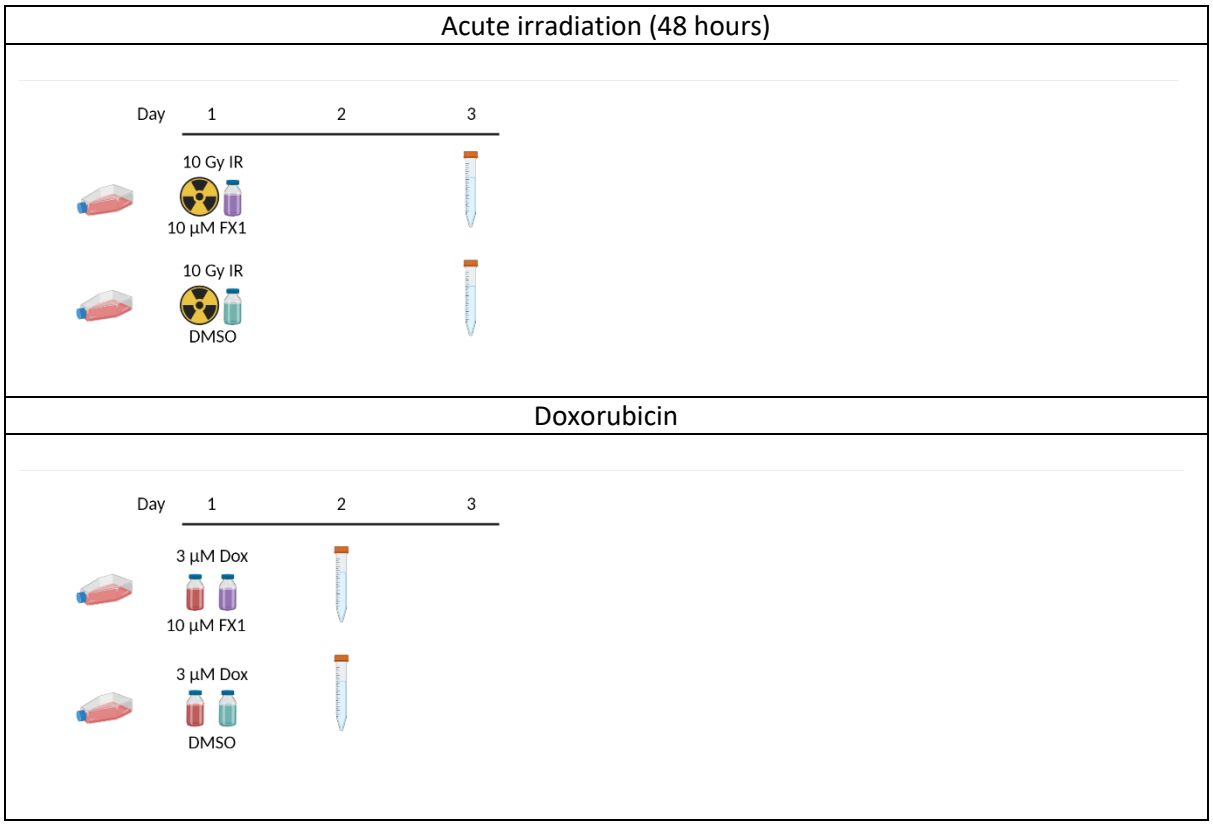


Figure 3.1: Treatment schedules

Schedules for the treatment of LN18 GBM cells before harvesting (indicated with the orange-capped tube), freezing and processing for proteomic analysis. Images produced using BioRender.

## 3.2: Aims

The objective of this chapter was to investigate the role of BCL6 in the response of LN18 GBM cells to different DNA-damaging therapies. This objective consisted of three aims. The first aim was to gain a broad understanding of how each treatment affected the whole proteome of LN18 cells. Secondly, this chapter investigated how inhibition of BCL6 affected the proteome of untreated LN18 cells. The last aim was to compare the whole proteome response of LN18 GBM cells to therapy with and without BCL6 inhibition in order to achieve the overall objective of the chapter.

## 3.3: Results

### 3.3.1: Determination of treatment concentrations

Western blot analysis was used to confirm that the acute treatments upregulated BCL6 expression in LN18 cells as expected and to investigate the effects of the clinically relevant treatments on BCL6 expression (Figure 3.2). There was a lot of background noise in the blot for BCL6 due to the promiscuity of commercially available BCL6 antibodies for western blotting. Multiple rounds of optimisation and the use of alternative antibodies did not improve the level of background (data not shown). However, a band at the expected molecular weight for BCL6 could be distinguished. Although the high background prevented any strong claims being made, western blots for BCL6 were a useful indication of BCL6 protein expression changes in response to treatment.

As expected, doxorubicin treatment strongly upregulated BCL6 expression, as did treatment with TMZ. At 48 hours after 10 Gy IR, BCL6 upregulation equivalent to that induced by the two chemotherapies was observed. The upregulation of BCL6 24 hours after acute IR was more variable. Fractionated IR treatment did not appear to upregulate BCL6 expression, however it was retained in the study because of its clinical relevance. None of these changes to BCL6 expression were statistically significant ($p \geq 0.05$), likely due to the variability of the data.

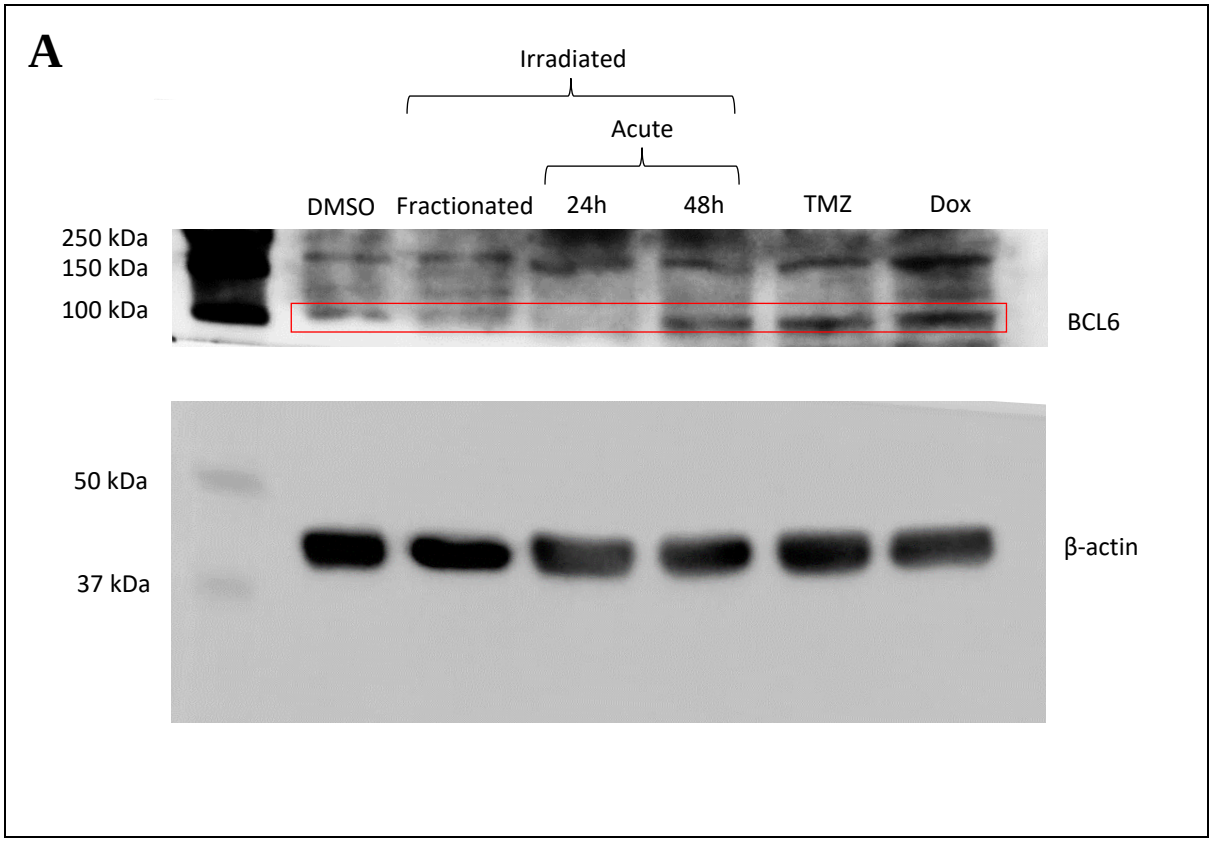

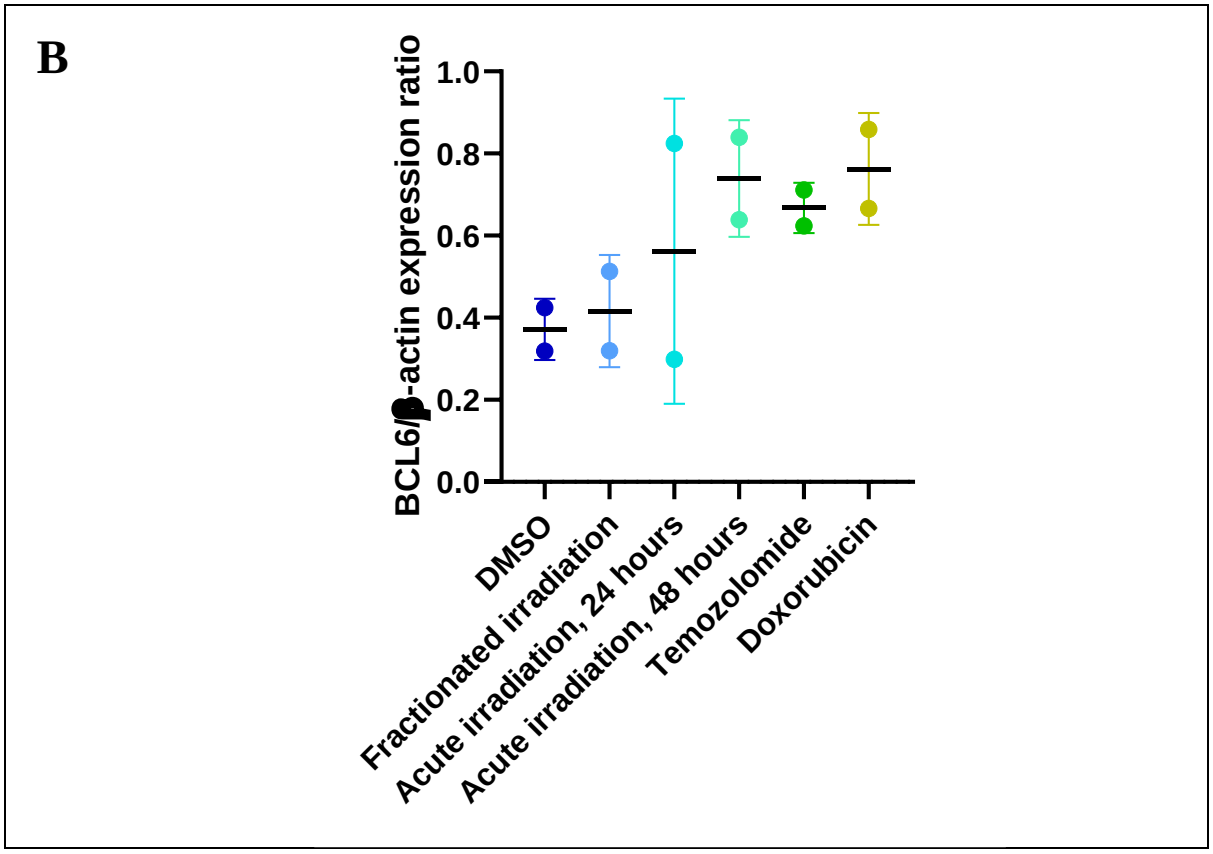


Figure 3.2: Western blot analysis of BCL6 expression in untreated and treated LN18 cells

A) Representative Western blot for BCL6 and β-actin in LN18 cells treated with DMSO, fractioned IR, acute IR 24 hours, acute IR 48 hours, TMZ and doxorubicin (Dox). The western blot for BCL6 was imaged with a 5 second exposure. The membrane was stripped and re-blotted for β-actin. The western blot for β-actin was imaged with a 0.2 second exposure. B) Quantitative analysis of BCL6 protein relative to β-actin protein from two Western blots. Black lines show mean and error bars show standard deviation (n=2).

To investigate the effect of BCL6 inhibition, the desirable FX1 concentration was one that affected cell function but did not kill all of the cells. Therefore, a clonogenic assay was used to determine the concentration of FX1 which markedly decreased the plating efficiency of LN18 cells, as observed in a previous study.[322] There was a clear decrease in average plating efficiency from 60% in untreated cells to 26% in cells treated with 10 μM FX1 (

Figure 3.3). The aberrantly high plating efficiency at 15 μM FX1 may be because the solubility limit of FX1 in DMSO had been reached. This could result in FX1 precipitating out of solution and decreasing the effective concentration. Indeed, the plating efficiency seen at 15 μM was similar to that caused by DMSO alone (46%, shown in red in

Figure 3.3) indicating that at least some of the decrease in plating efficiency seen was due to effects of DMSO.

FX1 at 10 µM was used to inhibit BCL6 in LN18 cells as this concentration significantly ($p \leq 0.05$, Dunnet's T3 multiple comparisons testing) decreased the plating efficiency of LN18 cells compared to DMSO alone. The effects of DMSO were corrected for in all experiments by adding DMSO as a vehicle control to all cells not treated with FX1.

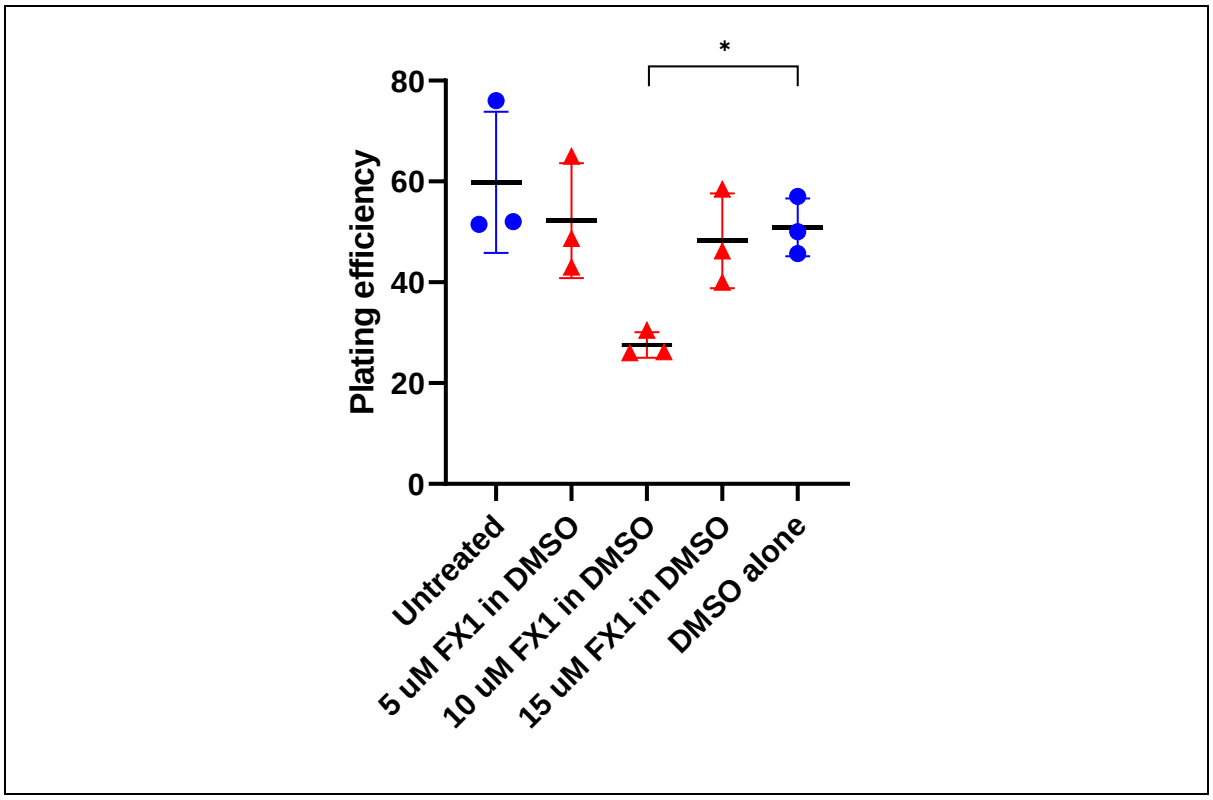


Figure 3.3: Plating efficiency of LN18 cells treated with FX1

Plating efficiency of LN18 cells treated with 5 µM, 10 µM and 15 µM FX1 in a clonogenic assay (red). Plating efficiency of untreated LN18 cells and LN18 cells treated with a DMSO concentration matching that of the 15 µM FX1 treatment (blue). Plating efficiencies were calculated from duplicate experiments. The three replicates shown for each concentration represent the average (n=2) plating efficiencies of cells plated at starting concentrations of 25, 50 and 100 cells per well. Black lines show mean and error bars show standard deviation (n=3). * = $p \leq 0.05$ (Dunnet's T3 multiple comparisons testing).

## 3.3.2: Effects of treatment on LN18 GBM cells

The first aim of this chapter was to determine the effects of each chemo- and radiotherapy treatment alone on the whole proteome of LN18 GBM cells. This established a baseline from which the effects of BCL6 inhibition on the therapy response of LN18 cells could be analysed. LN18 GBM cells were treated with each treatment regime (Figure 3.1) in biological triplicate. Proteins were extracted from the harvested cells and processed for whole proteome mass spectrometry analysis.

### 3.3.2.1 Quantitative analysis

The effects of each treatment on the whole proteome of LN18 GBM cells were investigated by quantitative analysis of protein expression in treated cells (+ DMSO vehicle) compared to untreated cells (+ DMSO vehicle). Protein abundance ratios were calculated by pairwise comparison between each set of treated replicates and the untreated replicates (three biological and two technical replicates each). Proteins were considered differentially expressed if their expression was changed more than two-fold compared to the DMSO controls with an adjusted p value $\leq 0.05$ (Benjamini-Hochberg multiple comparisons testing).

All five treatments resulted in changes in the expression of several hundred proteins (Table 3.1). The numbers of proteins up- and downregulated by each treatment were not vastly different in general. However, it is notable that more proteins were upregulated 48 hours after acute IR than after any of the other treatments.

Table 3.1: Changes in protein expression in LN18 cells in response to chemo- and radiotherapy
Proteins up- or downregulated ≥ 2-fold, adj. p ≤ 0.05 (Benjamini-Hochberg multiple comparisons testing) compared to untreated control.

| Treatment | Number of proteins upregulated | Number of proteins downregulated |
|---|---|---|
| Fractionated irradiation | 156 | 324 |
| Acute irradiation (24 hours) | 242 | 234 |
| Acute irradiation (48 hours) | 404 | 345 |
| Temozolomide | 163 | 193 |
| Doxorubicin | 210 | 345 |

Further analysis showed that the differentially expressed proteins varied between the treatments (Figure 3.4). There was more overlap between the proteins downregulated by each treatment, with 1/3 or fewer of the proteins downregulated by fractionated IR, 24 hours after acute IR or doxorubicin unique to that treatment (Table 3.2). This indicated that some proteins are downregulated in response to multiple

treatments, suggesting a common stress response. The upregulated proteins seemed to be more specific to each treatment. More than 40% of proteins upregulated by each treatment were unique to that treatment. Strikingly, the proteome changes 48 hours after acute IR and in response to TMZ were the most unique, suggesting that LN18 cells mount a specific response to these treatments.

Table 3.2: Uniqueness of LN18 whole proteome changes in response to each treatment

Proteins only up- or downregulated ≥ 2-fold, adj. p ≤ 0.05 (Benjamini-Hochberg multiple comparisons testing) compared to untreated control by each treatment.

| Treatment | Percentage of proteins only upregulated by this treatment | Percentage of proteins only downregulated by this treatment |
|---|---|---|
| **Fractionated irradiation** | 46% | 33% |
| **Acute irradiation 24 hours** | 47% | 13% |
| **Acute irradiation 48 hours** | 77% | 54% |
| **Temozolomide** | 60% | 37% |
| **Doxorubicin** | 42% | 26% |

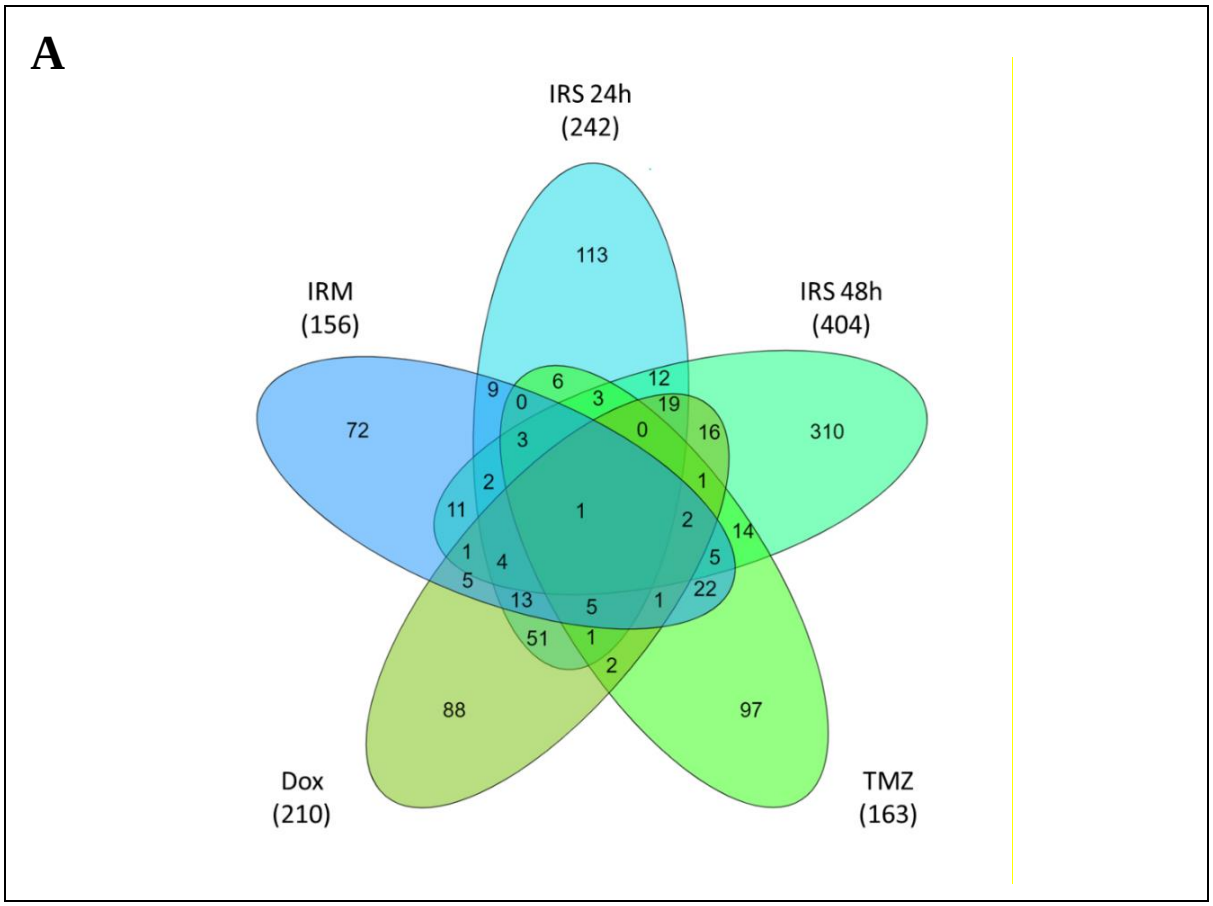

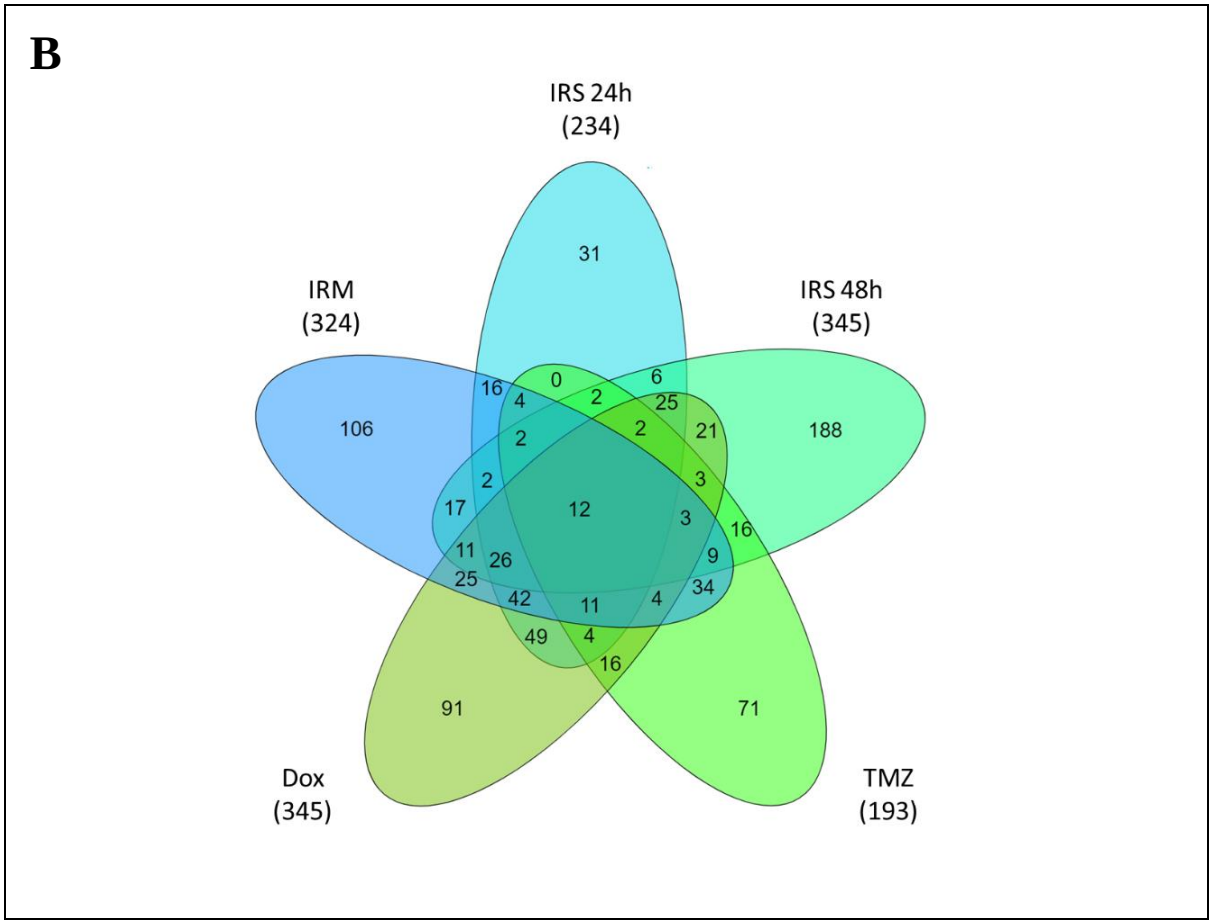


Figure 3.4: Overlap between proteins up- and downregulated by treatments.

Venn diagrams comparing proteins (A) upregulated and (B) downregulated by fractionated multiple doses of IR (IRM), 24 hours after single dose acute IR (IRS 24h), 48 hours after single dose acute IR (IRS 48h), TMZ and doxorubicin (Dox). Venn diagrams made using InteractiVenn.[358]

### 3.3.2.2: Functional enrichment analysis

The proteins differentially expressed in response to each treatment were interrogated using g:Profiler to identify significantly enriched ($p \leq 0.05$) gene ontology biological process (GO:BP) and cellular component (GO:CC) terms.[330] Statistical significance was calculated using the g:Profiler specific multiple comparisons testing algorithm g:SCS. The top 5 (if applicable) enriched parent GO:BP and GO:CC terms for proteins up- and downregulated by each treatment are displayed in Figures 3.5-3.9.

#### Treatment with fractionated irradiation

Fractionated IR treatment of LN18 cells resulted in downregulation of DNA replication and repair proteins (Figure 3.5). Downregulated proteins annotated to the enriched GO:BP term *negative regulation of DNA-dependent DNA replication* (p = 1.55E-2) included TIMELESS and TIPIN. These proteins form a complex involved in control of DNA repair, DNA replication and maintenance of replication fork stability.[359,360] Additionally, BLM, a DNA helicase involved in double strand break (DSB) repair, mismatch repair protein MSH3 and other proteins involved in DNA replication and repair were downregulated and annotated to this term.[361,362] The enriched GO:BP terms *cell division* (p – 1.56E-2) and *replication fork arrest* (p = 4.39E-2) contained downregulated proteins involved in the kinetochore, formation and function of mitotic spindles and in passing through cell cycle checkpoints. Similarly, proteins downregulated by fractionated IR were enriched for GO:CC terms *microtubule organising centre* (p = 5.37E-4) and *centrosome* (p = 1.32E-3). The downregulation of proteins involved in both DNA replication and mitosis suggested that in response to fractionated IR, LN18 cells reduced cell division. However, the downregulation of proteins involved in multiple stages of the cell cycle did not indicate arrest at any particular stage. Indeed, cells treated with fractionated IR continued to proliferate, suggesting that perhaps their rate of cell division was merely reduced rather than arrested.

The proteins downregulated by fractionated IR were also enriched for the GO:BP term *P-body* (p = 6.83E-3). Processing (P) bodies are foci of mRNA transcripts and mRNA decay proteins, so as such this term contained several downregulated proteins involved in mRNA silencing and decay.[363] Conversely, proteins upregulated by fractionated IR were enriched for the GO:CC term *ribosome* (p = 9.41E-3), which contained various ribosomal proteins and proteins involved in ribosome biogenesis and protein synthesis. Together this may indicate an upregulation of mRNA translation. Furthermore, proteins upregulated by fractionated IR were enriched for the GO:CC term *integral component of organelle membrane* (p = 4.78E-3). This term included mitochondrial membrane proteins and proteins involved in translocation into the endoplasmic reticulum (ER). Additionally, components of the ER-associated degradation (ERAD) Hrd1p ubiquitin ligase complex were upregulated by fractionated IR, resulting in enrichment of this GO:CC term (p = 8.00E-3). This suggests that fractionated IR induced increased protein trafficking across organelle membranes and an ER stress response.

Overall, fractionated IR of LN18 cells appeared to induce reduced cell division but increased protein translation and trafficking. This may have enabled LN18 cells to survive the long-term but mild therapy by slowing cell division and producing proteins needed to adapt to stress. Strangely, fractionated IR also caused downregulation of DNA repair proteins, suggesting that allowing time for DNA repair was not the reason for the apparent decrease in cell cycling.

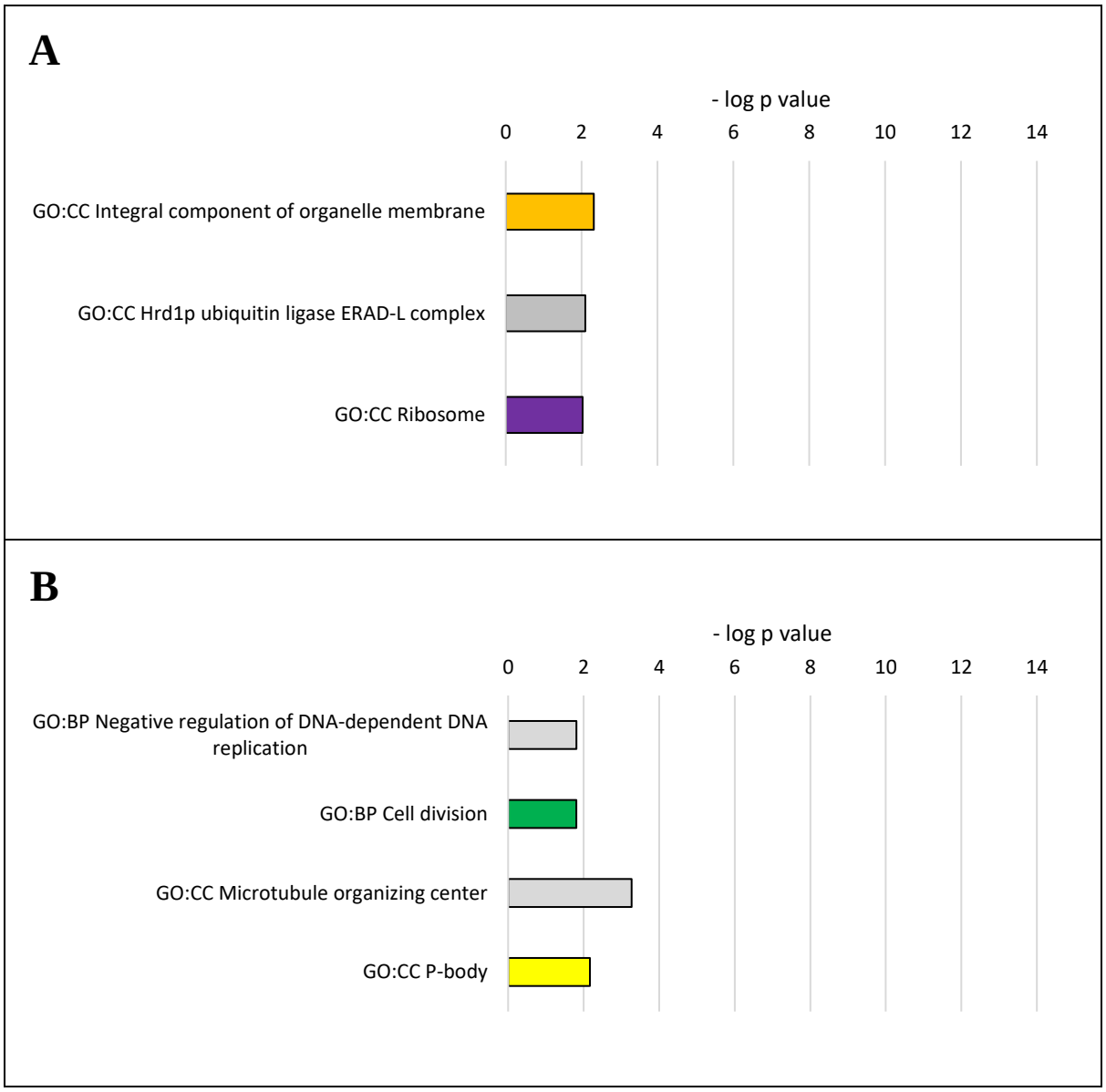


Figure 3.5: Functional enrichment of proteins up- and downregulated by fractionated IR in LN18 cells

Up to five most significantly enriched (highest – log p value) parent GO:BP and GO:CC terms from analysis of proteins (A) up- and (B) downregulated by fractionated IR. Common enrichments between treatments colour coded for comparison (colours correspond to Figures 3.5-3.9): orange = organelle membrane component, purple = ribosome or ribosome biogenesis, green = cell division, yellow = ribonucleoprotein complex, red = mitochondrial, light blue = protein transport or targeting, dark blue = transferase complex, purple = chromosome, pink = nuclear body.

Treatment with temozolomide

Functional enrichment analysis revealed that TMZ induced upregulation of proteins involved in telomere maintenance and mitosis, particularly the spindle assembly checkpoint (Figure 3.6). These proteins were annotated to the enriched GO:BP term *regulation of chromosome organisation* (p = 1.20E-2). mRNA splicing proteins were also upregulated by TMZ and annotated to the enriched GO:CC term *ribonucleoprotein complex* (p = 1.61E-2). Other upregulated proteins were annotated to the GO:CC term *nuclear body* (p = 6.19E-5). This broad term encompasses all types of membrane-less nuclear structures, so unsurprisingly the upregulated proteins annotated to it were varied and included histone modifiers and mRNA splicing proteins.

TMZ treatment resulted in downregulation of E3 ubiquitin-protein ligases, 26S proteasome subunits and inhibitors of protein ubiquitination and degradation annotated to the enriched GO:BP terms *regulation of cellular protein catabolic process* (p = 5.19E-3) and *regulation of cellular catabolic process* (p = 3.82E-2). This indicated a general reduction of the regulation of protein degradation, suggesting that protein degradation may be decreased in response to TMZ.

Proteins involved in vesicle trafficking and exocytosis were also downregulated by TMZ and were annotated to the enriched GO:BP terms *exocytic process* ( p = 3.41E-2) and *post-Golgi vesicle-mediated transport* (p = 3.60E-2). Additionally, proteins involved in RNA polymerase III-mediated transcription were downregulated by TMZ, resulting in enrichment for GO:BP term *rRNA transcription* (p = 4.96E-2) and GO:CC terms *transcription factor TFIIIC complex* (p = 6.34E-3) and *RNA polymerase III transcription regulator complex* (p = 2.60E-2).

Overall, TMZ downregulated expression of proteins involved in regulation of protein degradation and transcription of non-coding RNA required for translation. This suggested a decrease in the turnover of proteins in response to TMZ. Furthermore, the trafficking of proteins appeared to be decreased by TMZ. This suggested a general decrease in cellular activity in response to TMZ which may have enabled the LN18 cells to survive the long-term treatment. This was supported by the continued proliferation of the LN18 cells throughout the TMZ treatment regime. mRNA splicing proteins and proteins involved in histone modification and telomere regulation were upregulated in response to TMZ treatment. This suggested changes in the regulation of chromatin organisation and gene expression in response to treatment. Additionally, proteins involved in the spindle assembly checkpoint were upregulated, perhaps indicating G2/M arrest.

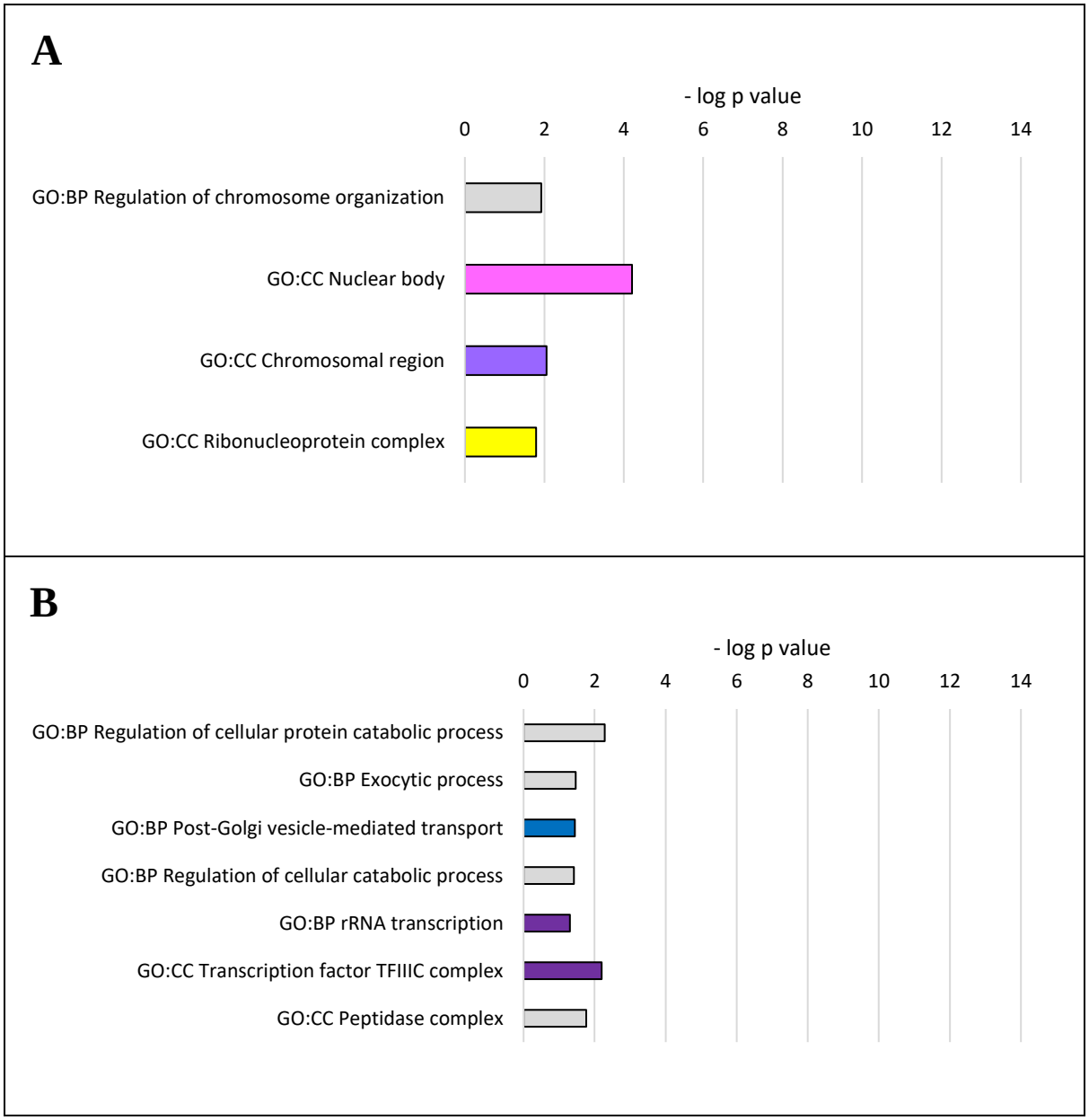


Figure 3.6: Functional enrichment of proteins up- and downregulated by TMZ in LN18 cells

Up to five most significantly enriched (highest – log p value) parent GO:BP and GO:CC terms from analysis of proteins (A) up- and (B) downregulated by TMZ. Common enrichments between treatments colour coded for comparison (colours correspond to Figures 3.5-3.9): orange = organelle membrane component, purple = ribosome or ribosome biogenesis, green = cell division, yellow = ribonucleoprotein complex, red = mitochondrial, light blue = protein transport or targeting, dark blue = transferase complex, purple = chromosome, pink = nuclear body.

Treatment with acute irradiation 24 hours

Functional enrichment analysis showed that acute exposure to 10 Gy IR treatment induced a very different response in LN18 cells compared to low dose fractionated IR (Figure 3.7). Whereas fractionated IR downregulated cell division proteins, proteins upregulated 24 hours after acute IR were enriched for the GO:BP term *cell division* (p = 4.67E-2). These upregulated proteins were involved in ensuring correct chromosome segregation during mitosis and in regulation of cytokinesis. Two cyclins involved in the G2/M transition, CCNA2 and CCNB1, were upregulated and annotated to this term.[364] Additionally, TIPIN, which is important for cell survival after DNA damage but was downregulated by fractionated IR, was upregulated by acute IR.[359,360] It is likely that the upregulation of these mitotic proteins represented cell cycle arrest at G2/M in response to the acute IR treatment.

Acute IR also resulted in the upregulation of mitochondrial proteins at 24 hours after treatment. These proteins were annotated to the enriched GO:BP term *mitochondrial organisation* (p = 2.89E-2) as well as to several more significantly enriched mitochondrial GO:CC terms (p values as low as 1.62E-6). The upregulated mitochondrial proteins were involved in structural organisation and insertion of proteins into the mitochondrial inner membrane. Two of these proteins, OPA1 and GHITM, are also involved in releasing cytochrome c during apoptosis.[365,366] The *mitochondrial organisation* term also included subunits of respiratory chain complexes. This functional enrichment suggests that acute IR induces changes to mitochondrial structure and function, likely due to cellular stress.

Proteins upregulated 24 hours after acute IR were also involved in protein targeting and transport into the ER and mitochondria. These proteins were annotated to the *mitochondrial organisation* term, as well as to the enriched GO:BP term *protein targeting* (p = 3.74E-2). Upregulation of mitochondrial and ER membrane proteins was also seen with fractionated IR treatment, suggesting that increased protein trafficking is part of the LN18 cellular response to IR-induced DNA damage.

Additionally, proteins upregulated 24 hours after acute IR were annotated to the enriched term *ribosomal small subunit biogenesis* (p = 1.07E-2). However, other ribosomal proteins were downregulated 24 hours after acute IR and annotated to the GO:CC term *ribonucleoprotein complex* (p = 9.63E-3). This suggested that there were changes in ribosome production in response to acute IR but did not clearly indicate whether translation was likely to increase or decrease. Furthermore, proteins involved in mRNA splicing were downregulated 24 hours after acute IR. These proteins were annotated to the enriched GO:BP parent term *mRNA metabolic process* (p = 1.48E-3).

Overall, by 24 hours after acute IR treatment, LN18 cells had upregulated G2/M phase proteins, suggesting G2/M cell cycle arrest. They also upregulated mitochondrial organisation and respiratory chain proteins, as well as proteins involved in protein transport into the ER and mitochondria. mRNA splicing was decreased 24 hours after acute IR and ribosome production appeared to be altered.

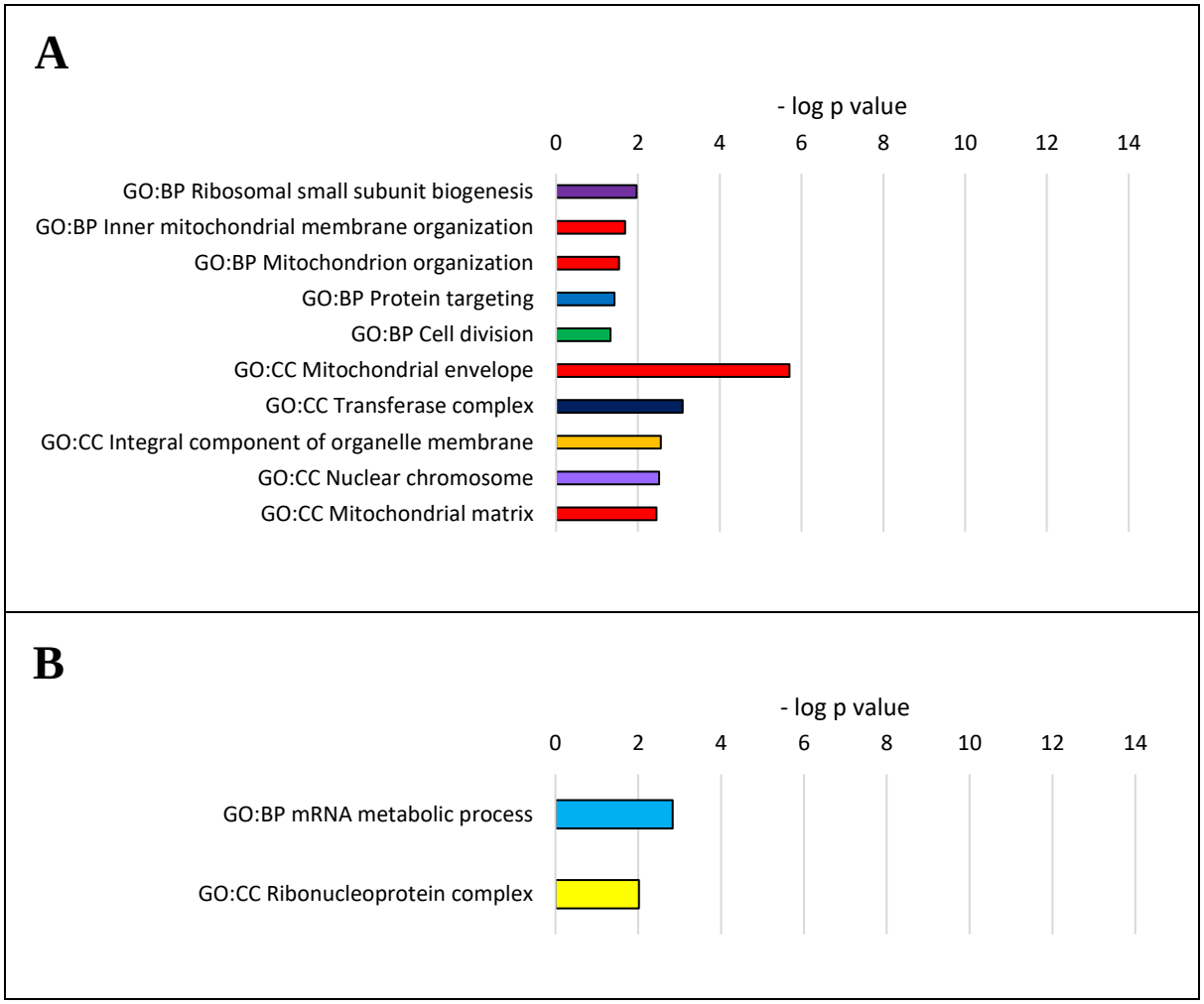


Figure 3.7: Functional enrichment of proteins up- and downregulated 24 hours after acute IR in LN18 cells

Up to five most significantly enriched (highest – log p value) parent GO:BP and GO:CC terms from analysis of proteins (A) up- and (B) downregulated 24 hours after acute IR. Common enrichments between treatments colour coded for comparison (colours correspond to Figures 3.5-3.9): orange = organelle membrane component, purple = ribosome or ribosome biogenesis, green = cell division, yellow = ribonucleoprotein complex, red = mitochondrial, light blue = protein transport or targeting, dark blue = transferase complex, purple = chromosome, pink = nuclear body.

Treatment with acute irradiation 48 hours

There were many similarities between proteins up- and downregulated at 24 and 48 hours after acute IR (Figure 3.8). At both time points, G2/M phase proteins were upregulated, suggesting that the LN18 cells remained arrested in that phase at 48 hours. These proteins were annotated to the enriched GO:BP terms *cell division* (p = 1.77E-2) and *mitotic nuclear division* (p = 1.69E-2) and included the two G2/M transition cyclins, CCNA2 and CCNB1, which were also upregulated 24 hours after acute IR.[364] At 48 hours, far more proteins involved in mitosis were upregulated. These included CDK1, which promotes G2/M transition, key mitotic regulator AURKA, proteins involved in the spindle assembly checkpoint MAD2L1, ZW10, TRIP13 and NUF2, as well as APC/C component CDC23.[367–372] Tumour suppressor and cell cycle checkpoint protein RB1 was also upregulated 48 hours after acute IR and annotated to the enriched *cell division* term.[373,374] This suggested the progression of the process of cell cycle arrest in G2/M phase over the 48 hours after treatment.

Furthermore, mitochondrial proteins were upregulated both 24 and 48 hours after acute IR and were annotated to the GO:BP term *mitochondrial organisation* (p = 5.92E-4) and to several mitochondrial GO:CC terms (p values as low as 8.69E-5). At both time points, the upregulated mitochondrial proteins included respiratory chain proteins and proteins involved in protein import into the mitochondria. In addition to mitochondrial changes, other metabolic alterations had occurred by 48 hours after acute IR. The GO:BP term *ribose phosphate metabolic process* was enriched (p = 3.33E-2) and contained upregulated proteins involved in metabolism and homeostasis of nucleotides and nucleoside phosphates, as well as proteins involved in lipid metabolism and the γ subunit of the master metabolic regulator AMPK.[375]

The most striking difference at 48 hours after acute IR compared to at 24 hours was the upregulation of proteins involved in autophagy. These proteins were annotated to the enriched GO:BP term *macroautophagy* (p = 8.59E-4). Additionally, protein quality control was upregulated, with proteins annotated to the GO:BP term *protein quality control for misfolded or incompletely synthesised proteins* (p = 5.34E-3). Notably, the tumour suppressor p53 and its functional enhancer TP53BP, were upregulated 48 hours after acute IR.[376,377] These changes at 48 hours indicated that while cell cycle arrest and changes to mitochondrial organisation and protein trafficking were initiated rapidly after acute IR treatment, autophagy and p53 expression were part of a longer-term program of responses.

As at 24 hours, at 48 hours after acute IR, proteins involved in mRNA splicing were downregulated and annotated to the GO:BP parent term *mRNA metabolic process* (p = 2.84E-5). Proteins downregulated 48 hours after acute IR were also annotated to the daughter term *RNA export from nucleus* (p = 6.80E-3). While the changes to ribosome production were unclear 24 hours after acute IR, at 48 hours, ribosome biogenesis proteins were downregulated and annotated to the enriched GO:BP term

*ribonucleoprotein complex biogenesis* (p = 5.29E-5) and daughter term *ribosome biogenesis* (p = 6.89E-5).

In summary, the biggest changes at 48 hours after acute IR compared to at 24 hours were the induction of autophagy and the p53 pathway, along with related metabolic changes such as upregulation of AMPK. Autophagy appeared to be a longer-term response to IR treatment which was initiated after the more rapid responses of cell cycle arrest in G2/M phase, increased protein trafficking, decreased mRNA splicing and changes to mitochondrial organisation and function. These initial responses were still evident at 48 hours after acute IR. Another longer-term response to acute IR was the downregulation of ribosome biogenesis which appeared to be in progress at 24 hours but less evident. This contrasted with the upregulation of ribosome proteins in response to fractionated IR.

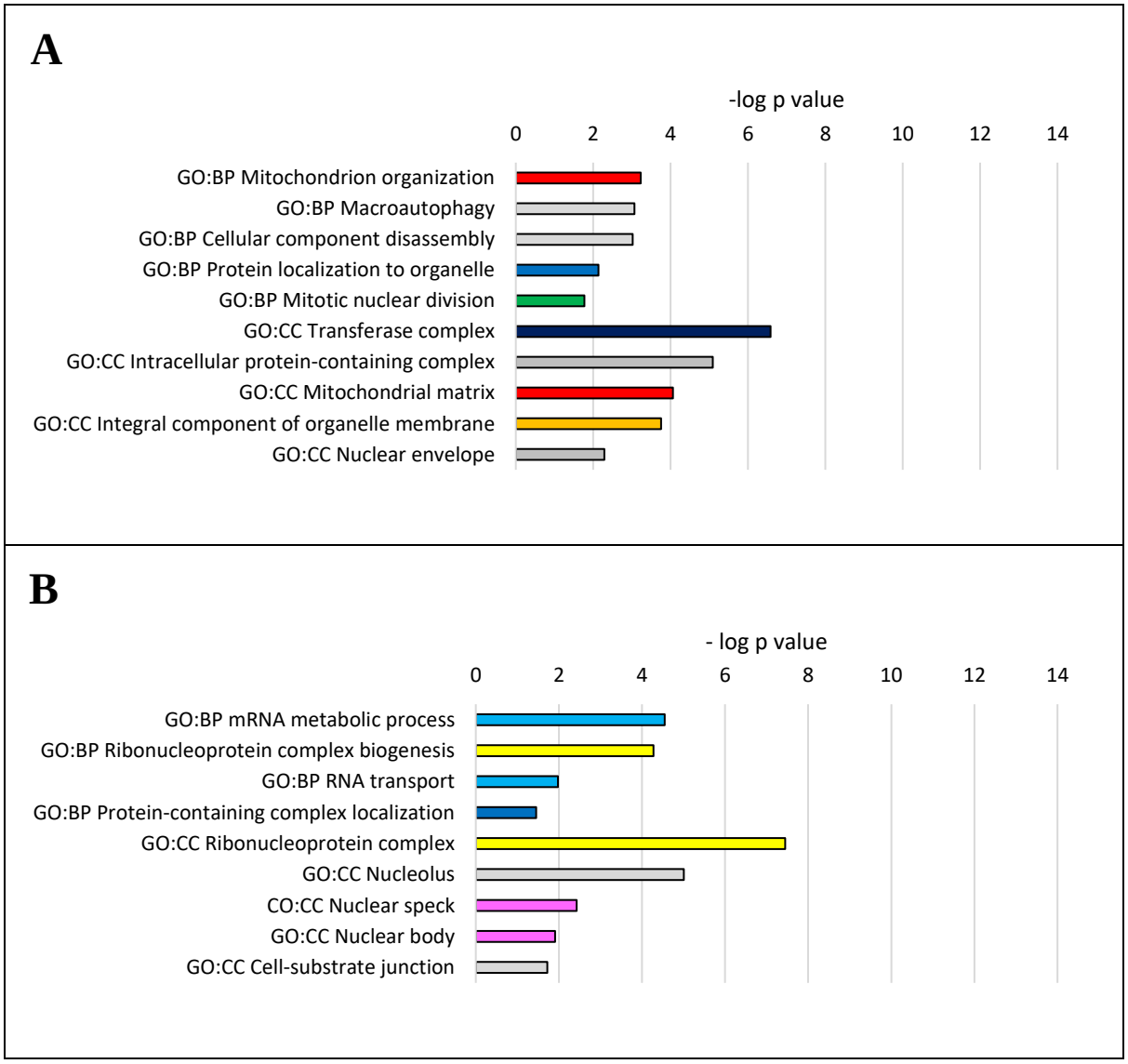

Figure 3.8: Functional enrichment of proteins up- and downregulated 48 hours after acute IR in LN18 cells

Up to five most significantly enriched (highest – log p value) parent GO:BP and GO:CC terms from analysis of proteins (A) up- and (B) downregulated 48 hours after acute IR. Common enrichments between treatments colour coded for comparison (colours correspond to Figures 3.5-3.9): orange = organelle membrane component, purple = ribosome or ribosome biogenesis, green = cell division, yellow = ribonucleoprotein complex, red = mitochondrial, light blue = protein transport or targeting, dark blue = transferase complex, purple = chromosome, pink = nuclear body.

## Treatment with doxorubicin

Functional enrichment analysis of proteins up- and downregulated by doxorubicin is shown in Figure 3.9. The most striking effect of doxorubicin on LN18 cells was the downregulation of ribosome biogenesis. This resulted in the highly significant enrichment for the GO:BP term *ribonucleoprotein complex biogenesis* (p = 5.05E-14) and GO:CC term *ribonucleoprotein complex* (p = 7.98E-9), including daughter terms *rRNA metabolic process* (p = 3.59E-13), *ribosome biogenesis* (p = 2.03E-12) and *nucleolus* (p = 2.52E-9). Both acute IR treatment and TMZ treatment also led to downregulation of proteins involved in ribosome biogenesis and translation. However, the proteins downregulated by doxorubicin were enriched for ribosome related terms with far greater significance than proteins up- or downregulated by the other treatments. Furthermore, some proteins involved in regulation of translation, including DNAJC3 and UNK, were upregulated by doxorubicin and annotated to the enriched term *peptide metabolic process* (p = 3.26E-2).[378,379] As with fractionated and acute IR, doxorubicin treatment also downregulated proteins involved in mRNA splicing. These proteins were annotated to GO:BP terms *mRNA metabolic process* (p = 7.25E-5) and *RNA splicing* (p = 3.77E-4) as well as to GO:CC term *nuclear body* (p = 1.13E-2). This suggests that there was a strong global suppression of translation in response to doxorubicin.

In contrast to acute IR, proteins involved in cell division were downregulated by doxorubicin and annotated to the GO:BP term *cell division* (p = 5.24E-3) and the GO:CC term *centrosome* (p = 4.05E-4). Proteins annotated to this term were largely involved in mitosis, indicating that unlike acute IR, doxorubicin did not arrest LN18 cells in G2/M phase. Other proteins annotated to this term were involved in DNA replication and repair, including TIMELESS and BLM which were also downregulated by fractionated IR.[359–362] However, TIPIN, which forms a complex with TIMELESS, was upregulated by doxorubicin along with other proteins annotated to the enriched GO:CC term *replication fork* (p = 3.64E-2).[359,360] Therefore, it was unclear whether doxorubicin arrested LN18 cells in another phase of the cell cycle, although there were clearly alterations to DNA replication and repair. Additionally, the tumour suppressor p53 was upregulated by doxorubicin treatment, as it was at 48 hours after acute IR.[377]

Like acute IR, doxorubicin treatment upregulated mitochondrial proteins annotated to enriched GO:BP term *mitochondrial organisation* (p = 1.01E-2) and several mitochondrial-related GO:CC terms (p values up to 2.73E-4). Again, these proteins were involved in membrane organisation, protein import into the mitochondria and the respiratory chain. Additionally, some other mitochondrial proteins, including some involved in biogenesis of respiratory chain complexes, were downregulated by doxorubicin and annotated to the enriched GO:CC term *mitochondrial intermembrane space* (p = 3.59E-2). As with fractionated and acute IR, mitochondrial and ER membrane proteins were upregulated by doxorubicin. These proteins were annotated to GO:CC terms *integral component of organelle membrane* (p = 1.04E-2) and *endoplasmic reticulum protein-containing complex* (p = 3.31E-2). Upregulated proteins were also enriched for the GO:CC term *primary lysosome* (p = 2.01E-2). Again, this suggested that the increase in protein trafficking between organelles was a common stress response in LN18 cells.

Unlike the other four treatments, proteins upregulated by doxorubicin were enriched for GO:BP terms related to regulation of gene silencing, including by miRNAs (p = 8.01E-4). Upregulated proteins annotated to this term included two transcription factors: OCT4, which is important for embryonic stem cell pluripotency, and SIN3A, a multifunctional transcriptional repressor known to associate with BCL6.[225,380] This suggested changes in the regulation of gene expression in response to doxorubicin treatment.

Overall, the downregulation of ribosome biogenesis and mRNA splicing and the upregulation of mitochondrial and ER membrane proteins appeared to be stress responses common to multiple treatments, including doxorubicin. However, doxorubicin led to far broader downregulation of ribosome biogenesis proteins than any of the other treatments. Unlike acute IR, acute doxorubicin treatment did not appear to arrest LN18 cells in G2/M phase. Instead, downregulation of proteins from this phase was seen, suggesting that doxorubicin led to cell cycle arrest in a different phase. Unlike the other treatments, upregulation of proteins involved in gene silencing was seen in response to doxorubicin, including upregulation of BCL6 corepressor SIN3A.

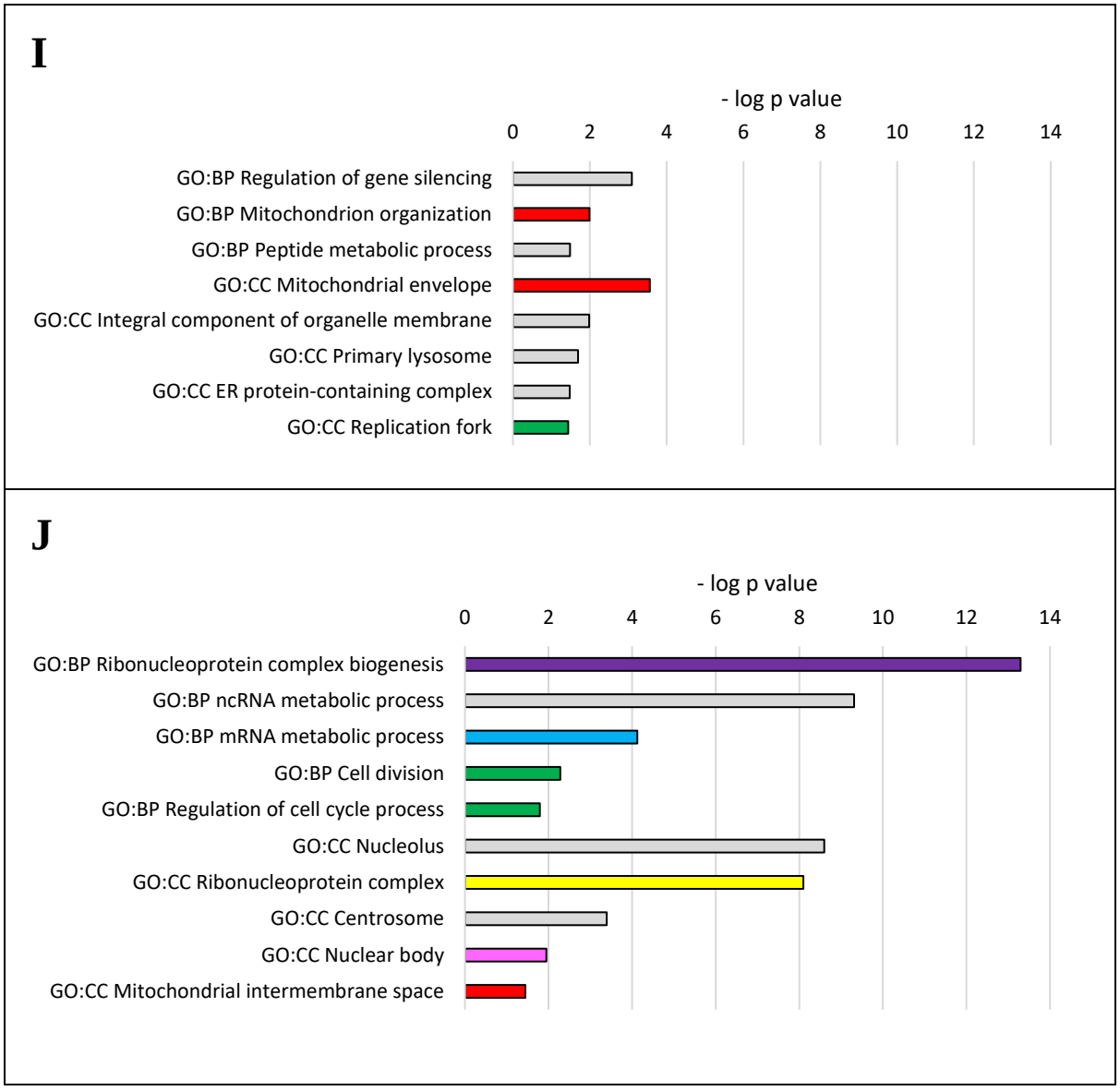


Figure 3.9: Functional enrichment of proteins up- and downregulated by doxorubicin in LN18 cells

Up to five most significantly enriched (highest – log p value) parent GO:BP and GO:CC terms from analysis of proteins (A) up- and (B) downregulated by doxorubicin. Common enrichments between treatments colour coded for comparison (colours correspond to Figures 3.5-3.9): orange = organelle membrane component, purple = ribosome or ribosome biogenesis, green = cell division, yellow = ribonucleoprotein complex, red = mitochondrial, light blue = protein transport or targeting, dark blue = transferase complex, purple = chromosome, pink = nuclear body.

### 3.3.2.3: Summary of effects of treatments on the proteome of LN18 cells

Functional enrichment analysis of the whole proteome changes induced by each treatment revealed differences in the LN18 cellular response to the clinically relevant treatments and the more acute treatments. Fractionated IR and TMZ appeared to cause LN18 cells to reduce their cellular activity, although in different ways. LN18 cells adapted to fractionated IR treatment by reducing cell division and DNA repair, but increasing protein translation and trafficking, perhaps enabling them to adapt to repeated stress. Conversely, LN18 cells adapted to TMZ treatment by reducing protein turnover and trafficking and upregulating telomere regulation and mitotic checkpoint proteins, perhaps indicating arrest in G2/M phase.

The acute treatments resulted in more distinct stress responses. Within 24 hours, acute IR clearly arrested LN18 cells in G2/M phase and upregulated mitochondrial organisation and respiratory chain proteins, as well as proteins involved in transport into the ER and mitochondria. Additionally, mRNA splicing was downregulated. These changes were maintained 48 hours after treatment. By 48 hours, autophagy was induced as part of a longer-term recovery process and ribosome biogenesis was downregulated. The downregulation of ribosome biogenesis and mRNA splicing and the upregulation of mitochondrial and ER membrane proteins appeared to be general responses to acute stress, as these changes were also seen with doxorubicin treatment. However, unlike acute IR, doxorubicin treatment did not arrest LN18 cells in G2/M phase and perhaps led to arrest in a different phase of the cell cycle.

### 3.3.2.4: Common responses to treatment

The downregulation of ribosome biogenesis and mRNA splicing and the upregulation of mitochondrial proteins were effects induced by all three of the acute treatments. Figure 3.10 shows that the majority of differentially expressed proteins annotated to these sets of terms were unique to each treatment. This may have been caused by technical differences between sample runs leading to proteins fluctuating above and below the threshold of detection but the overall functional enrichment remaining the same. However, where the differences are large it is more likely that there is some genuine biological difference. For example, very large, distinct sets of proteins annotated to these common terms were up- or downregulated only by doxorubicin and 48 hours after acute IR, suggesting differences in the therapy responses to these acute treatments.

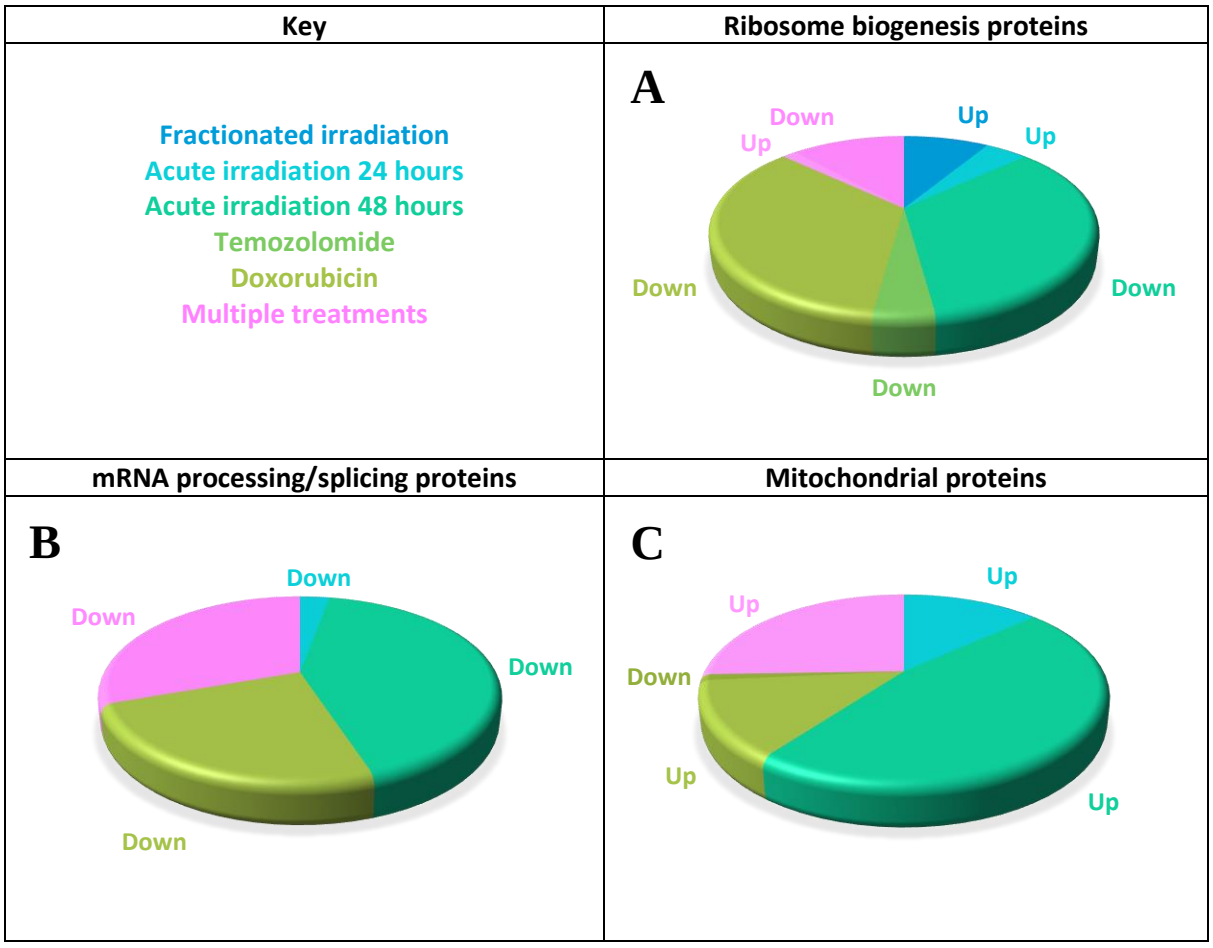


Figure 3.10: Differentially expressed proteins annotated to functional enrichment terms common to the acute treatments

Pie charts comparing the differentially expressed proteins annotated to terms enriched by multiple acute treatments: A) Ribosome biogenesis proteins, B) mRNA processing/splicing proteins and C) Mitochondrial proteins. Treatments colour coded as shown in the key.

## 3.3.3: The effect of FX1 on LN18 GBM cells

The overall objective of this chapter was to investigate the effects of BCL6 inhibition by FX1 on the therapy response of LN18 GBM cells. Before this was possible, it was necessary to investigate the effects of each therapy and of BCL6 inhibition separately on the whole proteome of LN18 cells. Section 3.3.2 established how each treatment affected the whole proteome of LN18 cells when BCL6 was not inhibited. The aim of this section (3.3.3) was to establish the effect of BCL6 inhibition on the whole proteome of untreated LN18 cells.

LN18 cells were treated with the BCL6 inhibitor FX1 in DMSO or with an equivalent volume of DMSO in biological triplicate. The cells were harvested 24 hours after treatment and proteins were extracted and processed for whole proteome mass spectrometry analysis.

### 3.3.3.1: Quantitative analysis

To investigate the effect of BCL6 inhibition on the whole proteome of LN18 cells, quantitative analysis of protein expression in FX1 treated cells (+DMSO vehicle) compared to untreated cells (+DMSO vehicle) was performed. Protein abundance ratios were calculated by pairwise comparison between the FX1 and DMSO treated replicates (three biological and two technical replicates each). Proteins were considered differentially expressed if their expression was changed more than two-fold compared to the DMSO controls with an adjusted p value $\leq 0.05$ (Benjamini-Hochberg multiple comparisons testing). FX1 treatment resulted in upregulation of 230 proteins and downregulation of 263 proteins.

### 3.3.3.2: Functional enrichment analysis

Functional enrichment analysis of the proteins up- and downregulated by FX1 treatment of LN18 GBM cells revealed some similar trends to the effects of the chemo- and radiotherapy treatments (Figure 3.11). Like the acute IR and doxorubicin treatments, FX1 treatment upregulated mitochondrial proteins. These were annotated to the enriched GO:CC terms *mitochondrial-protein containing complex* (p = 1.59E-6), *mitochondrial envelope* (p = 3.14E-5) and *mitochondrial matrix* (1.84E-3). As with the acute IR and doxorubicin treatments, mitochondrial proteins upregulated by FX1 included proteins involved in protein import into the mitochondria and subunits of respiratory chain complexes. FX1 treatment also upregulated mitochondrial ribosome subunits and proteins involved in mitochondrial metabolism. Interestingly, proteins downregulated by FX1 treatment were enriched for the GO:CC term *mitochondrial intermembrane space* (p = 5.59E-3). The eight downregulated proteins annotated to this term were involved in respiratory chain assembly, protein import and folding, protection against

mitochondrial stress and the mitochondrial apoptotic pathway. As with the acute treatments, this suggested changes in mitochondrial activity to manage stress.

Like acute IR, FX1 upregulated proteins enriched for GO:BP terms *intracellular protein transport* (p = 3.87E-3) and *protein targeting* (p = 5.43E-3) as well as ER membrane proteins annotated to the enriched GO:CC term *intrinsic component of endoplasmic reticulum membrane* (p = 3.04E-4). Like both acute IR and doxorubicin, proteins downregulated by FX1 in LN18 cells showed enrichment for the GO:BP term *mRNA metabolic process* (p = 1.99E-3), which contained several proteins involved in mRNA splicing. These common themes indicated that FX1 induced the same general stress responses common to the acute chemo- and radiotherapy treatments.

In contrast to the acute treatments, proteins upregulated by FX1 were enriched for the GO:BP terms *ribosome* (p = 2.05E-3) and *ribonucleoprotein complex biogenesis* (p = 1.47E-2). Downregulation of proteins annotated to these terms was seen in response to TMZ, doxorubicin and 48 hours after acute IR. This suggested that the cellular response to FX1 was not exactly like the responses seen with the acute treatments.

Microtubule-related proteins were also downregulated by FX1 in LN18 cells. These proteins were annotated to the enriched GO:BP term *microtubule-based process* (p = 1.65E-2) and GO:CC terms *centrosome* (p = 3.01-3) and *microtubule organising centre* (p = 4.02E-3). Several of the microtubule-related proteins were also involved in mitotic spindle processes, including those annotated to the enriched GO:CC terms *condensed chromosome, centromeric region* (p = 6.93E-3) and *kinetochore* (2.16E-2). This may indicate that FX1 caused arrest in another stage of the cell cycle, thereby downregulating proteins required in M phase. Proteins downregulated by FX1 also included proteins involved in transcription, DNA replication and DNA repair and annotated to the enriched term *nuclear body* (p = 1.44E-3) along with mRNA splicing proteins.

FX1 is designed to be selective for BCL6, however it could have off-target effects. This was assessed using the chronic myeloid leukaemia cell line K562. This cell line is commonly used as a *BCL6-null* control and was shown to have 3.6-fold lower expression of BCL6 mRNA than LN18 cells, with expression barely above background noise (Appendix). Treatment of K562 cells with FX1 suggested that most of the response of LN18 cells to FX1 was likely due to inhibition of BCL6 activity, rather than due to off-target effects (Appendix).[381–383] Proteins upregulated by FX1 in K562 cells were enriched for ribosome biogenesis, chromatin organisation, mRNA processing and mitosis. Apart from ribosome biogenesis, these functional groups of proteins were downregulated by FX1 in LN18 cells. The proteins downregulated by FX1 in K562 cells were enriched for mRNA processing, vesicle transport terms and DNA replication. Contrastingly, vesicle transport proteins were upregulated by FX1 in LN18 cells. Reassuringly, the striking upregulation of mitochondrial proteins was not observed in the K562 cell line.

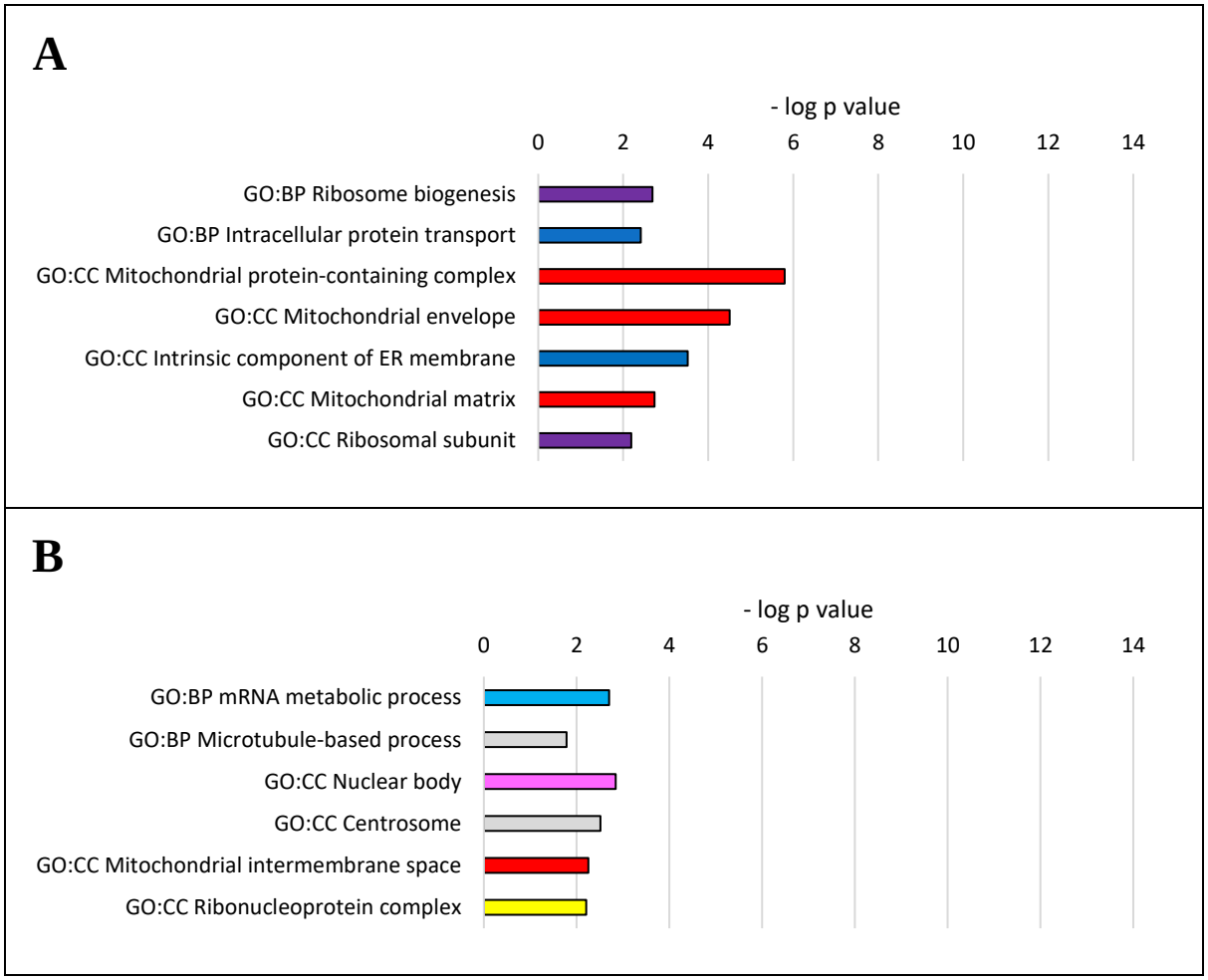


Figure 3.11: Functional enrichment of proteins up- and downregulated by FX1 treatment in LN18 cells

Up to five most significantly enriched (highest – log p value) parent GO:BP and GO:CC terms from analysis of proteins (A) upregulated and (B) downregulated by FX1. Common enrichments between treatments colour coded for comparison with figures in section 3.3.2.2: orange = organelle membrane component, purple = ribosome or ribosome biogenesis, green = cell division, yellow = ribonucleoprotein complex, red = mitochondrial, light blue = protein transport or targeting, dark blue = transferase complex, purple = chromosome, pink = nuclear body.

#### 3.3.3.2 Summary of effects of FX1 on the proteome of LN18 cells

In response to BCL6 inhibition by FX1, LN18 GBM cells upregulated mitochondrial proteins and proteins involved in protein transport and ribosome biogenesis. Additionally, BCL6 inhibition led to the downregulation of proteins involved in mRNA processing, microtubule proteins and a variety of nuclear proteins involved in transcription, DNA repair and DNA replication. The downregulation of mRNA processing and DNA replication proteins and the upregulation of ribosome biogenesis proteins may be at least partly due to off-target effects of FX1 as proteins annotated to these terms were also affected by FX1 in *BCL6-null* K562 cells. The upregulation of mitochondrial and protein transport proteins observed in the LN18 cells in response to FX1 was not seen in the K562 cells. The upregulation of proteins in these terms and the downregulation of mRNA processing were commonly seen in response to the acute treatments. This suggested that these are common stress responses. Assuming that these were not off-target effects of FX1, the differential expression of proteins in these same functional terms in response to FX1 implied that inhibition of BCL6 activity led to cell stress comparable to that caused by acute IR and doxorubicin treatment in LN18 cells. This reinforces the importance of BCL6 for the survival of GBM cells.

## 3.3.4: Effects of FX1 on treated LN18 GBM cells

Sections 3.3.2 and 3.3.3 investigated the effects of five treatments and of BCL6 inhibition separately on the whole proteome of LN18 GBM cells. With these effects established, this section examines the effect of BCL6 inhibition on the whole proteome response of LN18 cells to each therapy. LN18 cells were treated with each therapy + DMSO vehicle or with each therapy + the BCL6 inhibitor FX1 in DMSO vehicle. Proteins were extracted from the harvested cells and processed for whole proteome mass spectrometry analysis. This enabled quantitative comparison of protein expression in treated LN18 cells with and without BCL6 inhibition.

### 3.3.4.1: Comparison of proteins up- and downregulated by treatments with and without FX1

There were two main datasets generated in this chapter (listed below). To decipher the role of BCL6 in the therapy response of LN18 GBM cells, it was useful to compare the dataset analysed in section 3.3.2 (dataset 1 below) to the dataset generated in this section (dataset 2 below).

1. Differential protein expression in treated LN18 cells compared to in untreated LN18 cells (section 3.3.2).
2. Differential protein expression in treated LN18 cells with inhibited BCL6 (FX1-treated) compared to in untreated LN18 cells.

For each dataset, proteins were considered differentially expressed if proteins had a $\geq$ 2-fold change in abundance with adjusted p value $\leq$ 0.05 (Benjamini-Hochberg multiple comparisons testing). A generalised example of the comparison of these two datasets is shown in Figure 3.12. This analysis enabled the division of proteins up- or downregulated by treatment compared to control into those that were only differentially expressed in response to treatment when BCL6 was not inhibited (section i) and those that were differentially expressed in response to treatment regardless of BCL6 activity (section iii).

As the proteins in section i were only differentially expressed in response to treatment when BCL6 was not inhibited (i.e. they were not in section ii or iii), these proteins were good candidates for revealing the role of BCL6 in the therapy response of GBM cells. It must be kept in mind that BCL6 may regulate some of these proteins directly, but others may change in expression due to downstream effects of BCL6 activity. Additionally, the level of dependence on BCL6 activity is likely to vary, with other protein activities being important alongside BCL6. Nevertheless, for ease of description, the proteins that were only differentially expressed in response to treatment when BCL6 was not inhibited are referred to as ‘BCL6-dependent’ in this thesis.

The proteins in section iii were not informative for this study as they represented the treatment responses that occurred regardless of BCL6 activity. The proteins in section ii were not informative for the purposes of this chapter either as they were only differentially expressed when BCL6 was inhibited in treated cells compared to control and so were not part of the usual response to therapy. The comparison demonstrated in Figure 3.12 was made for each of the five treatments and the proteins in the informative section i were investigated further.

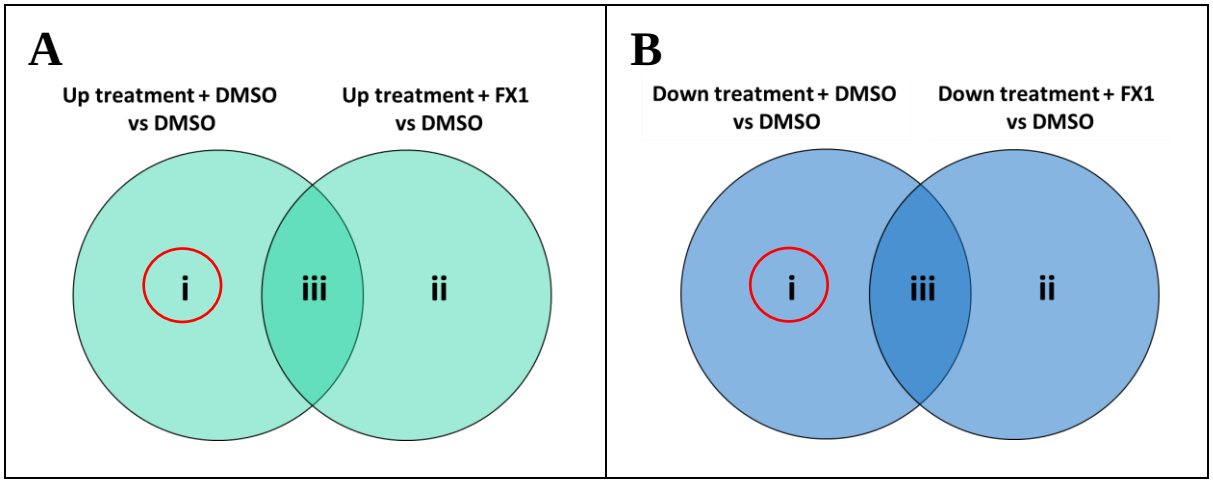


Figure 3.12: Example comparison between whole proteome datasets

General example of the comparison made for proteins (A) up- and (B) downregulated by each treatment in the two datasets discussed above. The sections of interest are circled in red.

The percentage of proteins up- or downregulated by each treatment (sections i + iii) and that were only up- or downregulated when BCL6 was uninhibited (section i) are shown in Table 3.3. Higher percentages of the proteins upregulated by fractionated IR and TMZ were dependent on BCL6 activity. This suggested that the responses of LN18 cells to the more clinically relevant treatments were more reliant on BCL6 activity than the responses to the three acute treatments.

For each treatment, g:Profiler multi-queries were used to compare the number of proteins annotated to enriched functional terms when analysing the total response compared to the BCL6-dependent response. An example of this comparison and its implications is shown in Figure 3.13. When the two bars were similar in size (for example Figure 3.13, top category), this indicated that the up- or downregulation of these proteins was dependent on BCL6. However, if the dark blue bar was longer than the light blue bar (for example Figure 3.13, bottom category), this indicated that the up- or downregulation of these proteins was largely independent of BCL6 activity.

STRING analysis was used to visualise the functional networks of proteins whose differential expression in response to treatment was dependent on BCL6 activity.[332] As the STRING analysis used

a different version of g:Profiler to calculate functional enrichment, the p values were different to when the proteins were analysed directly with g:Profiler. Therefore, p values were not stated when describing functional clusters seen with STRING.

Table 3.3: Percentage of treatment responses dependent on BCL6

Percentages calculated from the number of proteins in section i compared to in sections i + iii (Figure 3.12) in each treatment comparison.

| Treatment | Percentage of proteins dependent on BCL6 for upregulation by treatment (Figure 3.12A, section i) | Percentage of proteins dependent on BCL6 for downregulation by treatment (Figure 3.12B, section i) |
|---|---|---|
| **Fractionated irradiation** | 63% | 68% |
| **24 hours after acute irradiation** | 47% | 34% |
| **48 hours after acute irradiation** | 52% | 39% |
| **Temozolomide** | 65% | 55% |
| **Doxorubicin** | 42% | 28% |

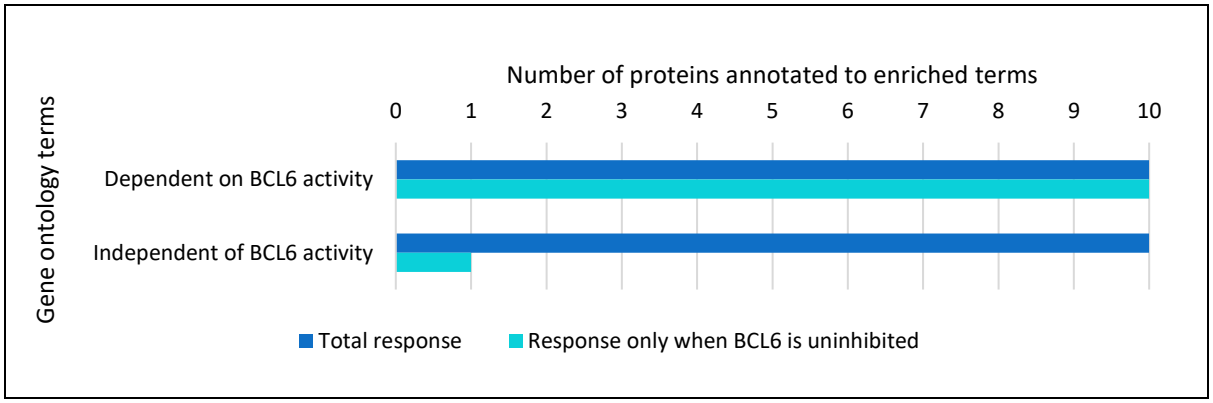


Figure 3.13: Example of g:Profiler multi-query data indicating that a response is dependent or independent of BCL6 activity

General example of the comparison of proteins up- or downregulated in the total treatment response (Figure 3.12A and B section i + iii, shown here in dark blue bars) to the proteins up- or downregulated by treatment only when BCL6 was uninhibited (Figure 3.12A and B section i, shown here in light blue bars). Enriched gene ontology terms are listed on the y axis and the number of proteins annotated to each term in section i + iii compared to section i are shown on the x axis.

### 3.3.4.2: The role of BCL6 in the whole proteome response of LN18 cells to fractionated irradiation

The comparisons demonstrated in Figure 3.12 were made for the fractionated IR datasets (Figure 3.14).

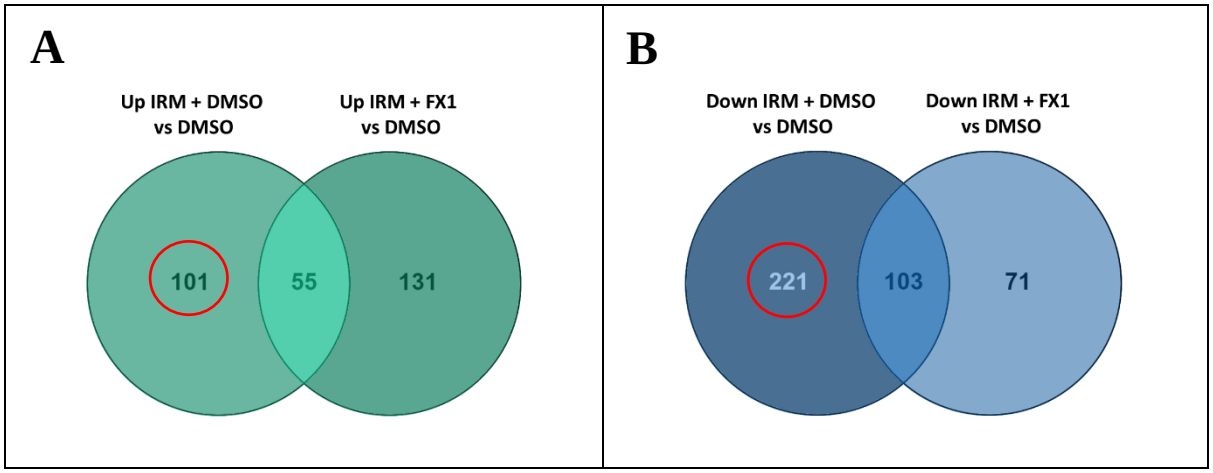


Figure 3.14: Comparison of +/- FX1 datasets to examine the role of BCL6 in the whole proteome response of LN18 cells to fractionated IR

Comparison of A) Proteins upregulated by fractionated multiple dose IR (IRM) + DMSO compared to DMSO alone vs proteins upregulated by fractionated multiple dose IR (IRM) + FX1 compared to DMSO; B) Proteins downregulated by fractionated multiple dose IR (IRM) + DMSO compared to DMSO alone vs proteins downregulated by fractionated multiple dose IR (IRM) + FX1 compared to DMSO. The BCL6-dependent proteins suggested by this comparison are circled in red.

Fractionated IR treatment of LN18 cells upregulated proteins involved in protein trafficking and translation and downregulated proteins involved in cell division and DNA repair (section 3.3.2). Table 3.3 shows that 63% of the proteins upregulated by fractionated IR were only upregulated when BCL6 was not inhibited (i.e. BCL6-dependent upregulation). Similarly, 68% of the proteins downregulated by fractionated IR were only downregulated when BCL6 was not inhibited (i.e. BCL6-dependent downregulation). This suggested that BCL6 had an important role in the response of LN18 cells to fractionated IR.

Functional enrichment analysis of the 101 proteins dependent on BCL6 for upregulation by fractionated IR (Figure 3.14A) did not reveal enrichment of protein trafficking and translation terms. However, comparative g:Profiler multi-query analysis (Figure 3.15A) revealed that some proteins annotated to GO:BP terms *integral component of organelle membrane* (p = 4.78E-3) and *integral component of ER membrane* (p = 1.41E-2) were BCL6-dependent. This suggested that BCL6 was involved in the upregulation of some of the proteins in these terms, but other proteins involved in trafficking across organelle membranes were upregulated independently of BCL6 activity. Additionally, some of the

ribosome-related proteins upregulated by fractionated IR were dependent on BCL6 (Figure 3.15A). The STRING analysis also revealed a small cluster of proteins involved in ribosome biogenesis.

The GO:BP term *mitotic spindle midzone assembly* (p = 1.37E-2), containing three upregulated proteins, was dependent on BCL6 for upregulation by fractionated IR (Figure 3.15A). Additionally, STRING analysis (Figure 3.15B) revealed BCL6-dependent upregulation of a larger cluster of proteins involved in cell division (Figure 3.15B: red), especially in promotion of mitosis (Figure 3.15B: blue). These and other proteins in the STRING network were also annotated to the GO:BP term *chromosome organisation* (Figure 3.15B: green). Some of these proteins were involved in DNA replication. These results were surprising, as findings in section 3.3.2 indicated that LN18 cells downregulated cell division proteins involved in promotion of mitosis, spindle organisation and DNA replication in response to fractionated IR. Furthermore, g:Profiler multi-query analysis of the proteins downregulated in response to fractionated IR revealed that the downregulation of several proteins involved in cell division was dependent on BCL6, while others were downregulated regardless of BCL6 inhibition. Therefore, while there was an overall downregulation of cell division proteins in response to fractionated IR, BCL6 was involved in both up- and downregulation of cell division proteins within this response.

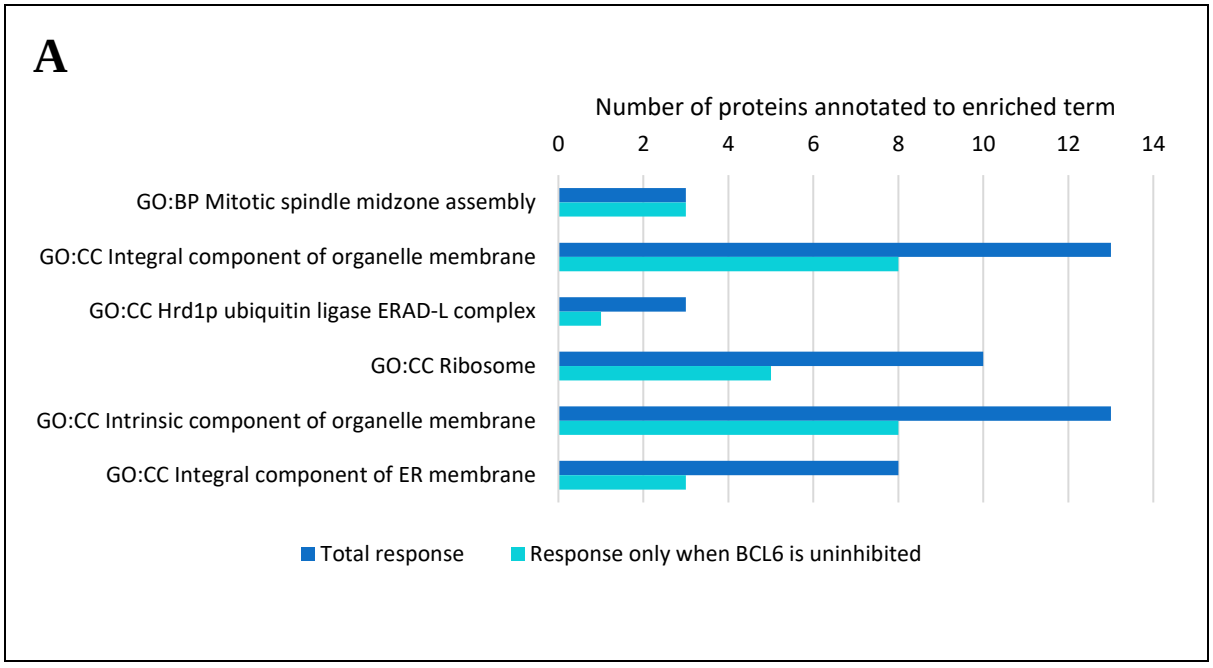

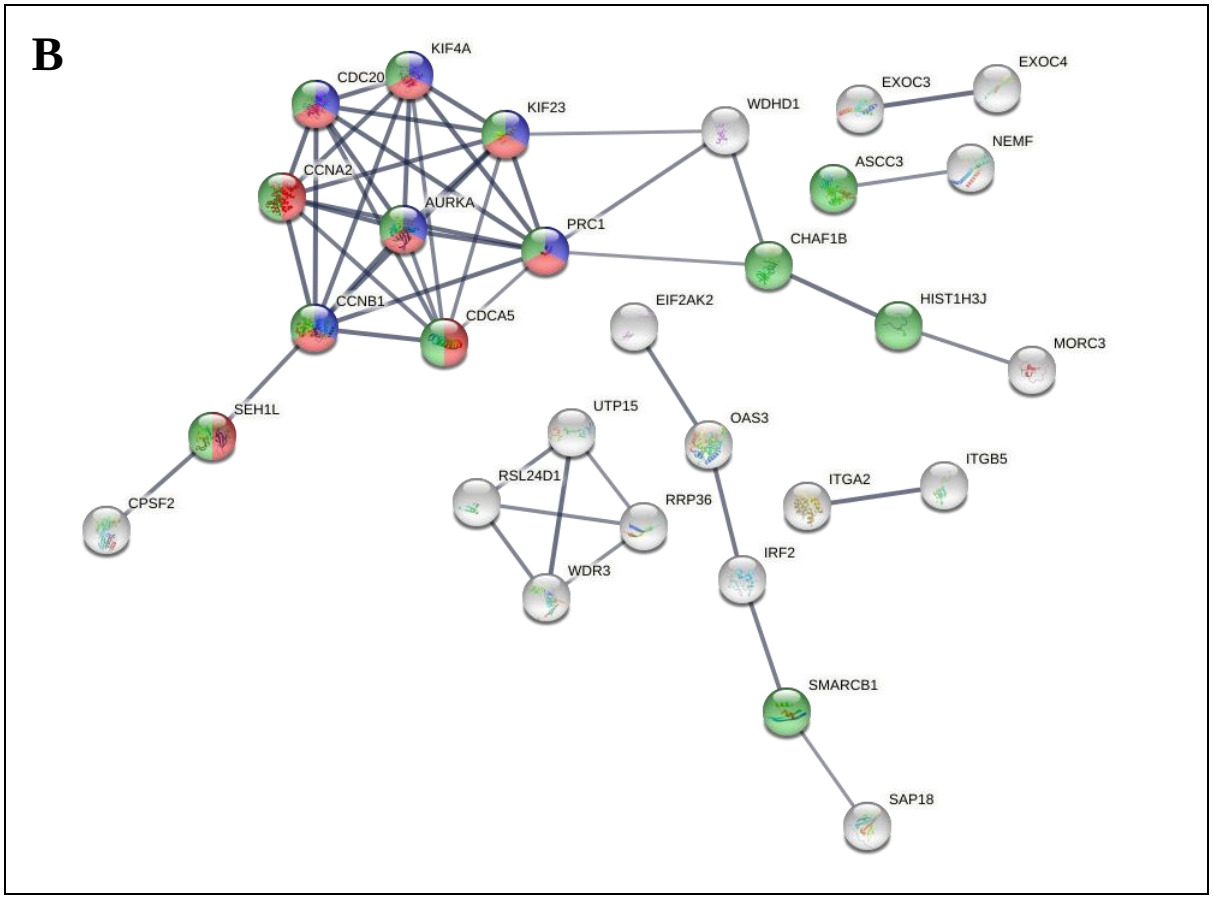


Figure 3.15: Proteins dependent on BCL6 for upregulation by fractionated IR

A) Plot comparing the number of upregulated proteins annotated to each enriched functional term in the total LN18 whole proteome response to fractionated IR (dark blue) compared to the LN18 whole proteome response to fractionated IR that only occurred when BCL6 was uninhibited (light blue). B) STRING network of proteins dependent on BCL6 for upregulation by fractionated IR in LN18 cells. Red = *cell division*, blue = *spindle organisation* and green = *chromosome organisation*. Edges indicate both functional and physical protein interactions and the thickness of the edges indicates confidence. Only edges with high confidence (minimum required interaction score 0.7) are shown and disconnected nodes are hidden. Interactions are sourced from textmining, experiments, databases, co-expression, neighbourhood and co-occurrence.

Functional enrichment analysis of the 221 proteins dependent on BCL6 for downregulation by fractionated IR (Figure 3.14B) revealed enrichment for the GO:BP term *cellular response to DNA damage stimulus* (p = 1.47E-2). g:Profiler multi-query analysis (Figure 3.16A) showed that the downregulation of almost all of the proteins annotated to this term was dependent on BCL6 activity. Furthermore, STRING analysis (Figure 3.16B) showed a cluster of proteins involved in the DNA damage response (Figure 3.16B: blue), especially in DNA repair (Figure 3.16B: red). These included TIMELESS and TIPIN, which are important for cell survival after DNA damage, and proteins involved in double strand break repair, such as BLM, RMI2 and NBN.[359–362,384,385] Enrichment for this term was masked by the greater number of proteins when all of the proteins downregulated in response to

fractionated IR were analysed. Therefore, in response to DNA damage by fractionated IR, BCL6 repressed the DNA damage response, as it does in GC B cells (section 1.2.2).

Functional enrichment analysis of the proteins dependent on BCL6 for downregulation by fractionated IR also revealed enrichment for the GO:BP term *positive regulation of gene silencing by miRNA* (p = 2.61E-2). The five downregulated proteins annotated to this term were only downregulated by fractionated IR when BCL6 was uninhibited, indicating that BCL6 was important for this response. STRING analysis of the proteins dependent on BCL6 for downregulation by fractionated IR revealed that many were annotated to the term *gene expression* and *nucleic acid binding* (Figure 3.16B: green and yellow respectively). These included proteins involved in RNA processing and in transcriptional regulation, including RNF2 which is shown in Chapter 4 to be associated with BCL6 in untreated GBM cells.[386]

The proteins dependent on BCL6 for differential expression in response to fractionated IR were revealing of the role of BCL6 in the response of LN18 cells to this therapy. In this context, BCL6 retained its known function as a repressor of the DNA damage response, particularly of DNA repair proteins (see section 1.2.2). Additionally, in response to fractionated IR, BCL6 was involved in regulating gene expression by downregulating expression of transcription factors, RNA processing factors and proteins involved in gene silencing by miRNA. While cell division proteins were generally downregulated in response to fractionated IR, BCL6 was involved in both up- and downregulation of cell division proteins within this response. It is possible that BCL6 was involved in the complex balance that is likely required to keep LN18 cells proliferating but perhaps at a slower rate.

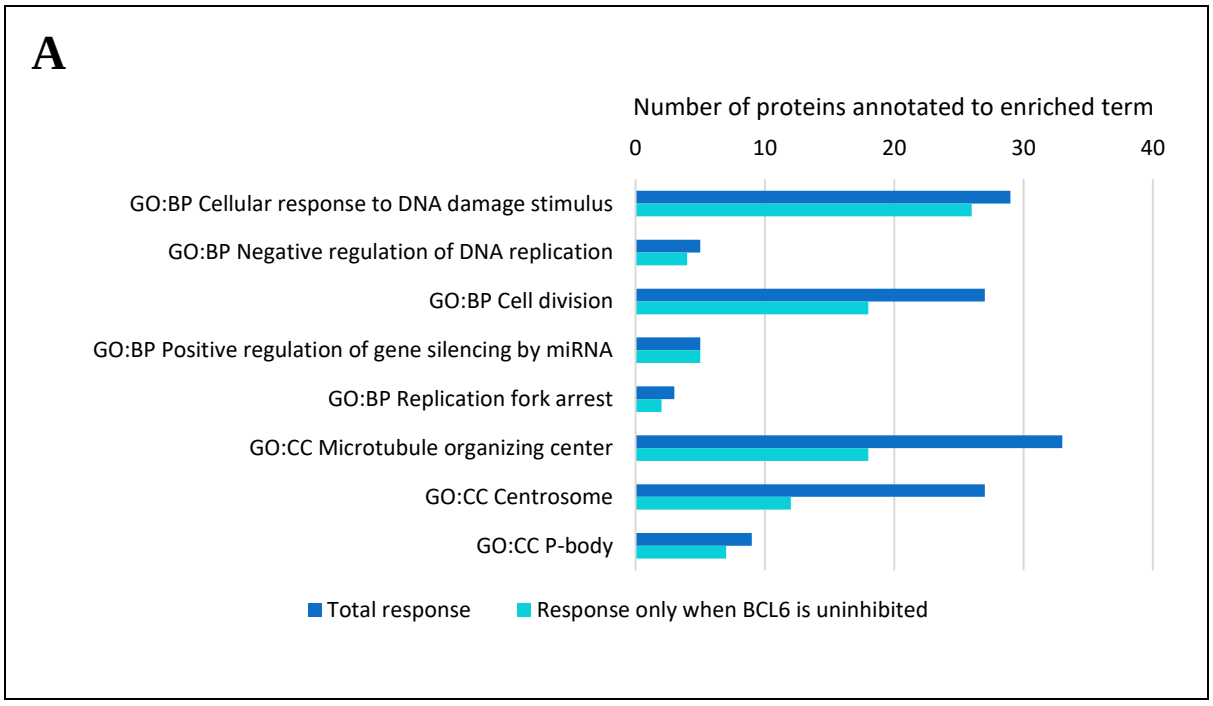

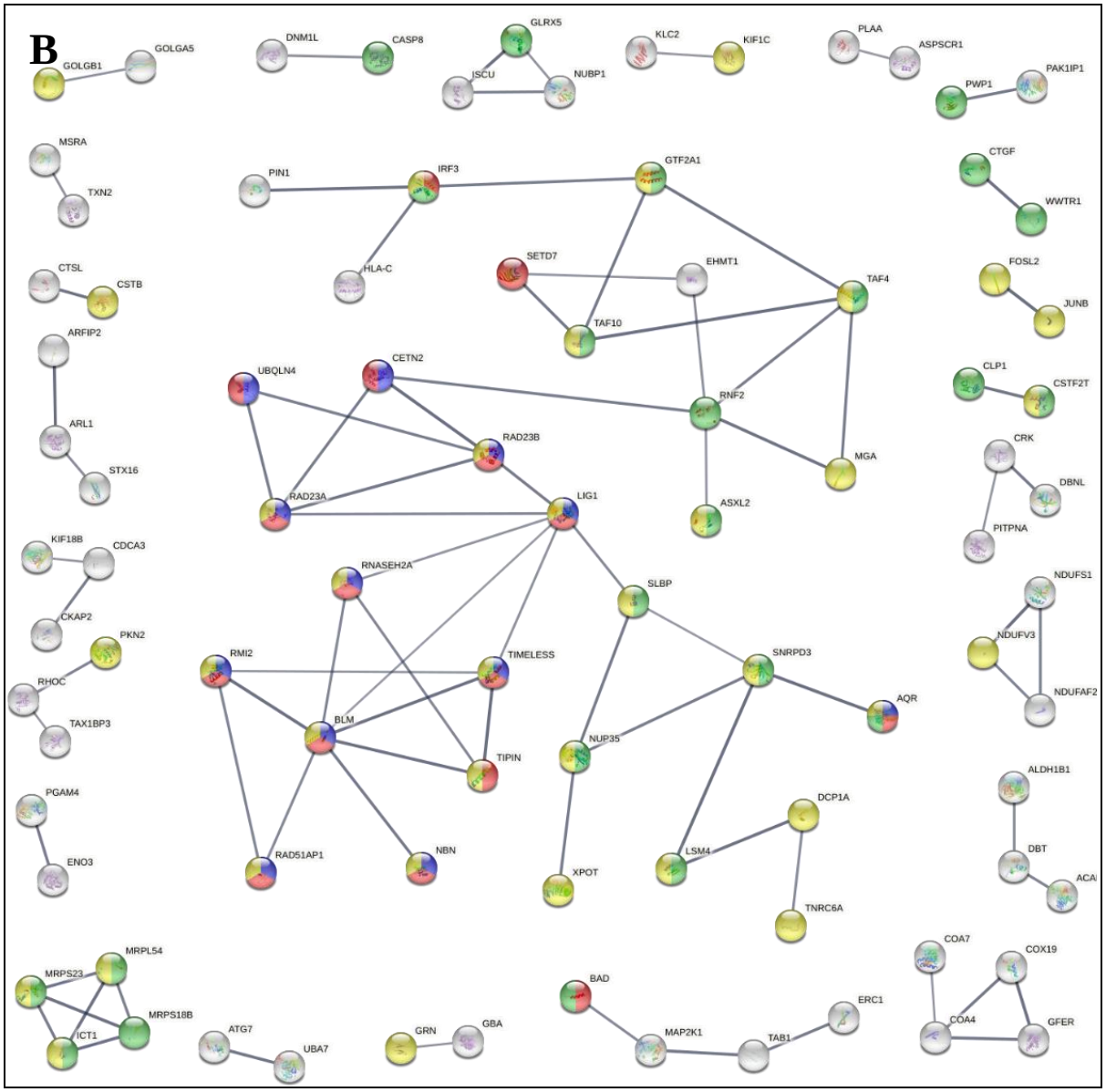


Figure 3.16: Proteins dependent on BCL6 for downregulation by fractionated IR

A) Plot comparing the number of downregulated proteins annotated to each enriched functional term in the total LN18 whole proteome response to fractionated IR (dark blue) compared to the LN18 whole proteome response to fractionated IR that only occurred when BCL6 was uninhibited (light blue). B) STRING network of proteins dependent on BCL6 for downregulation by fractionated IR in LN18 cells. Red = *cellular response to DNA damage stimulus*, blue = *DNA repair*, green = *gene expression* and yellow = *nucleic acid binding.* Edges indicate both functional and physical protein interactions and the thickness of the edges indicates confidence. Only edges with high confidence (minimum required interaction score 0.7) are shown and disconnected nodes are hidden. Interactions are sourced from textmining, experiments, databases, co-expression, neighbourhood and co-occurrence.

### 3.3.4.3: The role of BCL6 in the whole proteome response of LN18 cells to temozolomide

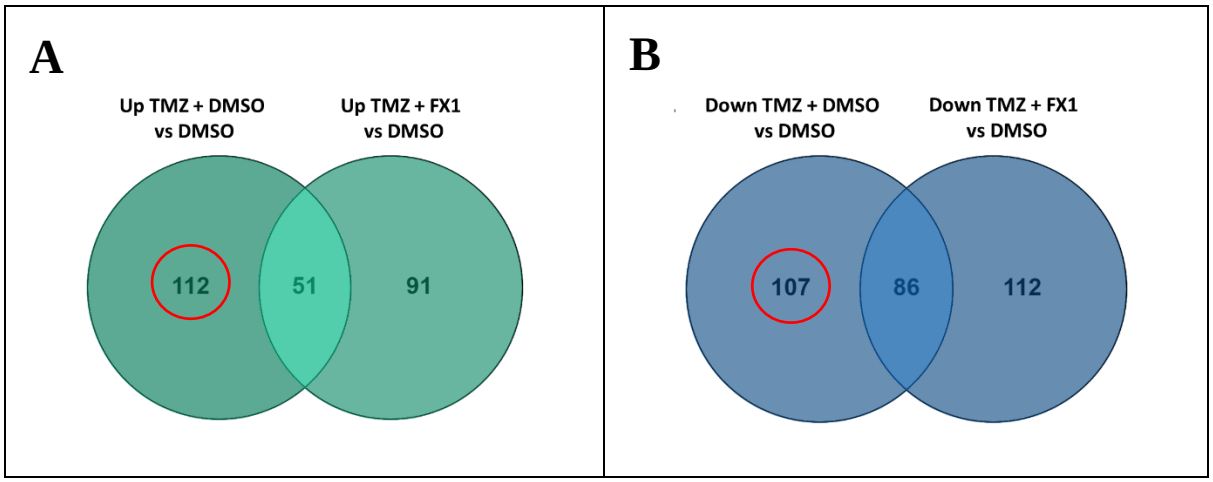


Figure 3.17: Comparison of +/- FX1 datasets to examine the role of BCL6 in the whole proteome response of LN18 cells to TMZ

Comparison of A) Proteins upregulated by TMZ + DMSO compared to DMSO alone vs proteins upregulated by TMZ + FX1 compared to DMSO; B) Proteins downregulated by TMZ + DMSO compared to DMSO alone vs proteins downregulated by TMZ + FX1 compared to DMSO. The BCL6-dependent proteins suggested by this comparison are circled in red.

TMZ treatment of LN18 cells caused downregulation of proteins involved in protein degradation, ribosome biogenesis and protein trafficking, suggesting decreased protein turnover and transport (section 3.3.2). TMZ treatment also upregulated proteins involved in mRNA splicing, histone modification, mitotic checkpoints and the maintenance of telomeres (section 3.3.2). Table 3.3 shows that 65% of the proteins upregulated by TMZ and 55% of the proteins downregulated by TMZ were dependent on BCL6 for differential expression in response to TMZ. As with fractionated IR, this suggested that BCL6 was important in the response of LN18 cells to TMZ.

Functional enrichment analysis of the 112 proteins dependent on BCL6 for upregulation by TMZ (Figure 3.17A) revealed enrichment for the same chromosomal and ribonucleoprotein complex terms observed in the total whole proteome response to TMZ. Indeed, g:Profiler multi-query analysis showed that most of the chromosomal and ribonucleoprotein proteins upregulated by TMZ were dependent on BCL6 activity (Figure 3.18A). The chromosome-related terms contained proteins involved in mitosis, telomere regulation and transcriptional regulation, including histone modifiers. The ribonucleoprotein term contained a handful of proteins involved in mRNA splicing. Furthermore, the proteins only upregulated by TMZ when BCL6 was uninhibited were enriched for the GO:MF term *telomeric DNA binding* ($p = 2.39E\text{-}2$). These four regulators of telomere length and protection, ROA1, TERF2, EST1A and ACD were only upregulated by TMZ when BCL6 was uninhibited, indicating that this response was dependent on BCL6 activity.[387–390]

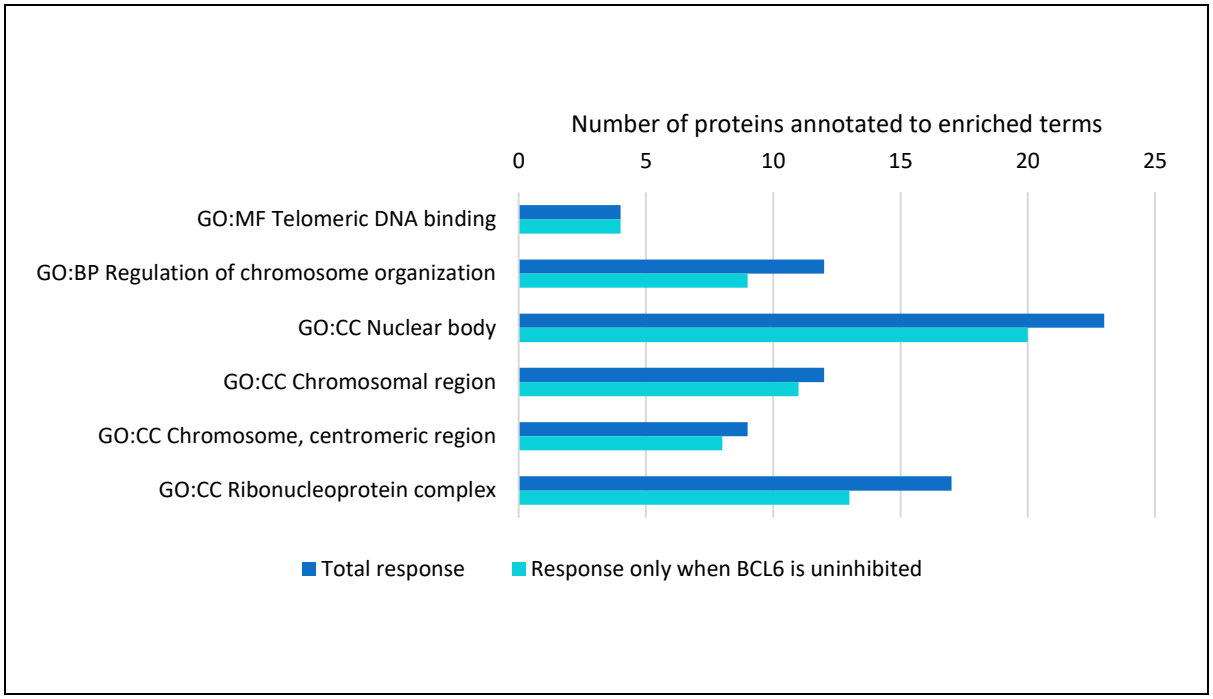


Figure 3.18: Proteins dependent on BCL6 for upregulation by TMZ

Plot comparing the number of upregulated proteins annotated to each enriched functional term in the total LN18 whole proteome response to TMZ (dark blue) compared to the LN18 whole proteome response to TMZ that only occurred when BCL6 was uninhibited (light blue). STRING analysis for the proteins upregulated by TMZ was not informative and so is not included as a figure.

Similarly, a large amount of the TMZ-induced downregulation of ribosome biogenesis, protein trafficking and protein degradation was dependent on BCL6 activity (Figure 3.19A). The STRING analysis showed that of the 107 proteins dependent on BCL6 for downregulation by TMZ, 34 were annotated to the GO:BP term *cellular localisation* (Figure 3.19B: red) and 23 to the more specific terms *cellular protein localisation* (Figure 3.19B: blue) and *intracellular protein transport* (Figure 3.19B: green). Furthermore, proteins dependent on BCL6 for downregulation by TMZ were enriched for the GO:BP term *nucleocytoplasmic transport* (p = 1.59E-3). g:Profiler multi-query analysis indicated that the downregulation of nucleocytoplasmic transport proteins in response to TMZ was dependent on BCL6-activity (Figure 3.19A). STRING analysis showed a handful of proteins involved in the export of mRNA (THOC6, DDX39A and SLBP) and tRNA (XPOT) from the nucleus to the cytoplasm and the import of proteins into the nucleus (IPO5 and IPO9) scattered throughout the STRING clusters and annotated to the *nucleocytoplasmic transport* term (Figure 3.19B: yellow).[391–395] Additionally, g:Profiler multi-query analysis (Figure 3.19A) showed that many but not all of the proteins annotated to GO:BP terms *exocytic process* (p = 3.41E-2) were only downregulated when BCL6 was uninhibited. This indicated that the downregulation of protein trafficking resulting from TMZ treatment of LN18 cells was at least partly dependent on the activity of BCL6.

Some of the proteins involved in nucleocytoplasmic transport (XPOT, IPO5 and IPO9) were linked to a small cluster of proteins involved in ribosome biogenesis (KRI1, PAK1IP1, GLTSCR2 and DNAJC21).[396–398] g:Profiler multi-query analysis showed that many but not all of the proteins annotated to GO:BP term *rRNA transcription* (p = 4.96E-2) and GO:CC term *transcription factor TFIIC complex* (p = 6.34E-3) were dependent on BCL6 for downregulation by TMZ (Figure 3.19A). Additionally, many of the proteins annotated to GO:BP term *regulation of proteolysis* (p = 4.05E-2) and GO:CC term *peptidase complex* (p = 1.72E-2) were dependent on BCL6 for downregulation by TMZ. This suggested that BCL6 was involved in the downregulation of ribosome biogenesis and protein degradation proteins seen in response to TMZ, although it was not fully responsible. Additionally, a variety of transcription factors were downregulated in response to TMZ only when BCL6 was uninhibited and were annotated to the enriched GO:MF term *transcription factor binding* (p = 3.87E-2).

Interestingly, the role of BCL6 in the response of LN18 GBM cells to TMZ was quite different to its role in the response to fractionated IR. In response to fractionated IR, BCL6 appeared to repress the DNA damage response, as it does canonically. This was not seen in response to TMZ. Instead, BCL6 was involved in most of the whole proteome functional changes seen in response to TMZ, including the downregulation of protein trafficking, protein degradation and ribosome biogenesis and the upregulation of mRNA splicing, histone modification and mitotic proteins. BCL6 was required for the downregulation of nucleocytoplasmic transport and the upregulation of telomere regulatory proteins. Additionally, the altered expression of several transcription factors in response to TMZ was dependent on BCL6, suggesting alteration of the transcriptional program along with reduced protein trafficking and turnover.

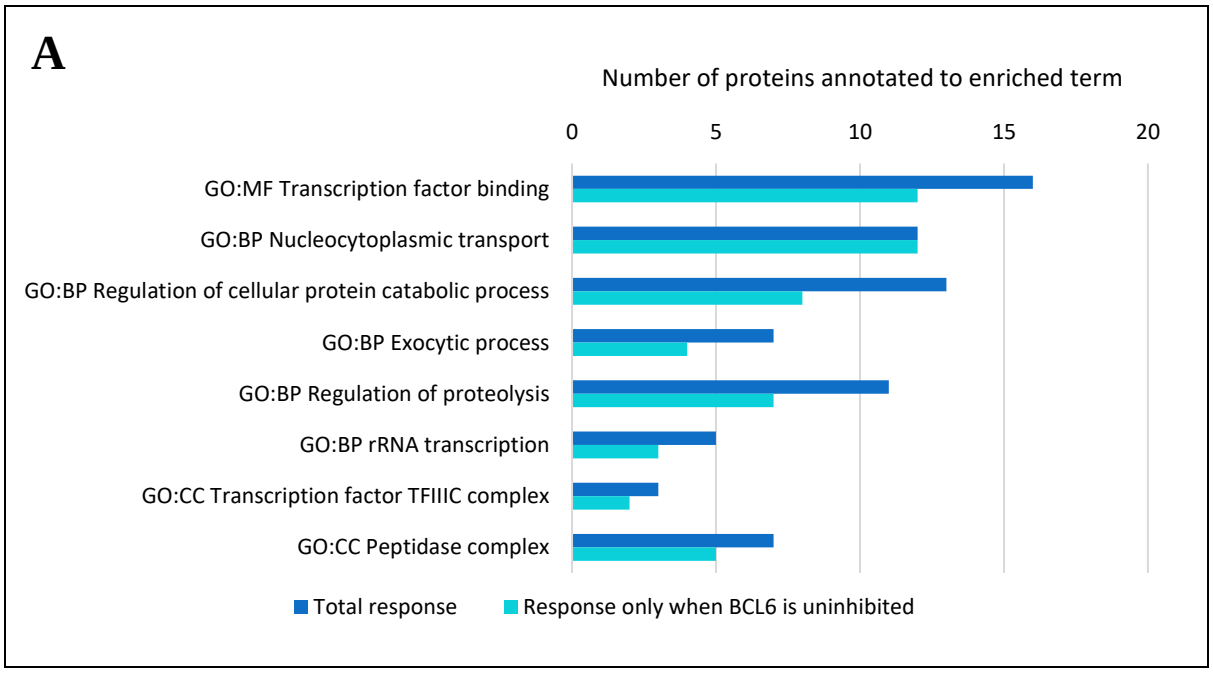

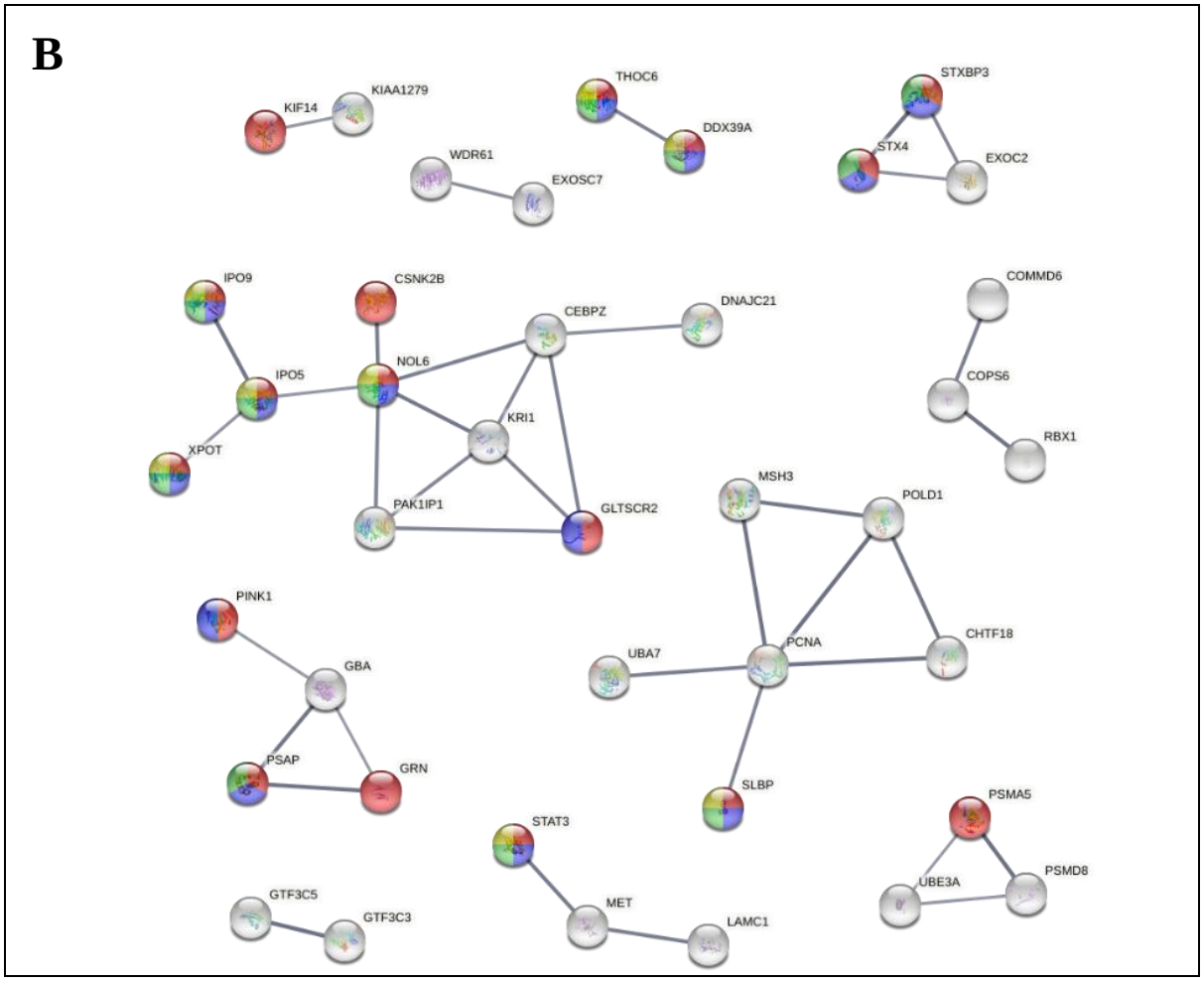


Figure 3.19: Proteins dependent on BCL6 for downregulation by TMZ

A) Plot comparing the number of downregulated proteins annotated to each enriched functional term in the total LN18 whole proteome response to TMZ (dark blue) compared to the LN18 whole proteome response to TMZ that only occurred when BCL6 was uninhibited (light blue). B) STRING network of proteins dependent on BCL6 for downregulation by TMZ in LN18 cells. Red = *cellular localisation*, blue = *cellular protein localisation*, green = *intracellular protein transport* and yellow = *nucleocytoplasmic transport*. Edges indicate both functional and physical protein interactions and the thickness of the edges indicates confidence. Only edges with high confidence (minimum required interaction score 0.7) are shown and disconnected nodes are hidden. Interactions are sourced from textmining, experiments, databases, co-expression, neighbourhood and co-occurrence.

### 3.3.4.4: The role of BCL6 in the whole proteome response of LN18 cells 24 hours after acute irradiation

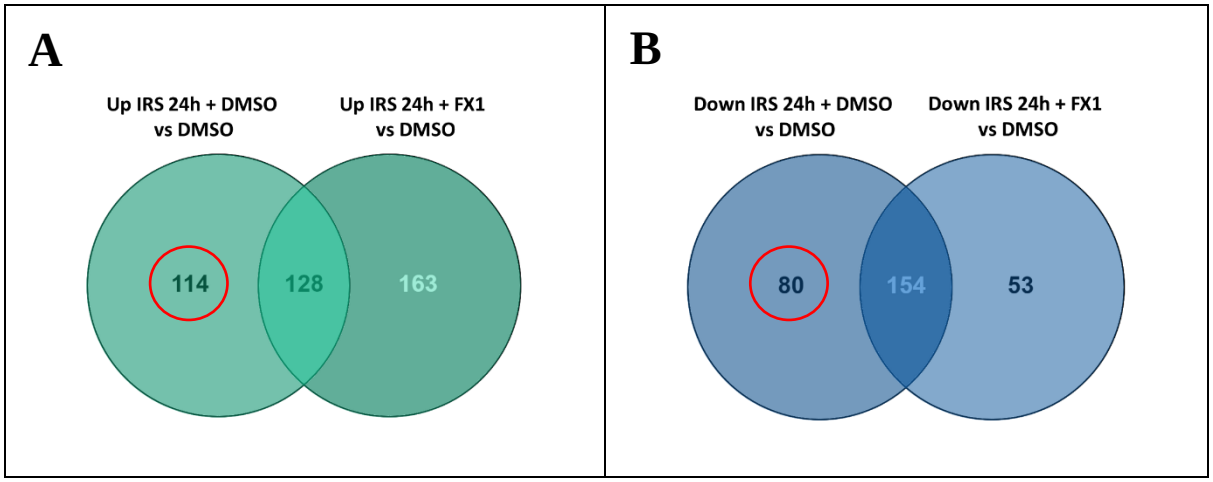


Figure 3.20: Comparison of +/- FX1 datasets to examine the role of BCL6 in the whole proteome response of LN18 cells 24 hours after acute IR

Comparison of A) Proteins upregulated 24 hours after single dose acute IR (IRS 24h) + DMSO compared to DMSO alone vs proteins upregulated 24 hours after single dose acute IR (IRS 24h) + FX1 compared to DMSO; B) Proteins downregulated 24 hours after single dose acute IR (IRS 24h) + DMSO compared to DMSO alone vs proteins downregulated 24 hours after single dose acute IR (IRS 24h) + FX1 compared to DMSO. The BCL6-dependent proteins suggested by this comparison are circled in red.

Section 3.3.2 showed that by 24 hours after acute IR, LN18 cells had upregulated mitotic proteins, suggesting cell cycle arrest at G2/M. Mitochondrial and ER proteins were also upregulated, including proteins involved in transport into these organelles. Proteins involved in mRNA splicing were downregulated 24 hours after acute IR. Unlike with the two longer-term treatments, more than 50% of the proteins up- and downregulated 24 hours after acute IR were not dependent on BCL6 activity (Table 3.3). However, 47% of the proteins upregulated and 34% of the proteins downregulated 24 hours after acute IR were dependent on BCL6 (Table 3.3). Therefore, BCL6 did have some role in the response of LN18 cells to acute IR.

However, g:Profiler multi-query analysis revealed that only around 50% of the proteins annotated to the protein targeting, mitochondrial and cell division terms were dependent on BCL6 (Figure 3.21A). Even fewer of the upregulated ER and ribosome biogenesis proteins were dependent on BCL6 activity. The exception to this was the proteins annotated to the GO:BP term *protein transmembrane transport* ($p = 3.91E\text{-}2$), which was only significantly enriched when the proteins dependent on BCL6 for upregulation were analysed. This suggested that BCL6 was required for the increase in protein transport across the mitochondrial and ER membranes. STRING analysis showed that upregulated proteins scattered between multiple clusters were involved in establishment of protein localisation (Figure 3.21B: red). One STRING cluster contained several proteins annotated to the *mitochondrial envelope*

(Figure 3.21B: blue). These included proteins involved in protein transport across the inner mitochondrial membrane (TIMM44, TIMM22, TIMM23B and AGK), mitochondrial ribosome proteins (MRPL37, MRPL18 and MRPS7) and a subunit of respiratory chain complex I (NDUFA9).[399–401] Other proteins in this and other clusters were annotated to the ER (Figure 3.21B: green). This confirmed that BCL6 was involved in the upregulation of at least some of the mitochondrial and ER proteins upregulated 24 hours after acute IR.

Another STRING cluster contained several upregulated proteins annotated to the microtubule cytoskeleton (Figure 3.21B: yellow). Several of these were involved in chromosome alignment and segregation in mitosis. This confirmed that BCL6 had a role in the arrest of LN18 cells at G2/M phase by 24 hours after acute IR, although many M phase proteins were upregulated regardless of BCL6 inhibition. Furthermore, 60% of the proteins annotated to the GO:CC term *nuclear chromosome* (p = 3.03E-3) were BCL6-dependent. STRING analysis showed that these upregulated proteins included SIN3A, a known part of BCL6 corepressor complexes, and four proteins involved in DNA replication and repair, TIPIN, BLM, POLD1 and SMARCAD1.[225,359–362,402,403] This contrasted with the response to fractionated IR, in which the downregulation of TIPIN and BLM was dependent on BCL6.

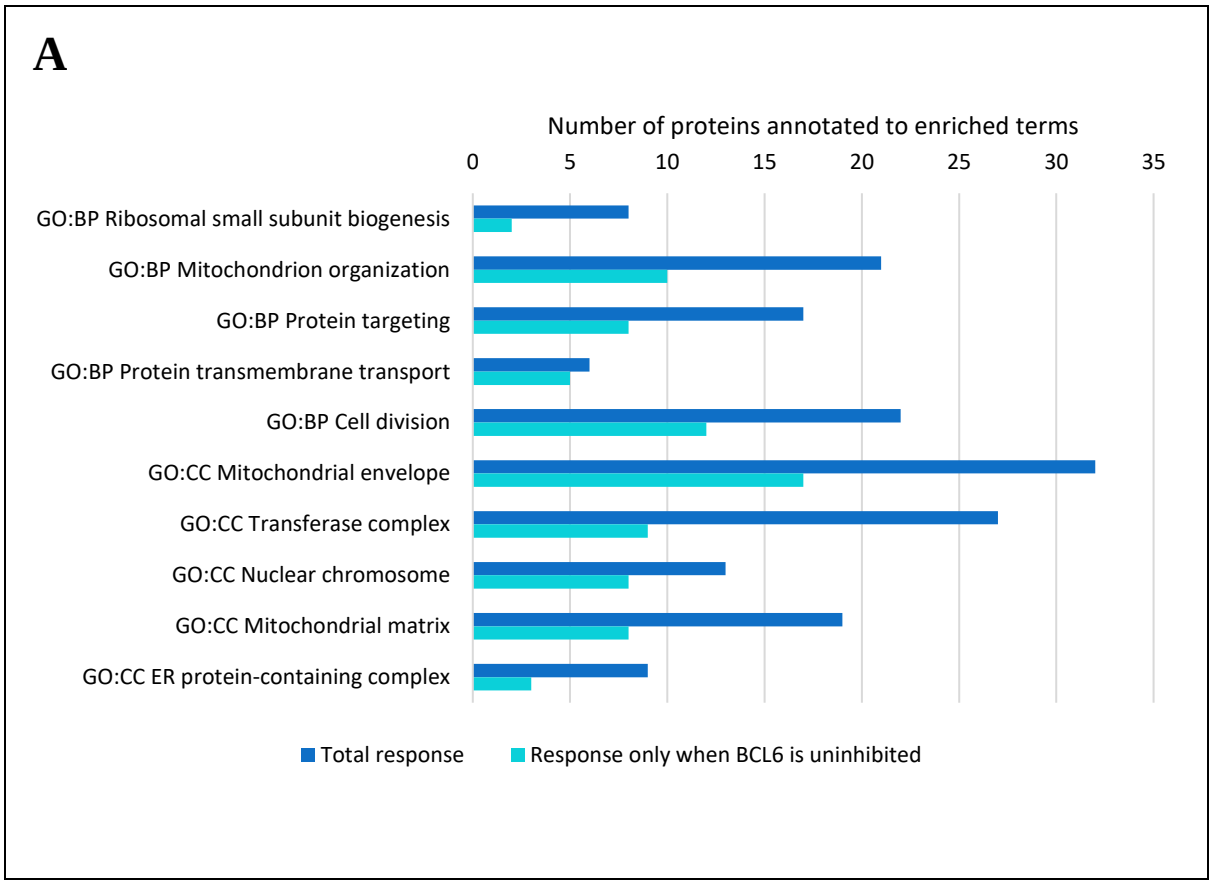

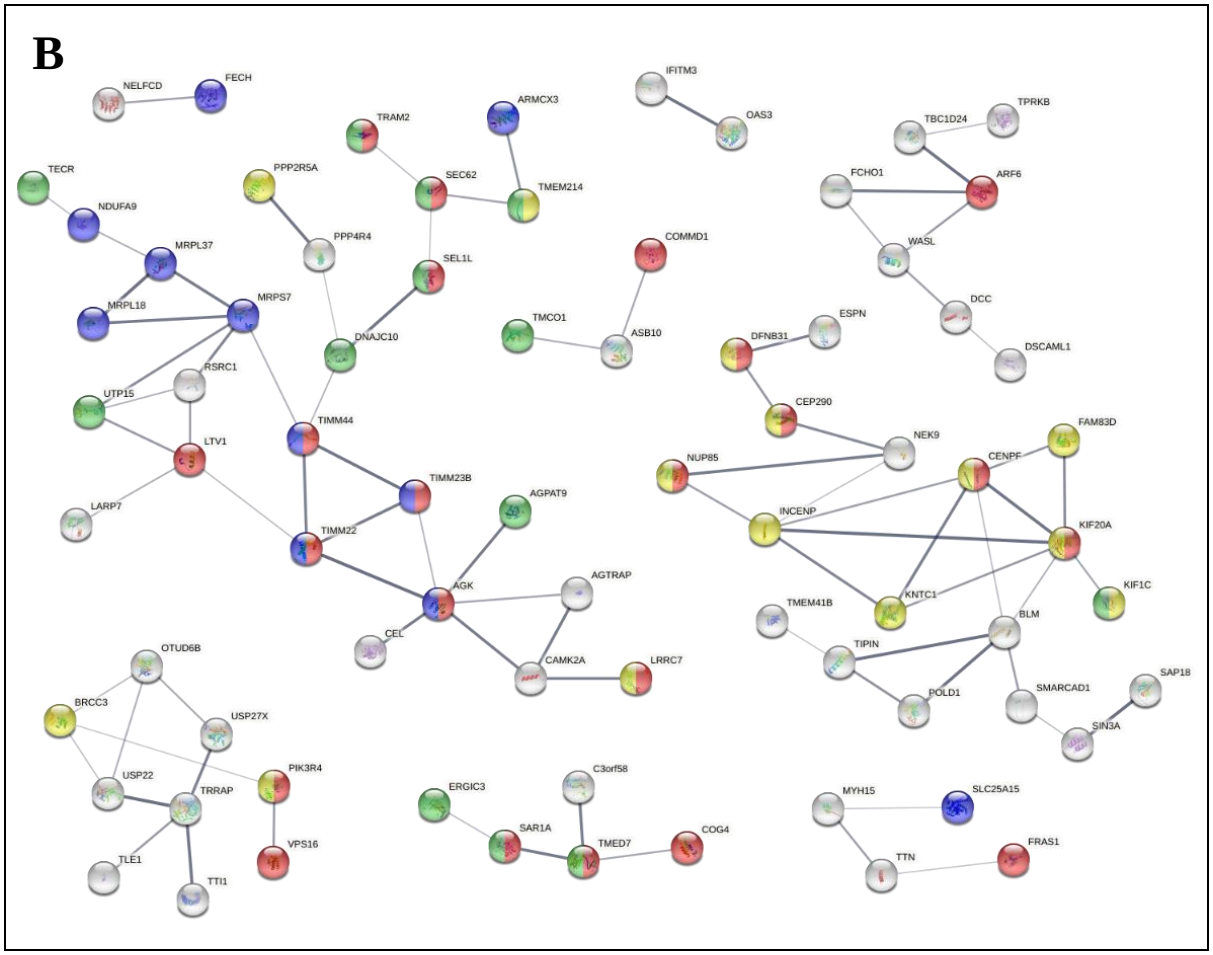


Figure 3.21: Proteins dependent on BCL6 for upregulation 24 hours after acute IR

A) Plot comparing the number of upregulated proteins annotated to each enriched functional term in the total LN18 whole proteome response 24 hours after acute IR (dark blue) compared to the LN18 whole proteome response 24 hours after acute IR that only occurred when BCL6 was uninhibited (light blue). B) STRING network of proteins dependent on BCL6 for upregulation 24 hours after acute IR in LN18 cells. Red = *establishment of protein localisation*, blue = *mitochondrial envelope*, green = *endoplasmic reticulum*, yellow = *microtubule cytoskeleton*. Edges indicate both functional and physical protein interactions and the thickness of the edges indicates confidence. Only edges with high confidence (minimum required interaction score 0.7) are shown and disconnected nodes are hidden. Interactions are sourced from textmining, experiments, databases, co-expression, neighbourhood and co-occurrence.

Functional enrichment analysis of the proteins dependent on BCL6 for downregulation 24 hours after acute IR showed enrichment for only one GO:BP term: *covalent chromatin modification* (p = 1.37E-2). This term contained proteins involved in histone methylation, demethylation and acetylation, along with other proteins involved general transcriptional regulation. g:Profiler multi-query analysis showed that this response to acute IR was mostly BCL6-dependent (Figure 3.22). BCL6-dependent downregulation of proteins involved in transcription was also seen in response to fractionated IR and TMZ. This indicated that BCL6 was involved in altering the transcriptional program of LN18 cells in response to DNA damaging therapies. g:Profiler multi-query analysis showed that BCL6 was involved in the

downregulation of some of the mRNA processing proteins downregulated 24 hours after acute IR but that many others were downregulated regardless of BCL6 inhibition (Figure 3.22).

The role of BCL6 in the response of LN18 cells to acute IR appeared to differ from its roles in response to fractionated IR and TMZ treatments. The only similarity between all three treatments was that BCL6 appeared to have some involvement in upregulation of mitotic proteins and downregulation of proteins involved in transcriptional regulation. The latter observation is likely to reflect transcriptional repression by BCL6 to reprogram the gene expression of the LN18 cells to deal with the stress of the treatment. Unexpectedly, while BCL6 downregulated the DNA damage response after fractionated IR, BCL6 activity appeared to lead to upregulation of some of the same proteins 24 hours after acute IR. This suggested that BCL6 has different roles in response to different levels of IR. Additionally, the upregulation of mitochondrial and ER proteins and the downregulation of mRNA processing proteins in response to acute IR appeared to be at least partly reliant on BCL6 activity.

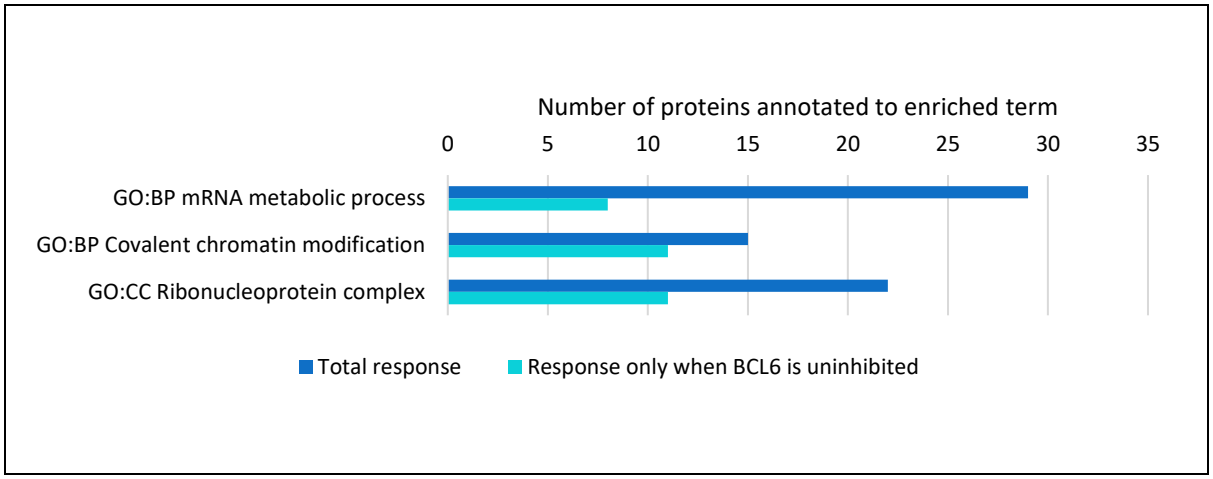


Figure 3.22: Proteins dependent on BCL6 for downregulation 24 hours after acute IR

Plot comparing the number of downregulated proteins annotated to each enriched functional term in the total LN18 whole proteome response 24 hours after acute IR (dark blue) compared to the LN18 whole proteome response 24 hours after acute IR that only occurred when BCL6 was uninhibited (light blue). STRING analysis for the proteins dependent on BCL6 for downregulation 24 hours after acute IR was not informative and so is not included as a figure.

### 3.3.4.5: The role of BCL6 in the whole proteome response of LN18 cells 48 hours after acute irradiation

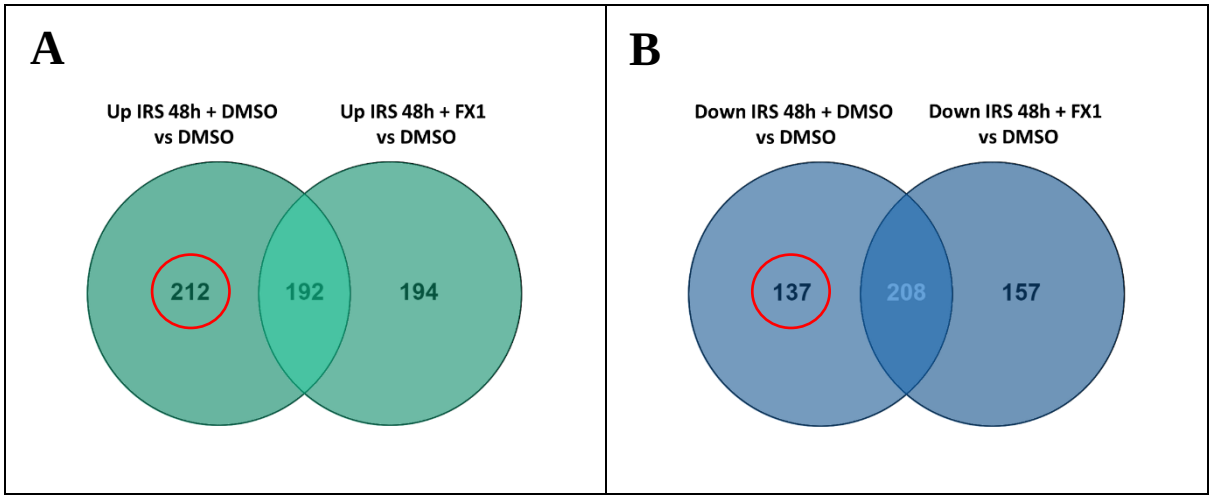


Figure 3.23: Comparison of +/- FX1 datasets to examine the role of BCL6 in the whole proteome response of LN18 cells 48 hours after acute IR

Comparison of A) Proteins upregulated 48 hours after single dose acute IR (IRS 48h) + DMSO compared to DMSO alone vs proteins upregulated 48 hours after single dose acute IR (IRS 48h) + FX1 compared to DMSO; B) Proteins downregulated 48 hours after single dose acute IR (IRS 48h) + DMSO compared to DMSO alone vs proteins downregulated 48 hours after single dose acute IR (IRS 48h) + FX1 compared to DMSO. The BCL6-dependent proteins suggested by this comparison are circled in red.

Many of the functional changes induced 24 hours after acute IR, including arrest at G2/M, increased protein trafficking, decreased mRNA splicing and increased expression of mitochondrial proteins, were still evident 48 hours after acute IR (section 3.3.2). However, by 48 hours after acute IR, autophagy had been induced and ribosome biogenesis was downregulated. Compared to fractionated IR and TMZ, smaller but still noteworthy percentages of the proteins upregulated (52%) and downregulated (39%) 48 hours after acute IR were dependent on BCL6 (Table 3.3).

g:Profiler multi-query analysis showed that the IR-induced upregulation of some of the mitochondrial, protein trafficking, autophagy and G2/M phase proteins was dependent on BCL6 (Figure 3.24). Nearly 60% of the upregulated proteins annotated to the GO:BP *macroautophagy* term were dependent on BCL6 activity. The STRING analysis of the proteins dependent on BCL6 for upregulation 48 hours after IR shows the proteins involved in autophagy in red (Figure 3.24B). This suggested that BCL6 activity was important in this longer-term response to acute IR. However, none of the responses were fully dependent on BCL6 activity.

STRING analysis of the proteins dependent on BCL6 for upregulation 48 hours after acute IR revealed a complex network of proteins, with four clear hub proteins: p53, AKT1, CCNA2 and CCNB2 (Figure

3.24B). The BCL6-dependence of p53 upregulation 48 hours after acute IR was surprising, as BCL6 represses p53 expression in GC B cells, lymphoma and other cancers.[240,302,303,305,310,311] AKT is known to be important in the radioresistance of GBM, so while its upregulation in response to acute IR was unsurprising, its dependence on BCL6 was.[53,91,93,96–101,110] In the STRING network, both p53 and AKT1 had interactions with many other proteins, several of which were annotated to enriched GO:MF terms *transferase activity* (Figure 3.24B: blue) and *nucleotide binding* (Figure 3.24B: green). The multi-query analysis showed that nearly 60% of the upregulated proteins annotated to the GO:CC term *transferase complex* (2.61E-7) were dependent on BCL6 (Figure 3.24A). AKT1 was connected to various kinases and phosphatases and the p105 subunit of NFκB (NFκB1). BCL6 is also known to repress the NFκB pathway, so BCL6-dependent upregulation of NFκB1 was unexpected.[227] p53 also connected to kinases, as well as to E3 ubiquitin-protein ligases, transcriptional regulators and the γ subunit of master metabolic regulator AMPK. Several of these proteins were involved in regulation of cell cycle phase transition and so were also connected to the cyclins CCNA2 and CCNB2 and other proteins involved in cell cycle control and mitosis. This upregulation of a network of signalling proteins centred around p53, AKT1 and cell cycle regulators suggested that BCL6 was involved in the upregulation of stress response signalling in response to the DNA damage induced by acute IR.

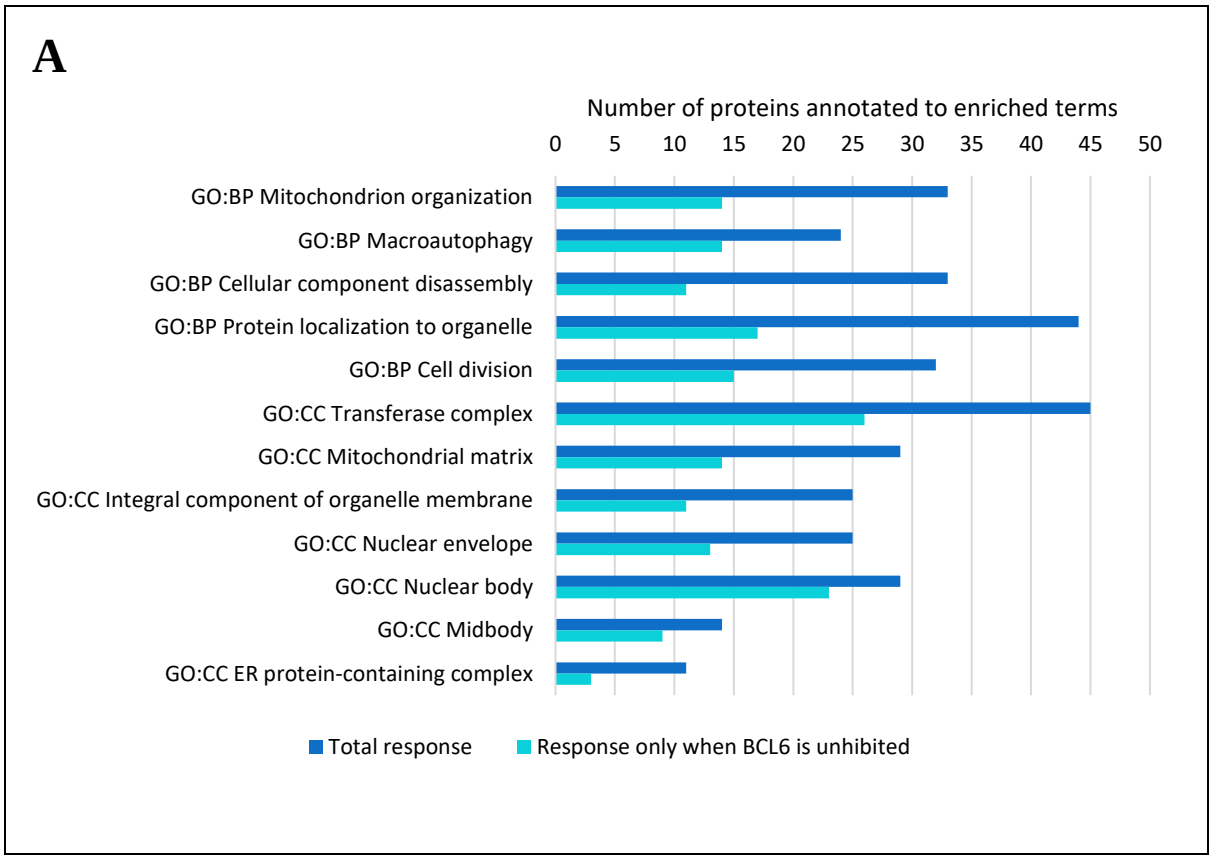

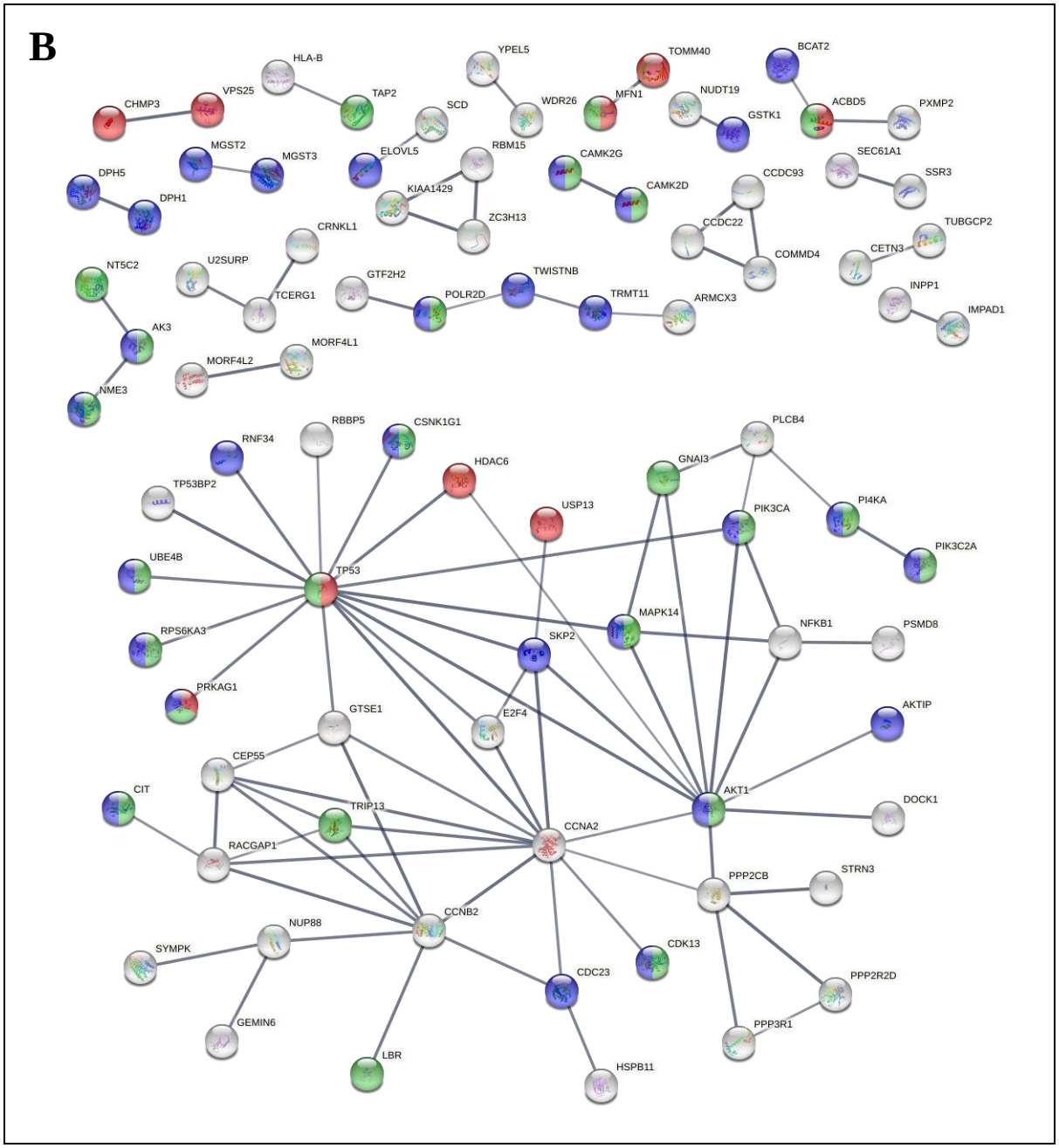


Figure 3.24: Proteins dependent on BCL6 for upregulation 48 hours after acute IR

A) Plot comparing the number of upregulated proteins annotated to each enriched functional term in the total LN18 whole proteome response 48 hours after acute IR (dark blue) compared to the LN18 whole proteome response 48 hours after acute IR that only occurred when BCL6 was uninhibited (light blue). B) STRING network of proteins dependent on BCL6 for upregulation 48 hours after acute IR in LN18 cells. Red = *autophagy*, blue = *transferase activity*, green = *nucleotide binding*. Edges indicate both functional and physical protein interactions and the thickness of the edges indicates confidence. Only edges with high confidence (minimum required interaction score 0.7) are shown and disconnected nodes are hidden. Interactions are sourced from textmining, experiments, databases, co-expression, neighbourhood and co-occurrence.

g:Profiler multi-query analysis showed that BCL6 was involved in the downregulation of mRNA processing and ribosome biogenesis proteins in response to acute IR (Figure 3.25A). Proteins annotated to the GO:MF term *RNA binding* (red) and the GO:CC terms *ribonucleoprotein complex* (blue) and *nucleolus* (green) are shown in the STRING network in Figure 3.25B. However, the majority of the downregulated proteins annotated to these terms were downregulated regardless of BCL6 activity (Figure 3.25A).

The most obvious difference between the whole proteome changes at 24 and 48 hours after acute IR was the initiation of autophagy by 48 hours. It seemed that BCL6 was important for the upregulation of some but not all of the proteins involved in autophagy. Additionally, BCL6 was involved in the downregulation of ribosome biogenesis proteins seen 48 hours after acute IR. However, the most striking impact of BCL6 activity 48 hours after acute IR was the upregulation of proteins involved in signalling, transcriptional regulation and cell cycle checkpoints, including hub proteins p53, AKT1, CCNA2 and CCNB2. BCL6 canonically suppresses DNA damage response pathways and appeared to do so in response to fractionated IR (sections 1.2.2 and 3.3.4.2). However, these results suggested that BCL6 had a very different function in the response of GBM cells to acute IR.

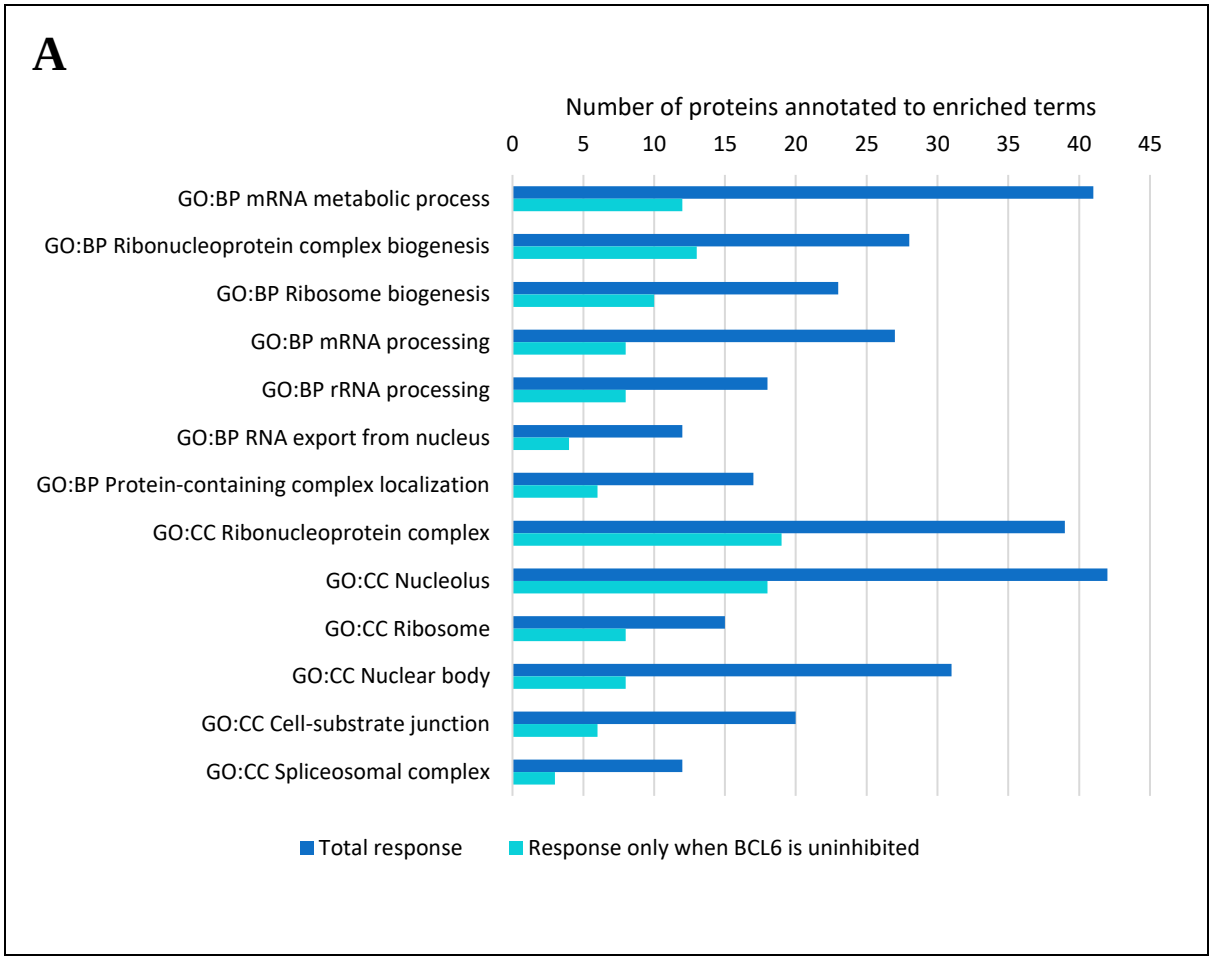

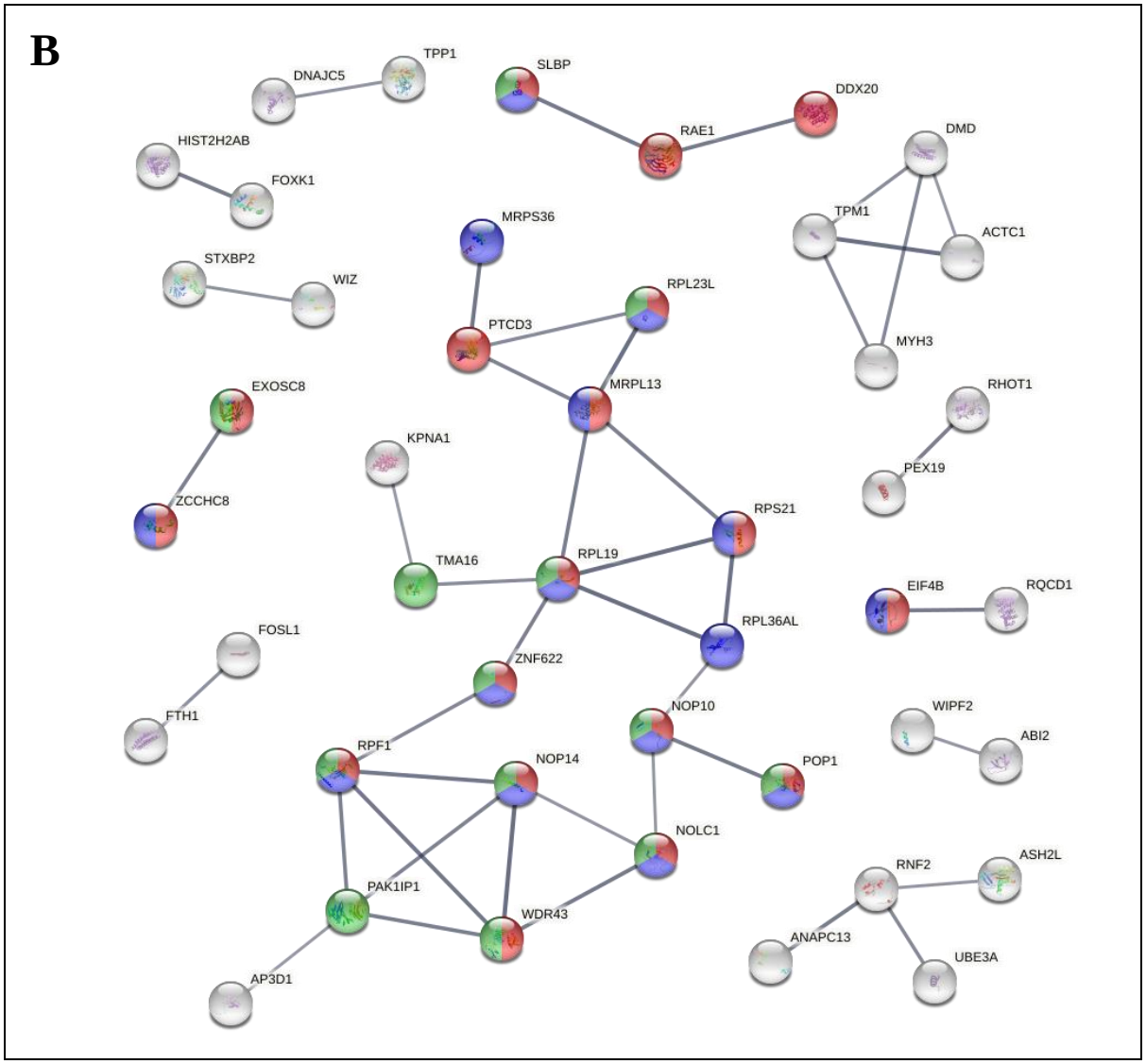


Figure 3.25: Proteins dependent on BCL6 for downregulation 48 hours after acute IR

A) Plot comparing the number of downregulated proteins annotated to each enriched functional term in the total LN18 whole proteome response 48 hours after acute IR (dark blue) compared to the LN18 whole proteome response 48 hours after acute IR that only occurred when BCL6 was uninhibited (light blue). B) STRING network of proteins dependent on BCL6 for downregulation 48 hours after acute IR in LN18 cells. Red = *RNA binding*, blue = *ribonucleosome complex*, green = *nucleolus*. Edges indicate both functional and physical protein interactions and the thickness of the edges indicates confidence. Only edges with high confidence (minimum required interaction score 0.7) are shown and disconnected nodes are hidden. Interactions are sourced from textmining, experiments, databases, co-expression, neighbourhood and co-occurrence.

### 3.3.4.6: The role of BCL6 in the whole proteome response of LN18 cells to doxorubicin

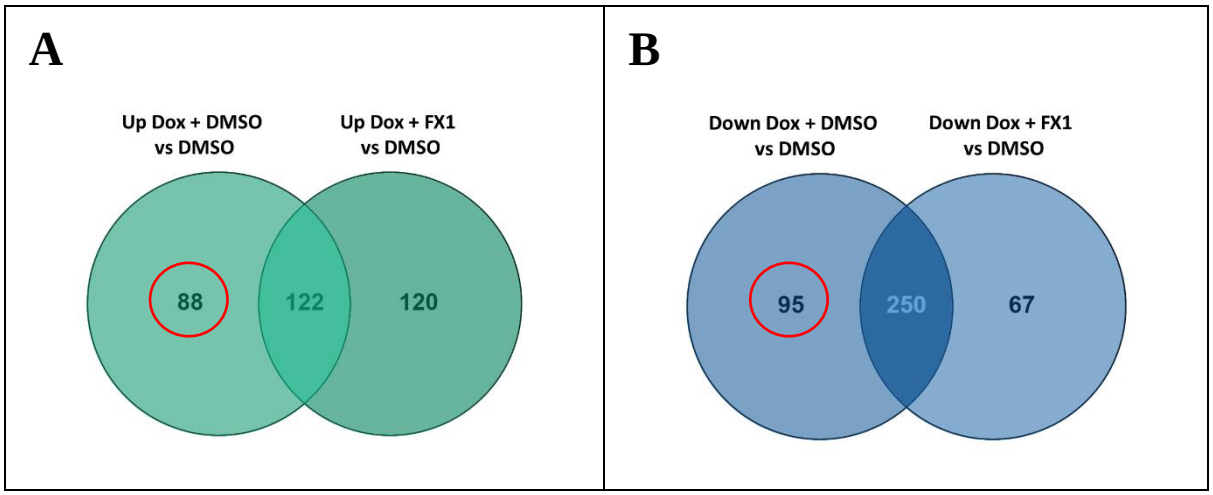


Figure 3.26: Comparison of +/- FX1 datasets to examine the role of BCL6 in the whole proteome response of LN18 cells to doxorubicin treatment

Comparison of A) Proteins upregulated by doxorubicin (Dox) + DMSO compared to DMSO alone vs proteins upregulated by doxorubicin (Dox) + FX1 compared to DMSO; B) Proteins downregulated by doxorubicin (Dox) + DMSO compared to DMSO alone vs proteins downregulated by doxorubicin (Dox) + FX1 compared to DMSO. The BCL6-dependent proteins suggested by this comparison are circled in red.

Like acute IR, doxorubicin treatment of LN18 cells downregulated mRNA splicing and upregulated mitochondrial and ER membrane proteins (section 3.3.2). Additionally, doxorubicin resulted in a far broader downregulation of ribosome biogenesis proteins than acute IR. Doxorubicin also downregulated mitotic proteins and upregulated proteins involved in gene silencing. The whole proteome response of LN18 cells to doxorubicin appeared to be less dependent on BCL6 than the responses to any of the other treatments tested. Only 42% and 28% of the proteins up- and downregulated by doxorubicin respectively were dependent on BCL6 activity (Table 3.3). These proteins had very little informative functional enrichment and g:Profiler multi-query analysis indicated that most of the functional changes in response to doxorubicin were independent of BCL6 activity (Figure 3.27).

Only the downregulation of proteins annotated to GO:BP term *regulation of histone methylation* (p = 4.41E-2) and GO:CC term *cell cortex* (p = 9.85E-3) seemed to mainly depend on BCL6 activity. These terms were only significantly enriched when the proteins dependent on BCL6 for downregulation by doxorubicin were analysed. The former term contained five proteins involved in regulation of transcription and chromatin structure. BCL6-dependent downregulation of transcriptional regulation proteins was also seen in response to fractionated and acute IR and TMZ treatment. It was notable that known BCL6 corepressor SIN3A and a component of the SIN3A complex, SAP18, were dependent on BCL6 for upregulation by doxorubicin.[225,404] This was also seen 24 hours after acute IR.

The *cell cortex* term contained a variety of proteins involved in signalling, vesicle trafficking and the cytoskeleton, including RHOB, which mediates apoptosis in cancer cells.[405] Therefore, while BCL6 seemed to have little role in the response of LN18 cells to doxorubicin treatment, it may have had some involvement in transcriptional regulation, modulation of cell signalling and preventing cell death.

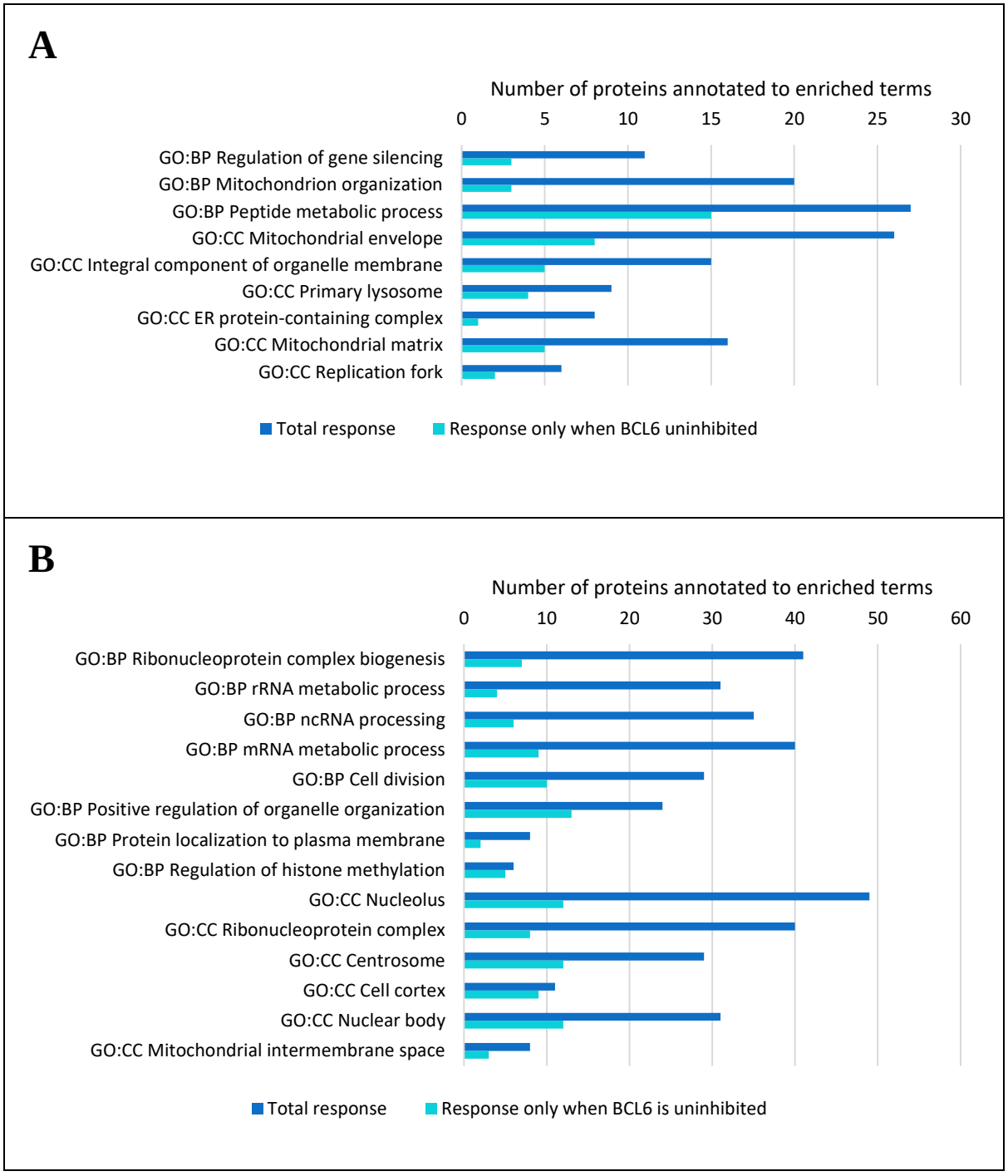


Figure 3.27: Proteins dependent on BCL6 for up- and downregulation by doxorubicin

Plots comparing the number of A) upregulated and B) downregulated proteins annotated to each enriched functional term in the total LN18 whole proteome response to doxorubicin (dark blue) compared to the LN18

whole proteome response to doxorubicin that only occurred when BCL6 was uninhibited (light blue). STRING analyses for the proteins dependent on BCL6 for up- and downregulation by doxorubicin were not informative and so are not included as figures.

### 3.3.4.7 Summary of proteins differentially expressed in response to treatment only when BCL6 was uninhibited

This section analysed the proteins only differentially expressed in response to treatment of LN18 cells when BCL6 was not inhibited. The rationale for this was that the differential expression of these proteins was dependent upon BCL6 being uninhibited and so BCL6 must be involved in these parts of the response to therapy. This analysis implicated BCL6 in various aspects of the response to each treatment. However, Figure 3.28 emphasises that there was no universal BCL6 response to therapy revealed by the whole proteome analysis. Instead, BCL6 appeared to play different roles depending on the treatment. The whole proteome response of LN18 cells to each treatment was very different (section 3.3.2), so it is perhaps unsurprising that BCL6 appeared to modify its activity to assist with the different treatment responses.

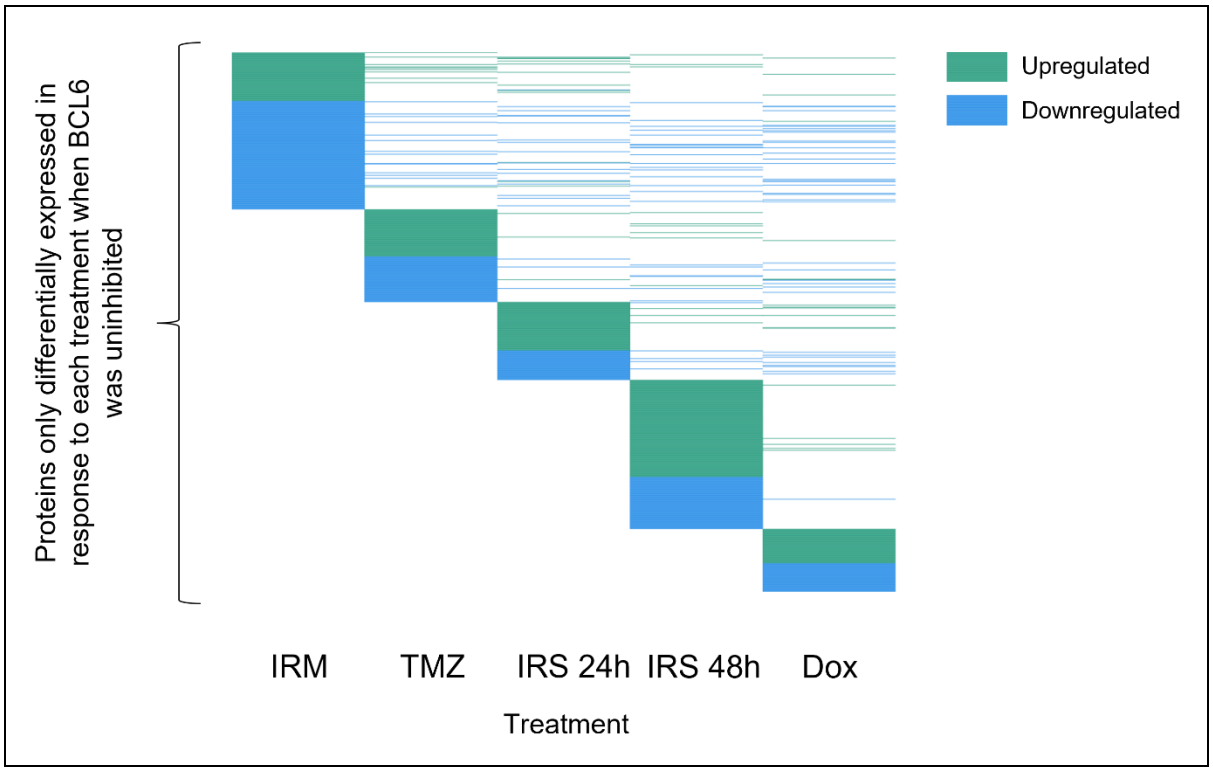

Figure 3.28: Comparison of proteins dependent on BCL6 for up- and downregulated by each treatment
'Heat map' showing proteins up- and downregulated by each treatment only when BCL6 was uninhibited. Treatments on the x axis are fractionated multiple dose IR (IRM), TMZ, acute single dose IR 24 hours (IRS 24h), acute single dose IR 48 hours (IRS 48h) and doxorubicin (Dox). Proteins listed on the y axis (not shown). Upregulated proteins shown in green and downregulated proteins shown in blue.

Table 3.4 summarises the whole proteome response to each treatment and how BCL6 appeared to be involved in these responses. In most cases, BCL6 was involved in the up- or downregulation of some but not all proteins in each functional term. This suggested that BCL6 was broadly involved in responses to DNA damaging therapy but tailored its function to each different treatment response. The level of BCL6 involvement in the response of LN18 cells also varied between the treatments.

BCL6 was involved in most of the proteome changes seen in response to TMZ treatment and seemed to be particularly important for the upregulation of telomere regulation proteins and the downregulation of nucleocytoplasmic transport proteins. BCL6 was also involved in a large proportion of the proteome changes seen in response to fractionated IR treatment. Most notably, BCL6 appeared to be almost fully responsible for downregulating DNA damage response proteins in response to fractionated IR treatment of LN18 cells. Hence the activity of BCL6 in response to fractionated IR in GBM cells was similar to its canonical role. This was not observed in response to any of the other treatments.

While BCL6 was at the heart of the response of LN18 cells to fractionated IR and TMZ treatment, it appeared to play only a supportive role in the response of LN18 cells to acute IR and doxorubicin. The role of BCL6 in the response to doxorubicin treatment was minor, although it was involved in downregulating promoter of cell death RHOB. BCL6 did appear to be important in the response of LN18 cells to acute IR, as it was involved in up- and downregulation of proteins in each altered functional group. However, many other proteins in these groups were differentially expressed independent of BCL6 activity. At 24 hours after acute IR, BCL6 was important for the upregulation of a cluster of DNA repair proteins. At 48 hours after acute IR, BCL6 was involved in the upregulation of a network of stress response signalling proteins, including p53, AKT1, NFκB1 and proteins involved in cell cycle checkpoints. This suggested that in response to acute IR, BCL6 performed essentially the opposite function to its canonical role as a suppressor of cellular stress responses.

Table 3.4: Summary of the whole proteome response of LN18 cells to each treatment and BCL6 involvement in each response

Functional groups of proteins up- and downregulated by each treatment are listed in the second column. Functional groups of proteins which were only up- or downregulated by each treatment when BCL6 was uninhibited are listed in the third column adjacent to matching terms in the second column. When BCL6 had some involvement in the up- or downregulation of proteins in a functional group but was not required for all of the changes seen, the functional group is listed in the fourth column adjacent to matching terms in the second and/or third columns. Notable features not picked up by gene ontology enrichment are shown in brackets.

| Treatment | Response to treatment | Response to treatment dependent on BCL6 activity | BCL6 involved in some aspects of the response |
|---|---|---|---|
| **Fractionated irradiation** | Up | Up | Up |
| | Protein trafficking | | Protein trafficking |
| | Ribosome biogenesis/translation | | Ribosome biogenesis |
| | | Cell division (spindle) | |
| | Down | Down | Down |
| | Cell division - mitosis and DNA replication | | Cell division - mitosis and DNA replication |
| | | DNA damage response - DNA repair and apoptosis | |
| | | Gene silencing by miRNA | |
| **Temozolomide** | Up | Up | Up |
| | mRNA splicing | | mRNA splicing |
| | Histone modification and transcriptional regulation | | Histone modification and transcriptional regulation |
| | Mitosis | | Mitosis |
| | Maintenance of telomeres | Maintenance of telomeres | |
| | Down | Down | Down |
| | Protein trafficking | Protein trafficking | Protein trafficking |
| | | Nucleocytoplasmic transport | |
| | Ribosome biogenesis | | Ribosome biogenesis |
| | Protein degradation | | Protein degradation |
| **Acute irradiation 24 hours** | Up | Up | Up |
| | G2/M phase proteins | | G2/M phase proteins, particularly microtubule-related |
| | Mitochondrial proteins | | Mitochondrial proteins |
| | ER proteins | | ER proteins |
| | | (DNA repair and replication) | |
| | Down | Down | Down |
| | mRNA splicing | | mRNA splicing |
| | Histone modification and transcriptional regulation | Histone modification and transcriptional regulation | Histone modification and transcriptional regulation |
| | (SIN3A) | (SIN3A) | |
| **Acute irradiation 48 hours** | Up | Up | Up |
| | Cell division - G2/M phase proteins | Cell cycle control | Cell division - G2/M phase proteins |
| | Mitochondrial proteins | | Mitochondrial proteins |
| | Autophagy | | Autophagy |
| | Transferase complexes | Transferase complexes (signalling – p53, AKT1, NFκB1, AMPK-γ1, other kinases/phosphatases) | Transferase complexes |

| | | | |
|---|---|---|---|
| | Down | Down | Down |
| | mRNA splicing | | mRNA splicing |
| | Ribosome biogenesis | | Ribosome biogenesis |
| **Doxorubicin** | Up | Up | Up |
| | Mitochondrial proteins | | Mitochondrial proteins |
| | ER proteins | | ER proteins |
| | Gene silencing by miRNA | | Gene silencing by miRNA |
| | (SIN3A) | (SIN3A) | |
| | Down | Down | Down |
| | Ribosome biogenesis | | Ribosome biogenesis |
| | G2/M phase proteins | | G2/M phase proteins |
| | Transcriptional regulation | Transcriptional regulation | Transcriptional regulation |
| | | (Apoptosis protein RHOB) | |

## 3.4: Discussion

### 3.4.1 Advantages of whole proteome analysis of LN18 GBM cells

Previous studies have indicated that BCL6 is important in the response of GBM and other cancer cell types to therapy.[207,295,406] However, these studies focused on specific measures of GBM survival, such as markers of apoptosis, inhibition of proliferation and the level of DNA damage, providing a limited view of BCL6 function.[207,295,406] In contrast, whole proteomics analysis of the response of LN18 cells to therapy with and without BCL6 inhibition provided a broad, unbiased view of the role of BCL6 in the therapy response. This revealed that although BCL6 was involved in the response to each treatment, its role in each treatment response was very different. This context specificity may not have been apparent with a more targeted experiment such as the measurement of survival.

Whole proteomics was chosen over whole transcriptomics as proteomics is a much better measure of functional changes. It is well established that transcript abundance often does not correlate with protein expression, due to multiple levels of post-transcriptional and post-translational regulation.[407,408] Therefore, to understand the functional consequences of BCL6 inhibition on the response of LN18 cells to therapy, proteomics was the superior choice.

### 3.4.2 Limitations of whole proteome analysis of LN18 GBM cells

This study identified which proteins were only differentially expressed in response to treatment of LN18 cells when BCL6 was not inhibited. It was reasonable to conclude that those proteins depended on BCL6 activity for their up- or downregulation in response to treatment. However, this analysis could not distinguish which proteins were directly up- or downregulated by BCL6 transcriptional activity and which had their expression altered downstream of BCL6 activity. Instead, the whole proteome data provided an overview of which processes BCL6 appeared to be involved in. This was vital to give context to previous experiments and to generate new hypotheses for further investigation of BCL6 function in GBM therapy responses.

While biological variability was mitigated by performing each experiment in biological triplicate, this study was only performed in one GBM cell line (LN18). GBM is an extremely heterogeneous cancer and other studies in this thesis were carried out in three different GBM cell lines to account for this variability. However, the number of treatments investigated in this chapter meant that access to the mass spectrometer and the scale of the data analysis limited this study to a single cell line. While investigating the effects of fewer treatments on more cell lines may have improved the applicability of these results to GBM in general, there were compelling reasons to investigate all of the treatments used. The acute treatments were known to strongly upregulate BCL6 expression and it was useful to include these treatments to provide context for previous results.[207,322] However, it was also important to include the

two longer-term and more clinically relevant treatments, fractionated IR and TMZ, to increase the applicability of the results to the clinic. This allowed an interesting comparison of the role of BCL6 in the responses of LN18 cells to acute and longer-term treatments. Therefore, the breadth of treatments studied was judged more important than repeating the experiment in multiple cell lines for this thesis. Future work should prioritise validating the results of this whole proteome analysis in other GBM cell lines to determine whether BCL6 is involved in the same treatment responses in multiple GBM cell lines.

This study was carried out in a human GBM cell line rather than in a mouse model or human GBM tissue. A two-dimensional mono-culture of GBM cells omits the three-dimensional interactions of GBM tumour cells with each other and with other cells in their environment. Additionally, *in vitro* models lack the complex interactions of multiple organ systems within the human body which may impact treatment responses. On some occasions, these factors can be modelled in animals, however the current lack of a murine *in vivo* system which accurately models human GBM made *in vitro* work in cell lines preferable to mouse models for this study.[409] Additionally, the broad, hypothesis-generating nature of this chapter meant that cell lines were a more cost effective and ethical model. It would be beneficial to repeat or validate the results of this study in low passage GBM cell lines derived from untreated GBM tissue, as these would better model GBM tumours. The LN18 GBM cell line was selected for this study to complement and provide context to previous findings using this cell line in the McConnell lab group.

### 3.4.3 Advantages and limitations of inhibition of BCL6 with FX1

BCL6 functions as a transcriptional repressor in GC B cells and lymphoma.[232] This activity is dependent on interactions with corepressors including BCOR, NCOR1 and NCOR2, which bind to the lateral groove in the BCL6 N-terminal BTB/POZ domain.[215,217,219] FX1 is a small molecule inhibitor that binds to the lateral groove with 4-fold greater affinity than the endogenous corepressors.[295] This blocks the binding of corepressors and therefore prevents BCL6 from repressing its target genes.[295] FX1 increases the efficacy of DNA-damaging and other cytotoxic therapies in multiple cancer cell lines, including lymphoma, leukaemia, breast cancer, lung cancer and GBM.[207,295,311,406] This indicates that BCL6 is involved in cancer cell resistance to therapy and that the recruitment of binding partners to the lateral groove is required for this activity. Therefore, FX1 was selected to inhibit BCL6 activity in LN18 GBM cells to investigate the role of BCL6 in the therapy responses of these cells.

There are some limitations to this approach. Firstly, if BCL6 had any functions which were independent of corepressor binding to the lateral groove, FX1 treatment would not inhibit this activity. Therefore, this whole proteomics study was limited to investigating the role of BCL6 *mediated by the recruitment of binding partners to the lateral groove* in the therapy response of LN18 GBM cells. As FX1 treatment

has been shown to improve the efficacy of TMZ and IR in GBM cells, the whole proteome analysis of treated GBM cells with and without FX1 at least investigated the reason for this observation.[207]

The second limitation of using FX1 to inhibit BCL6 activity was the possibility of off-target effects. FX1 is commercially available and has been branded as a BCL6-selective inhibitor.[410,411] Indeed, many publications have used FX1 to inhibit BCL6 without any discussion about whether FX1 might have off-target effects.[207,305,310,311,406,412–414] However, there is evidence that FX1 may have effects on other proteins, so some of the proteome changes seen in response to FX1 treatment could be due to off-target effects.[295] It would have been ideal to use matched BCL6-expressing and BCL6-knockout GBM cell lines for this work; however BCL6 knockout renders GBM cells non-viable (section 1.2.8). Therefore, as FX1 is a commonly used and well-accepted method of inhibiting BCL6, it was chosen as the best alternative.

The lack of FX1-induced de-repression of known BCL6 target genes in LN18 cells prompted a more thorough literature search of the effects of FX1. This revealed that molecules based on rhodanine, as FX1 is, are known as pan assay interference compounds (PAINS) as they frequently act on multiple targets.[415,416] Furthermore, although not explicitly mentioned in the text of the paper, McCoull et al. (2017) showed that the $IC_{50}$ of FX1 for the kinase CK2 was > 40 times lower than for BCL6.[417] Indeed, even the higher affinity BCL6 inhibitors designed by McCoull et al. still had activity against CK2.[417] This suggests that it may be difficult to disentangle the impact of BCL6 and CK2 inhibition when using inhibitors against the BCL6 lateral groove. However, this finding does not seem to have been picked up on by the multiple studies that have used FX1 to inhibit BCL6 since the 2017 paper was published and it has not been independently verified. Further work is required to determine whether FX1 is as selective for BCL6 as is generally assumed, as this could have large implications for the published literature on the activity of BCL6.

The specificity of FX1 for BCL6 was investigated by comparing the whole proteome response of K562 cells to FX1 treatment to the whole proteome response of LN18 cells (section 3.3.3). K562 is commonly considered a *BCL6-null* cell line due to having undetectable BCL6 expression compared to BCL6-dependent lymphoma cell lines.[381–383] It was confirmed that K562 cells had much lower BCL6 mRNA expression than LN18 cells (Appendix). Therefore, it was hoped that if FX1 was selective for BCL6, few whole proteome changes would be seen in response to FX1 treatment of the K562 cell line. While many proteins were up- and downregulated in K562 cells in response to FX1, they lacked the upregulation of mitochondrial and protein trafficking proteins seen in LN18 cells. This adds tentative support to the assumption that the main whole proteome changes seen in response to FX1 in LN18 cells are due to BCL6 inhibition. However, the different cellular context of K562 cells limits the usefulness of this comparison. Future work should validate the results of this chapter with a different method of

BCL6 inhibition, such as the peptide inhibitor RI-BPI or a BCL6-siRNA. This would increase the confidence that the changes observed in response to FX1 were due to BCL6 inhibition.

### 3.4.4 The responses of LN18 GBM cells to treatment

All five treatments used in this chapter were DNA damaging therapies, however each induced a different proteome response in LN18 cells. Nevertheless, the responses to each treatment were mainly expected on the basis of previous literature. As this was not the main purpose of this chapter, discussion of the effects of each treatment will be kept relatively brief.

The whole proteome responses induced by the three acute treatments were expected cellular responses to stress. The integrated stress response (ISR) describes the complex network of signalling pathways activated by eukaryotic cells in response to stress.[418–420] A key feature of the ISR is the downregulation of global protein synthesis by the inhibition of translation.[418–420] All three acute treatments downregulated both mRNA splicing and ribosome biogenesis proteins, consistent with a decrease in global protein production. As has previously been observed, the downregulation of ribosome biogenesis proteins was particularly striking in response to doxorubicin.[421,422] TMZ also decreased ribosome biogenesis proteins and protein degradation, indicating reduced protein turnover. Another key feature of the ISR is the induction of survival pathways such as autophagy.[418] Autophagy is a known mechanism of therapy resistance in GBM and was induced by 48 hours after acute IR.[132,423] Furthermore, mitochondrial dysfunction and ER stress are two conditions that initiate the ISR.[419] Crosstalk between these two organelles is important in the regulation of reactive oxygen species (ROS) such as those produced by IR, so it is not surprising that the acute treatments, particularly IR, upregulated proteins involved in trafficking across mitochondrial and ER membranes.[420] Additionally, there is a complex interplay between nuclear and mitochondrial activity in DNA damage responses such as DNA repair, cell cycle checkpoints and apoptosis.[424] The upregulation of mitochondrial proteins in response to acute IR likely indicates reprogramming of mitochondrial activity to help the LN18 cells adapt to the stress of IR damage.

Cell cycle arrest is also an expected response to DNA damaging therapy. Acute IR treatment of LN18 cells clearly induced cell cycle arrest at G2/M whereas doxorubicin treatment caused a downregulation of mitotic proteins. IR is known to induce cell cycle arrest at G2/M in GBM cells, so upregulation of mitotic proteins after acute IR was anticipated.[88,89,425,426] Doxorubicin has also generally been shown to arrest cells at G2/M, however it does arrest some cell types at other phases of the cell cycle.[427,428] A study of doxorubicin-resistant lung cancer cells showed G2 arrest at 12-16 hours followed by accumulation in S phase by 24 hours.[429] It is possible that the LN18 cells were arrested by doxorubicin soon after treatment, synchronising the cells to the same phase of the cell cycle, before resuming the cycling. This would explain the decrease in mitotic proteins by 24 hours after acute IR. Fractionated IR

and TMZ have also been shown to induce G2/M arrest in GBM cells.[92,430,431] TMZ treatment of LN18 cells did result in upregulation of a handful of proteins involved in the spindle assembly checkpoint, perhaps indicating some level of arrest at G2/M phase. This was not observed in the whole proteome response of LN18 cells to fractionated IR. Instead, cell cycle proteins in general were downregulated by fractionated IR. Additionally, unlike all of the other treatments, protein translation was upregulated in response to fractionated IR. It may be that LN18 GBM cells are resistant enough to fractionated IR to avoid cell cycle arrest and the ISR. This is discussed further in section 3.4.6.

The response of LN18 cells to TMZ was particularly unique compared to the other treatments. The downregulation of protein trafficking, ribosome biogenesis and protein degradation suggested a general decrease in cellular activity. However, the upregulation of nuclear proteins involved in telomere maintenance, histone modification and transcriptional regulation suggested changes to chromatin architecture. This could be indicative of senescence, which is known to be induced in GBM cells by TMZ.[155,156,432] However, no senescence-related terms were enriched in response to TMZ treatment and a manual search found that markers of senescence were not differentially expressed in response to TMZ. The upregulation of a handful of proteins involved in telomere maintenance may be indicative of resistance to TMZ. While the mechanism of resistance is unclear, inhibition of telomerase or telomere protection proteins like TERF2 sensitises GBM cells to DNA damage by TMZ.[433–435] This appears to be due to inhibition of DNA repair and prevention of G2/M arrest, which leads to DNA damage-induced senescence or apoptosis.[435] Therefore, the upregulation of telomere regulators ROA1, EST1A, TERF2 and ACD in response to TMZ may indicate that the LN18 cells activated a defence mechanism against TMZ-induced DNA damage.[389,434,436] The upregulation of spindle assembly checkpoint proteins BUB1 and ZW10 also indicated that at least some cell cycle checkpoint signalling was active, although the induction of G2/M arrest was not as clear as in the response to acute IR.[369,437]

In summary, the three acute treatments induced responses in LN18 GBM cells consistent with the eukaryotic ISR. The long-term TMZ treatment appeared to decrease cellular activity and induce mechanisms to protect against DNA damage-induced apoptosis, such as upregulation of telomere and cell cycle checkpoint proteins. In contrast, fractionated IR did not appear to induce cell cycle arrest or aspects of the ISR, suggesting that this therapy did not induce DNA damage stress in LN18 GBM cells. It is generally assumed that the DNA damage caused by the IR and TMZ treatments used clinically induces cell death to reduce tumour burden. However, LN18 GBM cells did not appear stressed by fractionated IR and appeared to initiate protective mechanisms against TMZ. This is consistent with the poor response of GBM patients to these treatments.

### 3.4.5 The response of LN18 GBM cells to BCL6 inhibition

BCL6 inhibition induced differential expression of similar functional sets of proteins to the acute chemo- and radiotherapy treatments, suggesting a common cellular stress response. Off-target effects of FX1 cannot be ruled out, however if future studies validate these results with another BCL6 inhibitor, this apparent stress response to BCL6 inhibition is revealing of the role of BCL6 in untreated GBM cells. Cancer cells are under stress caused by rapid proliferation, metabolic changes and DNA damage and mutations.[406] Therefore, under untreated conditions, BCL6 may act as a repressor of cellular responses to these stressors to allow GBM cells to continue to proliferate. Indeed, BCL6 has been characterised as an evolutionarily conserved mediator of adaptation to continued stress.[406] The BTB domain lateral groove, which is blocked by FX1, is vital for this role.[406] Therefore, the inhibition of BCL6 with FX1 in LN18 GBM cells would be expected to impede their ability to survive stress, explaining their reduced plating efficiency. This suggests that upon BCL6 inhibition, the stress that is usually masked by the activity of BCL6 is recognised by the GBM cells, which respond as if to an acute treatment stress.

BCL6 is known as a transcriptional repressor, however its inhibition with FX1 led to up- and downregulation of approximately equal numbers of proteins in LN18 cells. This was anticipated, as BCL6 is known to repress gene expression directly, but also to act as a repressor-of-repressors to induce expression of other genes.[256] In lymphoma cells, inhibition of BCL6 with FX1 induces de-repression of BCL6 target genes.[295] Comparison to known BCL6 target genes in GC B cells and $T_{FH}$ cells did not reveal de-repression of these BCL6 target genes by FX1 in LN18 cells (Appendix). This is not necessarily surprising, as BCL6 has very different patterns of DNA binding in different cell types, mediated by cell context-dependent chromatin architecture and corepressor binding (section 1.2). Additionally, it was anticipated that there would be a disconnect between the genes BCL6 targets in LN18 cells and the proteome changes that occurred in response to BCL6 inhibition. The proteome responses of LN18 cells to BCL6 inhibition and to several of the chemo- and radiotherapy treatments included changes to translation, mRNA splicing and protein trafficking and degradation. This indicated that there were multiple layers of proteostasis regulation between the transcriptional activity of BCL6 and the proteins consequently expressed.

As expected based on the changes to proteostasis regulation, the proteomic response to BCL6 inhibition differed greatly from the transcriptomic response observed in a previous study of the effect of FX1 on LN18 cells (Appendix).[207,322] The transcriptomic study used a higher concentration of FX1 (25 μM) than this study, which used 10 μM.[207,322] The concentration used in both studies was based on the reduction in plating efficiency observed in a clonogenic assay. The different clonogenic assay results obtained in the previous study may be due to changes to the LN18 cell line over time or to different experimental technique. Nevertheless, it was useful to compare the transcriptomic and proteomic responses to BCL6 inhibition by FX1 seen in LN18 cells.

The transcriptomic study performed gene set enrichment using the 'hallmarks of cancer' gene set in GSEA.[207,322] This revealed that inhibition of BCL6 upregulated transcripts involved in apoptosis, the TNFα/NFκB pathway and xenobiotic metabolism and downregulated transcripts involved in the hypoxia and glycolysis pathways.[207,322] The proteomics analysis carried out in this chapter did not find differential expression of proteins annotated to these terms in response to FX1 treatment. Comparison of the two datasets revealed almost no overlap between the up- and downregulated transcripts and proteins. The transcripts up- or downregulated ≥ 2-fold (q value ≤ 0.05) in the transcriptomic study data were re-analysed with gene ontology analysis as performed with the proteomic data in this chapter (Appendix) but this did not increase the similarity.

The differences in the proteomics and transcriptomics results could be partly due to the different concentrations of FX1, which may have resulted in different levels of BCL6 inhibition. However, this lack of correlation was not specific to the FX1 datasets. The transcriptomics study also analysed the transcriptome changes in LN18 cells 24 hours after acute IR.[322] Comparison of these changes to the proteomic changes observed with this treatment in this chapter revealed a similar lack of correlation. Additionally, a previous study found only a 24% correlation between transcripts and proteins deregulated by TMZ treatment of GBM tumours and often these transcripts and proteins were deregulated in opposite directions.[438] Therefore, as anticipated, it is likely that post-transcriptional and -translational regulation meant that the changes at the transcriptomic level did not reflect the proteins that were eventually expressed in response to treatment or FX1. The lack of correlation between transcriptome and proteome responses to BCL6 inhibition and IR may also be due to the temporal differences in mRNA expression changes and protein expression changes. As both of these treatments were acute, with transcriptome and proteome changes measured 24 hours after treatment, some changes to mRNA expression may not yet have translated into changes to protein expression.

The FX1-induced upregulation of transcripts involved in apoptosis suggested that BCL6 suppressed apoptosis in LN18 cells. Additionally, previous work showed that BCL6 inhibition induced apoptosis in a reproducible but very small proportion of GBM cells but significantly reduced long-term proliferative potential, suggesting a long-term rather than acute effect.[207] Therefore, it may be that inhibition of BCL6 with FX1 leads to upregulation of transcripts involved in apoptosis but that these transcripts are not yet translated into proteins 24 hours after treatment. The proteome changes that do occur initially in response to the acute stress of BCL6 inhibition may be more rapidly induced by other mechanisms such as protein or mRNA degradation. Future work could confirm this hypothesis by investigating the long-term effect of BCL6 inhibition on the proteome of LN18 cells.

### 3.4.6 BCL6 involvement in treatment responses

Previous studies have shown that BCL6 is involved in resistance to several types of anti-cancer therapies in multiple cancers.[207,210,295,302,309,311,350,351,406] In GBM cell lines, inhibition of BCL6 significantly increases the efficacy of TMZ and IR.[207,210] However, little was known about how BCL6 is involved in these therapy responses. This was investigated in this chapter by comparing the whole proteome response of LN18 cells to different therapies with and without BCL6 inhibition by FX1. The proteome changes which only occurred in response to treatment when BCL6 was not inhibited were likely dependent on BCL6 activity. It must be kept in mind that the changes apparently dependent on BCL6 could instead be due to off-target effects of FX1. Future work will prioritise the validation of BCL6-dependent responses to treatment with alternative BCL6-inhibitors.

One of the few BCL6-dependent responses observed across all the treatments was downregulation of transcriptional regulator proteins. Fractionated and acute IR, TMZ and doxorubicin led to BCL6-dependent downregulation of general transcriptional regulators, such as components of RNA polymerase transcriptional machinery. Fractionated IR and TMZ also resulted in BCL6-dependent downregulation of a range of transcriptional factors, while 24 hours after acute IR, BCL6 was involved in downregulation of histone modifiers. Despite this similarity, there was almost no overlap in the transcriptional proteins downregulated by each treatment. However, this common theme did indicate that BCL6 was involved in modulation of transcriptional activity in response to each treatment.

Although BCL6 had some involvement in the response of LN18 cells to every treatment, its greatest involvement was in the responses to the two longer-term, clinically relevant treatments: fractionated IR and TMZ. This corresponds to the characterisation of BCL6 as a protein important for adaptation to long-term, repeated stress.[406] Indications of the canonical role of BCL6 as a repressor of the DNA damage response were only seen in the response of LN18 cells to fractionated IR. Interestingly, fractionated IR was also the only treatment which did not upregulate BCL6 protein expression in LN18 cells, according to western blot analysis. This suggests that BCL6 was already present at sufficient abundance to carry out its role in the response of LN18 cells to fractionated IR.

Like fractionated IR, the TMZ treatment regime consisted of repeated doses of a relatively mild therapy. Based on the conclusions above, it would be reasonable to expect BCL6 to play a similar role in the responses of LN18 cells to fractionated IR and TMZ. However, this was not the case. In response to TMZ, BCL6 was involved in the differential expression of most of the enriched functional groups of proteins, however none of these were directly related to the DNA damage response. The upregulation of telomere proteins was dependent on BCL6, suggesting that BCL6 promoted their role in cell cycle arrest and DNA repair in response to TMZ.[433–435] Therefore, BCL6 appeared to play a very different role in the response of LN18 GBM cells to TMZ than it does canonically and in untreated and fractionated IR-treated cells. In light of other data in this chapter, this conclusion may not be as

surprising as it first appears. TMZ strongly upregulated BCL6 expression in LN18 cells, whereas fractionated IR did not. This suggested a different need for BCL6 protein levels in response to the two long-term treatments. Additionally, the whole proteome response induced by TMZ was very different to the other treatments. Changes to chromatin modification and corepressor recruitment have been shown to mediate the alternative roles of BCL6 in different cell type contexts (section 1.2). It is possible that similar mechanisms caused the activity of BCL6 to adapt to the context of TMZ treatment in LN18 cells.

BCL6, which was strongly upregulated by acute IR and doxorubicin, also had some involvement in most of the whole proteome responses to these treatments. In response to acute IR, some of the apparent functions of BCL6 were the opposite of its canonical role as a repressor of cellular stress responses. At 24 hours after acute IR, BCL6 was involved in the upregulation of a cluster of DNA repair proteins, some of which BCL6 was involved in downregulating in response to fractionated IR. At 48 hours after acute IR, BCL6 was involved in the upregulation of a network of signalling proteins including p53, AKT1, NFκB1 and several proteins involved in cell cycle checkpoints. This suggested that BCL6 was involved in the upregulation of stress response pathways in response to acute IR, especially in the longer-term response (48 hours). Strangely, this included the upregulation of pathways canonically suppressed by BCL6, such as p53 and NFκB.[240,245]

Previous research found that 48 hours after acute IR, BCL6 no longer behaved as a transcriptional repressor and may have behaved as a transcriptional activator.[207] Such alteration of BCL6 transcriptional function could explain the upregulation of this stress response signalling network, including the upregulation of p53, which is canonically directly repressed by BCL6.[240] A previous study found that BCL6 did not bind to the *TP53* locus in untreated LN18 cells and that FX1 did not de-repress *TP53* transcription.[322] Another study showed that BCL6 did repress p53 signalling in response to 6 Gy IR in GBM cells, but not in response to 12 Gy IR.[209] This suggests changes in the role of BCL6 in response to different levels of stress. Furthermore, it has been shown that while BCL6 repressed p53 expression in GC B cells, the inhibition of DNA damage repair mediated by BCL6 overexpression in naïve B cells and fibroblasts led to increased cell stress and the induction of p53 expression.[439] This suggests that the repression of p53 by BCL6 in context-specific, including in GBM cells.

BCL6 was only involved in a small proportion of the whole proteome response to doxorubicin. Aside from the BCL6-dependent downregulation of apoptotic protein RHOB, there was little indication that BCL6 was involved in either up- or downregulation of stress or DNA damage response signalling in response to doxorubicin treatment. However, the whole proteome response of LN18 cells to doxorubicin was only examined 24 hours after treatment. BCL6 had much greater involvement in the upregulation of stress response signalling proteins 48 hours after acute IR than it did at 24 hours. Additionally, previous research showed that 48 hours after doxorubicin treatment of LN18 cells, BCL6

lost its transcriptional repression activity and perhaps gained transcriptional activation activity, just as it did 48 hours after acute IR.[207] Therefore, it may be that BCL6 does induce a stress response to doxorubicin, but this is not yet evident at 24 hours. Whole proteome analysis of LN18 cells 48 hours after doxorubicin treatment could verify this supposition.

Overall, this chapter revealed that BCL6 was important in the responses of LN18 GBM cells to multiple treatments. However, apart from downregulation of transcriptional regulators, the role of BCL6 varied depending on the conditions. In untreated GBM cells, there were indications that BCL6 suppressed cellular stress responses to allow continued survival and proliferation. In response to fractionated IR, BCL6 suppressed the DNA damage response, as it does canonically. In response to TMZ treatment, there were indications that BCL6 may contribute to resistance by upregulating telomere maintenance proteins which promote DNA repair and checkpoint signalling. Furthermore, in response to acute IR, there were indications that the role of BCL6 underwent a dramatic change, switching from a repressor of the DNA damage response to an activator of stress response signalling. This may indicate that BCL6 behaves as a molecular switch, repressing cellular responses to stresses as long as they are mild enough to manage but then initiating stress response pathways when they become too harsh and acute.

### 3.4.7 Future directions

This chapter provided insight into the role of BCL6 in the responses of LN18 GBM cells to different therapies. However, the data generated was dependent on the selectivity of FX1 for BCL6, which is not guaranteed (section 3.4.3). Therefore, the priority for future work will be to validate the results of this chapter with an alternative BCL6 inhibitor. To confirm that the whole proteome changes of LN18 cells in response to FX1 were due to inhibition of BCL6 corepressor recruitment, it would be useful validate the results with another lateral groove-blocking inhibitor, such as peptidomimetic RI-BPI.[291] Furthermore, to determine whether any of the activity of BCL6 in response to therapy is independent of corepressor recruitment to the BTB domain, it would be informative to repeat the experiments in this chapter with a BCL6-depleting siRNA.

It is also important that these results are validated in other GBM cell lines. There is vast heterogeneity in GBM tumours and therefore in the GBM cell lines derived from them, so future work will need to confirm that the role of BCL6 in the response of other GBM cell lines to treatment is the same as in LN18 cells. It would be particularly useful to validate the results of this chapter in low passage tumour-derived cell lines, which are more likely to accurately represent GBM tumours than the LN18 cell line.

If the results of this chapter can be validated with another BCL6 inhibitor and in other GBM cell lines, these results can be used to generate hypotheses for future research into the role of BCL6 in GBM therapy responses. The most interesting outcome of this study was the indication that in response to

acute IR treatment, BCL6 switched roles from a repressor of the DNA damage response to a promotor of stress response signalling. This adds to previous research showing that BCL6 induced by acute IR and doxorubicin treatment loses its transcriptional repressor activity.[207] BCL6 is known to be an evolutionarily conserved stress response protein and to be important in the survival of cancer cells and resistance to therapy.[406] However, this research indicated that the role of BCL6 may change depending on the type or level of cell stress. Future work should investigate whether this extends to other types of stress. For example, the role of BCL6 in the response to doxorubicin 48 hours after treatment should be investigated to determine whether BCL6 is involved in the activation of stress response signalling by that time point. Additionally, it would be interesting to investigate the role of BCL6 at different points during the fractionated IR and TMZ treatment courses to determine whether the role of BCL6 in the response of LN18 cells to these long-term treatments changes over time.

Previous research has shown that BCL6 inhibition enhances the efficacy of fractionated IR, TMZ and doxorubicin in the treatment of GBM cells.[207,440] No research has investigated whether BCL6 inhibition enhances the efficacy of acute IR in the treatment of GBM cells. Future work should investigate this to determine whether the apparent switch of BCL6 activity confers resistance or sensitivity to GBM cells. It may be that in response to relatively mild stress, BCL6 represses the DNA damage response to allow GBM cells to continue to proliferate. However, when the stress is intense enough, this may be detrimental to the survival of the GBM cells. In this case, the activation of stress response signalling may allow the GBM cells to recover from the acute stress and survive. Hence, although performing very different functions, it is possible that BCL6 confers resistance to both levels of stress. If this is the case, then inhibition of BCL6 is a promising target to improve the sensitivity of GBM to treatment. However, if higher levels of stress can cause BCL6 to switch to a role that increases the sensitivity of cancer cells to therapy, this could complicate the clinical targeting of BCL6.

The involvement of BCL6 in the responses of LN18 cells to fractionated IR and TMZ appeared to be very different. TMZ treatment strongly upregulated expression of BCL6 protein, however fractionated IR did not induce a change in expression of BCL6. In response to fractionated IR, BCL6 inhibited the DNA damage response by repressing expression of DNA repair proteins. However, BCL6 appeared to be important in proteome changes suggestive of decreased cellular activity and increased expression of telomere proteins in response to long-term TMZ treatment. Clinically, fractionated IR and TMZ treatments are usually administered together.[4] As the role of BCL6 in response to each treatment was so different, it is difficult to predict what its role in response to the two treatments combined would be. Therefore, these experiments should be repeated with fractionated IR and TMZ administered together, to investigate the role of BCL6 in the response to the combination of these two treatments.

Comparison of the role of BCL6 in the response of LN18 GBM cells to different therapies revealed the context-dependency of BCL6 activity. Most striking was the dramatic change in the apparent role of

BCL6 in response to acute treatment. This has important implications for our current understanding of the role of BCL6 in the treatment resistance of GBM and as a stress-response protein in general. The remainder of this thesis focuses on investigating the change in BCL6 function in response to acute IR treatment of GBM cells by using targeted approaches to look more directly at the role of BCL6.

# 4: Identification of BCL6-associated proteins in GBM using RIME

## 4.1: Introduction

In GC B cells and B cell lymphoma, BCL6 represses the transcription of genes involved in the DNA damage response and differentiation.[232,382] In response to fractionated IR treatment of LN18 GBM cells, BCL6 repressed expression of proteins involved in DNA repair as anticipated (Chapter 3). However, Chapter 3 suggested a change in BCL6 activity in response to acute IR. Instead of repressing the DNA damage response, BCL6 promoted the upregulation of stress response signalling proteins in response to acute IR. This added to previous evidence that after acute IR treatment of GBM cells, BCL6 does not act as a transcriptional repressor and may act as a transcriptional activator.[207]

The transcriptional repressor activity of BCL6 is dependent on the recruitment of corepressors.[216,217] The corepressors BCOR, NCOR1 and NCOR2 bind to the lateral groove in the BTB/POZ domain of BCL6.[215,217,219,220,441] These and other BCL6 corepressors, MTA3 and CTBP1, recruit complexes containing HDACs and SIN3A to enable transcriptional repression.[221,223–225,442] BCL6 recruits different sets of corepressors to repress different target genes.[221,228,260] It is not known whether BCL6 binds to its canonical corepressors in GBM cells. Therefore, the apparent change in BCL6 activity in response to acute IR could be mediated by alternative BCL6 binding partners. This chapter aimed to identify the proteins BCL6 associated with in untreated and irradiated GBM cells to elucidate the activity of BCL6 in each context.

This aim was made challenging by the very low abundance of BCL6 in GBM cells. Notably, endogenous BCL6 cannot be identified in whole proteome analysis of GBM cells. The conventional approach would be to overexpress tagged BCL6 to allow affinity purification. However, the proven differences between artificially overexpressed and endogenous BCL6 induced by therapy in GBM made this approach unsuitable.[322] Therefore, enrichment of the endogenous protein was necessary.

Rapid immunoprecipitation mass spectrometry of endogenous proteins (RIME) is a recently developed technique for the identification of the proteins associated with an endogenous target protein (Figure 4.1).[335,443] RIME is based on the protocol for chromatin immunoprecipitation (ChIP), in which proteins are crosslinked to the DNA they are bound to, followed by nuclear enrichment, fragmentation of the DNA and extraction of the target protein and its associated DNA sequences by immunoprecipitation. In ChIP, the DNA sequences bound by the protein of interest are examined by PCR or sequencing. In RIME, the importance of the crosslinking step is the crosslinking of the target protein to the proteins it is associated with.[335] As with ChIP, the nuclear fraction is enriched, the DNA is fragmented and the target protein is enriched by immunoprecipitation, along with the proteins it is crosslinked to.[335] Unlike

in ChIP, the DNA is discarded. Instead, the target protein and the proteins crosslinked to it are digested for analysis by mass spectrometry.[335]

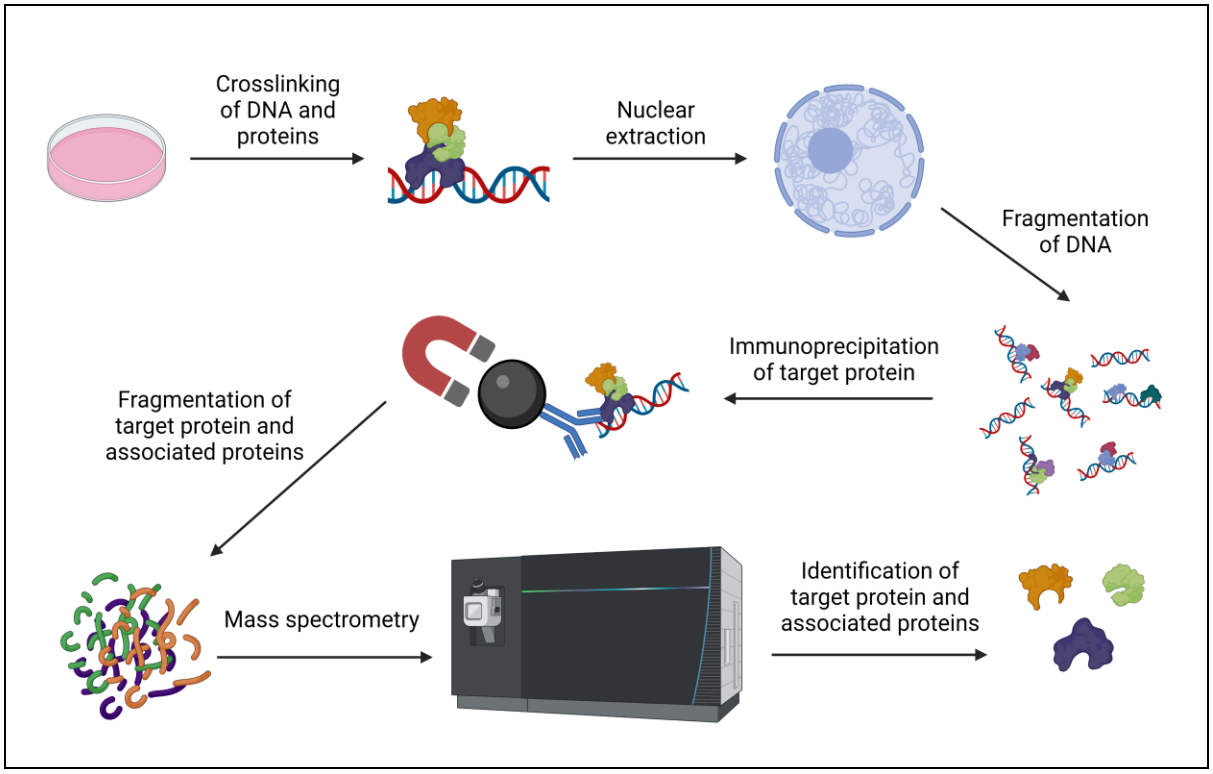


Figure 4.1: Schematic of RIME protocol
As described in Mohammed et al. (2016).[335] Image generated using BioRender.

RIME boasts several advantages over conventional immunoprecipitation. First, it allows enrichment of endogenous proteins and the proteins associated with them, which avoids the possible introduction of artifacts caused by overexpression of the protein of interest.[335] The nuclear enrichment step is beneficial for low abundance transcription factors like BCL6 and allows the capture of proteins bound to DNA which might be more easily lost in normal proteomic processing. Furthermore, the protein of interest is crosslinked to its associated proteins. This allows stringent washes to remove non-specific proteins without disrupting the interactions of interest.[335] This reduces the impact of one of the main limitations of immunoprecipitation experiments: the challenge of distinguishing genuine binding partners from non-specific proteins. The maintenance of protein associations by crosslinking also allows the capture of transient as well as high affinity interactions, which might usually be lost during wash steps.[335] This provides a more complete picture of the proteins associated with the protein of interest than immunoprecipitation alone can accomplish.

The crosslinking is achieved using formaldehyde, which due to its small size and short spacer-arm (2.3-2.7 Å) only crosslinks proteins in close association.[444] Formaldehyde is able to cross the membranes of living cells and the crosslinking reaction is quick enough to capture transient interactions.[444] Thus, RIME enables examination of the protein 'nano-environment' of the protein of interest by capturing the proteins associated with it at a moment in time.

## 4.2: Aims

The aims of this chapter were to identify the proteins BCL6 associated with in GBM cell lines and to examine whether these associations changed in response to acute IR treatment. It was of particular interest whether BCL6 associated with its known corepressors, which would suggest that it retained its transcriptional repressor role in GBM, or whether it had any novel associations that could provide insight into the role of BCL6 in GBM and in GBM treatment response.

## 4.3: Results

### 4.3.1: Validation of the RIME protocol

#### 4.3.1.1: RNA polymerase II

Chromatin immunoprecipitation (ChIP) for BCL6 in GBM cells had already been established by the McConnell lab group.[322] The established ChIP protocol was merged with the RIME methodology described by Mohammed et al. (2016).[335] This included changes to the length of formaldehyde treatment to favour modification of lysine side chains rather than the less specific modification expected to occur with longer treatment times.[335,444] Additionally, the steps of the RIME protocol designed to prepare the captured proteins for mass spectrometry replaced the DNA purification steps of the ChIP protocol.[335]

This merged protocol was verified using an antibody to the abundant protein RNA polymerase II. LN18 GBM cells were fixed with formaldehyde before being lysed, sonicated and added to beads coated with the RNA polymerase II antibody to immunoprecipitate RNA polymerase II and its associated proteins. The proteins were digested on the beads and then analysed by LC-MS/MS. A total of 770 proteins were identified with high confidence. This was within the expected range stated by Mohammed et al. (2016).[335] Reassuringly, RNA polymerase II subunits RPB1 (POLR2A) and RPB2 (POLR2B) were the highest and third highest confidence proteins identified (Table 4.1). Many of the other identified proteins, such as transcription elongation factors (including SUPT5H and SUPT6H) and histones, were known to interact with RNA polymerase II. This verified that the RIME protocol was able to enrich for the protein of interest along with expected associated proteins.

Cytoskeletal proteins such as keratin were also identified. The high abundance of keratin in human hair and skin makes it likely that these were contaminants from dust and particles in the air. Subsequently, this was minimised by performing the whole experiment in a laminar flow hood, however the identification of some contaminating cytoskeletal proteins seemed unavoidable. This is likely because the high abundance of these proteins resulted in some carry-over from the cell preparation into the crosslinked sonicated samples added to the beads. As the proteins of interest were a small, relatively low abundance fraction of the whole proteome, there were enough of these cytoskeletal proteins carried over to be identified by mass spectrometry.

Table 4.1: Top ten proteins identified by RIME in LN18 cells with RNA polymerase II antibody

From left to right, the columns show the following parameters: Uniprot accession number; protein name; false discovery rate (q value) calculated using decoy search; sum posterior error probability (PEP) score; the percentage of the protein covered by the identified peptides; the number of peptides identified which mapped to the protein; the number of peptide spectrum matches (PSMs) that mapped to the protein. The PEP score is a measure of the likelihood of a PSM being a random event. The sum PEP score is the negative logarithm of the sum of the PEP scores for the PSMs mapping to a protein (higher PEP score indicates higher confidence in the protein identification). q values < 0.001 are shown as 0.

| Protein Accession | Protein Name | q value | Sum PEP Score | Coverage (%) | Peptides | PSMs |
|---|---|---|---|---|---|---|
| P24928 | POLR2A | 0 | 436.752 | 46 | 77 | 174 |
| Q7KZ85 | SUPT6H | 0 | 278.433 | 42 | 60 | 106 |
| P30876 | POLR2B | 0 | 266.992 | 43 | 49 | 104 |
| P04264 | KRT1 | 0 | 265.014 | 58 | 46 | 116 |
| P35908 | KRT2 | 0 | 260.744 | 75 | 41 | 91 |
| O00267 | SUPT5H | 0 | 238.568 | 43 | 43 | 85 |
| P35527 | KRT9 | 0 | 235.872 | 73 | 33 | 95 |
| P13645 | KRT10 | 0 | 181.422 | 47 | 29 | 77 |
| P08670 | VIM | 0 | 124.011 | 65 | 31 | 52 |
| P60709 | ACTB | 0 | 121.545 | 58 | 18 | 37 |

#### 4.3.1.2: RIME for BCL6 in a human B cell lymphoma cell line

RIME for BCL6 was first performed in the Raji Burkitt's lymphoma cell line. BCL6 is well characterised in B cell lymphoma cells, which express higher levels of BCL6 than GBM.[207,445] This experiment aimed to confirm that RIME could identify BCL6 and the proteins it is known to bind to in lymphoma.

##### 4.3.1.2.1: Identification of BCL6 in Raji cells

Raji cells were fixed, lysed and sonicated and BCL6 and its associated proteins pulled down by a BCL6 antibody. The immunoprecipitated proteins were digested and analysed by LC-MS/MS. Unlike RNA polymerase II, BCL6 was not the most confident protein identification, reflecting the lower abundance of BCL6. Nonetheless, BCL6 was identified with high confidence (decoy search false discovery rate (q) < 0.001) and reasonable coverage in all replicates (Table 4.2).

Raji replicates 1 and 2 were run on the Orbitrap Fusion™ Lumos™ Tribrid™ Mass Spectrometer at Victoria University of Wellington, New Zealand. Due to problems with the Lumos™ mass spectrometer over the course of this project, replicate 3 was run on the Q Exactive™ Plus Mass Spectrometer at the Bio21 Molecular Science and Biotechnology Institute Mass Spectrometry and Proteomics Facility at the University of Melbourne, Australia. The instrument used at the Bio21 Institute was more sensitive, resulting in the identification of more proteins in the sample analysed on that instrument. Additionally, BCL6 was identified with greater coverage and a larger sum PEP score in replicate 3 (Table 4.2).

Table 4.2: Parameters of BCL6 identification in Raji RIME experiments

From left to right, the columns show the following parameters: biological replicate; position of BCL6 in the list of identified proteins ranked by sum posterior error probability (PEP) score; false discovery rate (q value) calculated using decoy search; sum PEP score; the percentage of the protein covered by the identified peptides; the number of peptides identified which mapped to the protein; the number of peptide spectrum matches (PSMs) that mapped to the protein. The PEP score is a measure of the likelihood of a PSM being a random event. The sum PEP score is the negative logarithm of the sum of the PEP scores for the PSMs mapping to a protein (higher PEP score indicates higher confidence in the protein identification). q values < 0.001 are shown as 0.

| Replicate | Position in list | q value | Sum PEP score | Coverage (%) | Peptides | PSMs |
|---|---|---|---|---|---|---|
| **1** | 96/588 | 0 | 17.369 | 15 | 9 | 10 |
| **2** | 32/466 | 0 | 32.873 | 22 | 12 | 17 |
| **3** | 30/993 | 0 | 91.974 | 27 | 17 | 26 |

#### 4.3.1.2.2: Known BCL6 binding partners in Raji cells

Five known BCL6 binding partners, BCOR, NCOR1, NCOR2, HDAC1 and HDAC2, were identified as BCL6-associated proteins in Raji BCL6 RIME replicate 3 (Table 4.3). HDAC1 and another known BCL6 corepressor MTA3 were also identified as BCL6-associated proteins in replicate 1. This supported the hypothesis that RIME is able to pull down BCL6 and its known corepressors when they are bound to it. However, none of the major BCL6 corepressors, BCOR, NCOR1 or NCOR2, were identified in Raji replicates 1 or 2. As these corepressors were identified with low coverage (≤ 3%) in replicate 3, it may be that they could only be identified by the more sensitive instrument at the Bio21 Institute. These corepressors likely fell below the threshold of detection on the Lumos™ mass spectrometer.

Table 4.3: Parameters of known BCL6 binding partner identification in Raji RIME experiments

From left to right, the columns show the following parameters: biological replicate (1-3); protein name; position of BCL6 in the list of identified proteins ranked by sum posterior error probability (PEP) score; false discovery rate (q value) calculated using decoy search; sum PEP score; the percentage of the protein covered by the identified peptides; the number of peptides identified which mapped to the protein; the number of peptide spectrum matches (PSMs) that mapped to the protein. The PEP score is a measure of the likelihood of a PSM being a random event. The sum PEP score is the negative logarithm of the sum of the PEP scores for the PSMs mapping to a protein (higher PEP score indicates higher confidence in the protein identification). q values < 0.001 are shown as 0.

| Raji rep. | Protein name | Position in list | q value | Sum PEP score | Coverage (%) | Peptides | PSMs |
|---|---|---|---|---|---|---|---|
| **3** | BCL6 corepressor (BCOR) | 622/993 | 0 | 5.529 | 2 | 2 | 2 |
| **3** | Nuclear receptor corepressor 1 (NCOR1) | 274/993 | 0 | 19.584 | 3 | 5 | 6 |
| **3** | Nuclear receptor corepressor 2 (NCOR2) | 444/993 | 0 | 9.548 | 2 | 4 | 4 |
| **1** | Metastasis-associated protein MTA3 | 350/588 | 0 | 4.488 | 5 | 2 | 2 |
| **1** | Histone deacetylase 1 (HDAC1) | 560/588 | 0.005 | 1.623 | 2 | 1 | 1 |
| **3** | Histone deacetylase 1 (HDAC1) | 352/993 | 0 | 13.301 | 15 | 6 | 6 |
| **3** | Histone deacetylase 2 (HDAC2) | 340/993 | 0 | 13.694 | 13 | 5 | 5 |

## 4.3.2: RIME for BCL6 in untreated and irradiated GBM cell lines

RIME for BCL6 was performed in biological triplicate with LN18, NZG0906 and NZG1003 GBM cell lines. Repetition within and between GBM cell lines accounted for biological variation and the heterogeneity of GBM tumours and cell lines. To examine the effect of acute IR on BCL6 activity, the GBM cells were either untreated or treated with 10 Gy acute IR 48 hours before RIME.

The identification of false positives is a known limitation of affinity purification experiments.[446] Therefore, to control for non-specific binding of proteins to the beads and antibodies, cells were processed as described in sections 4.3.1.1 and 4.3.1.2 before being split equally between tubes containing magnetic beads bound to either the anti-BCL6 antibody or a non-specific IgG antibody. The proteins pulled down with the anti-BCL6 antibody-coated beads and the IgG-coated beads were processed and analysed in parallel. Only proteins identified with high confidence (decoy search false discovery rate (q) $\leq 0.01$) were included in further analysis.

### 4.3.2.1: Variation between replicates

There were unfortunate but unavoidable changes to the mass spectrometer used for the analysis of the RIME experiments. The irradiated LN18 replicates, irradiated NZG0906 replicates 1 and 2 and untreated NZG1003 replicate 1 were run on the Orbitrap Fusion™ Lumos™ Tribrid™ Mass Spectrometer at Victoria University of Wellington, New Zealand. The RIME protocol was optimised using this instrument and the number of proteins identified in the samples run on the Lumos™ mass spectrometer were within the expected 300-900 range stated by Mohammed et al. (2016). However, due to long-term instrument failure, the remaining samples were shipped to the Bio21 Institute in Melbourne, Australia. The number of proteins identified in RIME samples run on the Q Exactive™ Plus instrument at the Bio21 Institute often exceeded the expected range due to its greater sensitivity.

This led to notable variability between replicates. Figure 4.2 examines the overlap between the proteins pulled down by the anti-BCL6 antibody in the three replicates for each untreated and irradiated GBM cell line. The samples run at the Bio21 Institute are marked with an asterisk (*). For most of the cell lines and treatments, between 30% and 50% of the proteins identified in the three replicates overlapped. However, although 35% of the proteins pulled down in the three irradiated NZG0906 RIME replicates overlapped, a further 32.8% of the total proteins were only identified in replicate 3, which was run at the Bio21 Institute (Figure 4.2D). Additionally, the untreated NZG1003 replicates had a smaller overlap of just 21.5% between the three replicates but had a large overlap of 37.8% between replicates 2 and 3, which were run at the Bio21 Institute (Figure 4.2E).

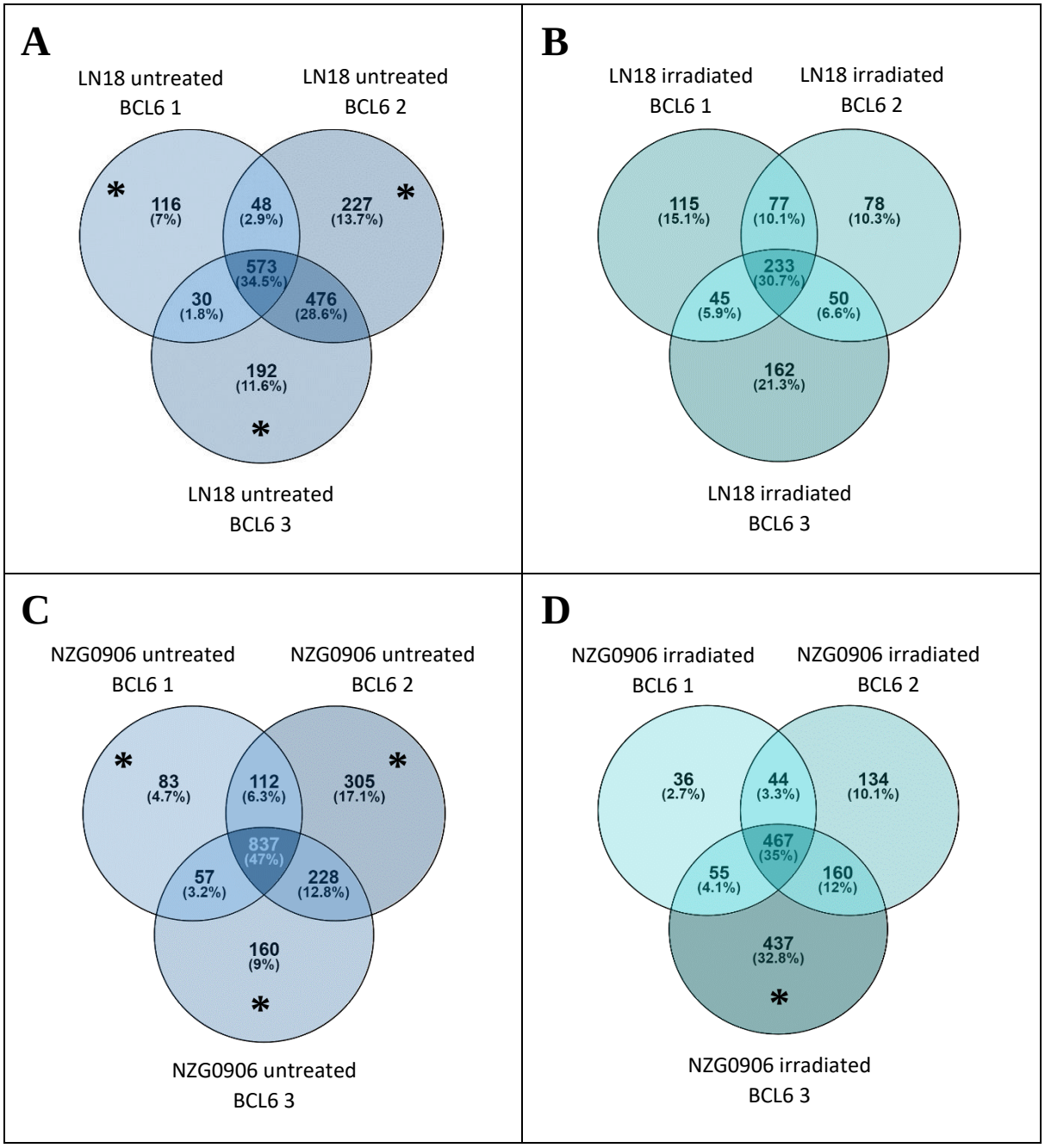
A
LN18 untreated
BCL6 1
LN18 untreated
BCL6 2
116
(7%)
48
(2.9%)
227
(13.7%)
573
(34.5%)
30
(1.8%)
476
(28.6%)
192
(11.6%)
LN18 untreated
BCL6 3
B
LN18 irradiated
BCL6 1
LN18 irradiated
BCL6 2
115
(15.1%)
77
(10.1%)
78
(10.3%)
233
(30.7%)
45
(5.9%)
50
(6.6%)
162
(21.3%)
LN18 irradiated
BCL6 3
C
NZG0906 untreated
BCL6 1
NZG0906 untreated
BCL6 2
83
(4.7%)
112
(6.3%)
305
(17.1%)
837
(47%)
57
(3.2%)
228
(12.8%)
160
(9%)
NZG0906 untreated
BCL6 3
D
NZG0906 irradiated
BCL6 1
NZG0906 irradiated
BCL6 2
36
(2.7%)
44
(3.3%)
134
(10.1%)
467
(35%)
55
(4.1%)
160
(12%)
437
(32.8%)
NZG0906 irradiated
BCL6 3

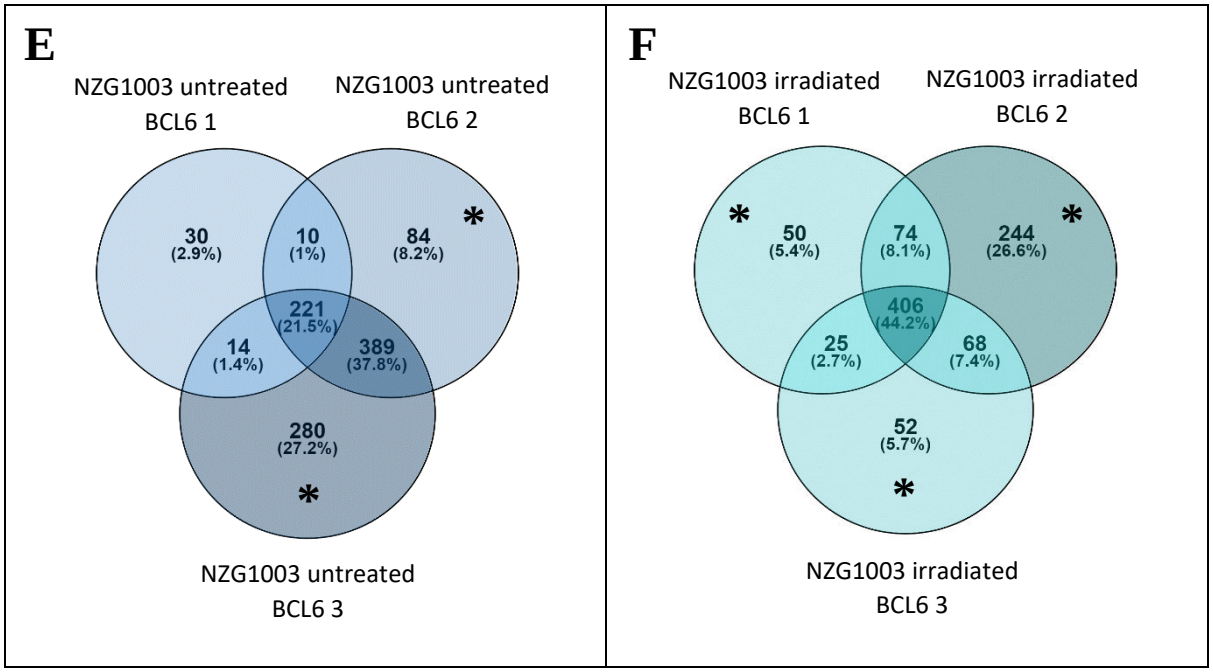


Figure 4.2: Overlap of proteins pulled down in BCL6 RIME replicates

In untreated LN18 (A), NZG0906 (C) and NZG1003 (E) cell lines and irradiated LN18 (B), NZG0906 (D) and NZG1003 (F) cell lines. Samples run at the Bio21 Institute indicated with an asterisk (*). Venn diagrams produced using Venny 2.1.[447]

### 4.3.2.1: Identification of BCL6

BCL6 was identified in all experimental replicates and no IgG control replicates. The parameters of BCL6 identification are displayed in Table 4.4. Despite the variation caused by instrument changes, it was clear that BCL6 was identified with greater coverage in the irradiated NZG0906 and NZG1003 samples than in the corresponding untreated samples. This was anticipated, as BCL6 is upregulated by acute IR treatment (section 3.3.1). BCL6 was also identified with greater coverage in the untreated and irradiated NZG0906 samples and in the irradiated NZG1003 samples than in the corresponding LN18 samples, suggesting lower BCL6 expression in that cell line.

Table 4.4: Parameters of BCL6 identification in GBM RIME experiments

From left to right, the columns show the following parameters: treatment; cell line; biological replicate; position of BCL6 in the list of identified proteins ranked by sum posterior error probability (PEP) score; false discovery rate (q value) calculated using decoy search; sum PEP score; the percentage of the protein covered by the identified peptides; the number of peptides identified which mapped to the protein; the number of peptide spectrum matches (PSMs) that mapped to the protein. The PEP score is a measure of the likelihood of a PSM being a random event. The sum PEP score is the negative logarithm of the sum of the PEP scores for the PSMs mapping to a protein (higher PEP score indicates higher confidence in the protein identification). Samples run at the Bio21 Institute indicated with an asterisk (*). q values < 0.001 are shown as 0.

| Treatment | Cell line | Replicate | Position in list | q value | Sum PEP score | Coverage (%) | Peptides | PSMs |
|---|---|---|---|---|---|---|---|---|
| Untreated | LN18 | 1* | 495/768 | 0 | 4.342 | 3 | 2 | 2 |
| | | 2* | 1156/1330 | 0 | 2.952 | 2 | 1 | 1 |
| | | 3* | 1142/1278 | 0.001 | 2.675 | 2 | 1 | 1 |
| | NZG 0906 | 1* | 294/1092 | 0 | 18.585 | 7 | 5 | 5 |
| | | 2* | 578/1490 | 0 | 17.549 | 9 | 5 | 5 |
| | | 3* | 562/1287 | 0 | 12.229 | 5 | 3 | 3 |
| | NZG 1003 | 1 | 270/276 | 0.009 | 1.135 | 2 | 1 | 1 |
| | | 2* | 207/706 | 0 | 17.593 | 10 | 7 | 7 |
| | | 3* | 725/907 | 0 | 3.382 | 2 | 2 | 2 |
| Irradiated | LN18 | 1 | 329/470 | 0 | 3.053 | 3 | 2 | 2 |
| | | 2 | 344/439 | 0.003 | 2.717 | 1 | 1 | 1 |
| | | 3 | 342/490 | 0 | 2.595 | 2 | 1 | 1 |
| | NZG 0906 | 1 | 83/603 | 0 | 22.924 | 12 | 8 | 13 |
| | | 2 | 159/806 | 0 | 20.793 | 11 | 8 | 8 |
| | | 3* | 83/1122 | 0 | 56.327 | 16 | 9 | 13 |
| | NZG 1003 | 1* | 108/557 | 0 | 20.667 | 12 | 10 | 10 |
| | | 2* | 255/793 | 0 | 14.567 | 12 | 8 | 8 |
| | | 3* | 118/552 | 0 | 22.24 | 14 | 9 | 10 |

### 4.3.2.2: Identification of known BCL6 binding partners

Table 4.5 lists the corepressors which bind to BCL6 in GC B cells and in B cell lymphoma. NCOR2, HDAC1 and HDAC2 were commonly identified in the BCL6 RIME data, especially in untreated GBM cells. NCOR1 was only identified in one untreated NZG0906 replicate and CTPB1 was only identified in two irradiated NZG0906 replicates. BCL6 corepressors BCOR, SIN3A and MTA3 were not identified in any GBM RIME replicates. Neither were any other HDAC proteins.

BCL6 corepressors were most commonly identified in the NZG0906 replicates. This may be because the highest coverage of BCL6 was seen in samples from this cell line and therefore the coverage of the low abundance corepressors was also increased. Meanwhile the lower coverage of BCL6 in the LN18 and NZG1003 samples may have caused the corepressor proteins to drop below the threshold of detection in some samples. NCOR2, HDAC1 and HDAC2 were only identified in untreated LN18 and NZG1003 replicates. This suggested that BCL6 bound to these corepressors more commonly in untreated GBM cells compared to after acute IR treatment. However, this interpretation must be treated with caution as NCOR2, HDAC1 and HDAC2 may have fallen below the threshold of detection in the irradiated LN18 samples as they were run on the less sensitive mass spectrometer.

Table 4.5: Identification of known BCL6 binding partners in BCL6 RIME data from GBM cell lines
Replicates in which each protein was identified highlighted in dark blue (untreated) or light blue (irradiated).

| Protein Accession | Protein name | Untreated | | | | | | | | | Irradiated | | | | | | | | |
|---|---|---|---|---|---|---|---|---|---|---|---|---|---|---|---|---|---|---|---|
| | | LN18 | | | NZG 0906 | | | NZG 1003 | | | LN18 | | | NZG 0906 | | | NZG 1003 | | |
| | | 1 | 2 | 3 | 1 | 2 | 3 | 1 | 2 | 3 | 1 | 2 | 3 | 1 | 2 | 3 | 1 | 2 | 3 |
| Q6W2J9 | BCOR | | | | | | | | | | | | | | | | | | |
| O75376 | NCOR1 | | | | | | | | | | | | | | | | | | |
| Q9Y618 | NCOR2 | | | | | | | | | | | | | | | | | | |
| Q96ST3 | SIN3A | | | | | | | | | | | | | | | | | | |
| Q13363 | CTBP1 | | | | | | | | | | | | | | | | | | |
| Q9BTC8 | MTA3 | | | | | | | | | | | | | | | | | | |
| Q13547 | HDAC1 | | | | | | | | | | | | | | | | | | |
| Q92769 | HDAC2 | | | | | | | | | | | | | | | | | | |

## 4.3.3: Identification-based determination of BCL6-associated proteins

### 4.3.3.1: Subtraction of non-specific proteins

Mohammed et al. (2016) recommended the exclusion of all proteins identified in the corresponding IgG replicates from the lists of proteins identified in each BCL6 replicate.[335] This method risked the loss of true positives, however its stringency assured the confident identification of BCL6-associated proteins with low risk of false positives. Therefore, for each cell line and treatment, a compiled list of non-specific proteins was created by combining the lists of proteins identified in the three IgG replicates and removing duplicates. These compiled lists of proteins were subtracted from each BCL6 replicate to leave only BCL6-specific proteins (Table 4.6).

After subtraction of non-specific proteins, few proteins overlapped between all three replicates for each cell line and treatment (Figure 4.3). This indicated that a large proportion of the similarity between replicates was due to non-specific proteins also found in the IgG replicates.

Table 4.6: Subtraction of non-specific proteins from proteins pulled down with the BCL6 antibody

The number of proteins identified with high confidence in each BCL6 and IgG replicate are shown. The number of proteins identified in total across the three IgG replicates after removal of duplicates (compiled) for each cell line and treatment are shown below the IgG replicates. The compiled lists of proteins identified in the IgG samples were subtracted from each corresponding BCL6 replicate. The number of proteins remaining in each BCL6 sample list after this are shown in the "BCL6-specific" column.

| Treatment | Cell line | Replicate | Number of proteins | | |
|---|---|---|---|---|---|
| | | | BCL6 | IgG | BCL6-specific |
| Untreated | LN18 | 1 | 768 | 851 | **140** |
| | | 2 | 1330 | 1122 | **295** |
| | | 3 | 1278 | 435 | **244** |
| | | Compiled | | 1365 | |
| | NZG0906 | 1 | 1092 | 932 | **84** |
| | | 2 | 1490 | 1569 | **143** |
| | | 3 | 1287 | 1292 | **93** |
| | | Compiled | | 1819 | |
| | NZG1003 | 1 | 276 | 830 | **37** |
| | | 2 | 706 | 650 | **50** |
| | | 3 | 907 | 1096 | **70** |
| | | Compiled | | 1229 | |
| Irradiated | LN18 | 1 | 470 | 334 | **147** |
| | | 2 | 439 | 473 | **80** |
| | | 3 | 490 | 245 | **183** |
| | | Compiled | | 548 | |
| | NZG0906 | 1 | 603 | 670 | **32** |
| | | 2 | 806 | 1157 | **54** |
| | | 3 | 1122 | 724 | **243** |
| | | Compiled | | 1335 | |
| | NZG1003 | 1 | 557 | 751 | **65** |
| | | 2 | 793 | 527 | **129** |
| | | 3 | 552 | 568 | **46** |
| | | Compiled | | 884 | |

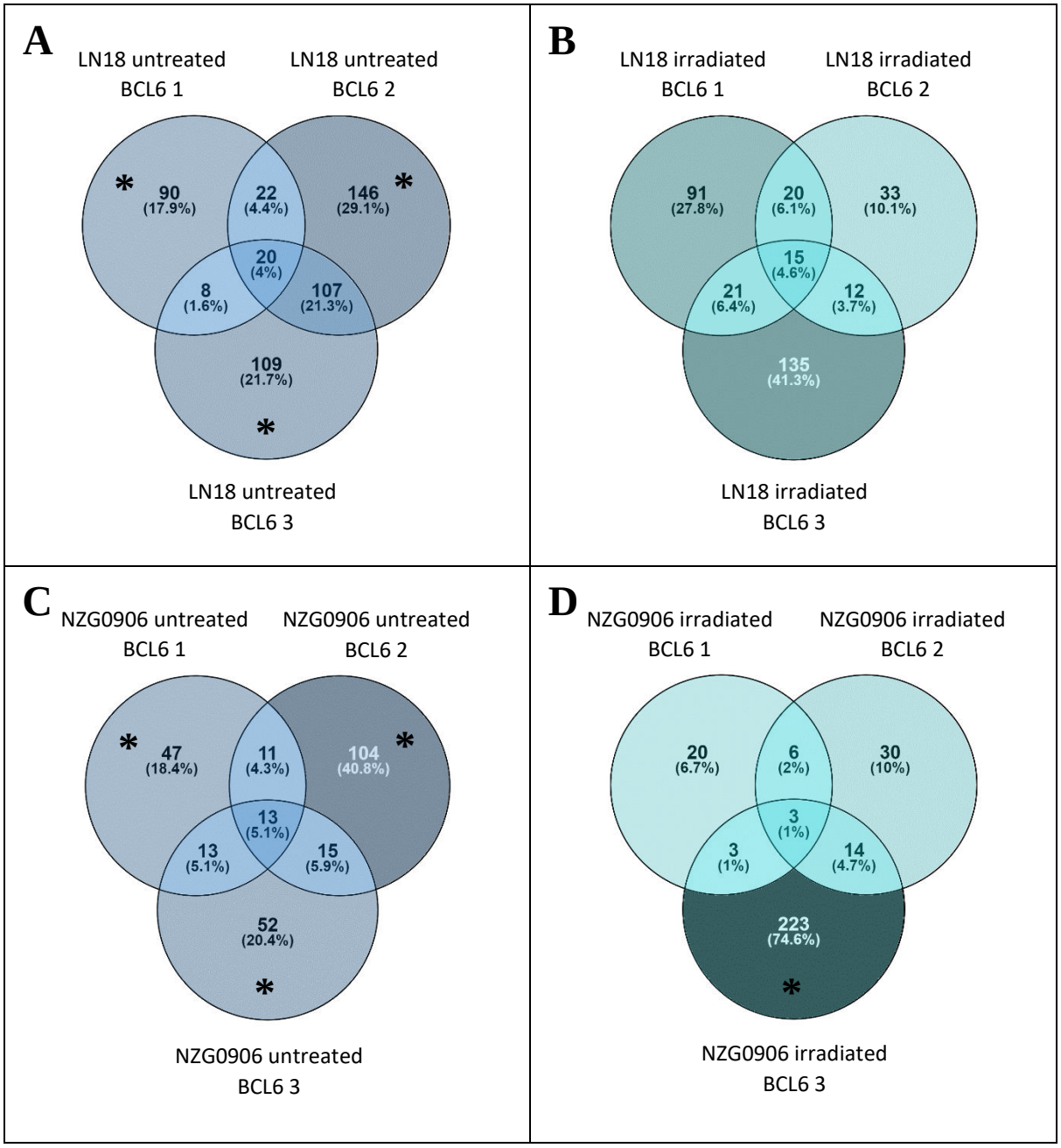
A
LN18 untreated BCL6 1
LN18 untreated BCL6 2
LN18 untreated BCL6 3
90 (17.9%)
22 (4.4%)
146 (29.1%)
20 (4%)
8 (1.6%)
107 (21.3%)
109 (21.7%)
B
LN18 irradiated BCL6 1
LN18 irradiated BCL6 2
LN18 irradiated BCL6 3
91 (27.8%)
20 (6.1%)
33 (10.1%)
15 (4.6%)
21 (6.4%)
12 (3.7%)
135 (41.3%)
C
NZG0906 untreated BCL6 1
NZG0906 untreated BCL6 2
NZG0906 untreated BCL6 3
47 (18.4%)
11 (4.3%)
104 (40.8%)
13 (5.1%)
13 (5.1%)
15 (5.9%)
52 (20.4%)
D
NZG0906 irradiated BCL6 1
NZG0906 irradiated BCL6 2
NZG0906 irradiated BCL6 3
20 (6.7%)
6 (2%)
30 (10%)
3 (1%)
3 (1%)
14 (4.7%)
223 (74.6%)

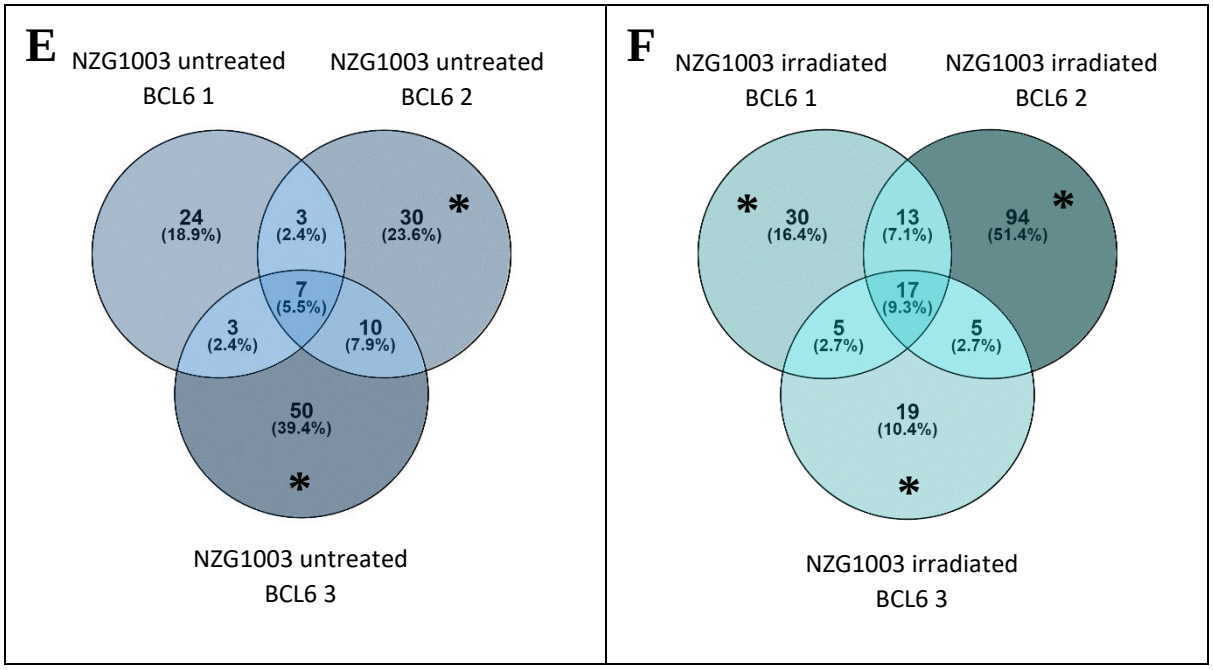


Figure 4.3: Overlap of proteins pulled down in BCL6 RIME replicates after subtraction of non-specific proteins found in IgG replicates

Overlap between replicates shown for untreated LN18 (A), NZG0906 (C) and NZG1003 (E) cell lines and irradiated LN18 (B), NZG0906 (D) and NZG1003 (F) cell lines. Samples run at the Bio21 Institute indicated with an asterisk (*). Venn diagrams produced using Venny 2.1.[447]

### 4.3.3.2: Commonly identified proteins

There was also substantial variation between the proteins pulled down by the BCL6 antibody in the different cell lines (Figure 4.4) as well as in each replicate, reinforcing the importance of repeating the RIME experiments in multiple GBM cell lines. However, there was some overlap. To confidently identify BCL6-associated proteins, only proteins identified in ≥ 3 untreated or irradiated GBM replicates of any of the cell lines were considered. By this definition, there were 67 commonly identified BCL6-associated proteins in untreated GBM cells and 44 commonly identified BCL6-associated proteins in irradiated GBM cells.

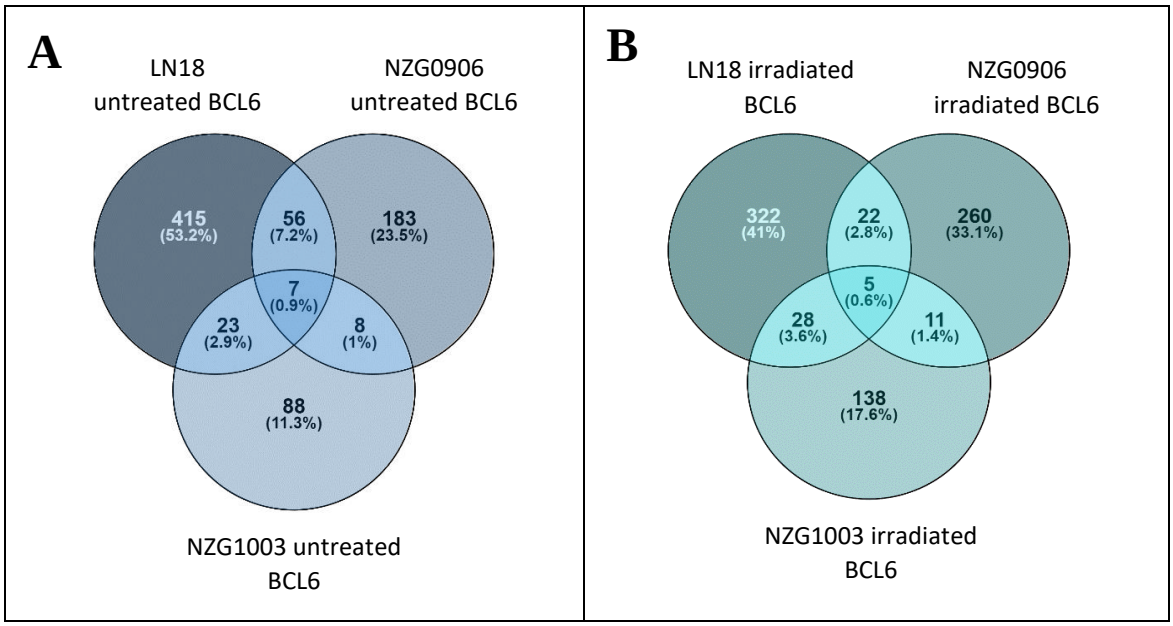


Figure 4.4: Overlap between cell lines

Overlap of proteins identified in any of the BCL6 replicates for each untreated (A) and irradiated (B) cell line, after subtraction of non-specific proteins found in IgG replicates. Venn diagrams produced using Venny 2.1.[447]

#### 4.3.3.3: Subtraction of proteins with high CRAPome scores

The CRAPome is a repository of lists of proteins identified in the negative controls of affinity purification mass spectrometry (AP-MS) experiments submitted by users of the repository.[448] The lists of BCL6-associated proteins identified in treated and untreated GBM cells were entered into the CRAPome 2.0 Workflow 1: "Query proteins and retrieve profiles". In the absence of a RIME-specific database, the proteins were searched against the CRAPome "H. sapiens Single Step Epitope Tag AP-MS" database. This database contained the proteins identified in 716 negative control AP-MS experiments. The CRAPome output showed how many of these negative control experiments each BCL6-associated protein had been identified in (Appendix).

Proteins that were identified in > 10% of the experiments in the database were excluded. While this was an arbitrary cut off, it ensured that only proteins that were infrequently identified in AP-MS experiments, which were therefore unlikely to be contaminants, were retained. This risked the loss of genuine BCL6-associated proteins that were commonly found in contaminant lists. However, the aim was to exclude all possible non-specific proteins to be as confident as possible in the identification of BCL6-associated proteins.

After subtraction of proteins identified in > 10% of CRAPome AP-MS experiments, there were 32 BCL6-associated proteins in untreated GBM cells and 20 BCL6-associated proteins in irradiated GBM cells.

#### 4.3.3.4: Known BCL6 binding partners

The stringency of the data processing methods used to remove false positives from the lists of BCL6-associated proteins resulted in the loss of all of the known BCL6 corepressor binding partners except NCOR2. NCOR2 was identified in two untreated LN18 replicates, one untreated NZG1003 replicate and three irradiated NZG0906 replicates. Although NCOR2 was also found in all three untreated NZG0906 replicates (Table 4.5), it was also found in one of the untreated NZG0906 IgG control replicates, meaning that it was eliminated from the list of BCL6-associated proteins found in the untreated NZG0906 replicates.

NCOR1 and CTBP1 were eliminated as they were identified in fewer than three replicates. HDAC1 and HDAC2 were excluded from the list of BCL6-associated proteins as they were found in IgG replicates and in 43% and 44% of the negative control experiments in the CRAPome database respectively. As HDAC1 and HDAC2 are known BCL6 binding partners, it is likely that they are genuine BCL6-associated proteins in GBM cells but are also common contaminant proteins.

The EMBL-EBI tool PSICQUIC View version 1.4.11 was used to search databases conforming to the Human Proteome Organisation (HUPO) Proteomics Standard Initiative for known BCL6 protein-protein interactions (PPIs).[449] PSICQUIC View clustered the evidence for each PPI, allowing comparison of known BCL6-associated proteins with the RIME results. This revealed that in addition to the corepressors described above, two other proteins known to interact with BCL6 were identified by RIME in GBM cells. NCOR complex component TBL1XR1 was identified as a BCL6-associated protein in all untreated NZG0906 replicates and one untreated LN18 replicate.[450] Additionally, FBXO11, the substrate-recognition component of an E3 ubiquitin-protein ligase complex known to mediate ubiquitination and degradation of BCL6, was identified as a BCL6-associated protein in almost all irradiated replicates and in all untreated NZG1003 replicates and one untreated NZG0906 replicate.[255] The identification of these known BCL6 binding partners helped to verify that the RIME technique was successful.

### 4.3.3.5: BCL6-associated proteins in untreated and irradiated GBM cells

After the data processing described above, there were 11 proteins commonly identified as BCL6-associated in both untreated and irradiated GBM cells (Table 4.7). There were also 21 BCL6-associated proteins specific to untreated GBM cells (Table 4.8) and nine BCL6-associated proteins specific to irradiated GBM cells (Table 4.9).

Table 4.7: BCL6-associated proteins commonly identified in both untreated and irradiated GBM cell lines

Replicates in which each protein was identified as a BCL6-associated protein highlighted in dark blue (untreated) or light blue (irradiated).

| Protein Accession | Protein name | Untreated | | | | | | | | | Irradiated | | | | | | | | |
|---|---|---|---|---|---|---|---|---|---|---|---|---|---|---|---|---|---|---|---|
| | | LN18 | | | NZG 0906 | | | NZG 1003 | | | LN18 | | | NZG 0906 | | | NZG 1003 | | |
| | | 1 | 2 | 3 | 1 | 2 | 3 | 1 | 2 | 3 | 1 | 2 | 3 | 1 | 2 | 3 | 1 | 2 | 3 |
| P04196 | HRG | | | | | | | | | | | | | | | | | | |
| P01024 | C3 | | | | | | | | | | | | | | | | | | |
| Q96LD4 | TRIM47 | | | | | | | | | | | | | | | | | | |
| P27169 | PON1 | | | | | | | | | | | | | | | | | | |
| Q86XK2 | FBXO11 | | | | | | | | | | | | | | | | | | |
| P54619 | PRKAG1 | | | | | | | | | | | | | | | | | | |
| Q13131 | PRKAA1 | | | | | | | | | | | | | | | | | | |
| P02461 | COL3A1 | | | | | | | | | | | | | | | | | | |
| Q9Y618 | NCOR2 | | | | | | | | | | | | | | | | | | |
| O75146 | HIP1R | | | | | | | | | | | | | | | | | | |
| P02647 | APOA1 | | | | | | | | | | | | | | | | | | |

Table 4.8: BCL6-associated proteins commonly identified only in untreated GBM cells

Replicates in which each protein was identified as a BCL6-associated protein highlighted in dark blue.

| Protein Accession | Protein name | LN18 | | | NZG0906 | | | NZG1003 | | |
|---|---|---|---|---|---|---|---|---|---|---|
| | | 1 | 2 | 3 | 1 | 2 | 3 | 1 | 2 | 3 |
| Q01433 | AMPD2 | | | | | | | | | |
| P02458 | COL2A1 | | | | | | | | | |
| Q9BZK7 | TBL1XR1 | | | | | | | | | |
| P19823 | ITIH2 | | | | | | | | | |
| Q9UBF1 | MAGEC2 | | | | | | | | | |
| P01599 | IGKV1-17 | | | | | | | | | |
| O75351 | VPS4B | | | | | | | | | |
| P17931 | LGALS3 | | | | | | | | | |
| P29508 | SERPINB3 | | | | | | | | | |
| P04114 | APOB | | | | | | | | | |
| P48735 | IDH2 | | | | | | | | | |
| Q86WA8 | LONP2 | | | | | | | | | |
| Q9HD26 | GOPC | | | | | | | | | |
| P51530 | DNA2 | | | | | | | | | |
| O00625 | PIR | | | | | | | | | |
| Q8IXK0 | PHC2 | | | | | | | | | |
| P42765 | ACAA2 | | | | | | | | | |
| Q99661 | KIF2C | | | | | | | | | |
| P04040 | CAT | | | | | | | | | |
| P12273 | PIP | | | | | | | | | |
| Q13043 | STK4 | | | | | | | | | |

Table 4.9: BCL6-associated proteins commonly identified only in irradiated GBM cell lines

Replicates in which each protein was identified as a BCL6-associated protein highlighted in light blue.

| Protein Accession | Protein name | LN18 | | | NZG0906 | | | NZG1003 | | |
|---|---|---|---|---|---|---|---|---|---|---|
| | | 1 | 2 | 3 | 1 | 2 | 3 | 1 | 2 | 3 |
| P83111 | LACTB | | | | | | | | | |
| P02452 | COL1A1 | | | | | | | | | |
| Q86SE5 | RALYL | | | | | | | | | |
| Q06033 | ITIH3 | | | | | | | | | |
| P61764 | STXBP1 | | | | | | | | | |
| P01023 | A2M | | | | | | | | | |
| P53680 | AP2S1 | | | | | | | | | |
| P02790 | HPX | | | | | | | | | |
| Q969G5 | CAVIN3 | | | | | | | | | |

## 4.3.4: Quantification-based determination of BCL6-associated proteins

In the follow-up to the 2016 RIME protocol publication, Papachristou et al. (2018) recommended an alternative method of removing non-specific proteins which reduces the loss of true positives.[443] In this method, proteins identified in experimental and IgG control replicates are quantitatively compared and proteins not at ≥ 2-fold higher abundance in the experimental samples are excluded. Hence proteins that would be excluded by subtraction of proteins identified in IgG replicates are retained if they are differentially pulled down by the target protein antibody compared to the IgG antibody. The RIME data was re-analysed with this method to identify the true positives lost in the more stringent method used in section 4.3.3.

The BCL6 and IgG replicates for each cell line were quantitatively compared. To be considered BCL6-associated, proteins had to be identified with high confidence (decoy search false discovery rate (q) ≤ 0.01) and upregulated ≥ 2-fold ($p \leq 0.05$, Benjamini-Hochberg multiple comparisons testing) in the BCL6 samples compared to the IgG samples. Proteins were excluded if they were identified at high abundance in any of the IgG replicates. As there were insufficient background proteins in the irradiated LN18 samples for a background-based t-test to be performed, proteins were considered BCL6-associated proteins on the basis of fold-change alone in those samples. Encouragingly, none of the upregulated proteins in the irradiated NZG0906 and NZG1003 samples had adjusted p values > 0.05. The lists of proteins upregulated ≥ 2-fold in the BCL6 samples were entered into the CRAPome 2.0 Workflow 1: "Query proteins and retrieve profiles".[448] Any proteins identified in > 10% of the 716 negative control AP-MS experiments were excluded from further analysis.

The BCL6-associated proteins commonly identified in both untreated and irradiated GBM cell lines were also upregulated in the BCL6 samples compared to the IgG samples in at least one untreated and one irradiated GBM cell line (Table 4.10). A handful of proteins only identified as BCL6-associated in either untreated or irradiated GBM cells with the identification-based method (COLA2, IGKV1-17, HPX and A2M) were identified in both untreated and irradiated GBM cells when the lists of proteins identified by the two methods were combined. Furthermore, GOLGA2, was identified as a BCL6-associated protein in two untreated and two irradiated GBM cell lines using the quantification-based method, despite not being commonly identified using the identification-based method. The PSICQUIC View search for BCL6 PPIs revealed that GOLGA2 has been shown to bind to BCL6 in two large-scale yeast-two-hybrid human interactome studies.[449,451,452] This thesis provides the first validation of this association in an endogenous context. GOLGA2 is involved in Golgi structure, vesicle transport and mitotic spindle pole assembly, so it is intriguing to see it associated with BCL6.[453,454]

Known BCL6 binding partner NCOR2 was not identified as a BCL6-associated protein in untreated LN18 or NZG1003 cells using the quantification-based method, despite being identified in these cells using the identification-based method. In untreated LN18 cells, the abundance ratio for NCOR2 was

just below the 2-fold threshold. Meanwhile, the NCOR2 peptides identified in the NZG1003 samples were filtered out by the settings of the quantitative analysis. The quantitative analysis settings specified that only unique or razor peptides were used for quantification. Unique peptides were those not shared by any other protein groups, while razor peptides were shared with other protein groups but were assigned to the protein group with the highest number of identified peptides. All other shared peptides were excluded from quantification. Other peptides were excluded from quantification because the consensus features associated with them could be assigned to more than one peptide.

NCOR2 was identified by both methods in irradiated NZG0906 cells. Surprisingly, NCOR2 was also identified by this method in irradiated NZG1003 cells, even though it was not identified with high confidence in any of the irradiated NZG1003 replicates. Closer inspection revealed that one NCOR2 peptide was identified and quantified in one irradiated NZG1003 replicate, while none were detected in the IgG replicates. Therefore, this identification seems tentative and should be interpreted with caution.

The quantification-based method identified many BCL6-associated proteins that were not identified using the identification-based method. Those that were upregulated in the BCL6 samples compared to the IgG samples in at least two untreated GBM cell lines are displayed in Table 4.11 below the BCL6-associated proteins identified in untreated GBM cells in section 4.3.3.5. The BCL6-associated proteins that were upregulated in the BCL6 samples compared to the IgG samples in at least two irradiated GBM cell lines are displayed in Table 4.12 below the BCL6-assocaited proteins identified in irradiated GBM cells in section 4.3.3.5.

Table 4.10: BCL6-associated proteins identified in both untreated and irradiated GBM cell lines using the identification-based and/or quantification-based methods

Replicates in which each protein was identified as a BCL6-associated protein using the identification-based method highlighted in dark blue (untreated) or light blue (irradiated) as in Table 4.7. ↑ columns filled with pink (untreated) or purple (irradiated) indicate that the protein was upregulated in the experimental (anti-BCL6) samples compared to the control (IgG) samples for that cell line (quantification-based method).

| Accession | Protein names | Untreated | | | | | | | | | | | | Irradiated | | | | | | | | | | | |
|---|---|---|---|---|---|---|---|---|---|---|---|---|---|---|---|---|---|---|---|---|---|---|---|---|---|
| | | LN18 | | | | NZG0906 | | | | NZG1003 | | | | LN18 | | | | NZG0906 | | | | NZG1003 | | | |
| | | 1 | 2 | 3 | ↑ | 1 | 2 | 3 | ↑ | 1 | 2 | 3 | ↑ | 1 | 2 | 3 | ↑ | 1 | 2 | 3 | ↑ | 1 | 2 | 3 | ↑ |
| P04196 | HRG | | | | | | | | | | | | | | | | | | | | | | | | |
| P01024 | C3 | | | | | | | | | | | | | | | | | | | | | | | | |
| Q96LD4 | TRIM47 | | | | | | | | | | | | | | | | | | | | | | | | |
| P27169 | PON1 | | | | | | | | | | | | | | | | | | | | | | | | |
| Q86XK2 | FBXO11 | | | | | | | | | | | | | | | | | | | | | | | | |
| P54619 | PRKAG1 | | | | | | | | | | | | | | | | | | | | | | | | |
| Q13131 | PRKAA1 | | | | | | | | | | | | | | | | | | | | | | | | |
| P02461 | COL3A1 | | | | | | | | | | | | | | | | | | | | | | | | |
| Q9Y618 | NCOR2 | | | | | | | | | | | | | | | | | | | | | | | | |
| O75146 | HIP1R | | | | | | | | | | | | | | | | | | | | | | | | |
| P02647 | APOA1 | | | | | | | | | | | | | | | | | | | | | | | | |
| Q08379 | GOLGA2 | | | | | | | | | | | | | | | | | | | | | | | | |
| P02458 | COL2A1 | | | | | | | | | | | | | | | | | | | | | | | | |
| P01599 | IGKV1-17 | | | | | | | | | | | | | | | | | | | | | | | | |
| P02790 | HPX | | | | | | | | | | | | | | | | | | | | | | | | |
| P01023 | A2M | | | | | | | | | | | | | | | | | | | | | | | | |

Table 4.11: BCL6-associated proteins identified only in untreated GBM cell lines using the identification-based and/or quantification-based methods

Replicates in which each protein was identified as a BCL6-associated protein using the identification-based method highlighted in dark blue as in Table 4.8. ↑ columns filled with pink indicate that the protein was upregulated in the experimental (anti-BCL6) samples compared to the control (IgG) samples for that cell line (quantification-based method).

| Protein Accession | Protein name | LN18 | | | | NZG0906 | | | | NZG1003 | | | |
|---|---|---|---|---|---|---|---|---|---|---|---|---|---|
| | | 1 | 2 | 3 | ↑ | 1 | 2 | 3 | ↑ | 1 | 2 | 3 | ↑ |
| Q01433 | AMPD2 | | ■ | ■ | | ■ | ■ | ■ | | | | | |
| Q9BZK7 | TBL1XR1 | | | ■ | | ■ | ■ | ■ | | | | | |
| P19823 | ITIH2 | | ■ | ■ | | | ■ | | | | | | |
| Q9UBF1 | MAGEC2 | ■ | ■ | ■ | | | | | | | | | |
| O75351 | VPS4B | ■ | ■ | ■ | | | | | | | | | |
| P17931 | LGALS3 | ■ | ■ | ■ | | | | | | | | | |
| P29508 | SERPINB3 | ■ | | | | ■ | | ■ | | | | | |
| P04114 | APOB | | ■ | ■ | | ■ | | | | | | | |
| P48735 | IDH2 | | ■ | ■ | | ■ | | | | | | | |
| Q86WA8 | LONP2 | | ■ | ■ | | ■ | | | | | | | |
| Q9HD26 | GOPC | | ■ | ■ | | | ■ | | | | | | |
| P51530 | DNA2 | | ■ | ■ | | | | | | | ■ | | |
| O00625 | PIR | | | ■ | | ■ | ■ | | | | | | |
| Q8IXK0 | PHC2 | | | ■ | | | ■ | ■ | | | | | |
| P42765 | ACAA2 | | | | | ■ | ■ | ■ | | | | | |
| Q99661 | KIF2C | | | | | ■ | ■ | | | | | ■ | |
| P04040 | CAT | ■ | | ■ | | | | | | ■ | | | |
| P12273 | PIP | ■ | | | | | | | | ■ | ■ | | |
| Q13043 | STK4 | ■ | | | | | | ■ | | ■ | | | |
| O60306 | AQR | | ■ | | | | | | | | | | |
| O76031 | CLPX | | ■ | ■ | | | | | | | | | |
| O94925 | GLS | | ■ | | | | | | | | | | |
| P01834 | IGKC | | | | | | | | | | | | |
| Q13098 | GPS1 | | | | | | ■ | ■ | | | | | |
| Q6ZSZ5 | ARHGEF18 | | | ■ | | ■ | | | | | | | |
| Q86VS8 | HOOK3 | | | | | | | | | | | | |
| Q8IY37 | DHX37 | | | | | | | | | | | | |
| Q8IZL2 | MAML2 | | | ■ | | ■ | | | | | | | |
| Q8NEM2 | SHCBP1 | | | | | ■ | | | | | | | |
| Q96KP1 | EXOC2 | | | ■ | | | ■ | | | | | | |
| Q99496 | RNF2 | ■ | | | | | ■ | | | | | | |
| Q9HC35 | EML4 | | ■ | | | | ■ | | | | | | |
| Q9UHA3 | RSL24D1 | | ■ | ■ | | | | | | | | | |
| O60701 | UGDH | | | | | | | | | | | | |
| P20930 | FLG | ■ | | | | | | | | | | | |
| Q92504 | SLC39A7 | | | ■ | | | | | | | ■ | | |
| Q9HCD5 | NCOA5 | | ■ | | | | | | | | | | |

Table 4.12: BCL6-associated proteins identified only in irradiated GBM cell lines using the identification-based and/or quantification-based methods

Replicates in which each protein was identified as a BCL6-associated protein using the identification-based method highlighted in light blue as Table 4.9. ↑ columns filled with purple indicate that the protein was upregulated in the experimental (anti-BCL6) samples compared to the control (IgG) samples for that cell line (quantification-based method).

| Protein Accession | Protein name | LN18 | | | | NZG0906 | | | | NZG1003 | | | |
|---|---|---|---|---|---|---|---|---|---|---|---|---|---|
| | | 1 | 2 | 3 | ↑ | 1 | 2 | 3 | ↑ | 1 | 2 | 3 | ↑ |
| P83111 | LACTB | | | | | | | | | | | | |
| P02452 | COL1A1 | | | | | | | | | | | | |
| Q86SE5 | RALYL | | | | | | | | | | | | |
| Q06033 | ITIH3 | | | | | | | | | | | | |
| P61764 | STXBP1 | | | | | | | | | | | | |
| P53680 | A2M | | | | | | | | | | | | |
| Q969G5 | CAVIN3 | | | | | | | | | | | | |
| P08123 | COL1A2 | | | | | | | | | | | | |
| Q03135 | CAV1 | | | | | | | | | | | | |
| O75955 | FLOT1 | | | | | | | | | | | | |
| O94811 | TPPP | | | | | | | | | | | | |
| P21579 | SYT1 | | | | | | | | | | | | |
| P51674 | GPM6A | | | | | | | | | | | | |
| P63098 | PPP3R1 | | | | | | | | | | | | |
| Q08188 | TGM3 | | | | | | | | | | | | |
| Q6UWE0 | LRSAM1 | | | | | | | | | | | | |
| P16070 | CD44 | | | | | | | | | | | | |
| Q04323 | UBXN1 | | | | | | | | | | | | |
| Q6NZI2 | CAVIN1 | | | | | | | | | | | | |
| P05026 | ATP1B1 | | | | | | | | | | | | |

## 4.3.5: Differential association of proteins with BCL6 in untreated and irradiated GBM cells

### 4.3.5.1: Quantitative analysis

To determine whether acute IR treatment changed the amount of each protein associated with BCL6, the proteins pulled down by the BCL6 antibody in untreated and irradiated GBM samples for each cell line were quantitatively analysed and compared using Proteome Discoverer 2.4. Protein abundances were normalised to the abundance of BCL6. This ensured that the ratio of BCL6 abundance between the irradiated and untreated samples was 1. Any proteins that remained bound to BCL6 in equal amounts in both conditions would also have an abundance ratio of 1. Proteins were considered to have their association with BCL6 increased or decreased by acute IR if they had an abundance ratio $\geq 2$ ($\log_2$-fold change $\geq 1$) or $\leq 0.5$ ($\log_2$-fold change $\leq -1$) respectively, with an adjusted p value $\leq 0.05$ (Benjamini-Hochberg multiple comparisons testing). Only proteins identified with high confidence ($q \leq 0.01$) were included. The proteins meeting these criteria fall into the coloured boxes in Figure 4.5.

The majority of proteins with $\log_2$-fold change $\leq -1$ were downregulated at least 100-fold ($\log_2$-fold change = -6.64) and had very low p values (E-17). Hence the points for several hundred proteins overlap in the upper left corner of Figure 4.5A-C. This suggested that a large number of proteins were only associated with BCL6 in the untreated GBM cells, resulting in a > 100-fold decrease in association in the irradiated GBM cells. Table 4.13 shows the number of proteins that had either increased or decreased association with BCL6 in response to IR in each cell line.

Table 4.13: Changes to BCL6 protein associations in response to IR

The number of proteins which had their association with BCL6 increased by IR in each cell line is shown in the middle column ('Increased'). The number of proteins which had their association with BCL6 decreased by IR in each cell line is shown in the right-hand column ('Decreased').

| Cell lines | Increased | Decreased |
|---|---|---|
| **LN18** | 153 | 523 |
| **NZG0906** | 127 | 462 |
| **NZG1003** | 186 | 131 |

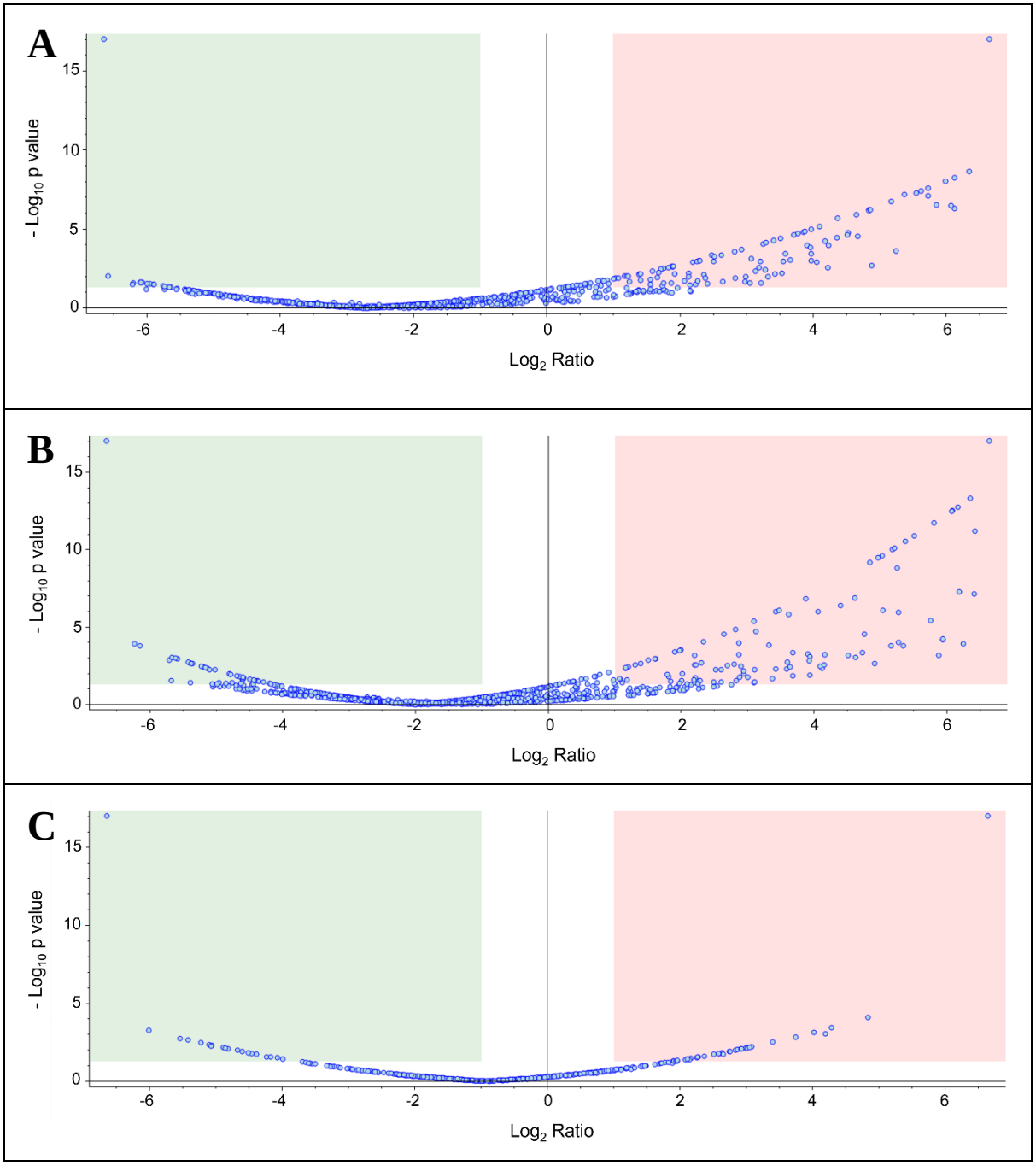


Figure 4.5: Quantitative analysis volcano plots

Volcano plots of the $\log_2$ abundance ratios of proteins in the irradiated BCL6 RIME samples compared to the untreated BCL6 RIME samples from A) LN18, B) NZG0906 and C) NZG1003 cells.

### 4.3.5.2: Differential association of commonly identified BCL6-associated proteins

As anticipated, the proteins only commonly identified in untreated GBM cells (Table 4.11) tended to have their association with BCL6 decreased by acute IR in at least one cell line. Similarly, the proteins only commonly identified in irradiated GBM cells (Table 4.12) tended to have their association with BCL6 increased by acute IR in at least one cell line. The proteins commonly identified in both untreated and irradiated GBM cells are shown in Table 4.14. These proteins all had their association with BCL6 increased or decreased by acute IR in one GBM cell line but there was little consistency between the cell lines. The two subunits of AMPK (PRKAG1 and PRKAA1) both had their association with BCL6 increased by acute IR but in different cell lines. NCOR2 had its association with BCL6 decreased by acute IR in LN18 and NZG0906 cells, but the decrease was not statistically significant ($p > 0.05$) in NZG0906 cells.

Table 4.14: Acute irradiation-induced changes in the BCL6 association of proteins commonly identified as BCL6-associated in both untreated and irradiated GBM cells

Proteins with increased and decreased association with BCL6 after acute IR ($p \leq 0.05$) highlighted in red and green respectively. Proteins with increased or decreased association with BCL6 after acute IR ($p > 0.05$) are not coloured. 'No values' indicates proteins which were identified but did not have abundance values associated with them (as described in section 4.3.4).

| Protein Accession | Protein name | Abundance ratio (irradiated/untreated) | | |
|---|---|---|---|---|
| | | LN18 | NZG0906 | NZG1003 |
| P04196 | HRG | 1.3 | 1.6 | 6.8 |
| Q96LD4 | TRIM47 | 0.03 | 0.12 | 8.5 |
| Q86XK2 | FBXO11 | 1.1 | 7.7 | 0.053 |
| P54619 | PRKAG1 | 0.95 | 3.5 | 0.56 |
| Q13131 | PRKAA1 | 0.54 | 0.61 | 100 |
| P02461 | COL3A1 | 100 | 0.71 | 1.0 |
| Q9Y618 | NCOR2 | 0.01 | 0.151 | No values |
| O75146 | HIP1R | 0.048 | 100 | Not found |
| P02647 | APOA1 | 0.01 | No values | 0.03 |
| Q08379 | GOLGA2 | 0.01 | 0.30 | 0.57 |
| P02458 | COL2A1 | 3.22 | 0.62 | 0.3 |

### 4.3.6.3: Subtraction of non-specific proteins

To further investigate the changes in the proteins associated with BCL6 after acute IR, non-specific proteins were removed. The compiled lists of proteins pulled down with the IgG antibody in each cell line were subtracted from the lists of up- and downregulated proteins. This introduced the risk of eliminating true BCL6-associated proteins with altered association with BCL6 in response to acute IR. This risk was accepted to confidently identify BCL6-associated proteins which changed their level of association with BCL6 in response to acute IR. In all three cell lines, subtraction of non-specific proteins reduced the number proteins considered to have their association with BCL6 increased or decreased in response to acute IR. This decrease was most pronounced in the NZG1003 cell line (Table 4.15).

Table 4.15: Effect of subtraction of non-specific proteins on the apparent changes to BCL6 protein associations in response to acute IR

The number of proteins which appeared to have their association with BCL6 increased by IR in each cell line before and after subtraction of non-specific proteins are shown in the second and third columns respectively ('Increased'). The number of proteins which appeared to have their association with BCL6 decreased by IR in each cell line before and after subtraction of non-specific proteins are shown in the fourth and fifth columns respectively ('Decreased').

| Cell lines | Increased | | Decreased | |
|---|---|---|---|---|
| | Before subtraction | After subtraction | Before subtraction | After subtraction |
| **LN18** | 153 | **86** | 523 | **212** |
| **NZG0906** | 127 | **26** | 462 | **73** |
| **NZG1003** | 186 | **23** | 131 | **8** |

### 4.3.5.4: Subtraction of proteins with high CRAPome scores

The remaining lists of proteins which had their association with BCL6 increased or decreased by acute IR were run through the CRAPome 2.0 "Query proteins and retrieve profiles" workflow. Proteins that were identified in > 10% of the 716 negative control AP-MS experiments in the database were excluded on the basis that they were more likely to be contaminants. After subtraction of both non-specific and likely contaminant proteins, far more proteins had their association with BCL6 increased or decreased by acute IR in LN18 cells than in NZG0906 cells or NZG1003 cells (Table 4.16).

The irradiated LN18 RIME samples were run on the Lumos™ mass spectrometer at Victoria University of Wellington, whereas the untreated LN18 RIME samples were run on the more sensitive instrument at the Bio21 Institute. Therefore, some caution must be taken with the proteins that had their association with BCL6 decreased in response to acute IR in LN18 cells, as they may have dropped below the threshold of detection on the less sensitive instrument. However, more confidence can be placed in the

proteins that had their association with BCL6 increased by acute IR in LN18 cells. As more proteins had their association with BCL6 increased *or* decreased by acute IR in LN18 cells compared to the other cell lines, this is likely to be at least partly due to a biological difference in LN18 cells rather than due only to the mass spectrometers used.

Table 4.16: Effect of subtraction of CRAPome proteins on the apparent changes to BCL6 protein associations in response to acute IR

The number of proteins which appeared to have their association with BCL6 increased by IR in each cell line before and after subtraction of proteins found in >10% of CRAPome AP-MS experiments are shown in the second and third columns respectively ('Increased'). The number of proteins which appeared to have their association with BCL6 decreased by IR in each cell line before and after subtraction of non-specific proteins found in >10% of CRAPome AP-MS experiments are shown in the fourth and fifth columns respectively ('Decreased').

| Cell lines | Increased | | Decreased | |
|---|---|---|---|---|
| | Before subtraction | After subtraction | Before subtraction | After subtraction |
| **LN18** | 86 | **56** | 212 | **116** |
| **NZG0906** | 26 | **19** | 73 | **47** |
| **NZG1003** | 23 | **15** | 8 | **6** |

### 4.3.6.5: Known BCL6 binding partners

Known BCL6 binding partners NCOR1, NCOR2 and HDAC1 had their association with BCL6 decreased ≥ 100-fold in irradiated compared to untreated LN18 cells. HDAC2 also had its association with BCL6 decreased by acute IR in LN18 cells, however this was not statistically significant ($p > 0.05$). NCOR2 and HDAC2 had their association with BCL6 decreased by acute IR in NZG0906 cells compared to untreated NZG0906 cells however the adjusted p values were > 0.05. NCOR2 was identified with medium confidence in one NZG1003 untreated sample, however it was excluded from further analysis as it did not meet the confidence threshold and did not have abundance values associated with it (as described in section 4.3.4).

NCOR1, HDAC1 and HDAC2 were found in > 10% of the control experiments in the CRAPome database and so were excluded from the final results, although it is likely that they are true BCL6-associated proteins in LN18 cells. Interestingly HDAC1 had its association with BCL6 increased by acute IR in NZG0906 cells compared to in untreated NZG0906 cells, however the p value was > 0.05. Contrastingly, HDAC1 was found at comparable levels in BCL6 RIME experiments in irradiated and untreated NZG1003 cells.

Hence it appeared that acute IR treatment of LN18 cells resulted in the loss of NCOR1, NCOR2 and HDAC1 from BCL6 complexes. The evidence was weaker that BCL6 also lost its association with NCOR2 in irradiated NZG0906 cells.

### 4.3.5.6: Functional enrichment analysis of proteins that had their association with BCL6 increased or decreased by acute IR

#### 4.3.5.6.1: LN18 cells

The proteins that had their association with BCL6 increased or decreased by acute IR were investigated using Gene Ontology functional enrichment analysis. In LN18 cells, the proteins that had their association with BCL6 increased by acute IR (Figure 4.6) were strongly enriched for GO:BP and GO:CC terms relating to synaptic activity, including *vesicle-mediated transport in synapse* (p = 1.01E-11), *chemical synaptic transmission* (p = 3.11E-9), *presynapse* (p = 1.38EE-11) and *synaptic vesicle* (p = 6.82E-10). While some of the proteins annotated to these terms were involved in general exocytosis and vesicle transport, others such as SYT1, STX1B, SYN2 and DLG4 were specific to synapses. Two major myelin proteins, PLP1 and CNP, also had their association with BCL6 increased by acute IR, as did TPPP, which promotes elongation of the myelin sheath.[455,456] Glutamate metabolism proteins GAD2 and GLUL also had their association with BCL6 increased by acute IR in LN18 cells.[457,458] Other enriched terms related to neuron morphogenesis, including the GO:BP term *neuron projection development* (1.14EE-4), which included two proteins, CTNNA2 and NCAM1, involved in cell-cell adhesion in the nervous system.[459,460] The GO:CC term *axon* (p = 1.07E-7) was also enriched. The same synaptic and neuronal proteins were also annotated to the enriched Gene Ontology Molecular Function (GO:MF) terms *SNARE binding* and *cytoskeletal protein binding.*

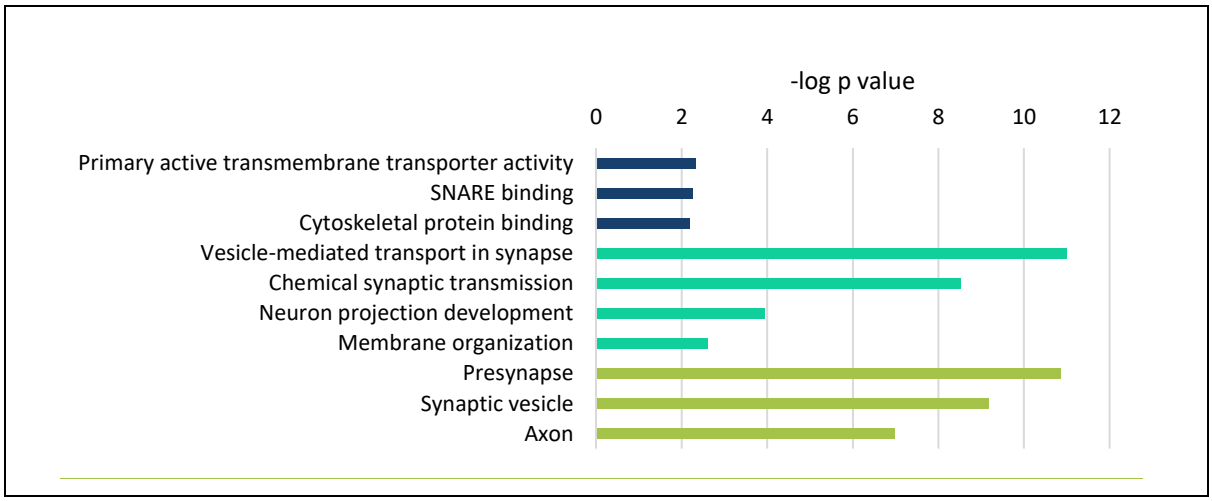

Figure 4.6: Functional enrichment of proteins that had their association with BCL6 increased by acute IR

Up to five most significantly enriched (highest – log p value) parent GO:MF (dark blue) GO:BP (turquoise) and GO:CC (green) terms from analysis of proteins that had their association with BCL6 increased by acute IR (48 hours) in LN18 cells.

The proteins that had their association with BCL6 decreased by acute IR (Figure 4.7) were enriched for the GO:MF terms *transcriptional corepressor activity* (p = 7.50E-3) and *transcriptional coregulator activity* (p = 2.00E-2). The proteins annotated to these terms included known BCL6 binding partner NCOR2, component of NCOR complexes TBL1XR1, and other corepressors RCOR1, DRAP1 and NCOA5.[217,450] The *transcriptional coregulator activity* term also contained transcriptional coactivators MAML2 and PIR.[461–463] The enriched GO:MF term *mRNA binding* contained a handful of proteins involved in regulation of mRNA splicing and stability.

Proteins that had their association with BCL6 decreased by acute IR were also enriched for GO:BP terms related to *ribosome biogenesis* (p = 1.4E-5). Most proteins annotated to this term were also annotated to *ncRNA metabolic process* (p = 2.86E-4). Other proteins that had their association with BCL6 decreased by acute IR were annotated to the enriched term *Golgi vesicle transport* (p = 1.36E-3), while four proteins involved in ubiquitin-ligase activity were annotated to the enriched term *positive regulation of ubiquitin-protein transferase activity* (p = 4.21E-2). Furthermore, there was enrichment for the GO:CC term *spindle* (p = 3.80E-2). Proteins annotated to the *spindle* term included spindle assembly checkpoint proteins MAD1L1, EML4 and APC/C component CDC20.[368,464,465]

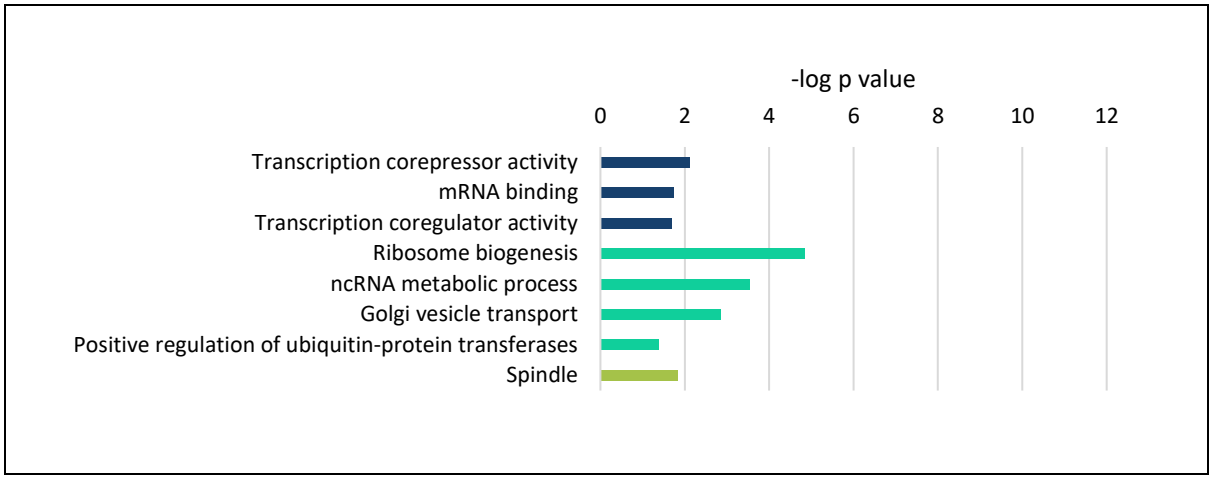


Figure 4.7: Functional enrichment of proteins that had their association with BCL6 decreased by acute IR

Up to five most significantly enriched (highest – log p value) parent GO:MF (dark blue) GO:BP (turquoise) and GO:CC (green) terms from analysis of proteins that had their association with BCL6 decreased by acute IR (48 hours) in LN18 cells.

Overall, in LN18 cells acute IR appeared to increase the association of BCL6 with synaptic proteins but decrease its association with transcriptional regulators and proteins related to ribosome biogenesis, vesicle transport, ubiquitin-ligase activity and the spindle. The reduction of BCL6 association with transcriptional regulators in response to acute IR fits with previous research showing that BCL6 induced by acute IR does not repress transcription.[207] However, it must be kept in mind that the proteins which appeared to have their BCL6-association decreased by acute IR could be artefacts caused by the different mass spectrometers used. More confidence can be placed in the proteins that had their association with BCL6 increased by acute IR. The increased association of BCL6 with synaptic proteins after acute IR was unanticipated and could indicate that BCL6 relocates to the plasma membrane in response to acute IR.

#### 4.3.5.6.2: NZG0906 and NZG1003 cells compared to LN18 cells

In contrast to the LN18 cells, the proteins that had their association with BCL6 increased or decreased by acute IR in NZG0906 cells or decreased by acute IR in NZG1003 cells had no significant enrichment for any Gene Ontology terms. This is likely due to the lower numbers of proteins which had their association with BCL6 altered by acute IR in NZG0906 and NZG1003 cells. However, a handful of proteins that had their association with BCL6 increased by acute IR in NZG1003 cells were annotated to the enriched GO:CC term *vesicle lumen* (p = 6.40E-6). This term overlapped with the two enriched GO:BP terms *blood coagulation* (p = 2.23E-2) and *negative regulation of peptidase activity* (3.32E-2). These proteins had roles in the extracellular matrix or in the blood.

Despite the striking increase in association of synaptic and neuronal proteins with BCL6 after acute IR in LN18 cells, no functional enrichment for similar terms was seen with the NZG0906 or NZG1003 cell lines. However, STXBP1, which is involved in synaptic vesicle docking and exocytosis, had its association with BCL6 increased by acute IR in both NZG0906 and NZG1003 cell lines. Additionally, two coregulators, RCOR1 and MAML2, had their association with BCL6 decreased by acute IR in both LN18 and NZG0906 cells. Another protein involved in transcriptional repression, PHC2, also had its association with BCL6 decreased by acute IR in both LN18 and NZG0906 cells.[466,467] Therefore, while there were some similar trends in the three cell lines, the lower number of proteins which had their association with BCL6 significantly altered by acute IR in NZG0906 and NZG1003 cells precluded informative functional enrichment analysis for these cell lines.

### 4.3.5.7: Proteins that commonly had their association with BCL6 increased or decreased by acute IR across GBM cell lines

Despite the differences between the GBM cell lines, some proteins had their association with BCL6 altered by acute IR in multiple cell lines (Table 4.17). Most were also commonly identified BCL6-associated proteins (sections 4.3.3 and 4.3.4). Those that were not also commonly identified are indicated with an asterisk (*).

Table 4.17: Proteins with increased or decreased association with BCL6 in response to acute IR

Proteins that were not also commonly identified as BCL6-associated proteins indicated with *. Proteins up- or downregulated ≥ 100-fold given abundance ratios 100 and 0.01 respectively.

| Protein Accession | Protein Name | Abundance ratio of proteins increased by acute IR (irradiated/untreated) | | | Abundance ratio of proteins decreased by acute IR (irradiated/untreated) | | |
|---|---|---|---|---|---|---|---|
| | | LN18 | NZG0906 | NZG1003 | LN18 | NZG0906 | NZG1003 |
| Q13043 | STK4 | 100 | 100 | | | | |
| P63098 | PPP3R1 | 36.0 | 40.8 | | | | |
| P61764 | STXBP1 | | 3.06 | 100 | | | |
| Q16610 | ECM1* | | 8.05 | 100 | | | |
| Q8IXK0 | PHC2 | | | | 0.01 | 0.01 | |
| P04114 | APOB | | | | 0.01 | 0.01 | |
| Q9UKL0 | RCOR1* | | | | 0.01 | 0.01 | |
| Q8IZL2 | MAML2 | | | | 0.01 | 0.01 | |
| Q6ZSZ5 | ARHGEF18 | | | | 0.01 | 0.01 | |
| Q9Y6D9 | MAD1L1* | | | | 0.01 | 0.01 | |
| Q9UHA3 | RSL24D1 | | | | 0.01 | 0.01 | 0.01 |
| Q96KP1 | EXOC2 | | | | 0.01 | 0.01 | |
| P02647 | APOA1 | | | | 0.01 | | 0.03 |

## 4.3.6: Comparison of RIME and whole proteome results

This chapter has demonstrated that the proteins associated with BCL6 changed in response to acute IR treatment of GBM cells. The effect of acute IR (48 hours) on the expression of each BCL6-associated protein identified using RIME was investigated using the whole proteome data from Chapter 3. This was useful to investigate whether the altered association of BCL6 with proteins after acute IR was mediated by changes in the abundance of its associated proteins or by other factors.

Many BCL6-associated proteins identified by RIME were not found in untreated or irradiated LN18 cells in the whole proteome analysis (Table 4.18). This confirmed that these proteins were enriched by RIME, along with BCL6. Furthermore, many of the proteins that were only associated with BCL6 in either untreated or irradiated GBM cells did not change in abundance in response to acute IR (Table 4.18). This suggests that their altered association with BCL6 was mediated by factors other than their abundance. These factors could include increased or decreased affinity between the proteins, competition with other proteins for BCL6 binding, or changes in their localisation which prevented or promoted association.

In contrast, PRKAG1 and LACTB were upregulated by acute IR and their association with BCL6 increased in response to this treatment in at least one cell line. This could suggest that the increased association of BCL6 with these proteins in irradiated GBM cells was driven by the increase in PRKAG1 and LACTB expression. Similarly, ARHGEF18, RNF2 and SLC39A7 were downregulated by acute IR. The association of BCL6 with ARHGEF18 was decreased in LN18 and NZG0906 cells after acute IR, while RNF2 and SLC29A7 were only commonly identified as BCL6-associated proteins in untreated GBM cells. This suggests that their association with BCL6 may decrease somewhat in irradiated cells due to their decreased expression.

In contrast, MAGEC2 and LONP2 both had their association with BCL6 decreased by acute IR in LN18 cells but had their expression upregulated 48 hours after acute IR in LN18 cells. Therefore, factors other than abundance, such as reduced affinity or increased competition, must have decreased the association of these proteins with BCL6 in response to acute IR. C3, HIP1R and PPP3R11 were upregulated by acute IR in the whole proteome analysis, however their association with BCL6 was unaffected by acute IR. It is possible that this was because BCL6 was also upregulated by acute IR and so the amount of association remained constant relative to the amount of BCL6, or simply that these proteins did not further associate with BCL6 even through their abundance had increased.

This analysis indicated that altered abundance was not the main factor mediating the changes in BCL6-associated proteins in response to acute IR. This confirmed that RIME was able to identify true changes in protein associations rather than being confounded by changing protein abundances.

### Table 4.18: Effect of acute IR (48h) on expression of BCL6-associated proteins in LN18 cells

BCL6-associated proteins commonly identified in both untreated and irradiated GBM cells (left-hand two columns), BCL6-associated proteins commonly identified in only untreated GBM cells (middle two columns) and BCL6-associated proteins commonly identified in only irradiated GBM cells (right-hand two columns). Proteins were considered up- or downregulated by acute IR if their abundance changed ≥ 2-fold, adj. $p \leq 0.05$ (Benjamini-Hochberg multiple comparisons testing).

| **Untreated and irradiated** | | **Untreated only** | | **Irradiated only** | |
|---|---|---|---|---|---|
| **Accession** | **Protein name** | **Accession** | **Protein name** | **Accession** | **Protein name** |
| **Expression upregulated by acute IR** | | | | | |
| P01024 | C3 | Q9UBF1 | MAGEC2 | P83111 | LACTB |
| P54619 | PRKAG1 | Q86WA8 | LONP2 | P63098 | PPP3R1 |
| O75146 | HIP1R | | | | |
| **Expression downregulated by acute IR** | | | | | |
| | | Q6ZSZ5 | ARHGEF18 | | |
| | | Q99496 | RNF2 | | |
| | | Q92504 | SLC39A7 | | |
| **Not found in whole proteome analysis** | | | | | |
| P04196 | HRG | P19823 | ITIH2 | P02452 | COL1A1 |
| P27169 | PON1 | P29508 | SERPINB3 | Q86SE5 | RALYL |
| Q86XK2 | FBXO11 | P04114 | APOB | Q06033 | ITIH3 |
| Q13131 | PRKAA1 | Q9HD26 | GOPC | P53680 | AP2S1 |
| P02461 | COL3A1 | P51530 | DNA2 | Q969G5 | CAVIN3 |
| P02647 | APOA1 | Q8IXK0 | PHC2 | P08123 | COL1A2 |
| P02458 | COL2A1 | P12273 | PIP | O94811 | TPPP |
| P01599 | IGKV1-17 | P01834 | IGKC | P21579 | SYT1 |
| P02790 | HPX | Q13098 | GPS1 | P51674 | GPM6A |
| P01023 | A2M | Q8IY37 | DHX37 | Q08188 | TGM3 |
| | | Q8IZL2 | MAML2 | Q6UWE0 | LRSAM1 |
| | | P20930 | FLG | | |
| **No significant change in expression** | | | | | |
| Q9Y618 | NCOR2 | Q01433 | AMPD2 | P61764 | STXBP1 |
| Q08379 | GOLGA2 | Q9BZK7 | TBL1XR1 | Q03135 | CAV1 |
| | | O75351 | VPS4B | O75955 | FLOT1 |
| | | P17931 | LGALS3 | P16070 | CD44 |
| | | P48735 | IDH2 | Q04323 | UBXN1 |
| | | O00625 | PIR | Q6NZI2 | CAVIN1 |
| | | P42765 | ACAA2 | P05026 | ATP1B1 |
| | | Q99661 | KIF2C | | |
| | | P04040 | CAT | | |
| | | Q13043 | STK4 | | |
| | | O60306 | AQR | | |
| | | O76031 | CLPX | | |
| | | O94925 | GLS | | |
| | | Q86VS8 | HOOK3 | | |
| | | Q8NEM2 | SHCBP1 | | |
| | | Q96KP1 | EXOC2 | | |
| | | Q9HC35 | EML4 | | |
| | | Q9UHA3 | RSL24D1 | | |
| | | O60701 | UGDH | | |
| | | Q9HCD5 | NCOA5 | | |
| **No abundance values** | | | | | |
| Q96LD4 | TRIM47 | | | | |

## 4.3.7: Selection of BCL6-associated proteins of interest

### 4.3.7.1: Summary of BCL6 RIME data

In this chapter, several methods have been used to investigate the proteins pulled down in BCL6 RIME experiments in untreated and irradiated GBM cell lines. Combining the results of the identification-based method described in section 4.3.3 with the quantification-based method described in section 4.3.4 revealed a total of 37 BCL6-associated proteins only found in untreated GBM cells, 20 BCL6-associated proteins only found in irradiated GBM cells and 16 BCL6-associated proteins identified in both untreated and irradiated GBM cells. In addition, differential expression analysis in section 4.3.5 identified four proteins which commonly had their association with BCL6 upregulated by acute IR in GBM cells. One of these had not already been identified in sections 4.3.3 and 4.3.4. Differential expression analysis in section 4.3.5 also identified nine proteins which commonly had their association with BCL6 downregulated by acute IR in GBM cells. Two of these had not already been identified in sections 4.3.3 and 4.3.4. This total of 76 BCL6-associated proteins are displayed in Table 4.19, which summarises all of the GBM BCL6 RIME data from this chapter. These proteins were submitted to the IMEx (http://www.imexconsortium.org) consortium through IntAct [X] and assigned the identifier IM-29565.[336]

Table 4.19: Summary of GBM BCL6 RIME data

Columns 3-6: Proteins commonly identified as BCL6-associated by the identification-based or quantification-based method in untreated (dark blue and pink respectively) or irradiated (light blue and purple respectively) GBM cell lines. Where proteins were identified but not in enough replicates to be considered 'commonly identified' the number of replicates they were identified in is shown with no colour. Column 7: Increased (red) or decreased (green) association with BCL6 in response acute IR (48 hours) in stated GBM cell lines. 'No change' indicates that the association of that protein with BCL6 did not change ≥2-fold, $p \leq 0.05$ (Benjamini-Hochberg multiple comparisons testing) in response to acute IR in any of the cell lines (after IgG subtraction). Column 8: Up- (red) or downregulation (green) of expression 48 hours after acute IR in LN18 cells (from whole proteome data, Chapter 3). 'No change' indicates that the expression of that protein in LN18 cells did not change >2-fold, $p \leq 0.05$ (Benjamini-Hochberg multiple comparisons testing) in response to acute IR. 'Not found' indicates that the protein was not identified in the control or irradiated LN18 cells or was not able to be quantified (as described in section 4.3.4).

| Protein Accession | Protein name | Identification-based method (number of replicates identified in) | | Quantification-based method (number of replicates identified in) | | Quantitative analysis (IRS 48h/untreated) | |
|---|---|---|---|---|---|---|---|
| | | Untreated (/9) | Irradiated (/9) | Untreated (/3) | Irradiated (/3) | RIME (association with BCL6) | LN18 whole proteome (expression) |
| P04196 | HRG | 9 | 8 | 3 | 3 | NZG1003 | Not found |
| P01024 | C3 | 8 | 4 | 3 | 2 | No change | |
| Q96LD4 | TRIM47 | 8 | 5 | 3 | 2 | NZG1003 | Not found |
| P27169 | PON1 | 7 | 3 | 3 | 2 | No change | Not found |
| Q86XK2 | FBXO11 | 4 | 8 | 3 | 3 | NZG0906 | Not found |
| P54619 | PRKAG1 | 3 | 8 | 3 | 3 | NZG0906 | |
| Q13131 | PRKAA1 | 4 | 4 | 1 | 2 | NZG1003 | Not found |
| P02461 | COL3A1 | 4 | 3 | 3 | 3 | LN18 | Not found |
| Q9Y618 | NCOR2 | 3 | 3 | 0 | 2 | LN18 | No change |
| O75146 | HIP1R | 3 | 3 | 1 | 1 | No change | |
| P02647 | APOA1 | 3 | 3 | 1 | 1 | LN18 NZG1003 | Not found |
| Q08379 | GOLGA2 | 2 | 2 | 2 | 2 | LN18 | No change |
| Q01433 | AMPD2 | 5 | 0 | 2 | 0 | No change | No change |
| P02458 | COL2A1 | 5 | 0 | 3 | 3 | LN18 | Not found |
| Q9BZK7 | TBL1XR1 | 4 | 0 | 1 | 0 | LN18 | No change |
| P19823 | ITIH2 | 3 | 0 | 1 | 0 | No change | Not found |
| Q9UBF1 | MAGEC2 | 3 | 0 | 1 | 0 | LN18 | |
| P01599 | IGKV1-17 | 3 | 0 | 0 | 2 | No change | Not found |
| O75351 | VPS4B | 3 | | 1 | | No change | No change |
| P17931 | LGALS3 | 3 | 0 | 1 | 0 | No change | No change |
| P29508 | SERPINB3 | 3 | 0 | 0 | 0 | No change | Not found |
| P04114 | APOB | 3 | 0 | 2 | 0 | LN18 NZG0906 | Not found |
| P48735 | IDH2 | 3 | 0 | 2 | 0 | LN18 | No change |
| Q86WA8 | LONP2 | 3 | 0 | 1 | 0 | LN18 | |
| Q9HD26 | GOPC | 3 | 0 | 2 | 0 | No change | Not found |
| P51530 | DNA2 | 3 | 0 | 0 | 0 | No change | Not found |
| O00625 | PIR | 3 | 0 | 2 | 0 | LN18 | No change |
| Q8IXK0 | PHC2 | 3 | 0 | 2 | 0 | LN18 NZG0906 | Not found |
| P42765 | ACAA2 | 3 | 0 | 1 | 0 | No change | No change |
| Q99661 | KIF2C | 3 | 0 | 1 | 0 | LN18 NZG0906 | No change |
| P04040 | CAT | 3 | 0 | 2 | 0 | NZG1003 | No change |
| P12273 | PIP | 3 | 0 | 1 | 0 | NZG1003 | Not found |
| Q13043 | STK4 | 3 | 0 | 1 | 0 | LN18 NZG0906 | No change |
| O60306 | AQR | 1 | 0 | 2 | 0 | LN18 | No change |
| O76031 | CLPX | 2 | 0 | 2 | 0 | No change | No change |
| O94925 | GLS | 1 | 0 | 2 | 0 | LN18 | No change |
| P01834 | IGKC | 0 | 0 | 2 | 0 | No change | Not found |
| Q13098 | GPS1 | 2 | | 2 | | NZG0906 | Not found |
| Q6ZSZ5 | ARHGEF18 | 2 | 0 | 2 | 0 | LN18 | |

| | | | | | | | |
|---|---|---|---|---|---|---|---|
| | | | | | | NZG0906 | |
| Q86VS8 | HOOK3 | 0 | 0 | 2 | 0 | No change | No change |
| Q8IY37 | DHX37 | 0 | 0 | 2 | 0 | LN18 | Not found |
| Q8IZL2 | MAML2 | 2 | 0 | 2 | 0 | LN18 NZG0906 | Not found |
| Q8NEM2 | SHCBP1 | 1 | 0 | 2 | 0 | No change | No change |
| Q96KP1 | EXOC2 | 2 | 0 | 2 | 0 | LN18 NZG0906 | No change |
| Q99496 | RNF2 | 2 | 0 | 2 | 0 | No change | |
| Q9HC35 | EML4 | 2 | 0 | 2 | 0 | No change | No change |
| Q9UHA3 | RSL24D1 | 2 | 0 | 2 | 0 | LN18 NZG0906 | No change |
| O60701 | UGDH | 0 | 0 | 2 | 0 | No change | No change |
| P20930 | FLG | 1 | 0 | 2 | 0 | No change | Not found |
| Q92504 | SLC39A7 | 2 | 0 | 2 | 0 | No change | |
| Q9HCD5 | NCOA5 | 1 | 0 | 2 | 0 | No change | No change |
| P02790 | HPX | 2 | 3 | 3 | 1 | No change | Not found |
| P01023 | A2M | 0 | 3 | 2 | 2 | No change | Not found |
| P83111 | LACTB | 0 | 4 | 0 | 2 | LN18 | |
| P02452 | COL1A1 | 0 | 3 | 0 | 2 | No change | Not found |
| Q86SE5 | RALYL | 0 | 3 | 0 | 0 | Not found | Not found |
| Q06033 | ITIH3 | 0 | 3 | 0 | 1 | LN18 NZG1003 | Not found |
| P61764 | STXBP1 | 0 | 3 | 0 | 2 | NZG0906 NZG1003 | No change |
| P53680 | AP2S1 | 0 | 3 | 0 | 1 | No change | Not found |
| Q969G5 | CAVIN3 | 0 | 3 | 0 | 1 | No change | Not found |
| P08123 | COL1A2 | 0 | 0 | 0 | 3 | No change | Not found |
| Q03135 | CAV1 | 0 | 0 | 0 | 3 | No change | No change |
| O75955 | FLOT1 | 0 | 2 | 0 | 2 | No change | No change |
| O94811 | TPPP | 0 | 2 | 0 | 2 | LN18 | Not found |
| P21579 | SYT1 | 0 | 2 | 0 | 2 | LN18 | Not found |
| P51674 | GPM6A | 0 | 1 | 0 | 2 | No change | Not found |
| P63098 | PPP3R1 | 0 | 2 | 0 | 2 | LN18 NZG0906 | |
| Q08188 | TGM3 | 0 | 0 | 0 | 2 | No change | Not found |
| Q6UWE0 | LRSAM1 | 0 | 0 | 0 | 2 | No change | Not found |
| P16070 | CD44 | 0 | 2 | 0 | 2 | No change | No change |
| Q04323 | UBXN1 | 0 | 2 | 0 | 2 | No change | No change |
| Q6NZI2 | CAVIN1 | 0 | 0 | 0 | 2 | No change | No change |
| P05026 | ATP1B1 | 0 | 1 | 0 | 2 | LN18 | No change |
| Q16610 | ECM1 | 2 | 1 | 1 | 1 | NZG0906 NZG1003 | Not found |
| Q9UKL0 | RCOR1 | 2 | 1 | 0 | 0 | LN18 NZG0906 | No change |
| Q9Y6D9 | MAD1L1 | 2 | 1 | 1 | 0 | LN18 NZG0906 | No change |

### 4.3.7.2: Identification of BCL6-associated proteins of interest

Of the 76 BCL6-associated proteins shown in Table 4.19, six were identified in at least half (≥ 9/18) of the RIME replicates (Table 4.20). These six proteins were identified in both untreated and irradiated GBM cells. As the most commonly identified proteins in the GBM RIME samples, these six proteins are the most confident BCL6-associations.

Additionally, as well as being commonly identified, seven proteins commonly (in ≥ 2/3 GBM cell lines) had their association with BCL6 decreased by acute IR (Table 4.20). A further three proteins commonly had their association with BCL6 increased by acute IR (Table 4.20). These proteins were also of interest as they indicated changes to BCL6 activity in response to treatment.

#### Table 4.20: BCL6-associated proteins of interest

BCL6-associated proteins of interest determined by how commonly they were identified or by how commonly they were found to have their association with BCL6 increased or decreased by acute IR. The most commonly identified proteins were those found in ≥ 9/18 RIME replicates. The proteins considered commonly increased or decreased by acute IR were identified as such in ≥ 2/3 GBM cell lines. Of these proteins, only those which were also commonly identified (in ≥ 3 untreated or ≥ 3 irradiated RIME replicates or upregulated in BCL6 vs IgG replicates in ≥ 2 untreated or ≥ 2 irradiated cell lines) were included in this table.

| Protein Accession | Protein Name |
|---|---|
| **Most commonly identified** | |
| P04196 | HRG |
| P01024 | C3 |
| Q96LD4 | TRIM47 |
| P27169 | PON1 |
| Q86XK2 | FBXO11 |
| P54619 | PRKAG1 |
| **Association with BCL6 commonly increased by acute IR** | |
| Q13043 | STK4 |
| P61764 | STXBP1 |
| P63098 | PPP3R1 |
| **Association with BCL6 commonly decreased by acute IR** | |
| P02647 | APOA1 |
| P04114 | APOB |
| Q8IXK0 | PHC2 |
| Q6ZSZ5 | ARHGEF18 |
| Q8IZL2 | MAML2 |
| Q96KP1 | EXOC2 |
| Q9UHA3 | RSL24D1 |

### 4.3.7.3: Subcellular location of BCL6-associated proteins

The subcellular location of each of the BCL6-associated proteins shown in Table 4.19 was identified using the Uniprot Subcellular Location Annotation.[329] Strikingly, 11 proteins (32%) associated with BCL6 in irradiated GBM cells were annotated to the plasma membrane (Figure 4.8). No proteins associated with BCL6 in untreated GBM cells were annotated to this subcellular location. Meanwhile, 19 proteins (36%) associated with BCL6 in untreated GBM cells were annotated to the nucleus or nucleus and cytoplasm, compared to just 6 proteins (18%) in irradiated GBM cells. Surprisingly, a large proportion of BCL6-associated proteins were annotated as secreted, both in untreated and irradiated GBM cells.

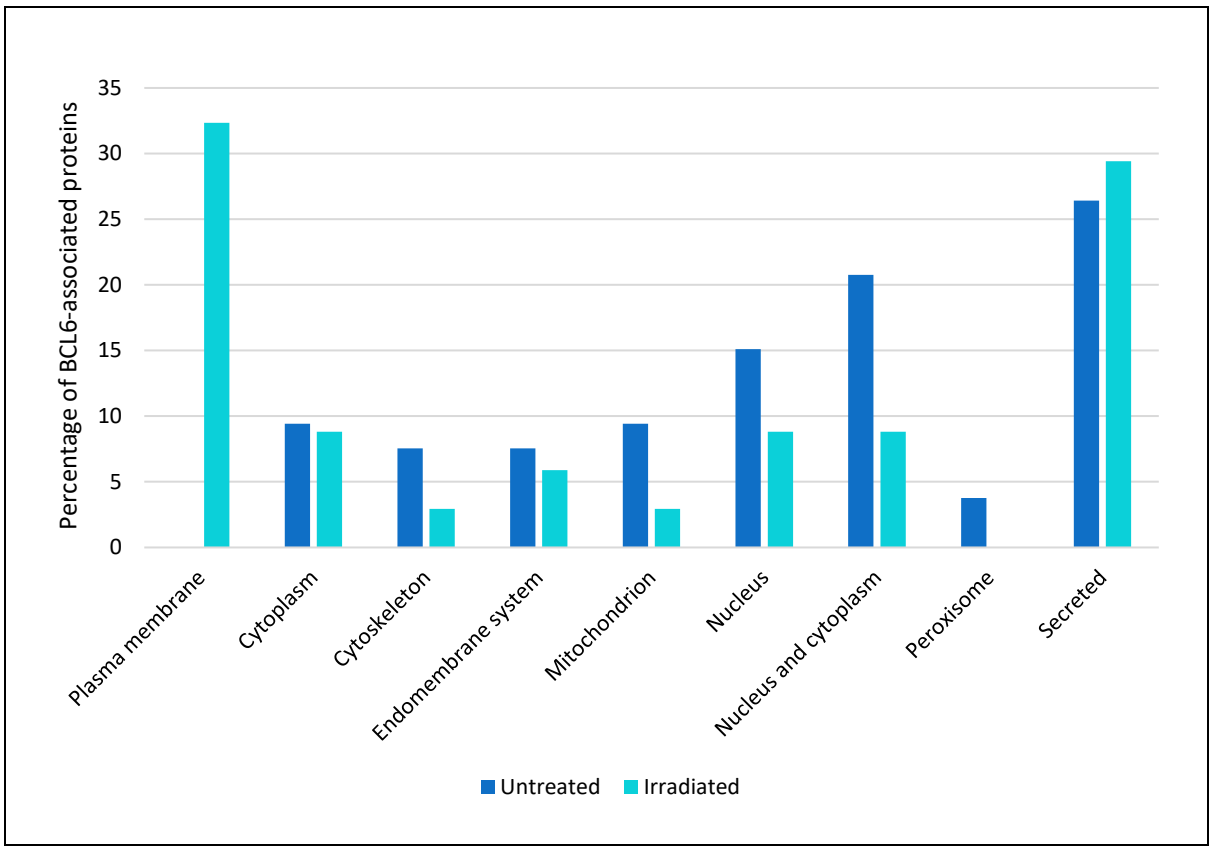


Figure 4.8: Subcellular location of BCL6-associated proteins

The percentage of BCL6-associated proteins in untreated and irradiated GBM cells which were annotated to each subcellular compartment listed.

### 4.3.7.4: Identification of interesting STRING clusters of BCL6-associated proteins

The 76 BCL6-associated proteins identified in Table 4.19 were entered into STRING along with BCL6.[332] STRING interaction sources 'experimentally determined interaction', 'database annotated' and 'automated textmining' were used to identify both functional and physical interactions between the proteins. The high confidence interactions (STRING score (SSc) > 0.7 out of a maximum of 1) are shown in Figure 4.9A and B.

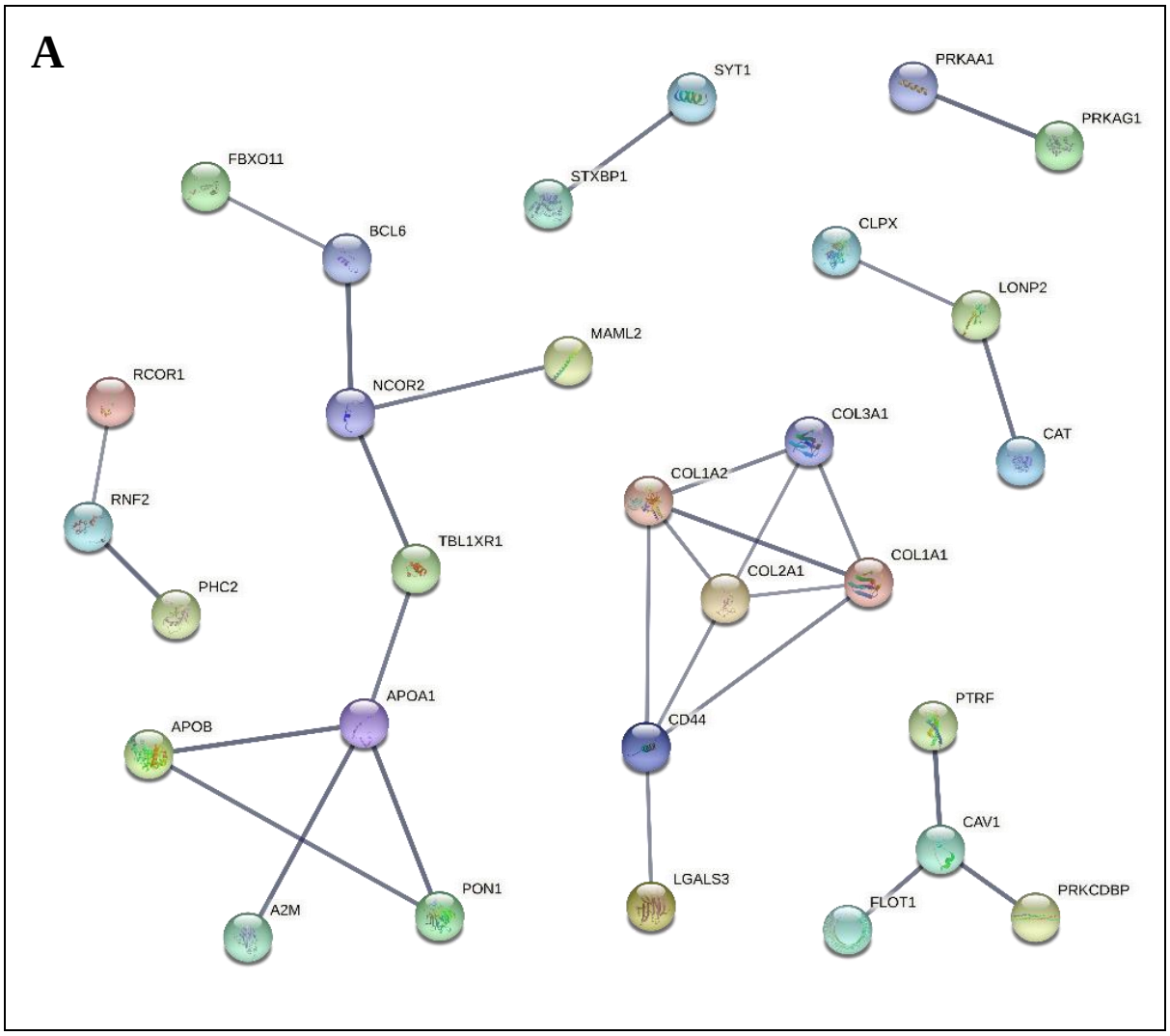

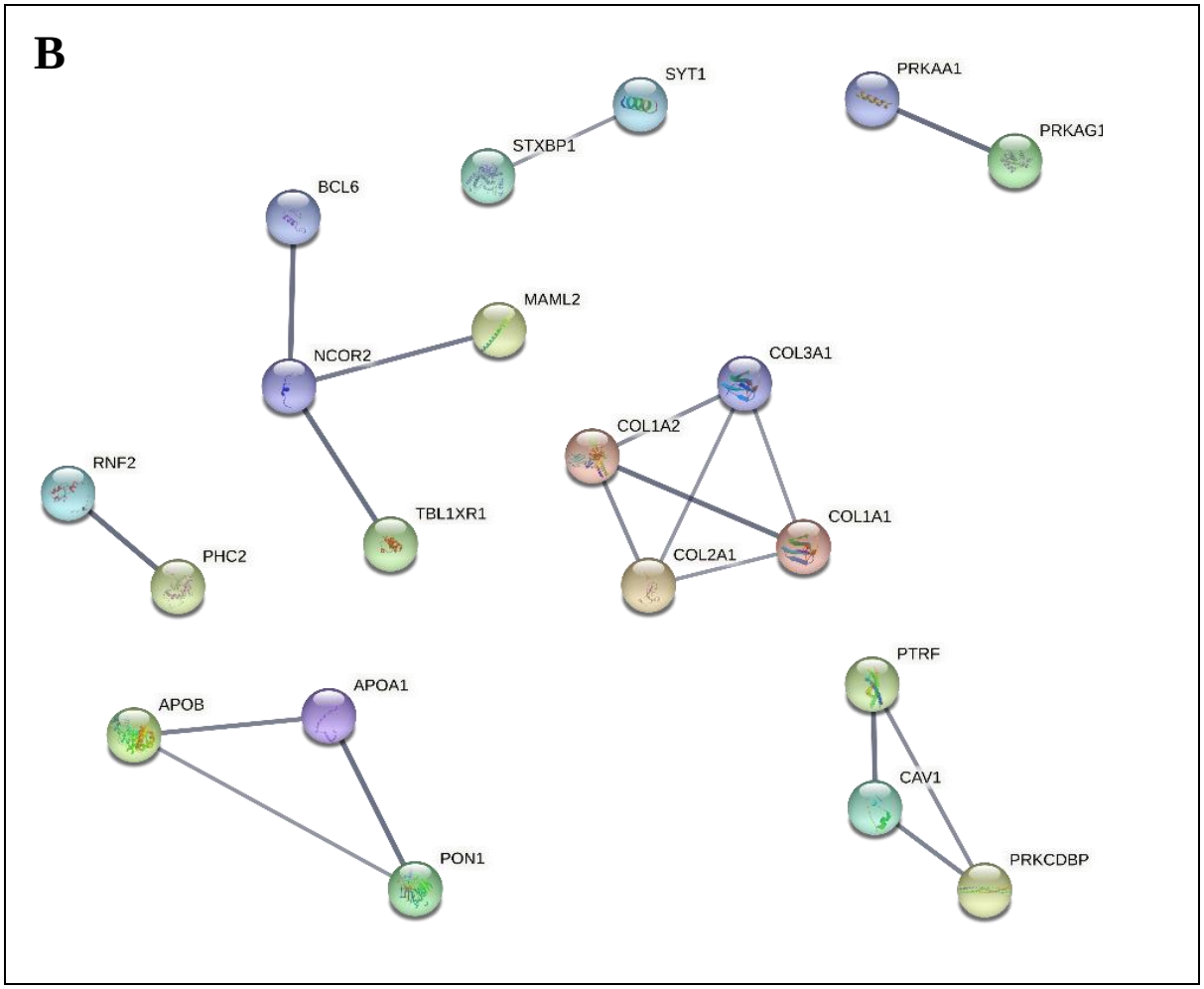


Figure 4.9: STRING network of BCL6-associated proteins

A) Both functional and physical interactions included. B) Only physical interactions included. Nodes with no connections are hidden. Interaction sources: experimentally determined interaction, database annotated and automated textmining. Minimum required interaction score = 0.7 (high confidence). Line thickness indicates confidence of interaction.

BCL6 was only linked to two nodes: corepressor NCOR2 (SSc = 0.999) and E3 ubiquitin-protein ligase FBXO11 (SSc = 0.775). NCOR2 had interactions with Notch coactivator MAML2 (SSc = 0.916) and NCOR complex component TBL1XR1 (0.997).[468,469450] Although the PSICQUIC search in section 4.3.3.4 identified an interaction between BCL6 and TBL1XR1, this interaction was only considered medium confidence by STRING (STRING score = 0.470) and so was excluded from Figure 4.9.

The cluster of proteins connected to the BCL6 node were linked to a lipid-related cluster via APOA1. This was due to the annotation of both TBL1XR1 and APOA1 to the Reactome pathway *APOA1 expression* in the 'database annotated' source. When only physical interactions were examined (Figure 4.9B), the high confidence interaction between TBL1XR1 and APOA1 was lost.

PHC2, RNF2 and RCOR1 formed a small cluster of proteins involved in transcriptional repression (Figure 4.9A). The interactions between RNF2 and PHC2 and between RNF2 and RCOR1 had SSc = 0.999 and SSc = 0.744 respectively. The interaction between RNF2 and RCOR1 was lost when only physical interactions were examined (Figure 4.9B). The two AMPK subunits PRKAA1 and PRKAG1 were connected with SSc = 0.999. Two proteins involved in synaptic signalling, STXBP1 and SYT1 were also connected (SSc = 0.912).

Four caveolae-associated proteins formed another cluster with CAV1 as the central node (CAV1-PTRF(CAVIN1) SSc = 0.995, CAV1-PRKCDBP(CAVIN3) SSc = 0.956, CAV1-FLOT1 SSc = 0.926). The interaction between CAV1 and FLOT1 was only found when functional as well as physical interactions were examined (Figure 4.9A) rather than only physical interactions (Figure 4.9B). Three of the cluster of four collagen proteins had evidence of interaction with CD44 (Figure 4.9A), but this connection was lost when only physical interactions were examined (Figure 4.9B). Two proteases, LONP2 and CLPX were found in another cluster (SSc = 0.787) (Figure 4.9A).[470,471] LONP2 was also connected to CAT, which breaks down hydrogen peroxide (SSc = 0.945) (Figure 4.9A).[470,472] This whole cluster was lost when only physical interactions were considered (Figure 4.9B).

In summary, the STRING analysis identified five main clusters of interest (Table 4.21). The first was proteins already known to interact with BCL6 (FBXO11 and NCOR2), as well as proteins which interact with NCOR2 (TBL1XR1 and MAML2). The small cluster of transcriptional repressor proteins, PHC2, RNF2 and RCOR1 was interesting due to the role of BCL6 as a transcriptional repressor in GC B cells and in B cell lymphoma. Two additional transcriptional regulators PIR and NCOA5, were also commonly associated with BCL6 but were not connected to any of the STRING clusters. The third cluster of interest was the cluster of two synaptic proteins: STXBP1 and SYT1 and the fourth was the cluster of four caveolae proteins: CAV1, CAVIN1 (PTRF), CAVIN3 (PRKCDBP) and FLOT1. Finally, the presence of the two AMPK subunits was also noteworthy.

The apolipoproteins and collagen proteins were some of the proteins annotated as secreted in the subcellular location analysis (section 4.3.7.3). Some of these were associated with BCL6 regardless of treatment, whereas others were only BCL6-associated in untreated or irradiated GBM cells. The association of BCL6 with secreted proteins was unexpected. These proteins were not found in whole proteome analysis of LN18 cells, so it seemed unlikely that they contaminated the RIME samples due to high abundance. However, it is possible that the RIME process enriched for these proteins non-specifically. Further work is required to determine the relevance of these secreted proteins.

Several of the proteins in these interesting functional clusters had already been identified as proteins of interest in section 4.3.7.2. These are highlighted in blue in Table 4.21.

Table 4.21: BCL6-associated proteins within interesting STRING clusters

BCL6-association proteins from the interesting STRING clusters identified above. Proteins already identified as proteins of interest in section 4.3.7.2 highlighted in blue.

| **Known BCL6 binding partners and their binding partners** | | **Transcriptional repression** | |
|---|---|---|---|
| Q9Y618 | NCOR2 | Q99496 | RNF2 |
| Q86XK2 | FBXO11 | Q8IXK0 | PHC2 |
| Q9BZK7 | TBL1XR1 | Q9UKL0 | RCOR1 |
| Q8IZL2 | MAML2 | | |
| **AMPK subunits** | | **Synaptic transmission** | |
| P54619 | PRKAG1 | P61764 | STXBP1 |
| Q13131 | PRKAA1 | P21579 | SYT1 |
| **Caveolae** | | | |
| Q03135 | CAV1 | | |
| Q6NZI2 | CAVIN1 | | |
| Q969G5 | CAVIN3 | | |
| O75955 | FLOT1 | | |

### 4.3.7.5: Indicated BCL6 activity in GBM cells

The BCL6-associated proteins of interest identified in section 4.3.7.2 and the STRING clusters identified in section 4.3.7.4 pointed to four main categories of BCL6 activity in GBM cells (Table 4.22). As would be expected for BCL6, these included transcriptional activity, mediated by interaction with known and novel associated proteins. These proteins appeared to be predominantly associated with BCL6 in untreated GBM cells. This was supported by the greater number of nuclear proteins associated with BCL6 in untreated GBM cells compared to in irradiated GBM cells (section 4.3.7.3). Additionally, BCL6 in GBM cells appeared to be regulated by two E3 ubiquitin-protein ligases, FBXO11 and TRIM47. Association of BCL6 with transcriptional cofactors and ubiquitin-protein ligases was unsurprising and provided confidence that the RIME technique was sound. More surprisingly, BCL6 was commonly associated with two subunits of AMPK in both untreated and irradiated GBM cells, and with exocytosis machinery and caveolae components in irradiated GBM cells. The IR-induced association of BCL6 with plasma membrane proteins was also seen when the subcellular localisation of BCL6-associated proteins was analysed (section 4.3.7.3). This supported the hypothesis that BCL6 has novel roles in GBM and that it may have altered activity in response to acute IR treatment.

Table 4.22: BCL6-associated proteins indicative of BCL6 activity in GBM cells

| **Transcriptional activity** | |
|---|---|
| Q9Y618 | NCOR2 |
| Q9BZK7 | TBL1XR1 |
| Q8IZL2 | MAML2 |
| Q99496 | RNF2 |
| Q8IXK0 | PHC2 |
| O00625 | PIR |
| Q9HCD5 | NCOA5 |
| **Regulation of BCL6** | |
| Q86XK2 | FBXO11 |
| Q96LD4 | TRIM47 |
| **AMPK** | |
| P54619 | PRKAG1 |
| Q13131 | PRKAA1 |
| **Exocytosis** | |
| P61764 | STXBP1 |
| P21579 | SYT1 |
| Q96KP1 | EXOC2 |
| **Caveolae** | |
| Q03135 | CAV1 |
| Q6NZI2 | CAVIN1 |
| Q969G5 | CAVIN3 |
| O75955 | FLOT1 |

## 4.4: Discussion

### 4.4.1: Use of RIME for BCL6 in GBM

#### 4.4.1.1: Success of RIME

RIME enabled the successful examination of the protein 'nano-environment' of BCL6 in untreated and irradiated GBM cell lines. BCL6 is known to associate with a variety of corepressors in different contexts and these interactions mediate the repression of different target genes (section 1.2). The results of Chapter 3 suggested that preventing corepressors from binding to the BCL6 BTB domain inhibited some of the responses of GBM cells to treatment. RIME provided unbiased insight into which proteins BCL6 associated with in GBM cells, regardless of whether they bound to the BTB domain. Furthermore, RIME allowed closer examination of the apparent change in BCL6 activity in response to acute IR, as suggested in Chapter 3 and by previous research.[207]

The use of RIME overcame several challenges that were faced when aiming to identify the proteins that associated with BCL6 in GBM. The low abundance of BCL6 in GBM cells makes study of the BCL6 protein difficult. As previous research indicated that the activity of endogenous BCL6 in GBM differs from that of overexpressed exogenous BCL6, transfection of BCL6 into GBM cells for affinity purification was not a viable option.[322] Endogenous BCL6 cannot be detected in the whole proteome of GBM cells, so it was necessary to enrich for BCL6 from large numbers of cells to obtain enough of the protein to identify it using mass spectrometry. For each RIME experiment, ten 15 cm plates of GBM cells at 80-90% confluence were used as starting material. Half of the crosslinked lysate was added to magnetic beads coated with the BCL6 antibody, while the other half was used as an IgG control. Despite the large amount of starting material, the protein yield from these RIME experiments was generally in the range of 0.5-2.5 μg, most of which consisted of non-specific proteins also found in the IgG control experiments.

BCL6 was identified with high confidence in every BCL6 RIME experiment, despite low coverage in the GBM cells (2-16%) compared to in the positive control Raji lymphoma cells (15-27%). Furthermore, known binding partners of BCL6 were detected by RIME, confirming the success of the technique. BCOR, NCOR1, NCOR2, MTA3, HDAC1 and HDAC2 were identified in at least one positive control Raji BCL6 RIME experiment, although the former three were only identified in the sample run on the more sensitive instrument at the Bio21 Institute. Meanwhile, NCOR2, HDAC1 and HDAC2 were commonly identified across the BCL6 RIME experiments in GBM cells. NCOR1 and CTBP1 were identified in one and two samples respectively, but likely fell below the threshold of detection in the other samples. Additionally, FBXO11, TBL1XR1 and GOLGA2, which have all been shown to interact with BCL6, were commonly identified as BCL6-associated proteins in GBM cells. The identification of these known BCL6-associated proteins in the RIME experiments confirmed that

the RIME technique was able to identify BCL6 and the proteins it associates with. This increased the confidence that the other proteins identified were true BCL6-associated proteins.

The stringent methods used to filter out non-specific proteins also conferred confidence in the proteins identified as BCL6-associated. IgG control experiments were run in parallel with the BCL6 experiments so that proteins pulled down non-specifically could be subtracted. In the most stringent method applied, for each untreated or irradiated cell line, proteins identified in any of the three corresponding IgG replicates were subtracted from the list of proteins identified in each BCL6 replicate. This ensured that any protein that was ever pulled down in the control experiments was not considered a BCL6-associated protein. This method was recommended in the original RIME protocol publication and required acceptance that some genuine BCL6-associated proteins would be lost in order to ensure high confidence in those that remained.[335] In a later publication, the same research group proposed a less stringent method in which proteins not ≥ 2-fold higher in abundance in the BCL6 replicates than in the IgG replicates were excluded.[443] Use of this technique allowed the retention of proteins which were pulled down non-specifically, but were also pulled down specifically with BCL6 and so were higher in abundance in those replicates. Both methods were used in this chapter and the results combined. High confidence could be placed in the BCL6-associated proteins identified using the first method. Although those identified using the second method should be treated with more caution, it was useful to include these proteins to add to the informative data.

The proteins remaining after subtraction of non-specific proteins were queried in CRAPome 2.0.[448] Proteins found in > 10% of the negative control AP-MS experiments in the CRAPome database were excluded on the basis that they were more likely to be contaminants. Again, this required acceptance that some genuine BCL6-associated proteins, such as HDAC1 and HDAC2, would be lost to increase the confidence in the remaining proteins.

The identification of common BCL6-associated proteins across replicates and GBM cell lines revealed proteins which were commonly associated with BCL6 in GBM regardless of treatment and other proteins which were only commonly associated with BCL6 in either untreated or irradiated GBM. Many of these associations were novel, with little to no previous evidence in the literature. The BCL6-associated proteins considered to be of most interest (section 4.3.7.5) are discussed in section 4.4.4. The success of RIME for BCL6 in both untreated and irradiated GBM cell lines also enabled quantitative analysis of how these associations changed in response to acute IR. This helped to elucidate the acute IR-induced changes to BCL6 activity observed in Chapter 3 and in previous research.[207]

#### 4.4.1.2 Limitations of RIME

While RIME is a valuable technique, it does have limitations and the results should be treated with some caution until validated by independent methods. RIME relies upon the specificity of the antibody used. While the enrichment for BCL6 observed in the RIME data demonstrated that the antibody bound to BCL6, it is possible that it could also bind to off-target proteins. However, despite its low abundance, BCL6 was the only protein found in all of the RIME replicates and none of the IgG replicates. This strongly suggests that the antibody used at least had a greater affinity for BCL6 than any other protein. HRG was the only contender for off-target antibody binding, as it was identified with low coverage (≤ 3%) in all but one GBM replicate and in two of the three Raji replicates. It was surprising to find this plasma glycoprotein commonly associated with BCL6, especially as The Human Protein Atlas showed no expression of HRG transcript or protein in glioma tissue or brain cancer cell lines.[473] Although HRG may be a genuine BCL6-associated protein, it is possible that the anti-BCL6 antibody used may non-specifically bind HRG as well as BCL6. Future work could verify whether HRG associates with BCL6 to clarify this matter.

The impact of formaldehyde modifications to proteins was minimised by selecting the length of the formaldehyde crosslinking reaction to favour modification of lysine side chains rather than more non-specific interactions.[335,444] However, as trypsin cleaves at arginine and lysine residues, this introduced the possibility of missed cleavages which may have impacted protein identification.[474] This was mitigated by allowing two missed cleavages in the analysis settings. Additionally, a polyclonal antibody was used to overcome the possibility of epitope-masking by the crosslinking. Mohammed et al. (2016) recommended the omission of the usual proteomic processing steps for reduction of disulfide bonds to decrease detection of antibody peptides.[335] Therefore peptides containing disulfide-linked cysteine amino acids were excluded from the RIME analysis, reducing the coverage of the proteins identified. However, this was considered acceptable as it prevented the signal from BCL6 and its associated proteins from being swamped by antibody peptides.[335]

In the case of BCL6, another limitation of RIME was that BCL6 coverage was low. Due to the great difficulty in identifying endogenous BCL6 from GBM cells by mass spectrometry, this was acceptable. However, as BCL6 itself was only just above the threshold of detection, it is likely that BCL6-associated proteins which only interacted with a fraction of BCL6 molecules per cell sometimes or always fell below the threshold of detection. This explains the variable identification of known BCL6 binding partners, even in the Raji positive control experiments. It also means that known binding partners such as BCOR, or other proteins which were not detected, may associate with BCL6 in GBM cells, but did not rise above the threshold of detection in any of the replicates. While this is important to consider, it does not negate the relevance of the BCL6-associated proteins which could be detected using RIME.

RIME detected any proteins associated with BCL6 at the time of formaldehyde crosslinking. Hence the BCL6-associated proteins identified likely represent multiple different complexes formed by BCL6, possibly in different subcellular locations. Further experiments would be required to distinguish the different complexes. Additionally, it is possible that some of the proteins shown to be associated with BCL6 were captured by crosslinking due to their proximity to BCL6 but did not interact with it or its binding partners. Furthermore, the crosslinking of the target protein to the DNA it was bound to meant that any other proteins crosslinked to that fragment of DNA could be pulled down by RIME. However, the identification of proteins bound to regions of DNA distant from the target protein was minimised by the fragmentation of DNA by micrococcal nuclease digestion and sonication. Despite these limitations, interpretation of the BCL6-associated proteins as the 'nano-environment' of BCL6 instead of as definite BCL6 binding partners still provides insight into which proteins BCL6 was localised with and therefore what its roles in untreated and irradiated GBM might be.

### 4.4.2: Limitations caused by mass spectrometer changes

Due to the time constraints of a PhD project, the long-term failure of the Lumos™ mass spectrometer at Victoria University of Wellington, compounded by repair delays caused by Covid-19, meant that an alternative had to be found. Therefore, while some samples were run on the Lumos™ mass spectrometer at Victoria University of Wellington, others were run on the Q Exactive Plus™ mass spectrometer at the Bio21 Molecular Science and Biotechnology Institute Mass Spectrometry and Proteomics Facility at the University of Melbourne, Australia. The problem with this was demonstrated in the Raji positive control replicates. Many of the known BCL6 binding partners fell below the threshold of detection in the Raji BCL6 RIME samples run on the less sensitive instrument in New Zealand but were detected in the sample run on the more sensitive instrument in Australia.

This was primarily a problem for the LN18 samples as the three irradiated replicates were run at Victoria University of Wellington and the three untreated replicates were run at the Bio21 Institute. Hence it was difficult to conclude whether NCOR2 was identified only in the untreated LN18 replicates due to instrument sensitivity or an effect of treatment. Similarly, the quantitative analysis results for LN18 samples should be treated with caution. Proteins found to have their association with BCL6 increased by acute IR could be trusted as these proteins were more abundant in the irradiated samples despite the lower instrument sensitivity. However, the proteins found to have their association with BCL6 decreased by acute IR could be explained by the differences in instrument sensitivity instead of by an effect of treatment.

The three untreated NZG0906 replicates and one irradiated NZG0906 replicate were run at the Bio21 Institute, whereas the other two irradiated replicates were run at Victoria University of Wellington.

Nevertheless, NCOR2 was identified in all six replicates. However, the irradiated NZG0906 IgG replicate run at the Bio21 Institute caused another issue, as far more non-specific proteins were identified in this control sample than in the two IgG samples run at Victoria University of Wellington. Hence proteins which otherwise would not have been identified as non-specific may have been subtracted from the NZG0906 replicates run on the less sensitive instrument. This problem was solved by the inclusion of the less stringent method for removing non-specific proteins, which allowed the inclusion of proteins ≥ 2-fold higher in abundance in the BCL6 replicates compared to the IgG replicates. All but one NZG1003 replicate were run on the more sensitive instrument at the Bio21 Institute so the effect on the NZG1003 results is likely to be minor.

### 4.4.3: Heterogeneity of cell lines and biological replicates

GBM tumours are notoriously heterogenous and so the cell lines derived from GBM tumours also vary dramatically [52] To account for this, RIME for BCL6 was performed on three GBM cell lines: LN18, NZG0906 and NZG1003. The NZG0906 and NZG1003 cells lines were low passage cell lines derived from patient tumour tissue and so were more likely to be representative of GBM tumours. The high level of variability in the proteins identified in each cell line highlighted the heterogeneity of GBM. Additionally, to account for biological and technical variability, each experiment was carried out in biological triplicate. After subtraction of non-specific proteins, there was a high level of variability between replicates of the same cell line. This is likely to be because BCL6, and therefore the proteins associated with it, were low abundance, meaning that they were detected in some replicates, whereas in others they fell below the threshold of detection. Due to this variability, only proteins commonly identified as BCL6-associated across the cell lines and replicates were considered. This meant that BCL6-associated proteins that often fell below the threshold of detection may have been excluded, however it increased the confidence that the results were more broadly applicable to GBM.

### 4.4.4: Indicated BCL6 activity in GBM

The aim of this chapter was to determine whether the proteins associated with BCL6 changed in response to acute IR treatment, perhaps explaining its apparently altered activity in this context (Chapter 3). It was of particular interest whether BCL6 bound to known transcriptional corepressors in GBM or whether it had novel associations. Identification of proteins commonly associated with BCL6 across GBM cell lines and replicates and investigation of functional clusters among these proteins provided insight into the roles of BCL6 in GBM.

#### 4.4.4.1: Transcriptional activity

The identification of known BCL6 corepressor NCOR2 as a BCL6-associated protein suggested that BCL6 may retain its transcriptional repressor function in GBM. While it was previously shown that GBM cell lines and tumours express NCOR2, along with other BCL6 corepressors, this thesis provided the first evidence that BCL6 binds to NCOR2 in GBM.[207,475] However, the variability of its identification suggested that NCOR2 was not bound to all BCL6 dimers in GBM and therefore sometimes fell below the threshold of detection. This was consistent with ChIP-seq analysis in GC B cells and DLBCL cells which found that while 90% of NCOR2 peaks were also occupied by BCL6, only 27% of BCL6 peaks were also occupied by NCOR2, indicating that not all BCL6 activity involves NCOR2.[228]

Furthermore, TBL1XR1, also identified as a BCL6-associated protein in GBM, is a known component of the NCOR complexes that bind to BCL6.[450] Some studies have found that TBL1XR1 recruits the 19S proteosome complex to either degrade or otherwise remove NCOR1 and NCOR2 from transcription factors, allowing the exchange of transcriptional corepressors for transcriptional coactivators.[476,477] However, other studies appeared to disprove these claims.[478,479] Nevertheless, the identification of TBL1XR1 as a BCL6-associated protein in four untreated GBM cell line replicates, along with the common identification of NCOR2, enabled the confident assertion that BCL6 was bound to the NCOR2 corepressor complex in GBM.

The RIME experiments also identified two components of the gene-silencing Polycomb group (PcG) multiprotein PRC1-like complex, RNF2 and PHC2, as BCL6-associated proteins. RNF2 and PHC2 are commonly found together in the same PRC1 complexes.[466,467,480] PcG proteins, including the histone H2A ubiquitin ligase RNF2, form complexes with BCL6 corepressor BCOR and are recruited to BCL6 target genes.[480,481] BCOR was not identified as a BCL6-associated protein in any of the RIME replicates, however it is possible that RNF2 is part of another repressive complex which binds to BCL6. There is no direct evidence that RNF2 is part of the NCOR2 complex, however NCOR1 and RNF2 have been shown to bind to the same proteins and another histone H2A ubiquitin ligase, DZIP3, is recruited by a NCOR1/HDAC3 complex.[482–484] While there does not appear to be any previous evidence of the presence of PHC2 in BCL6 corepressor complexes, it is reasonable that the two PcG proteins RNF2 and PHC2 could associate with a transcriptional repressor like BCL6.

Four other transcriptional cofactors were identified as BCL6-associated proteins in the RIME analysis: MAML2, RCOR1, PIR and NCOA5. RCOR1, a corepressor involved in repression of neuronal genes, was excluded from Table 4.22 as it was only identified through the differential association analysis, which found that association of BCL6 with RCOR1 was decreased by acute IR, but was not commonly identified as a BCL6-associated protein.[485]

MAML2 was only identified as a BCL6-associated protein in untreated GBM cells and its association with BCL6 was decreased by acute IR in LN18 and NZG0906 cells. NCOR2 and MAML2 were connected in the STRING analysis as they are part of the alternative corepressor and coactivator complexes that bind to the Notch signalling transcription factor RBPJ.[468,469] In the absence of Notch signalling, RBPJ binds to corepressor complexes, some of which include NCOR2, to suppress the expression of Notch genes.[468,469] Upon Notch signalling, the cleaved Notch intracellular domain (NICD) translocates to the nucleus and binds to RBPJ along with coactivators, including MAML2, to activate Notch genes.[468] Notch signalling has been implicated in both oncogenic and tumour suppressor contexts in glioma.[486] BCL6 represses the transcription of Notch genes in follicular lymphoma and during neurogenesis.[272,487] In neurogenesis and other aspects of embryonic development, BCL6 competes with MAML1 for binding to the NICD.[272,488] Therefore it is possible that BCL6 may be localised close to MAML2 without interacting directly with it and hence be picked up by RIME. However, the potential cofactor-exchange function of TBL1XR1 makes it tempting to speculate that BCL6 itself might interact with the coactivator MAML2 in untreated GBM cells. While originally identified in the context of Notch signalling, MAML proteins have since been shown to interact with multiple transcription factors as part of Hippo, Hedgehog and Wnt/β-catenin pathways, so it is possible that MAML2 may interact directly with BCL6.[489]

PIR promotes the binding of NFκB to its target genes in response to an oxidative cell state, thus promoting NFκB-mediated transcriptional activation.[463,490] Canonically, BCL6 represses NFκB pathway genes and is in turn repressed by NFκB signalling.[227,245] Additionally, inhibition of BCL6 has been shown to upregulate expression of NFκB pathway genes in LN18 GBM cells.[207] It is possible that BCL6 competes with NFκB for binding to target genes and hence is in close proximity to PIR. Alternatively, BCL6 may bind directly to PIR, either to competitively inhibit promotion of NFκB activity or because PIR promotes the binding of BCL6 to its target genes. In Chapter 3, it was discovered that in response to acute IR, BCL6 activity was required for the upregulation of NFκB1, suggesting that BCL6 switched from a repressor to a promotor of NFκB signalling. BCL6 was only associated with PIR in untreated GBM cells. This supported the suggestion that BCL6 changes its activity in response to acute IR and may even activate pathways it canonically suppresses.

NCOA5 is a nuclear receptor coregulator with both transcriptional coactivator and corepressor functions in different contexts.[491–494] There is no previous evidence of an interaction between BCL6 and NCOA5, however other nuclear receptor corepressors, NCOR1 and NCOR2, are important BCL6 corepressors.[217,218] Therefore, it is possible that NCOA5 promotes BCL6-mediated transcriptional regulation of its target genes. NCOA5 was only identified as a BCL6-associated protein in untreated GBM cells, again suggesting a loss of BCL6 association with transcriptional coregulators in response to acute IR.

While identification of NCOR2, TBL1XR1, RNF2 and PHC2 reinforce the known role of BCL6 as a transcriptional repressor, the identification of Notch and NFκB coactivators MAML2 and PIR hints at the possibility of BCL6 involvement in other transcriptional pathways in GBM. Notably, TBL1XR1, RNF2, PHC2, MAML2, PIR and NCOA5 were only identified as BCL6-associated proteins in untreated GBM replicates, while NCOR2 was also more commonly identified in the untreated replicates. Furthermore, TBL1XR1, PHC2, MAML2, PIR, RCOR1 and NCOR2 all had their association with BCL6 decreased by acute IR in at least one GBM cell line. This fits with the subcellular location analysis, which found that BCL6 associated with more nuclear proteins in untreated GBM cells than it did in irradiated GBM cells. The functional enrichment of the GO:MF term *transcriptional corepressor activity* in the analysis of proteins which had their association with BCL6 decreased by acute IR in LN18 cells added to these trends. Together this evidence suggested that BCL6 is a transcriptional regulator in untreated GBM cells but that its function changes in response to acute IR. However, due to the problems caused by mass spectrometer changes discussed above, these results should be treated with caution until verified by other methods.

#### 4.4.4.2: Regulation of BCL6

Two E3 ubiquitin-protein ligases, FBXO11 and TRIM47, were commonly identified as BCL6-associated proteins in GBM using RIME. While both proteins were identified in untreated and irradiated replicates, FBXO11 was identified in more irradiated replicates while TRIM47 was identified in more untreated replicates. However, both E3 ubiquitin-protein ligases had their association with BCL6 increased by acute IR in different GBM cell lines. As acute IR has been shown to increase BCL6 expression in GBM cells, this increased association of E3 ubiquitin-protein ligases with BCL6 apparently does not lead to decreased BCL6 levels.[207] It may be that the increased association does lead to increased BCL6 degradation, but that this is outweighed by the increase in BCL6 expression such that overall BCL6 abundance increases.

Along with NCOR2, FBXO11 was a key protein in showing the success of the RIME technique in this thesis. FBXO11 is the substrate recognition component of a Skp1-Cul1-F-box protein (SCF) ubiquitin-protein ligase complex known to mediate ubiquitination and subsequent degradation of BCL6.[255] FBXO11 is deleted or mutated in some DLBCL cell lines and DLBCL and Burkitt's lymphoma tumours and these mutations correlate with higher BCL6 expression.[255,495] Furthermore, expression of FBXO11 is inversely correlated with survival in GBM, which could be due to its role in negative regulation of BCL6.[496] However, another study showed that FBXO11 expression was increased in a treatment-resistant GBM cell line compared to the original cell line.[497] As BCL6 is known to contribute to the therapy resistance of GBM, it is possible that this increase in FBXO11 occurs alongside an increase in BCL6 expression and therefore has no net effect on BCL6 activity.

TRIM47 has not been previously linked with BCL6, however its overexpression and activity has been linked to cancer progression, therapy resistance or poorer prognosis in multiple cancer types.[498–507] TRIM47 has a wide variety of targets and promotes cancer through several pathways, including PI3K/AKT, NFκB, p53 and glycolysis.[498,499,501,502,504] In glioma, TRIM47 expression has been linked to inhibition of the Wnt/β-catenin pathway and knockdown was shown to inhibit proliferation and migration of glioma cells.[507] BCL6 is canonically involved in suppression of the NFκB and p53 signalling pathways and inhibition of BCL6 has been shown to upregulate genes involved in NFκB and apoptotic signalling in GBM cells.[207,240,245] Conversely, Chapter 3 showed that BCL6 appeared to be involved in upregulation of PI3K/AKT, NFκB and p53 pathway proteins in response to acute IR. Therefore, it is possible that TRIM47 may be involved in modulating the regulation of these pathways by BCL6.

#### 4.4.4.3: AMPK

AMPK subunits α1 and γ1 (PRKAA1 and PRKAG1) were two of the most commonly identified BCL6-associated proteins in both untreated and irradiated GBM cell lines. AMPK is the master regulator of the response to energetic and mitochondrial stress.[375] Upon activation by low cellular ATP levels, AMPK phosphorylates enzymes and transcription factors to promote catabolic processes, such as glycolysis and autophagy, and inhibit anabolic processes, such as protein and lipid synthesis, in order to restore ATP levels.[375] The binding of AMP or ADP instead of ATP to the γ subunit activates AMPK and the catalytic α subunit mediates phosphorylation of target proteins.[375,508,509] Both of these subunits were commonly identified as BCL6-associated, while the scaffolding β subunit, was not.[510] It may be that crosslinking between the β subunit and the other two AMPK subunits prevented detection of sufficient numbers of β subunit peptides for identification. The γ subunit was also found in two of the three Raji replicates. Therefore, although the association of BCL6 with AMPK is novel, it does not appear to be GBM-specific. It seems likely that the interaction between BCL6 and AMPK is transient and therefore could be identified by RIME but not by other methods lacking crosslinking.

It has been shown that AMPK transcript levels are upregulated in GBM compared to normal brain.[511] However, in a recent meta-analysis of GBM whole proteomics carried out alongside this thesis, there was no evidence of consistent upregulation of AMPK protein levels in GBM compared to normal brain.[64] Nonetheless, the abundance of activated AMPK is convincingly upregulated in GBM compared to normal brain.[511] This uniformly high activation, regardless of nutrient levels, has been linked to oncogene-associated stress.[511] AMPK activity in GBM promotes glycolysis and mitochondrial function via positive regulation of the HIF-1α and GABPA transcriptional pathways.[511] Additionally, AMPK is activated by IR in lung, breast and prostate cancer cell lines and contributes to the DNA damage

response.[512–514] AMPK is also activated in response to TMZ in GBM cells and contributes to apoptosis by inhibiting mTORC1 activity and downstream BCL2 expression and by phosphorylating p53.[515]

Chapter 3 revealed BCL6-dependent upregulation of AMPK-γ1 in response to acute IR treatment of LN18 cells. This suggests that in response to acute IR, BCL6 directly or indirectly mediates increased transcription or stabilisation of AMPK as well as interacting with it itself. Despite this, the association of BCL6 with AMPK-γ1 was not increased by acute IR in LN18 cells. Contrastingly, association of AMPK-α1 with BCL6 was increased by acute IR in NZG1003 cells, while association of AMPK-γ1 with BCL6 was increased by acute IR in NZG0906 cells. Thus, although BCL6 is associated with AMPK in untreated as well as irradiated GBM cells, this association may be increased by IR in some GBM cell lines.

AMPK is known to regulate BCL6 expression indirectly. AMPK upregulates BCL6 expression in glucose-deprived T cells and exerts anti-inflammatory effects in endothelial cells by phosphorylating PARP1 to prevent its inhibitory action on BCL6 transcription.[516,517] Furthermore, glucose deprivation of pancreatic β-cells upregulates BCL6 expression via the activity of FOXO transcription factors.[518] The FOXO transcription factors are positively regulated by AMPK so it is likely that the upregulation of BCL6 by FOXO transcriptional activity in response to glucose deprivation may be promoted by AMPK.[519,520] However, this thesis provides the first evidence of a physical interaction between BCL6 and AMPK.

Hadri et al. (2015) found that AMPK expression in vascular smooth muscle cells led to upregulation of BCL6.[521] Expression of the sPLA2-IIA gene was inhibited by AMPK activity, but this inhibition was independent of the BCL6 binding site in the sPLA2-IIA promoter.[521] Hadri et al. hypothesised that AMPK-mediated phosphorylation of BCL6 might cause it to bind to NFκB and block it from activating the transcription of sPLA2-IIA.[521] They supported this hypothesis with the identification of a putative AMPK phosphorylation site at Ser16 of BCL6.[521]

The RIME analysis in this chapter was repeated with phosphorylation defined as a dynamic modification. No phosphorylation of Ser16 was observed in the four untreated and five irradiated RIME replicates in which a peptide containing the putative phosphorylation site was identified (Appendix). Instead, phosphorylation of BCL6 residue Ser404 was observed in all three untreated NZG0906 RIME replicates, in one irradiated NZG0906 replicate and in two irradiated NZG1003 replicates (Appendix). In the other samples, the peptide containing Ser404 was not identified and so phosphorylation status could not be determined. A search of PhosphoSitePlus® v6.6.0.4 revealed that phosphorylation of BCL6 Ser404 had been identified in breast cancer, lymphoma, leukemia, non-small cell lung cancer and ovarian cancer.[522–529] However, these identifications were confined to supplementary data tables and the functional significance of this post-translational modification has not been investigated. The amino acid sequence surrounding Ser404 in BCL6 did not match the AMPK consensus phosphorylation

site.[530,531] As only partial coverage of BCL6 was achieved through RIME, it is possible that AMPK phosphorylated another site in BCL6 which was not identified. It is also possible that AMPK phosphorylated another protein associated with BCL6 in GBM and that this close proximity resulted in its identification as a BCL6-associated protein.

#### 4.4.4.4: Exocytosis and caveolae

RIME also revealed the association of BCL6 with several proteins involved in exocytosis. STXBP1 is involved the docking of synaptic vesicles in the pre-synapse and is essential for neurotransmitter release, while SYT1 triggers neurotransmitter release in response to calcium levels.[532–535] Similarly, as part of the exocyst complex, EXOC2 is involved in the docking of exocytic vesicles at the plasma membrane and is important in brain development.[536,537] The synaptic proteins, STXBP1 and SYT1, were only commonly found associated with BCL6 in irradiated GBM cells and association with STXBP1 was increased $\geq$ 2-fold by acute IR in NZG0906 and NZG1003 cells. Additionally, the proteins that had their association with BCL6 increased by acute IR in LN18 cells were enriched for synaptic and neuronal functional terms. Conversely, EXOC2 was only commonly identified as a BCL6-associated protein in untreated GBM cells and its association with BCL6 was decreased by acute IR in LN18 and NZG0906 cells. While there is no known link between synaptic proteins and BCL6, SNARE-related proteins have been shown to have importance in GBM. Blockade of STX1 impairs GBM growth and invasiveness, while STX1, STXBP1 and SYN1 proteins and SYT1 and SYN2 transcripts are commonly upregulated in GBM recurrent tumours compared to the corresponding primary tumours.[538,539]

Additionally, four caveolae components, CAV1, CAVIN1, CAVIN3 and FLOT1, were commonly identified as BCL6-associated proteins only in irradiated GBM cells. CAV1 is essential for formation of caveolae and recruits the CAVIN proteins.[540–543] CAVIN1 and CAVIN2 compete for binding to CAV1, forming distinct CAV1/CAVIN1/CAVIN3 and CAV1/CAVIN1/CAVIN2 complexes which bind to the same caveolae in separate striations.[542,544] CAVIN2 was not identified in any of the RIME replicates, suggesting that only the former complex is associated with BCL6 in irradiated GBM cells. There is no known link between BCL6 and caveolae, however CAV1 and CAVIN1 are upregulated in GBM and their expression is correlated with increased invasiveness in GBM cell lines and poorer patient survival.[545] Additionally, CAV1 expression increases in response to TMZ in GBM cells and in response to acute IR in a range of cell types.[546,547] One of these studies found that the CAV1 protein was stabilised in irradiated cells in order to promote DNA repair. However, CAV1 was not upregulated by acute IR in LN18 GBM cells.

While BCL6 may associate with these two groups of plasma membrane proteins separately, synaptic and caveolae proteins are known to interact. CAV1 has been linked with synaptic vesicle exocytosis in hippocampal neurons.[548] Additionally, CAV1 has been shown to interact with and negatively regulate

the activity of the glutamate transporters EAAT1-4 which are downregulated in GBM, promoting GBM survival and invasion.[549–551] The association of BCL6 with caveolae and pre-synaptic proteins in irradiated GBM cells suggested that at least a fraction of BCL6 was localised to the plasma membrane after acute IR. This was supported by the association of BCL6 with 11 plasma membrane proteins only in irradiated GBM cells. BCL6 could be localised with these proteins due to an unknown role at the plasma membrane in response to acute IR. Alternatively, the induction of autophagy seen 48 hours after acute IR in GBM cells (Chapter 3) could result in BCL6 being localised near these plasma membrane proteins within autophagic vesicles.

It is also possible that the association of BCL6 with these plasma membrane proteins could indicate the packaging of BCL6 into exocytic vesicles in response to acute IR treatment of GBM cells. IR increases the secretion of extracellular vesicles (EVs) from GBM cells by 24 and 48 hours in a dose-dependent manner.[552] Furthermore, IR changes the proteome of cancer-secreted EVs, so it is possible that BCL6 may be secreted from GBM cells in EVs in response to acute IR.[553] This was not observed in EVs secreted from irradiated GBM cells in a previous study, however it is likely that BCL6 was either not included in the microarray assay or was not detected due to its low abundance.[552] EVs secreted by irradiated cancer cells mediate bystander effects on other tumour cells, contributing to stress signalling, DNA repair and migration.[552–555] As BCL6 appeared to upregulate stress response signalling proteins in response to acute IR (Chapter 3), its export to surrounding GBM cells could help to induce stress responses in these cells.

The exocytosis of BCL6 could potentially explain the apparent association of BCL6 with secreted proteins such as collagen and apolipoproteins. However, BCL6 association with secreted proteins was observed in both untreated and irradiated GBM cells, whereas association with plasma membrane proteins was only observed in irradiated GBM cells. Future RIME experiments targeting other proteins in GBM cells could determine whether the secreted proteins are simply enriched by the RIME process rather than truly associated with BCL6.

#### 4.4.4.5: Summary of indicated BCL6 activity in GBM

Chapter 3 revealed that BCL6 appeared to switch from a repressor of the DNA damage response to a promoter of stress response signalling after acute IR treatment. This added to previous data showing that BCL6 induced by therapy did not act as a transcriptional repressor and may have acted as a transcriptional activator.[207] The RIME data supported these findings, as while BCL6 associated with transcriptional coregulator proteins in untreated GBM cells, these associations appeared to be lost or reduced in response to acute IR. Hence in untreated GBM cells, BCL6 may retain its known transcriptional repressor function but this seemed to change in response to irradiation.

The association of BCL6 with metabolic stress response protein AMPK concurred with characterisation of BCL6 as an evolutionarily conserved component of the cellular stress response.[406] AMPK may phosphorylate BCL6 to alter its function in response to stress. Although AMPK was found associated with BCL6 in both untreated and irradiated GBM cells, its association with BCL6 was increased in irradiated NZG0906 and NZG1003 cells, suggesting increased interaction in response to stress.

The association of BCL6 with plasma membrane proteins in irradiated GBM cells may indicate a further role for BCL6 in the stress response. BCL6 is important for adaptation to long-term stress in multiple cancer types.[406] Previous studies have focused on the transcriptional regulation role of BCL6 in stress adaptation, but it is possible that BCL6 may be packaged into vesicles and released into the tumour microenvironment to communicate stress to nearby cells. Cell-cell communication via exosomes is important in the cellular response to multiple types of stress and is involved in drug resistance in multiple cancer types, including GBM.[556,557] Therefore the release of BCL6 in EVs may help nearby GBM cells to respond to the stress induced by therapy as well as communicating with other cells in the microenvironment to enlist their help in surviving therapy. Alternatively, BCL6 may have another function at the plasma membrane or be taken up by autophagic vesicles along with plasma membrane proteins.

The results of this chapter indicated that investigation of the role of BCL6 in cellular responses to stress needs to be re-examined with a broader outlook. As well as its transcriptional regulation activity, BCL6 may be involved in other aspects of the response to stress such as interacting with AMPK and being released in vesicles as part of cell-cell communication.

### 4.4.5: Future directions

RIME for BCL6 identified numerous proteins associated with BCL6 in untreated and irradiated GBM cells. While many of these associations suggested exciting directions for follow-up work, it was necessary to consider which would be the most informative. NCOR2 was selected for validation as it is a known binding partner of BCL6. Therefore, demonstration that NCOR2 is associated with BCL6 using both RIME and another assay would provide confidence that BCL6 forms transcriptional repressor complexes in GBM. Moreover, the RIME study provided tentative evidence that BCL6 association with NCOR2 and other transcriptional corepressors may decrease in response to acute IR. Validation of this finding would have implications for the role of BCL6 in the response of GBM cells to therapy. The other transcriptional cofactors identified as BCL6-associated proteins also merit further investigation as some have not been previously linked directly to BCL6 activity. However, this will be an area for future study.

The identification of AMPK as a BCL6-associated protein was a novel finding with intriguing implications. The α1 and γ1 subunits of AMPK were commonly identified as BCL6-associated proteins across GBM cell lines, replicates and treatments, while the γ1 subunit was also associated with BCL6 in the Raji lymphoma cell line, making the finding robust as well as novel. Therefore, AMPK was the second BCL6-associated protein selected for validation. Verification of the association of BCL6 with AMPK would provide a solid basis for future studies to investigate the specifics of this interaction and its implications for the role of BCL6.

The association of BCL6 with synaptic and caveolae proteins in response to acute IR was also a fascinating finding and may be important in the role of BCL6 in the therapy resistance of GBM. However, this would require more extensive follow-up studies to validate as multiple proteins were involved. Additionally, the consequences are harder to interpret without follow-up experiments, whereas the connection of BCL6 with AMPK provides a clear link between BCL6 activity and the metabolic stress response. Furthermore, the association of BCL6 with E3 ubiquitin-protein ligases also warrants future work, as this may be important in regulation of BCL6 levels and particularly in the upregulation of BCL6 protein expression in response to treatment. However, the novelty of the AMPK association was deemed more suitable for validation.

Communication with Soleilmane Omarjee from the group who developed the RIME protocol (Carroll Lab, Cancer Research Institute UK, Cambridge) determined that proximity ligation assays (PLAs) are considered the best validation method for RIME results.[338,443] Chapter 5 describes preliminary work using PLA assays to validate the association of BCL6 with NCOR2 and AMPK.

# 5: Preliminary validation of the association of BCL6 with NCOR2 and AMPK in GBM cells

## 5.1: Introduction

RIME for BCL6 in GBM cells provided a list of candidate BCL6-associated proteins in untreated and irradiated GBM cells (Chapter 4). Extensive efforts were made to eliminate false positives from the RIME data. This included the use of multiple replicates, comparison to IgG controls and the use of the CRAPome database. However, false positives are a well-known issue with affinity purification mass spectrometry (AP-MS) experiments.[446] This emphasised the importance of validation to confirm that the RIME results identified true BCL6-associated proteins.

Two candidate BCL6-associated proteins identified using RIME were chosen for validation. These proteins were NCOR2 and AMPK. NCOR2 is a known BCL6-binding protein so further validation of this interaction in GBM cells would provide robust evidence that BCL6 retains its association with NCOR2 in GBM cells. The RIME data indicated that BCL6 may lose or reduce its interaction with NCOR2 by 48 hours after acute IR. Validation of this finding would support indications in Chapters 3 and 4 that the activity of BCL6 changes in response to acute IR. In contrast to NCOR2, the association of BCL6 with AMPK was a novel finding. Validation of this association would strengthen the evidence that these two proteins interact in GBM cells.

In this chapter, initial experiments aimed to identify and compare the subcellular localisation of the proteins of interest using immunofluorescence microscopy. Co-localisation was then examined in a preliminary study using proximity ligation assays (PLA). PLAs are superior to immunofluorescence co-localisation for the verification of protein associations as signal is only seen if the proteins of interest are within 40 nm of each other.[338] The primary antibodies used for immunofluorescence staining were also used for the PLAs (Figure 5.1A). In PLAs, two oligonucleotide-bound probes, one for each primary antibody species, are added (Figure 5.1B).[338] If the two proteins of interest are within 40 nm of each other, the oligonucleotides from the two probes hybridise and are ligated together (Figure 5.1C).[338] The resulting circular DNA is then amplified by DNA polymerase (Figure 5.1D).[338] Complementary fluorescent oligonucleotide probes then bind to the amplified circular DNA and produce a fluorescent signal when excited (Figure 5.1E), allowing detection of the protein-protein association by fluorescence microscopy (Figure 5.1F).[338]

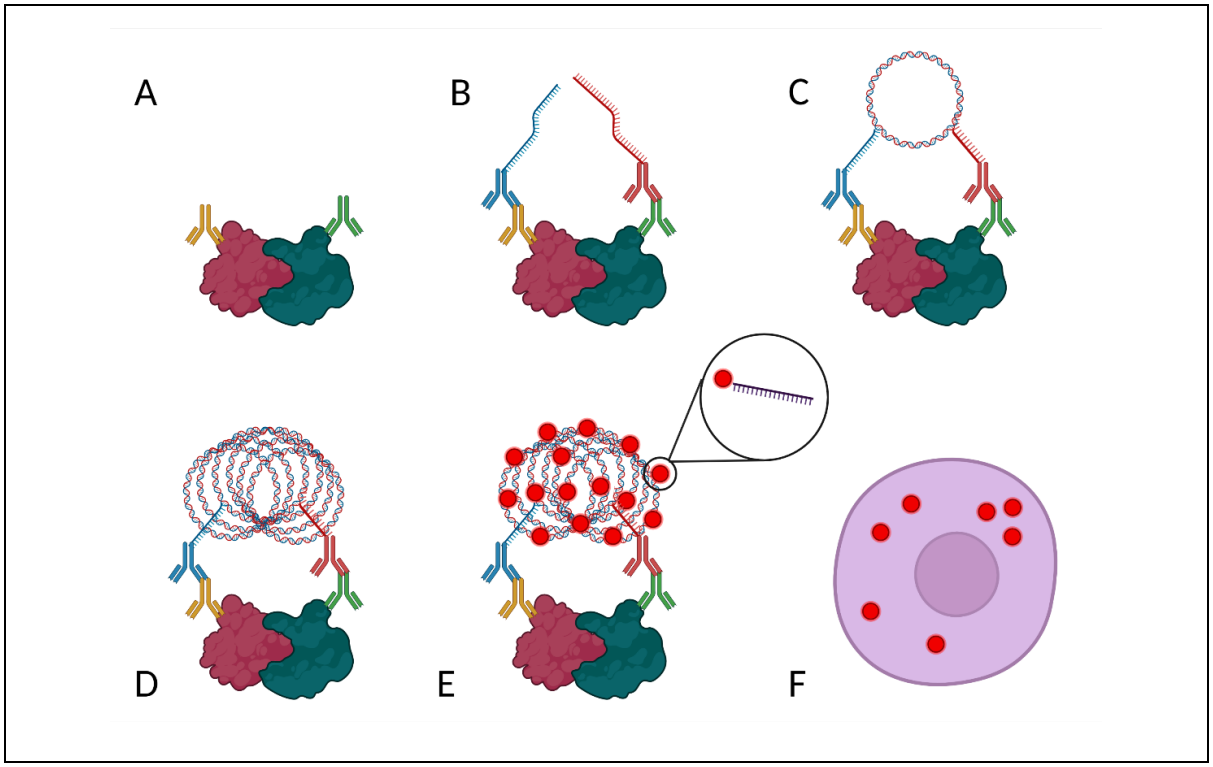


Figure 5.1: Schematic of the proximity ligation assay protocol

Steps A-F are as described in the paragraph above. Created using BioRender.

## 5.2: Aims

The primary aim of this chapter was to perform preliminary studies to validate the association of BCL6 with NCOR2 and AMPK in GBM cells by using microscopy techniques. The secondary aim was to investigate the effect of acute IR on these associations.

## 5.3: Results

### 5.3.1 The subcellular location of BCL6, NCOR2 and AMPK in LN18 GBM cells

#### 5.3.1.1: Selection of controls for immunofluorescence microscopy

For each antibody used (anti-BCL6, anti-NCOR2 and anti-AMPK), two types of control experiments were carried out. The first control assessed the specificity of antibody binding using non-specific IgG antibodies. As a control for the mouse anti-BCL6 antibody, an equal concentration of non-specific mouse IgG antibody was used, along with the same concentration of AF488 secondary antibody used for BCL6. As controls for the rabbit anti-NCOR2 and anti-AMPK antibodies, the concentration of non-specific rabbit IgG antibody matching the concentration of each specific antibody was used, along with the same concentration of AF568 antibody used for NCOR2 and AMPK. If the same signal was seen in the corresponding experimental and IgG samples, this would suggest that the experimental antibodies could also be binding to the LN18 cells non-specifically.

The second control investigated whether the antibodies bound only to the expected proteins. Cell lines with low mRNA expression of the proteins of interest were identified using the Human Protein Atlas.[558] The leukaemia cell line K562 was selected as a negative control for BCL6 expression due to its low expression of BCL6 mRNA and its common use as a *BCL6-null* cell line.[381–383] LN18 cells expressed 3.6-fold more BCL6 mRNA than K562 cells and transcript level in K562 cells was close to background (Appendix). NCOR2 and AMPK were problematic as they are widely expressed. The hepatocellular carcinoma HepG2 cell line was selected as a negative control for AMPK due to its relatively low AMPK mRNA expression. Doxorubicin-treated LN18 cells were used as a negative control for NCOR2 as this treatment had previously been shown to downregulate NCOR2 expression in LN18 cells.[322]

#### 5.3.1.2: Localisation of BCL6 in LN18 GBM cells

Immunofluorescence staining for BCL6 was made challenging by its low abundance. Figure 5.2 shows representative images of BCL6 staining in untreated LN18 cells (A and B) compared to staining with a non-specific mouse IgG antibody at the same concentration (C and D). A 1:50 antibody concentration was necessary to observe BCL6 staining, however at this high concentration there was often signal in the IgG control. However, the signal in the IgG control was typically made up of large speckles whereas the signal in the BCL6 sample was much more diffuse. This difference in appearance was considered sufficient to indicate that the BCL6 antibody was binding specifically. Furthermore, there was no signal observed in the K562 negative control with the BCL6 antibody. This increased the confidence in the BCL6-specificity of the BCL6 antibody.

The BCL6 staining (Figure 5.2A and B) showed that BCL6 was concentrated around the edge of the LN18 nuclei, with some fainter staining further inside the nucleus and in the cytoplasm.

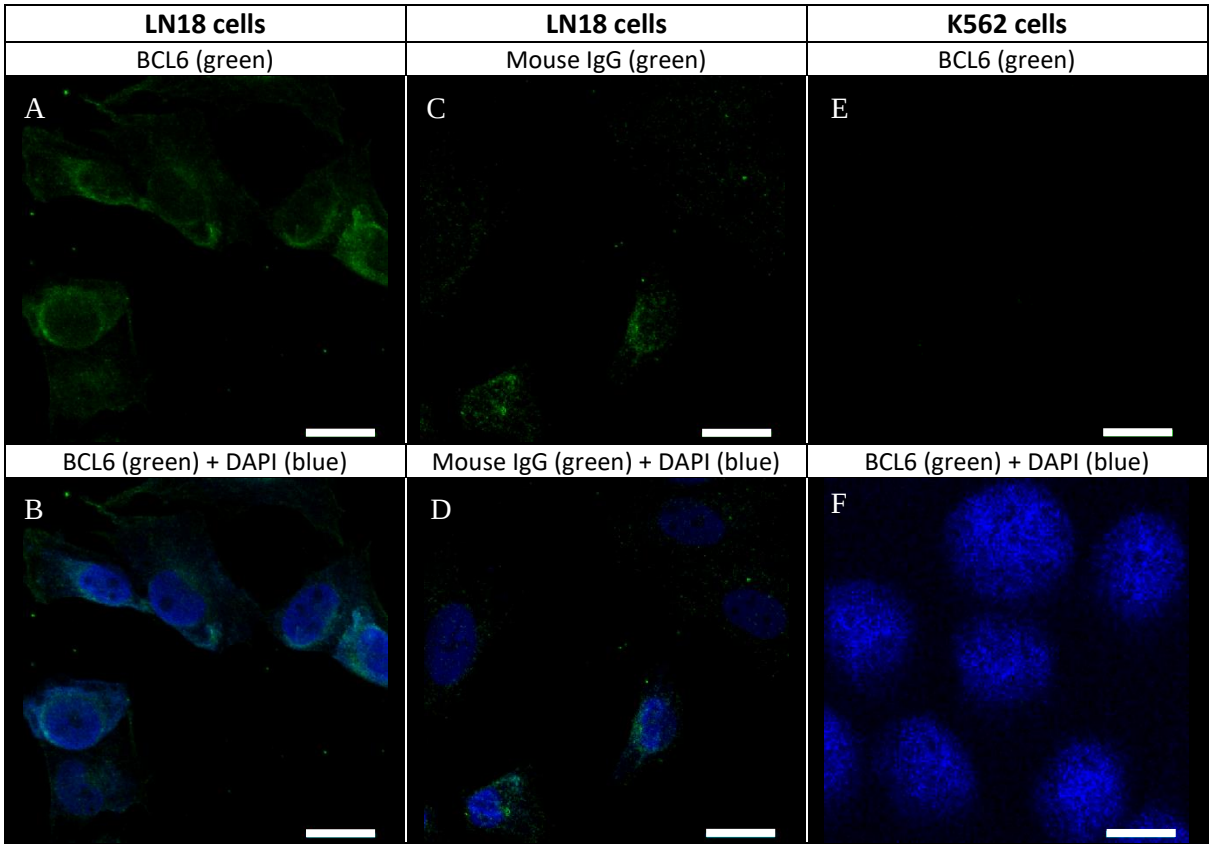


Figure 5.2: Specificity of BCL6 immunofluorescence

Comparison of staining for A&B) BCL6 (green) in untreated LN18 cells; C&D) non-specific mouse IgG antibody (green) in untreated LN18 cells; E&F) BCL6 (green) in the negative control K562 cell line. An AlexaFluor488 secondary antibody was used at the same concentration for all samples and images were taken with the same acquisition settings. Figures B, D and F show DAPI staining (blue) of nuclei as well as BCL6/IgG staining (green). Z-stack images (8 slices) taken using 40x objective followed by 3x digital zoom and Z-projection in Fiji (ImageJ). Relative brightness of colours adjusted equally in each image (green = 2.0, blue = 1.0) in CellProfiler. Images representative of A&B) 1 biological replicate (rep), 17 images (im); C&D) 1 rep, 14 im; E&F) 1 rep, 8 im. Scale bars = 20 µm.

### 5.3.1.3: Localisation of NCOR2 in LN18 GBM cells

NCOR2 stained brightly throughout the nucleus of LN18 cells (Figure 5.3A and B). There was very little non-specific signal observed in the IgG control (Figure 5.3C and D) and NCOR2 staining was markedly reduced in the doxorubicin-treated cells as expected (Figure 5.3E and F). This gave high confidence that the anti-NCOR2 antibody bound specifically to NCOR2 in LN18 cells.

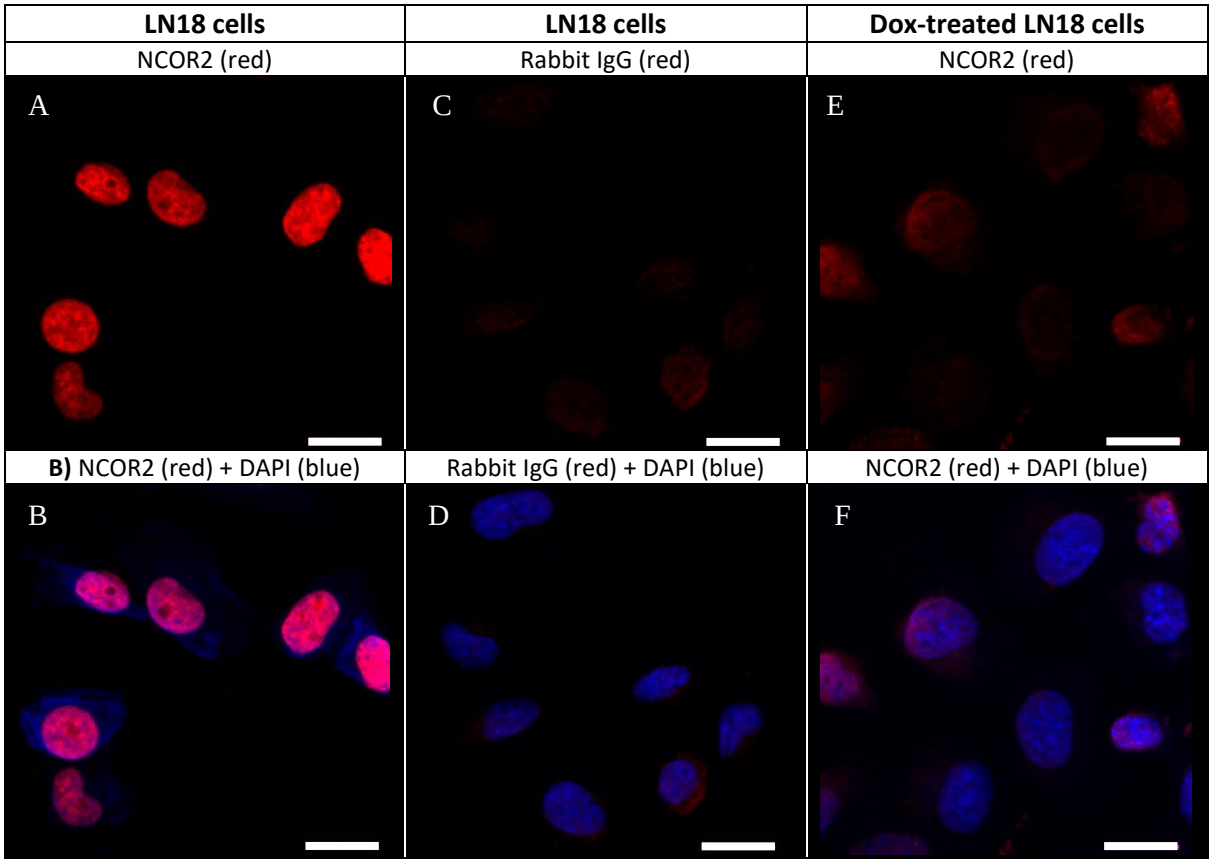


Figure 5.3: Specificity of NCOR2 immunofluorescence

Comparison of staining for A&B) NCOR2 (red) in untreated LN18 cells; C&D) non-specific rabbit IgG antibody (red) in untreated LN18 cells; E&F) NCOR2 (red) in the negative control doxorubicin-treated LN18 cells. An AlexaFluor568 secondary antibody was used at the same concentration for all samples and images were taken with the same acquisition settings. Figures B, D and F show DAPI staining (blue) of nuclei as well as NCOR2/IgG staining (red). Z-stack images (8 slices) taken using 40x objective followed by 3x digital zoom and Z-projection in Fiji (ImageJ). Relative brightness of colours adjusted equally in each image (red = 1.0, blue = 1.0) in CellProfiler. Images representative of A&B) 1 biological replicate (rep), 15 images (im); C&D) 1 rep, 8 im; E&F) 1 rep, 8 im. Scale bars = 20 µm.

### 5.3.1.4: Localisation of AMPK in LN18 GBM cells

The AMPK signal was dimmer than the NCOR2 signal, necessitating brightening of the image during processing. As the IgG control images were processed in the same way, this led to some visible signal in a few cells in the IgG control (Figure 5.4C and D). However, the rabbit IgG signal was much more speckled than the signal with the AMPK antibody. It was also concentrated in the nuclei whereas the AMPK signal was spread more diffusely throughout the nuclei and cytoplasm (Figure 5.4A and B). Therefore, it was concluded that the AMPK signal was likely to be genuine, although some caution should be taken when interpreting the nuclear signal. Additionally, AMPK signal was much lower in the negative control HepG2 cell line than in the LN18 cells (Figure 5.4E and F). This was expected as The Human Protein Atlas showed relatively low, but not absent, AMPK mRNA expression in HepG2 cells.

In LN18 cells, AMPK appeared to be spread throughout the nuclei and cytoplasm but was also concentrated in brighter punctate structures in the nuclei. This punctate signal could be due to non-specific signal, however the spots were much larger than the speckles seen in the IgG control and so may represent a genuine concentration of AMPK protein.

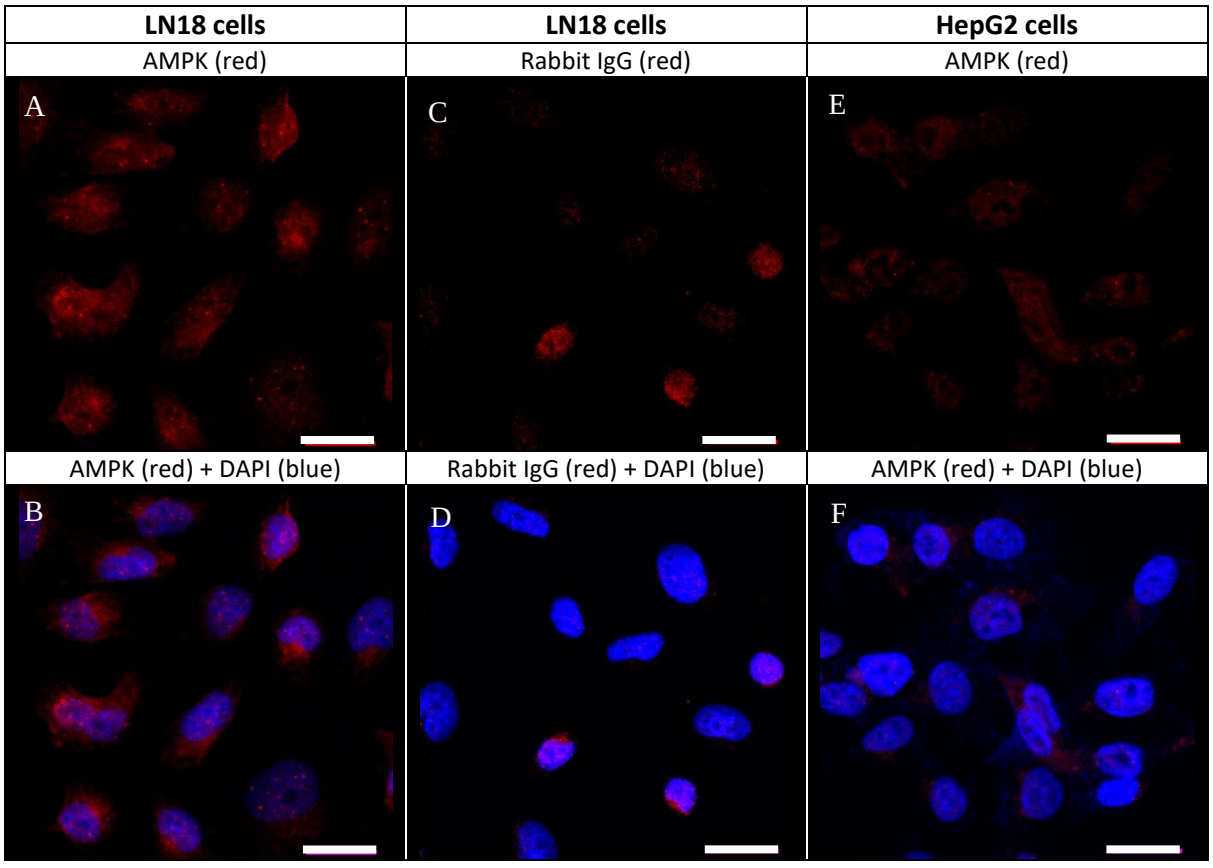


Figure 5.4: Specificity of AMPK immunofluorescence

Comparison of staining for A&B) AMPK (red) in untreated LN18 cells; C&D) non-specific rabbit IgG antibody (red) in untreated LN18 cells; E&F) AMPK (red) in the negative control HepG2 cell line. An AlexaFluor568 secondary antibody was used at the same concentration for all samples and images were taken with the same acquisition settings. Figures B, D and F show DAPI staining of nuclei (blue) as well as AMPK/IgG staining (red). Z-stack images (8 slices) taken using 40x objective followed by 3x digital zoom and Z-projection in Fiji (ImageJ). Relative brightness of colours adjusted equally in each image (red = 2.0, blue = 1.0) in CellProfiler. Images representative of A&B) 1 biological replicate (rep), 17 images (im); C&D) 1 rep, 8 im; E&F) 1 rep, 8 im. Scale bars = 20 µm.

### 5.3.1.5: Comparison of BCL6, NCOR2 and AMPK localisation in untreated and irradiated LN18 GBM cells

To determine whether the localisation of BCL6, NCOR2 and AMPK was altered by acute IR, the staining was repeated in irradiated LN18 cells. Figure 5.5A-F show the staining of untreated LN18 cells for BCL6 (A and B), NCOR2 (C and D) and AMPK (E and F) respectively, as displayed in the previous sections. Below, Figure 5.5G-L show the staining of irradiated LN18 cells for BCL6 (G and H), NCOR2 (I and J) and AMPK (K and L).

Staining for BCL6 was generally fainter in the irradiated LN18 cells. This contradicted previous research and the western blot results from Chapter 3 which showed that BCL6 expression was upregulated 48 hours after acute IR treatment.[207] As in the untreated LN18 cells, the distribution of BCL6 after IR was concentrated around the edge of the nucleus with some fainter staining in the nuclei and cytoplasm.

NCOR2 staining was also decreased in irradiated LN18 cells, although it was not as faint as in doxorubicin treated LN18 cells (Figure 5.3E and F). This fits with previous research showing a strong downregulation of NCOR2 protein expression by doxorubicin and a slight downregulation by IR.[322]

In untreated LN18 cells, AMPK was spread diffusely through the nucleus and cytoplasm, with some punctate localisation in the nucleus (Figure 5.5E and F). While there was still some cytoplasmic staining, AMPK seemed to concentrate in the nucleus after IR (Figure 5.5K and L). Additionally, the spots of AMPK signal in the nucleus were brighter and larger in the irradiated LN18 cells suggesting increased recruitment of AMPK to these locations.

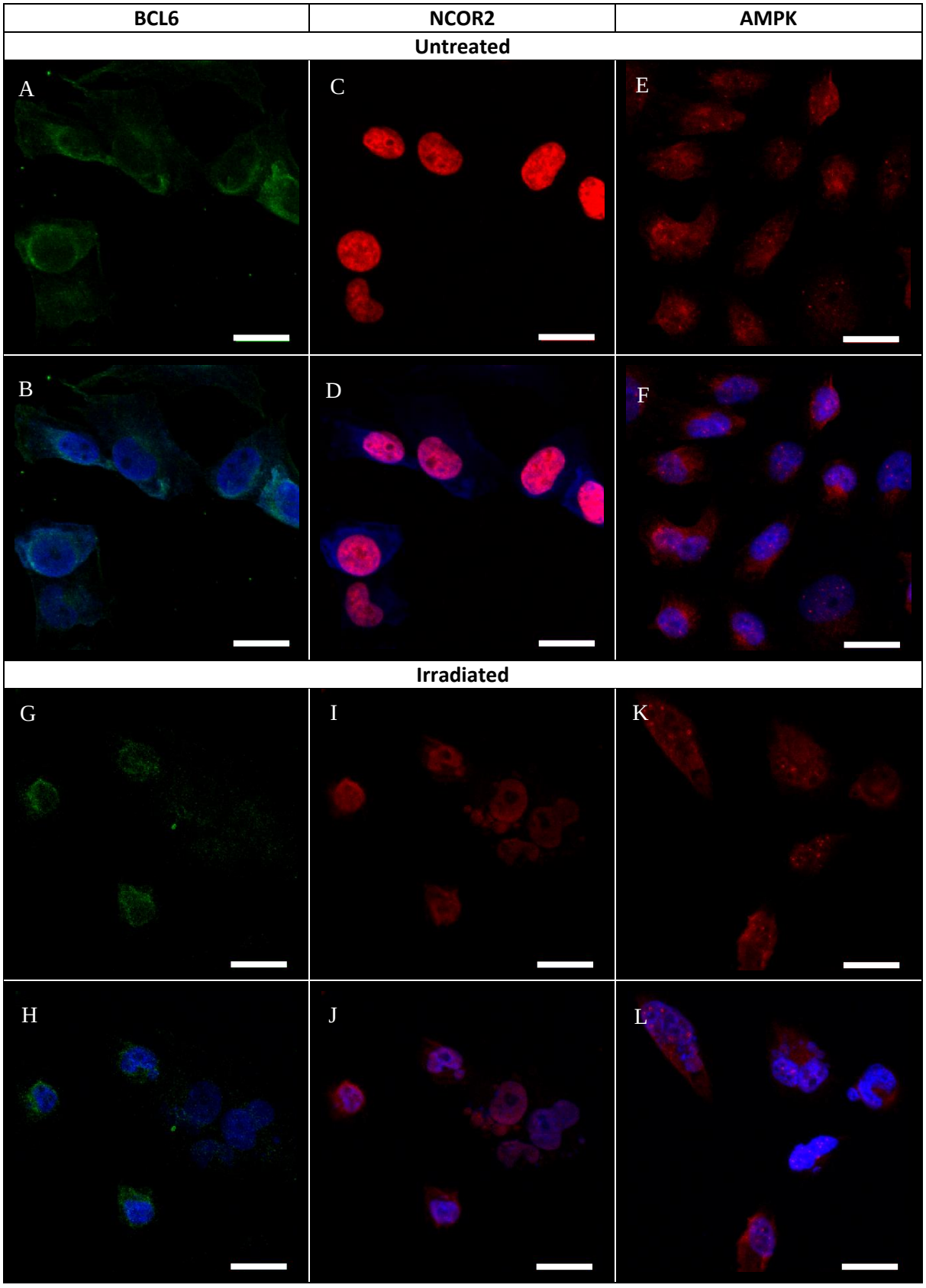


Figure 5.5: Effect of irradiation on BCL6, NCOR2 and AMPK localisation in LN18 cells

Comparison of staining for BCL6 (green) in untreated (A&B) and irradiated (G&H) LN18 cells; comparison of staining for NCOR2 (red) in untreated (C&D) and irradiated (I&J) LN18 cells; and comparison of staining for AMPK

(red) in untreated (E&F) and irradiated (K&L) LN18 cells. Figures B, D, F, H, J & L show DAPI staining of nuclei (blue) as well as BCL6/NCOR2/AMPK staining. Z-stack images (8 slices) taken using 40x objective followed by 3x digital zoom and Z-projection in Fiji (ImageJ). Relative brightness of colours adjusted equally in each image (green = 2.0, red(NCOR2) = 1.0, red(AMPK) = 2.0, blue = 1.0) in CellProfiler. Images representative of A&B) 1 biological replicate (rep), 17 images (im); C&D) 1 rep, 15 im; E&F) 1 rep, 17 im; G&H) 1 rep, 8 im; I&J) 1 rep, 8 im; K&L) 1 rep, 6 im. Scale bars = 20 µm.

## 5.3.2: Proximity ligation assays for BCL6 with NCOR2 and AMPK

### 5.3.2.1: Verification of the proximity ligation assay technique

The immunofluorescence experiments indicated that the location of NCOR2 and AMPK overlapped with the location of BCL6 at the edge of the nucleus, suggesting that it would be possible for them to associate. PLAs were chosen to verify these associations as signal is only seen in PLAs if the two target proteins are closely associated (within 40 nm), making it a high resolution technique.[338] This chapter describes PLA experiments investigating the co-localisation of BCL6 with NCOR2 and AMPK. These experiments aimed to determine the feasibility of PLA assays for the validation of RIME results and to obtain some initial data.

To account for biological and technical variation, the experimental and negative control staining was repeated in at least two biological replicates and several images were acquired from each sample at different points on the slide. These points were reasonably distant from each other but were selected because the field of view contained cells. The level of PLA signal was not checked before image acquisition, making the image selection relatively non-biased.

First, the PLA technique was verified in LN18 cells by staining for two proteins known to interact: NFκB subunits p65 and p50. As negative controls, each specific antibody was paired with the appropriate non-specific IgG control to ensure that the co-localisation seen was specific. Bright co-localisation signal was observed in the cytoplasm of LN18 cells stained for p65 and p50 (Figure 5.6A). In contrast, a small amount of non-specific signal was seen scattered across the LN18 cells stained for p65 with a non-specific mouse IgG antibody and p50 with a non-specific rabbit IgG antibody (Figure 5.6B and C). This demonstrated that the PLA technique could identify known interactions and that a positive result was easily differentiable from the control.

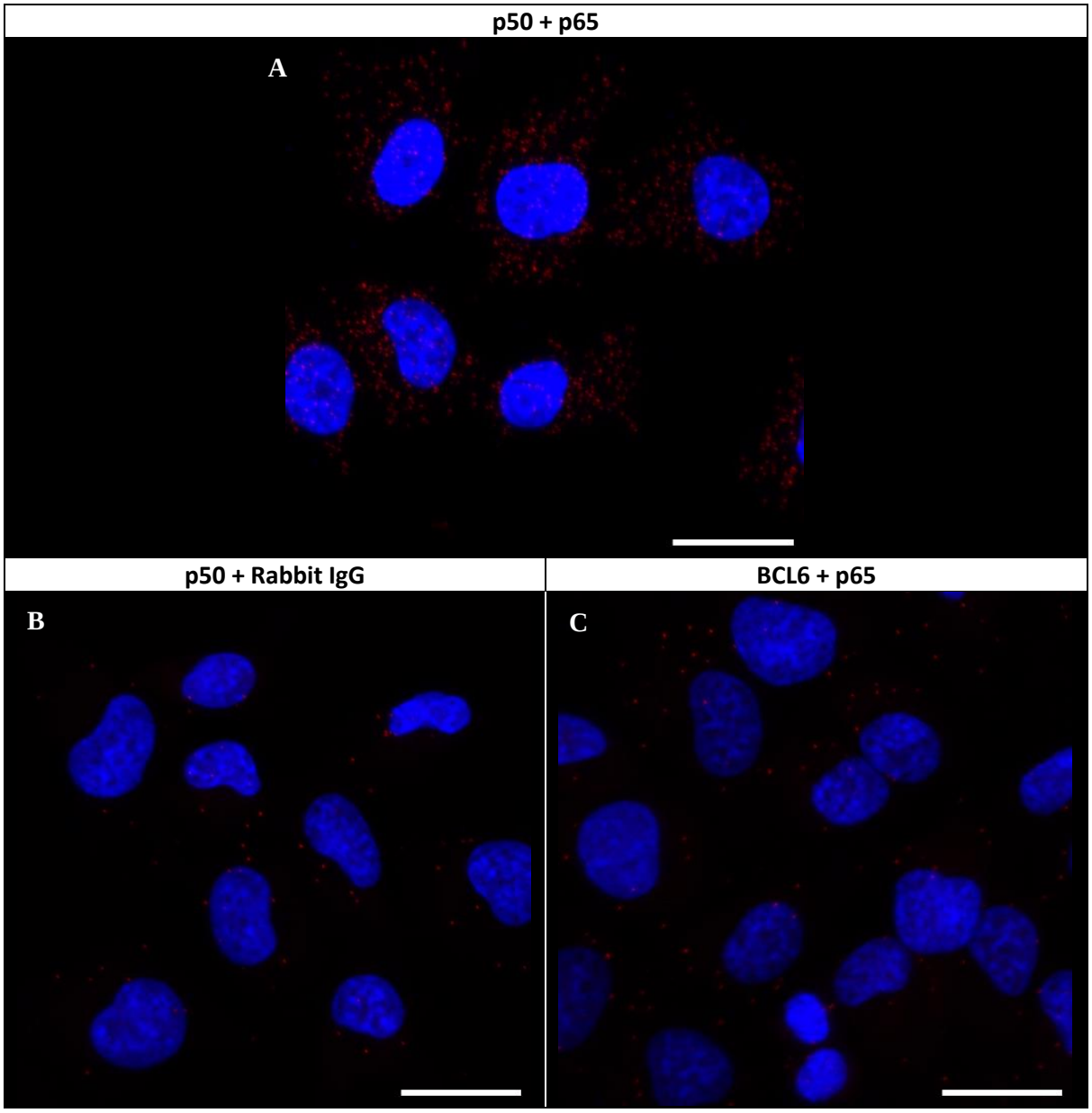


Figure 5.6: NFκB positive control for PLAs

PLA assays for A) NFκB subunits p50 and p65, B) p50 and non-specific rabbit IgG and C) p65 and non-specific mouse IgG. Co-localisation is shown in red and DAPI staining for nuclei is shown in blue. Z-stack images (10 slices) taken using 40x objective with 3.73x digital zoom. Z-projection was performed in Fiji (ImageJ). Scale bars = 20 µm.

A numerical measure of signal compared to background was generated. Two methods were compared: 1) the ratio of red to blue pixels in each image and 2) the ratio of red pixels to the number of nuclei in each image. The two methods were found to produce comparable results (Figure 5.7A and B), so the ratio of red to blue pixels was used for the rest of this chapter. The signal in the NFκB positive control images was much greater than the background signal, indicating that the co-localisation signal was specific (Figure 5.7).

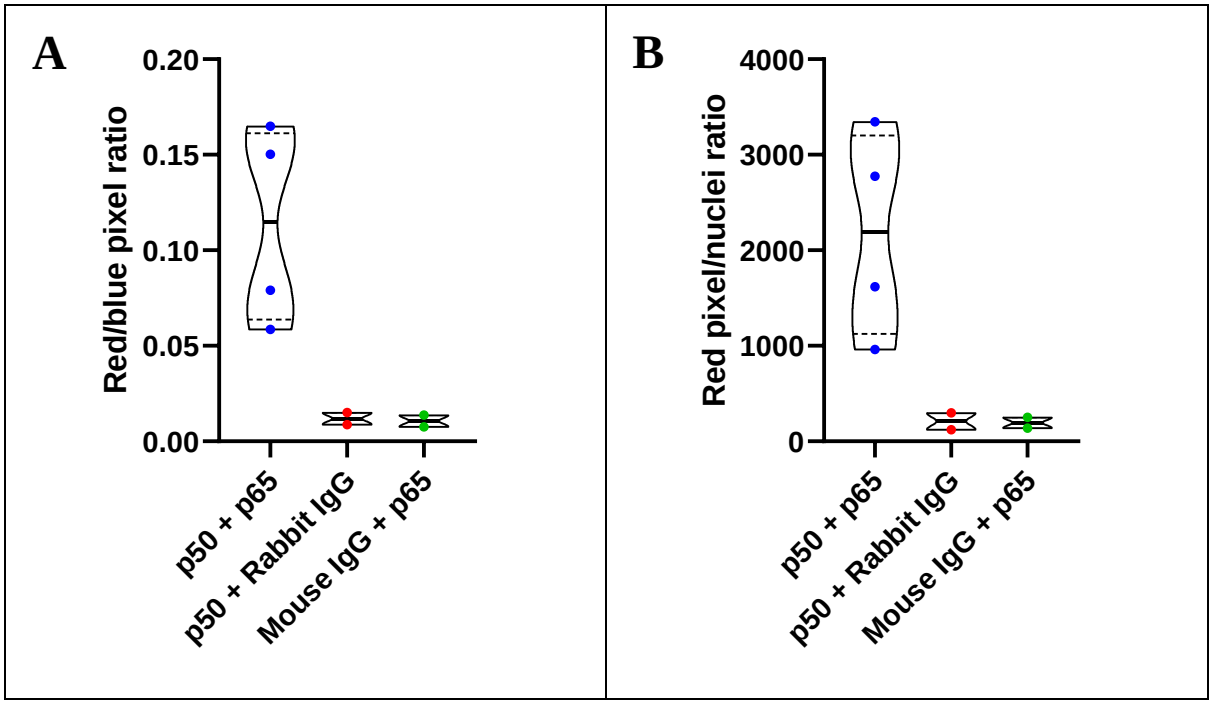


Figure 5.7: Co-localisation signal in NFκB positive control compared to negative controls

A) Violin plots comparing the ratio of red to blue pixels and B) Violin plots comparing the ratio of red pixels to number of nuclei in the following samples: p50 + p65 (blue, 1 biological replicate (rep), 4 images (im)), p50 + Rabbit IgG (red, 1 rep, 2 im) and Mouse IgG + p65 (green, 1 rep, 2 im). Solid line = median, dashed lines = quartiles.

### 5.3.2.2 Establishment of controls for proximity ligation assays

The same negative controls used for the immunofluorescence co-localisation staining were used for the PLA assays. As BCL6 is a low abundance protein and it is likely that only a fraction of it associates with NCOR2 or AMPK, the amplification time was doubled for the BCL6 PLAs. This enabled better differentiation between the experimental and control samples, however it resulted in non-specific signal in many control images.

Figure 5.8 shows that the level of non-specific signal ranged from bright to non-detectable in different areas of the slide for each replicate experiment. Figure 5.9 shows that the median ratio of red to blue pixels for every group of controls in LN18 cells was below 0.02. This was similar to the negative controls for the NFκB PLA (Figure 5.7). The lower quartile of every control had low variability, indicating that half of the images had consistently low signal. However, the spread of the upper quartiles of most of the controls was much higher, suggesting a high level of variability. Overall, this suggested that the signal in the controls was generally low, however a few images had unusually high signal.

These images were distributed throughout the replicates, suggesting that they were not caused by a difference in the processing of a single replicate.

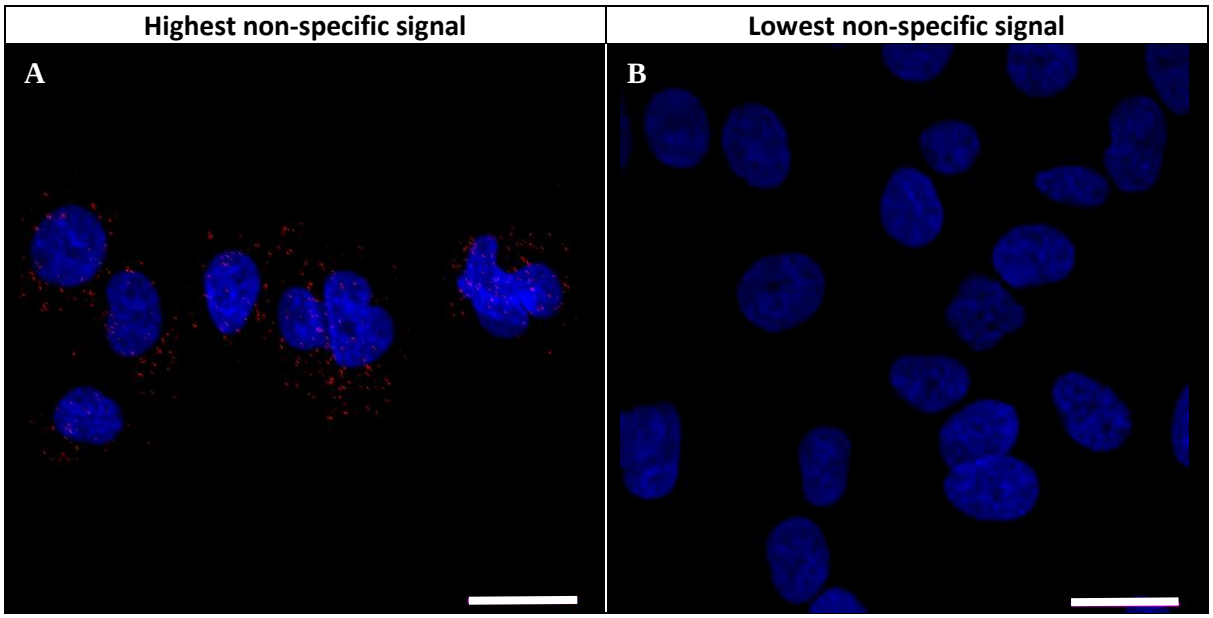


Figure 5.8: Range of signal in PLA assay negative controls

Highest and lowest non-specific signal seen in two images from biological replicate 2 of untreated LN18 cells stained with Mouse IgG (at the concentration of the BCL6 antibody used) and AMPK antibodies. These images had the highest and lowest amounts of non-specific signal seen in any of the LN18 control replicates (biological replicates 3, images 67). Co-localisation is shown in red and DAPI staining for nuclei is shown in blue. Z-stack images (10 slices) taken using 30x objective with 2x digital zoom and further zoomed in 2x using Fiji (ImageJ). Z-projection was performed in Fiji (ImageJ). Relative brightness of colours adjusted in CellProfiler (red =4.0, blue = 1.0). Scale bars = 20 µm.

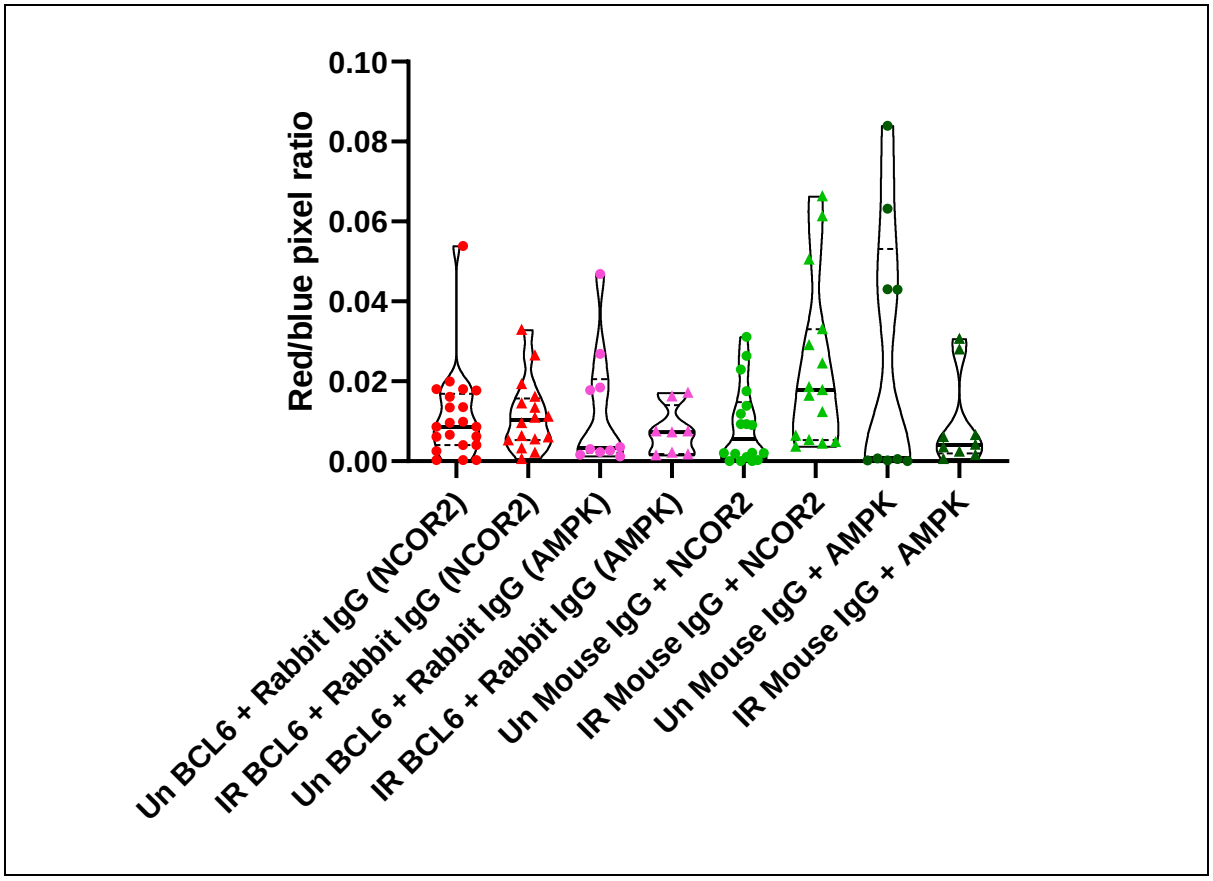


Figure 5.9: Ratio of red to blue pixels in negative controls

Violin plots comparing the ratio of red to blue pixels in the untreated (circles) and irradiated (triangles) control samples in LN18 cells. Untreated BCL6 + Rabbit IgG (NCOR2) (red, biological replicates (rep) 3, images (im) 21); ); Irradiated BCL6 + Rabbit IgG (NCOR2) (red, rep 4, im 16); Untreated BCL6 + Rabbit IgG(AMPK) (pink, rep 2, im 10); Irradiated BCL6 + Rabbit IgG(AMPK) (pink, rep 3, im 8); Untreated Mouse IgG + NCOR2 (light green, rep 4, im 16); Irradiated Mouse IgG + NCOR2 (light green, rep 4, im 15); Untreated Mouse IgG + AMPK (dark green, rep 2, im 9); Irradiated Mouse IgG + AMPK (dark green, rep 3, im 9). Solid line = median, dashed lines = quartiles.

### 5.3.2.3: Proximity ligation assays for BCL6 and NCOR2 in untreated and irradiated GBM cells

PLAs were carried out using the BCL6 and NCOR2 antibodies together to assess the association of these proteins. Figure 5.10 displays the spread of the BCL6 + NCOR2 signal compared to the negative controls in untreated and irradiated LN18, NZG0906 and NZG1003 cells. Statistical comparisons were made using a linear mixed model with antibody pairs and treatment as fixed effects, replicates as a random effect and images within replicates as repeated measurements with compound symmetry. Pairwise comparisons between antibody pairs and between treatments were made using sequential Bonferroni multiple comparisons adjustment.

In the untreated LN18 and NZG0906 cells, the PLA signal was significantly higher ($p \leq 0.05$) in the BCL6 + NCOR2 samples compared to the corresponding negative controls. A similar trend was seen in the NZG1003 cells, although the difference between the BCL6 + NCOR2 and negative control signal was not statistically significant ($p \geq 0.05$). Overall, this supports the RIME results and indicates that BCL6 associates with its known corepressor NCOR2 in GBM cells.

Contrastingly, the BCL6 + NCOR2 signal was not significantly different to the negative control signal in any of the irradiated GBM cell lines. However, the BCL6 + NCOR2 signal was only significantly decreased by irradiation in the NZG0906 cell line ($p \leq 0.01$). Therefore, the PLA results provide tentative but inconclusive support for the loss of BCL6 association with NCOR2 in response to irradiation which was suggested by the RIME results.

In the untreated GBM cell lines, there was some BCL6 and NCOR2 co-localisation in the nuclei, as expected for a transcription factor complex, however most of the signal was cytoplasmic (Figure 5.11). This corresponded with the immunofluorescence staining in Figure 5.2, which showed that while BCL6 was concentrated around the periphery of the nucleus, some localised to the cytoplasm and the nuclear lumen. However, the location of the PLA staining differed from the immunofluorescence staining in Figure 5.3, which showed apparently exclusive localisation of NCOR2 to the nucleus. As the PLA method only identified BCL6 and NCOR2 when they were closely associated, it is possible that the strong nuclear staining for NCOR2 in the immunofluorescence experiments prevented detection of the smaller amounts of NCOR2 in the cytoplasm.

**A**

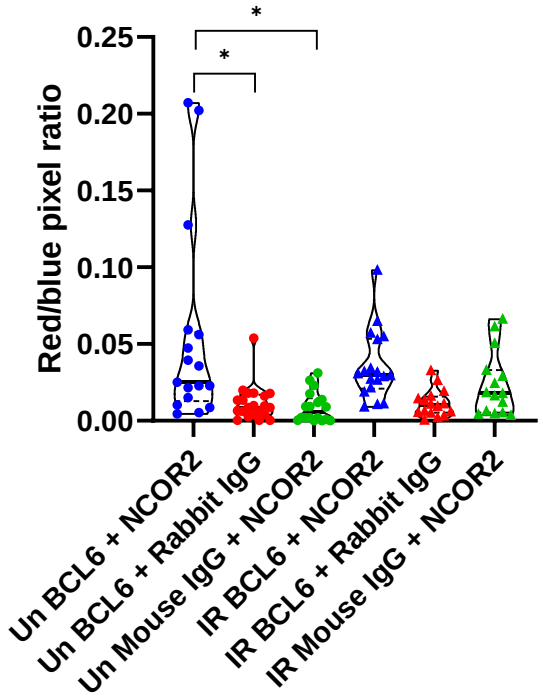
*
*
0.25
0.20
0.15
0.10
0.05
0.00
Red/blue pixel ratio
Un BCL6 + NCOR2
Un BCL6 + Rabbit IgG
Un Mouse IgG + NCOR2
IR BCL6 + NCOR2
IR BCL6 + Rabbit IgG
IR Mouse IgG + NCOR2

**B**

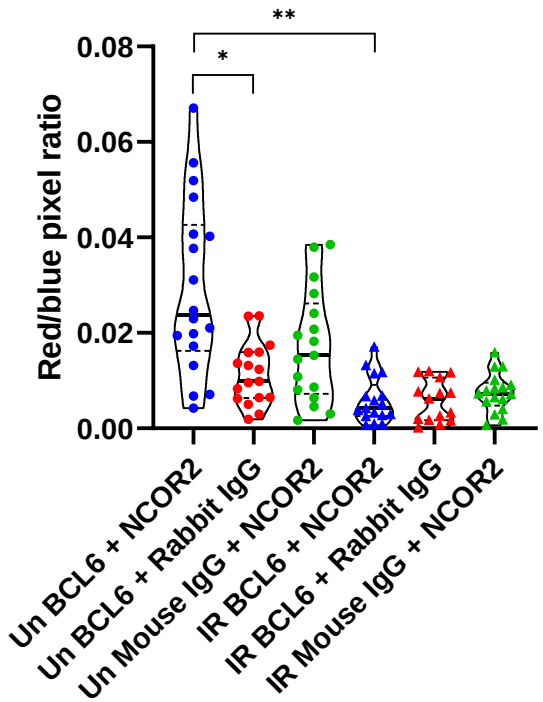
**
*
0.08
0.06
0.04
0.02
0.00
Red/blue pixel ratio
Un BCL6 + NCOR2
Un BCL6 + Rabbit IgG
Un Mouse IgG + NCOR2
IR BCL6 + NCOR2
IR BCL6 + Rabbit IgG
IR Mouse IgG + NCOR2

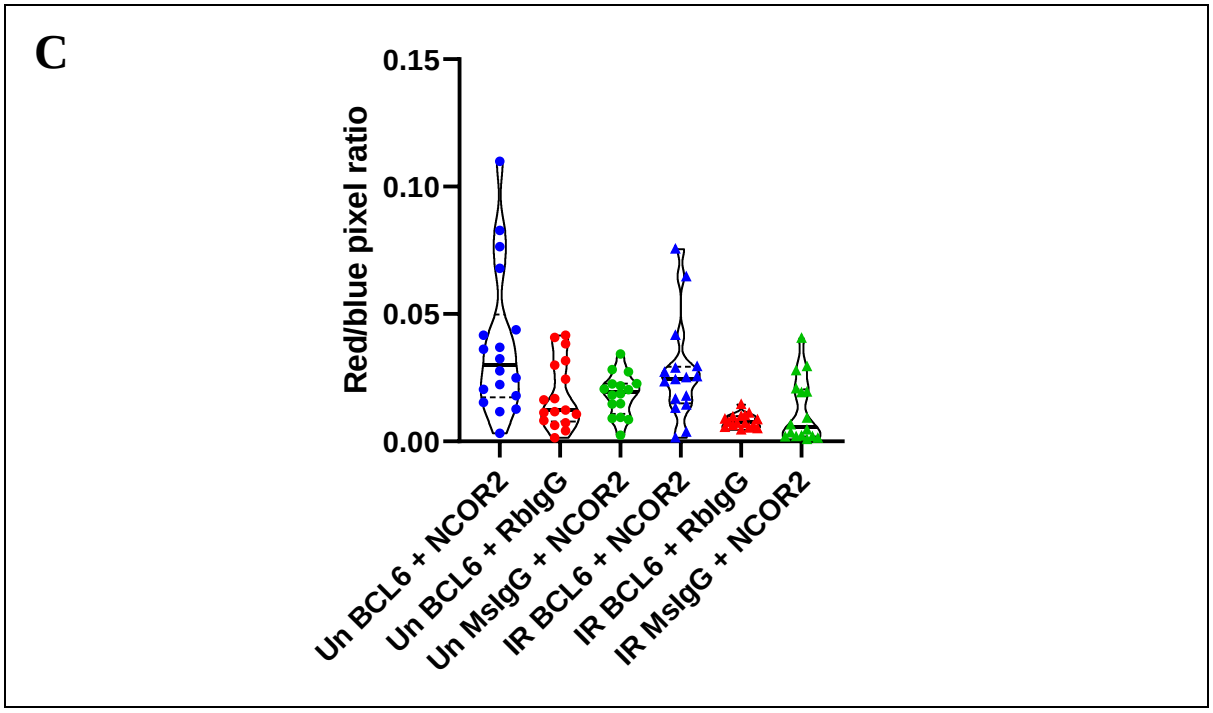


Figure 5.10: Ratio of red to blue pixels in BCL6 + NCOR2 PLAs in untreated and irradiated GBM cells compared to controls

Violin plots comparing the ratio of red to blue pixels in experimental BCL6 + NCOR2 (blue) and control BCL6 + Rabbit IgG (red) and Mouse IgG + NCOR2 (green) samples in untreated (circles) and irradiated (triangles) A) LN18 cells, B) NZG0906 cells and C) NZG1003 cells. A) Untreated BCL6 + NCOR2 (biological replicates (rep) 4, images (im) 17); Untreated BCL6 + Rabbit IgG (rep 4, im 21); Untreated Mouse IgG + NCOR2 (rep 4, im 18); Irradiated BCL6 + NCOR2 (rep 4, im 18); Irradiated BCL6 + Rabbit IgG (rep 4, im 16); Irradiated Mouse IgG + NCOR2 (rep 4, im 15). B) Untreated BCL6 + NCOR2 (biological replicates (rep) 3, images (im) 18); Untreated BCL6 + Rabbit IgG (rep 3, im 17); Untreated Mouse IgG + NCOR2 (rep 3, im 17); Irradiated BCL6 + NCOR2 (rep 3, im 17); Irradiated BCL6 + Rabbit IgG (rep 3, im 15); Irradiated Mouse IgG + NCOR2 (rep 3, im 17). C) Untreated BCL6 + NCOR2 (biological replicates (rep) 3, images (im) 18); Untreated BCL6 + Rabbit IgG (rep 3, im 17); Untreated Mouse IgG + NCOR2 (rep 3, im 16); Irradiated BCL6 + NCOR2 (rep 3, im 16); Irradiated BCL6 + Rabbit IgG (rep 3, im 16); Irradiated Mouse IgG + NCOR2 (rep 3, im 16). Solid line = median, dashed lines = quartiles. Statistical comparisons made as described in the text above. * = $p \leq 0.05$, ** = $p \leq 0.01$.

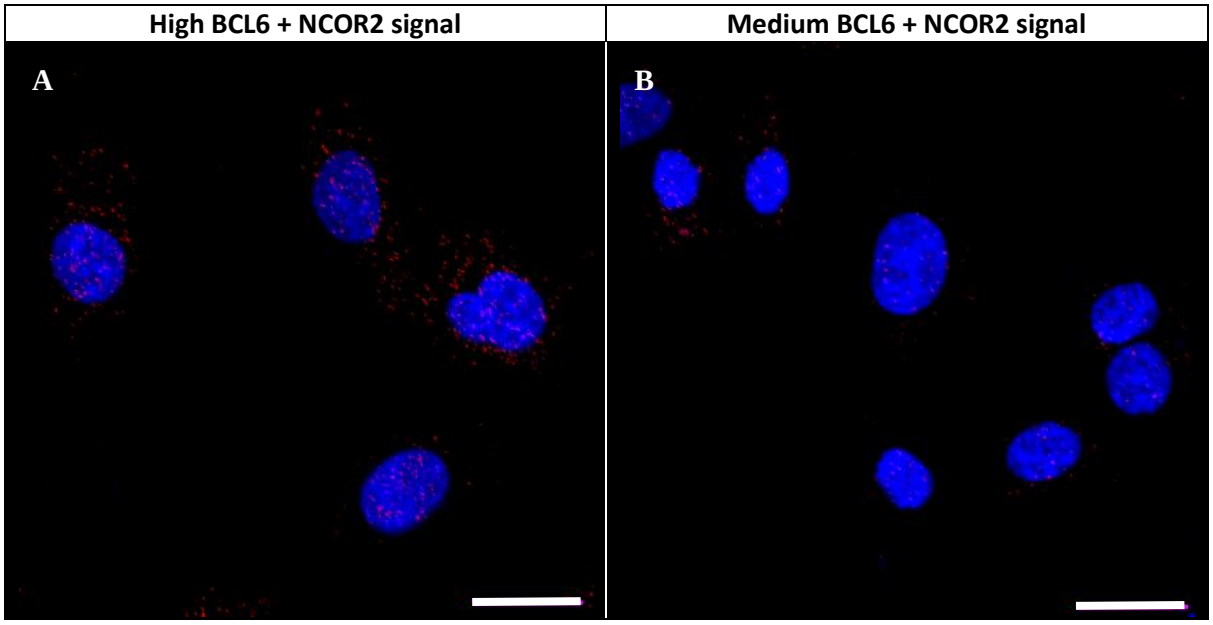


Figure 5.11: Location of BCL6 + NCOR2 signal in untreated LN18 cells

Images representative of a high (A) and medium (B) level of BCL6 + NCOR2 PLA staining are shown (biological replicates 3, images 11). Co-localisation is shown in red and DAPI staining for nuclei is shown in blue. Z-stack images (10 slices) taken using 30x objective with 2x digital zoom and further zoomed in 2x using Fiji (ImageJ). Z-projection was performed in Fiji (ImageJ). Relative brightness of colours adjusted in CellProfiler (red =4.0, blue = 1.0). Scale bars = 20 µm.

### 5.3.2.4: Proximity ligation assay for BCL6 and AMPK in untreated and irradiated LN18 GBM cells

PLAs for BCL6 with AMPK were also carried out in untreated and irradiated LN18 cells. Statistical comparisons were carried out as described for the BCL6 + NCOR2 data in section 5.3.2.3. The median red to blue pixel ratio in the BCL6 + AMPK PLAs was higher than the controls, however this difference was not statistically significant ($p \geq 0.05$) (Figure 5.12). This is likely because although the lowest amount of signal in the BCL6 + AMPK samples (red/blue pixel ratio = 9.3E-4) was higher than > 50% of the Mouse IgG + AMPK images (red/blue pixel ratio = 4.5E-6 to 7.1E-4), the upper quartile of the Mouse IgG + AMPK data had a large spread and overlapped with the BCL6 + AMPK data. Therefore, the signal in the BCL6 + AMPK images could not be confidently distinguished from the signal in the controls.

Contrastingly, there was a clearer although not statistically significant ($p \geq 0.05$) trend towards higher signal in the BCL6 + AMPK PLAs in irradiated LN18 cells compared to in the controls (**Error! Reference source not found.**3). As in the untreated cells, the upper quartile of the BCL6 + AMPK PLAs in irradiated cells had a large spread, indicating variability in the data. However, the signal in the controls was consistently low and there was very little overlap between the interquartile range of the BCL6 + AMPK PLA data and those of the controls. This provides tentative support for the association between BCL6 and AMPK in GBM cells suggested by RIME but will need to be confirmed in the other GBM cell lines.

There was no statistically significant difference ($p \geq 0.05$) between the BCL6 + AMPK PLA signal in the untreated and irradiated LN18 cells. This also supported the RIME results, which showed no quantitative difference in BCL6 association with AMPK between untreated and irradiated LN18 cells. However, due to the high level of signal in some of the untreated control images, the association between BCL6 and AMPK could not be confidently verified in this preliminary study.

The co-localisation of BCL6 and AMPK seen in irradiated LN18 cells appeared to be both nuclear and cytoplasmic (Figure 5.133). Although immunofluorescence staining showed that AMPK became predominantly nuclear after IR and BCL6 was concentrated around the periphery of the nucleus, there was also staining for both in the cytoplasm, in agreement with the PLA data (Figure 5.5).

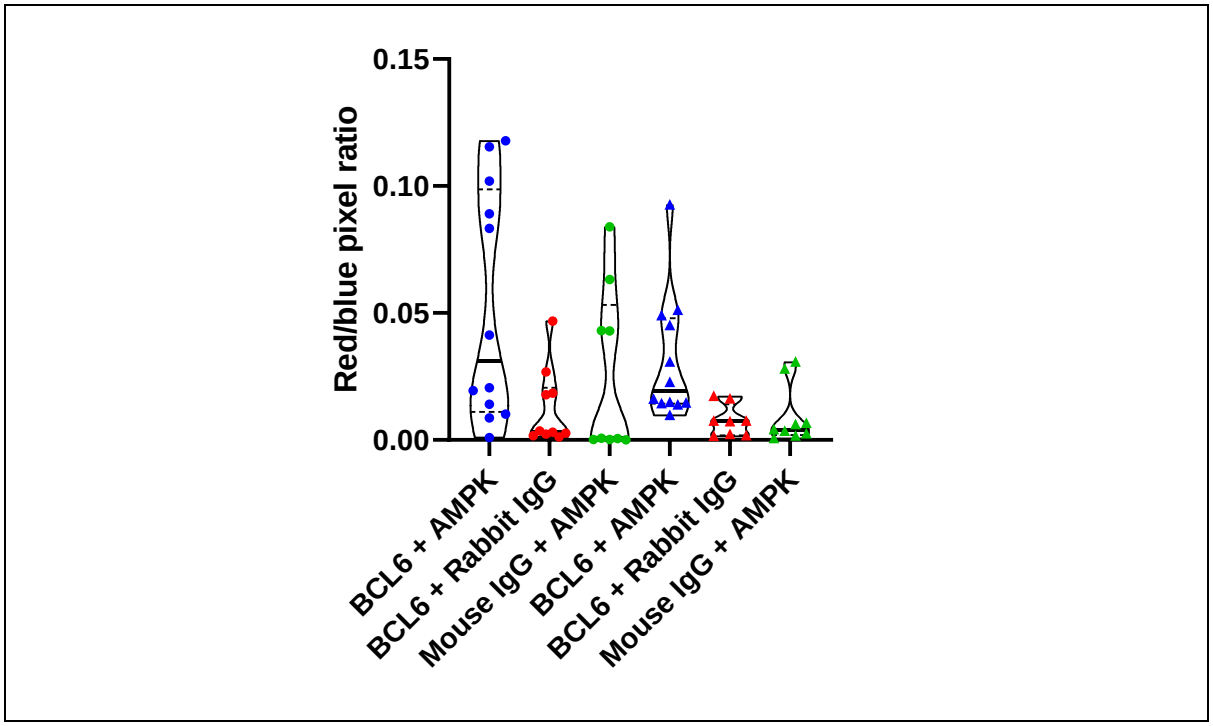


Figure 5.12: Ratio of red to blue pixels in BCL6 + AMPK PLAs in untreated LN18 GBM cells compared to controls

Violin plots comparing the ratio of red to blue pixels in experimental BCL6 + AMPK (blue) and control BCL6 + Rabbit IgG (red) and Mouse IgG + AMPK (green) samples in untreated (circles) and irradiated (triangles) LN18 cells. Untreated BCL6 + AMPK (biological replicates (rep) 3, images (im) 12); Untreated BCL6 + Rabbit IgG (rep 2, im 10); Untreated Mouse IgG + NCOR2 (rep 2, im 9). Solid line = median, dashed lines = quartiles. Statistical comparisons made as described in the text above (not shown as there were no statistically significant differences).

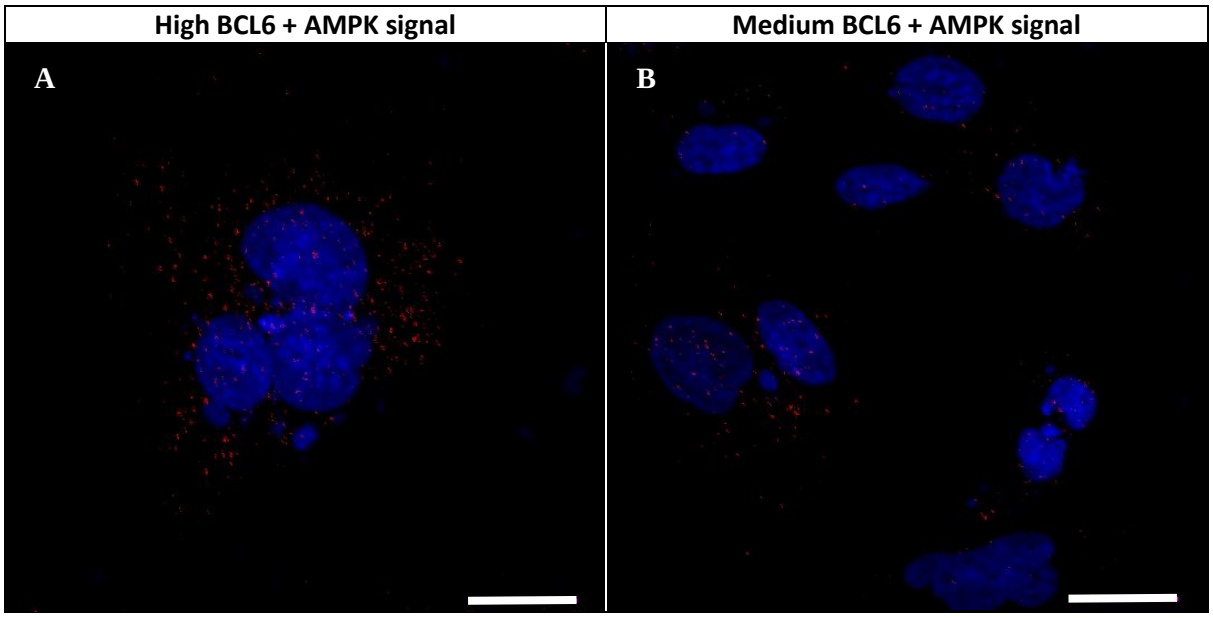


Figure 5.13: Location of BCL6 + AMPK signal in irradiated LN18 cells

Images representative of a high (A) and medium (B) level of BCL6 + AMPK PLA staining are shown (biological replicates 3, images 12). Co-localisation is shown in red and DAPI staining for nuclei is shown in blue. Z-stack images (10 slices) taken using 30x objective with 2x digital zoom and further zoomed in 2x using Fiji (ImageJ). Z-projection was performed in Fiji (ImageJ). Relative brightness of colours adjusted in CellProfiler (red =4.0, blue = 1.0). Scale bars = 20 µm.

## 5.4: Discussion

### 5.4.1: Advantages and limitations of immunofluorescence staining

The RIME results indicated that BCL6 associated with very different sets of proteins in untreated and irradiated GBM cells. Furthermore, RIME suggested that BCL6 may leave the nucleus in response to acute IR and associate with plasma membrane proteins. However, these inferences were based on the assumption that the proteins BCL6 associated with were in their usual subcellular compartment. Immunofluorescence staining was used to visualise the location of BCL6 within untreated and irradiated LN18 GBM cells.

Surprisingly, BCL6 staining was concentrated around the periphery of the nucleus in both untreated and irradiated LN18 GBM cells, with no visible change in localisation. This appeared to contradict the RIME results. Additionally, the level of BCL6 staining decreased after acute IR, contradicting western blot results showing that BCL6 protein expression was robustly upregulated 48 hours after acute IR (Chapter 3).[207] This suggested that not all of the BCL6 protein was detected by immunofluorescence staining in the irradiated LN18 cells or alternatively that irradiation somehow increased the extraction of BCL6 from LN18 cells for western blotting without a change in BCL6 abundance. It is possible that the altered location or protein associations of BCL6 in the irradiated cells prevented the monoclonal BCL6 antibody used for immunofluorescence from binding to its epitope at the BCL6 N-terminus. Therefore, the staining of BCL6 around the periphery of the nucleus may show the BCL6 that did not alter its function after acute IR, whereas the BCL6 associated with plasma membrane proteins may not have been detected.

BCL6 has various distributions in the nucleus and cytoplasm in different cell types.[207,316,559–561] Even in different GBM cell lines, BCL6 may be predominantly nuclear or cytoplasmic or present in both.[207] The distribution of overexpressed BCL6 has been shown to change over the cell cycle in an osteosarcoma cell line, with a diffuse nuclear distribution during G1 phase and localisation to replication foci during S phase.[561] The untreated LN18 cells in this chapter were likely in a range of phases of the cell cycle, while Chapter 3 and previous research indicated that at least a portion of the irradiated LN18 cells were arrested at G2/M.[88,89,425,426] However, no change in the localisation of BCL6 was observed in response to acute IR. The localisation of endogenous BCL6 (lung cancer cells) and overexpressed BCL6 (muscle, fibroblast and embryonic kidney cells) to membrane-less subnuclear organelles known as nuclear

bodies has also been associated with corepressor recruitment.[215,218,290,562,563] No punctate nuclear staining for BCL6 was observed in LN18 cells, however it is possible that the low abundance of BCL6 prevented clear resolution of its nuclear distribution.

RIME indicated that BCL6 associated with NCOR2 and AMPK in GBM cells, as these proteins were consistently pulled down with the BCL6 antibody. The subcellular localisation of NCOR2 and AMPK was established by immunofluorescence in LN18 GBM cells, allowing comparison to the location of BCL6. Both proteins had the potential to colocalise with BCL6, as their location overlapped with BCL6 at the periphery of and within the nucleus, and BCL6 and AMPK both had some cytoplasmic staining.

NCOR2 was distributed throughout the nucleus of LN18 cells, as has been observed in other cell types.[559,564–566] Like BCL6, overexpressed NCOR2 has been shown to localise to bright speckles within the nucleus in muscle and kidney cell lines and studies have demonstrated the co-localisation of overexpressed BCL6 and NCOR2 in nuclear bodies.[215,218,290,565] There were brighter and dimmer patches of NCOR2 staining in the nuclei of LN18 cells, however there were no punctate structures visible.

AMPK staining was distributed throughout the nucleus and cytoplasm of untreated LN18 cells, corresponding with its wide range of targets in different subcellular compartments.[567] After IR, AMPK became predominantly nuclear and was concentrated in bright speckles. Punctate nuclear staining of AMPK has been observed in several cell types and is induced by IR in lung cancer cells.[512,568,569] AMPK has also been shown to localise to the nucleus in cells in G2 arrest and to be important in the DNA damage response.[512–514] Therefore, it is likely that AMPK preferentially localises to the nucleus in irradiated LN18 cells to participate in G2 arrest and DNA repair processes.

## 5.4.2: Advantages and limitations of PLAs

PLAs were ideal for validation of the BCL6 RIME results for several reasons. This thesis aimed to study the activity of endogenous BCL6 protein in GBM cells, as previous work had indicated that BCL6 transfected into GBM cells did not behave the same as endogenous BCL6 induced by therapy.[207] In contrast to other methods such as FRET, PLAs allow the detection of association between endogenous, unmodified proteins.[338] Additionally, BCL6 is a very low abundance protein. Therefore, it was expected that the detection of its association with particular proteins would be even more infrequent than detection of the BCL6 protein itself. The amplification step in the PLA protocol meant that even a low amount of signal would be amplified. PLAs also removed the problem of the widespread localisation of NCOR2 and AMPK, as they would only be detected if they were within 40 nm of BCL6. While proteins at this distance were not guaranteed to be interacting, they were certainly in very close proxmity.[570]

PLAs successfully detected the interaction of NFκB subunits p50 and p65. However, the variability of the PLA signal and the low abundance of BCL6 made its association with NCOR2 and AMPK more difficult to distinguish from the non-specific signal in the controls. Nevertheless, the PLA experiments provided some initial validation of the RIME results.

NCOR2 was at low abundance in the RIME data and may have fluctuated above and below the threshold of detection of the mass spectrometer. However, the co-localisation signal of BCL6 and NCOR2 in the untreated LN18 and NZG0906 cells was significantly higher than the non-specific signal in the controls. This supported the finding that BCL6 retains its known association with NCOR2 in GBM cells. Contrastingly, in the irradiated GBM cells, the co-localisation signal of BCL6 and NCOR2 was not significantly higher than the signal in the controls. This suggested that the acute IR-induced decrease in the association of BCL6 with NCOR2 indicated by RIME may be genuine. However, there was only a statistically significant decrease in BCL6 + NCOR2 PLA signal in irradiated NZG0906 cells compared to untreated NZG0906 cells so further work is required to confirm this.

Although the co-localisation of BCL6 and NCOR2 in untreated LN18 cells was supported by this validation study, the location of this association was surprising. Previous literature has shown that BCL6 and NCOR2 colocalise in nuclear bodies.[215,218,290] While there was some BCL6 and NCOR2 association detected in the nuclei of LN18 cells, the majority of the signal was cytoplasmic. As the signal in the negative controls had a similar distribution, this could indicate that the BCL6 + NCOR2 signal was non-specific. However, as experimental samples had robustly higher signal intensity, this seemed unlikely. The studies identifying BCL6 and NCOR2 co-localisation in nuclear bodies overexpressed BCL6 and therefore its localisation may not have been representative of endogenous BCL6.[215,218,290] It is possible that most BCL6-NCOR2 complexes are sequestered in the cytoplasm and imported into the nucleus when their transcriptional activity is required. Indeed, NCOR2 is known to be regulated in this way by MAPK, NFκB and CD40 pathway signalling and by ubiquitination.[254,565,571–574] While this has generally been shown to remove NCOR2 from its nuclear transcription factor partners, it is possible that BCL6 could be exported from the nucleus along with NCOR2.

The association of BCL6 with AMPK could not be confidently validated in untreated LN18 cells with the preliminary data generated in this chapter. However, the BCL6 + AMPK co-localisation signal in irradiated LN18 cells was generally higher than in the controls, although this was not statistically significant. This provided some tentative support for the association of BCL6 with AMPK. The association of BCL6 with AMPK was both nuclear and cytoplasmic. Although AMPK was predominantly nuclear after IR, some remained in the cytoplasm. It is possible that phosphorylation of the BCL6-NCOR2 complex by AMPK contributes to its nuclear-cytoplasmic shuttling, as has been observed in the regulation of NCOR2 by other kinases.[254,565,571–573] The level of co-localisation signal for BCL6 and AMPK did not differ between untreated and irradiated GBM cells, further supporting the

detection of this association in both conditions by RIME. However, the high non-specific signal in some untreated controls confounded any confident conclusions about this intriguing interaction.

It is possible that the failure to confidently validate the BCL6-AMPK interaction could be due to the use of an anti-AMPK-γ1 antibody. RIME identified BCL6 association with the α1 and γ1 subunits of AMPK. The γ1 subunit was identified in more replicates and so was chosen for validation. However, if AMPK phosphorylates BCL6, it is likely to be the catalytic α1 subunit that interacts with BCL6.[93] Therefore, while crosslinking allowed identification of the γ1 subunit by RIME, the γ1 subunit may be too far away from BCL6 for consistent detection by PLAs. Repetition of the PLAs for BCL6 and AMPK with an anti-AMPK-α1 antibody may enable validation of this interaction.

### 5.4.3: Use of antibodies

Like RIME, immunofluorescence staining and PLAs both relied on antibodies. A polyclonal BCL6 antibody was used for RIME while a different, monoclonal BCL6 antibody was used for the PLA experiments. The association between BCL6 and NCOR2 in untreated LN18 cells was detected by both experiments. As this was seen with two very different techniques using different BCL6 antibodies, the confidence in this association is high.

Antibodies are valuable biological tools as they enable targeting of proteins of interest. However, if antibodies are not specific for their target, confounding results are generated. Therefore, the use of controls to assess non-specific binding was critical for this chapter. The specificity of each antibody was assessed by comparing the staining in untreated LN18 cells to two negative controls. Comparison to staining with a non-specific IgG antibody of the same species as the experimental antibody detected non-specific binding. Efforts were made to optimise the antibody concentrations and acquisition settings so that there was no signal in the control but detectable signal in the experimental samples. This was successful for the NCOR2 antibody. However, the low abundance of BCL6 meant that a high concentration of anti-BCL6 antibody had to be used to detect it. At this concentration, there was non-specific signal in the IgG controls. A similar problem was encountered in the IgG controls for AMPK due to the need to brighten the images to visualise the AMPK signal. However, there was a marked difference in the appearance of the staining with the non-specific compared to experimental antibodies. This suggested that the staining in the experimental samples was specific for BCL6 and AMPK, although it was necessary take some caution with interpretation.

To confirm that the antibodies were specific for the expected proteins, the ideal negative control would have been matched knockout cell lines. This would have allowed examination of the difference in staining when the protein of interest was and was not expressed. However, it was not possible to generate a knockout model for BCL6 in GBM cells as this renders GBM cells non-viable.[207]

Furthermore, due to limited time and resources, knockout or knockdown controls were not feasible. Therefore, cell lines known to have low expression of the proteins of interest were compared to the LN18 cells to examine the difference in staining. These cell lines were selected based on their low mRNA expression shown in the Human Protein Atlas, experiments carried out in the McConnell lab and their use as negative controls in the literature. The lack or lower amount of staining in these negative controls compared to in untreated LN18 cells increased the confidence that the BCL6, NCOR2 and AMPK antibodies were binding to their target proteins.

The antibodies already verified and optimised for immunofluorescence staining were used for the PLA experiments. IgG controls were also performed for these experiments. The high level of signal in some IgG controls meant that the signal in the irradiated BCL6 + NCOR2 samples and the untreated BCL6 + AMPK samples could not be distinguished from the controls. Due to the low concentration of BCL6, a longer amplification time than in the standard protocol was used. This is known to increase background signal. Additionally, there was substantial variability in the level of signal between images within both the experimental and control replicates. Further optimisation of this protocol could improve the difference between signal and background to enable more confident assessment of the association of BCL6 with NCOR2 and AMPK.

### 5.4.4: Future directions

RIME indicated that BCL6 in GBM cells has both known and novel associations with other proteins. It was encouraging that the known BCL6 corepressor NCOR2 was identified as a BCL6-associated protein by RIME. The preliminary PLA validation experiments in this chapter found support for the association of BCL6 with NCOR2 in untreated LN18 cells. This suggests that BCL6 may have transcriptional repressor activity in untreated GBM cells. Combined with the BCL6-mediated repression of the DNA damage response to fractionated IR observed in Chapter 3, this indicates that in untreated and fractionated IR-treated GBM cells, BCL6 retains at least some of its canonical functions known from GC B cells and lymphoma. The cytoplasmic location of much of the BCL6-NCOR2 co-localisation suggested that the transcriptional activity of this complex may be regulated by cytoplasmic sequestration. While it is known that NCOR2 is regulated in this way, the finding that BCL6 may be exported from the nucleus with NCOR2 warrants further investigation.

Previous evidence and results from Chapters 3 and 4 indicated that the function of BCL6 changes in response to acute IR. RIME suggested that in response to acute IR, BCL6 reduces its association with transcriptional regulators including NCOR2. Unlike in untreated LN18 and NZG0906 cells, the BCL6 + NCOR2 PLA signal in irradiated GBM cells was not significantly higher than the non-specific signal in the controls. Furthermore, there was a statistically significant decrease in BCL6 + NCOR2 PLA

signal in irradiated NZG0906 cells compared to in untreated NZG0906 cells. This provided further support for the loss of BCL6 transcriptional activity in response to acute IR.

RIME identified the association of BCL6 with AMPK in GBM cell lines and in the Raji lymphoma cell line. This novel association has interesting implications for the role of BCL6 in the metabolic stress response. The association of BCL6 with the γ subunit of AMPK was investigated with preliminary PLA experiments. There was tentative evidence that BCL6 and AMPK were associated in LN18 cells, however the high non-specific signal in the untreated controls prevented a confident conclusion. The PLAs for BCL6 and AMPK should be repeated with an anti-AMPK-α1 antibody, as BCL6 is more likely to be close to the catalytic α1 subunit. This may produce higher co-localisation signal which could be distinguished from the background.

Future work should further optimise the PLA protocol to reduce non-specific signal. This could be achieved by changing the duration of blocking, washes or the amplification step or by further optimising the antibody concentrations. Additionally, the variability in the signal within replicates could be improved by repeating the PLA assays with a greater volume per well so that all cells were evenly exposed to the reagents. It would also be useful to repeat the PLA experiments on additional GBM cell lines and on patient tissue to ensure that the results are applicable to GBM more generally.

Although the conclusions that could be drawn from these preliminary PLA experiments were somewhat limited, they added to the accumulating evidence that BCL6 has altered activity after acute IR treatment of GBM cells.

# 6: BCL6 transcript variants in untreated and irradiated GBM

## 6.1 Introduction

Chapters 3-5 suggested that in response to acute IR treatment of GBM cells, BCL6 has a different function from its canonical role in GC B cells and from its apparent activity in untreated and fractionated IR-treated GBM. This adds to previous evidence that BCL6 induced by therapy does not behave as a transcriptional repressor and may act as a transcriptional activator in GBM.[207,322] A possible explanation for this change in behaviour is that in response to therapy, BCL6 transcripts are alternatively spliced to produce a variant BCL6 transcript. This could be translated into a BCL6 isoform with a different structure and function. Alternative splicing is known to be important in cancer and over 1000 alternative splicing events have been shown to correlate with prognosis in GBM.[575,576] Therefore, it was hypothesised that BCL6 transcripts are alternatively spliced in GBM cells in response to therapy, resulting in a BCL6 protein isoform which has lost its transcriptional repressor function and perhaps gained other functions.

Four BCL6 transcript variants are annotated in the University of California Santa Cruz (UCSC) Genome Browser.[577] These are all also annotated in the National Centre for Biotechnology Information (NCBI) Gene Tool and Ensembl.[331,578] These three genome browsers also record variations in the length of the 5' and 3' untranslated regions (UTRs). NCBI contains two variations of one of the transcripts annotated to UCSC, which differ only in the length of the 3' UTR. NCBI also annotates another transcript variant not found in the UCSC Genome Browser. Most of the variation between the transcripts occurs in the UTRs. The only difference that affects the protein code is the lack of one exon in some of the transcript variants. Thus, the transcripts in NCBI and UCSC encode two variant proteins: BCL6, which has 706 amino acids encoded by eight translated exons, and BCL6S (short BCL6), which has 650 amino acids encoded by seven translated exons. BCL6S is missing the first two zinc fingers, however these are not required for nuclear localisation or DNA binding and their loss does not seem to alter BCL6 function.[579,580] Additionally, two of the seven partial transcripts annotated by Ensembl are predicted to be protein coding as they contain an open-reading frame.[331] BCL6-205 has 121 amino acids encoded by the two 5' coding exons.[331] BCL6-204 is missing part of the second exon and is 104 amino acids long.[331] These proteins contain only the BTB domain, so they may be able to bind co-repressors but they are unable to bind DNA.[331] Whether they have any function is unknown.

The recent development of long-read sequencing technologies enables the sequencing of whole transcripts.[581] This has enormous advantages over short-read sequencing, in which transcripts are fragmented and sequenced before the reads are assembled to a reference genome.[582] The assembly of transcript sequences from short-reads makes it difficult to identify splice variants, as fragments are assembled against the known reference sequence.[582,583] On the other hand, long-read sequencing enables

the comparison of intact transcripts, meaning that any differences are clear in the sequence.[582,583] One of the major long-read sequencing technologies is offered by Oxford Nanopore Technologies (ONT). ONT MinION sequencing involves application of a constant voltage across a membrane containing nanopores.[582] Each nucleotide sequence is fed through the nanopore one base at a time by a motor protein and the characteristic disruptions to the current caused by each base are used to determine the base sequence (Figure 6.1).[582]

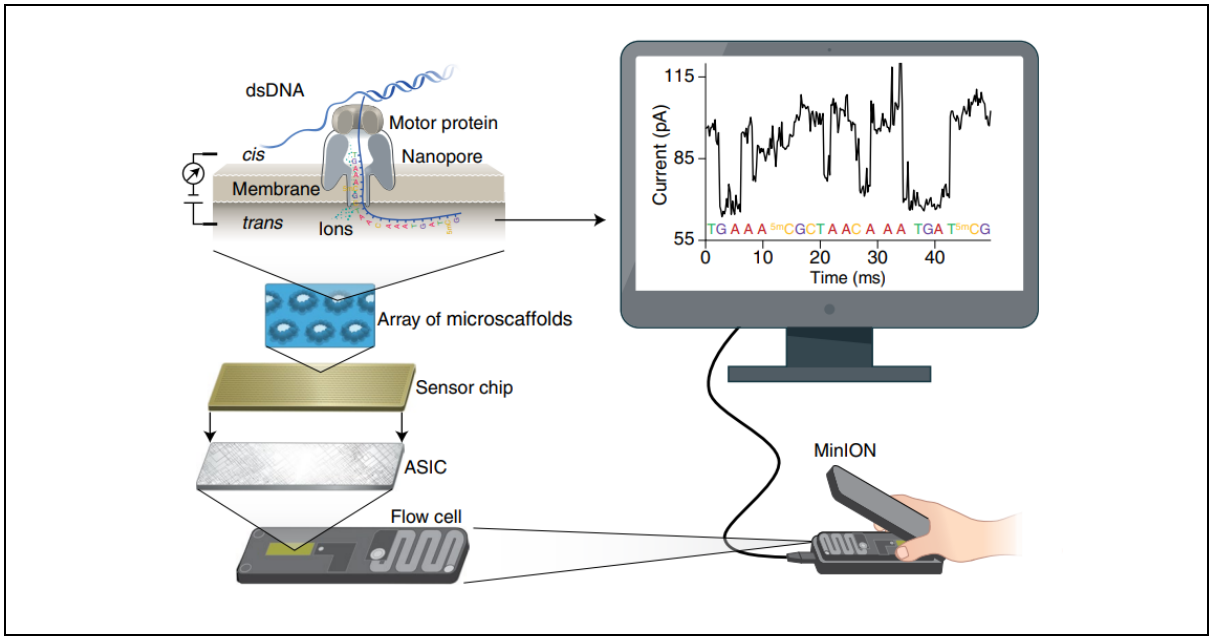


Figure 6.1: Oxford Nanopore Technologies MinION function

An illustration of ONT MinION function. Within the MinION flow cell, nanopores are embedded in a membrane across which a constant voltage is applied. The DNA or cDNA is unwound and a single strand is fed through the nanopore by the motor protein. As the bases pass through the nanopore one-by-one, they disrupt the current in a manner characteristic of each base, allowing the sequence to be determined. Reprinted by permission from Springer Nature Customer Service Centre GmbH: Springer Nature, Nature Biotechnology, Nanopore sequencing technology, bioinformatics and applications, Yunhao Wang et al., 2021.

There is no published data on the expression of BCL6 transcript variants in GBM. Therefore, it is unknown whether the altered activity of BCL6 in GBM cells treated with acute IR could be explained by alternative splicing. ONT MinION technology has been established in the McConnell lab group and has been used to perform whole transcriptome sequencing of GBM cell lines (unpublished data). It was noted that these experiments included very little coverage of the BCL6 transcript sequence, meaning that no conclusions could be drawn about transcript variants. Therefore, it was necessary to optimise a method for the enrichment of BCL6 transcripts to obtain enough coverage to identify different transcript variants.

Three methods for sequencing only the BCL6 transcript family were considered. The first was to perform reverse-transcription with sequence-specific primers, so that only BCL6 transcripts were reverse-transcribed into cDNA. The second was to perform general reverse-transcription and then amplify the cDNA with sequence-specific primers so that only BCL6 cDNA was amplified. These options both had merit, however they required defined 3' and 5' sequences of the BCL6 transcripts to be reverse-transcribed or amplified. This meant that any novel transcripts in which these chosen sequences were not conserved would be missed.

A third alternative was to reverse-transcribe all mRNA and then semi-specifically amplify the cDNA using one sequence-specific primer and one universal primer. Therefore, to enrich for BCL6 transcripts without excluding unknown variants, two different sets of primers were used. First, BCL6 was semi-specifically amplified with a BCL6-specific primer at the 3' end and a universal primer at the 5' end. Next, BCL6 was semi-specifically amplified with a BCL6-specific primer at the 5' end and a universal primer at the 3' end. This ensured that most variation at both ends of the BCL6 transcripts should have been captured. This enrichment method was used to enable long-read sequencing of the BCL6 transcript variants expressed in untreated and irradiated GBM cells.

## 6.2: Aim

The aim of this chapter was to use ONT MinION long-read sequencing to determine whether novel BCL6 transcript variants were produced in response to acute IR in GBM cells and whether this could explain the altered behaviour of BCL6 induced by therapy in GBM cells.

## 6.3: Results

### 6.3.1: Primer design

To enrich for BCL6 transcripts, two semi-specific sets of primers were designed. This required understanding of the reverse transcription reaction carried out using the ONT cDNA-PCR Sequencing Kit (SQK-PCS109). This reaction results in all fully reversed-transcribed mRNA transcripts having an added VN primer (VNP) sequence at the 3' end of the top strand and an added strand-switch primer (SSP) sequence at the 5' end of the top strand (Figure 6.2).

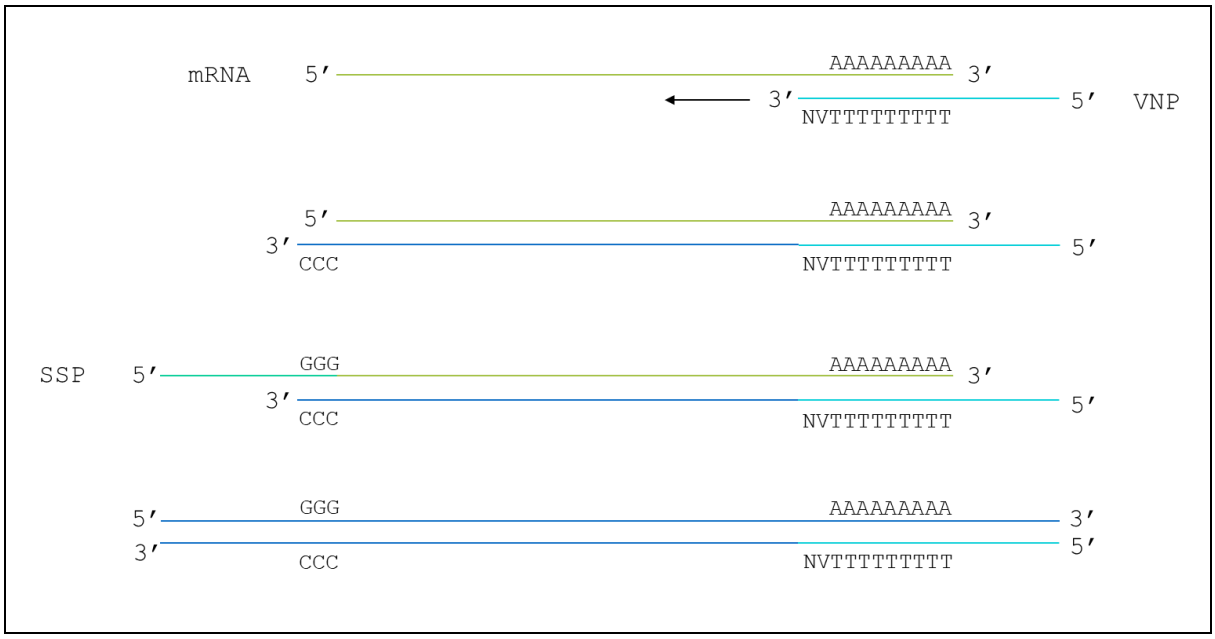


Figure 6.2: Schematic of reverse transcription of mRNA using the Oxford Nanopore Technologies SQK-PCS109 kit

The VNP primer binds to the poly-A tail of mRNA and the reverse transcriptase forms the DNA sequence complementary to each mRNA strand. At the end of the mRNA template, the reverse transcriptase adds three cytosine nucleotides. The three guanines on the end of the SSP sequence bind to the three cytosine nucleotides allowing the reverse transcriptase to switch strands.

In the SQK-PCS109 protocol, universal cDNA primers complementary to the VNP and SSP sequences are then added to amplify all fully reverse-transcribed transcripts. However, to investigate the BCL6 transcript variants in GBM, semi-specific amplification of BCL6 was performed in place of the general PCR with the universal primers.

First, a primer complementary to a 3' region of BCL6 mRNA was designed and paired with a primer complementary to the SSP sequence to semi-specifically amplify BCL6 mRNA (Figure 6.3A). Secondly, a primer complementary to a 5' region of BCL6 mRNA was designed and paired with a primer complementary to the VNP sequence to semi-specifically amplify BCL6 mRNA from the other end (Figure 6.3B).

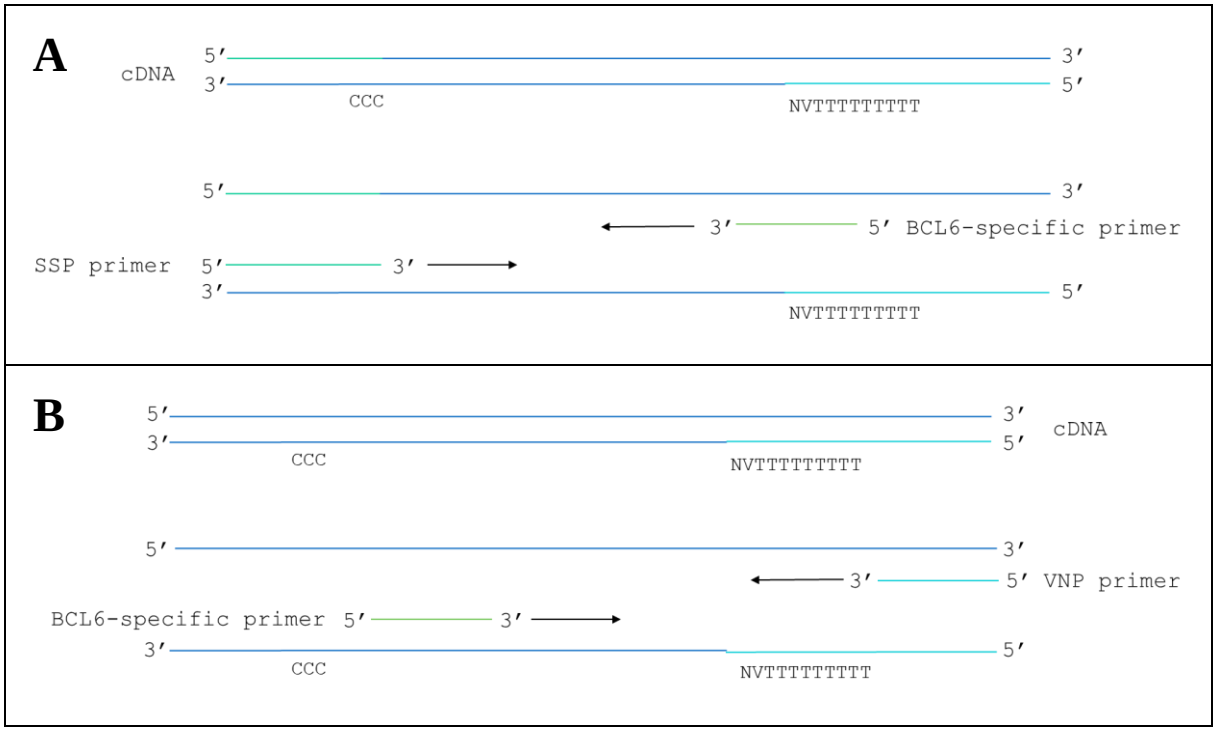


Figure 6.3: Schematic of semi-specific amplification of BCL6 cDNA

A) Semi-specific amplification of BCL6 cDNA using a BCL6-specific primer complementary to a 3' region of BCL6 mRNA and the universal SSP primer complementary to the SSP sequence added to the 5' end of the BCL6 cDNA during reverse transcription. B) Semi-specific amplification of BCL6 cDNA using a BCL6-specific primer complementary to a 5' region of BCL6 mRNA and the universal VNP primer complementary to the VNP sequence added to the 3' end of the BCL6 cDNA during reverse transcription.

The UCSC Genome Browser was used to visualise the known BCL6 transcript variants (Figure 6.4)[326] The coding portion of the 3' BCL6 exon and the first 25 bases of the 3'-UTR were conserved between all known variants. However, the rest of the 3'-UTR varied considerably between transcript variants. Therefore, the 3'-end specific primer was designed to be complementary to the conserved 25 bases at the start of the 3'-UTR. This primer would be paired with the universal SSP primer to amplify all BCL6 transcripts containing the 3'-end primer sequence regardless of the transcript sequence upstream.

There were several exons at the 5' ends of the different BCL6 transcript variants which were not conserved between all of the variants. The first conserved sequence occurred in an untranslated exon which was truncated in one variant but fully conserved in the other three variants. This conserved sequence was only 14 base pairs long due to the truncated variant. As this was too short, the selected 5'-end primer was complementary to these 14 bases plus the ten bases upstream to produce a primer with more favourable characteristics. This means that variants with the truncated exon will not necessarily have been captured in this experiment. The 5'-end primer was paired with the universal VNP primer to amplify all BCL6 transcripts containing the 5'-end primer sequence regardless of the transcript sequence downstream. Hence variation at both the 3'- and 5'-ends would be captured.

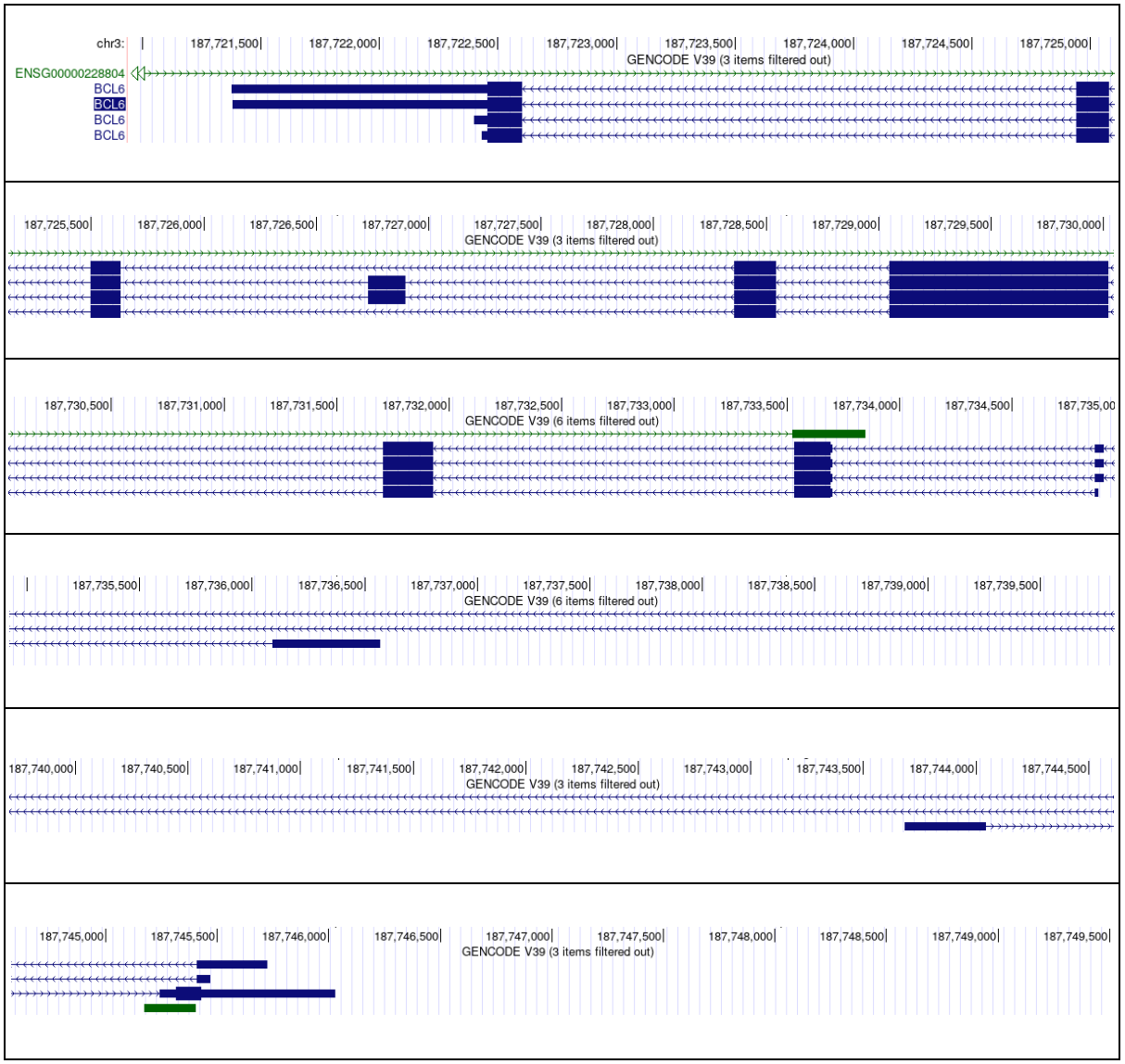


Figure 6.4: Known BCL6 transcript variants visualised using the UCSC Genome Browser

BCL6 is encoded on the bottom strand of DNA so the 3'ends of the transcript are at the top left of the figure and the 5' ends of the transcript are at the bottom of the figure. BCL6 transcripts are shown in blue while a long non-coding RNA encoded on the top strand at the same locus is shown in green.

## 6.3.2: Confirmation of enrichment for BCL6

RNA was extracted from LN18 cells, reverse-transcribed and amplified using the two sets of semi-specific amplification primers. As a quality control check, the amplified cDNA was visualised on an agarose gel. The amount of BCL6 transcript in the cDNA was quantified by qPCR compared to the amount of the housekeeping gene HPRT. To determine the efficacy of the semi-specific amplification, the amount of BCL6 transcript in the amplified cDNA was also quantified by qPCR compared to the amount of HPRT. The threshold cycle (Ct) difference between BCL6 and HPRT in each comparison indicated whether the amount of BCL6 had been enriched relative to the amount of HPRT by semi-specific amplification.

Representative gel images and qRT-PCR results from after optimisation of PCR parameters are displayed in Figure 6.5 and Figure 6.6. The semi-specific amplification using the 3'-end primer produced a band just smaller than 1500 base pairs, indicating enrichment for cDNA of this length (Figure 6.5A). This is about half the length of most known BCL6 transcripts, however the design of the primers meant that most of the BCL6 3'-UTR was not amplified. Considering that the 3'-UTR of some of the known transcripts is around 1000 base pairs in length, this brought the amplified band closer to the expected length. When qRT-PCR was performed on the cDNA before amplification, HPRT crossed the threshold 6.5 cycles before BCL6, indicating that HPRT was much more abundant than BCL6 (Figure 6.5B). Contrastingly, after semi-specific amplification using the 3'-end primer, BCL6 crossed the threshold 3.4 cycles before HPRT, indicating that BCL6 was now more abundant than HPRT, confirming strong enrichment (Figure 6.5C).

The semi-specific amplification using the 5'-end primer produced a band of about 6000 base pairs long, indicating enrichment for cDNA of this length (Figure 6.6A). This was about double the length of most known BCL6 transcripts and so was unexpected. It is possible that the primers enriched for a transcript of this length more strongly than they enriched for BCL6. However, the q-RT-PCR demonstrated that BCL6 was nonetheless enriched in the cDNA. When qRT-PCR was performed on the cDNA before amplification, HPRT crossed the threshold 7.4 cycles before BCL6, indicating that HPRT was much more abundant than BCL6 (Figure 6.6B). Contrastingly, after semi-specific amplification using the 5'-end primer, BCL6 crossed the threshold 1.1 cycles before HPRT, again showing that BCL6 was now more abundant than HPRT, indicating enrichment for BCL6 cDNA (Figure 6.6C).

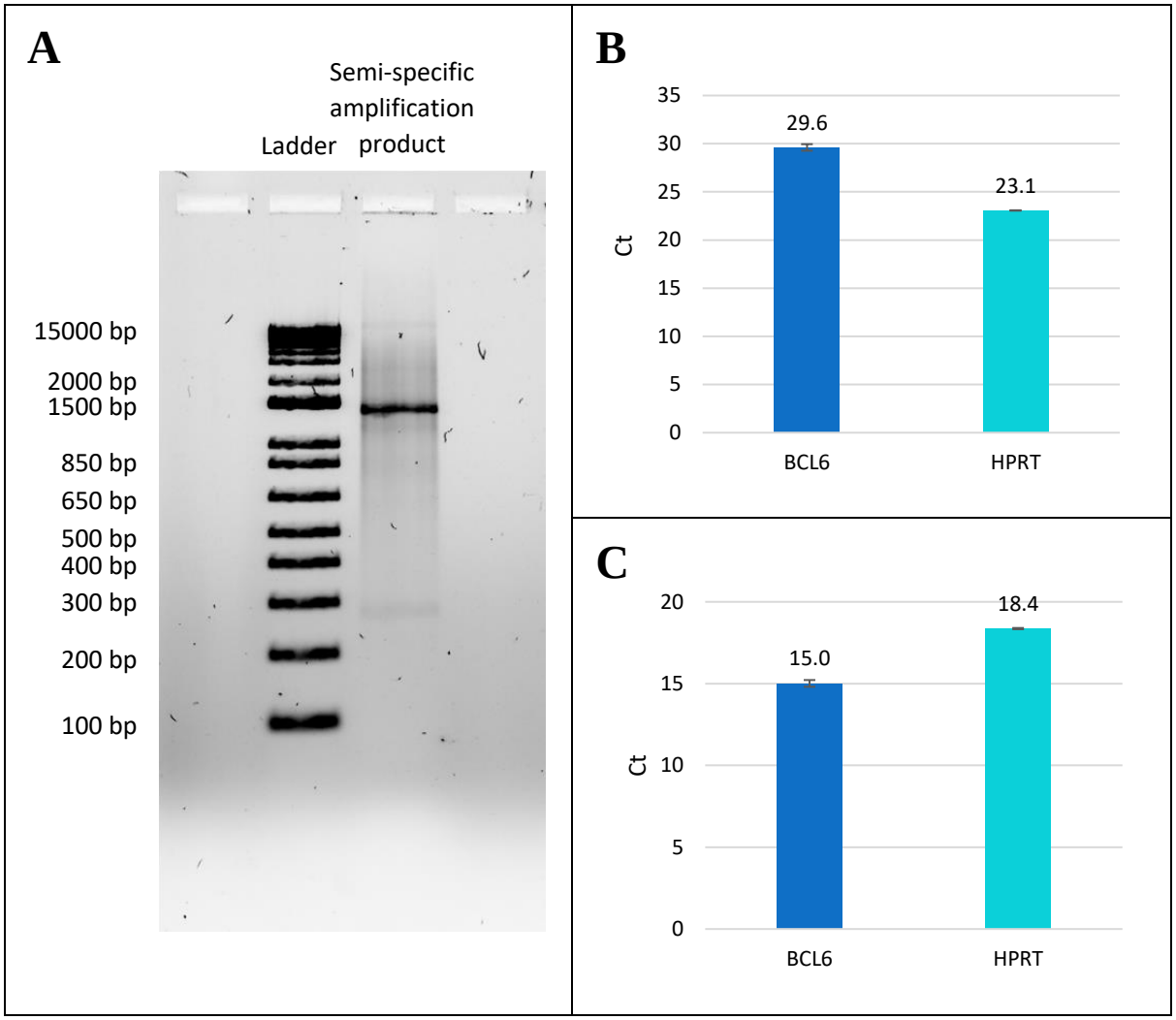


Figure 6.5: Semi-specific amplification for BCL6 cDNA using the 3'-end primer and the SSP primer

A) Agarose gel image of amplified product. B) qRT-PCR threshold cycle (Ct) values for BCL6 and HPRT in cDNA before amplification. C) qRT-PCR Ct values for BCL6 and HPRT in cDNA after semi-specific amplification for BCL6. Error bars show standard deviation of three qPCR technical replicates.

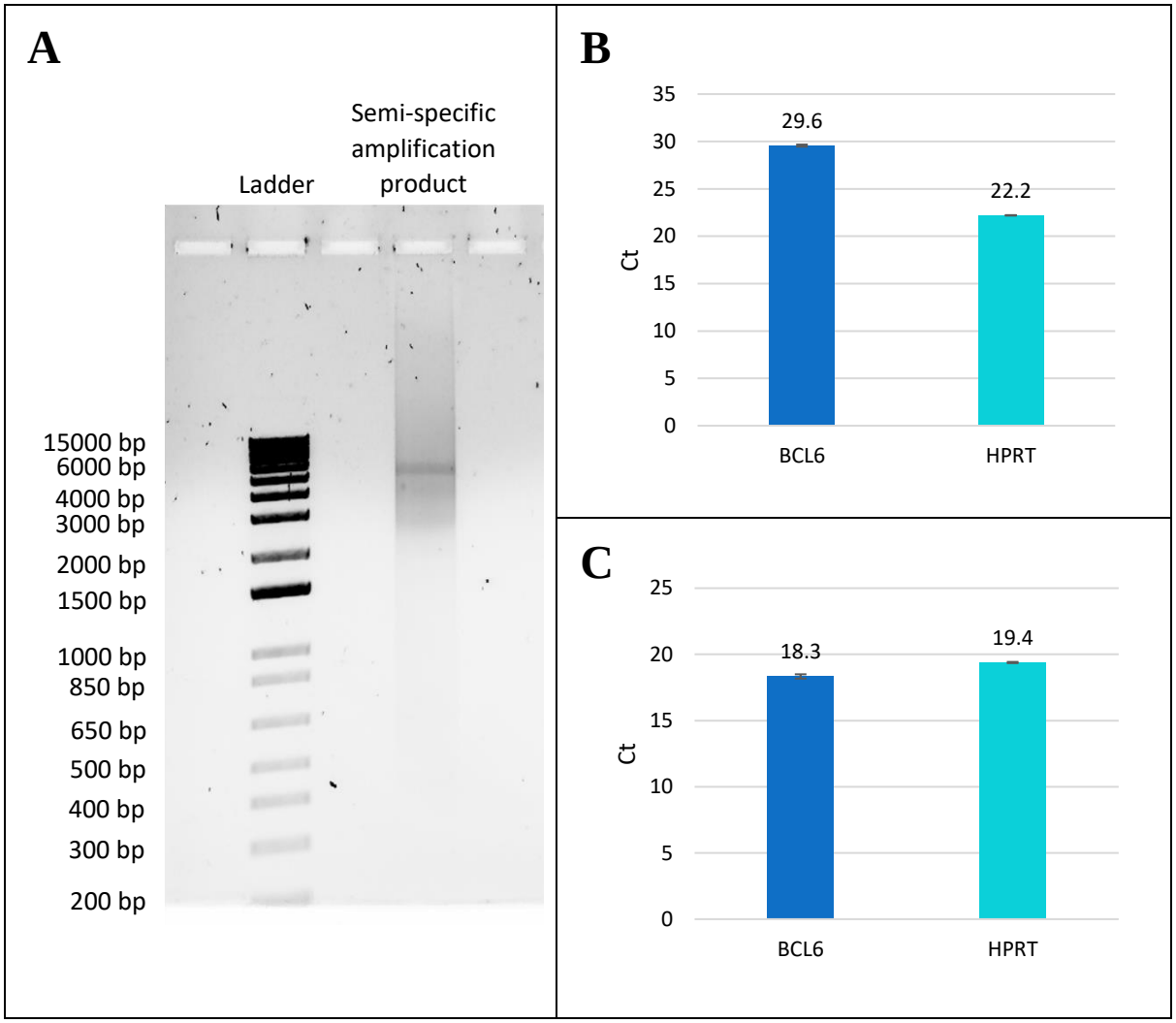


Figure 6.6: Semi-specific amplification for BCL6 cDNA using the 5'-end primer and the VNP primer

A) Agarose gel image of amplified product. B) qRT-PCR threshold cycle (Ct) values for BCL6 and HPRT in cDNA before amplification. C) qRT-PCR Ct values for BCL6 and HPRT in cDNA after semi-specific amplification for BCL6. Error bars show standard deviation of three qPCR technical replicates.

## 6.3.3: ONT MinION long-read sequencing of semi-specifically amplified cDNA from untreated and irradiated GBM cell lines

Once the semi-specific amplification of BCL6 had been optimised, these primer sets were used to amplify and sequence BCL6 transcripts in GBM cells. This was done in three cell lines (LN18, NZG0906 and NZG1003) to increase the applicability of the results to GBM in general. Additionally, the NZG0906 and NZG1003 cell lines were low passage, tumour-derived cell lines and therefore likely to be more representative of GBM tumours than the commercially available LN18 cell line.

In triplicate, RNA was extracted from the three GBM cell lines which were either untreated or had been treated with 10 Gy IR 24 hours previously. The ONT SQK-PCS109 kit was used to reverse transcribe the RNA, semi-specifically amplify the BCL6 cDNA with either the 3'-end specific primer or the 5'-end specific primer and prepare the cDNA for long-read sequencing on the MinION. For each primer (3'- and 5'-ends), the three untreated and irradiated replicates for each cell line were barcoded and multiplexed together for sequencing. The three sample sets amplified with the 3'-end specific primer (LN18, NZG0906 and then NZG1003 multiplexed samples) were run sequentially on the same MinION flow cell, which was washed in between. This flow cell had already been used and washed once previously for another experiment. The same procedure was used with a different MinION flow cell for the three sample sets amplified with the 5'-end specific primer.

Reuse of the flow cells reduced the cost of the experiments. This worked well as the washes tended to regenerate some pores which were lost over the previous run. However, as pores were lost over successive runs, fewer reads were obtained. This introduced variability in the number of reads for each run (Appendix). The NZG1003 samples had fewer reads (< 1 million) than the other samples as they were run last on the flow cells.

## 6.3.4: Bioinformatics analysis

Bioinformatics analysis of the data generated by the MinION sequencing runs was performed by Leticia Castro (McConnell lab group, Victoria University of Wellington, New Zealand). The sequencing data was quality control filtered and basecalled. Transcript variants were identified using FLAIR (Full-Length Alternative Isoform analysis of RNA).[345] FLAIR is a pipeline specifically developed to analyse long-read RNA sequencing data obtained using ONT platforms.[345] The FLAIR modules diffExp and diffSplice were kindly run by George Wiggins (Logan lab group, University of Otago, Christchurch, New Zealand).

As depicted in Figure 6.7, FLAIR used minimap2 to align the raw reads with a reference sequence (flair align).[345] Misaligned splice junctions were corrected to a reference genome (flair correct).[345] The reads

with the same splice junctions were grouped into isoform groups to form a first-pass assembly (flair collapse).[345] The raw reads were then re-aligned to this first-pass assembly.[345] The number of reads corresponding to each isoform were quantified and isoforms with fewer than three supporting reads were discarded to create a confident isoform assembly.[345] The primary read alignments were then quantified using minimap2 (flair quantify).[345] The FLAIR module flair diffExp analysed differential gene expression, isoform expression and isoform usage between samples, in this case between the untreated and irradiated replicates in each cell line.[345] Differential isoform usage, which analyses the relative abundances of isoforms compared to total gene expression, was not useful for this study because it was not possible to compare to total gene expression in the BCL6-enriched samples. Finally, the FLAIR module flair diffSplice analysed alternative 3' splicing, alternative 5' splicing, intron retention and exon skipping.[345]

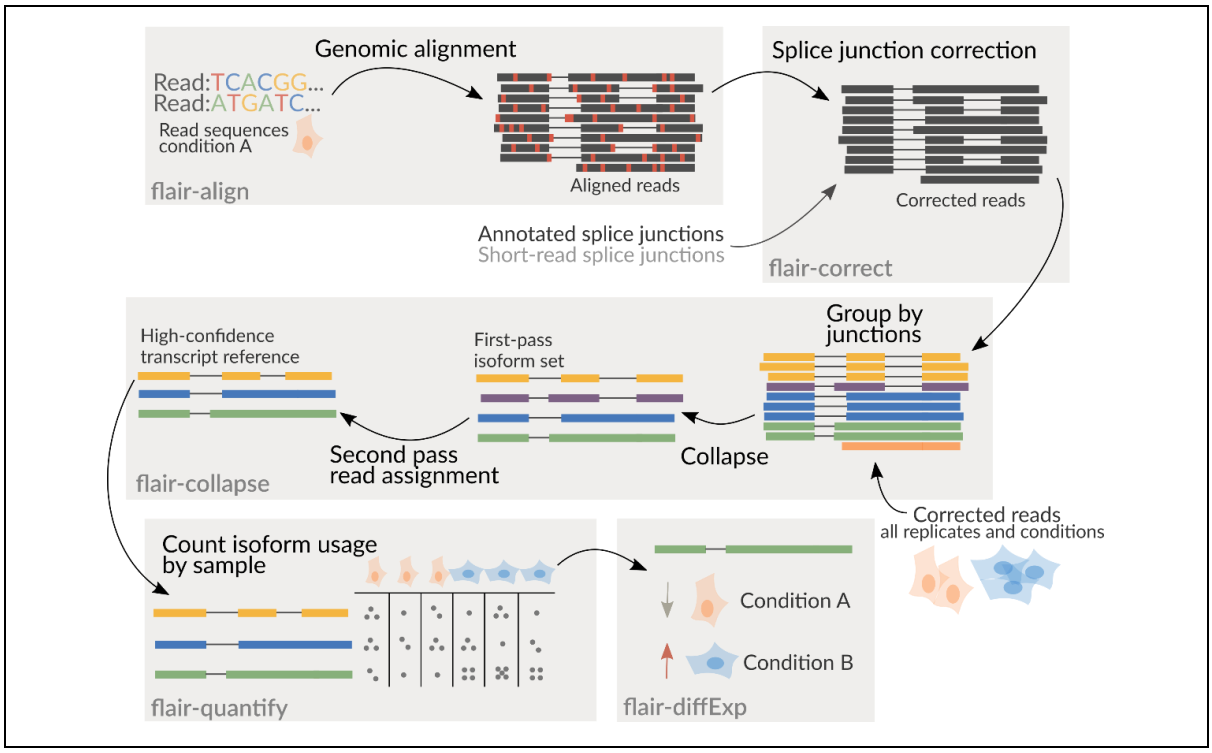


Figure 6.7: Flow diagram of the FLAIR pipeline

Figure from GitHub BrooksLabUCSC/flair[345]: https://github.com/BrooksLabUCSC/flair#readme. Image reproduced with permission from Angela Brooks.

## 6.3.5: Identification of BCL6 transcript variants

### 6.3.5.1: BCL6 coverage

The variability in the number of reads obtained for each sample had little impact on the coverage of the BCL6 sequence (Table 6.1, Appendix). The biggest differences in the coverage of BCL6 were due to which primer was used. Table 6.1 shows that 0.41-0.80% of reads in the 3'-end primer-amplified samples were mapped to BCL6. This emphasised that semi-specific amplification is only a technique for enrichment, not purification. Meanwhile, just 0.0014-0.059% of reads in the 5'-end primer-amplified samples were mapped to BCL6. This highlighted that enrichment with the 3' primer was far superior to enrichment with the 5' primer. The number of transcript variants identified correlated with the coverage of BCL6 (Appendix). Therefore, because the samples in which BCL6 was amplified with the 5'-end primer had lower coverage of BCL6, fewer transcript variants were identified in these samples.

It was expected from previous results that acute IR would increase the abundance of BCL6 transcripts. Encouragingly, there was a trend towards acute IR increasing the coverage of BCL6 in LN18 and NZG1003 cells (Appendix).[322]

Table 6.1: Percentages of total reads mapping to BCL6

| Multiplexed sample | 3'-end primer | | | 5'-end primer | | |
|---|---|---|---|---|---|---|
| | Million reads | Total reads mapping to BCL6 | % of reads mapping to BCL6 | Million reads | Total reads mapping to BCL6 | % of reads mapping to BCL6 |
| **LN18** | 1.93 | 7,924 | 0.41% | 5.1 | 72 | 0.0014% |
| **NZG0906** | 1.46 | 11,701 | 0.80% | 2.0 | 342 | 0.017% |
| **NZG1003** | 0.748 | 4,423 | 0.59% | 0.195 | 116 | 0.059% |

### 6.3.5.2: Visualisation and analysis of BCL6 transcript variants

The results of the FLAIR pipeline were visualised in the Integrative Genomics Viewer (IGV) against a reference genome (Figure 6.8 and Figure 6.9) and the parameters of each transcript variant identified were exported and examined manually (Appendix).[346]

NCBI numbers the exons from the 5' to 3' end of each individual transcript, however this system is inadequate when discussing multiple transcript variants with different exons. There did not appear to be a standard system for approaching this problem, so the numbering system used in this thesis to discuss the exons in BCL6 transcript variants is defined in Figure 6.8.

.

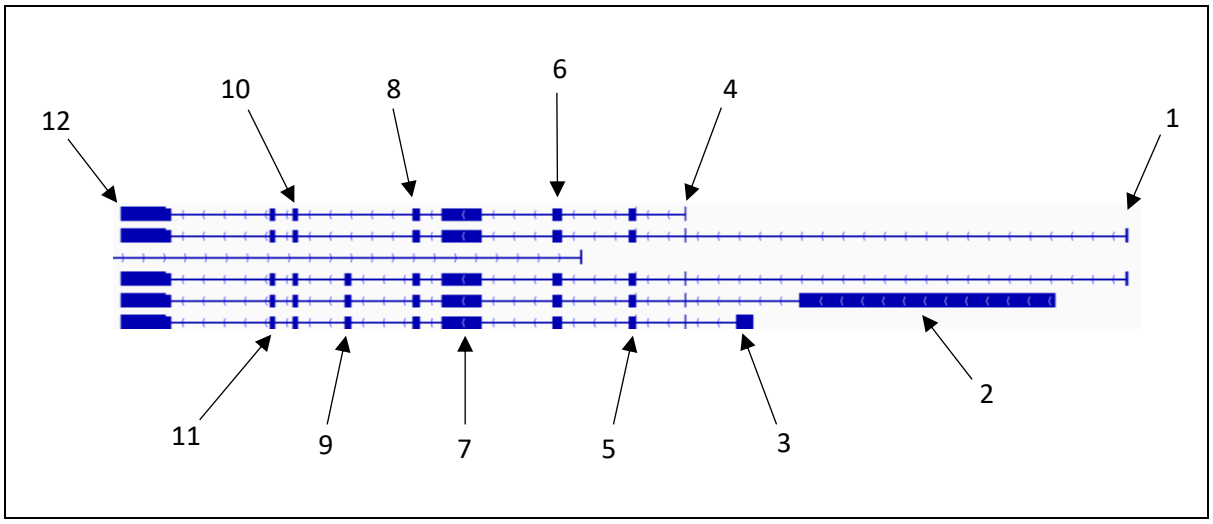


Figure 6.8: Numbering system for exons in BCL6 transcript variants

BCL6 transcript variants in human genome browser reference genome GRCh38.p13 (GCA_000001405.28) used in IGV. Exons labelled 1-12 from 5' to 3' end.

For ease of discussion, BCL6 transcripts annotated in NCBI are referred to by shortened names throughout the rest of this chapter. The NCBI transcript names and numbers are shown in Table 6.2 alongside the shortened names used and the exons in each transcript, as defined in Figure 6.8.

Table 6.2: Shortened NCBI transcript names

| NCBI transcript name | NCBI transcript number | Shortened name used | Exons in transcript |
|---|---|---|---|
| Transcript variant 1 | NM_001706.5 | Variant 1 | 1, 4-12 |
| Transcript variant 2 | NM_001130845.2 | Variant 2 | 3-12 |
| Transcript variant 3 | NM_001134738.1 | Variant 3 | 4-8, 10-12 |
| Predicted transcript variant X1 | XM_005247694.4 | Variant X1 | 2-12 |
| Predicted transcript variant X2 | XM_011513062.3 | Variant X2 | Extended exon 1, 4-12 |
| Predicted transcript variant X3 | XM_011513062.4 | Variant X3 | 1, 4-8, 10-12 |

### 6.3.5.4: BCL6 transcript variants identified with the 3'-end primer

The transcripts identified in the 18 GBM samples (triplicate untreated and irradiated LN18, NZG0906 and NZG1003 samples) were compared. Multiple BCL6 transcript variants were expressed in the GBM cell lines. However, no transcripts were commonly identified in the irradiated GBM cells but not in the untreated cells or vice versa. This suggests that acute IR does not induce alternative splicing of a BCL6 variant which is absent in untreated GBM cells.

Three transcript variants were identified in 17 of the 18 GBM samples with BCL6 amplified with the 3'-end primer. Two of these were known BCL6 variants: Variant 1 and Variant X3 (Figure 6.9A and B). Variant 1 contains exons 1 and 4-12. Variant X3 differs from Variant 1 because it is missing exon 9. The third BCL6 transcript variant identified in 17 of 18 samples was almost identical to Variant 1, except that exon 6 was only 160 bases long instead of 222 (Figure 6.9C). Another BCL6 transcript variant identical to Variant X3 except for the same deletion in exon 6 was identified in 9 of the 18 samples (Figure 6.9H). These two deletion variants will be referred to as Variant 1Δ6 and Variant X3Δ6.

There was also evidence for transcripts with apparent transcription start sites in exon 2 (Figure 6.9E), exon 3 (Figure 6.9G) and exon 7 (Figure 6.9D and F). This indicated that Variant X1, which has a transcription start site in exon 2, and Variant 2, which has a transcription start site in exon 3, were expressed in GBM cells. However, the apparent transcription start sites in 3 and 7 were extremely variable, with no clear pattern between cell lines and treatments. It is possible that there is a genuine transcription start site in exon 7 of BCL6, but it seems likely that these transcripts, and the variability

of the apparent start sites in Variant 2, were due to mRNA degradation or incomplete reverse transcription.

Variant 3 which contains exons 4-8 and 10-12 was not detected. The NCBI genome browser shows that this transcript had the shortest 3'-UTR, at only 25 bases. The 3'-specific primer was designed to bind to these 25 bases. It may be that the lack of bases flanking the primer sequence prevented capture of this transcript, whereas the transcripts with longer 3'-UTRs were captured. Alternatively Variant 3 may not be expressed in GBM cells. Variant X2, which is identical to Variant 1 except for a longer exon 1 was also not detected, suggesting that it is not expressed in GBM cells. Other transcript variants were identified but in fewer than half of the samples analysed and so were not investigated further.

#### 6.3.5.5: BCL6 transcript variants identified with the 5'-end primer

As so few transcript variants were identified per sample with the 5'-end primer, the results were not very informative. Variants 1 and X3 were the most commonly identified BCL6 transcripts with both the 3'- and 5'-end primers. Variant 1 was identified in 16 of the 18 samples amplified with the 5'-end primer (Figure 6.9A), while Variant X3 was identified in eight of the 18 samples Figure 6.9B). Variant 1Δ6 was not identified in any of the samples with the 5'-primer, despite being identified in almost all samples with the 3'-primer. However, Variant X3Δ6 was identified in one irradiated and one untreated NZG0906 sample (Figure 6.9H).

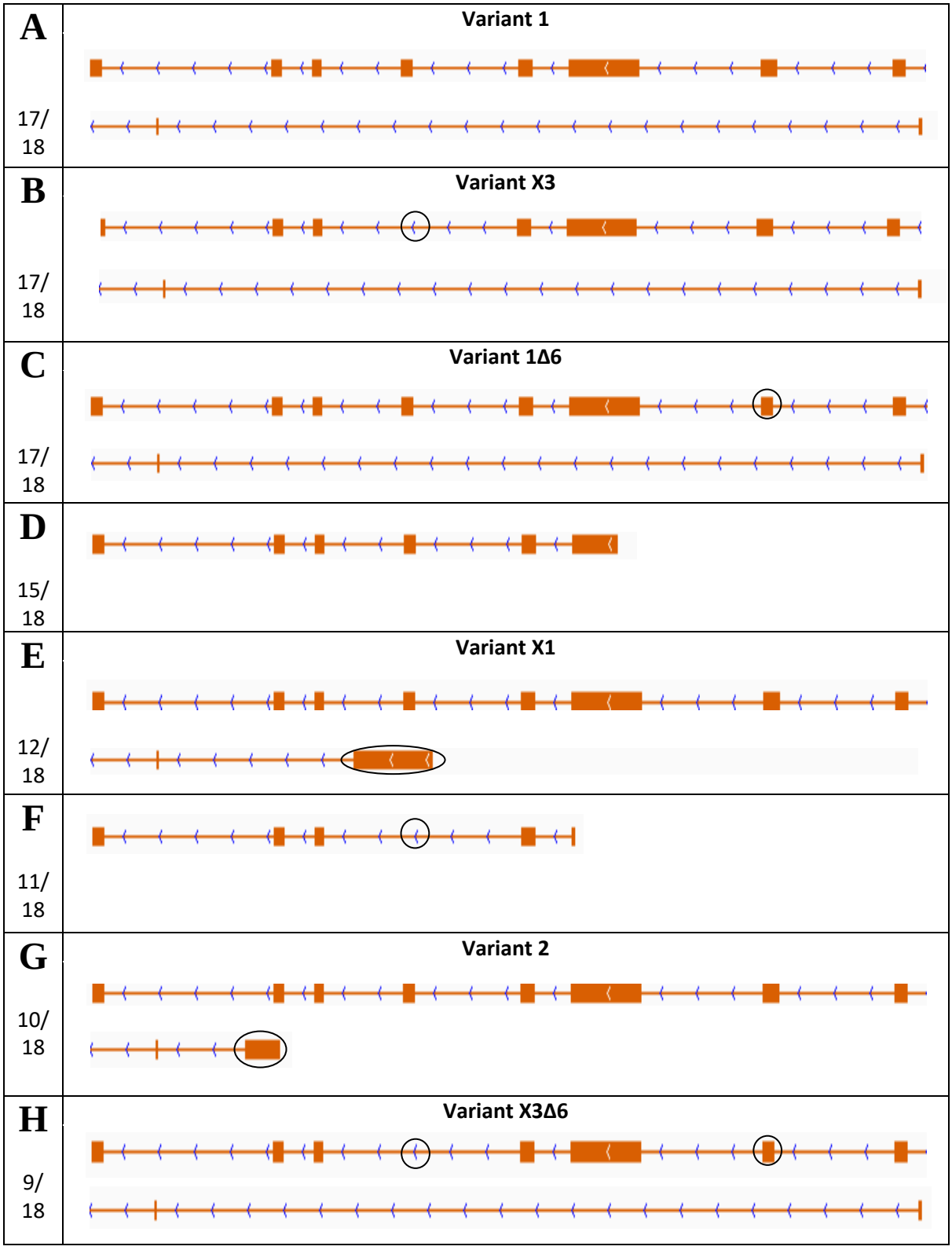


Figure 6.9: BCL6 transcript variants commonly identified across untreated and irradiated GBM cell lines

BCL6 transcript variants identified in at least half of the 18 untreated and irradiated GBM cell line samples analysed with BCL6 amplified using the 3'-end primer. Number of samples in which each transcript was identified shown in left column. Distinctive exons circled. Transcripts viewed in IGV.

### 6.3.5.6: 3’ and 5’ untranslated regions

In all BCL6 variants annotated in UCSC and NCBI, the transcription start site was ten bases into exon 5. Everything upstream was the 5’ UTR. As discussed above, the 5’ UTR of most of the transcripts identified in GBM cells consisted of exon 1, exon 4 and the first nine nucleotides of exon 5. While most of the commonly identified transcripts started in exon 1, the apparent transcription start site varied by up to 13 nucleotides. The transcripts starting in exon 2 had an apparent transcriptional start site further 5’ than that of Variant X1 in NCBI. However, the length of exon 2 in the transcripts observed matched a BCL6 transcript annotated in Ensembl. The 5’ end of the transcripts starting in exon 3 (Variant 2) varied by hundreds of nucleotides. Additionally, some transcripts containing exon 2 or 3 had apparent transcription start sites in the introns between NCBI-annotated exons 1 and 2 or between exons 2 and 3.

The 3’-end primer was designed to complement the first 25 bases of the 3’-UTR of BCL6, which was conserved in all BCL6 transcripts in the UCSC genome browser. Therefore, no more of the 3’-UTR could be sequenced with the 3’-end primer.

The limited data gathered using the 5’-end primer indicated that almost all of the BCL6 transcript variants identified had 3’-UTRs of 1077 bases. This corresponded to the 3’-UTRs annotated in NCBI for Variants 1 and 2. In the NCBI database, the 3’-UTRs of the other BCL6 transcript variants are 4 bases longer at 1081 bases. This was not observed in the data generated with the 5’-end primer. Some of the transcript variants identified had shorter 3’-UTRs, although these varied from a few hundred bases to 1071 bases long and were not consistently identified.

## 6.3.6: Differential splicing of BCL6 transcripts

The aim of this chapter was to determine whether acute IR induced alternative splicing of BCL6 transcripts, perhaps explaining the altered activity of BCL6 after treatment in GBM cells. This was investigated using the FLAIR diffSplice module to analyse the data generated using the 3'-end BCL6-specific primer. Alternative 3' splicing, alternative 5' splicing, exon skipping and intron retention were analysed. Alternative 3' splicing refers to a situation in which the 5'-splice site remains the same but the 3'-splice site changes.[584] Alternative 5' splicing is the opposite. Exon skipping and intron retention analysed inclusion or exclusion of whole exons and whole introns respectively.[584]

Only one alternative splicing event was detected. This was the alternative position of the 3' splice site 62 nucleotides into exon 6 rather than at the start of exon 6, leading to the transcripts with the short exon 6 (Variants 1Δ6 and X3Δ6). This alternative splicing event occurred in all three GBM cell lines and its frequency was very similar in untreated and irradiated GBM cells. There was slight variation between the cell lines, with the frequency of the alternative splicing event ranging from 10.1% in untreated NZG1003 cells to 4.2% in irradiated LN18 cells (Table 6.3). However, the untreated and irradiated GBM cell lines all had low but reproducible expression of the Δ6 transcripts.

Although diffSplice identified some transcripts with intron retention (Appendix), this occurred only in a handful of reads, meaning that very little information could be taken from these results.

Several different exon skipping events were identified by diffSplice (Appendix), however most were very infrequent. The frequent exon skipping events are displayed in Table 6.4. Again, they occurred at similar frequencies in both untreated and irradiated GBM cells. Skipping of exon 9, resulting in Variants X3 and X3Δ6, occurred in approximately 20% of transcripts in NZG0906 and NZG1003 cells and in around 13% of transcripts in LN18 cells. Skipping of exon 5 was also a fairly frequent event. None of the commonly identified transcripts (section 6.3.5.4) skipped exon 5, however several of the transcript variants only identified in one or two out of 18 replicates did not contain exon 5. The frequency of exon 5 skipping ranged from 10.6% in irradiated NZG0906 cells to 4.5% in irradiated NZG1003 cells. Again, this shows that while there was some variation between the cell lines, the frequency of BCL6 splicing events were fairly consistent and were not altered by IR.

### Table 6.3: Alternative 3' splicing

The number of BCL6 reads containing the two alternative splice sites in untreated and irradiated GBM cells are shown in columns 3 and 4 respectively. The frequency with which each alternative splice site occurred in BCL6 transcripts in untreated and irradiated GBM cells was calculated from the read numbers in columns 3 and 4 and is shown in columns 5 and 6 respectively.

| Cell line | Position of 3' splice site | Average reads | | Frequency of splice site (%) | |
|---|---|---|---|---|---|
| | | Untreated | Irradiated | Untreated | Irradiated |
| **Position of 3' splice site for splicing of intron between exons 5 and 6 (chr3:187733532-187731930_chr3:187733532-187731868)** | | | | | |
| **LN18** | Start of exon 6 | 591 | 1400 | 95.3 | 95.8 |
| | 62 nucleotides into exon 6 | 29 | 61 | 4.7 | 4.2 |
| **NZG0906** | Start of exon 6 | 1106 | 1125 | 93.7 | 93.1 |
| | 62 nucleotides into exon 6 | 74 | 84 | 6.3 | 6.9 |
| **NZG1003** | Start of exon 6 | 596 | 636 | 89.9 | 91.6 |
| | 62 nucleotides into exon 6 | 67 | 58 | 10.1 | 8.4 |

### Table 6.4: Exon skipping

The number of BCL6 reads with inclusion or exclusion of exons 9 and 5 in untreated and irradiated GBM cells are shown in columns 3 and 4 respectively. The frequency with which exons 9 and 5 were included or excluded from BCL6 transcripts was calculated from the read numbers in columns 3 and 4 and is shown in columns 5 and 6 respectively.

| Cell line | Inclusion or exclusion | Average reads | | Frequency of exon inclusion/exclusion (%) | |
|---|---|---|---|---|---|
| | | Untreated | Irradiated | Untreated | Irradiated |
| **Exon 9 (chr3:187726730-187726898)** | | | | | |
| **LN18** | Inclusion | 644 | 1476 | 86.1 | 87.2 |
| | Exclusion | 104 | 217 | 13.9 | 12.8 |
| **NZG0906** | Inclusion | 1268 | 1405 | 80.1 | 81.0 |
| | Exclusion | 316 | 330 | 19.9 | 19.0 |
| **NZG1003** | Inclusion | 663 | 660 | 79.5 | 78.4 |
| | Exclusion | 171 | 182 | 20.5 | 21.6 |
| **Exon 5 (chr3:187733532-187733703)** | | | | | |
| **LN18** | Inclusion | 620 | 1461 | 91.4 | 92.9 |
| | Exclusion | 58 | 111 | 8.6 | 7.1 |
| **NZG0906** | Inclusion | 1209 | 1242 | 91.6 | 89.4 |
| | Exclusion | 111 | 148 | 8.4 | 10.6 |
| **NZG1003** | Inclusion | 663 | 695 | 93.8 | 95.5 |
| | Exclusion | 44 | 33 | 6.2 | 4.5 |

## 6.3.7: Quantification of BCL6 transcript variants

Differential splicing analysis did not indicate any BCL6 alternative splicing events unique to or more common in irradiated GBM cells. However, diffSplice did not examine the frequency of combinations of splicing events. Therefore, it was possible that acute IR treatment caused changes to the relative abundance of the different BCL6 variants present in the GBM cells. This was assessed by quantitative analysis.

### 6.3.7.1 FLAIR quantify

FLAIR quantify was used to quantify the transcripts identified by the sequencing of the cDNA amplified with the 3'-end primer, including the > 99% which were not annotated to BCL6. The quantification values for the commonly identified BCL6 transcript variants shown in Figure 6.9 were extracted and are displayed in Figure 6.10. The transcript variants beginning at varying locations within exon 7 were not examined further as it was likely that these were present due to incomplete reverse transcription or degradation of the mRNA. Variants 1 and X3 were far more abundant than the other commonly identified transcripts and so are displayed separately in Figure 6.10A. Similarly, Variants 1Δ6 and X3Δ6 were much more abundant than Variants 2 and X1 and so these are displayed separately in Figure 6.10B and C.

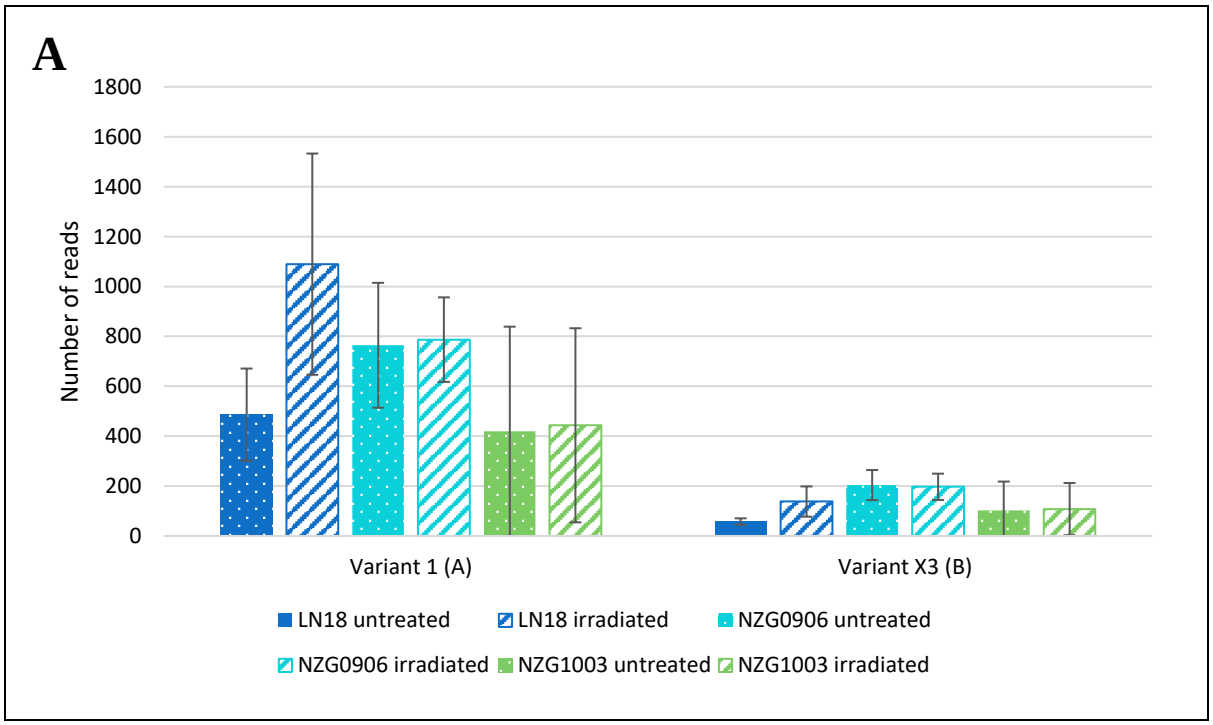

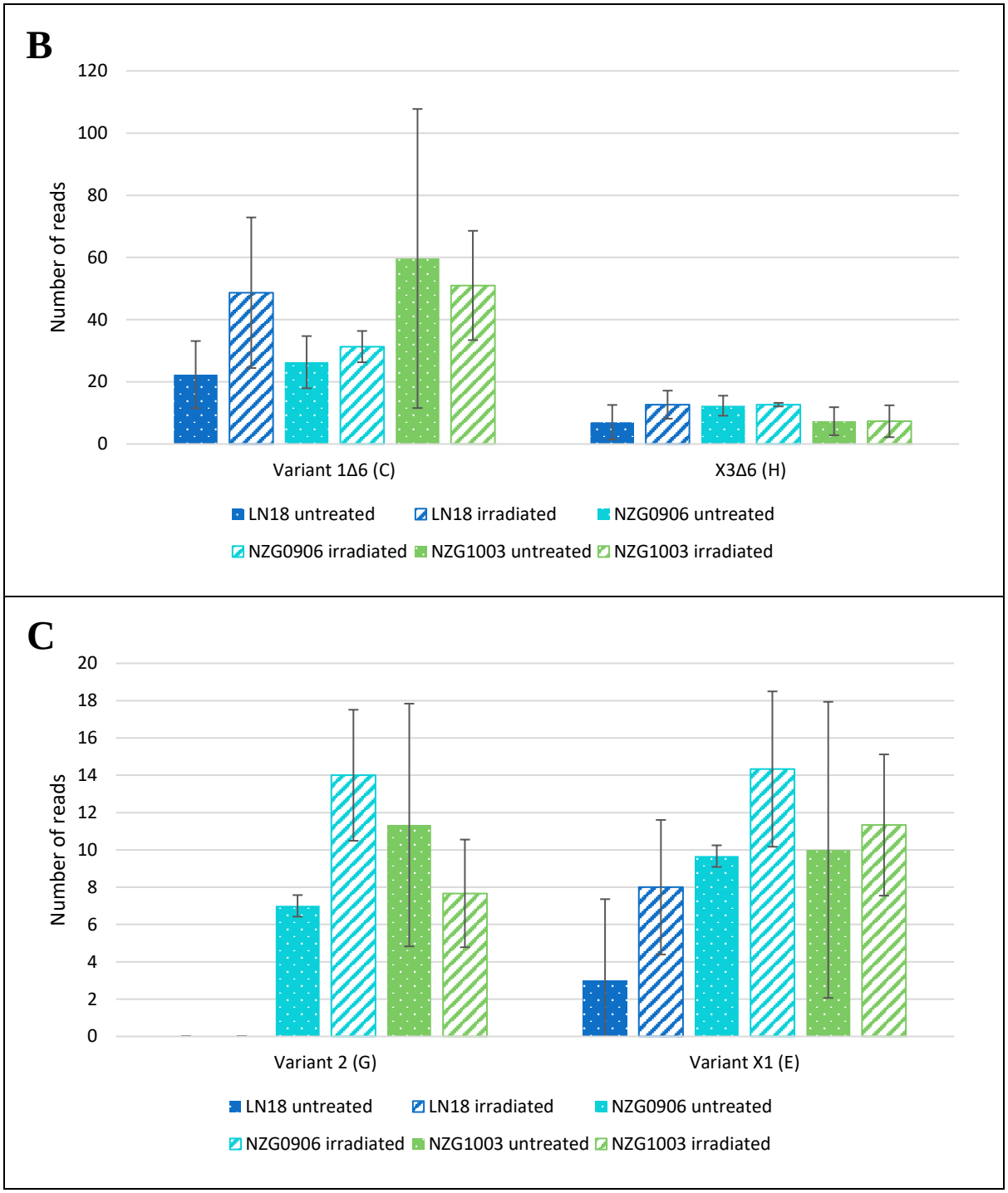


## Figure 6.10: Quantification of BCL6 transcript variants

Number of reads of each BCL6 transcript variant commonly identified across sequenced samples, as shown in Figure 6.9. Average number of reads shown for untreated and irradiated LN18, NZG0906 and NZG1003 samples. A) Quantification of Variants 1 and X3 (corresponding to Figure 6.9A and B). B) Quantification of Variants 1Δ6 and X3Δ6 (corresponding to Figure 6.9C and H). C) Quantification of BCL6 Variants 2 and X1 (corresponding to Figure 6.9G and E). Error bars show standard deviation of the three biological replicates.

### 6.3.7.2: FLAIR diffExp

The FLAIR module diffExp was used to calculate the effect of acute IR on the abundance of BCL6 transcripts. Most of the differential expression observed was not statistically significant, likely due to the variability of the data. To minimise the impact of this variability, a shrinkage step was included to correct the fold-changes calculated for transcripts with high variability in their expression to a background distribution.[585,586]

diffExp calculated the differential expression of all BCL6 transcripts collectively and of each variant transcript separately (Appendix). Every BCL6 transcript variant had one of two BCL6 Uniprot accession numbers as a suffix. Most transcript variants were given the suffix P41182, which represented the canonical BCL6 protein. A few were given the suffix A0A0C4DH53, which represented the variant with the short exon 6. Each group included a variety of isoforms with no clear indication of how they were sorted. However, the collective differential expression of each group was very similar.

P41182 BCL6 mRNA expression was upregulated 1.8-fold (adjusted p = 1.49E-2) by acute IR in LN18 cells. A0A0C4DH53 BCL6 mRNA expression was upregulated 1.6-fold by acute IR in LN18 cells however did not reach statistical significance (adjusted p = 9.38E-2). P41182 and A0A0C4DH53 BCL6 mRNA expression was upregulated 1.3-1.4-fold in NZG0906 or NZG1003 cells but without statistical significance.

Differential expression analysis of the different BCL6 transcript variants revealed that Variant 1, the most abundant BCL6 transcript, was upregulated 1.8-fold (adjusted p = 5.05E-2) by acute IR in LN18 cells. Many of the other transcript variants were upregulated between 1.4- and 1.7-fold by acute IR in LN18 cells, however without statistical significance. Slight upregulation of most transcript variants was also seen in the NZG0906 cells, but without statistical significance. There were too few reads mapping to BCL6 for flair diffExp to calculate differential expression of BCL6 transcript variants in the irradiated compared to untreated NZG1003 samples.

In summary, there is evidence that BCL6 mRNA expression and expression of most BCL6 transcript variants was slightly upregulated by acute IR in GBM cell lines. These changes were not statistically significant in most cases, likely due to the variability of the data. However, the aim of the differential expression analysis was to determine whether the *relative abundance* of BCL6 transcript variants was altered in response to acute IR. There was no evidence that this was the case. Therefore, any changes in BCL6 function after acute IR are likely not due to changes to the sequence and structure of the BCL6 protein.

### 6.3.8: BCL6 transcript variants with short exon 6

The expression of the BCL6Δ6 transcript variants in GBM cells was an intriguing finding. Variant 1Δ6 was found in 17 of the 18 GBM cell line samples sequenced with the 3'-end primer. Variant X3Δ6 was found in half of the GBM cell line samples sequenced with the 3'-end primer. These variants were expressed regardless of treatment. Although these Δ6 transcripts were a small proportion of the BCL6 transcripts in the GBM cells analysed, they may have an important role in BCL6 function.

#### 6.3.8.1: Effect of deletion on BCL6Δ6 transcript and protein

The deletion in the Δ6 transcripts causes a frame-shift and introduces a stop-codon at the start of the Δ6 exon (Figure 6.11A and B). Therefore, the proteins resulting from transcript variants 1Δ6 and X3Δ6 would be identical, as the downstream exons are irrelevant to the protein sequence. This BCL6Δ6 protein would be severely truncated. The serine amino acid encoded at the join of exons 5 and 6 would be replaced by an arginine, followed by a serine instead of a glycine (Figure 6.11C and D). Therefore, the BCL6Δ6 protein would be only 55 amino acids long, with a predicted weight of 6.2 kDa.

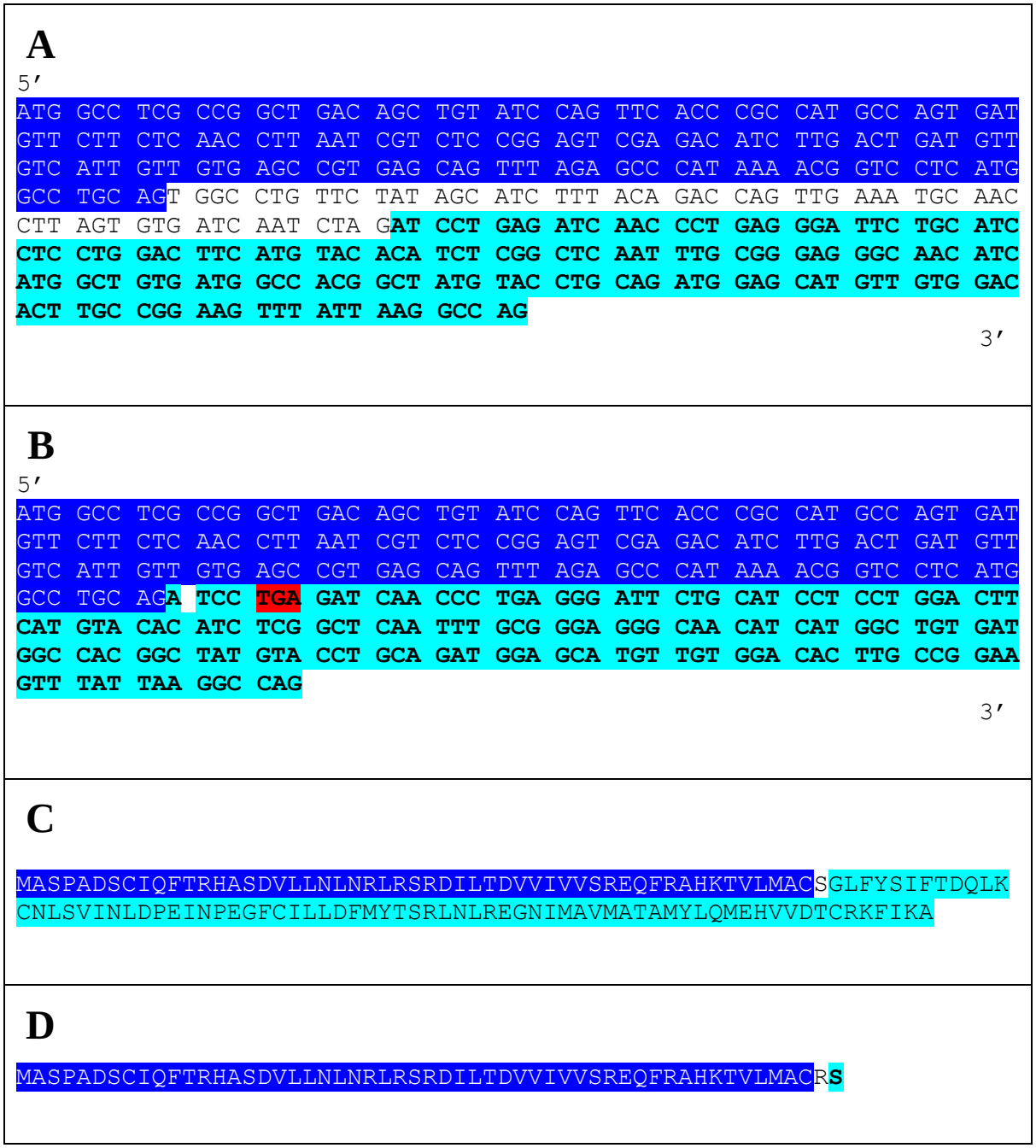


Figure 6.11: Effect of deletion on BCL6Δ6 transcript and protein

A) Base sequence of BCL6 exons 5 (highlighted in dark blue and white font) and 6 from 5' to 3' on the bottom strand of DNA (which encodes BCL6). Region retained in Δ6 transcripts highlighted in light blue and bold font. Reverse complement sequence obtained from UCSC Genome Browser using the View DNA reverse complement function.[326] B) Base sequence of BCL6 exon 5 (highlighted in dark blue and white font) joined to the Δ6 exon (highlighted in light blue and bold font). Premature stop codon highlighted in red. C) Amino acid sequence encoded by BCL6 exons 5 and 6, obtained from UCSC Genome Browser.[326] D) Amino acid sequence encoded by BCL6 exons 5 and Δ6. C&D) Amino acids encoded by exon 5 highlighted in dark blue and white font, amino acids encoded by exon 6 or Δ6 highlighted in light blue and amino acids partly encoded by both exons not highlighted.

### 6.3.8.2: Validation of BCL6Δ6 transcript expression

Expression of the BCL6Δ6 transcript variants was validated by designing primers to amplify the region around the exon 5 to exon 6 junction (Figure 6.13A and B). If both full-length BCL6 and BCL6Δ6 were expressed, there would be two amplification products, one 62 base pairs shorter than the other. The predicted amplification products were 217 base pairs long for the BCL6Δ6 transcript variants and 279 base pairs long for the BCL6 transcript variants with full-length exon 6.

RNA from two replicates each of untreated and irradiated LN18, NZG0906 and NZG1003 samples were reverse-transcribed and an endpoint PCR was carried out (Figure 6.12). As expected, in every sample there was an intense band of approximately 279 base pairs due to the full-length exon 6 present in the majority of BCL6 transcripts. In every sample, there was also a much fainter but distinct band slightly below the intense band. This corresponded to the 217 base pair amplification product expected for the BCL6Δ6 transcript variants.

Both amplification products were extracted from the gel and underwent Sanger sequencing. This confirmed that the longer band was BCL6 with the full-length exon 6, while the shorter band was missing 62 nucleotides of exon 6 as expected (Figure 6.13C and D).

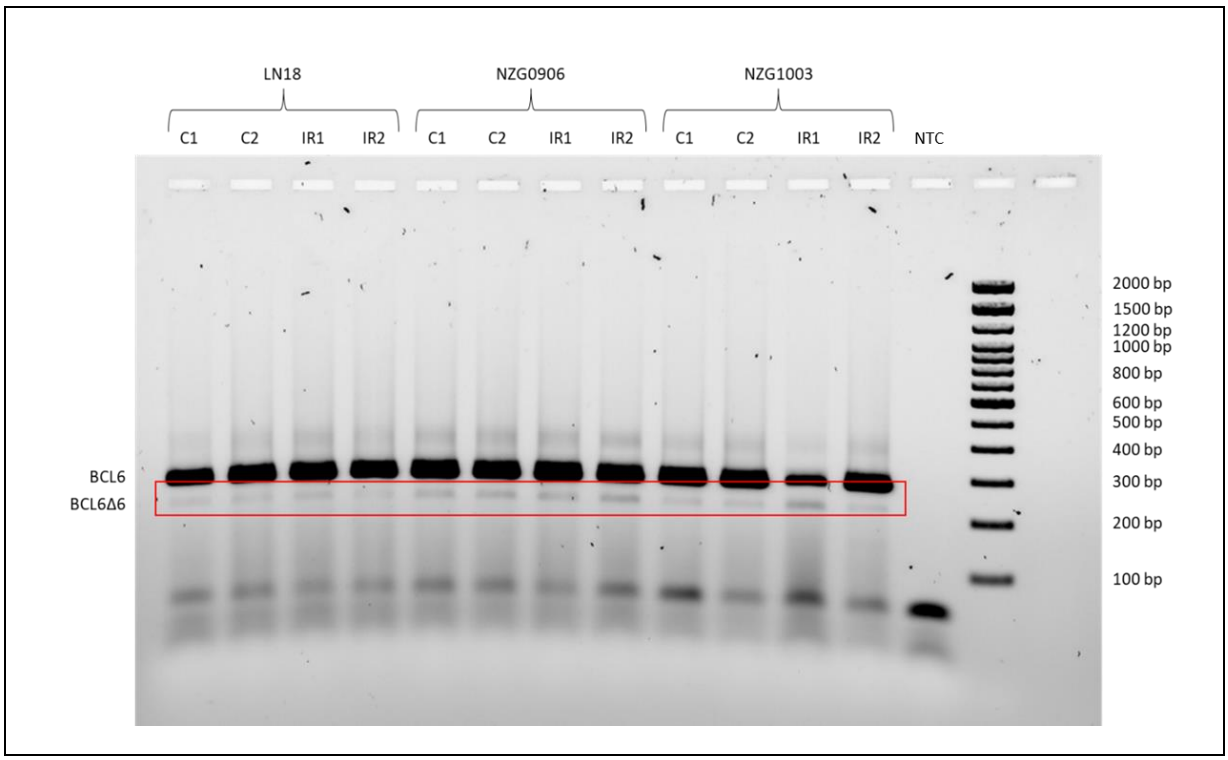


Figure 6.12: Amplification products with primers across BCL6 exon 5 to exon 6 junction

Agarose gel showing base pair lengths of the products of amplification with PCR primers spanning the BCL6 exon 5 to exon 6 junction. PCR amplification performed on cDNA from two untreated (C) and two irradiated (IR) replicates each of LN18, NZG0906 and NZG1003 GBM cell lines. Amplification product from BCL6Δ6 transcript variants indicated by red box. NTC = no template control.

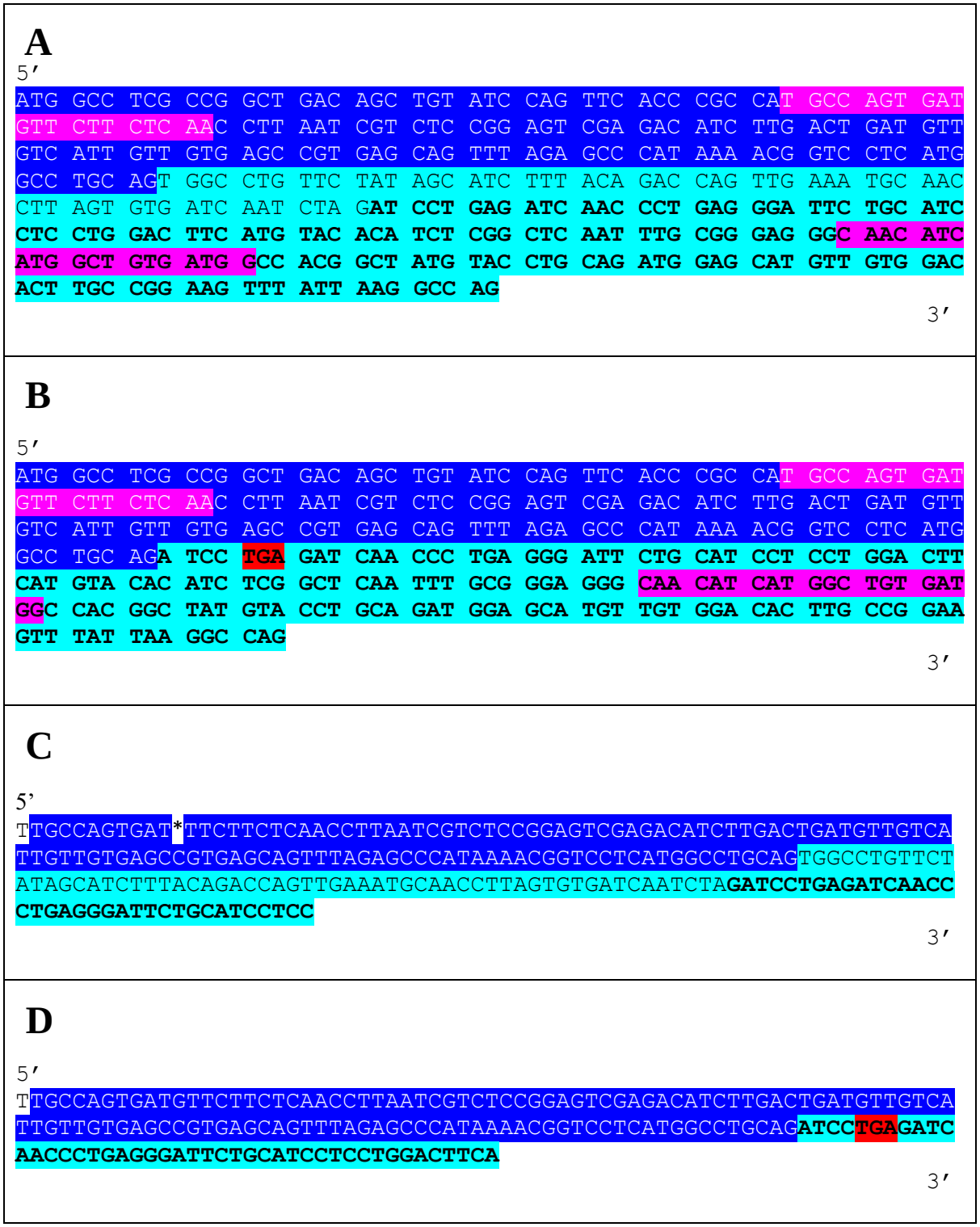


Figure 6.13: Sanger sequencing of BCL6 and BCL6Δ6 PCR products

A-D) BCL6 exon 5 highlighted in dark blue and white font and BCL6 exon 6 highlighted in light blue. Short exon 6 sequence in bold. Premature stop codon highlighted in red. A&B) PCR primers used highlighted in pink. A) Nucleotide sequence of BCL6 exons 5 and 6. B) Nucleotide sequence of BCL6 exon 5 and Δ6. C) Sanger sequencing of longer amplification product. Missing G base present in sequencing of the shorter product (D) indicated with a *. D) Sanger sequencing of shorter amplification product. Sequencing products from the forward primer only are shown for simplicity.

## 6.4: Discussion

### 6.4.1: Use of MinION cDNA sequencing with semi-specific amplification

#### 6.4.1.1: Advantages and disadvantages of ONT MinION sequencing

Chapters 3-5 added to previous research indicating that in response to acute IR, BCL6 loses its transcriptional repressor function.[207,322] After acute IR, BCL6 appeared to interact with different proteins and to promote expression of proteins it canonically suppresses. It was hypothesised that BCL6 transcripts are alternatively spliced in response to therapy, resulting in translation of a BCL6 protein which has lost its transcriptional repressor function and perhaps gained other functions. Therefore, the aim of this chapter was to identify the BCL6 transcript variants present in GBM cells and to determine whether the expression of transcript variants changed with treatment.

Long-read cDNA sequencing enabled the sequencing of full-length BCL6 transcripts. Long-read technologies are superior to short-read sequencing technologies like Illumina for the identification of transcript variants.[587] This is because short-read sequencing requires the assembly of multiple sequence fragments to a reference genome, whereas long-read technologies sequence the intact transcript.[588] Conversely, because long-read sequencing technologies lack the amplification and repeated sequencing of Illumina, they have higher signal-to-noise ratios and therefore much higher error rates.[581,589] These errors mostly consist of indels of single bases.[590] They also have lower throughput, which reduces the accuracy of quantitative analysis.[587] The two major long-read sequencing technologies are available from ONT and Pacific BioSciences. While historically, the former provided lower accuracy results with higher throughput, a recent study showed that ONT devices now produce higher quality, although shorter length, reads than Pacific BioSciences devices.[591] Moreover, ONT devices were better than Pacific BioSciences devices for identifying known gene variants and for quantification of transcript abundance, although worse at identification of alternative splicing events.[591] Additionally, ONT devices and reagents are more affordable than those offered by Pacific BioSciences.[591]

The ONT R9.4 MinION was used for this study. This version of the ONT sequencing technology has a lower error rate (6-15%) than previous versions, however this is still much higher than Illumina (0.1-1%).[581,589] As ONT devices work by feeding a nucleotide molecule through a nanopore and measuring the characteristic disruption to current caused by each base, errors can be introduced due to structural similarities between nucleotides or by homopolymers which confuse the signal.[581,589,592] However, for this study, the suitability of ONT long-read technology for the identification of transcript variants overcame concerns about its high error rates.

Steps were taken during the data processing to reduce the error as much as possible. Basecalling was performed using Guppy version 6.1 set to the high accuracy configuration. Guppy is considered to be the fastest and most accurate basecaller available for long-read sequencing.[581] Additionally, qscore

filtering was used so that only reads above a standard quality threshold were accepted. The FLAIR pipeline which was used to identify transcript variants corrected splice junctions to reference annotations to reduce the error rate.[345] These splice-corrected reads were then grouped by their unique splice junctions and collapsed into one representative transcript variant based on the density of reads starting and ending at the same position.[345] This further mitigates sequencing errors between different reads of the same transcript variant. Transcript variants were filtered out if they did not have at least three supporting reads, further increasing confidence.[345]

#### 6.4.1.2: Success and limitations of semi-specific amplification

BCL6 is a low abundance transcript in GBM cells and whole transcriptome sequencing of GBM cells in the McConnell lab group achieved very low coverage of BCL6. To identify and quantify the BCL6 transcript variants present in GBM cells, it was important to have good coverage of the BCL6 sequence. Therefore, semi-specific amplification was used to enrich for BCL6 transcripts. BCL6 was amplified using a primer specific for the 3' end of BCL6 paired with a universal primer at the 5' end. Repetition of the sequencing with a primer specific for the 5' end of BCL6 with a universal primer at the 3' end meant that these experiments should have captured any BCL6 transcripts which had at least one of the BCL6 primer sequences, thereby capturing almost all possible variants.

Semi-specific amplification with the BCL6-specific 3'-end primer proved successful. q-RT-PCR showed that BCL6 was enriched such that it crossed the threshold 3.4 cycles before HPRT, compared to 6.5 cycles after HPRT in the original sample. Most samples semi-specifically amplified with this primer had more than 500 reads annotated to BCL6, while some had as many as 2500. This enabled the confident identification of the BCL6 transcript variants present in GBM cells, as well as analysis of differential splicing and expression.

Unfortunately, semi-specific amplification with the BCL6-specific 5'-end primer was less successful. q-RT-PCR showed that BCL6 transcripts were enriched using this primer, with BCL6 crossing the threshold 1 cycle before HPRT after amplification. However, the superior enrichment obtained with the 3'-end primer made a large difference to the sequencing results. Most samples semi-specifically amplified with the 5'-end primer had 10-fold fewer reads annotated to BCL6 than the 3'-end primer-amplified samples with the fewest BCL6 reads. There was a strong relationship between the coverage of BCL6 and the number of transcript variants identified. In the GBM RNA samples semi-specifically amplified with the 3'-end primer, between five and 18 transcript variants were identified in each sample. Meanwhile, six transcript variants were identified in one sample amplified with the 5'-end primer, with three or fewer identified in the rest. The data gathered using the 5'-end primer was useful for confirmation of some of the results obtained with the 3'-end primer and to provide some information about the 3'-UTR of the BCL6 transcripts. However, the limitations of the data from the 5'-end primer

experiments meant that only the data obtained using the 3'-end primer was carried forward for further analysis.

While semi-specific amplification enriched BCL6 transcripts sufficiently for them to be sequenced, > 99% of the transcripts sequenced were not annotated to BCL6. Further investigation showed coverage of genes across most of the genome. This suggested that the combination of one specific primer with one universal primer allowed amplification of a wide range of transcripts. However, most genes did not have as much coverage as BCL6, indicating that the enrichment was successful. There were a handful of genes with similar coverage, suggesting that the specific primer likely had some off-target affinity for these transcripts. This explains the intense band at around 6000 base pairs in the 5'-end amplified cDNA, which did not correspond to the expected length of BCL6 transcripts. Therefore, it is possible that the primers could have been further optimised to reduce enrichment for these other transcripts and increase coverage of BCL6. However, the enrichment for BCL6 with the 3'-end primer was sufficient for the purposes of this experiment.

A limitation of the semi-specific amplification results was that it was difficult to determine if the differences seen at the ends of the transcripts were due to genuine differences, degradation, incomplete reverse-transcription or sequencing artifacts. While most of the commonly identified transcripts started in exon 1, the length of exon 1 sequenced varied between 50, 59 and 63 nucleotides. Both UCSC and NCBI genome browsers annotate a BCL6 variant with a 59-nucleotide exon 1.[326,578] The transcripts in which exon 1 was 50 or 63 nucleotides in length could be due to sequencing aberrations, degradation of the 59-nucleotide exon or the longer 316-nucleotide exon 1 annotated by UCSC, or due to genuine variants.

Additionally, it is known that ONT MinION sequencing is unable to read the 5'-end 10-15 nucleotides of nucleotide sequences.[593] The motor protein which drives the nucleotide strand through the nanopore is 10-15 nucleotides from the sensor, so when the strand is released by the motor protein, it passes the sensor too quickly to be read.[593] This should not have caused any loss of BCL6 sequence in the transcripts amplified with the 3'-end primer, as the 22 base pair SSP primer sequence was at the 5' end. However, the loss of 5' nucleotides may explain oddities in the 5'-end of the transcripts sequenced using the 5'-end primer. The 5'-end primer was designed to be complementary to the last 24 bases of exon 4. Interestingly, all BCL6 transcripts sequenced with the 5'-end primer had a 14 base long exon 4, suggesting that 10 nucleotides were lost from the 5'-end of the sequence. A few BCL6 transcripts identified using the 5'-end primer were missing exon 4 all-together and started from exon 5. As these sequences could not have been amplified without exon 4 being present, it is likely that the distance of the motor protein from the sensor resulted in exon 4 being missed entirely in some transcripts and shortened in others. Alternatively, it is possible that some or all of the transcripts sequenced did have a 14 base long exon 4, as a transcript with this variation is annotated to the UCSC Genome Browser.

However, this would necessitate all of the 5'-end bases being read, which goes against findings reported in the literature.[593]

The variation in the apparent transcriptional start sites in exons 3 and 7 was much larger than the variation seen in exon 1, varying by hundreds or thousands of nucleotides compared to less than 15 nucleotides. It seems likely that this variation was due to degradation of the mRNA or incomplete reverse transcription. Alternatively, it is possible that a disruption to sequencing caused the truncation of these reads, as has been previously observed.[593–595] ONT direct RNA and cDNA sequencing tends to produce less coverage of the 5'-ends of transcripts, which are sequenced from 3' to 5', making this a possible explanation for the 5'-end variability.[596] However, the coverage of PCR amplified transcripts tends to be more even, so degradation or incomplete reverse transcription seem more likely explanations.[596]

There was less variation in the 3'-ends of the transcripts sequenced with the 5'-end BCL6-specific primer, with most transcripts having a 3'-UTR of the same length. This is likely because reverse-transcription could only occur if the poly-A tail was present for the VNP sequence to bind to, so any transcripts degraded at the 3' end would not have been reverse-transcribed. Additionally, as reverse-transcription started from the 3'-end, incomplete reverse-transcription would not cause loss of the 3' end of the transcript. Therefore, the few transcripts identified with varying lengths of shorter 3'-UTRs, could be genuine variants.

The difficulty in determining the cause of differences in the 3' and 5' ends of BCL6 transcripts limited the conclusions that could be drawn about variations in the 3'- and 5'-UTRs. Therefore, the technique was more suited to the identification of variants with differences within the transcript, such as exon skipping and alternative splicing, rather than differences in the 3'- and 5' ends of transcripts. As the aim of this chapter was to identify splice variants which could impact the structure of the translated protein, this technique was suitable.

## 6.4.2: BCL6 transcripts in GBM

Three BCL6 transcripts were identified in 17/18 replicates. Two were known BCL6 transcript variants 1 and X3. Variant 1 was the most abundant BCL6 transcript in all untreated and irradiated GBM cell lines tested. This variant encoded the canonical BCL6 protein. Variant X3 was the second most abundant transcript, at an average of 5-fold lower abundance than Variant 1. This transcript was missing exon 9 and therefore would be translated into the known BCL6S protein which is missing two zinc fingers without apparent impact on function.[579,580] The exon-skipping event that resulted in loss of exon 9 occurred at a frequency of about 20% in NZG0906 and NZG1003 cells and about 13% in LN18 cells.

Although expressed at 17-fold lower abundance than Variant 1, Variant 1Δ6 was identified in almost all of the replicates. Furthermore, Variant X3Δ6 was identified in half of the replicates. This alternative splicing event was detected at a frequency of 4.2-10.1% in the GBM cells. If translated, these two transcripts would produce the same severely truncated BCL6 isoform.

The four transcripts discussed so far contained exons 1 and 4-12 or exons 1, 4-8 and 10-12. Therefore, the vast majority of BCL6 transcripts expressed by GBM cells contain the BCL6 auto-regulatory binding sites in exon 1.[251] Exon 1 is commonly lost due to translocation of the BCL6 gene in lymphoma, resulting in deregulation of BCL6 expression.[251] This does not seem to be the case in GBM.

Transcripts containing exon 2 (Variant X1) were identified in 12/18 GBM samples and transcripts containing exon 3 (Variant 2) were identified in 10/18 GBM samples. However, these transcripts were low in abundance and the lengths of exon 3 sequenced varied. As exons 2 and 3 are non-coding, these transcripts would be translated into the canonical BCL6 protein, however their inclusion may affect regulation of transcript stability or translation. Furthermore, transcripts starting at various locations within exon 7 were commonly identified. These were assumed to be due to degradation of the mRNA, incomplete reverse-transcription or sequencing artifacts, however it is possible that BCL6 transcripts starting from exon 7 are expressed in GBM cells. Additionally, skipping of BCL6 exon 5 occurred with an average frequency of 4.5-10.6% in GBM cells. However, transcripts with this exon skipping event were not commonly detected across the replicates.

The results of this chapter indicated that transcripts encoding the canonical BCL6 protein were by far the most abundant BCL6 transcripts in GBM cells. Meanwhile 13-20% of transcripts underwent an exon skipping event that resulted in loss of exon 9, resulting in a functional BCL6 protein missing the first two zinc fingers. Interestingly, an alternative splicing event causing a deletion in BCL6 exon 6 occurred consistently in GBM cells. A couple of other BCL6 transcript variants containing non-coding exons 2 or 3 or missing exon 5 were also expressed at a very low level in GBM.

## 6.4.3: Effect of acute IR on BCL6 transcripts in GBM

### 6.4.3.1: Effect of acute IR on BCL6 expression

Chapters 3-5 suggested that BCL6 protein function 48 hours after acute IR was very different to in untreated GBM cells. Chapter 3 also indicated that BCL6 protein function had changed by 24 hours after acute IR, however the difference was less striking. As there is a time delay between transcription and protein expression, the transcript variants expressed in GBM cells 24 hours after acute IR were investigated.[597]

BCL6 mRNA was upregulated between 1.4 and 1.8-fold after acute IR in all three GBM cell lines. Most of these changes were not statistically significant, likely due to the variability of the data. Although western blot analysis showed that BCL6 protein expression in LN18 cells is upregulated 48 hours after 10 Gy IR (Figure 3.2), the expression detected at 24 hours was too variable to make any confident conclusions. Previous results showed that BCL6 transcript levels 48 hours after 10 Gy IR in LN18 cells were similar to in untreated LN18 cells.[322] Together these results suggest that BCL6 mRNA expression in LN18 cells is increased around 1.5-2-fold 24 hours after 10Gy IR but returns to baseline expression by 48 hours after IR. This appears to correspond to an upregulation of BCL6 protein expression by 48 hours after 10 Gy IR, likely representing the time-delay between increased transcription of BCL6 and translation of those transcripts into BCL6 protein.

### 6.4.3.2: Effect of acute IR on splicing of BCL6 transcripts

Differential splicing and differential expression analysis revealed no changes to the frequency of splicing events or the relative expression of BCL6 transcript variants in irradiated GBM cells compared to untreated GBM cells. This disproved the hypothesis that the altered function of BCL6 after acute IR treatment was due to alternative splicing of the BCL6 transcript. Therefore, the loss of association with transcription coregulators and apparent change in BCL6 location is likely not mediated by changes to the BCL6 protein sequence. Instead, these changes must be controlled by other factors such as post-translational modifications.

## 6.4.4: Speculation on the functional capabilities of BCL6Δ6

Although IR-induced alternative splicing of BCL6 was not observed, the frequent expression of BCL6Δ6 transcript variants in GBM cells was intriguing. While no literature exists around BCL6Δ6, it is annotated as a BCL6 isoform in Uniprot with the accession number A0A0C4DH53 and included in NCBI GenBank as a cDNA clone (DKFZp686M22130) isolated from human uterus tissue, with the accession number BX649185.[331,598] A transcript similar to BCL6Δ6 is also annotated as a BCL6 transcript variant in Ensembl (release 105) with the ID ENST00000419510.6. This transcript is the same as that of BCL6Δ6 except that it starts at exon 3 instead of exon 1. None of these entries include any information about the protein function and the protein sequence seems to be predicted from sequencing of transcripts rather than observed directly.

The Ensembl entry predicts that BCL6Δ6 is degraded by nonsense-mediated decay (NMD). There does not seem to be any literature supporting this, however it is a reasonable prediction due to the introduction of the premature stop codon (PTC) in the BCL6Δ6 sequences. It is well established that when a ribosome reaches a PTC during translation, NMD is triggered, resulting in degradation of the transcript.[599,600] However, there is evidence that when a PTC is in close proximity to the start codon, transcripts can escape NMD.[600–602] Lindeboom et al. (2016) analysed a large human cancer genome dataset and reported a 35% NMD efficiency when PTCs were located within 200 nucleotides of the start codon compared to a 93% NMD efficiency when PTCs were located further away.[600] There were 162 nucleotides between the start codon and the PTC in the BCL6Δ6 transcript variants, so it is possible that it at least partially escapes NMD. A proposed mechanism for NMD escape is translation re-initiation at a start codon downstream of the PTC. The first in-frame start codon downstream of the PTC in the BCL6Δ6 transcript variants is 462 nucleotides downstream, however Lindeboom et al. (2016) showed that the distance did not appear to impact escape from NMD.[600]

Lindeboom et al. (2016) proposed a model which explained 74% of the variance in NMD efficiency, however much is still unknown about why NMD is more efficient for some transcripts with PTCs than others.[600] In a later paper, Lindeboom et al. (2019) found that based on the rules they had defined in their 2016 paper, only 51% of possible PTCs in the human genome are likely to result in efficient NMD.[603] Therefore, it is impossible to predict whether or not the BCL6Δ6 transcript variants are efficiently degraded by NMD.

If the BCL6Δ6 transcript variants escape NMD and are translated in GBM cells, the BCL6Δ6 protein would be unable to bind to DNA due to the absence of the C-terminal zinc-finger region. However, a portion of the N-terminal BTB/POZ domain (circled in Figure 6.14B) would be retained. The predicted structure of the BCL6Δ6 protein, obtained from AlphaFold, is shown in Figure 6.14C.[604,605]

The BTB/POZ domain is involved in both homodimerization of BCL6 proteins and binding to corepressors. Although no detailed data is available for dimerisation of the BCL6 BTB/POZ domain, the similar BTB/POZ domain-containing zinc-finger protein PLZF has been studied in detail.[606] Residues along the length of the PLZF BTB/POZ domain, some of which are conserved in the BCL6 BTB/POZ domain, are involved in homodimerization.[606] It was shown that deletion of 31 residues at the C-terminus of the PLZF BTB/POZ domain abolished homodimerization of the deletion mutants and abolished heterodimerisation of the deletion mutant with the full length BTB/POZ domain.[606] This suggests that BCL6Δ6, which is missing the C-terminal half of the BTB/POZ domain, may be unable to homodimerize or to dimerise with the full-length BCL6 proteins present in GBM cells.

Ahmad et al. (2003) investigated the binding of corepressor NCOR2 to the BCL6 BTB/POZ domain.[215] Figures of interest are reproduced in Figure 6.14. Figure 6.14A shows the crystal structure of the BCL6 BTB/POZ domain homodimer on the left, with monomers indicated in blue and red. On the right of Figure 6.14A, the NCOR2 peptides used to investigate binding of this corepressor to the BCL6 BTB/POZ domain are shown in green and yellow. Figure 6.14B shows the residues of the BCL6 BTB/POZ domain that are buried when interacting with NCOR2. NCOR2 interacts with the β1 and α1 regions of one BCL6 monomer and with the α2, α3 and α6 regions of the other BCL6 monomer. Figure 6.14C shows that the β1 and α1 regions are retained in the predicted structure of BCL6 (circled in red in Figure 6.14B), however the α2, α3 and α6 regions are not.[604,605] Thus, whether or not BCL6Δ6 can bind to NCOR2 depends on whether the interactions with the β1 and α1 regions are sufficient for the interaction to occur. The β1 and α1 regions contain most of the residues which contribute the largest amounts to the buried interface surface, except for histidine-116 (Figure 6.14B). Mutation of histidine-116 to alanine significantly reduced the affinity of the BCL6 BTB/POZ domain for the NCOR2 peptide but did not abolish binding.[215] Hence it is possible that BCL6Δ6 may retain some weakened affinity for NCOR2.

If the β1 and α1 regions in BCL6Δ6 are sufficient for weakened binding to corepressors, homodimerisation, which usually provides the α2, α3 and α6 regions for the rest of the BTB/POZ-corepressor interactions, may not be a requirement. Hence, if transcript variants 1Δ6 and X3Δ6 are not degraded by NMD and are translated into the BCL6Δ6 protein, it is possible that the BCL6Δ6 protein might be able to bind corepressors, although with lower affinity than the full-length protein.

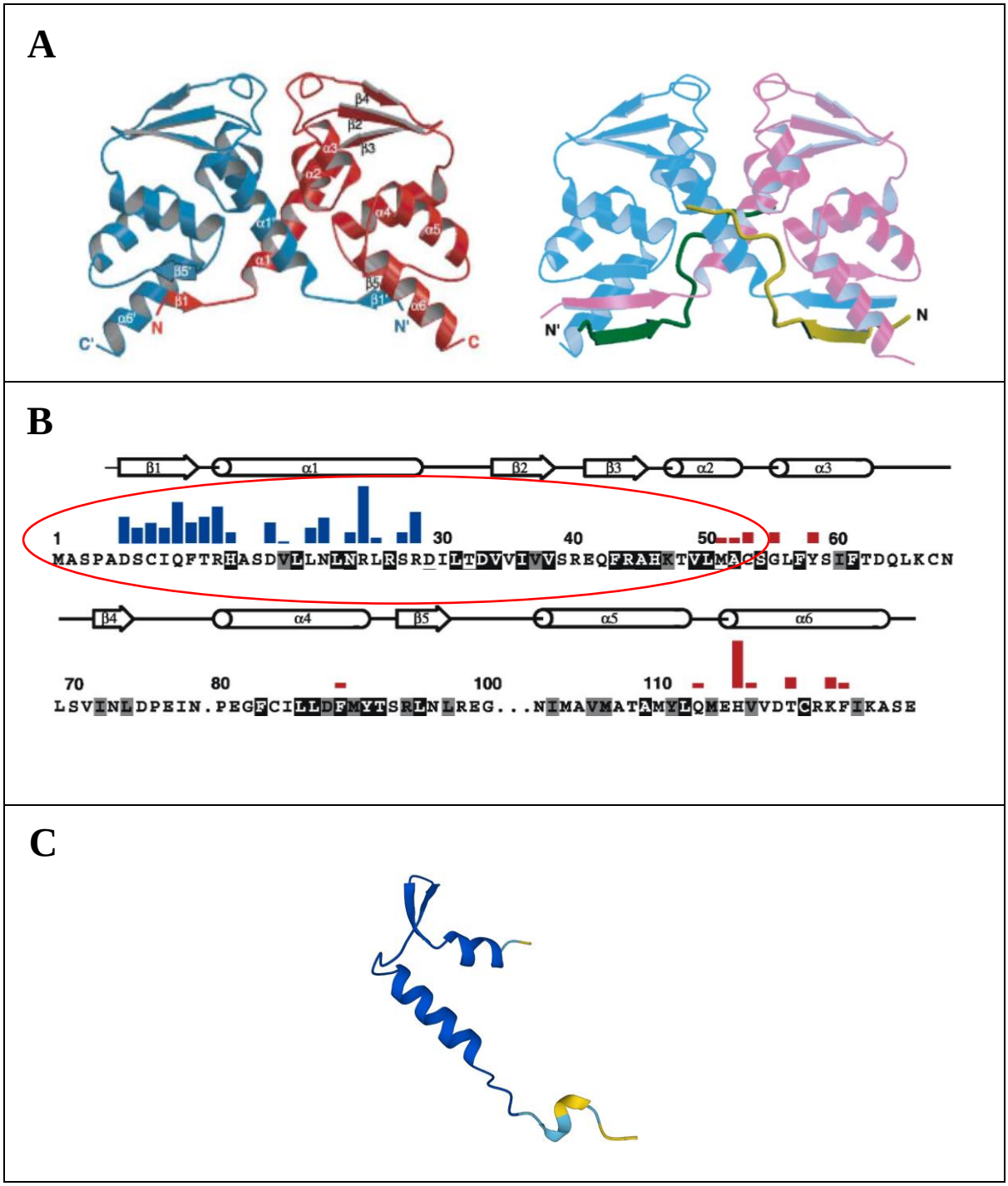


Figure 6.14: Corepressor binding to the BTB domain of BCL6

A) The image on the left shows the crystal structure of the BCL6 BTB domain homodimer (monomers indicated in blue and red). The image on the right shows the crystal structure of the BCL6 BTB domain homodimer bound to two NCOR2 corepressors (NCOR2 peptides indicated in green and yellow). B) BCL6 BTB domain homodimer residue interactions with the yellow NCOR2 peptide shown in (A). BCL6 monomers indicated in blue (corresponding to the blue monomer in (A)) and red (corresponding to the red monomer in (A)). Contribution of each residue to the buried interface surface indicated by the size of the bars. Region of BTB domain retained in BCL6Δ6 circled in red. Figure C) AlphaFold prediction of the structure of the BCL6Δ6 protein.[604,605] A and B reprinted from Molecular Cell, Vol 12, Ahmad et al. Mechanism of SMRT Corepressor Recruitment by the BCL6 BTB Domain, 1551-1564, 2003, with permission from Cell Press.

## 6.4.5: Future directions

The aim of this chapter was to determine which BCL6 transcript variants were expressed in GBM cells and whether the transcript variants expressed changed in response to IR. It was hypothesised that in response to IR, alternative splicing of BCL6 led to the translation of a BCL6 protein with an altered structure and function. BCL6 mRNA expression was slightly upregulated by IR, but the proportion of each transcript variant remained constant, proving this hypothesis false. Therefore, the apparent loss of transcriptional repressor function in BCL6 induced by acute IR cannot be explained by alternative splicing of the BCL6 transcript.

However, the expression of the two BCL6Δ6 transcript variants in GBM is intriguing. As discussed above, if translated, this BCL6Δ6 protein would be unable to bind DNA and would probably be unable to dimerise. However, it is possible that the BCL6Δ6 protein would be able to bind to corepressors, albeit with likely weakened affinity. While only a small proportion of the BCL6 transcripts present in GBM cells contained the Δ6 alternative splicing event, it was consistently identified. Therefore, while likely to be at much lower abundance than the canonical BCL6 protein, if the BCL6Δ6 protein is expressed it may have an important function in GBM cells. For example, if BCL6Δ6 can recruit corepressors, it may compete with BCL6 for corepressor binding and hence modulate BCL6-mediated transcriptional repression.

Consequently, it would be valuable to determine whether the BCL6Δ6 transcripts are translated in GBM cells. Future studies could transfect BCL6Δ6 cDNA into GBM cells and analyse expression by western blot. This method been used previously to show that an alternative splice variant of GFAP expressed in GBM cells is translated into a severely truncated GFAP protein isoform despite the introduction of a PTC.[607] While this truncated protein was larger than the predicted BCL6Δ6 protein (21 kDa compared to 6.2 kDa), this confirms that alternatively spliced transcripts containing PTCs may be translated in GBM cells, even if they produce extremely truncated proteins.[607] If BCL6Δ6 was translated, it would be interesting to investigate its role. This could include assessing the effect of transfected BCL6Δ6 on the response of GBM cells to therapy and determining whether co-transfection of BCL6 and BCL6Δ6 into GBM cells alters the ability of BCL6 to repress transcription of a reporter. Additionally, further experiments could determine whether BCL6Δ6 is commonly expressed in multiple cell types or is GBM-specific.

In summary, the loss of BCL6 transcriptional repressor function in response to acute IR did not appear to be due to alternative splicing of the transcript. This was a valuable finding as it showed that the majority of BCL6 protein expressed in GBM cells is likely to be the canonical protein. Therefore, the apparent changes in BCL6 function in response to acute IR are likely to be due to modulation of the activity of the canonical BCL6 protein. Future studies should focus on investigating post-translational

modifications which may alter the affinity of BCL6 for corepressors and drive its change in function in response to acute IR.

# 7: Discussion

## 7.1: Aims of this thesis

GBM is a deadly disease with no effective treatments. Decades of research have been unable to greatly improve the prognosis of patients due to the robust treatment resistance of GBM tumours. It is likely that the route to improved treatments involves targeting GBM from multiple angles to prevent it from initiating the pathways that lead to resistance. There is evidence that BCL6 is critical in the survival and therapy resistance of GBM cells. Therefore, inhibition of BCL6 could improve the effectiveness of treatments such as IR and TMZ. While it is clear that BCL6 is important in GBM therapy resistance, studies in this area remain sparse and little is understood about the role of BCL6 in this context.

This thesis aimed to clarify the role of BCL6 in the therapy resistance of GBM cells. First, proteomics was used to gain an overview of which GBM cellular responses to treatment were dependent on BCL6 activity (Chapter 3). These results indicated that BCL6 may change its function in response to acute IR treatment. Therefore, more targeted approaches, RIME and validation by PLAs, were used to investigate which proteins BCL6 associates with in irradiated compared to untreated GBM cells (Chapters 4 and 5). This confirmed that BCL6 appeared to change its activity in response to acute IR and gave some indications of the functions of BCL6 in each context. It was hypothesised that alternative splicing of BCL6 may lead to the expression of different BCL6 protein isoforms after IR, resulting in altered BCL6 activity. This hypothesis was investigated and proved false in Chapter 6. Therefore, while the function of BCL6 changes in response to acute IR treatment, these changes are not likely to be due to changes to the structure of the BCL6 protein.

Overall, this thesis successfully established which GBM therapy responses are dependent on BCL6 activity and confirmed previous indications that the role of BCL6 changes in response to acute treatment. This thesis further elucidated how the ‘nano-environment’ of proteins associated with BCL6 may mediate these functional changes and confirmed that these different roles are carried out by the canonical BCL6 protein. These results are discussed in more detail in the next few sections.

## 7.2: The role of BCL6 is context-specific

Previous studies have shown that inhibition of BCL6 in GBM cells and mouse models increased the efficacy of treatments such as IR and TMZ.[207,210] However, these studies used measures such as plating efficiency and tumour growth to assess the consequences of BCL6 inhibition. These studies gave no indication of how BCL6 contributes to the therapy resistance of GBM. Therefore, the first aim of this thesis was to determine how BCL6 inhibition affects the whole proteome response of GBM cells to therapy. Proteomics was chosen over transcriptomics because the analysis of changes in protein

abundance more directly measured the functional changes that occurred in response to treatment and BCL6 inhibition.

### 7.2.1 LN18 GBM cells have distinct responses to different treatments

A handful of previous studies investigated the effects of IR and TMZ on the whole proteome of GBM cells.[608–613] However, these studies often used supra-physiological doses and only looked at the effect of one treatment.[608–613] As far as could be ascertained, this thesis is the first study to compare the whole proteome response of a GBM cell line to multiple treatments, including two given at clinically relevant doses. This revealed the striking differences in the responses of LN18 GBM cells to fractionated IR, TMZ, acute IR and doxorubicin.

The three acute treatments, acute IR 24 and 48 hours and doxorubicin, all induced recognisable components of the integrated stress response.[418] These included downregulation of ribosome biogenesis and mRNA processing proteins, indicating a global reduction in protein synthesis, and upregulation of ER and mitochondrial transport proteins. Acute IR also caused upregulation of mitotic proteins, indicating arrest at G2/M, while doxorubicin had a much larger effect on downregulation of ribosome biogenesis than acute IR. Additionally, the comparison of the proteome response at 24 and 48 hours after acute IR demonstrated the progression of the cellular response to IR. This revealed that by 48 hours after acute IR, a network of stress response signalling proteins, including p53, AKT1, NFκB1, AMPK and cell cycle checkpoint signalling, was upregulated and autophagy had been induced.

Similarly, TMZ treatment of LN18 cells resulted in downregulation of ribosome biogenesis and mRNA processing, as well as downregulation of protein trafficking and degradation, suggesting a reduction in protein turnover. Although not as obvious as with acute IR, there were indications that TMZ induced G2/M arrest. Interestingly, a handful of telomere maintenance proteins were upregulated by TMZ, linking to the known role of telomere proteins in promoting DNA repair and cell cycle arrest in TMZ-resistant cells.[433–435]

In contrast to the other treatments, fractionated IR led to upregulation of translation and downregulation of cell cycle proteins from multiple phases. Fractionated IR also caused LN18 cells to upregulate protein trafficking. Most strikingly, LN18 cells downregulated DNA damage repair in response to fractionated IR. This indicated that in response to fractionated IR, LN18 GBM cells decreased but did not arrest proliferation, inhibited the DNA damage response and upregulated protein turnover. This is a surprising response to a DNA damaging therapy. Upregulation of the DNA damage response has typically been linked to GBM resistance to IR treatment.[93,94] However, these results suggest that at a clinically relevant dose of IR, the DNA damage response is suppressed. This may indicate that masking the DNA damage to avoid cell cycle arrest and apoptosis is favoured in response to this low dose, long-term stress.

### 7.2.2 BCL6 inhibition does not induce de-repression of known BCL6 target genes in LN18 GBM cells

The small molecule BCL6 inhibitor FX1 was used to suppress BCL6 activity. FX1 was designed to bind to the corepressor recruitment site in the lateral groove of the BCL6 BTB domain.[295] Blocking the lateral groove prevents recruitment of important BCL6 corepressors such as BCOR, NCOR1 and NCOR2 and has been shown to cause de-repression of BCL6 target genes in lymphoma and breast cancer.[228,295] However, the differential expression of proteins in response to FX1 treatment of LN18 GBM cells did not indicate de-repression of known BCL6 target genes. This was not unexpected as BCL6 has been shown to have diverse roles in different contexts, including in different immune cells, in neurogenesis and in different cancer types (see section 1.2). There are suggestions that these varying roles may be mediated by changes in chromatin modification and corepressor recruitment.[258,260,273,307]

The main effects of FX1 treatment of LN18 GBM cells were reminiscent of the responses to the acute treatments (10 Gy IR and doxorubicin). Specifically, FX1 also caused upregulation of mitochondrial and protein transport proteins and downregulation of mRNA processing. Unlike the acute treatments, FX1 treatment did not downregulate ribosome biogenesis, suggesting that there are some differences between BCL6 inhibition and acute treatment stress. However, the similarities may indicate that the inhibition of BCL6 has a similar effect to an acute environmental stress. BCL6 is an evolutionarily conserved stress response protein and appears to be particularly important in adaptation to long-term stress.[406] Cancer cells, including in GBM, are under substantial stress due to their rapid proliferation rate, oncogene expression and altered metabolism.[406] Additionally, BCL6 inhibition reduces the viability of untreated GBM cells and BCL6 knockout renders GBM cells completely non-viable.[207,209–211] This may suggest that BCL6 is critical for the suppression of cellular responses to the basal level of stress that GBM cells are under. Therefore, the inhibition of BCL6 releases this suppression, causing the GBM cells to react to BCL6 inhibition as an acute stress. Inhibition of BCL6 also downregulated microtubule-related proteins, many of which were involved in cell division. This may indicate that BCL6 activity in untreated LN18 GBM cells suppresses stress responses to allow the cells to continue to proliferate.

As discussed in Chapter 3, the effects of FX1 must be treated with some caution. While FX1 is generally considered to be a BCL6-selective inhibitor, further literature review after completion of this study found evidence that FX1 may affect other proteins.[23] Therefore, some of the responses of LN18 cells to FX1 could be explained by off-target effects. This limitation must be kept in mind. However, in the absence of a feasible knockout control, the use of a BCL6 inhibitor was useful to gain a broad overview of the role of BCL6 in the therapy response of GBM cells.[207] Future studies should validate these experiments with an alternative BCL6 inhibitor to determine which effects are BCL6-specific. Later

experiments in this thesis investigated BCL6 activity more directly to avoid all conclusions being dependent on the specificity of FX1.

### 7.2.3 BCL6 has context-specific roles in the distinct responses of LN18 GBM cells to different treatments

Given the known tendency of BCL6 to alter its role in different cell contexts, it was unsurprising that BCL6 appeared to have different functions in the response of LN18 cells to each treatment. Activity reminiscent of the canonical role of BCL6 was only observed in response to fractionated IR. Canonically, in GC B cells, BCL6 suppresses DNA damage response signalling to allow GC B cells to proliferate and undergo somatic hypermutation without triggering cell cycle arrest and apoptosis.[232–234] Similarly, the suppression of the DNA damage response to fractionated IR was dependent on BCL6 activity. Interestingly, fractionated IR was also the only treatment not to upregulate BCL6 expression according to western blot analysis. This suggests that BCL6 is already abundant enough in LN18 GBM cells to mediate the suppression of DNA damage signalling in response to IR.

Contrastingly, the other treatments investigated all upregulated BCL6 expression. In TMZ-treated cells, BCL6 was involved in most aspects of the whole proteome response, including downregulation of protein turnover and upregulation of chromatin modification, transcriptional regulation and a handful of spindle-assembly checkpoint proteins. Most importantly, the upregulation of telomere-maintenance proteins, indicative of the promotion of DNA repair and TMZ resistance, was dependent on BCL6 activity.[433–435] This suggests that in response to TMZ treatment, BCL6 promotes DNA repair and cell cycle checkpoint signalling and inhibits proliferation and protein turnover. Similarly, at 24 hours after acute IR, the upregulation of a handful of proteins involved in DNA repair was dependent on BCL6. By 48 hours after acute IR, BCL6 was required for the induction of a network of stress response signalling proteins, including p53, AKT1, NFκB1, AMPK-γ1 and cell cycle checkpoint proteins. BCL6 represses p53 and NFκB signalling in GC B cells and lymphoma, so this indicated a complete reversal of BCL6 activity in the response of LN18 GBM cells to acute IR.[232–234]

Again, it must be kept in mind that some of the treatment responses considered ‘BCL6-dependent’ by this study may be due to off-target effects of FX1. However, the apparent switch in BCL6 activity from repression of the DNA damage response to promotion of stress response signalling fits with previous evidence that BCL6 may switch from a transcriptional repressor to a transcriptional activator in response to acute IR or doxorubicin treatment of GBM cells.[207] BCL6 did not appear to be greatly involved in the response of LN18 cells 24 hours after doxorubicin treatment. However, Fabre et al. (2020) observed the potential transcriptional activator function of BCL6 48 hours after doxorubicin

treatment.[207] Therefore, it would be worth investigating the role of BCL6 in the response of LN18 cells 48 hours after doxorubicin treatment in future work.

BCL6 is known to be important in adaptation to long-term stress.[406] This was demonstrated by the importance of BCL6 in the response of LN18 GBM cells to fractionated IR and TMZ. However, the role of BCL6 in the response of LN18 cells to acute IR suggests that BCL6 is also important for responding to single dose, high levels of stress, but that its role in these responses may be different. The subsequent chapters of this thesis investigated this change in BCL6 function in more detail.

## 7.3: The role of BCL6 changes in response to acute irradiation

The activity of BCL6 is mediated by the recruitment of corepressors.[215,217–222] It has been demonstrated that BCL6 may target different genes depending on which corepressors it is bound to.[221,228,260,273] Therefore, it is possible that BCL6 recruits alternative binding partners in response to acute IR treatment and that this enables it to change its activity. Chapter 4 used RIME to investigate which proteins BCL6 associated with in GBM cells treated with acute IR (48 hours) compared to in untreated GBM cells. While the number of treatments investigated limited the whole proteome analysis to one GBM cell line, RIME for BCL6 was performed in triplicate in three GBM cell lines and only the proteins commonly found associated with BCL6 were considered. This increased the likelihood that the results were applicable to GBM more generally. Additionally, the possible off-target effects of FX1 were not a factor in the RIME study. However, the RIME analysis did rely upon the specificity of the BCL6 antibody, which was not guaranteed. Nevertheless, BCL6 was the only protein identified in every experimental replicate and in none of the control replicates, indicating that the BCL6 antibody was at least more selective for BCL6 than for any other protein.

### 7.3.1: BCL6 loses its transcriptional regulatory function in response to irradiation

RIME demonstrated that the proteins associated with BCL6 were very different 48 hours after acute IR than in untreated GBM cells. In untreated GBM cells, BCL6 associated with far more nuclear proteins than after IR. These nuclear proteins included known BCL6 corepressor NCOR2 and NCOR complex component TBL1XR1.[450] Additionally, BCL6 was associated with two Polycomb group proteins, RNF2 and PHC2, transcriptional activator of NOTCH signalling MAML2, coactivator of NFκB transcriptional activity PIR, and multifunctional transcriptional coregulator NCOA5.[463,466–468,480,493] NCOR2 was associated with BCL6 in six untreated GBM replicates and three irradiated GBM replicates, suggesting that BCL6 may bind to this corepressor under both untreated and irradiated conditions. However, the association of BCL6 with NCOR2 was significantly downregulated by IR in

LN18 cells and was downregulated without reaching statistical significance in NZG0906 cells. Furthermore, association of BCL6 with the other six transcriptional regulators identified was only observed in untreated GBM cells. This and the decreased association of BCL6 with nuclear proteins in general after IR suggests that BCL6 loses or reduces its role in transcription in response to acute IR. PLA validation experiments supported the association between BCL6 and NCOR2 in untreated LN18 and NZG0906 GBM cells. The interaction could not be confidently validated in irradiated GBM cells and the interaction signal was significantly decreased in response to irradiation in NZG0906 cells, further supporting the idea that BCL6 loses its transcriptional activity in response to acute IR.

### 7.3.2: BCL6 may associate with AMPK in GBM and other cell types

Regardless of treatment, BCL6 in GBM cells was associated with two E3 ubiquitin-protein ligase proteins, FBXO11 and TRIM47, and two subunits of AMPK.[255,500] FBXO11 is known to mediate ubiquitination and degradation of BCL6 and TRIM47 is likely also involved in BCL6 regulation.[255] AMPK is a master regulator of the cellular response to metabolic stress.[375] AMPK is known to indirectly upregulate BCL6 expression and Chapter 3 revealed BCL6-dependent upregulation of AMPK-γ1 in response to acute IR in LN18 cells.[516–518,521] This suggests the possibility of a positive feedback loop between BCL6 and AMPK during cellular stress responses. Despite these indirect interactions, no previous literature has found a physical association between BCL6 and AMPK. Notably, this interaction was also identified by RIME in the Raji lymphoma cell line, so it is not specific to GBM cells. It is possible that BCL6 associates with AMPK in multiple cell types but that the interaction is transient and so was captured by RIME but not by traditional immunoprecipitation methods, which only capture strong interactions.

It may be that AMPK transiently interacts with BCL6 to phosphorylate it. Phosphorylation of the PEST domains of BCL6 by MAP kinases is known to target BCL6 for degradation.[214] It is possible that AMPK induces upregulation of BCL6 expression but is part of a regulatory feedback loop to control BCL6 abundance. Phosphorylation of the BCL6 PEST domains by AMPK may even recruit FBXO11 and TRIM47 to ubiquitinate BCL6. Alternatively, it is possible that AMPK could phosphorylate a different part of the BCL6 protein, leading to activation or some other modification of function. As both BCL6 and AMPK are known to be stress response proteins, this link between them may be an important part of stress response signalling that has so far been missed. In Chapter 5, validation of the association between BCL6 and AMPK was attempted in a preliminary study. While the background signal was too high to detect association in untreated LN18 GBM cells, there were indications that BCL6 and AMPK may be associated in irradiated LN18 GBM cells. While this validation was only tentative, the association of BCL6 and AMPK is an exciting area for future investigation.

### 7.3.3: BCL6 associates with plasma membrane proteins after irradiation

The association of BCL6 with plasma membrane proteins was only observed after acute IR. These plasma membrane proteins included proteins involved in exocytosis, particularly related to synaptic transmission, and caveolae proteins. The association of BCL6 with synaptic signalling membrane proteins was significantly upregulated by IR in LN18 cells. Strangely, immunofluorescence staining of LN18 GBM cells did not detect relocation of BCL6 to the plasma membrane. Instead, BCL6 remained concentrated around the periphery of the nucleus. However, it was notable that the level of BCL6 signal was lower in irradiated compared to untreated LN18 cells, despite western blots showing that BCL6 protein expression is strongly upregulated 48 hours after 10 Gy IR. It is possible that something about the localisation or activity of BCL6 after IR prevented the monoclonal antibody used for the immunofluorescence staining from binding to BCL6. Although the epitope sequence is proprietary, Santa-Cruz Biotechnology Inc. state that the anti-BCL6 antibody used in Chapter 5 of this thesis binds to the N-terminus of BCL6.[614] Therefore, it is conceivable that the epitope could be blocked in irradiated cells due to BCL6 binding to different proteins via its N-terminus BTB domain. The antibody used for RIME was polyclonal and so was less likely have this problem. Therefore, while BCL6 may be associated with the plasma membrane in irradiated cells as indicated by RIME, this may not have been detected in the microscopy experiments.

The apparent localisation of BCL6 with exocytic machinery at the plasma membrane has intriguing implications. IR is known to increase EV release from GBM cells.[552] In GBM and other cancers, IR-induced EVs are taken up by surrounding cancer cells, where they induce bystander effects such as activation of DNA repair pathways, stress signalling and migration.[552–555] Therefore, it is possible that BCL6 is secreted in EVs in response to acute IR treatment to transmit stress responses important for cell survival to surrounding GBM cells. It is also possible that BCL6 has another function at the plasma membrane, such as regulation of the exo- or endocytosis of signalling receptors. This could mediate the BCL6-dependent upregulation of AKT and NFκB signalling pathways in response to acute IR. Alternatively, as the whole proteomics analysis revealed that autophagy is induced by 48 hours after acute IR, it is also possible that BCL6 is caught up in autophagic vesicles with plasma membrane proteins rather than localising to the plasma membrane itself.

### 7.3.4: RIME results support the irradiation-induced changes to BCL6 function indicated by the whole proteome response

The RIME experiments confirmed previous indications that BCL6 does not behave as a transcriptional repressor 48 hours after acute IR.[207] The loss of association with nuclear proteins including transcriptional regulators explains the observation that BCL6 does not suppress the DNA damage

response 48 hours after acute IR as it does canonically and in response to fractionated IR in LN18 GBM cells. However, the previous study suggested that rather than only losing transcriptional repressor activity, BCL6 in irradiated GBM cells may behave as a transcriptional activator.[207] Therefore, it was anticipated that BCL6 may lose association with transcriptional corepressors and gain association with transcriptional coactivators. However, BCL6 was associated with both transcriptional corepressor and transcriptional coactivator proteins in untreated LN18 GBM cells. This suggested that BCL6 could behave as both an activator and a repressor of transcription in GBM cells, as has previously been suggested in both GBM and breast cancer.[209,307] However, in response to IR, BCL6 seemed to desert its transcriptional regulator function rather than gaining transcriptional activation activity.

The whole proteome analysis indicated that BCL6 switched to a promotor of stress response signalling in response to acute IR. It is possible that BCL6 upregulated these stress response signalling proteins indirectly rather than acting as a transcriptional activator itself. BCL6 may block the activity of other transcription factors in untreated GBM cells, as it does in macrophages and neurogenesis.[259,269,272,273] This could occur independently of the BTB domain, as has been observed in macrophages, perhaps explaining why FX1 treatment did not cause upregulation of these stress signalling proteins in untreated GBM cells.

The RIME data showed that BCL6 was associated with Notch and NFκB pathway transcriptional coactivators MAML2 and PIR in untreated GBM cells. This may indicate that BCL6 blocks transcriptional activation mediated by these coactivators in untreated GBM. Future work could further elucidate these interactions by comparing the ChIP profiles of BCL6, MAML2 and PIR in GBM cells to determine which genes may be regulated by these interactions. BCL6 lost association with the coactivators after acute IR, suggesting that it may have released its inhibition of transcription. Therefore, the upregulation of stress response signalling in response to acute IR may be due to BCL6 export from the nucleus to prevent it from blocking transcriptional activation of these genes. The upregulation of stress response signalling appeared to be dependent on BCL6 activity, as it was not observed when BCL6 was inhibited with FX1. This suggests that BCL6 actively promotes expression of these signalling proteins rather than simply being unable to suppress them. However, it is possible that the interaction of proteins with the BTB domain is required for removal of BCL6 from the nucleus. For example, the association of BCL6 with stress-responsive, pro-apoptotic kinase STK4 was increased after acute IR in LN18 and NZG0906 cells.[615] It is possible that an interaction with this or another protein leads to release of BCL6 from DNA, preventing it from repressing stress response pathways. This could explain why the upregulation of these stress signalling pathways was inhibited by blockage of the BTB domain.

Immunofluorescence microscopy indicated that BCL6 remained at the periphery of the nucleus after acute IR, however the decrease in BCL6 signal intensity conflicted with the upregulation of BCL6

observed by western blot analysis. Additionally, the RIME results showed that BCL6 lost its association with nuclear proteins and instead associated with plasma membrane proteins after acute IR. Together this suggested that not all of the BCL6 present in irradiated LN18 cells was successfully stained with the monoclonal antibody used. Future work will need to confirm whether BCL6 is exported from the nucleus, as suggested by the RIME results. If this is the case, it is possible that once exported from the nucleus, BCL6 may be taken up by autophagosomes for degradation, perhaps explaining its association with cell membrane proteins. However, upregulation of BCL6 protein expression has been observed in response to therapy.[207] It seems unlikely that GBM cells would upregulate BCL6 expression in response to acute IR but then export it to the cytoplasm for degradation. Nevertheless, it is possible that cytoplasmic BCL6 is more easily extracted for western blot analysis than nuclear BCL6, leading to the apparent increase in expression.

Therefore, it is possible that the upregulation of stress response signalling proteins 48 hours after acute IR is mediated by lack of BCL6 activity rather than by an IR-induced change in BCL6 activity. However, this explanation does not explain the apparent increase in the transcriptional activity of the BCL6 DNA binding motif in the luciferase assays performed in treated GBM cells.[207] While this activation was not statistically significant, it was striking and consistent between IR and doxorubicin treatments. It is possible that another transcriptional activator is able to bind to the BCL6 binding motif in its absence, perhaps explaining this observation.

It is also possible that rather than simply being unable to repress transcription after acute IR, BCL6 actively promotes upregulation of stress response signalling proteins. After IR, BCL6 was associated with ubiquitin-binding protein UBXN1. UBXN1 suppresses NFκB signalling by sequestering cellular inhibitors of apoptosis proteins (cIAPs) to inhibit TNFα signalling and by sequestering CUL1 to prevent the degradation of NFKBIA.[616,617] If BCL6 association with UBXN1 disrupts the sequestering of these proteins, this could lead to activation of NFκB signalling. NFκB targets a wide variety of genes and release of NFκB inhibition could conceivably be the mechanism by which BCL6 upregulates stress response signalling.[618] It is also possible that the association of BCL6 with plasma membrane proteins could indicate BCL6 involvement in plasma membrane functions such as exo- or endocytosis of signalling receptors, which may indirectly lead to upregulation of stress response signalling proteins.

Alternatively, it is possible that FX1 inhibits the upregulation of stress response signalling after acute IR through off-target effects. For example, CK2, which is known to be targeted by FX1, is involved in activation of these signalling pathways, although via phosphorylation rather than transcriptional activation.[417,619–621] Nevertheless, CK2 phosphorylates many proteins which themselves lead to transcriptional regulation and so could be responsible for the observed upregulation of stress response signalling proteins.[48–50] Validation of the whole proteome analysis results with an alternative BCL6

inhibitor would determine whether the upregulation of stress response signalling 48 hours after IR is dependent on the activity of BCL6. This will be a priority for future research.

## 7.4 The changes in BCL6 activity are not due to expression of BCL6 variants

The whole proteome and RIME results added to previous research showing that the role of BCL6 changes in response to acute IR in GBM cells. The RIME results confirmed that this is mediated at least in part by which proteins BCL6 associates with after IR. This change in protein-protein associations could be caused by multiple factors. The corepressor proteins that BCL6 binds to in untreated GBM may be downregulated by IR so that BCL6 can no longer bind to them. Meanwhile, other proteins which also have affinity for BCL6 may be upregulated and so replace the corepressors as BCL6 binding partners. RNF2 was downregulated 48 hours after acute IR, so this could explain the loss of this association. However, NCOR2, TBLXR1, PIR and NCOA5 had no change in abundance 48 hours after IR. Therefore, the loss of BCL6 association with these transcriptional regulator proteins must be mediated by factors other than abundance. Similarly, the synaptic and caveolae proteins which were found in the whole proteome analysis did not change in abundance, suggesting that their increased association with BCL6 was not mediated by abundance.

The RIME results suggested that BCL6 is exported from the nucleus after IR, although immunofluorescence staining showed that at least some BCL6 remained around the periphery of the nucleus. This change in location could also mediate the loss of transcriptional coregulator binding. Post-translational modifications of BCL6 or its corepressors could mediate the dissociation of BCL6 from its corepressors and its export from the nucleus. Alternatively, it is possible that the sequence of the BCL6 protein may change in response to IR, leading to changes in protein structure and interactions with different proteins. A previous study found that BCL6 was strongly upregulated by 10 Gy acute IR and did not act as a transcriptional repressor, whereas exogenous overexpression of BCL6 in untreated GBM cells did repress transcription.[207] Therefore, it was hypothesised that when BCL6 expression is upregulated in response to acute IR, the BCL6 transcript is alternatively spliced. This could lead to expression of a BCL6 variant or variants which do not bind to corepressors and therefore do not act as transcriptional repressors.

### 7.4.1: Alternative splicing of the BCL6 transcript does occur in GBM cells

Targeted long-read transcript sequencing in Chapter 6 revealed that several BCL6 transcript variants are expressed in GBM cells. The vast majority of BCL6 transcripts encoded the canonical BCL6 protein. These included the most abundant BCL6 transcript, containing exons 1 and 4-12, as well as far lower

abundance transcripts starting in non-coding exons 2 or 3 instead of 1. Transcripts missing exon 9, resulting in expression of BCL6 protein missing the first two zinc fingers (BCL6S) were also relatively abundant. This protein is thought to have the same function as BCL6 but has not been thoroughly investigated.[579] Additionally, GBM cells expressed BCL6 transcripts with a deletion of the first 62 bases of exon 6. The expression of these BCL6Δ6 variant transcripts was verified. As discussed in Chapter 6, this deletion leads to the introduction of a premature stop codon, which may cause the alternatively spliced transcript to undergo nonsense-mediated decay. However, this transcript variant was identified in almost all replicates, suggesting that it is a regularly produced transcript and could have a biological function. If this transcript was translated, it would produce a severely truncated BCL6 protein variant, containing only the N-terminal of the BTB domain. The possible functions of this truncated BCL6 protein are uncertain. It is possible that the BCL6Δ6 protein could bind to corepressors but not DNA, perhaps inhibiting the function of canonical BCL6. However, further research is needed to confirm whether this protein variant is expressed and to examine its function.

### 7.4.2: BCL6 is not alternatively spliced in response to irradiation in GBM cells

Despite the range of BCL6 transcript variants identified in GBM cells, there was no differential expression of the variants in response to acute IR. This discounts alternative splicing as a mechanism of BCL6 functional modulation in response to acute IR. While a negative result, this is a very useful finding as it directs future research towards investigating post-translational modifications to the canonical BCL6 protein or its binding partners in response to acute IR.

## 7.5: Outlook

This thesis successfully answered the questions it set out to investigate. However, the findings open up avenues of future research to further clarify the role of BCL6 in the therapy response of GBM.

### 7.5.1: Validation of results

All of the experiments in this thesis were carried out in GBM cell lines. This has inherent limitations as cell lines cannot accurately model the complex three-dimensional environment of a tumour. However, cell line studies were a cost-effective way to investigate the whole proteome response of GBM cells to multiple therapies with and without BCL6 inhibition. This large dataset can now be used to generate hypotheses into the role of BCL6 in the therapy resistance of GBM. It is important that the interesting results are validated in other GBM cell lines and in cells derived from primary tumour material. Further

investigation in appropriate mouse models of GBM would validate the effects of BCL6 inhibition on therapy response *in vivo*.

The apparent switch in the activity of BCL6 in response to acute IR meant that the RIME experiments prioritised the comparison of untreated GBM cells to GBM cells 48 hours after acute IR. The selection of one treatment meant that the RIME experiments could be repeated in three GBM cell lines, including two low passage, patient-derived cell lines. The use of cell lines was also critical for the RIME experiments, as the low abundance of BCL6 meant that the cell numbers required were far above what could be achieved with mouse or patient tissue. Preliminary validation of the RIME results was carried out using PLAs in LN18 cells. The PLA experiments supported the interaction of BCL6 and NCOR2 in untreated LN18 cells and also corroborated the observation that this interaction appeared to be reduced after acute IR. Validation of the interaction between BCL6 and AMPK was less successful but was tentatively supportive in the irradiated LN18 cells. The main problem with the PLA experiments was the high level of non-specific signal. More replicates are required to more confidently determine whether the co-localisation of BCL6 and AMPK rises above the background signal. Future work should also repeat the validation of the association of BCL6 with AMPK in other GBM cell lines to increase the applicability of the results. Furthermore, the identification of AMPK as a BCL6-associated protein in Raji cells suggested that this interaction may not be unique to GBM cells. Therefore, future work should validate and explore the implications of this interaction in other cell types.

The targeted BCL6 transcript sequencing indicated that future research should focus on modifications to the BCL6 protein, rather than on the alternative splicing of BCL6. However, although not differentially expressed in response to IR, the identification of the BCL6Δ6 variant was intriguing and warrants follow up studies.

### 7.5.2: BCL6 as a stress response protein

BCL6 has been identified as an evolutionarily conserved stress response protein.[406] BCL6 is canonically associated with repression of cellular stress responses and differentiation in GC B cells, to allow the GC reaction to occur.[232–234] BCL6 is also important in the suppression of differentiation and of inflammatory phenotypes in $T_{FH}$ cells, $T_{regs}$ and macrophages.[256,258,259,266] In the context of stress response, the upregulation of BCL6 expression in multiple types of cancer is not surprising. Cancer cells have inherently stressful cellular environments due to their high rates of proliferation, mutational burdens and altered metabolism.[406] Inhibition of BCL6 has been shown to increase the efficacy of stress-inducing treatments in multiple cancer types.[207,295,311,406] Therefore, evidence is mounting for a critical, widespread role for BCL6 in cellular stress responses.

BCL6 appears to retain its canonical role as a repressor of differentiation and the DNA damage response in lymphoma and leukaemia.[228,302–305] However, BCL6 binds to a very different set of genes in breast cancer, suggesting that BCL6 does not have the same function in every cell type.[307] This thesis demonstrates that the role of BCL6 in the stress response may be dynamic and may alter depending on the type or level of stress. BCL6 appeared to repress DNA damage repair in response to fractioned IR treatment of LN18 GBM cells. However, when BCL6 was upregulated by treatments such as acute IR and TMZ, it appeared to switch to promoting stress response signalling and pathways which promote DNA damage repair. This change was most striking 48 hours after acute IR treatment. Stress response signalling pathways such as p53 and NFκB, which are downregulated by BCL6 in other cancers and GC B cells, appeared to be dependent on BCL6 for upregulation 48 hours after acute IR treatment of GBM cells. RIME experiments confirmed that BCL6 associated with different proteins in untreated and irradiated GBM cells. This raises the question of whether BCL6 plays a different role in the response to acute, high levels of stress than it does in adaptation to long-term stress. The suppression of the DNA damage response may be beneficial to cancer cells when it enables them to continue to proliferate rather than undergoing cell cycle arrest or apoptosis. However, if DNA damage gets too severe, this may no longer be beneficial. Instead, the upregulation of stress response signalling could allow these cells to repair the damage and survive. Hence, it would make sense to have a mechanism to either suppress or change BCL6 function in response to high levels of stress. It is necessary to validate the whole proteome analysis results with an alternative BCL6 inhibitor to confirm that the upregulation of stress response signalling is dependent on BCL6 activity.

BCL6 was not upregulated by fractionated IR but appeared to be required for the repression of the DNA damage response to this treatment. In contrast, BCL6 was strongly upregulated by TMZ treatment. While not as evident as at 48 hours after acute IR, BCL6 upregulated by TMZ did appear to be required for upregulation of cell cycle checkpoint and DNA repair-promoting proteins. The response to TMZ treatment was assessed after seven doses administered over two weeks. The LN18 cells were visibly less viable at this stage of treatment and had perhaps reached a threshold of stress that induced the upregulation and switch of BCL6 activity. Future work could assess the role of BCL6 in the response to TMZ over the treatment time-course. It is possible that BCL6 initially represses the DNA damage response to help the cells adapt to long-term stress but as DNA damage accumulates, the stress level becomes high enough to switch the function of BCL6. Observation of this threshold would confirm the hypothesis that the role of BCL6 is mediated by the level of stress.

If the activity of BCL6 is mediated by the level of DNA damage-induced stress, it would be interesting to investigate whether a similar switch in activity occurs in response to different levels of other stresses. The paper that identified BCL6 as an evolutionarily conserved stress response protein demonstrated its role in adaptation to multiple doses of heat shock, as well as in the response of cancer cells to cytotoxic therapies.[406] While they identified the BCL6-mediated repression of the transcription factor TOX as

important in both stress responses, more in-depth proteome or transcriptome analysis could investigate the wider role of BCL6 in both responses, as well as in the responses to other types and levels of stress.[406] The association of BCL6 with master metabolic stress regulator AMPK in both GBM and lymphoma cell lines and the possible indications of BCL6 secretion in EVs in response to IR also indicate that BCL6 may have roles in cellular stress responses that are not yet appreciated.

### 7.5.3: BCL6 as a promising target for the treatment of GBM

This thesis has added to the evidence that BCL6 is a promising target for the treatment of GBM. BCL6 is clearly involved in the response of GBM cells to therapy and its inhibition has been shown to increase the efficacy of available treatments.[207–211] In this thesis, the role of BCL6 in the response of LN18 GBM cells to the two clinically relevant treatments, fractionated IR and TMZ, was examined separately. However, these treatments are usually given together in the clinic.[4] As BCL6 appeared to have very different roles in response to fractionated IR and TMZ, it is difficult to predict its function in response to combination treatment. Therefore, the analysis of the whole proteome effects of BCL6 inhibition on the response of GBM cells to fractionated IR and TMZ together will be a vital next step. Ideally, the role of BCL6 over a time-course of fractionated IR and TMZ treatment would be analysed in multiple GBM cell lines with different types of BCL6 inhibitor and later in mouse models. This would allow full understanding of how BCL6 is involved in the therapy response of GBM over time. In addition, it would be useful to repeat the RIME experiments to identify the proteins BCL6 associates with in response to fractionated IR and TMZ. It would be interesting to compare the proteins associated with BCL6 in untreated GBM cells and GBM cells treated with fractionated IR, to determine whether BCL6 activity is altered by fractionated IR. It would also be revealing to determine whether BCL6 in TMZ-treated GBM cells associates with proteins seen in untreated or irradiated cells, or with a different set of proteins entirely.

The role of BCL6 in the therapy response of GBM cells is more complicated and context-specific than expected. However, evidence is mounting that BCL6 is important for the survival of GBM cells and for their resistance to treatment. More research is needed to fully clarify the role of BCL6 in the response of GBM cells to different treatments, however BCL6 inhibitors in development hold great promise to improve the efficacy of currently available therapies such as fractionated IR and TMZ.

## 7.6 Conclusion

BCL6 is emerging as a critical protein for the survival of cancer cells. Previous research revealed that BCL6 is important in the therapy resistance of GBM and holds promise as a target to improve the dire prognosis of this disease. This thesis has expanded upon the evidence that BCL6 is important in the

response of GBM cells to multiple treatments and that its role is drastically altered in response to therapy. This strengthens the rationale for pursuing BCL6 inhibition to improve the efficacy of GBM treatment.

# 8: References


1. Public Health England. *Cancer Survival in England for Patients Diagnosed between 2014 and 2018, and Followed up to 2019*.; 2021. https://www.gov.uk/government/statistics/cancer-survival-in-england-for-patients-diagnosed-between-2014-and-2018-and-followed-up-until-2019/cancer-survival-in-england-for-patients-diagnosed-between-2014-and-2018-and-followed-up-to-2019.
2. Ostrom QT, Cioffi G, Gittleman H, et al. CBTRUS Statistical Report: Primary Brain and Other Central Nervous System Tumors Diagnosed in the United States in 2012-2016. *Neuro Oncol*. 2019;21(5):v1-v100. doi:10.1093/neuonc/noz150
3. Desouza RM, Shaweis H, Han C, et al. Has the survival of patients with glioblastoma changed over the years? *Br J Cancer*. 2016;114(2):146-150. doi:10.1038/bjc.2015.421
4. Stupp R, Mason WP, van den Bent MJ, et al. Radiotherapy plus concomitant and adjuvant temozolomide for glioblastoma. *N Engl J Med*. 2005;352(10):987-996. doi:10.4137/cmo.s390
5. Burnet NG, Jefferies SJ, Benson RJ, Hunt DP, Treasure FP. Years of life lost (YLL) from cancer is an important measure of population burden - And should be considered when allocating research funds. *Br J Cancer*. 2005;92(2):241-245. doi:10.1038/sj.bjc.6602321
6. Weller M, Wick W, Aldape K, et al. Glioma. *Nat Rev Dis Prim*. 2015;1(15017). doi:10.1038/nrdp.2015.17
7. Louis DN, Perry A, Reifenberger G, et al. The 2016 World Health Organization Classification of Tumors of the Central Nervous System: a summary. *Acta Neuropathol*. 2016;131(6):803-820. doi:10.1007/s00401-016-1545-1
8. Zong H, Verhaak RGW, Canoll P. The cellular origin for malignant glioma and prospects for clinical advancements. *Expert Rev Mol Diagn*. 2012;12(4):383-394. doi:10.1586/erm.12.30.
9. Llaguno SRA, Parada LF. Cell of origin of glioma: Biological and clinical implications. *Br J Cancer*. 2016;115(12):1445-1450. doi:10.1038/bjc.2016.354
10. Yao M, Li S, Wu X, et al. Cellular origin of glioblastoma and its implication in precision therapy. *Cell Mol Immunol*. 2018;15(8):737-739. doi:10.1038/cmi.2017.159
11. Fan X, Xiong Y, Wang Y. A reignited debate over the cell(s) of origin for glioblastoma and its clinical implications. *Front Med*. 2019;13(5):531-539. doi:10.1007/s11684-019-0700-1
12. Bachoo RM, Maher EA, Ligon KL, et al. Epidermal growth factor receptor and Ink4a/Arf. *Cancer Cell*. 2002;1(3):269-277. doi:10.1016/s1535-6108(02)00046-6
13. Irvin DM, McNeill RS, Bash RE, Miller CR. Intrinsic Astrocyte Heterogeneity Influences Tumor Growth in Glioma Mouse Models. *Brain Pathol*. 2017;27(1):36-50. doi:10.1111/bpa.12348
14. Friedmann-Morvinski D, Bushong EA, Ke E, et al. Dedifferentiation of Neurons and Astrocytes by Oncogenes Can Induce Gliomas in Mice. 2012;338(6110):1080-1084. doi:10.1126/science.1226929.

15. Joya A, Martín A. Evaluation of glial cell proliferation with non-invasive molecular imaging methods after stroke. *Neural Regen Res*. 2021;16(11):2209-2210. doi:10.4103/1673-5374.310681

16. Llaguno SA, Chen J, Kwon CH, et al. Malignant Astrocytomas Originate from Neural Stem/Progenitor Cells in a Somatic Tumor Suppressor Mouse Model. *Cancer Cell*. 2009;15(1):45-56. doi:10.1016/j.ccr.2009.02.008

17. Lee JH, Lee JE, Kahng JY, et al. Human glioblastoma arises from subventricular zone cells with low-level driver mutations. *Nature*. 2018;560(7717):243-247. doi:10.1038/s41586-018-0389-3

18. Liu C, Sage JC, Miller MR, et al. Mosaic Analysis with Double Markers (MADM) Reveals Tumor Cell-of-Origin in Glioma. *Cell*. 2011;146(2):209-221. doi:10.1016/j.cell.2011.06.014.

19. Llaguno SRA, Wang Z, Sun D, et al. Adult Lineage Restricted CNS Progenitors Specify Distinct Glioblastoma Subtypes. *Cancer Cell*. 2015;28(4):429-440. doi:10.1016/j.ccell.2015.09.007.

20. Ohgaki H, Kleihues P. The definition of primary and secondary glioblastoma. *Clin Cancer Res*. 2013;19(4):764-772. doi:10.1158/1078-0432.CCR-12-3002

21. Geisbrecht B V., Gould SJ. The human PICD gene encodes a cytoplasmic and peroxisomal NADP+- dependent isocitrate dehydrogenase. *J Biol Chem*. 1999;274(43):30527-30533. doi:10.1074/jbc.274.43.30527

22. Hurley JH, Dean AM, Koshland DE, Stroud RM. Catalytic Mechanism of NADP+-Dependent Isocitrate Dehydrogenase: Implications from the Structures of Magnesium-Isocitrate and NADP+ Complexes. *Biochemistry*. 1991;30(35):8671-8678. doi:10.1021/bi00099a026

23. Des Rosiers C, Fernandez CA, David F, Brunengraber H. Reversibility of the mitochondrial isocitrate dehydrogenase reaction in the perfused rat liver. Evidence from isotopomer analysis of citric acid cycle intermediates. *J Biol Chem*. 1994;269(44):27179-27182. doi:10.1016/s0021-9258(18)46965-7

24. Yan H, Parsons DW, Jin G, et al. IDH1 and IDH2 Mutations in Gliomas. *N Engl J Med*. 2009;360(8):765-773. doi:10.1056/NEJMoa0808710.

25. Dang L, White DW, Gross S, et al. Cancer-associated IDH1 mutations produce 2-hydroxyglutarate. *Nature*. 2009;462(7274):739-744. doi:10.1038/nature08617.

26. Leonardi R, Subramanian C, Jackowski S, Rock CO. Cancer-associated isocitrate dehydrogenase mutations inactivate NADPH-dependent reductive carboxylation. *J Biol Chem*. 2012;287(18):14615-14620. doi:10.1074/jbc.C112.353946

27. Xu W, Yang H, Liu Y, et al. Oncometabolite 2-hydroxyglutarate is a competitive inhibitor of α-ketoglutarate-dependent dioxygenases. *Cancer Cell*. 2011;19(1):17-30. doi:10.1016/j.ccr.2010.12.014

28. Chowdhury R, Yeoh KK, Tian YM, et al. The oncometabolite 2-hydroxyglutarate inhibits histone lysine demethylases. *EMBO Rep*. 2011;12(5):463-469. doi:10.1038/embor.2011.43

29. Lu C, Ward PS, Kapoor GS, et al. IDH mutation impairs histone demethylation and results in a block to cell differentiation. *Nature*. 2012;483(7390):474-478. doi:10.1038/nature10860

30. Turcan S, Rohle D, Goenka A, et al. IDH1 mutation is sufficient to establish the glioma hypermethylator phenotype. *Nature*. 2012;483(7390):479-483. doi:10.1038/nature10866

31. Noushmehr H, Weisenberger DJ, Diefes K, et al. Identification of a CpG Island Methylator Phenotype that Defines a Distinct Subgroup of Glioma. 2010;17(5):510-522. doi:10.1016/j.ccr.2010.03.017.

32. Ohm JE, Mcgarvey KM, Yu X, et al. A Stem Cell-Like Chromatin Pattern May Predispose

Tumor Suppressor Genes to DNA Hypermethylation and Silencing in Adult Cancers. 2007;39(2):237-242. doi:10.1038/ng1972.

33. Watanabe T, Nobusawa S, Kleihues P, Ohgaki H. IDH1 mutations are early events in the development of astrocytomas and oligodendrogliomas. *Am J Pathol*. 2009;174(4):1149-1153. doi:10.2353/ajpath.2009.080958

34. Lai A, Kharbanda S, Pope WB, et al. Evidence for sequenced molecular evolution of IDH1 mutant glioblastoma from a distinct cell of origin. *J Clin Oncol*. 2011;29(34):4482-4490. doi:10.1200/JCO.2010.33.8715

35. Rohle D, Popovici-Muller J, Palaskas N, et al. An Inhibitor of Mutant IDH1 Delays Growth and Promotes Differentiation of Glioma Cells. *Science (80- )*. 2013;340(6132):626-630. doi:10.1126/science.1236062.

36. Grassian AR, Parker SJ, Davidson SM, et al. IDH1 Mutations Alter Citric Acid Cycle Metabolism and Increase Dependence on Oxidative Mitochondrial Metabolism Authors' Contributions Conception and design: HHS Public Access. *Cancer Res*. 2014;74(12):3317-3331. doi:10.1158/0008-5472.CAN-14-0772-T

37. Chesnelong C, Chaumeil MM, Blough MD, et al. Lactate dehydrogenase A silencing in IDH mutant gliomas. *Neuro Oncol*. 2014;16(5):686-695. doi:10.1093/neuonc/not243

38. Hartmann C, Hentschel B, Wick W, et al. Patients with IDH1 wild type anaplastic astrocytomas exhibit worse prognosis than IDH1-mutated glioblastomas, and IDH1 mutation status accounts for the unfavorable prognostic effect of higher age: Implications for classification of gliomas. *Acta Neuropathol*. 2010;120(6):707-718. doi:10.1007/s00401-010-0781-z

39. Brada M, Ford D, Ashley S, et al. Risk of second brain tumour after conservative surgery and radiotherapy for pituitary adenoma. *Br Med J*. 1992;304(6838):1343-1346. doi:10.1136/bmj.304.6838.1343

40. Neglia JP, Robison LL, Stovall M, et al. New primary neoplasms of the central nervous system in survivors of childhood cancer: A report from the childhood cancer survivor study. *J Natl Cancer Inst*. 2006;98(21):1528-1537. doi:10.1093/jnci/djj411

41. Braganza MZ, Kitahara CM, Berrington De González A, Inskip PD, Johnson KJ, Rajaraman P. Ionizing radiation and the risk of brain and central nervous system tumors: A systematic review. *Neuro Oncol*. 2012;14(11):1316-1324. doi:10.1093/neuonc/nos208

42. Kinnersley B, Mitchell JS, Gousias K, et al. Quantifying the heritability of glioma using genome-wide complex trait analysis. *Sci Rep*. 2015;5(17267). doi:10.1038/srep17267

43. Ostrom QT, Fahmideh MA, Cote DJ, et al. Risk factors for childhood and adult primary brain tumors. *Neuro Oncol*. 2019;21(11):1357-1375. doi:10.1093/neuonc/noz123

44. Larjavaara S, Mäntylä R, Salminen T, et al. Incidence of gliomas by anatomic location. *Neuro Oncol*. 2007;9(3):319-325. doi:10.1215/15228517-2007-016

45. Oronsky B, Reid TR, Oronsky A, Sandhu N, Knox SJ. A Review of Newly Diagnosed Glioblastoma. *Front Oncol*. 2021;10(574012). doi:10.3389/fonc.2020.574012

46. Martínez-González A, Calvo GF, Pérez Romasanta LA, Pérez-García VM. Hypoxic Cell Waves Around Necrotic Cores in Glioblastoma: A Biomathematical Model and Its Therapeutic Implications. *Bull Math Biol*. 2012;74(12):2875-2896. doi:10.1007/s11538-012-9786-1

47. Brat DJ, Van Meir EG. Vaso-occlusive and prothrombotic mechanisms associated with tumor hypoxia, necrosis, and accelerated growth in glioblastoma. *Lab Investig*. 2004;84(4):397-405. doi:10.1038/labinvest.3700070

48. Hardee ME, Zagzag D. Mechanisms of glioma-associated neovascularization. *Am J Pathol*.

2012;181(4):1126-1141. doi:10.1016/j.ajpath.2012.06.030

49. Alexander H, Irwin C, Purdie G, Hunn M. Incidence and management of high grade glioma in Māori and non-Māori patients. *J Clin Neurosci*. 2010;17(9):1144-1147. doi:10.1016/j.jocn.2010.01.033

50. Ministry of Health - Manatū Hauora. New cancer registrations 2019. https://www.health.govt.nz/publication/new-cancer-registrations-2019. Published 2021.

51. McManus EJ, Frampton C, Tan A, Phillips MCL. Metabolics risk factors in a New Zealand glioblastoma cohort. *Neuro-Oncology Pract*. 2022;9(1):43-49. doi:10.1093/nop/npab064

52. Inda M del M, Bonavia R, Seoane J. Glioblastoma multiforme:A look inside its heterogeneous nature. *Cancers (Basel)*. 2014;6(1):226-239. doi:10.3390/cancers6010226

53. The Cancer Genome Atlas (TCGA) Research Network. Comprehensive genomic characterization defines human glioblastoma genes and core pathways. *Nature*. 2008;455(7216):1061-1068. doi:10.1038/nature07385.

54. Lee E, Yong RL, Paddison P, Zhu J. Comparison of glioblastoma (GBM) molecular classification methods. *Semin Cancer Biol*. 2018;53(May):201-211. doi:10.1016/j.semcancer.2018.07.006

55. Verhaak RGW, Hoadley KA, Purdom E, et al. Integrated Genomic Analysis Identifies Clinically Relevant Subtypes of Glioblastoma Characterized by Abnormalities in PDGFRA, IDH1, EGFR, and NF1. *Cancer Cell*. 2010;17(1):98-110. doi:10.1016/j.ccr.2009.12.020

56. Wang Q, Hu B, Hu X, et al. Tumor Evolution of Glioma-Intrinsic Gene Expression Subtypes Associates with Immunological Changes in the Microenvironment. *Cancer Cell*. 2017;32(1):42-56.e6. doi:10.1016/j.ccell.2017.06.003

57. Varn FS, Johnson KC, Martinek J, et al. Glioma progression is shaped by genetic evolution and microenvironment interactions. *Cell*. 2022;185(12):2184-2199.e16. doi:10.1016/j.cell.2022.04.038

58. Hegi ME, Diserens A-C, Gorlia T, et al. MGMT Gene Silencing and Benefit from Temozolomide in Glioblastoma . *N Engl J Med*. 2005;352(10):997-1003. doi:10.1056/nejmoa043331

59. Hermisson M, Klumpp A, Wick W, et al. O6-methylguanine DNA methyltransferase and p53 status predict temozolomide sensitivity in human malignant glioma cells. *J Neurochem*. 2006;96(3):766-776. doi:10.1111/j.1471-4159.2005.03583.x

60. Kitange GJ, Carlson BL, Schroeder MA, et al. Induction of MGMT expression is associated with temozolomide resistance in glioblastoma xenografts. *Neuro Oncol*. 2009;11(3):281-291. doi:10.1215/15228517-2008-090

61. Fan CH, Liu WL, Cao H, Wen C, Chen L, Jiang G. O6-methylguanine DNA methyltransferase as a promising target for the treatment of temozolomide-resistant gliomas. *Cell Death Dis*. 2013;4(10):e876. doi:10.1038/cddis.2013.388

62. Mun DG, Bhin J, Kim S, et al. Proteogenomic Characterization of Human Early-Onset Gastric Cancer. *Cancer Cell*. 2019;35(1):111-124.e10. doi:10.1016/j.ccell.2018.12.003

63. Satpathy S, Krug K, Jean Beltran PM, et al. A proteogenomic portrait of lung squamous cell carcinoma. *Cell*. 2021;184(16):4348-4371.e40. doi:10.1016/j.cell.2021.07.016

64. Tribe AKW, Mcconnell MJ, Teesdale-spittle PH. The Big Picture of Glioblastoma Malignancy: A Meta-Analysis of Glioblastoma Proteomics to Identify Altered Biological Pathways. *ACS Omega*. 2021;6(38):24535-24544. doi:10.1021/acsomega.1c02991

65. Oh S, Yeom J, Cho HJ, et al. Integrated pharmaco-proteogenomics defines two subgroups in isocitrate dehydrogenase wild-type glioblastoma with prognostic and therapeutic opportunities. *Nat Commun*. 2020;11(1). doi:10.1038/s41467-020-17139-y

66. Yanovich-Arad G, Ofek P, Yeini E, et al. Proteogenomics of glioblastoma associates molecular patterns with survival. *Cell Rep*. 2021;34(9):108787. doi:10.1016/j.celrep.2021.108787

67. Wang LB, Karpova A, Gritsenko MA, et al. Proteogenomic and metabolomic characterization of human glioblastoma. *Cancer Cell*. 2021;39(4):509-528.e20. doi:10.1016/j.ccell.2021.01.006

68. Grant R. Overview: Brain tumour diagnosis and management/Royal College of Physicians guidelines. *Neurol Pract*. 2004;75(2). doi:10.1136/jnnp.2004.040360

69. Kostaras X, Cusano F, Kline GA, Roa W, Easaw J. Use of dexamethasone in patients with high-grade glioma: A clinical practice guideline. *Curr Oncol*. 2014;21(3):493-503. doi:10.3747/co.21.1769

70. Pruitt AA. Medical management of patients with brain tumors. *Curr Treat Options Neurol*. 2011;13(4):413-426. doi:10.1007/s11940-011-0132-y

71. Abd-Elghany AA, Naji AA, Alonazi B, et al. Radiological characteristics of glioblastoma multiforme using CT and MRI examination. *J Radiat Res Appl Sci*. 2019;12(1):289-293. doi:10.1080/16878507.2019.1655864

72. Wei RL, Wei XT. Advanced Diagnosis of Glioma by Using Emerging Magnetic Resonance Sequences. *Front Oncol*. 2021;11(August). doi:10.3389/fonc.2021.694498

73. Gonçalves FG, Chawla S, Mohan S. Emerging MRI Techniques to Redefine Treatment Response in Patients With Glioblastoma. *J Magn Reson Imaging*. 2020;52(4):978-997. doi:10.1002/jmri.27105.

74. Lacroix M, Abi-Said D, Fourney DR, et al. A multivariate analysis of 416 patients with glioblastoma multiforme: prognosis, extent of resection, and survival. *J Neurosurg*. 2001;95(2):190-198. doi:10.3171/jns.2001.95.2.0190

75. Chaichana KL, Jusue-Torres I, Navarro-Ramirez R, et al. Establishing percent resection and residual volume thresholds affecting survival and recurrence for patients with newly diagnosed intracranial glioblastoma. *Neuro Oncol*. 2014;16(1):113-122. doi:10.1093/neuonc/not137

76. Tang L, Feng Y, Gao S, Mu Q, Liu C. Nanotherapeutics Overcoming the Blood-Brain Barrier for Glioblastoma Treatment. *Front Pharmacol*. 2021;12(786700). doi:10.3389/fphar.2021.786700

77. Daneman R, Prat A. The blood–brain barrier. *Cold Spring Harb Perspect Biol*. 2015;7(1). doi:10.36303/SAJAA.2020.26.6.S3.2533

78. Pardridge WM. Blood-brain barrier delivery. *Drug Discov Today*. 2007;12(1-2):54-61. doi:10.1016/j.drudis.2006.10.013

79. Patel M, McCully C, Godwin K, Balis FM. Plasma and cerebrospinal fluid pharmacokinetics of intravenous temozolomide in non-human primates. *J Neurooncol*. 2003;61(3):203-207. doi:10.1023/a:1022592913323

80. Erasimus H, Gobin M, Niclou S, Van Dyck E. DNA repair mechanisms and their clinical impact in glioblastoma. *Mutat Res - Rev Mutat Res*. 2016;769:19-35. doi:10.1016/j.mrrev.2016.05.005

81. Cheung-Ong K, Giaever G, Nislow C. DNA-damaging agents in cancer chemotherapy: Serendipity and chemical biology. *Chem Biol*. 2013;20(5):648-659. doi:10.1016/j.chembiol.2013.04.007

82. Sia J, Szmyd R, Hau E, Gee HE. Molecular Mechanisms of Radiation-Induced Cancer Cell

Death: A Primer. *Front Cell Dev Biol*. 2020;8(41). doi:10.3389/fcell.2020.00041

83. Verheij M. Clinical biomarkers and imaging for radiotherapy-induced cell death. *Cancer Metastasis Rev*. 2008;27(3):471-480. doi:10.1007/s10555-008-9131-1

84. Roninson IB, Broude E V., Chang BD. If not apoptosis, then what? Treatment-induced senescence and mitotic catastrophe in tumor cells. *Drug Resist Updat*. 2001;4(5):303-313. doi:10.1054/drup.2001.0213

85. Newlands ES, Stevens MFG, Wedge SR, Wheelhouse RT, Brock C. Temozolomide: A review of its discovery, chemical properties, pre-clinical development and clinical trials. *Cancer Treat Rev*. 1997;23(1):35-61. doi:10.1016/S0305-7372(97)90019-0

86. Stupp R, Gander M, Leyvraz S, Newlands E. Current and future developments in the use of temozolomide for the treatment of brain tumours. *Lancet Oncol*. 2001;2(9):552-560. doi:10.1016/S1470-2045(01)00489-2

87. Hickman MJ, Samson LD. Role of DNA mismatch repair and p53 in signaling induction of apoptosis by alkylating agents. *Proc Natl Acad Sci U S A*. 1999;96(19):10764-10769. doi:10.1073/pnas.96.19.10764

88. Herst PM, Broadley KWR, Harper JL, McConnell MJ. Pharmacological concentrations of ascorbate radiosensitize glioblastoma multiforme primary cells by increasing oxidative DNA damage and inhibiting G2/M arrest. *Free Radic Biol Med*. 2012;52(8):1486-1493. doi:10.1016/j.freeradbiomed.2012.01.021

89. Murad H, Alghamian Y, Aljapawe A, Madania A. Effects of ionizing radiation on the viability and proliferative behavior of the human glioblastoma T98G cell line. *BMC Res Notes*. 2018;11(1). doi:10.1186/s13104-018-3438-y

90. Hao J, Godley A, Shoemake JD, Han Z, Magnelli A, Yu JS. The effects of extra high dose rate irradiation on glioma stem-like cells. *PLoS One*. 2019;13(8). doi:10.1371/journal.pone.0202533

91. Chautard E, Loubeau G, Tchirkov A, et al. Akt signaling pathway: A target for radiosensitizing human malignant glioma. *Neuro Oncol*. 2010;12(5):434-443. doi:10.1093/neuonc/nop059

92. Rubner Y, Muth C, Strnad A, et al. Fractionated radiotherapy is the main stimulus for the induction of cell death and of Hsp70 release of p53 mutated glioblastoma cell lines. *Radiat Oncol*. 2014;9(1). doi:10.1186/1748-717X-9-89

93. Han X, Xue X, Zhou H, Zhang G. A molecular view of the radioresistance of gliomas. *Oncotarget*. 2017;8(59):100931-100941. doi:10.18632/oncotarget.21753

94. Ali MY, Oliva CR, Noman ASM, et al. Radioresistance in glioblastoma and the development of radiosensitizers. *Cancers (Basel)*. 2020;12(9):2511. doi:10.3390/cancers12092511

95. Li LY, Guan Y Di, Chen XS, Yang JM, Cheng Y. DNA Repair Pathways in Cancer Therapy and Resistance. *Front Pharmacol*. 2021;11(629266). doi:10.3389/fphar.2020.629266

96. Kao GD, Jiang Z, Fernandes AM, Gupta AK, Maity A. Inhibition of Phosphatidylinositol-3-OH Kinase/Akt Signaling Impairs DNA Repair in Glioblastoma Cells following Ionizing Radiation. *J Biol Chem*. 2007;282(29):21206-21212. doi:10.1074/jbc.M703042200.

97. Toulany M, Kasten-Pisula U, Brammer I, et al. Blockage of epidermal growth factor receptor-phosphatidylinositol 3-kinase-AKT signaling increases radiosensitivity of K-RAS mutated human tumor cells in vitro by affecting DNA repair. *Clin Cancer Res*. 2006;12(13):4119-4126. doi:10.1158/1078-0432.CCR-05-2454

98. Toulany M, Lee KJ, Fattah KR, et al. Akt promotes post-irradiation survival of human tumor cells through initiation, progression, and termination of DNA-PKcs-dependent DNA double-strand break repair. *Mol Cancer Res*. 2012;10(7):945-957. doi:10.1158/1541-7786.MCR-11-

0592

99. Golding SE, Morgan RN, Adams BR, Hawkins AJ, Povirk LF, Valerie K. Pro-survival AKT and ERK signaling from EGFR and mutant EGFRvIII enhances DNA double-strand break repair in human glioma cells. *Cancer Biol Ther*. 2009;8(8):730-738. doi:10.4161/cbt.8.8.7927

100. Chakravarti A, Zhai G, Suzuki Y, et al. The prognostic significance of phosphatidylinositol 3-kinase pathway activation in human gliomas. *J Clin Oncol*. 2004;22(10):1926-1933. doi:10.1200/JCO.2004.07.193

101. Li HF, Kim JS, Waldman T. Radiation-induced Akt activation modulates radioresistance in human glioblastoma cells. *Radiat Oncol*. 2009;4(43). doi:10.1186/1748-717X-4-43

102. Brognard J, Clark AS, Ni Y, Dennis PA. Akt/protein kinase B is constitutively active in non-small cell lung cancer cells and promotes cellular survival and resistance to chemotherapy and radiation. *Cancer Res*. 2001;61(10):3986-3997.

103. Bussink J, van der Kogel AJ, Kaanders JH. Activation of the PI3-K/AKT pathway and implications for radioresistance mechanisms in head and neck cancer. *Lancet Oncol*. 2008;9(3):288-296. doi:10.1016/S1470-2045(08)70073-1

104. Routhier A, Astuccio M, Lahey D, et al. Pharmacological inhibition of Rho-kinase signaling with Y-27632 blocks melanoma tumor growth. *Oncol Rep*. 2010;23(3):861-867. doi:10.3892/or

105. Lee CM, Fuhrman CB, Planelles V, et al. Phosphatidylinositol 3-kinase inhibition by LY294002 radiosensitizes human cervical cancer cell lines. *Clin Cancer Res*. 2006;12(1):250-256. doi:10.1158/1078-0432.CCR-05-1084

106. Tanno S, Yanagawa N, Habiro A, et al. Serine/threonine kinase AKT is frequently activated in human bile duct cancer and is associated with increased radioresistance. *Cancer Res*. 2004;64(10):3486-3490. doi:10.1158/0008-5472.CAN-03-1788

107. Toulany M, Peter Rodemann H. Potential of Akt mediated DNA repair in radioresistance of solid tumors overexpressing erbB-PI3K-Akt pathway. *Transl Cancer Res*. 2013;2(3):190-202. doi:10.3978/j.issn.2218-676X.2013.04.09

108. Nijkamp MM, Hoogsteen IJ, Span PN, et al. Spatial relationship of phosphorylated epidermal growth factor receptor and activated AKT in head and neck squamous cell carcinoma. *Radiother Oncol*. 2011;101(1):165-170. doi:10.1016/j.radonc.2011.06.022

109. Georgescu MM. Pten tumor suppressor network in PI3K-Akt pathway control. *Genes and Cancer*. 2010;1(12):1170-1177. doi:10.1177/1947601911407325

110. Yang JA, Liu BH, Shao LM, et al. LRIG1 enhances the radiosensitivity of radioresistant human glioblastoma U251 cells via attenuation of the EGFR/Akt signaling pathway. *Int J Clin Exp Pathol*. 2015;8(4):3580-3590.

111. Bao S, Wu Q, McLendon RE, et al. Glioma stem cells promote radioresistance by preferential activation of the DNA damage response. *Nature*. 2006;444(7120):756-760. doi:10.1038/nature05236

112. Walcher L, Kistenmacher AK, Suo H, et al. Cancer Stem Cells—Origins and Biomarkers: Perspectives for Targeted Personalized Therapies. *Front Immunol*. 2020;11(1280). doi:10.3389/fimmu.2020.01280

113. Sheila K. Singh, Cynthia Hawkins, Ian D. Clarke, et al. Identification of human brain tumour initiating cells. *Nature*. 2004;432(7015):396-401. doi:10.1038/nature03031.1.

114. Clément V, Dutoit V, Marino D, Dietrich PY, Radovanovic I. Limits of CD133 as a marker of glioma self-renewing cells. *Int J Cancer*. 2009;125(1):244-248. doi:10.1002/ijc.24352

115. Singh SK, Clarke ID, Terasaki M, et al. Identification of a cancer stem cell in human brain tumors. *Cancer Res*. 2003;63(18):5821-5828.

116. Chen W, Dong J, Haiech J, Kilhoffer MC, Zeniou M. Cancer stem cell quiescence and plasticity as major challenges in cancer therapy. *Stem Cells Int*. 2016;2016. doi:10.1155/2016/1740936

117. Xie XP, Laks DR, Sun D, et al. Quiescent human glioblastoma cancer stem cells drive tumor initiation, expansion, and recurrence following chemotherapy. *Dev Cell*. 2022;57(1):32-46.e8. doi:10.1016/j.devcel.2021.12.007

118. Jamal M, Rath BH, Tsang PS, Camphausen K, Tofilon PJ. The brain microenvironment preferentially enhances the radioresistance of CD133+ glioblastoma stem-like cells. *Neoplasia*. 2012;14(2):150-158. doi:10.1593/neo.111794

119. Crabtree HG, Cramer W. The action of radium on cancer cells. II. - Some factors determining the susceptivility of cancer cells to radium. *Proc R Soc B Biol Sci*. 1933;782:238-250. doi:10.3181/00379727-11-85

120. Boulefour W, Rowinski E, Louati S, et al. A review of the role of hypoxia in radioresistance in cancer therapy. *Med Sci Monit*. 2021;27:e934116-1–e934116-7. doi:10.12659/MSM.934116

121. Wang H, Jiang H, Van De Gucht M, De Ridder M. Hypoxic radioresistance: Can ROS be the key to overcome it? *Cancers (Basel)*. 2019;11(1):112. doi:10.3390/cancers11010112

122. Ratcliffe PJ, O'Rourke JF, Maxwell PH, Pugh CW. Oxygen sensing, hypoxia-inducible factor-1 and the regulation of mammalian gene expression. *J Exp Biol*. 1998;201(8):1153-1162. doi:10.1242/jeb.201.8.1153

123. Soeda A, Park M, Lee D, et al. Hypoxia promotes expansion of the CD133-positive glioma stem cells through activation of HIF-1α. *Oncogene*. 2009;28(45):3949-3959. doi:10.1038/onc.2009.252

124. Bar EE, Lin A, Mahairaki V, Matsui W, Eberhart CG. Hypoxia increases the expression of stem-cell markers and promotes clonogenicity in glioblastoma neurospheres. *Am J Pathol*. 2010;177(3):1491-1502. doi:10.2353/ajpath.2010.091021

125. Seidel S, Garvalov BK, Wirta V, et al. A hypoxic niche regulates glioblastoma stem cells through hypoxia inducible factor 2α. *Brain*. 2010;133(4):983-995. doi:10.1093/brain/awq042

126. Klionsky DJ, Abdel-Aziz AK, Abdelfatah S, et al. Guidelines for the use and interpretation of assays for monitoring autophagy (4th edition)1. *Autophagy*. 2021;17(1):1-382. doi:10.1080/15548627.2020.1797280

127. Daido S, Yamamoto A, Fujiwara K, Sawaya R, Kondo S, Kondo Y. Inhibition of the DNA-dependent protein kinase catalytic subunit radiosensitizes malignant glioma cells by inducing autophagy. *Cancer Res*. 2005;65(10):4368-4375. doi:10.1158/0008-5472.CAN-04-4202

128. Fujiwara K, Iwado E, Mills GB, Sawaya R, Kondo S, Kondo Y. Akt inhibitor shows anticancer and radiosensitizing effects in malignant glioma cells by inducing autophagy. *Int J Oncol*. 2007;31(4):753-760. doi:10.3892/ijo.31.4.753

129. Porta C, Paglino C, Mosca A. Targeting PI3K/Akt/mTOR signaling in cancer. *Front Oncol*. 2014;4(64). doi:10.3389/fonc.2014.00064

130. Ito H, Daido S, Kanzawa T, Kondo S, Kondo Y. Radiation-induced autophagy is associated with LC3 and its inhibition sensitizes malignant glioma cells. *J Oncol*. 2005;26(5):1401-1410.

131. Yuan X, Du J, Hua S, et al. Suppression of autophagy augments the radiosensitizing effects of STAT3 inhibition on human glioma cells. *Exp Cell Res*. 2015;330(2):267-276. doi:10.1016/j.yexcr.2014.09.006

132. Jandrey EHF, Bezerra M, Inoue LT, Furnari FB, Camargo AA, Costa ET. A Key Pathway to Cancer Resilience: The Role of Autophagy in Glioblastomas. *Front Oncol*. 2021;11(652133). doi:10.3389/fonc.2021.652133

133. He Y, Su J, Lan B, Gao Y, Zhao J. Targeting off-target effects: Endoplasmic reticulum stress and autophagy as effective strategies to enhance temozolomide treatment. *Onco Targets Ther*. 2019;12:1857-1865. doi:10.2147/OTT.S194770

134. Stupp R, Hegi ME, Mason WP, et al. Effects of radiotherapy with concomitant and adjuvant temozolomide versus radiotherapy alone on survival in glioblastoma in a randomised phase III study: 5-year analysis of the EORTC-NCIC trial. *Lancet Oncol*. 2009;10(5):459-466. doi:10.1016/S1470-2045(09)70025-7

135. Hegi ME, Genbrugge E, Gorlia T, et al. MGMT Promoter Methylation Cutoff with Safety Margin for Selecting Glioblastoma Patients into Trials Omitting Temozolomide: A Pooled Analysis of Four Clinical Trials. *Clin Cancer Res*. 2019;25(6):1809-1816. doi:10.1158/1078-0432.CCR-18-3181.

136. Mansouri A, Hachem LD, Mansouri S, et al. MGMT promoter methylation status testing to guide therapy for glioblastoma: Refining the approach based on emerging evidence and current challenges. *Neuro Oncol*. 2019;21(2):167-178. doi:10.1093/neuonc/noy132

137. Koike G, Maki H, Takeya H, Hayakawa H, Sekiguchi M. Purification, structure, and biochemical properties of human O6-methylguanine-DNA methyltransferase. *J Biol Chem*. 1990;265(25):14754-14762. doi:10.1016/s0021-9258(18)77177-9

138. Park CK, Kim JE, Kim JY, et al. The changes in MGMT promoter methylation status in initial and recurrent glioblastomas. *Transl Oncol*. 2012;5(5):393-397. doi:10.1593/tlo.12253

139. Feldheim J, Kessler AF, Monoranu CM, Ernestus R-I, Löhr M, Hagemann C. Methyltransferase ( MGMT ) Promoter Methylation in Literature Review. *Cancers (Basel)*. 2019;11(12):1837. doi:10.3390/cancers11121837

140. Lavon I, Fuchs D, Zrihan D, et al. Novel mechanism whereby nuclear factor κB mediates DNA damage repair through regulation of O6-methylguanine-DNA-methyltransferase. *Cancer Res*. 2007;67(18):8952-8959. doi:10.1158/0008-5472.CAN-06-3820

141. Wang X, Jia L, Jin X, et al. NF-κB inhibitor reverses temozolomide resistance in human glioma TR/U251 cells. *Oncol Lett*. 2015;9(6):2586-2590. doi:10.3892/ol.2015.3130

142. Kohsaka S, Wang L, Yachi K, et al. STAT3 inhibition overcomes temozolomide resistance in glioblastoma by downregulating MGMT expression. *Mol Cancer Ther*. 2012;11(6):1289-1299. doi:10.1158/1535-7163.MCT-11-0801

143. Trivedi RN, Almeida KH, Fornsaglio JL, Schamus S, Sobol RW. The role of base excision repair in the sensitivity and resistance to temozolomide-mediated cell death. *Cancer Res*. 2005;65(14):6394-6400. doi:10.1158/0008-5472.CAN-05-0715

144. Tang JB, Svilar D, Trivedi RN, et al. N-methylpurine DNA glycosylase and DNA polymerase β modulate BER inhibitor potentiation of glioma cells to temozolomide. *Neuro Oncol*. 2011;13(5):471-486. doi:10.1093/neuonc/nor011

145. Touat M, Li YY, Boynton AN, et al. Mechanisms and therapeutic implications of hypermutation in gliomas. *Nature*. 2020;580(7804):517-523. doi:10.1038/s41586-020-2209-9.

146. Singh N, Miner A, Hennis L, Mittal S. Mechanisms of temozolomide resistance in glioblastoma - a comprehensive review. *Cancer Drug Resist*. 2021;4(1):17-43. doi:10.20517/cdr.2020.79

147. Jiapaer S, Furuta T, Tanaka S, Kitabayashi T, Nakada M. Potential strategies overcoming the temozolomide resistance for glioblastoma. *Neurol Med Chir (Tokyo)*. 2018;58(10):405-421.

doi:10.2176/nmc.ra.2018-0141

148. Golden EB, Cho HY, Jahanian A, et al. Chloroquine enhances temozolomide cytotoxicity in malignant gliomas by blocking autophagy. *Neurosurg Focus*. 2014;37(6):E12. doi:10.3171/2014.9.FOCUS14504

149. Wen ZP, Zeng WJ, Chen YH, et al. Knockdown ATG4C inhibits gliomas progression and promotes temozolomide chemosensitivity by suppressing autophagic flux. *J Exp Clin Cancer Res*. 2019;38(1):298. doi:10.1186/s13046-019-1287-8

150. Zanotto-Filho A, Braganhol E, Klafke K, et al. Autophagy inhibition improves the efficacy of curcumin/temozolomide combination therapy in glioblastomas. *Cancer Lett*. 2015;358(2):220-231. doi:10.1016/j.canlet.2014.12.044

151. Zhang YB, Zhao W, Zeng RX. Autophagic Degradation of Caspase-8 Protects U87MG Cells Against H2O2-induced Oxidative Stress. *Asian Pacific J Cancer Prev*. 2013;14(7):4095-4099. doi:10.7314/APJCP.2013.14.7.4095

152. Johannessen TC, Hasan-Olive MM, Zhu H, et al. Thioridazine inhibits autophagy and sensitizes glioblastoma cells to temozolomide. *Int J Cancer*. 2019;144(7):1735-1745. doi:10.1002/ijc.31912

153. Josset E, Burckel H, Noël G, Bischoff P. The mTOR inhibitor RAD001 potentiates autophagic cell death induced by temozolomide in a glioblastoma cell line. *Anticancer Res*. 2013;33(5):1845-1851.

154. Liu T, Li A, Xu Y, Xin Y. Momelotinib sensitizes glioblastoma cells to temozolomide by enhancement of autophagy via JAK2/STAT3 inhibition. *Oncol Rep*. 2019;41(3):1883-1892. doi:10.3892/or.2019.6970

155. Beltzig L, Schwarzenbach C, Leukel P, et al. Senescence Is the Main Trait Induced by Temozolomide in Glioblastoma Cells. *Cancers (Basel)*. 2022;14(9):2233. doi:10.3390/cancers14092233

156. Aasland D, Gotzinger L, Hauck L, et al. Temozolomide induces senescence and repression of DNA repair pathways in glioblastoma cells via activation of ATR–Chk1, p21, and NF-kB. *Cancer Res*. 2019;79(1):99-113. doi:10.1158/0008-5472.CAN-18-1733

157. Fisher JP, Adamson DC. Current FDA-Approved Therapies for High-Grade Malignant Gliomas. *Biomedicines*. 2021;9(324). doi:10.3390/biomedicines9030324

158. Chen Y, Jia Y, Song W, Zhang L. Therapeutic Potential of Nitrogen Mustard Based Hybrid Molecules. *Front Pharmacol*. 2018;9(1453). doi:10.3389/fphar.2018.01453

159. Lawley PD, Brookes P. Molecular mechanism of the cytotoxic action of difunctional alkylating agents and of resistance to this action. *Nature*. 1965;206:480-483.

160. Kehrer JP. The effect of bcnu (carmustine) on tissue glutathione reductase activity. *Toxicol Lett*. 1983;17(1-2):62-68.

161. U.S. Food and Drug Administration. Gleostine (lomustine). 2016. https://www.accessdata.fda.gov/drugsatfda_docs/label/2016/017588s042lbl.pdf.

162. Weller M, van den Bent M, Tonn JC, et al. European Association for Neuro-Oncology (EANO) guideline on the diagnosis and treatment of adult astrocytic and oligodendroglial gliomas. *Lancet Oncol*. 2017;18(6):e315-e329. doi:10.1016/S1470-2045(17)30194-8

163. Keogh RJ, Aslam R, Hennessy MA, et al. One year of procarbazine lomustine and vincristine is poorly tolerated in low grade glioma: a real world experience in a national neuro-oncology centre. *BMC Cancer*. 2021;21(1):140. doi:10.1186/s12885-021-07809-5

164. Weller M, Le Rhun E. How did lomustine become standard of care in recurrent glioblastoma? *Cancer Treat Rev*. 2020;87(102029). doi:10.1016/j.ctrv.2020.102029

165. U.S. Food and Drug Administration. BiCNU. 2017. https://www.accessdata.fda.gov/drugsatfda_docs/label/2017/017422s055lbl.pdf.

166. Lin SH, Kleinberg LR. Carmustine wafers: Localized delivery of chemotherapeutic agents in CNS malignancies. *Expert Rev Anticancer Ther*. 2008;8(3):343-359. doi:10.1586/14737140.8.3.343

167. U.S. Food and Drug Administration. GLIADEL® WAFER (carmustine implant). 2018. https://www.accessdata.fda.gov/drugsatfda_docs/label/2018/020637s029lbl.pdf.

168. Xiao ZZ, Wang ZF, Lan T, et al. Carmustine as a Supplementary Therapeutic Option for Glioblastoma: A Systematic Review and Meta-Analysis. *Front Neurol*. 2020;11(1036). doi:10.3389/fneur.2020.01036

169. Brem H, Mahaley Jr. MS, Vick NA, et al. Interstitial chemotherapy with drug polymer implants for the treatment of recurrent gliomas. *J Neurosurg*. 1991;74(3):441-446. doi:10.3171/jns.1991.74.3.0441

170. Taal W, Oosterkamp HM, Walenkamp AME, et al. Single-agent bevacizumab or lomustine versus a combination of bevacizumab plus lomustine in patients with recurrent glioblastoma (BELOB trial): A randomised controlled phase 2 trial. *Lancet Oncol*. 2014;15(9):943-953. doi:10.1016/S1470-2045(14)70314-6

171. Metellus P, Coulibaly B, Nanni I, et al. Prognostic impact of O6-methylguanine-DNA methyltransferase silencing in patients with recurrent glioblastoma multiforme who undergo surgery and carmustine wafer implantation: A prospective patient cohort. *Cancer*. 2009;115(20):4783-4794. doi:10.1002/cncr.24546

172. Ferrara N, Hillan KJ, Gerber HP, Novotny W. Discovery and development of bevacizumab, an anti-VEGF antibody for treating cancer. *Nat Rev Drug Discov*. 2004;3(5):391-400. doi:10.1038/nrd1381

173. Xiao Q, Yang S, Ding G, Luo M. Anti-vascular endothelial growth factor in glioblastoma: a systematic review and meta-analysis. *Neurol Sci*. 2018;39(12):2021-2031. doi:10.1007/s10072-018-3568-y

174. Administration USF and D. AVASTIN (bevacizumab). 2014. https://www.accessdata.fda.gov/drugsatfda_docs/label/2014/125085s301lbl.pdf.

175. U.S. Food and Drug Administration. FDA approves bevacizumab in combination with chemotherapy for ovarian cancer. https://www.fda.gov/drugs/resources-information-approved-drugs/fda-approves-bevacizumab-combination-chemotherapy-ovarian-cancer#:~:text=FDA approves bevacizumab in combination with chemotherapy for ovarian cancer,-Share&text=On June 13%2C 2018%2C the,Avas. Published 2018. Accessed August 7, 2022.

176. Cohen MH, Shen YL, Keegan P, Pazdur R. FDA Drug Approval Summary: Bevacizumab (Avastin®) as Treatment of Recurrent Glioblastoma Multiforme. *Oncologist*. 2009;14(11):1131-1138. doi:10.1634/theoncologist.2009-0121

177. Roche. Avastin (bevacizumab). https://www.roche.com/solutions/pharma/productid-d263d2d3-708f-4fbd-87da-23364b2958f6#:~:text=In addition%2C Avastin is approved,progressive glioblastoma following prior therapy. Published 2022. Accessed August 7, 2022.

178. Medsafe.govt.nz. NEW ZEALAND DATA SHEET Avastin ® (bevacizumab) 1. 2021. https://www.medsafe.govt.nz/profs/Datasheet/a/Avastininf.pdf.

179. Zhang T, Xin Q, Kang JM. Bevacizumab for recurrent glioblastoma: A systematic review and

meta-analysis. *Eur Rev Med Pharmacol Sci*. 2021;25(21):6480-6491. doi:10.26355/eurrev_202111_27092

180. Giladi M, Schneiderman RS, Voloshin T, et al. Mitotic Spindle Disruption by Alternating Electric Fields Leads to Improper Chromosome Segregation and Mitotic Catastrophe in Cancer Cells. *Sci Rep*. 2015;5(18046). doi:10.1038/srep18046

181. Carrieri FA, Smack C, Siddiqui I, Kleinberg LR, Tran PT. Tumor Treating Fields: At the Crossroads Between Physics and Biology for Cancer Treatment. *Front Oncol*. 2020;10(575992). doi:10.3389/fonc.2020.575992

182. Berkelmann L, Bader A, Meshksar S, et al. Tumour-treating fields (TTFields): Investigations on the mechanism of action by electromagnetic exposure of cells in telophase/cytokinesis. *Sci Rep*. 2019;9(1). doi:10.1038/s41598-019-43621-9

183. U.S. Food and Drug Administration. Tumor Treatment Fields. 2015. https://www.accessdata.fda.gov/cdrh_docs/pdf10/P100034S013b.pdf.

184. Stupp R, Taillibert S, Kanner A, et al. Effect of tumor-treating fields plus maintenance temozolomide vs maintenance temozolomide alone on survival in patients with glioblastoma a randomized clinical trial. *JAMA - J Am Med Assoc*. 2017;318(23):2306-2316. doi:10.1001/jama.2017.18718

185. Mehta M, Wen P, Nishikawa R, Reardon D, Peters K. Critical review of the addition of tumor treating fields (TTFields) to the existing standard of care for newly diagnosed glioblastoma patients. *Crit Rev Oncol Hematol*. 2017;111:60-65. doi:10.1016/j.critrevonc.2017.01.005

186. Nabors LB, Portnow J, Ahluwalia M, et al. Central nervous system cancers, version 3.2020. *JNCCN J Natl Compr Cancer Netw*. 2020;18(11):1537-1570. doi:10.6004/JNCCN.2020.0052

187. Krigers A, Pinggera D, Demetz M, et al. The Routine Application of Tumor-Treating Fields in the Treatment of Glioblastoma WHO° IV. *Front Neurol*. 2022;13. doi:10.3389/fneur.2022.900377

188. Onken J, Staub-Bartelt F, Vajkoczy P, Misch M. Acceptance and compliance of TTFields treatment among high grade glioma patients. *J Neurooncol*. 2018;139(1):177-184. doi:10.1007/s11060-018-2858-9

189. Le Rhun E, Preusser M, Roth P, et al. Molecular targeted therapy of glioblastoma. *Cancer Treat Rev*. 2019;80(101896). doi:10.1016/j.ctrv.2019.101896

190. Pan PC, Magge RS. Mechanisms of egfr resistance in glioblastoma. *Int J Mol Sci*. 2020;21(22). doi:10.3390/ijms21228471

191. Colardo M, Segatto M, Di Bartolomeo S. Targeting rtk-pi3k-mtor axis in gliomas: An update. *Int J Mol Sci*. 2021;22(9). doi:10.3390/ijms22094899

192. Yang K, Wu Z, Zhang H, et al. Glioma targeted therapy: insight into future of molecular approaches. *Mol Cancer*. 2022;21(1). doi:10.1186/s12943-022-01513-z

193. Sim HW, Galanis E, Khasraw M. PARP Inhibitors in Glioma: A Review of Therapeutic Opportunities. *Cancers (Basel)*. 2022;14(4). doi:10.3390/cancers14041003

194. Maya-Mendoza A, Moudry P, Merchut-Maya JM, Lee M, Strauss R, Bartek J. High speed of fork progression induces DNA replication stress and genomic instability. *Nature*. 2018;559(7713):279-284. doi:10.1038/s41586-018-0261-5

195. Cong K, Peng M, Kousholt AN, et al. Replication gaps are a key determinant of PARP inhibitor synthetic lethality with BRCA deficiency. *Mol Cell*. 2021;81(15):3227. doi:10.1016/j.molcel.2021.07.015

196. Waldman AD, Fritz JM, Lenardo MJ. A guide to cancer immunotherapy: from T cell basic science to clinical practice. *Nat Rev Immunol*. 2020;20(11):651-668. doi:10.1038/s41577-020-0306-5

197. Cancer Research Institute. FDA Approval Timeline of Active Immunotherapies. https://www.cancerresearch.org/en-us/scientists/immuno-oncology-landscape/fda-approval-timeline-of-active-immunotherapies. Published 2022. Accessed August 7, 2022.

198. Bausart M, Préat V, Malfanti A. Immunotherapy for glioblastoma: the promise of combination strategies. *J Exp Clin Cancer Res*. 2022;41(1). doi:10.1186/s13046-022-02251-2

199. Himes BT, Geiger PA, Ayasoufi K, Bhargav AG, Brown DA, Parney IF. Immunosuppression in Glioblastoma: Current Understanding and Therapeutic Implications. *Front Oncol*. 2021;11(770561). doi:10.3389/fonc.2021.770561

200. Sanders S, Debinski W. Challenges to successful implementation of the immune checkpoint inhibitors for treatment of glioblastoma. *Int J Mol Sci*. 2020;21(8). doi:10.3390/ijms21082759

201. Platten M. EGFRvIII vaccine in glioblastoma-InACT-IVe or not ReACTive enough? *Neuro Oncol*. 2017;19(11):1425-1426. doi:10.1093/neuonc/nox167

202. Huang B, Li X, Li Y, Zhang J, Zong Z, Zhang H. Current Immunotherapies for Glioblastoma Multiforme. *Front Immunol*. 2021;11(603911). doi:10.3389/fimmu.2020.603911

203. Yu J, Sun H, Cao W, Song Y, Jiang Z. Research progress on dendritic cell vaccines in cancer immunotherapy. *Exp Hematol Oncol*. 2022;11(1). doi:10.1186/s40164-022-00257-2

204. Sterner RC, Sterner RM. CAR-T cell therapy: current limitations and potential strategies. *Blood Cancer J*. 2021;11(4). doi:10.1038/s41408-021-00459-7

205. Rong L, Li N, Zhang Z. Emerging therapies for glioblastoma: current state and future directions. *J Exp Clin Cancer Res*. 2022;41(1). doi:10.1186/s13046-022-02349-7

206. Yang L, Gu X, Yu J, Ge S, Fan X. Oncolytic Virotherapy: From Bench to Bedside. *Front Cell Dev Biol*. 2021;9. doi:10.3389/fcell.2021.790150

207. Fabre M, Stanton NM, Slatter TL, et al. The oncogene BCL6 is up-regulated in glioblastoma in response to DNA damage, and drives survival after therapy. *PLoS One*. 2020;15(4). doi:10.1371/journal.pone.0231470

208. Ruggieri S, Tamma R, Marzullo A, et al. Translocation of the proto-oncogene Bcl-6 in human glioblastoma multiforme. *Cancer Lett*. 2014;353(1):41-51. doi:10.1016/j.canlet.2014.06.017

209. Xu L, Chen Y, Dutra-Clarke M, et al. BCL6 promotes glioma and serves as a therapeutic target. *Proc Natl Acad Sci U S A*. 2017;114(15):3981-3986. doi:10.1073/pnas.1609758114

210. Song W, Wang Z, Kan P, et al. Knockdown of BCL6 inhibited malignant phenotype and enhanced sensitivity of glioblastoma cells to TMZ through AKt pathway. *Biomed Res Int*. 2018;2018(6953506). doi:10.1155/2018/6953506

211. Zhou J, Liu R. Upregulation of miR-144-3p expression attenuates glioma cell viability and invasion by targeting BCL6. *Exp Ther Med*. 2021;22(4). doi:10.3892/etm.2021.10591

212. Kerckaert J, Deweindt C, Tilly H, et al. LAZ3, a novel zinc-finger encoding gene, is disrupted by recurring chromosome 3q27 translocations in human lymphomas. 1993;5:66-70. doi:10.1038/ng0993-66.

213. Albagli O, Dhordain P, Deweindt C, Lecocq G, Leprince D. The BTB/POZ domain: A new protein-protein interaction motif common to DNA- and actin-binding proteins. *Cell Growth Differ*. 1995;6:1193-1198.

214. Niu H, Ye BH, Dalla-Favera R. Antigen receptor signaling induces MAP kinase-mediated phosphorylation and degradation of the BCL-6 transcription factor. *Genes Dev*. 1998;12(13):1953-1961. doi:10.1101/gad.12.13.1953

215. Ahmad KF, Melnick A, Lax S, et al. Mechanism of SMRT Corepressor Recruitment by the BCL6 BTB Domain. *Mol Cell*. 2003;12(6):1551-1564. doi:10.1016/S1097-2765(03)00454-4

216. Chang CC, Ye BH, Chaganti RSK, Dalla-Favera R. BCL-6, a POZ/zinc-finger protein, is a sequence-specific transcriptional repressor. *Proc Natl Acad Sci U S A*. 1996;93(14):6947-6952. doi:10.1073/pnas.93.14.6947

217. Huynh KD, Bardwell VJ. The BCL-6 POZ domain and other POZ domains interact with the co-repressors N-CoR and SMRT. *Oncogene*. 1998;17(19):2473-2484. doi:10.1038/sj.onc.1202197

218. Dhordain P, Albagli O, Lin RJ, et al. Corepressor SMRT binds the BTB/POZ repressing domain of the LAZ3/BCL6 oncoprotein. *Proc Natl Acad Sci U S A*. 1997;94(20):10762-10767. doi:10.1073/pnas.94.20.10762

219. Huynh KD, Fischle W, Verdin E, Bardwell VJ. BCoR, a novel corepressor involved in BCL-6 repression. *Genes Dev*. 2000;14(14):1810-1823. doi:10.1101/gad.14.14.1810

220. Ghetu AF, Corcoran CM, Cerchietti L, Bardwell VJ, Melnick A, Privé GG. Structure of a BCOR corepressor peptide in complex with the BCL6 BTB domain dimer. *Mol Cell*. 2008;29(3):384-391. doi:10.1016/j.molcel.2007.12.026.

221. Mendez LM, Polo JM, Yu JJ, et al. CtBP Is an Essential Corepressor for BCL6 Autoregulation. *Mol Cell Biol*. 2008;28(7):2175-2186. doi:10.1128/mcb.01400-07

222. Fujita N, Jaye DL, Geigerman C, et al. MTA3 and the Mi-2/NuRD complex regulate cell fate during B lymphocyte differentiation. *Cell*. 2004;119(1):75-86. doi:10.1016/j.cell.2004.09.014

223. Lemercier C, Brocard MP, Puvion-Dutilleul F, Kao HY, Albagli O, Khochbin S. Class II histone deacetylases are directly recruited by BCL6 transcriptional repressor. *J Biol Chem*. 2002;277(24):22045-22052. doi:10.1074/jbc.M201736200

224. Guenther MG, Barak O, Lazar MA. The SMRT and N-CoR Corepressors Are Activating Cofactors for Histone Deacetylase 3. *Mol Cell Biol*. 2001;21(18):6091-6101. doi:10.1128/mcb.21.18.6091-6101.2001

225. Dhordain P, Lin RJ, Quief S, et al. The LAZ3(BCL-6) oncoprotein recruits a SMRT/mSIN3A/histone deacetylase containing complex to mediate transcriptional repression. *Nucleic Acids Res*. 1998;26(20):4645-4651. doi:10.1093/nar/26.20.4645

226. Nagy L, Kao HY, Chakravarti D, et al. Nuclear receptor repression mediated by a complex containing SMRT, mSin3A, and histone deacetylase. *Cell*. 1997;89(3):373-380. doi:10.1016/S0092-8674(00)80218-4

227. Basso K, Saito M, Sumazin P, et al. Integrated biochemical and computational approach identifies BCL6 direct target genes controlling multiple pathways in normal germinal center B cells. *Blood*. 2010;115(5):975-984. doi:10.1182/blood-2009-06-227017

228. Hatzi K, Jiang Y, Huang C, et al. A hybrid mechanism of action for BCL6 in B-cells defined by formation of functionally distinct complexes at enhancers and promoters. *Cell Rep*. 2013;4(3):578-588. doi:10.1016/j.celrep.2013.06.016.A

229. Béguelin W, Teater M, Gearhart MD, et al. EZH2 and BCL6 Cooperate to Assemble CBX8-BCOR Complex to Repress Bivalent Promoters, Mediate Germinal Center Formation and Lymphomagenesis. *Cancer Cell*. 2016;30(2):197-213. doi:10.1016/j.ccell.2016.07.006

230. Baron BW, Nucifora G, Mccabe N, Espinosa R, Le Beau MM, Mckeithan TW. Identification of the gene associated with the recurring chromosomal translocations t(3;14)(q27;q32) and

t(3;22)(q27;q11) in B-cell lymphomas. *Proc Natl Acad Sci U S A*. 1993;90(11):5262-5266. doi:10.1073/pnas.90.11.5262

231. Ye BH, Rao PH, Chaganti RSK, Dalla-Favera R. Cloning of bcl-6, the Locus Involved in Chromosome Translocations Affecting Band 3q27 in B-Cell Lymphoma. *Cancer Res*. 1993;53(12):2732-2735.

232. Basso K, Dalla-Favera R. Roles of BCL6 in normal and transformed germinal center B cells. *Immunol Rev*. 2012;247(1):172-183. doi:10.1111/j.1600-065X.2012.01112.x

233. Song S, Matthias PD. The transcriptional regulation of germinal center formation. *Front Immunol*. 2018;9(2026). doi:10.3389/fimmu.2018.02026

234. Basso K. Biology of Germinal Center B Cells Relating to Lymphomagenesis. *HemaSphere*. 2021;5(6):E582. doi:10.1097/HS9.0000000000000582

235. Victoria GD, Schwickert TA, Fooksman DR, et al. Germinal Center Dynamics Revealed by Multiphoton Microscopy Using a Photoactivatable Fluorescent Reporter. *Cell*. 2010;143(4):592-605. doi:10.1016/j.cell.2010.10.032.

236. Di Noia JM, Neuberger MS. Molecular mechanisms of antibody somatic hypermutation. *Annu Rev Biochem*. 2007;76:1-22. doi:10.1146/annurev.biochem.76.061705.090740

237. Kitano M, Moriyama S, Ando Y, et al. Bcl6 Protein Expression Shapes Pre-Germinal Center B Cell Dynamics and Follicular Helper T Cell Heterogeneity. *Immunity*. 2011;34(6):961-972. doi:10.1016/j.immuni.2011.03.025

238. Ye BH, Cattoretti G, Shen Q, et al. The BCL-6 proto-oncogene controls germinal-centre formation and Th2-type inflammation. *Nat Genet*. 1997;16:161-170.

239. Jackson SP, Bartek J. The DNA-damage response in human biology and disease. *Nature*. 2009;461(7267):1071-1078. doi:10.1038/nature08467

240. Phan RT, Dalla-Favera R. The BCL6 proto-oncogene suppresses p53 expression in germinal-centre B cells. *Nature*. 2004;432(7017):630-635. doi:10.1038/nature03148

241. Ranuncolo SM, Polo JM, Dierov J, et al. Bcl-6 mediates the germinal center B cell phenotype and lymphomagenesis through transcriptional repression of the DNA-damage sensor ATR. *Nat Immunol*. 2007;8(7):705-714. doi:10.1038/ni1478

242. Ranuncolo SM, Polo JM, Melnick A. BCL6 represses CHEK1 and suppresses DNA damage pathways in normal and malignant B-cells. *Blood Cells, Mol Dis*. 2008;41(1):95-99. doi:10.1016/j.bcmd.2008.02.003

243. Phan RT, Saito M, Basso K, Niu H, Dalla-Favera R. BCL6 interacts with the transcription factor Miz-1 to suppress the cyclin-dependent kinase inhibitor p21 and cell cycle arrest in germinal center B cells. *Nat Immunol*. 2005;6(10):1054-1060. doi:10.1038/ni1245

244. Saito M, Novak U, Piovan E, et al. BCL6 suppression of BCL2 via Miz1 and its disruption in diffuse large B cell lymphoma. *Proc Natl Acad Sci U S A*. 2009;106(27):11294-11299. doi:10.1073/pnas.0903854106

245. Saito M, Gao J, Basso K, et al. A Signaling Pathway Mediating Downregulation of BCL6 in Germinal Center B Cells Is Blocked by BCL6 Gene Alterations in B Cell Lymphoma. *Cancer Cell*. 2007;12(3):280-292. doi:10.1016/j.ccr.2007.08.011

246. Tunyaplin C, Shaffer AL, Angelin-Duclos CD, Yu X, Staudt LM, Calame KL. Direct Repression of prdm1 by Bcl-6 Inhibits Plasmacytic Differentiation . *J Immunol*. 2004;173(2):1158-1165. doi:10.4049/jimmunol.173.2.1158

247. Ochiai K, Maienschein-Cline M, Simonetti G, et al. Transcriptional regulation of germinal

center B and plasma cell fates by dynamical control of IRF4. *Immunity*. 2013;38(5):918-929. doi:10.1016/j.immuni.2013.04.009.

248. Chu CS, Hellmuth JC, Singh R, et al. Unique Immune Cell Coactivators Specify Locus Control Region Function and Cell Stage. *Mol Cell*. 2020;80(5):845-861.e10. doi:10.1016/j.molcel.2020.10.036

249. Chang HL, Melchers M, Wang H, et al. Regulation of the germinal center gene program by interferon (IFN) regulatory factor 8/IFN consensus sequence-binding protein. *J Exp Med*. 2006;203(1):63-72. doi:10.1084/jem.20051450

250. Yoon J, Feng X, Kim YS, et al. Interferon regulatory factor 8 (IRF8) interacts with the B cell lymphoma 6 (BCL6) corepressor BCOR. *J Biol Chem*. 2014;289(49):34250-34257. doi:10.1074/jbc.M114.571182

251. Pasqualucci L, Migliazza A, Basso K, Houldsworth J, Chaganti RSK, Dalla-Favera R. Mutations of the BCL6 proto-oncogene disrupt its negative autoregulation in diffuse large B-cell lymphoma. *Blood*. 2003;101(8):2914-2923. doi:10.1182/blood-2002-11-3387

252. Bereshchenko OR, Gu W, Dalla-Favera R. Acetylation inactivates the transcriptional repressor BCL6. *Nat Genet*. 2002;32(4):606-613. doi:10.1038/ng1018

253. Jiang Y, Ortega-Molina A, Geng H, et al. CREBBP inactivation promotes the development of HDAC3 dependent lymphomas. *Cancer Discov*. 2017;7(1):38-53. doi:10.1158/2159-8290.CD-16-0975.CREBBP

254. Polo JM, Ci W, Licht JD, Melnick A. Reversible disruption of BCL6 repression complexes by CD40 signaling in normal and malignant B cells. *Blood*. 2008;112(3):644-651. doi:10.1182/blood-2008-01-131813

255. Duan S, Cermak L, Pagan JK, et al. FBXO11 targets BCL6 for degradation and is inactivated in diffuse large B-cell lymphomas. *Nature*. 2012;481(7379):90-94. doi:10.1038/nature10688

256. Choi J, Diao H, Faliti CE, et al. Bcl-6 is the nexus transcription factor of T follicular helper cells via repressor-of-repressor circuits. *Nat Immunol*. 2020;21(7):777-789. doi:10.1038/s41590-020-0706-5

257. Johnston RJ, Poholek AC, DiToro D, et al. Bcl6 and Blimp-1 Are Reciprocal and Antagonistic Regulators of T Follicular Helper Cell Differentiation. *Science (80- )*. 2009;325(5943):1006-1010. doi:10.1126/science.1175870

258. Hatzi K, Philip Nance J, Kroenke MA, et al. BCL6 orchestrates Tfh cell differentiation via multiple distinct mechanisms. *J Exp Med*. 2015;212(4):539-553. doi:10.1084/jem.20141380

259. Huang C, Hatzi K, Melnick A. Lineage-specific functions of Bcl-6 in immunity and inflammation are mediated through distinct biochemical mechanisms. *Nat Immunol*. 2013;14(4):380-388. doi:10.1016/j.physbeh.2017.03.040

260. Nance JP, Bélanger S, Johnston RJ, Hu JK, Takemori T, Crotty S. Bcl6 middle domain repressor function is required for T follicular helper cell differentiation and utilizes the corepressor MTA3. *Proc Natl Acad Sci U S A*. 2015;112(43):13324-13329. doi:10.1073/pnas.1507312112

261. Ichii H, Sakamoto A, Hatano M, et al. Role for BcL-6 in the generation and maintenance of memory CD8+ T cells. *Nat Immunol*. 2002;3(6):558-563. doi:10.1038/ni802

262. Liu Z, Guo Y, Tang S, et al. Cutting Edge: Transcription Factor BCL6 Is Required for the Generation, but Not Maintenance, of Memory CD8 + T Cells in Acute Viral Infection . *J Immunol*. 2019;203(2):323-327. doi:10.4049/jimmunol.1900014

263. Wu T, Ji Y, Moseman EA, et al. The TCF1-Bcl6 axis counteracts type I interferon to repress exhaustion and maintain T cell stemness. *Sci Immunol*. 2016;1(6).

doi:10.1126/sciimmunol.aai8593.

264. Yoshida K, Sakamoto A, Yamashita K, et al. Bcl6 controls granzyme B expression in effector CD8+ T cells. *Eur J Immunol*. 2006;36(12):3146-3156. doi:10.1002/eji.200636165

265. Josefowicz SZ, Lu L-F, Rudensky AY. Regulatory T Cells: Mechanisms of Differentiation and Function. *Annu Rev Immunol*. 2012;30:531-564. doi:10.1146/annurev.immunol.25.022106.141623.

266. Sawant D V., Wu H, Yao W, Sehra S, Kaplan MH, Dent AL. The transcriptional repressor Bcl6 controls the stability of regulatory T cells by intrinsic and extrinsic pathways. *Immunology*. 2015;145(1):11-23. doi:10.1111/imm.12393

267. Li Y, Wang Z, Lin H, et al. Bcl6 Preserves the Suppressive Function of Regulatory T Cells During Tumorigenesis. *Front Immunol*. 2020;11(806). doi:10.3389/fimmu.2020.00806

268. Chung Y, Tanaka S, Chu F, et al. Follicular regulatory T cells expressing Foxp3 and Bcl-6 suppress germinal center reactions. *Nat Med*. 2011;17(8):983-988. doi:10.1038/nm.2426

269. Li Q, Zhou L, Wang L, et al. Bcl6 modulates innate immunity by controlling macrophage activity and plays critical role in experimental autoimmune encephalomyelitis. *Eur J Immunol*. 2020;50(4):525-536. doi:10.1002/eji.201948299

270. Yu RYL, Wang X, Pixley FJ, et al. BCL-6 negatively regulates macrophage proliferation by suppressing autocrine IL-6 production. *Blood*. 2005;105(4):1777-1784. doi:10.1182/blood-2004-08-3171

271. Desai NN, Zhu B, Son Y, Sun J. Inhibition of effective anti-tumor immunity by macrophage Bcl6. *J Immunol*. 2019;202(1):135.28.

272. Tiberi L, Van Den Ameele J, Dimidschstein J, et al. BCL6 controls neurogenesis through Sirt1-dependent epigenetic repression of selective Notch targets. *Nat Neurosci*. 2012;15(12):1627-1635. doi:10.1038/nn.3264

273. Bonnefont J, Tiberi L, van den Ameele J, et al. Cortical Neurogenesis Requires Bcl6-Mediated Transcriptional Repression of Multiple Self-Renewal-Promoting Extrinsic Pathways. *Neuron*. 2019;103(6):1096-1108.e4. doi:10.1016/j.neuron.2019.06.027

274. Wiegraffe C, Wahl T, Joos NS, Bonnefont J, Liu P, Britsch S. Developmental cell death of cortical projection neurons is 2 controlled by a Bcl11a/Bcl6-dependent pathway. *EMBO Rep*. 2022;23:e54104. doi:10.15252/embr.202154104

275. Tiberi L, Bonnefont J, VandenAmeele J, et al. A BCL6/BCOR/SIRT1 Complex Triggers Neurogenesis and Suppresses Medulloblastoma by Repressing Sonic Hedgehog Signaling. *Cancer Cell*. 2014;26(6):797-812. doi:10.1016/j.ccell.2014.10.021

276. Chen W, Iida S, Louie DC, Dalla-Favera R, Chaganti RSK. Heterologous promoters fused to BCL6 by chromosomal translocations affecting band 3q27 cause its deregulated expression during B-cell differentiation. *Blood*. 1998;91(2):603-607. doi:10.1182/blood.v91.2.603.603_603_607

277. Ye BH. BCL-6 in the pathogenesis of non-Hodgkin's lymphoma. *Cancer Invest*. 2000;18(4):356-365. doi:10.3109/07357900009012179

278. Wang X, Li Z, Naganuma A, Ye BH. Negative autoregulation of BCL-6 is bypassed by genetic alterations in diffuse large B cell lymphomas. *Proc Natl Acad Sci U S A*. 2002;99(23):15018-15023. doi:10.1073/pnas.232581199

279. Lo Coco F, Ye BH, Lista F, et al. Rearrangements of the BCL6 gene in diffuse large cell non-Hodgkin's lymphoma. *Blood*. 1994;83(7):1757-1759.

280. Otsuki T, Yano T, Clark HM, et al. Analysis of LAZ3 (BCL-6) status in B-cell non-Hodgkin's lymphomas: Results of rearrangement and gene expression studies and a mutational analysis of coding region sequences. *Blood*. 1995;85(10):2877-2884. doi:10.1182/blood.v85.10.2877.bloodjournal85102877

281. Bastard C, Deweindt C, Kerckaert J, et al. LAZ3 rearrangements in non-Hodgkin's lymphoma: correlation with histology, immunophenotype, karyotype, and clinical outcome in 217 patients. *Blood*. 1994;83(9):2423-2427. doi:10.1182/blood.v83.9.2423.2423

282. Shen HM, Peters A, Baron B, Zhu X, Storb U. Mutation of BCL-6 gene in normal B cells by the process of somatic hypermutation of Ig genes. *Science (80- )*. 1998;280(5370):1750-1752. doi:10.1126/science.280.5370.1750

283. Pasqualucci L, Migliazza A, Fracchiolla N, et al. BCL-6 mutations in normal germinal center B cells: Evidence of somatic hypermutation acting outside Ig loci. *Proc Natl Acad Sci U S A*. 1998;95(20):11816-11821. doi:10.1073/pnas.95.20.11816

284. Pasqualucci L, Dominguez-Sola D, Chiarenza A, et al. Inactivating mutations of acetyltransferase genes in B-cell lymphoma. *Nature*. 2011;471(7337):189-196. doi:10.1038/nature09730

285. Schneider C, Kon N, Amadori L, et al. FBXO11 inactivation leads to abnormal germinal-center formation and lymphoproliferative disease. *Blood*. 2016;128(5):660-666. doi:10.1182/blood-2015-11-684357

286. Ying CY, Dominguez-Sola D, Fabi M, et al. MEF2B mutations lead to deregulated expression of the BCL6 oncogene in Diffuse Large B cell Lymphoma. *Nat Immunol*. 2013;14(10):1084-1092. doi:10.1038/ni.2688.

287. Li H, Kaminski MS, Li Y, et al. Mutations in linker histone genes HIST1H1 B, C, D, and E; OCT2 (POU2F2); IRF8; and ARID1A underlying the pathogenesis of follicular lymphoma. *Blood*. 2014;123(10):1487-1498. doi:10.1182/blood-2013-05-500264

288. Leeman-Neill RJ, Bhagat G. BCL6 as a therapeutic target for lymphoma. *Expert Opin Ther Targets*. 2018;22(2):143-152. doi:10.1080/14728222.2018.1420782

289. Dent AL, Shaffer AL, Yu X, Allman D, Staudt LM. Control of inflammation, cytokine expression, and germinal center formation by BCL-6. *Science (80- )*. 1997;276(5312):589-592. doi:10.1126/science.276.5312.589

290. Polo JM, Dell'Oso T, Ranuncolo SM, et al. Specific peptide interference reveals BCL6 transcriptional and oncogenic mechanisms in B-cell lymphoma cells. *Nat Med*. 2004;10(12):1329-1335. doi:10.1038/nm1134

291. Cerchietti LC, Yang SN, Shaknovich R, et al. A peptomimetic inhibitor of BCL6 with potent antilymphoma effects in vitro and in vivo. *Blood*. 2009;113(15):3397-3405. doi:10.1182/blood-2008-07-168773

292. Chattopadhyay A, Tate SA, Beswick RW, Wagner SD, Ko Ferrigno P. A peptide aptamer to antagonize BCL-6 function. *Oncogene*. 2006;25(15):2223-2233. doi:10.1038/sj.onc.1209252

293. Zacharchenko T, Kalverda AP, Wright SC. Structural basis of Apt48 inhibition of the BCL6 BTB domain. *Structure*. 2022;30(3):396-407.e3. doi:10.1016/j.str.2021.10.010

294. Cerchietti LC, Ghetu AF, Zhu X, et al. A small molecule inhibitor of BCL6 kills DLBCL cells in vitro and in vivo. *Cancer Cell*. 2010;17(4):400-411. doi:10.1016/j.ccr.2009.12.050.A

295. Cardenas MG, Yu W, Beguelin W, et al. Rationally designed BCL6 inhibitors target activated B cell diffuse large B cell lymphoma. *J Clin Invest*. 2016;126(9):3351-3362. doi:10.1172/JCI85795

296. Yasui T, Yamamoto T, Sakai N, et al. Discovery of a novel B-cell lymphoma 6 (BCL6)–corepressor interaction inhibitor by utilizing structure-based drug design. *Bioorganic Med Chem*. 2017;25(17):4876-4886. doi:10.1016/j.bmc.2017.07.037

297. Kamada Y, Sakai N, Sogabe S, et al. Discovery of a B-Cell Lymphoma 6 Protein-Protein Interaction Inhibitor by a Biophysics-Driven Fragment-Based Approach. *J Med Chem*. 2017;60(10):4358-4368. doi:10.1021/acs.jmedchem.7b00313

298. Evans SE, Goult BT, Fairall L, et al. The ansamycin antibiotic, rifamycin SV, inhibits BCL6 transcriptional repression and forms a complex with the BCL6-BTB/POZ domain. *PLoS One*. 2014;9(3). doi:10.1371/journal.pone.0090889

299. Kerres N, Steurer S, Schlager S, et al. Chemically Induced Degradation of the Oncogenic Transcription Factor BCL6. *Cell Rep*. 2017;20(12):2860-2875. doi:10.1016/j.celrep.2017.08.081

300. Xing Y, Guo W, Wu M, et al. An orally available small molecule BCL6 inhibitor effectively suppresses diffuse large B cell lymphoma cells growth in vitro and in vivo. *Cancer Lett*. 2022;529:100-111. doi:10.1016/j.canlet.2021.12.035

301. Dupont T, Yang SN, Patel J, et al. Selective targeting of BCL6 induces oncogene addiction switching to BCL2 in B-cell lymphoma. *Oncotarget*. 2016;7(3):3520-3532. doi:10.18632/oncotarget.6513

302. Duy C, Hurtz C, Shojaee S, et al. BCL6 enables Ph+ acute lymphoblastic leukaemia cells to survive BCR-ABL1 kinase inhibition. *Nature*. 2011;473(7347):384-391. doi:10.1038/nature09883

303. Hurtz C, Hatzi K, Cerchietti L, et al. BCL6-mediated repression of p53 is critical for leukemia stem cell survival in chronic myeloid leukemia. *J Exp Med*. 2011;208(11):2163-2174. doi:10.1084/jem.20110304

304. Hurtz C, Chan LN, Geng H, et al. Rationale for targeting BCL6 in MLL-rearranged acute lymphoblastic leukemia. *Genes Dev*. 2019;33(17-18):1265-1279. doi:10.1101/gad.327593.119

305. Kawabata KC, Zong H, Meydan C, et al. BCL6 maintains survival and self-renewal of primary human acute myeloid leukemia cells. *Blood*. 2021;137(6):812-825. doi:10.1182/blood.2019001745

306. Jantus Lewintre E, Reinoso Martín C, García Ballesteros C, et al. BCL6: Somatic mutations and expression in early-stage chronic lymphocytic leukemia. *Leuk Lymphoma*. 2009;50(5):773-780. doi:10.1080/10428190902842626

307. Walker SR, Liu S, Xiang M, et al. The transcriptional modulator BCL6 as a molecular target for breast cancer therapy. *Oncogene*. 2015;34(9):1073-1082. doi:10.1038/onc.2014.61

308. Wu Q, Liu X, Yan H, et al. B-cell lymphoma 6 protein stimulates oncogenicity of human breast cancer cells. *BMC Cancer*. 2014;14(1). doi:10.1186/1471-2407-14-418

309. Sultan M, Nearing JT, Brown JM, et al. An in vivo genome-wide shRNA screen identifies BCL6 as a targetable biomarker of paclitaxel resistance in breast cancer. *Mol Oncol*. 2021;15(8):2046-2064. doi:10.1002/1878-0261.12964

310. Tran YZ, Minozada R, Cao X, et al. Immediate adaptation analysis implicates BCL6 as an EGFR-TKI combination therapy target in NSCLC. *Mol Cell Proteomics*. 2020;19(6):928-943. doi:10.1074/mcp.RA120.002036

311. Guo J, Liu Y, Lv J, et al. BCL6 confers KRAS-mutant non-small-cell lung cancer resistance to BET inhibitors. *J Clin Invest*. 2021;131(1):e133090. doi:10.1172/JCI133090

312. Deb D, Rajaram S, Larsen JE, et al. Combination therapy targeting BCL6 and phospho-STAT3

defeats intra-tumor heterogeneity in a subset of non-small cell lung cancers. *Cancer Res*. 2017;77(11):3070-3081. doi:10.1158/0008-5472.CAN-15-3052

313. Wang YQ, Xu MD, Weng WW, Wei P, Yang YS, Du X. BCL6 is a negative prognostic factor and exhibits pro-oncogenic activity in ovarian cancer. *Am J Cancer Res*. 2015;5(1):255-266.

314. Zhu L, Feng H, Jin S, et al. High expressions of BCL6 and lewis y antigen are correlated with high tumor burden and poor prognosis in epithelial ovarian cancer. *Tumor Biol*. 2017;39(7). doi:10.1177/1010428317711655

315. Shen J, Hong L, Chen L. Ubiquitin-specific protease 14 regulates ovarian cancer cisplatin-resistance by stabilizing BCL6 oncoprotein. *Biochem Biophys Res Commun*. 2020;524(3):683-688. doi:10.1016/j.bbrc.2020.01.150

316. Sena P, Mariani F, Benincasa M, et al. Morphological and quantitative analysis of BCL6 expression in human colorectal carcinogenesis. *Oncol Rep*. 2014;31(1):103-110. doi:10.3892/or.2013.2846

317. Sun N, Zhang L, Zhang C, Yuan Y. MiR-144-3p inhibits cell proliferation of colorectal cancer cells by targeting BCL6 via inhibition of Wnt/β-catenin signaling. *Cell Mol Biol Lett*. 2020;25(19). doi:10.1186/s11658-020-00210-3

318. Hirata Y, Ogasawara N, Sasaki M, et al. BCL6 degradation caused by the interaction with the C-terminus of pro-HB-EGF induces cyclin D2 expression in gastric cancers. *Br J Cancer*. 2009;100(8):1320-1329. doi:10.1038/sj.bjc.6605010

319. Bahria-Sediki I Ben, Yousfi N, Paul C, et al. Clinical significance of T-bet, GATA-3, and Bcl-6 transcription factor expression in bladder carcinoma. *J Transl Med*. 2016;14(1):1-11. doi:10.1186/s12967-016-0891-z

320. Wu WR, Lin JT, Pan CT, et al. Amplification-driven BCL6-suppressed cytostasis is mediated by transrepression of FOXO3 and post-translational modifications of FOXO3 in urinary bladder urothelial carcinoma. *Theranostics*. 2020;10(2):707-724. doi:10.7150/thno.39018

321. Brennan CW, Verhaak RGW, McKenna A, et al. The Somatic Genomic Landscape of Glioblastoma. *Cell*. 2014;157(3):462-477. doi:10.1016/j.cell.2014.04.004

322. Jones NM. The Role of BCL6 in Glioblastoma. 2018.

323. Broadley KWR, Hunn MK, Farrand KJ, et al. Side population is not necessary or sufficient for a cancer stem cell phenotype in glioblastoma multiforme. *Stem Cells*. 2011;29(3):452-461. doi:10.1002/stem.582

324. Davarinejad H. Quantifications of Western Blots with ImageJ. York University, Toronto, Canada. http://www.yorku.ca/yisheng/Internal/Protocols/ImageJ.pdf. Accessed March 14, 2022.

325. Schindelin J, Arganda-Carreras I, Frise E, et al. Fiji: An open-source platform for biological-image analysis. *Nat Methods*. 2012;9(7):676-682. doi:10.1038/nmeth.2019

326. Kent WJ, Sugnet CW, Furey TS, et al. The Human Genome Browser at UCSC. *Genome Res*. 2002;12(6):996-1006. doi:10.1101/gr.229102

327. Untergasser A, Cutcutache I, Koressaar T, et al. Primer3-new capabilities and interfaces. *Nucleic Acids Res*. 2012;40(15):e115. doi:10.1093/nar/gks596

328. IDT, Coralville, Iowa U. PrimerQuest(R) program. https://www.idtdna.com/SciTools.

329. Bateman A, Martin MJ, Orchard S, et al. UniProt: the universal protein knowledgebase in 2021. *Nucleic Acids Res*. 2021;49(D1):D480-D489. doi:10.1093/nar/gkaa1100

330. Raudvere U, Kolberg L, Kuzmin I, et al. G:Profiler: A web server for functional enrichment analysis and conversions of gene lists (2019 update). *Nucleic Acids Res*. 2019;47(W1):W191-W198. doi:10.1093/nar/gkz369

331. Howe KL, Achuthan P, Allen J, et al. Ensembl 2021. *Nucleic Acids Res*. 2021;49(D1):D884-D891. doi:10.1093/nar/gkaa942

332. Szklarczyk D, Gable AL, Nastou KC, et al. The STRING database in 2021: Customizable protein-protein networks, and functional characterization of user-uploaded gene/measurement sets. *Nucleic Acids Res*. 2021;49(D1):D605-D612. doi:10.1093/nar/gkaa1074

333. Center for Computational Mass Spectrometry. MassIVE (Mass Spectrometry Interactive Virtual Environment). University of California, San Diego, USA. https://massive.ucsd.edu/ProteoSAFe/static/massive.jsp. Accessed September 2, 2022.

334. Foster ED, Deardorff A. Open Science Framework (OSF). *J Med Libr Assoc*. 2017;105(2):203-206. doi:dx.doi.org/10.5195/jmla.2017.88

335. Mohammed H, Taylor C, Brown GD, Papachristou EK, Carroll JS, D'Santos CS. Rapid immunoprecipitation mass spectrometry of endogenous proteins (RIME) for analysis of chromatin complexes. *Nat Protoc*. 2016;11(2):316-326. doi:10.1038/nprot.2016.020

336. Orchard S, Ammari M, Aranda B, et al. The MIntAct project - IntAct as a common curation platform for 11 molecular interaction databases. *Nucleic Acids Res*. 2014;42(D1):358-363. doi:10.1093/nar/gkt1115

337. Merck. Duolink® PLA Fluorescence Protocol. https://www.sigmaaldrich.com/NZ/en/technical-documents/protocol/protein-biology/protein-and-nucleic-acid-interactions/duolink-fluorescence-user-manual. Accessed August 23, 2022.

338. Alam MS. Proximity Ligation Assay (PLA). *Curr Protoc Immunol*. 2018;123(1):191-201. doi:10.1002/cpim.58.

339. Stirling DR, Swain-Bowden MJ, Lucas AM, Carpenter AE, Cimini BA, Goodman A. CellProfiler 4: improvements in speed, utility and usability. *BMC Bioinformatics*. 2021;22(1). doi:10.1186/s12859-021-04344-9

340. Pichette B. Color Pixel Counter. ImageJ Documentation Wiki. https://imagejdocu.list.lu/plugin/color/color_pixel_counter/start. Published 2010. Accessed August 3, 2022.

341. Altschul SF, Gish W, Miller W, Myers EW, Lipman DJ. Basic local alignment search tool. *J Mol Biol*. 1990;215(3):403-410. doi:10.1016/S0022-2836(05)80360-2

342. Oxford Nanopre Technologies. PCR-cDNA sequencing (SQK-PCS109). 2019. https://nanoporetech.com/resource-centre/knowledge.

343. Oxford Nanopre Technologies. Native barcoding amplicons (with EXP-NBD104 , EXP-NBD114, and SQK-LSK109). 2019.

344. Brooks Lab, University of Santa Cruz C. BrooksLabUCSC/flair/misc/flair_conda_env.yaml. GitHub.

345. Tang AD, Soulette CM, van Baren MJ, et al. Full-length transcript characterization of SF3B1 mutation in chronic lymphocytic leukemia reveals downregulation of retained introns. *Nat Commun*. 2020;11(1). doi:10.1038/s41467-020-15171-6

346. Robinson JT, Thorvaldsdóttir H, Winckler W, et al. Integrative Genome Viewer. *Nat Biotechnol*. 2011;29(1):24-26. doi:10.1038/nbt.1754.

347. Ostrom QT, Cioffi G, Gittleman H, et al. CBTRUS Statistical Report: Primary Brain and Other

Central Nervous System Tumors Diagnosed in the United States in 2012-2016. *Neuro Oncol*. 2019;21:V1-V100. doi:10.1093/neuonc/noz150

348. Witthayanuwat S, Pesee M, Supaadirek C, Supakalin N, Thamronganantasakul K, Krusun S. Survival analysis of Glioblastoma Multiforme. *Asian Pacific J Cancer Prev*. 2018;19(9):2613-2617. doi:10.22034/APJCP.2018.19.9.2613

349. Delgado-López PD, Corrales-García EM. Survival in glioblastoma: a review on the impact of treatment modalities. *Clin Transl Oncol*. 2016;18(11):1062-1071. doi:10.1007/s12094-016-1497-x

350. Cardenas MG, Oswald E, Yu W, Xue F, MacKerell Jr. AD, Melnick AM. The expanding role of the BCL6 oncoprotein as a cancer therapeutic target. *Clin Cancer Res*. 2017;23(4):885-893. doi:10.1586/1744666X.2014.967684.The

351. Liu Y, Feng J, Yuan K, et al. The oncoprotein BCL6 enables solid tumor cells to evade genotoxic stress. *Elife*. 2022;11. doi:10.7554/eLife.69255

352. Wu HB, Lv WF, Wang YX, Li YY, Guo W. BCL6 promotes the methotrexate-resistance by upregulating ZEB1 expression in children with acute B lymphocytic leukemia. *Eur Rev Med Pharmacol Sci*. 2018;22(16):5240-5247. doi:10.26355/eurrev_201808_15722

353. Kurosu T, Fukuda T, Miki T, Miura O. BCL6 overexpression prevents increase in reactive oxygen species and inhibits apoptosis induced by chemotherapeutic reagents in B-cell lymphoma cells. *Oncogene*. 2003;22(29):4459-4468. doi:10.1038/sj.onc.1206755

354. Slone WL, Moses BS, Hare I, Evans R, Piktel D, Gibson LF. Bcl6 modulation of acute lymphoblastic leukemia response to chemotherapy. *Oncotarget*. 2016;7(17):23439-23453. doi:10.18632/oncotarget.8273

355. Norouzi M, Yathindranath V, Thliveris JA, Kopec BM, Siahaan TJ, Miller DW. Doxorubicin-loaded iron oxide nanoparticles for glioblastoma therapy: a combinational approach for enhanced delivery of nanoparticles. *Sci Rep*. 2020;10(1). doi:10.1038/s41598-020-68017-y

356. Sohail M, Sun Z, Li Y, Gu X, Xu H. Research progress in strategies to improve the efficacy and safety of doxorubicin for cancer chemotherapy. *Expert Rev Anticancer Ther*. 2021;21(12):1385-1398. doi:10.1080/14737140.2021.1991316

357. Thorn CF, Oshiro C, Marsh S, et al. Doxorubicin pathways. *Pharmacogenet Genomics*. 2011;21(7):440-446. doi:10.1097/fpc.0b013e32833ffb56

358. Heberle H, Meirelles VG, da Silva FR, Telles GP, Minghim R. InteractiVenn: A web-based tool for the analysis of sets through Venn diagrams. *BMC Bioinformatics*. 2015;16(1). doi:10.1186/s12859-015-0611-3

359. Gotter AL, Suppa C, Emanuel BS. Mammalian TIMELESS and Tipin are Evolutionarily Conserved Replication Fork-Associated Factors. *J Mol Biol*. 2007;366(1):36-52. doi:10.1016/j.jmb.2006.10.097.Mammalian

360. Chou DM, Elledge SJ. Tipin and Timeless form a mutually protective complex required for genotoxic stress resistance and checkpoint function. *Proc Natl Acad Sci U S A*. 2006;103(48):18143-18147. doi:10.1073/pnas.0609251103

361. Wan L, Han J, Liu T, et al. Scaffolding protein SPIDR/KIAA0146 connects the Bloom syndrome helicase with homologous recombination repair. *Proc Natl Acad Sci U S A*. 2013;110(26):10646-10651. doi:10.1073/pnas.1220921110

362. Acharya S, Wilson T, Gradia S, et al. hMSH2 forms specific mispair-binding complexes with hMSH3 and hMSH6. *Proc Natl Acad Sci U S A*. 1996;93(24):13629-13634. doi:10.1073/pnas.93.24.13629

363. Luo Y, Na Z, Slavoff SA. P-Bodies: Composition, Properties, and Functions. *Biochemistry*. 2018;57(17):2424-2431. doi:10.1021/acs.biochem.7b01162

364. Hochegger H, Takeda S, Hunt T. Cyclin-dependent kinases and cell-cycle transitions: does one fit all? *Nat Rev Mol Cell Biol*. 2008;9(900-916). doi:10.1038/nrm2510.

365. Arnoult D, Grodet A, Lee YJ, Estaquier J, Blackstone C. Release of OPA1 during apoptosis participates in the rapid and complete release of cytochrome c and subsequent mitochondrial fragmentation. *J Biol Chem*. 2005;280(42):35742-35750. doi:10.1074/jbc.M505970200

366. Oka T, Sayano T, Tamai S, et al. Identification of a Novel Protein MICS1 that is Involved in Maintenance of Mitochondrial Morphology and Apoptotic Release of Cytochrome c. *Mol Biol Cell*. 2008;19:2597-2608. doi:10.1091/mbc.E07

367. Marumoto T, Hirota T, Morisaki T, et al. Roles of aurora-A kinase in mitotic entry and G2 checkpoint in mammalian cells. *Genes to Cells*. 2002;7(11):1173-1182. doi:10.1046/j.1365-2443.2002.00592.x

368. Ji W, Luo Y, Ahmad E, Liu ST. Direct interactions of mitotic arrest deficient 1 (MAD1) domains with each other and MAD2 conformers are required for mitotic checkpoint signaling. *J Biol Chem*. 2018;293(2):484-496. doi:10.1074/jbc.RA117.000555

369. Kops GJPL, Kim Y, Weaver BAA, et al. ZW10 links mitotic checkpoint signaling to the structural kinetochore. *J Cell Biol*. 2005;169(1):49-60. doi:10.1083/jcb.200411118

370. Yost S, De Wolf B, Hanks S, et al. Biallelic TRIP13 mutations predispose to Wilms tumor and chromosome missegregation. *Nat Genet*. 2017;49(7):1148-1151. doi:10.1038/ng.3883

371. Liu D, Ding X, Du J, et al. Human NUF2 interacts with centromere-associated protein E and is essential for a stable spindle microtubule-kinetochore attachment. *J Biol Chem*. 2007;282(29):21415-21424. doi:10.1074/jbc.M609026200

372. Thornton BR, Ng TM, Matyskiela ME, Carroll CW, Morgan DO, Toczyski DP. An architectural map of the anaphase-promoting complex. *Genes Dev*. 2006;20(4):449-460. doi:10.1101/gad.1396906

373. Dyson NJ. RB1: A prototype tumor suppressor and an enigma. *Genes Dev*. 2016;30(13):1492-1502. doi:10.1101/gad.282145.116

374. Mayhew CN, Perkin LM, Zhang X, Sage J, Jacks T, Knudsen ES. Discrete signaling pathways participate in RB-dependent responses to chemotherapeutic agents. *Oncogene*. 2004;23(23):4107-4120. doi:10.1038/sj.onc.1207503

375. Herzig S, Shaw RJ. AMPK: guardian of metabolism and mitochondrial homeostasis. 2018;19(2):121-135. doi:10.1038/nrm.2017.95.

376. Wang B, Matsuoka S, Carpenter PB, Elledge SJ. 53BP1, a mediator of the DNA damage checkpoint. *Science (80- )*. 2002;298(5597):1435-1438. doi:10.1126/science.1076182

377. Hafner A, Bulyk ML, Jambhekar A, Lahav G. The multiple mechanisms that regulate p53 activity and cell fate. *Nat Rev Mol Cell Biol*. 2019;20(4):199-210. doi:10.1038/s41580-019-0110-x

378. Murn J, Zarnack K, Yang YJ, et al. Control of a neuronal morphology program by an RNA-binding zinc finger protein, Unkempt. *Genes Dev*. 2015;29(5):501-512. doi:10.1101/gad.258483.115

379. Roobol A, Roobol J, Bastide A, Knight JRP, Willis AE, Smales CM. P58IPK is an inhibitor of the eIF2α kinase GCN2 and its localization and expression underpin protein synthesis and ER processing capacity. *Biochem J*. 2015;465:213-225. doi:10.1042/BJ20140852

380. Takahashi K, Tanabe K, Ohnuki M, et al. Induction of Pluripotent Stem Cells from Adult Human Fibroblasts by Defined Factors. *Cell*. 2007;131(5):861-872. doi:10.1016/j.cell.2007.11.019

381. Takenaga M, Hatano M, Takamori M, et al. Bcl6-dependent transcriptional repression by BAZF. *Biochem Biophys Res Commun*. 2003;303(2):600-608. doi:10.1016/S0006-291X(03)00396-6

382. Shaffer AL, Yu X, He Y, Boldrick J, Chan EP, Staudt LM. BCL-6 represses genes that function in lymphocyte differentiation, inflammation, and cell cycle control. *Immunity*. 2000;13(2):199-212. doi:10.1016/S1074-7613(00)00020-0

383. Arima M, Toyama H, Ichii H, et al. A Putative Silencer Element in the IL-5 Gene Recognized by Bcl6 . *J Immunol*. 2002;169(2):829-836. doi:10.4049/jimmunol.169.2.829

384. Xu D, Guo R, Sobeck A, et al. RMI, a new OB-fold complex essential for Bloom syndrome protein to maintain genome stability. *Genes Dev*. 2008;22(20):2843-2855. doi:10.1101/gad.1708608

385. Ikura M, Furuya K, Matsuda S, et al. Acetylation of Histone H2AX at Lys 5 by the TIP60 Histone Acetyltransferase Complex Is Essential for the Dynamic Binding of NBS1 to Damaged Chromatin. *Mol Cell Biol*. 2015;35(24):4147-4157. doi:10.1128/mcb.00757-15

386. Taherbhoy AM, Huang OW, Cochran AG. BMI1-RING1B is an autoinhibited RING E3 ubiquitin ligase. *Nat Commun*. 2015;6(7621). doi:10.1038/ncomms8621

387. Zaug AJ, Podell ER, Nandakumar J, Cech TR. Functional interaction between telomere protein TPP1 and telomerase. *Genes Dev*. 2010;24(6):613-622. doi:10.1101/gad.1881810

388. Ye J, Lenain C, Bauwens S, et al. TRF2 and Apollo Cooperate with Topoisomerase 2α to Protect Human Telomeres from Replicative Damage. *Cell*. 2010;142(2):230-242. doi:10.1016/j.cell.2010.05.032

389. Snow BE, Erdmann N, Cruickshank J, et al. Functional Conservation of the Telomerase Protein Est1p in Humans. *Curr Biol*. 2003;13:698-704. doi:10.1016/S

390. Zhang QS, Manche L, Xu RM, Krainer AR. hnRNP A1 associates with telomere ends and stimulates telomerase activity. *RNA*. 2006;12(6):1116-1128. doi:10.1261/rna.58806

391. Sullivan KD, Mullen TE, Marzluff WF, Wagner EJ. Knockdown of SLBP results in nuclear retention of histone mRNA. *RNA*. 2009;15(3):459-472. doi:10.1261/rna.1205409

392. Pryor A, Tung L, Yang Z, Kapadia F, Chang TH, Johnson LF. Growth-regulated expression and G0-specific turover of the mRNA that encodes URH49, a mammalian DExH/D box protein that is highly related to the mRNA export protein UAP56. *Nucleic Acids Res*. 2004;32(6):1857-1865. doi:10.1093/nar/gkh347

393. Masuda S, Das R, Cheng H, Hurt E, Dorman N, Reed R. Recruitment of the human TREX complex to mRNA during splicing. *Genes Dev*. 2005;19(13):1512-1517. doi:10.1101/gad.1302205

394. Kuersten S, Arts G-J, Walther TC, Englmeier L, Mattaj IW. Steady-State Nuclear Localization of Exportin-t Involves RanGTP Binding and Two Distinct Nuclear Pore Complex Interaction Domains. *Mol Cell Biol*. 2002;22(16):5708-5720. doi:10.1128/mcb.22.16.5708-5720.2002

395. Jäkel S, Mingot J-M, Schwarzmaier P, Hartmann E, Görlich D. Importins fulfil a dual function as nuclear import receptors and cytoplasmic chaperones for exposed basic domains. *EMBO J*. 2002;21(3):377-386. doi:10.1093/emboj/21.3.377

396. Sasaki T, Toh-e A, Kikuchi Y. Yeast Krr1p Physically and Functionally Interacts with a Novel Essential Kri1p, and Both Proteins Are Required for 40S Ribosome Biogenesis in the Nucleolus. *Mol Cell Biol*. 2000;20(21):7971-7979. doi:10.1128/.20.21.7971-7979.2000

397. Sloan KE, Bohnsack MT, Watkins NJ. The 5S RNP Couples p53 Homeostasis to Ribosome Biogenesis and Nucleolar Stress. *Cell Rep*. 2013;5(1):237-247. doi:10.1016/j.celrep.2013.08.049

398. Tummala H, Walne AJ, Williams M, et al. DNAJC21 Mutations Link a Cancer-Prone Bone Marrow Failure Syndrome to Corruption in 60S Ribosome Subunit Maturation. *Am J Hum Genet*. 2016;99(1):115-124. doi:10.1016/j.ajhg.2016.05.002

399. Sokol AM, Sztolsztener ME, Wasilewski M, Heinz E, Chacinska A. Mitochondrial protein translocases for survival and wellbeing. *FEBS Lett*. 2014;588(15):2484-2495. doi:10.1016/j.febslet.2014.05.028

400. Vukotic M, Nolte H, König T, et al. Acylglycerol Kinase Mutated in Sengers Syndrome Is a Subunit of the TIM22 Protein Translocase in Mitochondria. *Mol Cell*. 2017;67(3):471-483.e7. doi:10.1016/j.molcel.2017.06.013

401. Baertling F, Sánchez-Caballero L, van den Brand MAM, et al. NDUFA9 point mutations cause a variable mitochondrial complex I assembly defect. *Clin Genet*. 2018;93(1):111-118. doi:10.1111/cge.13089

402. Costelloe T, Louge R, Tomimatsu N, et al. The yeast Fun30 and human SMARCAD1 chromatin remodelers promote. *Nature*. 2012;489(7417):581-584. doi:10.1038/nature11353.

403. Ogi T, Limsirichaikul S, Overmeer RM, et al. Three DNA Polymerases, Recruited by Different Mechanisms, Carry Out NER Repair Synthesis in Human Cells. *Mol Cell*. 2010;37(5):714-727. doi:10.1016/j.molcel.2010.02.009

404. Zhang Y, Iratni R, Erdjument-Bromage H, Tempst P, Reinberg D. Histone deacetylases and SAP18, a novel polypeptide, are components of a human Sin3 complex. *Cell*. 1997;89(3):357-364. doi:10.1016/S0092-8674(00)80216-0

405. Srougi MC, Burridge K. The nuclear guanine nucleotide exchange factors Ect2 and Net1 regulate RhoB-mediated cell death after DNA damage. *PLoS One*. 2011;6(2). doi:10.1371/journal.pone.0017108

406. Fernando TM, Marullo R, Gresely BP, et al. BCL6 evolved to enable stress tolerance in vertebrates and is broadly required by cancer cells to adapt to stress. *Cancer Discov*. 2019;9(5):662-679. doi:10.1158/2159-8290.CD-17-1444.BCL6

407. Gunawardana Y, Niranjan M. Bridging the gap between transcriptome and proteome measurements identifies post-translationally regulated genes. *Bioinformatics*. 2013;29(23):3060-3066. doi:10.1093/bioinformatics/btt537

408. Wang D, Eraslan B, Wieland T, et al. A deep proteome and transcriptome abundance atlas of 29 healthy human tissues. *Mol Syst Biol*. 2019;15(2). doi:10.15252/msb.20188503

409. Haddad AF, Young JS, Amara D, et al. Mouse models of glioblastoma for the evaluation of novel therapeutic strategies. *Neuro-Oncology Adv*. 2021;3(1). doi:10.1093/noajnl/vdab100

410. Sigma-Aldrich (Merck). FX1 SML2074. https://www.sigmaaldrich.com/NZ/en/product/sigma/sml2074. Published 2022. Accessed August 13, 2022.

411. Selleckchem.com. FX1 S8591. https://www.selleckchem.com/products/fx1.html. Published 2022. Accessed August 13, 2022.

412. Ishikawa C, Mori N. FX1, a BCL6 inhibitor, reactivates BCL6 target genes and suppresses HTLV-1-infected T cells. *Invest New Drugs*. 2022;40(2):245-254. doi:10.1007/s10637-021-01196-1

413. Zhang H, Qi X, Wu J, et al. BCL6 inhibitor FX1 attenuates inflammatory responses in murine

sepsis through strengthening BCL6 binding affinity to downstream target gene promoters. *Int Immunopharmacol*. 2019;75(105789). doi:10.1016/j.intimp.2019.105789

414. Cai Y, Watkins MA, Xue F, et al. BCL6 BTB-specific inhibition via FX1 treatment reduces Tfh cells and reverses lymphoid follicle hyperplasia in Indian rhesus macaque (Macaca mulatta). *J Med Primatol*. 2020;49(1):26-33. doi:10.1111/jmp.12438

415. Baell JB, Holloway GA. New substructure filters for removal of pan assay interference compounds (PAINS) from screening libraries and for their exclusion in bioassays. *J Med Chem*. 2010;53(7):2719-2740. doi:10.1021/jm901137j

416. Ai Y, Hwang L, Mackerell AD, Melnick A, Xue F. Progress toward B-Cell Lymphoma 6 BTB Domain Inhibitors for the Treatment of Diffuse Large B-Cell Lymphoma and beyond. *J Med Chem*. 2021;64(8):4333-4358. doi:10.1021/acs.jmedchem.0c01686

417. McCoull W, Abrams RD, Anderson E, et al. Discovery of Pyrazolo[1,5-a]pyrimidine B-Cell Lymphoma 6 (BCL6) Binders and Optimization to High Affinity Macrocyclic Inhibitors. *J Med Chem*. 2017;60(10):4386-4402. doi:10.1021/acs.jmedchem.7b00359

418. Pakos-Zebrucka K, Koryga I, Mnich K, Ljujic M, Samali A, Gorman AM. The integrated stress response. *EMBO Rep*. 2016;17(10):1374-1395. doi:10.15252/embr.201642195

419. Bilen M, Benhammouda S, Slack RS, Germain M. The integrated stress response as a key pathway downstream of mitochondrial dysfunction. *Curr Opin Physiol*. 2022;27:100555. doi:10.1016/j.cophys.2022.100555

420. Bhattarai KR, Riaz TA, Kim HR, Chae HJ. The aftermath of the interplay between the endoplasmic reticulum stress response and redox signaling. *Exp Mol Med*. 2021;53(2):151-167. doi:10.1038/s12276-021-00560-8

421. Halim VA, García-Santisteban I, Warmerdam DO, et al. Doxorubicin-induced DNA damage causes extensive ubiquitination of ribosomal proteins associated with a decrease in protein translation. *Mol Cell Proteomics*. 2018;17(12):2297-2308. doi:10.1074/mcp.RA118.000652

422. Taymaz-Nikerel H, Karabekmez ME, Eraslan S, Kırdar B. Doxorubicin induces an extensive transcriptional and metabolic rewiring in yeast cells. *Sci Rep*. 2018;8(1). doi:10.1038/s41598-018-31939-9

423. Khan I, Hassan Baig M, Mahfooz S, et al. Resistance Mechanisms in Glioblastoma. *Int J Mol Sci*. 2021;22(1318). doi:10.3390/ijms22031318

424. McCann E, O'Sullivan J, Marcone S. Targeting cancer-cell mitochondria and metabolism to improve radiotherapy response. *Transl Oncol*. 2021;14(1):100905. doi:10.1016/j.tranon.2020.100905

425. Tachon G, Cortes U, Guichet PO, et al. Cell cycle changes after glioblastoma stem cell irradiation: The major role of rad51. *Int J Mol Sci*. 2018;19(10). doi:10.3390/ijms19103018

426. Alexiou GA, Vartholomatos E, Tsamis KI, et al. Combination treatment for glioblastoma with temozolomide, dfmo and radiation. *J BUON*. 2019;24(1):397-404.

427. Cao W qiang, Li Y, Hou Y jun, et al. Enhanced anticancer efficiency of doxorubicin against human glioma by natural borneol through triggering ROS-mediated signal. *Biomed Pharmacother*. 2019;118(109261). doi:10.1016/j.biopha.2019.109261

428. Levi M, Salaroli R, Parenti F, et al. Doxorubicin treatment modulates chemoresistance and affects the cell cycle in two canine mammary tumour cell lines. *BMC Vet Res*. 2021;17(1). doi:10.1186/s12917-020-02709-5

429. O'Loughlin C, Heenan M, Coyle S, Clynes M. Altered cell cycle response of drug-resistant lung carcinoma cells to doxorubicin. *Eur J Cancer*. 2000;36(9):1149-1160. doi:10.1016/S0959-

8049(00)00071-X

430. Hirose Y, Berger MS, Pieper RO. p53 effects both the duration of G2/M arrest and the fate of temozolomide-treated human glioblastoma cells. *Cancer Res*. 2001;61(5):1957-1963.

431. Shen W, Hu JA, Zheng JS. Mechanism of temozolomide-induced antitumour effects on glioma cells. *J Int Med Res*. 2014;42(1):164-172. doi:10.1177/0300060513501753

432. Herranz N, Gil J. Mechanisms and functions of cellular senescence. *J Clin Invest*. 2018;128(4):1238-1246. doi:10.1172/JCI95148

433. Kanzawa T, Germano IM, Kondo Y, Ito H, Kyo S, Kondo S. Inhibition of telomerase activity in malignant glioma cells correlates with their sensitivity to temozolomide. *Br J Cancer*. 2003;89(5):922-929. doi:10.1038/sj.bjc.6601193

434. Bai Y, Lathia JD, Zhang P, Flavahan W, Rich JN, Mattson MP. Molecular targeting of TRF2 suppresses the growth and tumorigenesis of glioblastoma stem cells. *Glia*. 2014;62(10):1687-1698. doi:10.1002/glia.22708

435. Amen AM, Fellmann C, Soczek KM, et al. Cancer-specific loss of TERT activation sensitizes glioblastoma to DNA damage. *Proc Natl Acad Sci U S A*. 2021;118(13). doi:10.1073/pnas.2008772118

436. Wang F, Podell ER, Zaug AJ, et al. The POT1-TPP1 telomere complex is a telomerase processivity factor. *Nature*. 2007;445(7127):506-510. doi:10.1038/nature05454

437. Tang Z, Shu H, Oncel D, Chen S, Yu H. Phosphorylation of Cdc20 by Bub1 provides a catalytic mechanism for APC/C inhibition by the spindle checkpoint. *Mol Cell*. 2004;16(3):387-397. doi:10.1016/j.molcel.2004.09.031

438. Lemée JM, Clavreul A, Aubry M, et al. Integration of transcriptome and proteome profiles in glioblastoma: Looking for the missing link. *BMC Mol Biol*. 2018;19(1):13. doi:10.1186/s12867-018-0115-6

439. Ranuncolo SM, Wang L, Polo JM, et al. BCL6-mediated attenuation of DNA damage sensing triggers growth arrest and senescence through a p53-dependent pathway in a cell context-dependent manner. *J Biol Chem*. 2008;283(33):22565-22572. doi:10.1074/jbc.M803490200

440. Gordon-Schneider RMA. The influence of BCL6 on the WNT pathway in glioblastoma therapy resistance. 2018.

441. Wong CW, Privalsky ML. Components of the SMRT corepressor complex exhibit distinctive interactions with the POZ domain oncoproteins PLZF, PLZF-RARØ, and BCL-6. *J Biol Chem*. 1998;273(42):27695-27702. doi:10.1074/jbc.273.42.27695

442. Jaye DL, Iqbal J, Fujita N, et al. The BCL6-associated transcriptional co-repressor, MTA3, is selectively expressed by germinal centre B cells and lymphomas of putative germinal centre derivation. *J Pathol*. 2007;213:106-115. doi:10.1002/path.2199

443. Papachristou EK, Kishore K, Holding AN, et al. A quantitative mass spectrometry-based approach to monitor the dynamics of endogenous chromatin-associated protein complexes. *Nat Commun*. 2018;9(1). doi:10.1038/s41467-018-04619-5

444. Sutherland BW, Toews J, Kast J. Utility of formaldehyde cross-linking and mass spectrometry in the study of protein-protein interactions. *J Mass Spectrom*. 2008;43(6):699-715. doi:10.1002/jms.1415

445. Yang H, Green MR. Epigenetic Programing of B-Cell Lymphoma by BCL6 and Its Genetic Deregulation. *Front Cell Dev Biol*. 2019;7(272). doi:10.3389/fcell.2019.00272

446. Meysman P, Titeca K, Eyckerman S, et al. Protein complex analysis: From raw protein lists to

protein interaction networks. *Mass Spectrom Rev*. 2017;36:600-614. doi:10.1002/mas

447. Oliveros JC. Venny. An interactive tool for comparing lists with Venn's diagrams. 2007. https://bioinfogp.cnb.csic.es/tools/venny/index.html.

448. Mellacheruvu D, Wright Z, Couzens AL, et al. The CRAPome: A contaminant repository for affinity purification-mass spectrometry data. *Nat Methods*. 2013;10(8):730-736. doi:10.1038/nmeth.2557

449. del-Toro N, Dumousseau M, Orchard S, et al. A new reference implementation of the PSICQUIC web service. *Nucleic Acids Res*. 2013;41:601-606. doi:10.1093/nar/gkt392

450. Yoon HG, Chan DW, Huang ZQ, et al. Purification and functional characterization of the human N-CoR complex: The roles of HDAC3, TBL1 and TBLR1. *EMBO J*. 2003;22(6):1336-1346. doi:10.1093/emboj/cdg120

451. Luck K, Kim D-K, Lambourne L, et al. A reference map of the human binary protein interactome. *Nature*. 2020;580(7803):402-408. doi:10.1038/s41586-020-2188-x.A

452. Yachie N, Petsalaki E, Mellor JC, et al. Pooled-matrix protein interaction screens using Barcode Fusion Genetics. *Mol Syst Biol*. 2016;12(4):863. doi:10.15252/msb.20156660

453. Wei J-H, Zhang ZC, Wynn RM, Seemann J. GM130 regulates Golgi-derived spindle assembly by activating TPX2 and capturing microtubules. *Cell*. 2015;162(2):287-299. doi:10.1016/j.cell.2015.06.014.

454. Puthenveedu MA, Bachert C, Puri S, Lanni F, Linstedt AD. GM130 and GRASP65-dependent lateral cisternal fusion allows uniform Golgi-enzyme distribution. *Nat Cell Biol*. 2006;8(3):238-248. doi:10.1038/ncb1366

455. Jahn O, Tenzer S, Werner HB. Myelin proteomics: Molecular anatomy of an insulating sheath. *Mol Neurobiol*. 2009;40(1):55-72. doi:10.1007/s12035-009-8071-2

456. Fu M, Mcalear TS, Nguyen H, et al. The Golgi Outpost Protein TPPP Nucleates Microtubules and is Critical for Myelination. 2019;179(1):132-146. doi:10.1016/j.cell.2019.08.025.

457. Erlander MG, Tillakaratne NJK, Feldblum S, Patel N, Tobin AJ. Two genes encode distinct glutamate decarboxylases. *Neuron*. 1991;7(1):91-100. doi:10.1016/0896-6273(91)90077-D

458. Castegna A, Menga A. Glutamine synthetase: Localization dictates outcome. *Genes (Basel)*. 2018;9(2). doi:10.3390/genes9020108

459. Schaffer AE, Breuss MW, Caglayan AO, et al. Bi-allelic loss of human CTNNA2, encoding αN-catenin, leads to ARP2/3 over-activity and disordered cortical neuronal migration. *Nat Genet*. 2018;50(8):1093-1101. doi:10.1038/s41588-018-0166-0.

460. Cunningham BA, Hemperly JJ, Murray BENA, Prediger EA, Brackenbury R, Edelman GM. Neural Cell Adhesion Molecule: Structure, Immunoglobulin-Like Domains, Cell Surface Modulation, and Alternative RNA Splicing. *Science (80- )*. 1987;236:799-806.

461. Waltzer L, Bourillot PY, Sergeant A, Manet E. RBP-Jkrepression activity is mediated by a co-repressor and antagonized by the epstein-barr virus transcription factor EBNA2. *Nucleic Acids Res*. 1995;23(24):4939-4945. doi:10.1093/nar/23.24.4939

462. Bray SJ. Notch signalling in context. *Nat Rev Mol Cell Biol*. 2016;17(11):722-735. doi:10.1038/nrm.2016.94

463. Liu F, Rehmani I, Esaki S, et al. Pirin is an iron-dependent redox regulator of NF-κB. *Proc Natl Acad Sci U S A*. 2013;110(24):9722-9727. doi:10.1073/pnas.1221743110

464. Fang G, Yu H, Kirschner MW. The checkpoint protein MAD2 and the mitotic regulator CDC20

form a ternary complex with the anaphase-promoting complex to control anaphase initiation. *Genes Dev*. 1998;12(12):1871-1883. doi:10.1101/gad.12.12.1871

465. Chen D, Ito S, Yuan H, et al. EML4 promotes the loading of NUDC to the spindle for mitotic progression. *Cell Cycle*. 2015;14(10):1529-1539. doi:10.1080/15384101.2015.1026514

466. Vandamme J, Völkel P, Rosnoblet C, Le Faou P, Angrand PO. Interaction proteomics analysis of polycomb proteins defines distinct PRC1 complexes in mammalian cells. *Mol Cell Proteomics*. 2011;10(4). doi:10.1074/mcp.M110.002642

467. Colombo M, Pessey O, Marcia M. Topology and enzymatic properties of a canonical Polycomb repressive complex 1 isoform. *FEBS Lett*. 2019;593(14):1837-1848. doi:10.1002/1873-3468.13442

468. Hori K, Sen A, Artavanis-Tsakonas S. Notch signaling at a glance. *J Cell Sci*. 2013;126(10):2135-2140. doi:10.1242/jcs.127308

469. Contreras-Cornejo H, Saucedo-Correa G, Oviedo-Boyso J, et al. The CSL proteins, versatile transcription factors and context dependent corepressors of the notch signaling pathway. *Cell Div*. 2016;11(12). doi:10.1186/s13008-016-0025-2

470. Okumoto K, Kametani Y, Fujiki Y. Two proteases, trypsin domain-containing 1 (Tysnd1) and peroxisomal lon protease (PsLon), cooperatively regulate fatty acid β-oxidation in peroxisomal matrix. *J Biol Chem*. 2011;286(52):44367-44379. doi:10.1074/jbc.M111.285197

471. Kang SG, Ortega J, Singh SK, et al. Functional proteolytic complexes of the human mitochondrial ATP-dependent protease, hClpXP. *J Biol Chem*. 2002;277(23):21095-21102. doi:10.1074/jbc.M201642200

472. Takeuchi A, Miyamoto T, Yamaji K, et al. A Human Erythrocyte-derived Growth-promoting Factor with a Wide Target Cell Spectrum: Identification as Catalase. *Cancer Res*. 1995;55(7):1586-1589.

473. HRG. The Human Protein Atlas Version 21.0.

474. Olsen J V., Ong SE, Mann M. Trypsin cleaves exclusively C-terminal to arginine and lysine residues. *Mol Cell Proteomics*. 2004;3(6):608-614. doi:10.1074/mcp.T400003-MCP200

475. Campos B, Bermejo JL, Han L, et al. Expression of nuclear receptor corepressors and class I histone deacetylases in astrocytic gliomas. *Cancer Sci*. 2011;102(2):387-392. doi:10.1111/j.1349-7006.2010.01792.x

476. Perissi V, Aggarwal A, Glass CK, Rose DW, Rosenfeld MG. A Corepressor/Coactivator Exchange Complex Required for Transcriptional Activation by Nuclear Receptors and Other Regulated Transcription Factors. *Cell*. 2004;116(4):511-526. doi:10.1016/S0092-8674(04)00133-3

477. Huang W, Ghisletti S, Perissi V, Rosenfeld MG, Glass CK. Transcriptional integration of TLR2 and TLR4 signaling at the NCoR de-repression checkpoint. *Mol Cell*. 2009;35(1):48-57. doi:10.1016/j.molcel.2009.05.023

478. Zhang XM, Chang Q, Zeng L, Gu J, Brown S, Basch RS. TBLR1 regulates the expression of nuclear hormone receptor co-repressors. *BMC Cell Biol*. 2006;7(31). doi:10.1186/1471-2121-7-31

479. Venturutti L, Teater M, Zhai A, et al. TBL1XR1 mutations drive extranodal lymphoma by inducing a pro-tumorigenic memory fate. *Cell*. 2020;182(2):297-316. doi:10.1016/j.cell.2020.05.049.

480. Sánchez C, Sánches I, Demmers JAA, Rodriguez P, Strouboulis J, Vidal M. Proteomics analysis of Ring1B/Rnf2 interactions identifies a novel complex with the Fbxl10/Jhdm1B histone

demethylase and the Bcl6 interacting corepressor. *Mol Cell Proteomics*. 2007;6(5):820-834. doi:10.1074/mcp.M600275-MCP200

481. Gearhart MD, Corcoran CM, Wamstad JA, Bardwell VJ. Polycomb Group and SCF Ubiquitin Ligases Are Found in a Novel BCOR Complex That Is Recruited to BCL6 Targets. *Mol Cell Biol*. 2006;26(18):6880-6889. doi:10.1128/mcb.00630-06

482. Gwak J, Shin JY, Lee K, et al. SFMBT2 (Scm-like with four mbt domains 2) negatively regulates cell migration and invasion in prostate cancer cells. *Oncotarget*. 2016;7(30):48250-48264. doi:10.18632/oncotarget.10198

483. Choi D, Lee SJ, Hong S, Kim IH, Kang S. Prohibitin interacts with RNF2 and regulates E2F1 function via dual pathways. *Oncogene*. 2008;27(12):1716-1725. doi:10.1038/sj.onc.1210806

484. Zhou W, Zhu P, Wang J, et al. Histone H2A monoubiquitination represses transcription by inhibiting RNA polymerase II transcriptional elongation. *Mol Cell*. 2008;29(1):69-80. doi:10.1074/jbc.M116.725879

485. Ballas N, Battaglioli E, Atouf F, et al. Regulation of neuronal traits by a novel transcriptional complex. *Neuron*. 2001;31(3):353-365. doi:10.1016/S0896-6273(01)00371-3

486. Parmigiani E, Taylor V, Giachino C. Oncogenic and Tumor-Suppressive Functions of NOTCH Signaling in Glioma. *Cells*. 2020;9(10). doi:10.3390/cells9102304

487. Valls E, Lobry C, Geng H, et al. BCL6 antagonizes NOTCH2 to maintain survival of human follicular lymphoma cells. *Cancer Discov*. 2017;7(5):506-521. doi:10.1158/2159-8290.CD-16-1189.

488. Sakano D, Kato A, Parikh N, et al. BCL6 canalizes Notch-dependent transcription, excluding Mastermind-like1 from selected target genes during left-right patterning. *Dev Cell*. 2010;18(3):450-462. doi:10.1016/j.devcel.2009.12.023.

489. Zema S, Pelullo M, Nardozza F, Felli MP, Screpanti I, Bellavia D. A Dynamic Role of Mastermind-Like 1: A Journey Through the Main (Path)ways Between Development and Cancer. *Front Cell Dev Biol*. 2020;8. doi:10.3389/fcell.2020.613557

490. Adeniran C, Hamelberg D. Redox-Specific Allosteric Modulation of the Conformational Dynamics of κb DNA by Pirin in the NF-κB Supramolecular Complex. *Biochemistry*. 2017;56(37):5002-5010. doi:10.1021/acs.biochem.7b00528

491. Sauvé F, McBroom LDB, Gallant J, Moraitis AN, Labrie F, Giguère V. CIA, a Novel Estrogen Receptor Coactivator with a Bifunctional Nuclear Receptor Interacting Determinant. *Mol Cell Biol*. 2001;21(1):343-353. doi:10.1128/mcb.21.1.343-353.2001

492. Gillespie MA, Gold ES, Ramsey SA, Podolsky I, Aderem A, Ranish JA. An LXR – NCOA 5 gene regulatory complex directs inflammatory crosstalk-dependent repression of macrophage cholesterol efflux . *EMBO J*. 2015;34(9):1244-1258. doi:10.15252/embj.201489819

493. Yuan X, Zhang L, Cui Y, Yu Y, Gao X, Ao J. NCOA5 is a master regulator of amino acid-induced mTOR activation and β-casein synthesis in bovine mammary epithelial cells. *Biochem Biophys Res Commun*. 2020;529(3):569-574. doi:10.1016/j.bbrc.2020.05.193

494. Jiang C, Ito M, Piening V, Bruck K, Roeder RG, Xiao H. TIP30 interacts with an estrogen receptor α-interacting coactivator CIA and regulates c-myc transcription. *J Biol Chem*. 2004;279(26):27781-27789. doi:10.1074/jbc.M401809200

495. Pighi C, Cheong TC, Compagno M, et al. Frequent mutations of FBXO11 highlight BCL6 as a therapeutic target in Burkitt lymphoma. *Blood Adv*. 2021;5(23):5239-5257. doi:10.1182/bloodadvances.2021005682

496. Yang CH, Pfeffer SR, Sims M, et al. The oncogenic microRNA-21 inhibits the tumor

suppressive activity of FBXO11 to promote tumorigenesis. *J Biol Chem*. 2015;290(10):6037-6046. doi:10.1074/jbc.M114.632125

497. Wen X, Li S, Guo M, et al. miR-181a-5p inhibits the proliferation and invasion of drug-resistant glioblastoma cells by targeting F-box protein 11 expression. *Oncol Lett*. 2020;20(5):1-9. doi:10.3892/ol.2020.12098

498. Wang Y, Liu C, Xie Z, Lu H. Knockdown of TRIM47 inhibits breast cancer tumorigenesis and progression through the inactivation of PI3K/Akt pathway. *Chem Biol Interact*. 2020;317(8):108960. doi:10.1016/j.cbi.2020.108960

499. Li L, Yu Y, Zhang Z, et al. TRIM47 accelerates aerobic glycolysis and tumor progression through regulating ubiquitination of FBP1 in pancreatic cancer. *Pharmacol Res*. 2021;166(105429). doi:10.1016/j.phrs.2021.105429

500. Liang Q, Tang C, Tang M, Zhang Q, Gao Y, Ge Z. TRIM47 is up-regulated in colorectal cancer, promoting ubiquitination and degradation of SMAD4. *J Exp Clin Cancer Res*. 2019;38(1). doi:10.1186/s13046-019-1143-x

501. Azuma K, Ikeda K, Suzuki T, Aogi K, Horie-Inoue K, Inoue S. TRIM47 activates NF-κB signaling via PKC-e/PKD3 stabilization and contributes to endocrine therapy resistance in breast cancer. *Proc Natl Acad Sci U S A*. 2021;118(35). doi:10.1073/pnas.2100784118

502. Chen J xin, Xu D, Cao J wei, et al. TRIM47 promotes malignant progression of renal cell carcinoma by degrading P53 through ubiquitination. *Cancer Cell Int*. 2021;21(1). doi:10.1186/s12935-021-01831-0

503. Fujimura T, Inoue S, Urano T, et al. Increased Expression of Tripartite Motif (TRIM) 47 Is a Negative Prognostic Predictor in Human Prostate Cancer. *Clin Genitourin Cancer*. 2016;14(4):298-303. doi:10.1016/j.clgc.2016.01.011

504. Han Y, Tian H, Chen P, Lin Q. TRIM47 overexpression is a poor prognostic factor and contributes to carcinogenesis in non-small cell lung carcinoma. *Oncotarget*. 2017;8(14):22730-22740. doi:10.18632/oncotarget.15188

505. Dai W, Wang J, Wang Z, et al. Comprehensive Analysis of the Prognostic Values of the TRIM Family in Hepatocellular Carcinoma. *Front Oncol*. 2021;11(767644). doi:10.3389/fonc.2021.767644

506. Xia Y, Wei Z, Huang W, Wei X, He Y. Trim47 overexpression correlates with poor prognosis in gastric cancer. *Neoplasma*. 2021;68(2):307-316. doi:10.4149/neo

507. Chen L, Li M, Li Q, Xu M, Zhong W. Knockdown of TRIM47 inhibits glioma cell proliferation, migration and invasion through the inactivation of Wnt/β-catenin pathway. *Mol Cell Probes*. 2020;53(101623). doi:10.1016/j.mcp.2020.101623

508. Stapleton D, Mitchelhill KI, Gao G, et al. Mammalian AMP-activated protein kinase subfamily. *J Biol Chem*. 1996;271(2):611-614. doi:10.1074/jbc.271.2.611

509. Cheung PCF, Salt IP, Davies SP, Hardie DG, Carling D. Characterization of AMP-activated protein kinase γ-subunit isoforms and their role in AMP binding. *Biochem J*. 2000;346(3):659-669. doi:10.1042/0264-6021:3460659

510. Wong KA, Lodish HF. A revised model for AMP-activated protein kinase structure: The α-subunit binds to both the β- and γ-subunits although there is no direct binding between the β- and γ-subunits. *J Biol Chem*. 2006;281(47):36434-36442. doi:10.1074/jbc.M607410200

511. Chhipa RR, Fan Q, Anderson J, et al. AMP kinase promotes glioblastoma bioenergetics and tumor growth. *Nat Cell Biol*. 2018;20(7):823-835. doi:10.1038/s41556-018-0126-z.

512. Sanli T, Rashid A, Liu C, et al. Ionizing radiation activates AMP-activated kinase (AMPK): A

target for radiosensitization of human cancer cells. *Int J Radiat Oncol Biol Phys*. 2010;78(1):221-229. doi:10.1016/j.ijrobp.2010.03.005

513. Sanli T, Steinberg GR, Singh G, Tsakiridis T. AMP-activated protein kinase (AMPK) beyond metabolism: A novel genomic stress sensor participating in the DNA damage response pathway. *Cancer Biol Ther*. 2014;15(2):156-169. doi:10.4161/cbt.26726

514. He P, Li Z, Xu F, et al. AMPK Activity Contributes to G2 Arrest and DNA Damage Decrease via p53/p21 Pathways in Oxidatively Damaged Mouse Zygotes. *Front Cell Dev Biol*. 2020;8. doi:10.3389/fcell.2020.539485

515. Zhang W Bin, Wang Z, Shu F, et al. Activation of AMP-activated protein kinase by temozolomide contributes to apoptosis in glioblastoma cells via p53 activation and mTORC1 inhibition. *J Biol Chem*. 2010;285(52):40461-40471. doi:10.1074/jbc.M110.164046

516. Xie MM, Amet T, Liu H, Yu Q, Dent AL. AMP kinase promotes Bcl6 expression in both mouse and human T cells. *Mol Immunol*. 2017;81:67-75. doi:10.1016/j.molimm.2016.11.020.

517. Gongol B, Marin T, Peng IC, et al. AMPKα2 exerts its anti-inflammatory effects through PARP-1 and Bcl-6. *Proc Natl Acad Sci U S A*. 2013;110(8):3161-3166. doi:10.1073/pnas.1222051110

518. Glauser DA, Schlegel W. The FoxO/Bcl-6/cyclin D2 pathway mediates metabolic and growth factor stimulation of proliferation in Min6 pancreatic β-cells. *J Recept Signal Transduct*. 2009;29(6):293-298. doi:10.3109/10799890903241824

519. Zhao Y, Hu X, Liu Y, et al. ROS signaling under metabolic stress: Cross-talk between AMPK and AKT pathway. *Mol Cancer*. 2017;16(1):79. doi:10.1186/s12943-017-0648-1

520. Greer EL, Banko MR, Brunet A. AMP-activated Protein Kinase and FoxO Transcription Factors in Dietary Restriction–induced Longevity. *Ann N Y Acad Sci*. 2009;1170:688-692. doi:10.1111/j.1749-6632.2009.04019.x.

521. Hadri K El, Denoyelle C, Ravaux L, et al. AMPK signaling involvement for the repression of the IL-1β-induced group IIA secretory phospholipase A2 expression in VSMCs. *PLoS One*. 2015;10(7). doi:10.1371/journal.pone.0132498

522. Mertins P, Mani DR, Ruggles K V, et al. Proteogenomics connects somatic mutations to signaling in breast cancer. *Nature*. 2016;534(7605):55-62. doi:10.1038/nature18003.

523. Sharma K, D'Souza RCJ, Tyanova S, et al. Ultradeep Human Phosphoproteome Reveals a Distinct Regulatory Nature of Tyr and Ser/Thr-Based Signaling. *Cell Rep*. 2014;8(5):1583-1594. doi:10.1016/j.celrep.2014.07.036

524. Mertins P, Yang F, Liu T, et al. Ischemia in tumors induces early and sustained phosphorylation changes in stress kinase pathways but does not affect global protein levels. *Mol Cell Proteomics*. 2014;13(7):1690-1704. doi:10.1074/mcp.M113.036392

525. Rolland D, Basrur V, Conlon K, et al. Global phosphoproteomic profiling reveals distinct signatures in B-cell non-hodgkin lymphomas. *Am J Pathol*. 2014;184(5):1331-1342. doi:10.1016/j.ajpath.2014.01.036

526. Kim JY, Welsh EA, Oguz U, et al. Dissection of TBK1 signaling via phosphoproteomics in lung cancer cells. *Proc Natl Acad Sci U S A*. 2013;110(30):12414-12419. doi:10.1073/pnas.1220674110

527. Mertins P, Qiao JW, Patel J, et al. Integrated proteomic analysis of post-translational modifications by serial enrichment. *Nat Methods*. 2013;10(7):634-637. doi:10.37936/ecti-cit.200622.53280

528. Klammer M, Kaminski M, Zedler A, et al. Phosphosignature predicts dasatinib response in non-small cell lung cancer. *Mol Cell Proteomics*. 2012;11(9):651-668.

doi:10.1074/mcp.M111.016410

529. Hornbeck P V., Zhang B, Murray B, Kornhauser JM, Latham V, Skrzypek E. PhosphoSitePlus, 2014: Mutations, PTMs and recalibrations. *Nucleic Acids Res*. 2015;43(D1):D512-D520. doi:10.1093/nar/gku1267

530. Hardie DG. AMP-activated protein kinase-an energy sensor that regulates all aspects of cell function. *Genes Dev*. 2011;25(18):1895-1908. doi:10.1101/gad.17420111

531. Schaffer BE, Levin RS, Hertz NT, et al. Identification of AMPK phosphorylation sites reveals a network of proteins involved in cell invasion and facilitates large-scale substrate prediction. 2015;22(5):907-921. doi:10.1016/j.cmet.2015.09.009.

532. Verhage M, Maia AS, Plomp JJ, et al. Synaptic assembly of the brain in the absence of neurotransmitter secretion. *Science (80- )*. 2000;287(5454):864-869. doi:10.1126/science.287.5454.864

533. Toonen RFG, Wierda K, Sons MS, et al. Munc18-1 expression level control synapse recovery by regulating readily releasable pool size. *Proc Natl Acad Sci U S A*. 2006;103(48):18332-18337. doi:10.1073/pnas.0608507103

534. Tucker WC, Weber T, Chapman ER. Reconstitution of Ca2+-Regulated Membrane Fusion by Synaptotagmin and SNAREs. *Science (80- )*. 2004;304(5669):435-438. doi:10.1126/science.1097196

535. Chen Y, Wang YH, Zheng Y, et al. Synaptotagmin-1 interacts with PI(4,5)P2 to initiate synaptic vesicle docking in hippocampal neurons. *Cell Rep*. 2021;34(11):108842. doi:10.1016/j.celrep.2021.108842

536. Mei K, Guo W. The exocyst complex. *Curr Biol*. 2018;28(17):R922-R925. doi:10.1016/j.cub.2018.06.042

537. Van Bergen NJ, Ahmed SM, Collins F, et al. Mutations in the exocyst component EXOC2 cause severe defects in human brain development. *J Exp Med*. 2020;217(10):e20192040. doi:10.1084/JEM.20192040

538. Ulloa F, Gonzàlez-Juncà A, Meffre D, et al. Blockade of the SNARE protein syntaxin 1 inhibits glioblastoma tumor growth. *PLoS One*. 2015;10(3). doi:10.1371/journal.pone.0119707

539. Dekker LJM, Kannegieter NM, Haerkens F, et al. Multiomics profiling of paired primary and recurrent glioblastoma patient tissues. *Neuro-Oncology Adv*. 2020;2(1):1-12. doi:10.1093/noajnl/vdaa083

540. Drab M, Verkade P, Elger M, et al. Loss of caveolae, vascular dysfunction, and pulmonary defects in caveolin-1 gene-disrupted mice. *Science (80- )*. 2001;293(5539):2449-2452. doi:10.1126/science.1062688

541. Hill MM, Bastiani M, Luetterforst R, et al. PTRF-Cavin, a Conserved Cytoplasmic Protein Required for Caveola Formation and Function. *Cell*. 2008;132(1):113-124. doi:10.1016/j.cell.2007.11.042

542. Mohan J, Morén B, Larsson E, Holst MR, Lundmark R. Cavin3 interacts with cavin1 and caveolin1 to increase surface dynamics of caveolae. *J Cell Sci*. 2015;128(5):979-991. doi:10.1242/jcs.161463

543. Bastiani M, Liu L, Hill MM, et al. MURC/Cavin-4 and cavin family members form tissue-specific caveolar complexes. *J Cell Biol*. 2009;185(7):1259-1273. doi:10.1083/jcb.200903053

544. Gambin Y, Ariotti N, McMahon K-A, et al. Single-molecule analysis reveals self assembly and nanoscale segregation of two distinct cavin subcomplexes on caveolae. *Elife*. 2014;3. doi:10.7554/elife.01434

545. Pu W, Nassar ZD, Khabbazi S, et al. Correlation of the invasive potential of glioblastoma and expression of caveola-forming proteins caveolin-1 and CAVIN1. *J Neurooncol*. 2019;143(2):207-220. doi:10.1007/s11060-019-03161-8

546. Bruyère C, Abeloos L, Lamoral-Theys D, et al. Temozolomide modifies caveolin-1 expression in experimental malignant gliomas in vitro and in vivo. *Transl Oncol*. 2011;4(2):92-100. doi:10.1593/tlo.10205

547. Zhu H, Yue J, Pan Z, et al. Involvement of caveolin-1 in repair of DNA damage through both homologous recombination and non-homologous end joining. *PLoS One*. 2010;5(8):e12055. doi:10.1371/journal.pone.0012055

548. Koh S, Lee W, Park SM, Kim SH. Caveolin-1 deficiency impairs synaptic transmission in hippocampal neurons. *Mol Brain*. 2021;14(53):1-10. doi:10.1186/s13041-021-00764-z

549. González MI, Krizman-Genda E, Robinson MB. Caveolin-1 regulates the delivery and endocytosis of the glutamate transporter, excitatory amino acid carrier. *J Biol Chem*. 2007;282(41):29855-29865. doi:10.1074/jbc.M704738200

550. Abousaab A, Warsi J, Elvira B, Lang F. Caveolin-1 Sensitivity of Excitatory Amino Acid Transporters EAAT1, EAAT2, EAAT3, and EAAT4. *J Membr Biol*. 2016;249(3):239-249. doi:10.1007/s00232-015-9863-0

551. Robert SM, Sontheimer H. Glutamate Transporters in the Biology of Malignant Gliomas. *Cell Mol Life Sci*. 2014;71(10):1839-1854. doi:10.1016/j.surg.2006.10.010.

552. Arscott WT, Tandle AT, Zhao S, et al. Ionizing radiation and glioblastoma exosomes: Implications in tumor biology and cell migration. *Transl Oncol*. 2013;6(6):638-648. doi:10.1593/tlo.13640

553. Abramowicz A, Wojakowska A, Marczak L, et al. Ionizing radiation affects the composition of the proteome of extracellular vesicles released by head-and-neck cancer cells in vitro. *J Radiat Res*. 2019;60(3):289-297. doi:10.1093/jrr/rrz001

554. Szatmári T, Kis D, Bogdándi EN, et al. Extracellular vesicles mediate radiation-induced systemic bystander signals in the bone marrow and spleen. *Front Immunol*. 2017;8(347). doi:10.3389/fimmu.2017.00347

555. Tortolici F, Vumbaca S, Incocciati B, et al. Ionizing Radiation-Induced Extracellular Vesicle Release Promotes AKT-Associated Survival Response in SH-SY5Y Neuroblastoma Cells. *Cells*. 2021;10(107). doi:https://doi.org/10.3390/cells10010107

556. O'Neill CP, Gilligan KE, Dwyer RM. Role of extracellular vesicles (EVs) in cell stress response and resistance to cancer therapy. *Cancers (Basel)*. 2019;11(136):1-14. doi:10.3390/cancers11020136

557. Bălasa A, Serban G, Chinezu R, Hurghis C, Tămas F, Manu D. The Involvement of Exosomes in Glioblastoma Development, Diagnosis, Prognosis, and Treatment. *Brain Sci*. 2020;10(8):553. doi:10.3390/brainsci10080553

558. Uhlén M, Fagerberg L, Hallström BM, et al. Tissue-based map of the human proteome. *Science (80- )*. 2015;347(6220). doi:10.1126/science.1260419

559. Uhlen M, Zhang C, Lee S, et al. A pathology atlas of the human cancer transcriptome. *Science (80- )*. 2017;357(6352). doi:10.1126/science.aan2507

560. BCL6. The Human Protein Atlas Version 21.0. https://www.proteinatlas.org/ENSG00000113916-BCL6/subcellular#human. Published 2021. Accessed August 20, 2022.

561. Albagli O, Lindon C, Lantoine D, et al. DNA Replication Progresses on the Periphery of Nuclear

Aggregates Formed by the BCL6 Transcription Factor. *Mol Cell Biol*. 2000;20(22):8560-8570. doi:10.1128/mcb.20.22.8560-8570.2000

562. Lemercier C, Brocard MP, Puvion-Dutilleul F, Kao HY, Albagli O, Khochbin S. Class II histone deacetylases are directly recruited by BCL6 transcriptional repressor. *J Biol Chem*. 2002;277(24):22045-22052. doi:10.1074/jbc.M201736200

563. Mao YS, Zhang B, Spector DL. Biogenesis and function of nuclear bodies. *Trends Genet*. 2011;27(8):295-306. doi:10.1016/j.tig.2011.05.006.Biogenesis

564. NCOR2. The Human Protein Atlas Version 21.0. https://www.proteinatlas.org/ENSG00000196498-NCOR2/pathology. Published 2021.

565. Jonas BA, Privalsky ML. SMRT and N-CoR corepressors are regulated by distinct kinase signaling pathways. *J Biol Chem*. 2004;279(52):54676-54686. doi:10.1074/jbc.M410128200

566. Chen JD, Evans RM. A transcriptional co-repressor that interacts with nuclear hormone receptors. *Nature*. 1995;377(6548):454-457. doi:10.1038/377454a0

567. Afinanisa Q, Cho MK, Seong HA. AMPK localization: A key to differential energy regulation. *Int J Mol Sci*. 2021;22(20). doi:10.3390/ijms222010921

568. Salt I, Celler JW, Hawley SA, et al. AMP-activated protein kinase: Greater AMP dependence, and preferential nuclear localization, of complexes containing the α2 isoform. *Biochem J*. 1998;334(1):177-187. doi:10.1042/bj3340177

569. Dzeja PP, Chung S, Faustino RS, Behfar A, Terzic A. Developmental enhancement of adenylate kinase-AMPK metabolic signaling axis supports stem cell cardiac differentiation. *PLoS One*. 2011;6(4). doi:10.1371/journal.pone.0019300

570. Erickson HP. Size and shape of protein molecules at the nanometer level determined by sedimentation, gel filtration, and electron microscopy. *Biol Proced Online*. 2009;11(1):32-51. doi:10.1007/s12575-009-9008-x

571. Mottis A, Mouchiroud L, Auwerx J. Emerging roles of the corepressors NCoR1 and SMRT in homeostasis. *Genes Dev*. 2013;27(8):819-835. doi:10.1101/gad.214023.113

572. Fernández-Majada V, Aguilera C, Villanueva A, et al. Nuclear IKK activity leads to dysregulated Notch-dependent gene expression in colorectal cancer. *Proc Natl Acad Sci U S A*. 2007;104(1):276-281. doi:10.1073/pnas.0606476104

573. Espinosa L, Inglés-Esteve J, Robert-Moreno A, Bigas A. IkBa and p65 Regulate the Cytoplasmic Shuttling of Nuclear Corepressors: Cross-talk between Notch and NFkB Pathways. *Mol Biol Cell*. 2003;14:491-502. doi:10.1091/mbc.E02

574. Perissi V, Scafoglio C, Zhang J, et al. TBL1 and TBLR1 Phosphorylation on Regulated Gene Promoters Overcomes Dual CtBP and NCoR/SMRT Transcriptional Repression Checkpoints. *Mol Cell*. 2008;29(6):755-766. doi:10.1016/j.molcel.2008.01.020

575. Climente-González H, Porta-Pardo E, Godzik A, Eyras E. The Functional Impact of Alternative Splicing in Cancer. *Cell Rep*. 2017;20(9):2215-2226. doi:10.1016/j.celrep.2017.08.012

576. Li Y, Ren Z, Peng Y, et al. Classification of glioma based on prognostic alternative splicing. *BMC Med Genomics*. 2019;12. doi:10.1186/s12920-019-0603-7

577. Kent WJ, Sugnet CW, Furey TS, et al. The Human Genome Browser at UCSC. *Genome Res*. 2002;12(6):996-1006. doi:10.1101/gr.229102

578. Agarwala R, Barrett T, Beck J, et al. Database resources of the National Center for Biotechnology Information. *Nucleic Acids Res*. 2018;46(D1):D8-D13. doi:10.1093/nar/gkx1095

579. Shen Y, Ge B, Ramachandrareddy, Himabindu, McKeithan T, Chan WC. Alternative splicing generates a short BCL6 (BCL6S) isoform encoding a compact repressor. *Biochem Biophys Res Commun*. 2008;375(2):190-193. doi:10.1038/jid.2014.371

580. Mascle X, Albagli O, Lemercier C. Point mutations in BCL6 DNA-binding domain reveal distinct roles for the six zinc fingers. *Biochem Biophys Res Commun*. 2003;300(2):391-396. doi:10.1016/S0006-291X(02)02873-5

581. Wang Y, Zhao Y, Bollas A, Wang Y, Au KF. Nanopore sequencing technology, bioinformatics and applications. *Nat Biotechnol*. 2021;39(11):1348-1365. doi:10.1038/s41587-021-01108-x

582. Jain M, Olsen HE, Paten B, Akeson M. The Oxford Nanopore MinION: delivery of nanopore sequencing to the genomics community. *Genome Biol*. 2016;17(1). doi:10.1186/s13059-016-1103-0

583. Bolisetty MT, Rajadinakaran G, Graveley BR. Determining exon connectivity in complex mRNAs by nanopore sequencing. *Genome Biol*. 2015;16(1). doi:10.1186/s13059-015-0777-z

584. Koren E, Lev-Maor G, Ast G. The emergence of alternative 3′ and 5′ splice site exons from constitutive exons. *PLoS Comput Biol*. 2007;3(5):0895-0908. doi:10.1371/journal.pcbi.0030095

585. Love MI, Huber W, Anders S. Moderated estimation of fold change and dispersion for RNA-seq data with DESeq2. *Genome Biol*. 2014;15(12). doi:10.1186/s13059-014-0550-8

586. Zhu A, Ibrahim JG, Love MI. Heavy-Tailed prior distributions for sequence count data: Removing the noise and preserving large differences. *Bioinformatics*. 2019;35(12):2084-2092. doi:10.1093/bioinformatics/bty895

587. Weirather JL, de Cesare M, Wang Y, et al. Comprehensive comparison of Pacific Biosciences and Oxford Nanopore Technologies and their applications to transcriptome analysis. *F1000Research*. 2017;6(1):100. doi:10.12688/f1000research.10571.1

588. Steijger T, Abril JF, Engström PG, et al. Assessment of transcript reconstruction methods for RNA-seq. *Nat Methods*. 2013;10(12):1177-1184. doi:10.1038/nmeth.2714

589. Lin B, Hui J, Mao H. Nanopore technology and its applications in gene sequencing. *Biosensors*. 2021;11(7). doi:10.3390/bios11070214

590. Tyler AD, Mataseje L, Urfano CJ, et al. Evaluation of Oxford Nanopore's MinION Sequencing Device for Microbial Whole Genome Sequencing Applications. *Sci Rep*. 2018;8(1). doi:10.1038/s41598-018-29334-5

591. Cui J, Shen N, Lu Z, Xu G, Wang Y, Jin B. Analysis and comprehensive comparison of PacBio and nanopore-based RNA sequencing of the Arabidopsis transcriptome. *Plant Methods*. 2020;16(1). doi:10.1186/s13007-020-00629-x

592. Tyler AD, Mataseje L, Urfano CJ, et al. Evaluation of Oxford Nanopore's MinION Sequencing Device for Microbial Whole Genome Sequencing Applications. *Sci Rep*. 2018;8(1). doi:10.1038/s41598-018-29334-5

593. Workman RE, Tang AD, Tang PS, et al. Nanopore native RNA sequencing of a human poly(A) transcriptome. *Nat M*. 2019;16(12):1297-1305. doi:10.1038/s41592-019-0617-2.Nanopore

594. Payne A, Holmes N, Rakyan V, Loose M. Bulkvis: A graphical viewer for Oxford nanopore bulk FAST5 files. *Bioinformatics*. 2019;35(13):2193-2198. doi:10.1093/bioinformatics/bty841

595. Soneson C, Yao Y, Bratus-Neuenschwander A, Patrignani A, Robinson MD, Hussain S. A comprehensive examination of Nanopore native RNA sequencing for characterization of complex transcriptomes. *Nat Commun*. 2019;10(3359). doi:10.1038/s41467-019-11272-z

596. Grünberger F, Ferreira-Cerca S, Grohmann D. Nanopore sequencing of RNA and cDNA

molecules in Escherichia coli. *RNA*. 2022;28(3):400-417. doi:10.1261/rna.078937.121

597. Josić K, López JM, Ott W, Shiau LJ, Bennett MR. Stochastic delay accelerates signaling in gene networks. *PLoS Comput Biol*. 2011;7(11). doi:10.1371/journal.pcbi.1002264

598. Sayers EW, Cavanaugh M, Clark K, et al. GenBank. *Nucleic Acids Res*. 2021;49(D1):D92-D96. doi:10.1093/nar/gkaa1023

599. Raimondeau E, Bufton JC, Schaffitzel C. New insights into the interplay between the translation machinery and nonsense-mediated mRNA decay factors. *Biochem Soc Trans*. 2018;46(3):503-512. doi:10.1042/BST20170427

600. Lindeboom RGH, Supek F, Lehner B. The rules and impact of nonsense-mediated mRNA decay in human cancers. *Nat Genet*. 2016;48(10):1112-1118. doi:10.1038/ng.3664

601. Inácios Â, Silva AL, Pinto J, et al. Nonsense mutations in close proximity to the initiation codon fail to trigger full nonsense-mediated mRNA decay. *J Biol Chem*. 2004;279(31):32170-32180. doi:10.1074/jbc.M405024200

602. Silva AL, Ribeiro P, Inácio Â, Liebhaber SA, Romão L. Proximity of the poly(A)-binding protein to a premature termination codon inhibits mammalian nonsense-mediated mRNA decay. *RNA*. 2008;14(3):563-576. doi:10.1261/rna.815108

603. Lindeboom RGH, Vermeulen M, Lehner B, Supek F. The impact of nonsense-mediated mRNA decay on genetic disease, gene editing and cancer immunotherapy. *Nat Genet*. 2019;51(11):1645-1651. doi:10.1038/s41588-019-0517-5

604. Jumper J, Evans R, Pritzel A, et al. Highly accurate protein structure prediction with AlphaFold. *Nature*. 2021;596(7873):583-589. doi:10.1038/s41586-021-03819-2

605. Varadi M, Anyango S, Deshpande M, et al. AlphaFold Protein Structure Database: Massively expanding the structural coverage of protein-sequence space with high-accuracy models. *Nucleic Acids Res*. 2022;50(D1):D439-D444. doi:10.1093/nar/gkab1061

606. Melnick A, Ahmad KF, Arai S, et al. In-Depth Mutational Analysis of the Promyelocytic Leukemia Zinc Finger BTB/POZ Domain Reveals Motifs and Residues Required for Biological and Transcriptional Functions. *Mol Cell Biol*. 2000;20(17):6550-6567. doi:10.1128/mcb.20.17.6550-6567.2000

607. van Bodegraven EJ, Sluijs JA, Tan AK, Robe PAJT, Hol EM. New GFAP splice isoform (GFAPμ) differentially expressed in glioma translates into 21 kDa N-terminal GFAP protein. *FASEB J*. 2021;35(3). doi:10.1096/fj.202001767R

608. Maachani UB, Shankavaram U, Kramp T, Tofilon PJ, Camphausen K, Tandle AT. FOXM1 and STAT3 interaction confers radioresistance in glioblastoma cells. *Oncotarget*. 2016;7(47):77365-77377. doi:10.18632/oncotarget.12670

609. Bassett EA, Palanichamy K, Pearson M, et al. Calpastatin phosphorylation regulates radiation-induced calpain activity in glioblastoma. *Oncotarget*. 2018;9(18):14597-14607. doi:10.18632/oncotarget.24523

610. Guo J, Yi G zhong, Liu Z, et al. Quantitative Proteomics Analysis Reveals Nuclear Perturbation in Human Glioma U87 Cells treated with Temozolomide. *Cell Biochem Funct*. 2020;38(2):185-194. doi:10.1002/cbf.3459

611. Yi GZ, Xiang W, Feng WY, et al. Identification of Key Candidate Proteins and Pathways Associated with Temozolomide Resistance in Glioblastoma Based on Subcellular Proteomics and Bioinformatical Analysis. *Biomed Res Int*. 2018;2018(5238760). doi:10.1155/2018/5238760

612. Li M, Ren T, Lin M, Wang Z, Zhang J. Integrated proteomic and metabolomic profiling the

global response of rat glioma model by temozolomide treatment. *J Proteomics*. 2020;211(103578). doi:10.1016/j.jprot.2019.103578

613. Pak O, Zaitsev S, Shevchenko V, Sharma A, Sharma HS, Bryukhovetskiy I. *Effectiveness of Bortezomib and Temozolomide for Eradication of Recurrent Human Glioblastoma Cells, Resistant to Radiation*. Vol 266. 1st ed. Elsevier B.V.; 2021. doi:10.1016/bs.pbr.2021.06.010

614. Santa Cruz Biotechnology Inc. Anti-Bcl-6 Antibody (D-8): sc-7388. https://www.scbt.com/p/bcl-6-antibody-d-8. Accessed August 16, 2022.

615. Yuan F, Xie Q, Wu J, et al. MST1 promotes apoptosis through regulating Sirt1-dependent p53 deacetylation. *J Biol Chem*. 2011;286(9):6940-6945. doi:10.1074/jbc.M110.182543

616. Hu Y, O'Boyle K, Auer J, et al. Multiple UBXN family members inhibit retrovirus and lentivirus production and canonical NFκB signaling by stabilizing IκBα. *PLoS Pathog*. 2017;13(2). doi:10.1371/journal.ppat.1006187

617. Wang YB, Tan B, Mu R, et al. Ubiquitin-associated domain-containing ubiquitin regulatory X (UBX) protein UBXN1 is a negative regulator of nuclear factor κB (NF-κB) signaling. *J Biol Chem*. 2015;290(16):10395-10405. doi:10.1074/jbc.M114.631689

618. Boston University Biology. NF-kB Target Genes. https://www.bu.edu/nf-kb/gene-resources/target-genes/. Accessed August 16, 2022.

619. Ji H, Lu Z. The Role of Protein Kinase CK2 in Glioblastoma Development. *Clin Cancer Res*. 2013;19(23):6335-6337. doi:10.1158/1078-0432.CCR-13-2478.

620. Borgo C, Ruzzene M. Role of protein kinase CK2 in antitumor drug resistance. *J Exp Clin Cancer Res*. 2019;38(287). doi:10.1007/BF01757347

621. Rabalski AJ, Gyenis L, Litchfield DW. Molecular pathways: Emergence of protein kinase CK2 (CSNK2) as a potential target to inhibit survival and DNA damage response and repair pathways in cancer cells. *Clin Cancer Res*. 2016;22(12):2840-2847. doi:10.1158/1078-0432.CCR-15-1314

# 9: Appendix

## 9.1: Tables and Figures

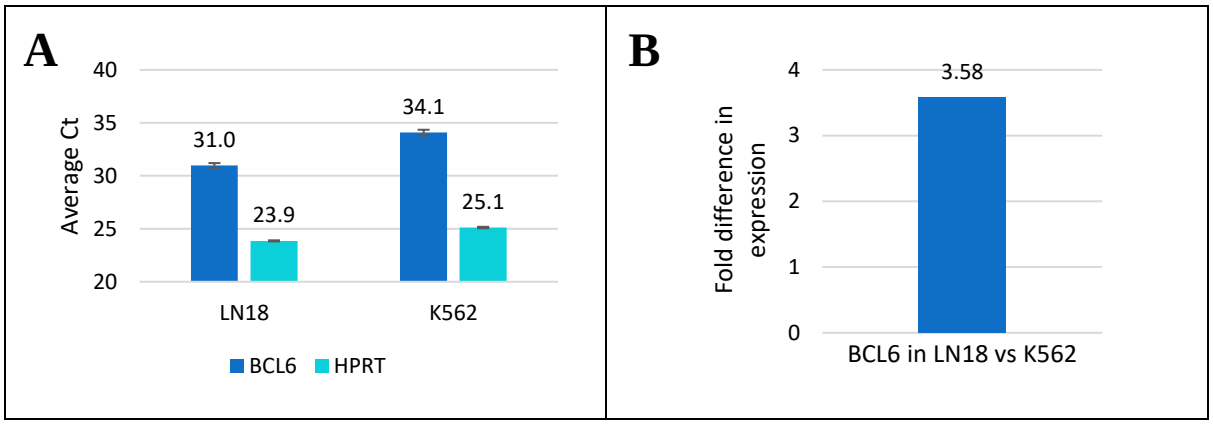


Figure 9.1: qRT-PCR for BCL6 in LN18 and K562 cells

A) Average Ct values for BCL6 and the housekeeping gene HPRT in LN18 and K562 cells. Error bars represent standard deviation (n = 3). B) Fold difference in BCL6 expression in LN18 cells compared to K562 cells, corrected to HPRT.

Table 9.1: Top ten enriched GO:BP terms for proteins up- and downregulated by FX1 in K562 cells

| GO:BP term | Adjusted p value |
|---|---|
| **Upregulated by FX1** | |
| Ribonucleoprotein complex biogenesis | 8.86E-12 |
| Ribosome biogenesis | 1.25E-11 |
| Regulation of chromatin organization | 2.53E-09 |
| rRNA processing | 2.70E-09 |
| rRNA metabolic process | 6.34E-09 |
| mRNA metabolic process | 5.75E-08 |
| ncRNA metabolic process | 1.89E-07 |
| Chromosome condensation | 2.79E-07 |
| ncRNA processing | 4.63E-07 |
| DNA packaging | 5.52E-06 |
| **Downregulated by FX1** | |
| Nucleotide metabolic process | 0.00888 |
| Regulation of mRNA stability | 0.00921 |
| Endoplasmic reticulum to Golgi vesicle-mediated transport | 0.0103 |
| Vesicle organization | 0.0107 |
| Nucleoside phosphate metabolic process | 0.0120 |
| Regulation of mRNA catabolic process | 0.0128 |
| Regulation of RNA stability | 0.0149 |
| Intracellular protein transport | 0.0176 |
| Golgi vesicle transport | 0.0220 |
| Regulation of mRNA metabolic process | 0.0396 |

### Table 9.2: Effect of FX1 on known BCL6 target genes in LN18 cells

BCL6 target genes identified in GC B cells and/or $T_{FH}$ cells for which the corresponding protein was identified in LN18 cells.[227,258] The abundance ratios and adjusted p values show the effect of FX1 treatment on the expression of these known BCL6 target genes in LN18 cells.

| Protein accession | Gene name | Abundance Ratio (FX1/DMSO) | Adj. p value |
|---|---|---|---|
| P05412 | JUN | 3.07 | 0.05390198 |
| P40763 | STAT3 | 1.729 | 0.567935303 |
| P63279 | UBE2I | 1.728 | 0.512605918 |
| P51572 | BCAP31 | 1.703 | 0.560432282 |
| O14647 | CHD2 | 1.412 | 0.826314131 |
| Q9BTC0 | DIDO1 | 0.977 | 0.99633457 |
| P28482 | MAPK1 | 0.97 | 0.970898342 |
| P42345 | MTOR | 0.792 | 0.926100018 |
| O14757 | CHEK1 | 0.778 | 0.913690155 |
| Q15628 | TRADD | 0.654 | 0.82046433 |
| P31749 | AKT1 | 0.648 | 0.780664267 |
| P53999 | SUB1 | 0.431 | 0.058426649 |
| P17535 | JUND | 0.01 | 9.2178E-17 |
| O00221 | NRKBIE | 0.01 | 9.2178E-17 |
| P63098 | PPP3R1 | No abundance values | |
| Q99836 | MYD88 | No abundance values | |
| P19838 | NFKB1 | No abundance values | |
| P04637 | TP53 | No abundance values | |
| O43524 | FOXO3 | No abundance values | |
| O94916 | NFAT5 | No abundance values | |

### Table 9.3: Genes up- or downregulated at both the transcript and protein level by FX1 treatment of LN18 cells

The commonly affected transcripts and proteins are out of 37 transcripts and 230 proteins upregulated by FX1 (≥2-fold, $p \leq 0.05$) and 55 transcripts and 263 proteins downregulated by FX1 (≥ 2-fold, $p \leq 0.05$). The transcriptome sequencing data is from previous research carried out by the McConnell lab group.[207,322]

| | | RNA sequencing | | Whole proteomics | |
|---|---|---|---|---|---|
| Protein accession | Gene name | Abundance Ratio (FX1/DMSO) | Adjusted p value | Abundance Ratio (FX1/DMSO) | Adjusted p value |
| O00767 | SCD | 2.16 | 0 | 100 | 9.22E-17 |
| Q9NP84 | TNFRSF12A | 0.457 | 0 | 0.01 | 9.22E-17 |
| Q8IVL0 | NAV3 | 0.401 | 0.002 | 0.01 | 9.22E-17 |
| Q9NX24 | NHP2 | 0.0743 | 0.033 | 0.32 | 0.0309 |

### Table 9.4: Top ten enriched GO:BP terms for transcripts downregulated by FX1 in LN18 cells

Transcript data from previous McConnell lab group research re-analysed using the same gene ontology analysis method used to analyse the whole proteome data.[322] There was no functional enrichment for the upregulated transcripts.

| GO:BP term | Adjusted p value |
|---|---|
| Secondary metabolic process | 0.000199 |
| Omega-hydroxylase P450 pathway | 0.002223 |
| Unsaturated fatty acid metabolic process | 0.004957 |
| Icosanoid metabolic process | 0.006681 |
| Cellular ketone metabolic process | 0.010532 |
| Cellular hormone metabolic process | 0.013801 |
| Carboxylic acid metabolic process | 0.018669 |
| Organic hydroxy compound metabolic process | 0.020406 |
| Oxoacid metabolic process | 0.023693 |
| Olefinic compound metabolic process | 0.025045 |

### Table 9.5: BCL6 peptides identified in RIME replicates

Peptides identified by which amino acids in the BCL6 protein sequence they covered (left-hand column). When a peptide was identified in a RIME sample, the box is marked with a tick. The total number of samples identifying each group of similar peptides is shown in the right-hand column.

| Peptide | LN18 Untreated | | | NZG0906 Untreated | | | NZG1003 Untreated | | | LN18 Irradiated | | | NZG0906 Irradiated | | | NZG1003 Irradiated | | | Total |
|---|---|---|---|---|---|---|---|---|---|---|---|---|---|---|---|---|---|---|---|
| | 1 | 2 | 3 | 1 | 2 | 3 | 1 | 2 | 3 | 1 | 2 | 3 | 1 | 2 | 3 | 1 | 2 | 3 | |
| 14-24 | ✓ | | | | ✓ | ✓ | | ✓ | | | | | ✓ | ✓ | | ✓ | ✓ | ✓ | 9 |
| 27-40 | | ✓ | | ✓ | ✓ | | ✓ | | | | | | | | | ✓ | ✓ | ✓ | 9 |
| 29-40 | | | | | | ✓ | | ✓ | | | | | | | | | | | |
| 148-170 | | | | ✓ | | | | ✓ | | | | | | | | ✓ | | | 11 |
| 148-158 | ✓ | | | | ✓ | ✓ | | | | | | | | | | | ✓ | | |
| 159-170 | | | | | | | | | | | | | ✓ | ✓ | | | | ✓ | |
| 161-170 | | | | | ✓ | | | | | | | | | | | | | | |
| 218-226 | | | | | | | | ✓ | ✓ | | | | | | | ✓ | | | 3 |
| 271-289 | | | | | | | | | | | | | | | | | | ✓ | 1 |
| 380-406 | | | | ✓ | ✓ | ✓ | | | | | | | ✓ | | | | ✓ | ✓ | 6 |
| 431-445 | | | ✓ | | | | | | | | | ✓ | | | | | | | 2 |
| 446-452 | | | | | | | | ✓ | ✓ | | ✓ | | ✓ | | | ✓ | ✓ | ✓ | 7 |
| 460-474 | | | | ✓ | ✓ | | | | | | | | | | | | | ✓ | 3 |
| 527-535 | | | | | | | | | | | | | | | | | ✓ | ✓ | 5 |
| 527-547 | | | | | | | | | | | | | | | | ✓ | | | |
| 536-547 | | | | | ✓ | | | | | | | | | ✓ | | | | | |
| 566-575 | | | | | | | | ✓ | | ✓ | ✓ | | ✓ | ✓ | | | | ✓ | 6 |
| 611-618 | | | | | | | | | | | | | | | | ✓ | ✓ | ✓ | 3 |
| 692-703 | | | | | | | | | | | | | ✓ | ✓ | | | ✓ | | 3 |

Table 9.6: CRAPome analysis of BCL6-associated proteins identified with the identification-based method

Proteins commonly pulled down with BCL6 in untreated and irradiated GBM cells (≥ 3 replicates) were searched against the 716 AP-MS negative control samples in the CRAPome database. The percentage columns show how frequently each BCL6-associated protein was found in these controls. Proteins found in ≥ 10% of the controls in the CRAPome database were excluded (grey).

| Untreated | | | Irradiated | | |
|---|---|---|---|---|---|
| **Accession** | **Name** | **Percentage** | **Accession** | **Name** | **Percentage** |
| P01599 | IGKV1-17 | 0 | Q86XK2 | FBXO11 | 0 |
| Q86XK2 | FBXO11 | 0 | P41182 | BCL6 | 0.27933 |
| Q86WA8 | LONP2 | 0.139665 | P61764 | STXBP1 | 0.27933 |
| P41182 | BCL6 | 0.27933 | Q96LD4 | TRIM47 | 0.418994 |
| P19823 | ITIH2 | 0.27933 | P02461 | COL3A1 | 0.558659 |
| O00625 | PIR | 0.27933 | Q06033 | ITIH3 | 0.558659 |
| Q96LD4 | TRIM47 | 0.418994 | Q969G5 | CAVIN3 | 1.117318 |
| P51530 | DNA2 | 0.418994 | P83111 | LACTB | 1.396648 |
| P02461 | COL3A1 | 0.558659 | O75146 | HIP1R | 1.396648 |
| Q9UBF1 | MAGEC2 | 0.837989 | P53680 | AP2S1 | 1.396648 |
| Q9HD26 | GOPC | 1.256983 | P27169 | PON1 | 1.396648 |
| P27169 | PON1 | 1.396648 | P04196 | HRG | 2.094972 |
| O75146 | HIP1R | 1.396648 | P02790 | HPX | 2.094972 |
| Q01433 | AMPD2 | 1.536313 | P02647 | APOA1 | 2.374302 |
| P02458 | COL2A1 | 1.536313 | Q13131 | PRKAA1 | 2.513966 |
| Q8IXK0 | PHC2 | 1.815642 | P02452 | COL1A1 | 2.932961 |
| P04196 | HRG | 2.094972 | P54619 | PRKAG1 | 6.005587 |
| P02647 | APOA1 | 2.374302 | P01024 | C3 | 6.284916 |
| Q13131 | PRKAA1 | 2.513966 | P01023 | A2M | 7.541899 |
| P04114 | APOB | 2.513966 | Q9Y618 | NCOR2 | 7.821229 |
| P17931 | LGALS3 | 2.793296 | Q86SE5 | RALYL | 8.240223 |
| Q13043 | STK4 | 3.351955 | P07954 | FH | 10.19553 |
| O75351 | VPS4B | 3.77095 | Q13492 | PICALM | 10.89385 |
| P54619 | PRKAG1 | 6.005587 | Q96FW1 | OTUB1 | 11.59218 |
| P01024 | C3 | 6.284916 | P0C0L4 | C4A | 12.15084 |
| Q9BZK7 | TBL1XR1 | 6.284916 | Q16891 | IMMT | 12.98883 |
| P29508 | SERPINB3 | 6.284916 | Q96EY1 | DNAJA3 | 16.20112 |
| Q99661 | KIF2C | 6.564246 | Q92900 | UPF1 | 16.34078 |
| P42765 | ACAA2 | 6.843575 | Q8WTT2 | NOC3L | 17.03911 |
| Q9Y618 | NCOR2 | 7.821229 | O00151 | PDLIM1 | 18.99441 |
| P04040 | CAT | 7.960894 | P30154 | PPP2R1B | 18.99441 |
| P12273 | PIP | 8.240223 | P06744 | GPI | 19.69274 |
| P48735 | IDH2 | 9.078212 | P04080 | CSTB | 22.90503 |
| P54132 | BLM | 10.61453 | P61604 | HSPE1 | 23.32402 |
| Q9BWD1 | ACAT2 | 10.61453 | O00487 | PSMD14 | 23.46369 |
| P51784 | USP11 | 10.89385 | Q5T9A4 | ATAD3B | 24.02235 |

| | | | | | |
|---|---|---|---|---|---|
| P00491 | PNP | 10.89385 | P63010 | AP2B1 | 25.55866 |
| P78332 | RBM6 | 11.17318 | P60900 | PSMA6 | 26.95531 |
| O43148 | RNMT | 11.31285 | Q9BRL6 | SRSF8 | 28.49162 |
| Q13045 | FLII | 11.31285 | Q9Y678 | COPG1 | 31.84358 |
| Q9BW27 | NUP85 | 11.31285 | Q9NVI7 | ATAD3A | 31.98324 |
| P0C0L4 | C4A | 12.15084 | P67936 | TPM4 | 43.43575 |
| Q9BTE3 | MCMBP | 12.84916 | P42677 | RPS27 | 57.40223 |
| Q03701 | CEBPZ | 13.68715 | P10599 | TXN | 60.3352 |
| P45973 | CBX5 | 13.96648 | P62987 | UBA52 | 64.52514 |
| Q8NB90 | SPATA5 | 14.94413 | | | |
| Q8N3U4 | STAG2 | 14.94413 | | | |
| Q96HC4 | PDLIM5 | 16.20112 | | | |
| Q15436 | SEC23A | 17.4581 | | | |
| Q14964 | RAB39A | 18.01676 | | | |
| P08243 | ASNS | 18.29609 | | | |
| Q8IX01 | SUGP2 | 18.99441 | | | |
| P06744 | GPI | 19.69274 | | | |
| P23258 | TUBG1 | 19.69274 | | | |
| Q14676 | MDC1 | 20.67039 | | | |
| P28070 | PSMB4 | 20.81006 | | | |
| Q8N684 | CPSF7 | 21.50838 | | | |
| Q9BR76 | CORO1B | 21.92737 | | | |
| Q08043 | ACTN3 | 23.74302 | | | |
| Q5T9A4 | ATAD3B | 24.02235 | | | |
| P33240 | CSTF2 | 26.25698 | | | |
| Q9Y2Z0 | SUGT1 | 26.53631 | | | |
| P55769 | SNU13 | 27.09497 | | | |
| P18669 | PGAM1 | 33.37989 | | | |
| P62304 | SNRPE | 36.17318 | | | |
| Q13547 | HDAC1 | 42.73743 | | | |
| P11498 | PC | 42.73743 | | | |
| P30048 | PRDX3 | 43.99441 | | | |

### Table 9.7: CRAPome analysis of BCL6-associated proteins identified with the quantification-based method

Proteins commonly pulled down by the BCL6 antibody at ≥ 2-fold greater abundance than by the IgG antibody in untreated and irradiated GBM cells (≥ 2 cell lines) were searched against the 716 AP-MS negative control samples in the CRAPome database. The percentage columns show how frequently each BCL6-associated protein was found in these controls. Proteins found in ≥ 10% of the controls in the CRAPome database were excluded (not shown).

| Untreated | | | Irradiated | | |
|---|---|---|---|---|---|
| **Accession** | **Name** | **Percentage** | **Accession** | **Name** | **Percentage** |
| Q8IZL2 | MAML2 | 0 | P01599 | IGKV1-17 | 0 |
| Q96KP1 | EXOC2 | 0.698324 | P21579 | SYT1 | 0 |
| Q8NEM2 | SHCBP1 | 0.977654 | P51674 | GPM6A | 0 |
| Q86VS8 | HOOK3 | 1.536313 | O94811 | TPPP | 0.139665 |
| P02790 | HPX | 2.094972 | P63098 | PPP3R1 | 0.139665 |
| Q9UHA3 | RSL24D1 | 2.234637 | Q6UWE0 | LRSAM1 | 0.27933 |
| O60701 | UGDH | 2.653631 | P05026 | ATP1B1 | 0.977654 |
| P01834 | IGKC | 5.027933 | P02458 | COL2A1 | 1.536313 |
| Q6ZSZ5 | ARHGEF18 | 5.726257 | P16070 | CD44 | 1.815642 |
| Q92504 | SLC39A7 | 5.726257 | P08123 | COL1A2 | 2.653631 |
| Q9HCD5 | NCOA5 | 6.145251 | Q6NZI2 | CAVIN1 | 3.77095 |
| O76031 | CLPX | 7.122905 | Q03135 | CAV1 | 4.329609 |
| O60306 | AQR | 7.26257 | O75955 | FLOT1 | 6.284916 |
| P01023 | A2M | 7.541899 | Q08188 | TGM3 | 6.564246 |
| O94925 | GLS | 7.541899 | Q04323 | UBXN1 | 8.798883 |
| P20930 | FLG | 7.541899 | Q08379 | GOLGA2 | 9.916201 |
| Q8IY37 | DHX37 | 9.078212 | | | |
| Q13098 | GPS1 | 9.357542 | | | |
| Q99496 | RNF2 | 9.357542 | | | |
| Q9HC35 | EML4 | 9.636872 | | | |
| Q08379 | GOLGA2 | 9.916201 | | | |

### Table 9.8: Phosphorylation of BCL6

Samples in which the putative AMPK phosphorylation site (Ser16) was identified without evidence of phosphorylation and samples in which phosphorylation of Ser404 was identified.

| **Serine residue** | **LN18 Untreated** | | | **NZG0906 Untreated** | | | **NZG1003 Untreated** | | | **LN18 Irradiated** | | | **NZG0906 Irradiated** | | | **NZG1003 Irradiated** | | |
|---|---|---|---|---|---|---|---|---|---|---|---|---|---|---|---|---|---|---|
| **Ser16** | ✓ | | | | ✓ | ✓ | | ✓ | | | | | ✓ | ✓ | | ✓ | ✓ | ✓ |
| **pSer404** | | | | ✓ | ✓ | ✓ | | | | | | | ✓ | | | | ✓ | ✓ |

Table 9.9: Red/blue pixel ratios for BCL6 + NCOR2 PLA assays and controls in untreated and irradiated LN18 cells

| Antibodies | Replicate | Field | Number of red pixels | Number of blue pixels | Ratio |
|---|---|---|---|---|---|
| **Untreated** | | | | | |
| **BCL6 + NCOR2** | 1 | 1 | 3787 | 165445 | 0.02289 |
| | 1 | 2 | 2808 | 270459 | 0.010382 |
| | 1 | 3 | 6499 | 115908 | 0.05607 |
| | 1 | 4 | 9053 | 70991 | 0.127523 |
| | 2 | 2 | 4030 | 67975 | 0.059287 |
| | 2 | 3 | 14530 | 70155 | 0.207113 |
| | 2 | 4 | 5010 | 24777 | 0.202204 |
| | 3 | 1 | 4233 | 89467 | 0.047314 |
| | 3 | 2 | 3510 | 231842 | 0.01514 |
| | 3 | 3 | 8505 | 238531 | 0.035656 |
| | 3 | 4 | 4963 | 216639 | 0.022909 |
| **BCL6 + Rabbit IgG** | 2 | 1 | 952 | 99197 | 0.009597 |
| | 2 | 2 | 753 | 122932 | 0.006125 |
| | 2 | 3 | 969 | 155336 | 0.006238 |
| | 3 | 1 | 753 | 187512 | 0.004016 |
| | 3 | 2 | 477 | 55469 | 0.008599 |
| | 3 | 3 | 54 | 183534 | 0.000294 |
| **Mouse IgG + NCOR2** | 2 | 1 | 380 | 180106 | 0.00211 |
| | 2 | 2 | 1090 | 120922 | 0.009014 |
| | 2 | 3 | 21 | 79419 | 0.000264 |
| | 3 | 1 | 643 | 68937 | 0.009327 |
| | 3 | 2 | 661 | 326887 | 0.002022 |
| **Irradiated** | | | | | |
| **BCL6 + NCOR2** | 1 | 1 | 3429 | 159064 | 0.021557 |
| | 1 | 2 | 1608 | 52301 | 0.030745 |
| | 1 | 3 | 4380 | 44609 | 0.098186 |
| | 1 | 4 | 2516 | 94822 | 0.026534 |
| | 2 | 1 | 1839 | 163561 | 0.011244 |
| | 2 | 2 | 2401 | 88241 | 0.02721 |
| | 2 | 3 | 1427 | 157805 | 0.009043 |
| | 2 | 4 | 1670 | 155158 | 0.010763 |
| | 3 | 1 | 1774 | 55662 | 0.031871 |
| | 3 | 2 | 3056 | 103463 | 0.029537 |
| | 3 | 3 | 4020 | 73335 | 0.054817 |
| | 3 | 4 | 1307 | 68970 | 0.01895 |
| **BCL6 + Rabbit IgG** | 1 | 1 | 934 | 28424 | 0.03286 |
| | 1 | 2 | 258 | 17879 | 0.01443 |
| | 2 | 1 | 540 | 99476 | 0.005428 |
| | 2 | 2 | 465 | 73704 | 0.006309 |

| | | | | | |
|---|---|---|---|---|---|
| | 2 | 3 | 342 | 57210 | 0.005978 |
| | 2 | 4 | 698 | 134425 | 0.005192 |
| | 3 | 1 | 41 | 74908 | 0.000547 |
| | 3 | 2 | 285 | 89309 | 0.003191 |
| | 3 | 3 | 1023 | 94046 | 0.010878 |
| | 3 | 4 | 123 | 58182 | 0.002114 |
| **Mouse IgG + NCOR2** | 1 | 1 | 4284 | 129679 | 0.033035 |
| | 1 | 2 | 5261 | 104240 | 0.05047 |
| | 2 | 1 | 160 | 36780 | 0.00435 |
| | 2 | 2 | 737 | 60140 | 0.012255 |
| | 2 | 3 | 359 | 75462 | 0.004757 |
| | 2 | 4 | 763 | 119590 | 0.00638 |
| | 3 | 1 | 714 | 195299 | 0.003656 |
| | 3 | 2 | 4048 | 61075 | 0.066279 |
| | 3 | 3 | 2850 | 46492 | 0.061301 |
| | 3 | 4 | 486 | 91251 | 0.005326 |

Table 9.10: Red/blue pixel ratios for BCL6 + AMPK PLA assays and controls in untreated and irradiated LN18 cells

| Antibodies | Replicate | Field | Red pixels | Blue pixels | Ratio |
|---|---|---|---|---|---|
| **Untreated** | | | | | |
| **BCL6 + AMPK** | 1 | 1 | 124 | 133672 | 0.000928 |
| | 1 | 2 | 5978 | 144867 | 0.041265 |
| | 1 | 3 | 5139 | 43602 | 0.117862 |
| | 1 | 4 | 1302 | 92675 | 0.014049 |
| | 2 | 1 | 8118 | 70360 | 0.115378 |
| | 2 | 2 | 3524 | 42296 | 0.083318 |
| | 2 | 3 | 6581 | 73879 | 0.089078 |
| | 2 | 4 | 5900 | 57896 | 0.101907 |
| | 3 | 1 | 2784 | 274406 | 0.010146 |
| | 3 | 2 | 2440 | 118516 | 0.020588 |
| | 3 | 3 | 1678 | 86482 | 0.019403 |
| | 3 | 4 | 2605 | 300031 | 0.008682 |
| **BCL6 + Rabbit IgG** | 2 | 1 | 837 | 47132 | 0.017759 |
| | 2 | 2 | 761 | 41225 | 0.01846 |
| | 2 | 3 | 732 | 15626 | 0.046845 |
| | 2 | 4 | 100 | 60864 | 0.001643 |
| | 2 | 5 | 672 | 25027 | 0.026851 |
| | 3 | 1 | 250 | 83302 | 0.003001 |
| | 3 | 2 | 947 | 345573 | 0.00274 |
| | 3 | 3 | 235 | 66396 | 0.003539 |
| | 3 | 4 | 379 | 312106 | 0.001214 |

| | | | | | |
|---|---|---|---|---|---|
| | 3 | 5 | 309 | 136838 | 0.002258 |
| **Mouse IgG + AMPK** | 2 | 1 | 4532 | 105493 | 0.04296 |
| | 2 | 2 | 4484 | 104106 | 0.043071 |
| | 2 | 3 | 2331 | 27767 | 0.083949 |
| | 2 | 4 | 4882 | 77254 | 0.063194 |
| | 3 | 1 | 30 | 173544 | 0.000173 |
| | 3 | 2 | 38 | 163320 | 0.000233 |
| | 3 | 3 | 153 | 214335 | 0.000714 |
| | 3 | 4 | 71 | 135796 | 0.000523 |
| | 3 | 5 | 1 | 221665 | 4.51E-06 |
| **Irradiated** | | | | | |
| **BCL6 + AMPK** | 1 | 1 | 4625 | 49959 | 0.092576 |
| | 1 | 2 | 2049 | 66746 | 0.030698 |
| | 1 | 3 | 1425 | 103127 | 0.013818 |
| | 1 | 4 | 4334 | 96211 | 0.045047 |
| | 2 | 1 | 1089 | 76413 | 0.014252 |
| | 2 | 2 | 1532 | 31298 | 0.048949 |
| | 2 | 3 | 1452 | 98385 | 0.014758 |
| | 2 | 4 | 1919 | 84644 | 0.022671 |
| | 3 | 1 | 1239 | 128377 | 0.009651 |
| | 3 | 2 | 3218 | 63074 | 0.051019 |
| | 3 | 3 | 2206 | 151092 | 0.0146 |
| | 3 | 4 | 1616 | 100786 | 0.016034 |
| **BCL6 + Rabbit IgG** | 1 | 1 | 479 | 64525 | 0.007423 |
| | 1 | 2 | 478 | 63775 | 0.007495 |
| | 2 | 1 | 153 | 103967 | 0.001472 |
| | 2 | 2 | 206 | 119474 | 0.001724 |
| | 2 | 3 | 185 | 86828 | 0.002131 |
| | 3 | 1 | 938 | 54690 | 0.017151 |
| | 3 | 2 | 859 | 119498 | 0.007188 |
| | 3 | 3 | 861 | 53101 | 0.016214 |
| **Mouse IgG + AMPK** | 1 | 1 | 2432 | 79377 | 0.030639 |
| | 1 | 2 | 2635 | 94157 | 0.027985 |
| | 2 | 1 | 204 | 31264 | 0.006525 |
| | 2 | 2 | 63 | 115904 | 0.000544 |
| | 2 | 3 | 65 | 42057 | 0.001546 |
| | 2 | 4 | 521 | 126867 | 0.004107 |
| | 3 | 1 | 275 | 115579 | 0.002379 |
| | 3 | 2 | 259 | 75297 | 0.00344 |
| | 3 | 3 | 406 | 66901 | 0.006069 |

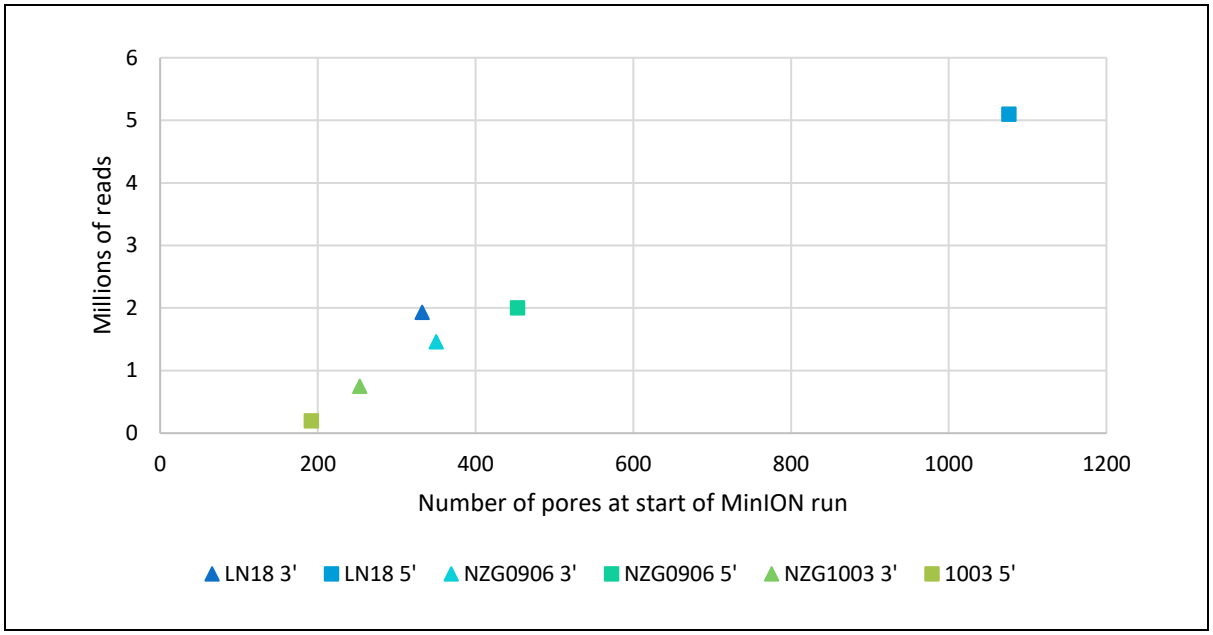


Figure 9.2: Effect of number of pores on number of reads

Millions of sequencing reads obtained from each multiplexed sample indicated in the key: LN18, NZG0906 and NZG1003, with BCL6 amplified using the 3'-end primer (triangles) or the 5'-end primer (squares).

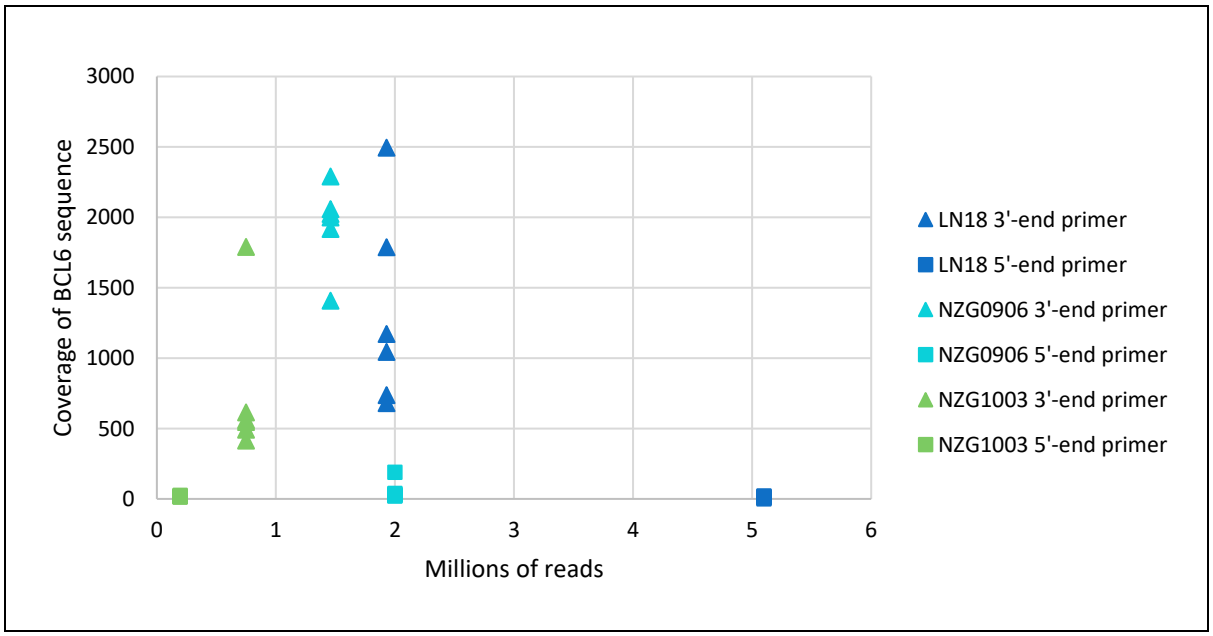


Figure 9.3: Effect of number of reads on coverage of BCL6

Number of total reads compared to number of reads mapping to BCL6 (coverage) for each multiplexed sample indicated in the key: LN18, NZG0906 and NZG1003, with BCL6 amplified using the 3'-end primer (triangles) or the 5'-end primer (squares).

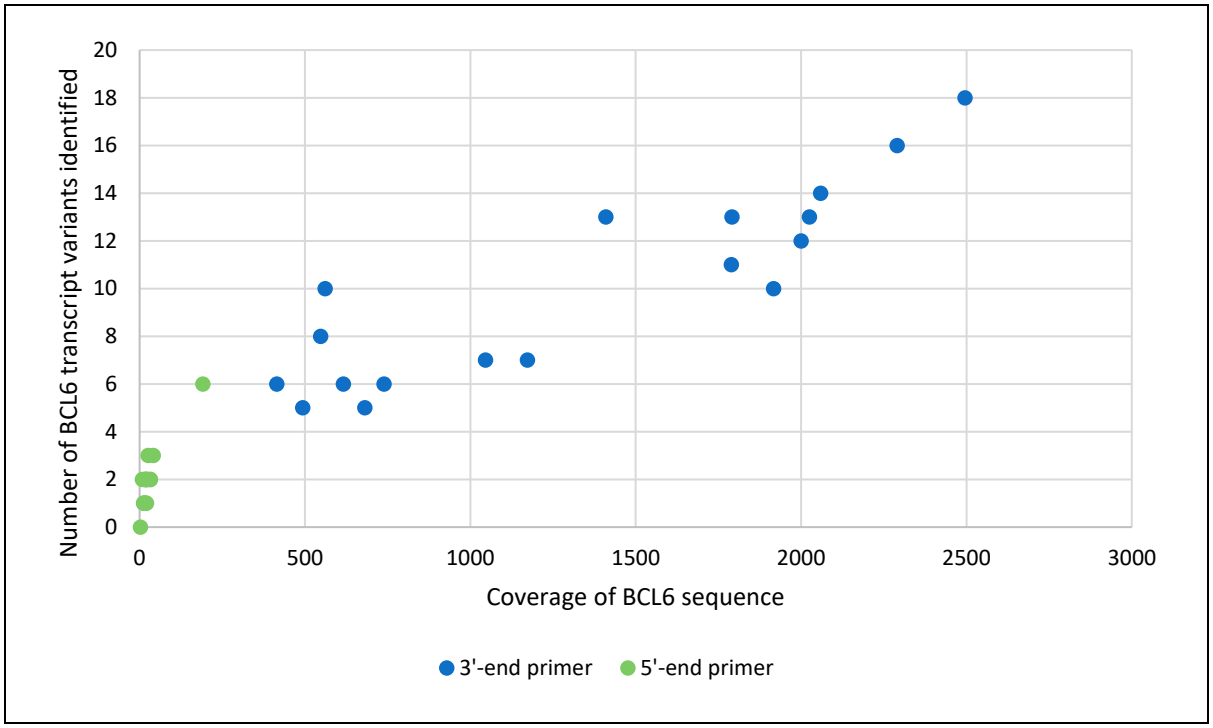


Figure 9.4: Effect of coverage of BCL6 on the number of different BCL6 transcript variants identified

Comparison shown for all samples in which BCL6 was amplified with the 3'-end primer (blue) and in which BCL6 was amplified with the 5'-end primer (green).

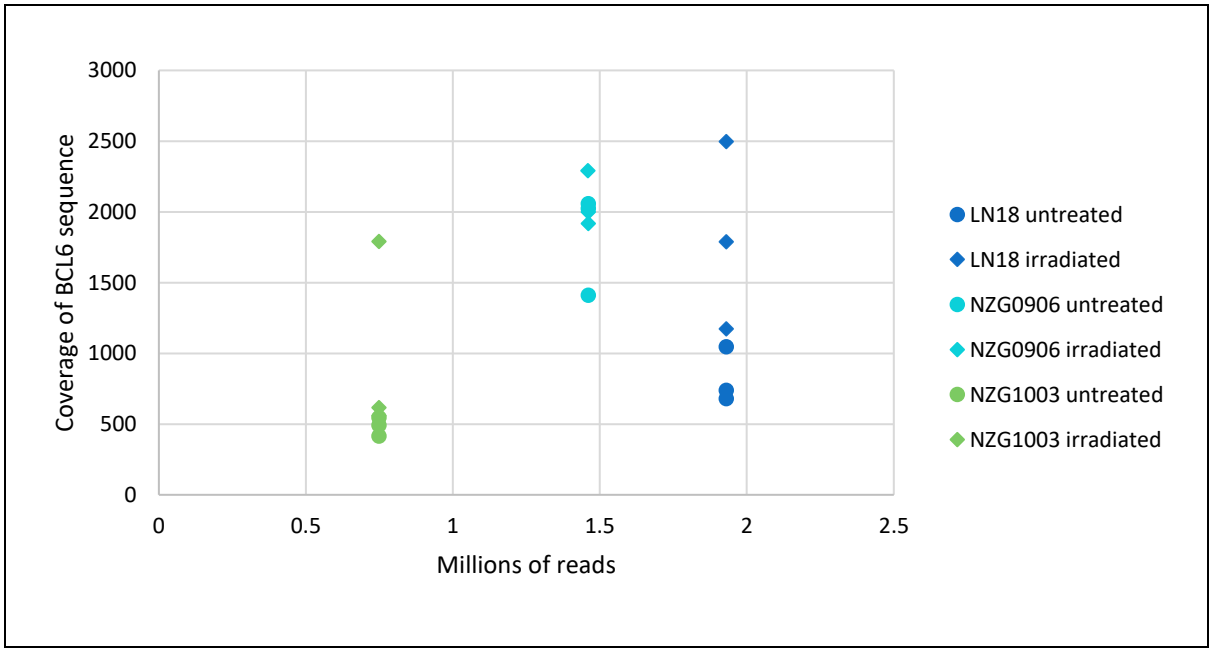


Figure 9.5: Effect of irradiation on coverage of BCL6

Number of total reads compared to number of reads mapping to BCL6 (coverage) for each multiplexed sample amplified with the 3'-end primer. The coverage of BCL6 in the untreated (circles) and irradiated (diamonds) samples are compared.

## 9.2: Code for bioinformatics analysis of MinION transcript sequencing output

### 9.2.1 Basecalling

# Basic configuration file for ONT Guppy basecaller software.

# Compatibility

compatible_flowcells = FLO-FLG001,FLO-MIN106,FLO-MINSP6

compatible_kits = SQK-CAS109,SQK-CS9109,SQK-DCS108,SQK-DCS109,SQK-LRK001,SQK-LSK108,SQK-LSK109,SQK-LSK109-XL,SQK-LSK110,SQK-LSK110-XL,SQK-LSK111,SQK-LSK111-XL,SQK-LWP001,SQK-PCS108,SQK-PCS109,SQK-PCS110,SQK-PCS111,SQK-PRC109,SQK-PSK004,SQK-RAD002,SQK-RAD003,SQK-RAD004,SQK-RAD111,SQK-RAS201,SQK-RLI001,SQK-ULK001,VSK-VBK001,VSK-VSK001,VSK-VSK002,VSK-VSK003,VSK-VSK004

compatible_kits_with_barcoding = OND-SQK-LP0096M,OND-SQK-LP0096MA,OND-SQK-LP0096S,OND-SQK-LP0768L,OND-SQK-LP1152S,OND-SQK-LP9216,OND-SQK-RP0096M,OND-SQK-RP0096MA,OND-SQK-RP0384L,SQK-16S024,SQK-MLK110-96-XL,SQK-MLK111-96-XL,SQK-NBD110-24,SQK-NBD110-96,SQK-NBD111-24,SQK-NBD111-96,SQK-PCB109,SQK-PCB110,SQK-PCB111-24,SQK-RBK001,SQK-RBK004,SQK-RBK110-96,SQK-RBK111-24,SQK-RBK111-96,SQK-RLB001,SQK-LWB001,SQK-PBK004,SQK-RAB201,SQK-RAB204,SQK-RPB004,VSK-PTC001,VSK-VMK001,VSK-VMK002,VSK-VMK003

# Data trimming

trim_strategy = dna

trim_threshold = 2.5

trim_min_events = 3

# Basecalling

model_file = template_r9.4.1_450bps_hac.jsn

chunk_size = 2000

gpu_runners_per_device = 4

chunks_per_runner = 256

chunks_per_caller = 10000

overlap = 50

qscore_offset = -0.1721

qscore_scale = 0.9356

builtin_scripts = 1

beam_width = 32

noisiest_section_scaling_max_size = 8000

# Calibration strand detection

calib_reference = lambda_3.6kb.fasta

calib_min_sequence_length = 3000

calib_max_sequence_length = 3800

calib_min_coverage = 0.6

# Output

records_per_fastq = 4000

min_qscore = 9.0

# Telemetry

ping_url = https://ping.oxfordnanoportal.com/basecall

ping_segment_duration = 60

## 9.2.2: Demultiplexing

The basecalled reads were demultiplexed using qcat in epi2me mode with the following additional settings:

--trim
--detect-middle
--kit NBD103/NBD104

## 9.2.3: FLAIR code

## `flair-align`

python ../flair.py align \

--genome
/hg38/GCA_000001405.15_GRCh38/GCA_000001405.15_GRCh38_no_alt_analysis_set/GRCh38_no_alt_analysis_set_ch

r_only.fa \

--reads sample_reads.fastq \

--threads 46 \

--output sample.aligned \

--version1.3

## `flair-correct`

```
python ../flair.py correct \
--query /sample.aligned.bed \
--genome
/hg38/GCA_000001405.15_GRCh38/GCA_000001405.15_GRCh38_no_alt_analysis_set/GRCh38_no_alt_analysis_set_ch
r_only.fa \
--gtf /hg38/unknown/hg38.knownGene.gtf \
--threads 46 \
--output sample \
--generate_map \
--print_check

## `flair-collapse`
python ../flair.py collapse \
--genome
/hg38/GCA_000001405.15_GRCh38/GCA_000001405.15_GRCh38_no_alt_analysis_set/GRCh38_no_alt_analysis_set_chr_only.fa \
--reads /sample_reads.fastq \
--query sample_all_corrected.bed \
--gtf /hg38/unknown/hg38.knownGene.gtf \
--trust_ends \
--no_redundant best_only \
--threads 46 \
--output sample_stringent \
--stringent \
--generate_map

## `flair-quantify`
python ../flair.py quantify \
--reads_manifest /sample_manifest.tsv \
--isoforms sample_stringent.isoforms.fa \
--threads 46 \
--output sample_quantify \
--trust_ends \
--tpm
```

```
## `flair-diffExp`
 python ../flair.py diffExp \
--counts_matrix /sample_quantify.tsv \
--threads 46 \
--out_dir sample_diffexp \

 ## `flair-diffSplice`
 python ../flair.py diffSplice \
--counts_matrix /sample_quantify.tsv \
--isoforms sample_stringent.isoforms.fa \
--threads 46 \
--output sample_diffsplice \
```

## 9.3: Data repositories

Proteome Discoverer results files, gProfiler analysis results and FLAIR output files are stored in Excel spreadsheet format on the Open Science Framework (OSF) repository: https://osf.io/hs627/?view_only=0563901eb9004de7a187b5f3912bb487.[334]

Mass spectrometry data is stored in the MassIVE data repository:[333]

Chapter 3: ftp://MSV000090274@massive.ucsd.edu

Chapter 4: ftp://MSV000090288@massive.ucsd.edu

The RIME results were submitted to the IMEx (http://www.imexconsortium.org) consortium through IntAct [X] and assigned the identifier IM-29565.[336]